Claudio Margottini
Paolo Canuti · Kyoji Sassa
Editors

Landslide Science and Practice

Volume 4
Global Environmental Change

Springer

Claudio Margottini • Paolo Canuti • Kyoji Sassa
Editors

Landslide Science and Practice

Volume 4: Global Environmental Change

Springer

Editors
Claudio Margottini
ISPRA - Italian Institute for
Environmental Protection and Research
Geological Survey of Italy
Rome, Italy

Paolo Canuti
ICL - International Consortium on Landslides
Florence, Italy

Kyoji Sassa
UNITWIN Headquarters Building
Kyoto University Uji Campus
Uji, Kyoto, Japan

Associate Editors
Filippo Catani
Department of Earth Sciences
University of Florence
Firenze, Italy

Alessandro Trigila
ISPRA - Italian Institute for
Environmental Protection and Research
Geological Survey of Italy
Rome, Italy

Additional material to Volume 1 can be downloaded from http://extras.springer.com

ISBN 978-3-642-31336-3 ISBN 978-3-642-31337-0 (eBook)
DOI 10.1007/978-3-642-31337-0
Springer Heidelberg New York Dordrecht London

Library of Congress Control Number: 2013932640

Printed on acid-free paper

Springer is part of Springer Science+Business Media (www.springer.com)

Preface

Landslide Science and Practice

Proceedings of the Second World Landslide Forum

The Second World Landslide Forum (**WLF**) was organized at the headquarters of the Food and Agriculture Organization of the United Nations (FAO), Rome, Italy, on 3–9 October 2011. WLF is a triennial mainstream conference of the International Programme on Landslides (**IPL**) which is jointly managed by the IPL Global Promotion Committee consisting of the International Consortium on Landslides (**ICL**), the United Nations Educational, Scientific and Cultural Organization (UNESCO), the World Meteorological Organization (WMO), the Food and Agriculture Organization of the United Nations (FAO), the United Nations International Strategy for Disaster Risk Reduction (UNISDR), the United Nations University (UNU), the International Council for Science (ICSU), and the World Federation of Engineering Organizations (WFEO).

Background to the World Landslide Forums

The International Consortium on Landslides (ICL) was established by the 2002 Kyoto Declaration "Establishment of an International Consortium on Landslides," with the Statutes adopted in January 2002. The Statutes defined the **General Assembly** of ICL: In order to report and disseminate the activities and achievements of the consortium, a General Assembly shall be convened every 3 years by inviting Members of the International Consortium on Landslides, individual members within those organizations, and all levels of cooperating organizations and individual researchers, engineers, and administrators. The General Assembly will receive reports on Consortium activities and provide a forum for open discussion and new initiatives from all participants.

The First General Assembly 2005 to the First World Landslide Forum 2008

The First General Assembly was organized at the Keck Center of the National Academy of Sciences in Washington D.C., USA, on 12–14 October 2005. At this Assembly, the first full-color book reporting consortium activities for the initial 3 years, 2002–2005, was published as "Landslides-Risk analysis and sustainable disaster management" through Springer. The 2006 Tokyo Round-Table Discussion – "Strengthening Research and Learning on Earth System Risk Analysis and Sustainable Disaster Management within UN-ISDR as Regards Landslides" – toward a dynamic global network of the International Programme on Landslides (IPL) was held at the United Nations University, Tokyo, on 18–20 January 2006. **The 2006 Tokyo**

Action Plan – *Strengthening research and learning on landslides and related earth system disasters for global risk preparedness* – was adopted. The Tokyo Action Plan established a new global International Programme on Landslides (IPL) including holding World Landslide Forums. Accordingly, the Second General Assembly 2008 was replaced by the **First World Landslide Forum** and held at the United Nations University, Tokyo, Japan, on 18–21 November 2008.

Report of the Second World Landslide Forum

The Second World Landslide Forum – *Putting Science into Practice* – was organized at the Headquarters of the Food and Agriculture Organization of the United Nations (FAO) on 3–9 October 2011. It was jointly organized by the IPL Global Promotion Committee (ICL, UNESCO, WMO, FAO, UNISDR, UNU, ICSU, WFEO) and two ICL members in Italy: the Italian Institute for Environmental Protection and Research (ISPRA) and the Earth Science Department of the University of Florence with support from the Government of Italy and many Italian landslide-related organizations.

- 864 people from 63 countries participated. Attendance was larger than expected, and twice the attendance at the First World Landslide Forum 2008 in Tokyo (430 participants: 175 from Japan and 255 from abroad).
- 25 technical sessions were held, and 465 full papers were submitted. All accepted papers were edited in 7 volumes including this volume:
  1. Landslide Inventory and Susceptibility and Hazard Zoning
  2. Early Warning, Instrumentation and Monitoring
  3. Spatial Analysis and Modeling
  4. **Global Environmental Change – this volume**
  5. Complex Environment
  6. Risk Assessment, Management and Mitigation
  7. Social and Economic Impact and Policies

Requests of Cooperation for Further Development of ICL and IPL

ICL and IPL are global multidisciplinary and cross-sectoral initiatives to promote landslide science and capacity-development to reduce landslide disasters. The core activities of ICL and IPL are ***Landslides:*** Journal of International Consortium on Landslides, World Landslide Forum, and IPL projects. Thanks to worldwide support of the journal, the Impact Factor of ***Landslides*** was 2.216 for 2011 which is the highest within 30 ISI journals in category of Engineering, Geological. The journal will develop from a quarterly journal to a bimonthly journal from Vol. 10 in 2013. The Third World Landslide Forum – Landslide risk mitigation toward a safer geo-environment – at the China National Convention Center, Beijing, China, on 2–6 June (conference) and 7–11 June (Field Trip) 2014. The ICL entered into the second decade of its activities and organized a 10th anniversary Conference on 17–20 January 2012, in Kyoto, Japan. ICL adopted the ICL Strategic Plan 2012–2021, *To create a safer geo-environment*- as an outcome of this conference.

ICL is an international nongovernmental and nonprofit scientific organization promoting landslide research and capacity-building for the benefit of society and the environment, and is

the thematic landslides platform in the UNISDR Global Platform for Disaster Risk Reduction. ICL activities are supported by voluntary efforts of ICL members and supporting organizations. All people involving in landslide research and landslide disaster mitigation activities are requested to cooperate for the development of this initiative through its second decade 2012–2021. (http://www.iplhq.org/ *and* http://icl.iplhq.org/).

We are deeply appreciative of all e Second World Landslide Forum participants and of the contributions from our UNESCO, WMO, FAO, UNISDR, UNU, ICSU, WFEO partners and all of our colleagues in ICL for the development of IPL up to now. Finally we address our sincere thanks to Filippo Catani and Alessandro Trigila (the associate editors) for their extensive efforts covering the technical sessions, and reviewing and editing the papers.

Claudio Margottini
Forum Chair

Paolo Canuti
President of ICL

Kyoji Sassa
Executive Director of ICL

ICL and IPL Secretariat

IPL office: UNITWIN headquarters Buildings, Kyoto University Uji Campus,
Uji, Kyoto 611-0011, Japan
ICL office: The Association for Diaster Prevention Research,
138-1 Tanaka Asukai-cho, Sakyo-ku, Kyoto 606-8226, Japan
Email: secretariat@iclhq.org
URL: http://www.iplhq.org/ and http://icl.iplhq.org/

Organizational Structure of the Second World Landslide Forum

Organizers

IPL Global Promotion Committee including:
- International Consortium on Landslides (ICL) *
- United Nations Educational, Scientific and Cultural Organization (UNESCO)
- World Meteorological Organization (WMO)
- Food and Agriculture Organization of the United Nations (FAO)
- United Nations International Strategy for Disaster Risk Reduction (UNISDR)
- United Nations University (UNU)
- International Council for Science (ICSU)
- World Federation of Engineering Organizations (WFEO)
- Italian Institute for Environmental Protection and Research (ISPRA)

(* Members are listed in the last page of this book)

Co-sponsors

- International Union of Geological Sciences (IUGS)
- International Union of Geodesy and Geophysics (IUGG)
- International Geographical Union (IGU)
- International Flood Initiative (IFI)

Under the Auspices of

- International Association for Engineering Geology and the Environment, Italian Section (IAEG)
- Italian Association of Engineering Geologists (AIGA)
- Italian Association of Geotechnique (AGI)
- Italian Association for Mining Engineers, Environment and Territory (ANIM)
- Italian Georesources and Environment Association (GEAM)

International Organizing Board

Honorary Chairpersons

- Irina BOKOVA (UNESCO Director-General)
- Catherine BRECHIGNAC (ICSU President)
- Jacques DIOUF (FAO Director-General)

- Michel JARRAUD (WMO Secretary-General)
- Maria P. LAFFARGUE (WFEO President)
- Konrad OSTERWALDER (UNU Rector)
- Bernardo DE BERNARDINIS (ISPRA President)
- UNISDR Director

Chairpersons

- Claudio MARGOTTINI (ISPRA, Forum Chair)
- Paolo CANUTI (ICL President)
- Kyoji SASSA (ICL Executive-Director)

Deputy Chairpersons

- Peter BOBROWSKY (IUGS Secretary General)
- Deliang CHEN (ICSU Executive Director)
- Peter LYTTLE (ICL Vice President, US Geological Survey)
- Eduardo ROJAS-BRIALES (Assistant Director General of FAO)
- Badaoui ROUHBAN (Director of UNESCO's Section for Disaster Reduction)
- Yueping YIN (ICL Vice President, China Geological Survey)

Scientific Advisory Board

Representing Organisation

- Irasema ALCANTARA-AYALA (Vice President of International Geographical Union - IGU)
- Walter AMMAN (President Davos Forum)
- Michael CROZIER (President of International Association of Geomorphologists - IAG)
- Carlos DELGADO (President of International Association of Engineering Geology - IAEG)
- Luca DEMICHELI (Secretary General of EuroGeoSurveys)
- John HARDING (United Nations Secretariat to International Strategy for Disaster Reduction - UNISDR)
- Srikantha HERATH (Senior Academic Programme Officer of the United Nations University - UNU)
- Thomas HOFER (Forestry officer, Food and Agriculture Organization of the United Nations - FAO)
- Yumio ISHII (Chair of the Committee on Disaster Risk Management of The World Federation of Engineering Organizations WFEO)
- Derek MARTIN (Vice President for North America of International Society for Rock Mechanics - ISRM)
- Howard MOORE (Senior Advisor, International Council for Science - ICSU)
- Pedro SECO E PINTO (Past President of International Society for Soil Mechanics and Geotechnical Engineering - ISSMGE)
- Luciano PICARELLI (Chairperson of the Joint Technical Committee on Landslides and Engineered slopes - JTC1 of ISSMGE, ISRM, IAEG)
- Kaoru TAKARA (Vice chairperson of the Intergovernmental Council of the International Hydrological Programme of UNESCO - IHP)
- Kuniyoshi TAKEUCHI (President of GeoRisk Commission of International Union of Geodesy and Geophysics - IUGG)

Landslide Experts

- Giovanni BARLA (Politecnico di Torino, Italy)
- R.K. BHANDARI (Consultant, India)
- Christophe BONNARD (Swiss Federal Institute of Technology, Lausanne, Switzerland)
- Nicola CASAGLI (University of Florence, Italy)
- Leonardo CASCINI (University of Salerno, Italy)
- Giovanni CROSTA (University of Milano Bicocca, Milano, Italy)
- Jordi COROMINAS (Technical University of Catalonia, Barcelona, Spain)
- Dave CRUDEN (University of Alberta, Edmonton, Alberta, Canada)
- Thomas GLADE (University of Vienna, Austria)
- Jerome DE GRAFF (United States Department of Agriculture , Fresno - Ca - USA)
- Michel HERMELIN (Universidad EAFIT, Medellin, Colombia)
- Ken HO (Hong Kong Geotechnical office, Hong Kong, China)
- Jurgen KROPP (Potsdam Institute for Climate Change - PIK, Potsdam, Germany)
- Richard M. IVERSON (United States Geological Survey - Vancouver, WA , USA)
- C. F. LEE (Hong Kong University, China)
- Jacques LOCAT (University of Laval, Canada)
- Paul MARINOS (University of Athens, Greece)
- Hideaki MARUI (Niigata University, Japan)
- Hormoz MODARESSI (BRGM, Orléans, France)
- Farrouk NADIM (Norwegian Geothecnical Institute - NGI, Oslo, Norway)
- Gabriele SCARASCIA MUGNOZZA (University of Rome, Italy)
- Wang SIJING (Tsinghua University, China)
- Vern SINGHROY (Canada Centre for Remote Sensing, Ottawa, Canada)
- Alexander STROM (Institute of Geospheres Dynamics, RAS, Moscow, Russia)
- Ikuo TOWHATA (University of Tokyo, Japan)
- Keith TURNER (Emeritus Professor, Colorado School of Mines, Denver, Colorado USA)
- Keizo UGAI (Gunma University, Kiryu,Gunma, Japan)
- Roger URGELES (Institut de Ciències del Mar - CSIC, Barcelona, Spain
- Yasser el SHAYEB (Cairo University, Egypt)
- Sergio SEPULVEDA (University of Chile, Santiago)
- Mauro SOLDATI (University of Modena and Reggio Emilia, Italy)
- Pasquale VERSACE (Calabria University, Cosenza, Italy)
- Cees van WESTEN (ITC, Enschede, Netherlands)
- Kifle WOLDEAREGAY (University of Mekelle, Ethiopia)

Local Organizing Board

Forum Chairs

- Paolo CANUTI (ICL President - WLF2 Chairperson)
- Claudio MARGOTTINI (ISPRA - WLF2 Chairperson)
- Kyoji SASSA (ICL Secretary General - WLF2 Chairperson)

Scientific Programme Committee

- Luciano PICARELLI (Second University of Napoli)
- Marco AMANTI (ISPRA)
- Filippo CATANI (University of Firenze)
- Fausto GUZZETTI (CNR-IRPI)
- Javier HERVAS (JRC)

- Thomas HOFER (FAO)
- Carla IADANZA (ISPRA)
- Claudio MARGOTTINI (ISPRA - WLF2 Chairperson)
- Paolo TOMMASI (CNR-IGAG)
- Alessandro TRIGILA (ISPRA)

Editorial Committee

- Filippo CATANI (University of Firenze)
- Riccardo FANTI (University of Firenze)
- Fausto GUZZETTI (CNR-IRPI)
- Javier HERVAS (JRC)
- Irene RISCHIA (ISPRA)
- Gabriele SCARASCIA MUGNOZZA (Università di Roma "La Sapienza")
- Alessandro TRIGILA (ISPRA)

Logistic Committee

- Thomas HOFER (FAO)
- Claudio MARGOTTINI (ISPRA - WLF2 Chairperson)
- Orlando PANDOLFI (ECN)
- Luna GUBINELLI

Field Trips

- Gabriele SCARASCIA MUGNOZZA (University of Roma "La Sapienza")
- Giuseppe DELMONACO (ISPRA)
- Riccardo FANTI (University of Firenze)
- Irene RISCHIA (ISPRA)
- Daniele SPIZZICHINO (ISPRA)
- Paolo TOMMASI (CNR-IGAG)

Fund Raising and Exhibition

- Claudio MARGOTTINI (ISPRA - WLF2 Chairperson)
- Paolo FARINA (IDS SpA)
- Giorgio LOLLINO (CNR-IRPI)

Secretariat

ISPRA, Italian Institute for Environmental Protection and Research
Dept. Geological Survey of Italy, Via Vitaliano Brancati, 48-00144 Rome, Italy.

Logistics and Administration

Orlando PANDOLFI - ECN yourLIFE Foundation

Contents

Part I

Landslide Scenarios Accounting for Climatic, Geomorphological and Geotechnical Contexts

Introduction by Luciano Picarelli[1] and Vit Vilímek[2]

1) Department of Civil Engineering, Seconda Università di Napoli, via Roma 29, Aversa, Italy
2) Department of Physical Geography and Geoecology, Charles University, Prague, Czech Republic

Opening Address

Meteorological factors are among the main causes of slope failure. Precipitations ad snow-melt, temperature fluctuations, air humidity and other factors can trigger landslides, directly, or through associated geological processes such as erosion, weathering ad so on. The geomorphological conditions and the nature and properties of outcropping soils, interacting with previously mentioned factors, play an important role too. As a matter of fact, in different geomorphological and geotechnical contexts similar weather conditions cannot cause the same effects. This suggests that incoming climate changes will produce a relevant impact on hydrogeological risks, but also that the geomorphological and geotechnical context should be properly accounted for when depicting scenarios aimed at a reliable land planning for the near future. Scientists and land planners are more and more aware of these problems and an increasing number of papers, reports, workshops and conferences is being devoted to this subject and to related topics. These have been good reasons to propose and organize in this World Landslide Forum the session titled "Landslide scenarios accounting for climatic, geomorphological and geotechnical contexts" which drew some interesting contributions part of which are briefly mentioned below.

Precipitations (rainfalls and snowfalls) represent the most evident and direct cause of weather-induced landslides. Water infiltration is responsible for increase in water content in unsaturated soils with consequent decrease in suction, for increase in pore pressures in saturated soils with consequent decrease in effective stresses, or even for cleft pressures building up in both fractured rocks and stiff fissured soils with consequent increase in destabilizing forces. The effects of rainfalls are delayed depending on the hydraulic diffusivity of shallowest soils and on the water paths (i.e. thickness of involved layers): the delay can range between hours and months (e.g. Klimeš and Vilímek 2011). However, the role of rainfall is generally very complex since the entire precipitations history and intensity and distribution of single downpours, as well as the duration of windows in between couples of them and the intensity of associated evapotranspiration, play a prominent role. In case of snowfalls, the role of temperature is still greater. Important quantitative contributions on the influence of precipitations on the stability of slopes have been published in the last 20 years (Brand et al. 1984; Guzzetti et al. 2008; Rahardjo et al. 2009) and well documented case histories provide useful data for a proper interpretation of landslides occurred in the past and for prediction of potential future events (Springman et al. 2003; Rahardjo et al. 2005; Zhan et al. 2007; Damiano et al. 2012; Pirone et al. 2012).

Naturally, the role of weather does not stop here since deglaciation, melting of frozen soils, erosion and other phenomena have a significant impact on the stability of slopes through different and complex mechanisms. On the other hand, in some cases further different factors

can interact with those associated with weather. For instance, in tectonically active areas, a combination of different impacts, as intense erosion, tectonically crushed zones, seismicity, can produce favourable conditions for slope deformations and failure. In addition, mostly in highly populated areas, anthropogenic impacts play a prominent role. In these cases, precipitations may be the triggering cause, but other factors, often difficult to be quantified, may act as preparatory causes; the opposite is also possible with precipitations acting as a preparatory cause. Sometimes, it is nearly impossible to classify the cause of a landslide, because there are too many potential triggers. Polemio and Lonigro in this session show that in the Apulia region (Italy), where climatic changes characterised by a decrease of rainfall should lead to higher slope stability, an increase of landslides has been observed and can be explained as a result of a worse land use. Gomez and Villarraga illustrate the same problem for the urban area of Medellin, Colombia, where both the effects of intense rainfalls and the anthropogenic activity are responsible for several landslides in residual soils.

Mechanisms and types of precipitation-induced landslides are being more and more discussed within the geo-scientific community in relation with climatic changes. These can produce uneasily quantifiable modifications of weather parameters playing a key role on individual types of slope movements. However, the stability conditions in single contexts are different. For instance regelation processes are of key importance on rock falls (e.g. Grøneng et al. 2011), increase in temperature govern shallow slope movements in periglacial zones and increased sea level affects the stability of costal areas. On the other hand, in some areas dryness can cause an increased frequency of fires and formation of debris flows. Therefore, the impact of climatic change on the stability of slopes must be investigated and understood in the context of the different geomorphological (e.g. fluvial, glacial or periglacial type of relief) and geotechnical conditions (e.g. in rock masses, weathered covers, coarse or fine grained soils and so on), in order to develop correct adaptation strategies (Allen et al. 2011). In this session Mateos et al. discuss the types and mechanisms of landslides triggered in the last years in the Mallorca island, Spain, during extremely wet and cold winters. The mechanisms of landslides in Canada due to valley erosion, are described by Geertsema based on previous models. He remarks that future climate changes could modify the valley evolution trends and the same landslide mechanisms. Bertolini and Fioroni report a nice discussion on the mechanisms of earthflows in Italian Apennines, highlighting the interaction processes which govern the landslide type with special reference to undrained conditions that establish within the earthflow body.

To correctly assess the relationship between precipitations and landslides, careful investigations are requested over long periods. An example is reported by Floris et al. for the Vicenza province, at the foothills of the Alps, North-East Italy, where long-term readings of temperature (since 1949), daily rainfall amounts (since 1920) and downpours in five minute intervals (since 1990) led to useful considerations about regional climate change. In particular, last 20 years have been characterised by an increase in temperature and a decrease in rainfalls which, in principle, should lead to an increase in stability conditions in landslide prone areas. However, a more detailed analysis shows an increase in rainfall and unchanged temperature in autumn, thus a worsening of stability conditions. Another interesting result is the increase of the number of short intense rainfall events which occurred in 1966, 1992 and 2010. Finally Khov and Hang report interesting observations about the evolution of the groundwater level in an area in Estonia, based on piezometer readings and groundwater monitoring wells.

The effects of future climate changes have been examined also by Damiano and Mercogliano and by Comegna et al. looking at the geotechnical context, considering the available scenarios for many parts of the Mediterranean basin where less rainfall with higher intensity are expected. Since landslides in clay are a consequence of cumulated rainfall over months due to their low hydraulic conductivity, according to Comegna et al., who report useful well documented data, landslide activity should be lower. In contrast, in regions covered by relatively permeable soils (as Campania where pyroclastic soils prevail, or South-East Asia

which is occupied by decomposed granites or China by loess), shallow covers should be more and more susceptible to landslide which can turn into rapid flowslides or debris flows. An interesting contribution on that has been provided by Damiano and Mercogliano in their report, where they have described some believable future scenarios in pyroclastic soils.

One of the key factors for real-time prediction of rainfall-induced slope movements is a deeper knowledge of precipitations threshold levels. In particular, it is necessary to differentiate extreme precipitations (for instance from the perspective of their hourly amount) and longer lasting rainfall (cumulative amount) accounting for the kinematics of movements (for instance continuous movement characterised by accelerations, seasonal movements) not neglecting temperature effects (evapotranspiration). On the other hand, in some areas it is necessary to consider large potential differences in precipitation even over very short distances due to landscape variability, slope orientation and high relative altitude differences (Vilímek et al. 2006). An in depth analysis of these problems was done by Tiranti and Rabuffetti (2011) in 160 landslide localities in Piedmont region in Italy. They analysed daily precipitation in the period 1990–2002 and 429 landslides. The result is a prediction model of shallow slides developed separately for two different regions in dependence on their geomorphological and lithologic predispositions.

An important issue for land managers is the capability to predict in due time landslide triggering induced by incoming precipitations. This has a fundamental importance for risk mitigation and people safety in those areas that are prone to rapid catastrophic landslides. Besides well know approaches as the one proposed by Caine (1980) based on empirical elaboration of previous events, or by Sirangelo and Versace which account of both the precipitation history and the triggering rain (1996), new procedures are being developed using real-time numerical analyses of infiltration (Pagano et al. 2010) or coupling of short-term weather forecasting and numerical analysis of the slope behaviour. Two on-going researchers on this subject have been presented by Mercogliano et al. and by Bailles et al. who describe codes available for both analyses (short-term weather forecasting and slope stability analysis) and report some simulations regarding landslides occurred in the recent past.

References

Allen SK, Cox SC, Owens IF (2011) Rock avalanches and other landslides in the central Southern Alps of New Zealand: a regional study considering possible climate change impats. Landslides 8(1):33–48

Bailles A, Vandromme R, Desramaut N, Sedan-Miegemolle O, Grandjean G (this session)

Bertolini G, Fioroni C (this session)

Brand EW, Premchitt J, Philipson HB (1984) Relationship between rainfall and landslides in Hong Kong. In: Proceedings of 4th international symposium on landslides, vol 1, Toronto, pp 377–384

Caine N (1980) The rainfall intensity-duration control of shallow landslides and debris flow. Geogr Ann A-Phys Geogr 62(1–2):23–27

Comegna L, Tommasi P, Picarelli L (this session)

Damiano E, Mercogliano P (this session)

Damiano E, Olivares L, Picarelli L (2012) Steep-slope monitoring in unsaturated pyroclastic soils. Eng Geol 137–138:1–12

Floris M, D'Alpaos A, De Agostini A, Tessari G, Genevois R (this session).

Geertsema M (this session)

Gomez E, Villarraga M (this session)

Grøneng G, Christiansen HH, Nilsen B, Blikra LH (2011) Meteorological effects on seasonal displacements of the Aknes rockslide, western Norway. Landslides 8(1):1–15

Guzzetti F, Peruccacci S, Rossi M, Stark CP (2008) The rainfall intensity-duration control of shallow landslides and debris flows: an update. Landslides 5(1):3–17

Khov M, Hang T (this session)

Klimeš J, Vilímek V (2011) A catastrophic landslide near Rampac Grande in the Cordillera Negra, northern Peru. Landslides 8(3):309–320

Mateos R M, Garcia-Moreno I, Herrera G, Mulas J (this session)

Mercogliano P, Casagli N, Catani F, Damiano E, Olivares L, Picarelli L, Rossi G, Schiano P, Segoni S, Sikorski B, Tofani V (this session)

Pagano L, Picarelli L, Rianna G, Urciuoli G (2010) A simplified approach for timely prediction of precipitation-induced landslides in unsaturated pyroclastic soils. Landslides 7(3):273–289

Pirone M, Damiano E, Picarelli L, Olivares L, Urciuoli G (2012) Groundwater-atmosphere interaction in unsaturated pyroclastic slopes. Field monitoring of two test sites. Rivista Italiana di Geotecnica, 3:29–49

Polemio M, Lonigro T (this session)

Rahardjo H, Lee TT, Leong EC, Reazour RB (2005) Response of a residual soil slope to rainfall. Can Geotech J 42(2):340–351

Rahardjo H, Reazour RB, Leong EC (2009) Mechanism of rainfall-induced slope failures in tropical regions. In: Picarelli L, Tommasi P, Urciuoli G, Versace P (eds) Proceedings of 1st Italian workshop on landslides, vol 1, Naples, pp 31–42

Sirangelo B, Versace P (1996) A real time forecasting for landslide triggered by rainfall. Meccanica 31:1–13

Springman SM, Jommi C, Teysseire P (2003) Instabilities on moraine slopes induced by loss of suction: a case hystory. Geotéchnique 53(1):3–10

Tiranti D, Rabuffetti D (2011) Estimation of rainfall thresholds triggering shallow landslides for an operational warning system implementation. Landslides 7(4):471–781

Vilímek V, Klimeš J, Vlčko V, Carreño R (2006) Catastrophic debris flows near Machu Picchu village (Aguas Calientes), Peru. Environ Geol 50(7):1041–1052

Zhan TLT, Ng CWW, Fredlund G (2007) Field study of rainfall infiltration into a grassed unsaturated expansive soil slope. Can Geotech J 44(4):392–408

Rock Glacier Degradation and Instabilities in the European Alps: A Characterisation and Monitoring Experiment in the Turtmanntal, CH

Sarah M. Springman, Yuko Yamamoto, Thomas Buchli, Marian Hertrich, Hansruedi Maurer, Kaspar Merz, Isabelle Gärtner-Roer, and Linda Seward

Abstract

Global climate change is impacting sensitive alpine cryogenic regions, through slope instabilities in rocks and soils. Significant temperature increase at the air-ground surface interface may be accompanied by increased rainfall, more extreme storms and additional severe rise in mean global temperatures in the coming decades, enhancing risk of mass movement hazards to human life and infrastructure. Rock glaciers and degrading permafrost on steep Alpine slopes are particularly susceptible to warming and phase change in either massive or interstitial ground ice, which may lead to release of water, accelerated motions, initiation of landslides and instabilities. Accumulated failure in soil elements, determined on artificial frozen specimens of rock glacier materials at temperatures below 0 °C, is linked to these processes at field scale. A geophysical and geotechnical field characterisation and monitoring experiment is being conducted on a rock glacier that is undergoing thermally induced creep and growth of thermokarst. Preliminary investigations are described in this contribution.

Keywords

Alpine permafrost • Rock glacier • Landslide • Thermal degradation • Characterisation • Geophysics

Introduction

Global climate change is estimated to impact mountainous cryogenic regions more than the global average (Vonder Mühll et al. 2008). IPCC reported temperature increase on top of the Arctic permafrost layer by up to 3 °C between 1980 and 2007, and thawing of the permafrost base at up to 0.04 m/year. Climate scenarios for the Swiss Alps (time horizon of 2050) indicate changes in temperature/precipitation by +2 °C/+10 % in winter and +3 °C/−20 % in summer, with predicted loss of ~75 % of glacier surface and deep warming of mountain permafrost, impacting landscape cover, hydrology and slope stability (Hohmann 2007; Haeberli and Hohmann 2008).

Rock glaciers and degrading permafrost on steep Alpine debris slopes are becoming more susceptible to melting of ice and initiation of landslides, debris flows and other instabilities associated with accelerated land motions, which introduce various forms of hazard to human life and infrastructure. The risk of mass movements due to degrading permafrost can be expected to increase over the next decades.

Permafrost is defined as soil/rock at, or below 0 °C for at least two consecutive winters and the intervening summer.

S.M. Springman (✉) • Y. Yamamoto • T. Buchli • L. Seward
Institute of Geotechnical Engineering, Swiss Federal Institute of Technology, Wolfgang-Pauli-Str. 15, Zurich 8093, Switzerland
e-mail: sarah.springman@igt.baug.ethz.ch

M. Hertrich • H. Maurer • K. Merz
Institute of Geophysics, Swiss Federal Institute of Technology, Sonnegg-Str. 5, Zurich 8092, Switzerland

I. Gärtner-Roer
Department of Geography, University of Zurich, Winterthur-Str. 190, Zurich 8057, Switzerland

Department of Geography, University of Bonn, Meckenheimer Allee 166, Bonn 53115, Germany

C. Margottini et al. (eds.), *Landslide Science and Practice*, Vol. 4,
DOI 10.1007/978-3-642-31337-0_1,

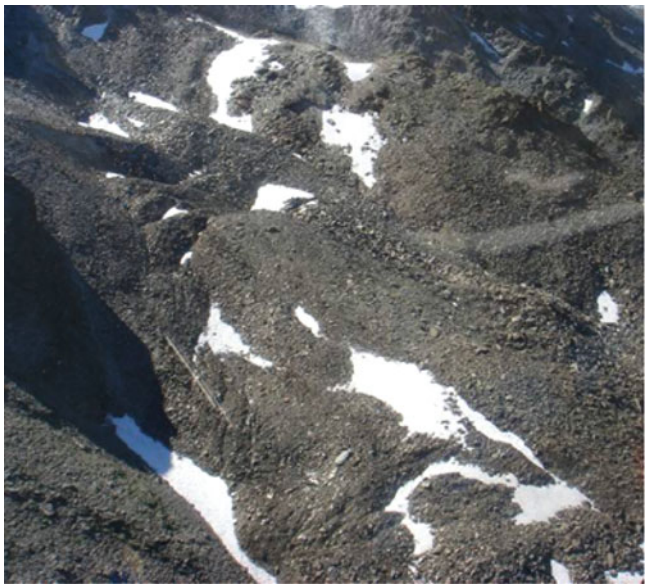

Fig. 1 Photograph of the Furggwanghorn rock glacier and environment (VS)

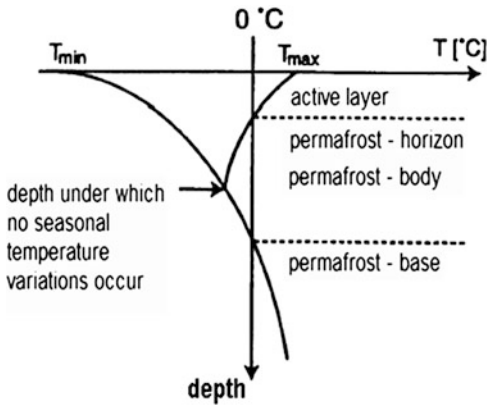

Fig. 2 Definition of permafrost (see also http://nsidc.org/fgdc/glossary) (After Brown et al. 1981)

Land mass on Earth (20 % area) and in Switzerland (~7 %) is covered by continuous and discontinuous permafrost, with extent varying with latitude, altitude, aspect and climate change. Alpine permafrost exists at high altitudes in lower latitude regions through rock glaciers (Giardino et al. 1987; Martin and Whalley 1987; Barsch 1996) creeping downslope and exhibiting evidence of a viscous geomorphological form (Fig. 1). An active layer lies above the permafrost layer (Fig. 2), cycling seasonally above and below freezing temperatures, with depth acutely sensitive to surface temperature and climate variability (Lachenbruch and Marshall 1986; Haeberli et al. 2006).

Mass Movements Triggered by Permafrost Degradation

Catastrophic slides have been triggered due to the reduction in strength as the ice phase warms, induced by climate change (e.g. Haeberli 1992; Zimmermann and Haeberli 1992; Haeberli et al. 1993a; 1997; Davies et al. 2001; Wuilloud, 2008, private communication). Many debris flows were attributed to have occurred due to melting ice at Val Pola (northern Italy south of Bormio, Crosta et al. 2004). Hundreds of landslides and severe flooding occurred between 15th and 22nd July 1987, causing loss of life and large scale economic damage. The temperature was reported to be unusually warm during this period, while the 0 °C isotherm shifted from a typical alpine value of 2,500 m (Vonder Mühll and Haeberli 1990; Arenson 2002; Maurer and Hauck 2007) to between 3,500 and 4,000 m. As well, abnormally high rainfall was noted (600 mm from 15–22/07/87: mean annual rainfall is generally 1,200 mm). The combination of heavy rainfall and exceptionally warm temperatures led to melting of frozen soil and interstitial ice, which in turn led to pore pressure build up, loss of strength, high runoff, severe flooding, which triggered landslides that were characterised by shallow failures, mostly becoming debris flows as they mobilised.

Numerous debris flows have also been recorded at Ritigraben in the Valais, CH (Rebetez et al. 1997), threatening roads, bridges, a railway line and two villages (Grächen and Sankt Niklaus). The Ritigraben torrent system is oriented WNW, is 3.5 km long and ranges from an altitude of 3,100 m at the ridge to 1,050 m in the valley floor. The upper part of the unstable system is in the alpine periglacial zone, with discontinuous frozen ground (King and Akerman 1993). Past studies (Pfister and Hächler 1990; Röthlisberger 1991; Mani 1994) have provided a record of floods from the Valais/Ritigraben area for the majority of the twentieth century, which indicate that the Ritigraben has been subject to nine large debris flows between 1921 (Schnydrig 1952) or 1922 (Mani 1994) and 1996 (Rebetez et al. 1997). These debris flows have become more frequent since the late 1980s (four major events have occurred between 1987 and 1994). A large scale debris flow occurred on September 24, 1993 at the Ritigraben torrent, and had a devastating effect on local infrastructure as it cut across two roads, a railway line and destroyed a bridge. All these debris flows (with the exception of the 1962 event) occurred at the end of summer/beginning of autumn, when the active layer of the permafrost is unfrozen in the periglacial belt. Seven of the nine debris flows were triggered by excessive rainfall events in the Alps, with the remaining two debris flows (1962 and 1994) being triggered by snowmelt. The flow has been shown to have begun at altitudes of above 2,400 m in the Alpine periglacial zone and within the zone of discontinuous permafrost

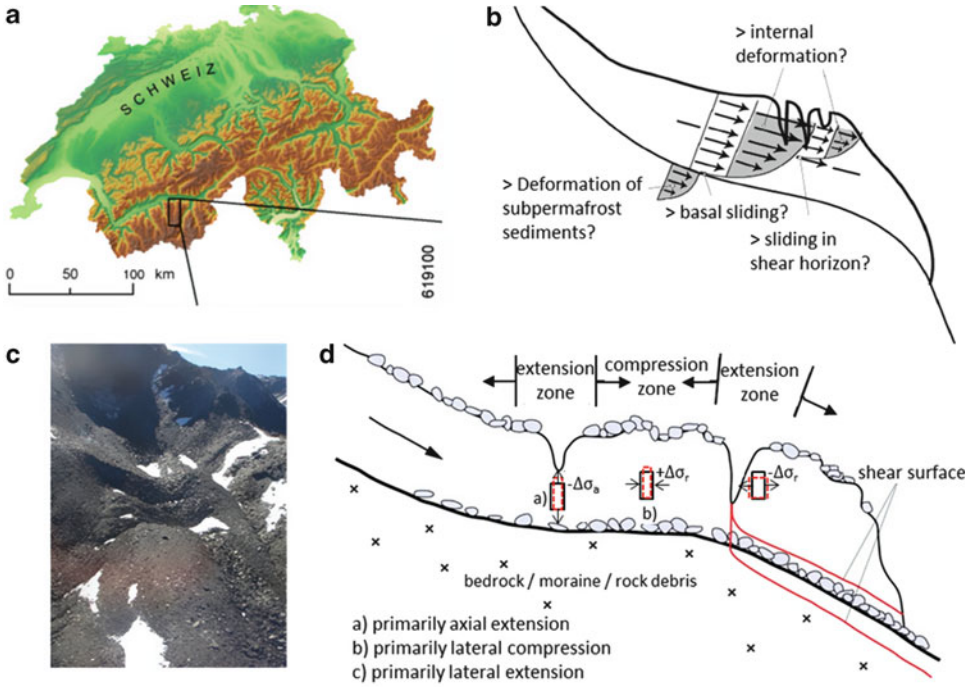

Fig. 3 (**a**) Turtmanntal enclosed within the rectangular box superimposed on the South West Alps (after Nyenhuis 2005); (**b**) cross sections during thermal degradation of mountain permafrost including formation of 'crevasses' (Roer et al. 2008); (**c**) Photograph of the rooting zone in the Furggwanghorn rock glacier in Turtmanntal, Valais (Sarah Springman); (**d**) possible zones of extension and compression with shear planes extending from the base of a crevasse as it deepens, as well as at the surface (within the active layer)

(Haeberli 1990) in the 1921/1922, 1953 and 1993 events (Mani 1994).

More recently, the Bèrard rock glacier in the Parpallion Range in the Southern French Alps has been subjected to a combination of slumping and debris flow due to extreme storm and rains, demonstrating the effect of permafrost degradation on mountain slope stability. It was described as quasi-complete destabilisation of the landform by Krysiecki et al. (2008), releasing about 1.5 million m^3 of material into the adjacent valley in summer 2006. Geomorphological studies revealed that the collapse was probably related to an underlying rockslide in the schist below (Krysiecki et al. 2008), which may have been activated by storms. Current studies are focusing on monitoring ongoing rock glacier movements using Electrical Resistance Tomography, Seismic Refraction Tomography and GPS measurements accompanied by a thermal monitoring weather station. No significant movement of the displaced mass was obtained during the first 3 months. The remaining rock glacier was subject to large movements (displacements of more than 5 m in 3 months). Studies are still being carried out, and once published, should give an interesting insight into mechanisms affecting rock glaciers in the warming French Alps.

The Grabengufer rock glacier is small, steep, 500 m long and 100 m wide. It is located close to the lower limit of the regional discontinuous permafrost belt in the Swiss Alps in the Valais. Analysis of 1-day ERS-1/2 differential SAR interferograms showed a displacement rate of 0.5–1 cm/day during 1993–1997. More recently, this rock glacier has

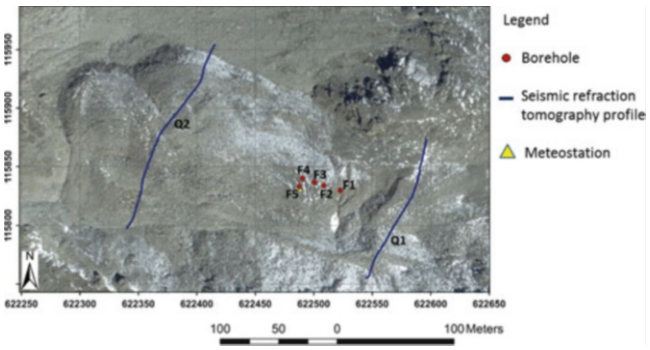

Fig. 4 Orthophoto with the position of boreholes, meteostation and seismic sections along profiles Q1 and Q2 (after Swisstopo)

accelerated, in common with many other small rock glaciers in the region (Delaloye et al. 2008; Roer et al. 2008). Several measurements series have been conducted since July 2009 (Delaloye et al. 2010), including lateral pictures, permanent GPS (June 2009–February 2010) and a ground-based InSAR survey. Results after 8 months of survey include extremely high surface velocities, ranging from 30 to more than 200 m/year in some rock glacier sections. Rapid erosion of the front has occurred in mid-February 2010, as new scarps developed, with surfaces tending to dip backwards, evidencing the development of rotational failures at the foot of the rock glacier combined with slumping. This is predicted to continue until a total amount of about 250,000 m^3 of rocky debris erodes into the gully beneath the rock glacier snout.

Rising temperatures have also induced rapid motion of other rock glaciers in the Turtmann valley in the Valais (CH), exposed through recent photogrammetric studies (Roer et al. 2005, 2008; Kääb et al. 2007) (Fig. 3a, c), which are compounding the urgency for improved understanding and predictability of rock glacier stability in the face of climate warming and will be investigated subsequently in this paper.

The existence and dynamics of unfrozen water in frozen soils within permafrost (Boike et al. 1998; Romanovsky and Osterkamp 2000) affect the hydro-thermal regime within rock glaciers (Rist and Phillips (2005) and Rist (2007)). They found that values for hydrological and thermal parameters in the ground, estimates of slope stability and meteorological parameters were closely correlated in time during thawing periods. Instantaneous increase in ground temperature was caused by convective heat transfer and latent heat was released due to phase change of infiltrating meltwater from surficial snow. Downslope displacement begun simultaneously. Their laboratory experiments showed that a slope failure is most likely in summer, when the thawing active layer deepens into finer grained materials, which is saturated, mainly due to heavy rainfall. Snowmelt was found to be less critical, because a large amount of the infiltrating water froze in the active layer, which was still cold, and the surficial deposits were stabilised by the ice. Ice formed during this period determined the water content during active layer thawing, which was found to be important for the disposition of slope failure in summer, as was the three dimensional nature of the active layer in degrading zones of rock glaciers (e.g. in Muragl, CH, after Arenson 2002).

The Furggwanghorn Rock Glacier Test Site

The Turtmann valley is located in the Western Swiss Alps. Numerous rock glaciers are found on its Eastern slope (Figs. 1 and 3a) (e.g. van Tatenhove and Dikau 1990; Nyenhuis 2005; Roer 2005) with the 0 °C isotherm at about 2,550 m.a.s l. Long period observations of air temperature and horizontal movements show clear correlation between air temperature variations and accelerated flow of assorted rock glacier units (e.g. Roer et al. 2005; Kääb et al. 2007). The increased flow rates, most probably combined with thermal degradation, have led to deep crevasses forming in the rock glacier bodies, which may lead to destabilising processes (Fig. 3b, Roer et al. 2008). Investigations are required to locate potential shear surfaces that could lead to formation of a detachment slide, either along the active layer or a deeper shear surface through the crevasses to the base of the rock glacier (Fig. 3d). Significant volumes of degrading frozen debris would be mobilised; either causing collapse (volume loss into existing thermokarst), translational sliding or debris flows, as probably occurred at the Bérard rock glacier.

Preliminary Geophysical Investigations

Several geophysical investigations have been performed to characterise critical subsurface structures, and primarily to locate permafrost, so that boreholes could be positioned and drilling depths decided. Two seismic refraction tomography profiles were acquired in spring 2010 to delineate the bedrock topography of the rock glacier and to map large-scale internal structures. The location of the profiles is shown in Fig. 4.

The active layer and the snow cover can be identified in both profiles by the 3–10 m thick layer with relatively low shear wave velocities between 500 m/s and 1,500 m/s near the surface of the rock glacier. Zones with velocities >4,500 m/s are indicative of bedrock or very large boulders, whereas the permafrost is expected to have velocities around 3,000–4,000 m/s. Zones with degraded permafrost show velocities around 2,000 m/s.

The thickness of the permafrost is less than 5 m with bedrock occurring at a depth of about 10 m in the southern part of profile Q1 (Fig. 5a). The bedrock is not clearly defined in the northern part. A permafrost body might exist and extend to a depth of around 15–20 m.

Profile Q2 in (Fig. 5b) shows a very heterogeneous internal structure of the rock glacier. A bedrock barrier in the centre of the profile seems to divide the rock glacier into two flow branches. High velocity anomalies within the rock glacier may indicate the presence of large boulders. Zones with lower velocities near the southern end of the profile are an indication of beginning of degradation of the permafrost.

In order to obtain more comprehensive subsurface information, additional geophysical measurements (ground-penetrating radar, electrical resistivity tomography, nuclear magnetic resonance) are currently being carried out and interpreted. A three-dimensional subsurface model will be established based on this information, as input to the geotechnical models.

Boreholes, Instrumentation, Meteorological Station

Two major zones of interest had been identified from field observations. Thermal degradation was apparent due to deepening troughs at the rock glacier root, running NNE-SSW (around 622,520 E, 115,830 N). The first drilling campaign was designed to investigate thermal response along a transect. The second area extends from the rooting

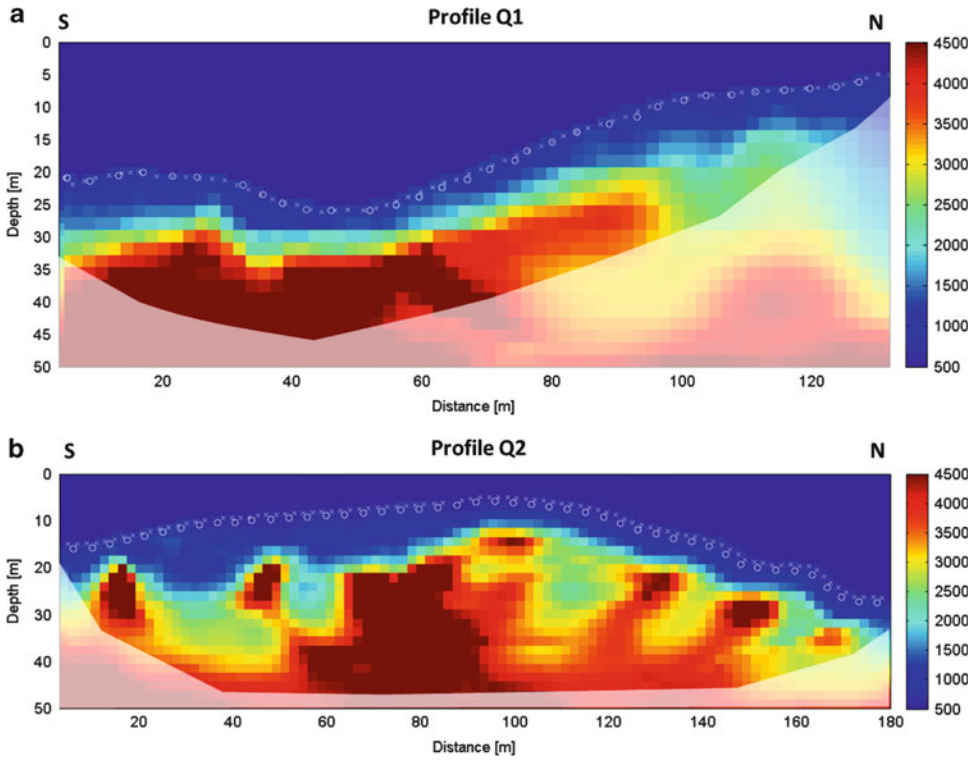

Fig. 5 Seismic sections along (**a**) profile Q1 and (**b**) profile Q2. The locations of the profiles are shown in Fig. 4. Source positions are indicated by *circles*, receiver positions by *crosses*. *Faint areas* are not well resolved by the data

zone to the WWN, where annual surface movements of over 3 m had been observed, and the causes of this high rate of strain were of interest.

Figures 5 and 6a show the position of five boreholes (F1–F5). Based on the data presented in Fig. 5a and b, these were drilled to 25 m depth in summer 2010 to try to locate active layer, permafrost and bedrock. The irregular surface indicates the different flow regimes in the rock glacier.

An inclinometer was manufactured from four chains, each with eight sections of rods of 0.5 m length and with rotary joints at each end, and installed in F5. Orthogonal tiltmeters in the vertical plane measured rotation of each section to determine displacement of the rock glacier with depth (www.terramonitoring.ch).

Monitoring results over the half year (Oct. 2010–Apr. 2011) show that the boreholes F3, F4 and F5 have moved downslope from F1 and F2. A movement of 1.5 m was measured at the surface during this time, accompanied by visible surface deformations. Several cracks were identified between F3 and F5, which may indicate seasonal movements of the active layer (Fig. 6b). Large displacements of the rock glacier, more or less at constant strain rate, were measured by the inclinometer as well, with a concentrated shear zone located between 14 and 15 m depth.

Thermistor chains have been installed in boreholes F1 to F4, with 30 temperature sensors spaced at either 0.5 or 1 m. The temperature distribution in F1 is shown in Fig. 7a for the first 6 months. The cooling effect during winter can be seen up to a depth of 8 m, below which the temperature remained just below zero, without significant seasonal change. The boreholes F2 and F3 show a similar temperature distribution as borehole F1 for the first 6 months. The winter cooling effect in F4 is not discernible (Fig. 7b). The temperature below 8 m depth remained close to 0 °C in all four boreholes during the measuring period. Measurements on the rock glacier were supplemented by a meteorological station that recorded wind speed and direction, long and shortwave radiation, water equivalent of snow and rain, humidity, air temperature and snow depth (Fig. 8). All data were registered by a logger located next to F5.

The meteorological data presented in Fig. 8 indicate a winter period 2010–2011 with early and continuous snow cover since mid-October, which decays, perhaps exponentially during periods in which mean air temperature exceeds 0 °C. Snow depths have persisted notwithstanding several - multi-day periods during which the air temperature exceeded 0 °C and increased up to just over 1 m on two separate occasions. The apparent loss in snow depth shortly after 10th March reflects anthropogenic effects due to excavation of snow around the meteorological station.

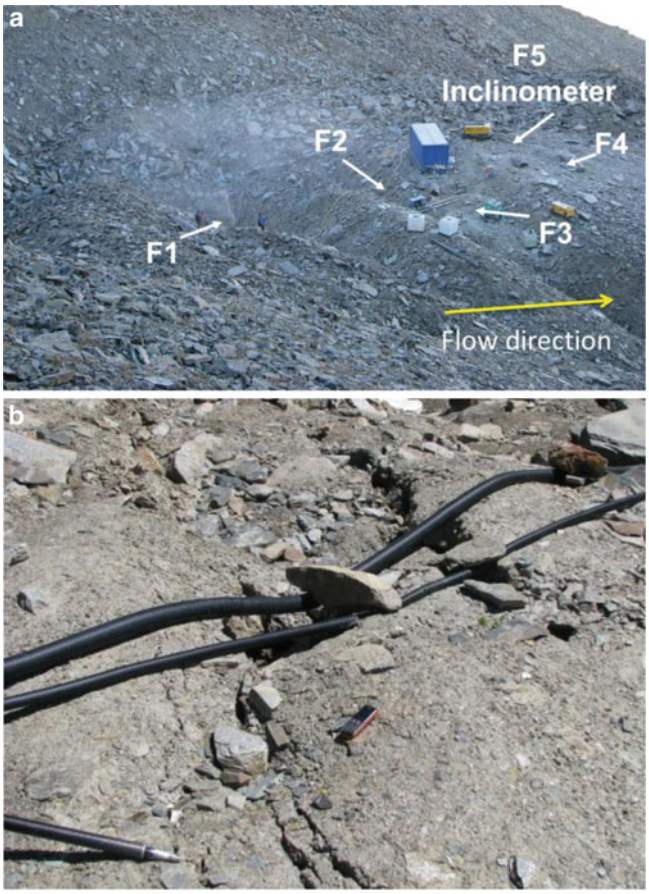

Fig. 6 (**a**) Irregular surface in the area of the field campaign; (**b**) surface tension cracks between boreholes F3 and F5

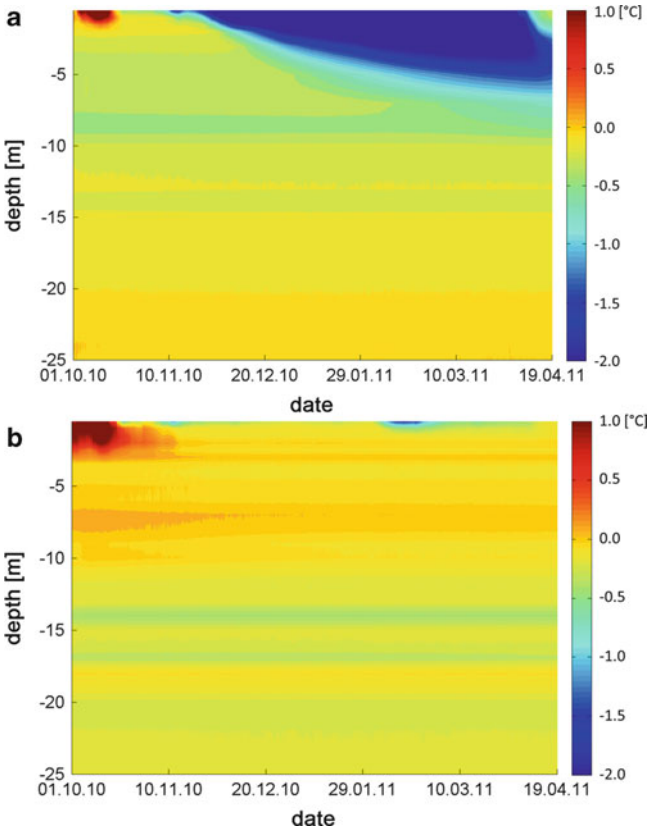

Fig. 7 Temperature distributions from October 2010 to April 2011 in boreholes (**a**) F1 (**b**) F4

Future Fieldwork

Since running water has been heard in the snow-filled depression 30 m due south of F1 (Fig. 4), the importance of investigating the hydrology is acknowledged. Measurements will be carried out in the active layer and around the flanks of the rock glacier.

Now that the monitoring is well underway, it should be possible to obtain multi-season data including the key meteorological records combined with spatial and temporal output from temperatures and displacements on the surface, and at depth in the boreholes.

Ongoing geophysical investigations using ground penetrating radar (GPR), electrical resistance tomography and nuclear magnetic resonance form a major part of the characterisation and monitoring threads of this project. GPR was most helpful in locating the next two boreholes to be drilled by a mixture of rotary coring and percussion midway between section Q2 and borehole F4 in August 2011 to 30 m depth. The focus will be to delineate any shear zones that have been implied by the preliminary GPR analyses (Notivol Lazaro, 2011, private communication) as well as determine strain rates with depth.

An inclinometer and 30 thermistors will be installed in each borehole after a series of monotonic and constant load (creep) pressuremeter tests have been carried out, similar to those conducted by Arenson et al. (2003). The pressuremeter tests are intended to obtain the local stress–strain response in situ as a function of time, and the limit pressures, for comparison with a study that is currently underway in the laboratory to determine creep and shear strength parameters.

Laboratory Characterisation

Laboratory characterisation is essential to select parameters for thermo-mechanical constitutive models to be used in subsequent numerical modelling. Stress paths experienced by soil elements along the shear planes are entirely different (Fig. 3d) from those in the conventional axial compression, which require investigation to establish whether failure will occur at lower values of deviator stress in radial and axial extension, where $q_{LE} < q_{AC}$ and $q_{AE} < q_{LC}$ (Fig. 9).

Yamamoto and Springman (2011) confirm that this concern should be taken seriously. Artificially frozen soil has

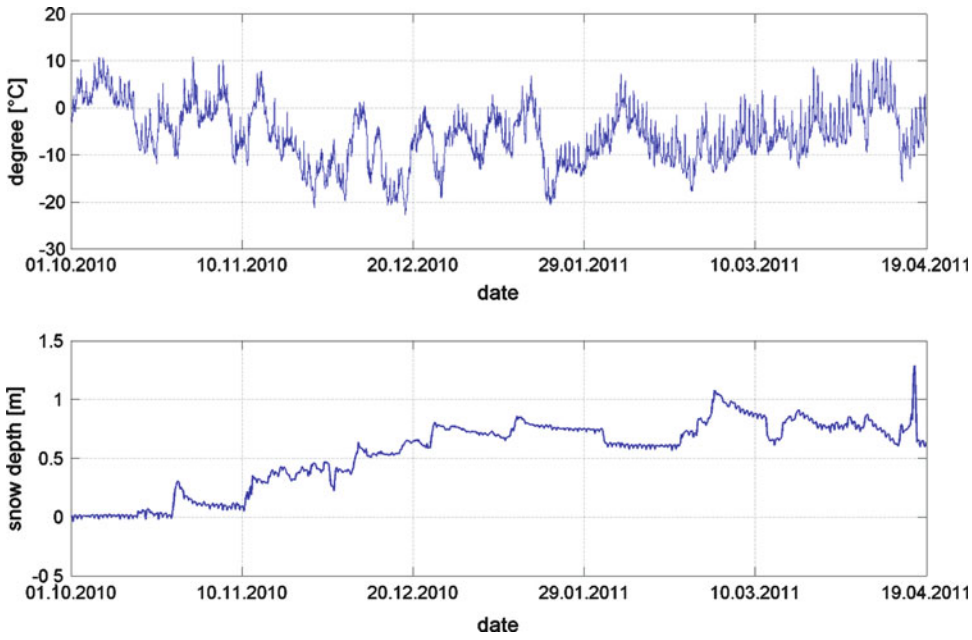

Fig. 8 Meteorological data from the first 6 months of monitoring for air temperature and snow depth

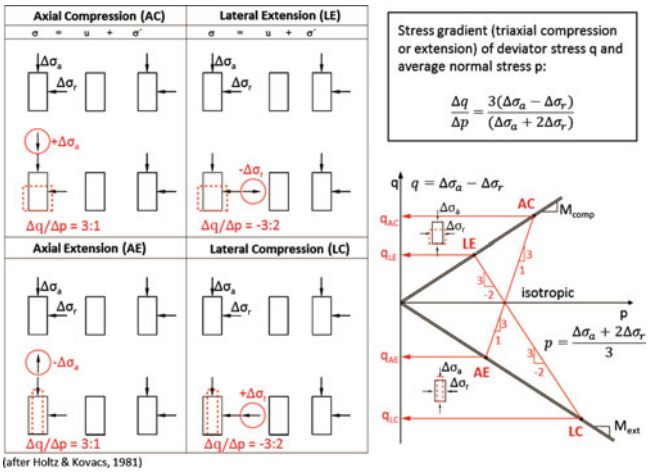

Fig. 9 Stress paths in a triaxial apparatus in deviator (axial – radial total stress, $\sigma_a - \sigma_r$) and mean total ($(\sigma_a + 2\sigma_r)/3$) stress space for axial and lateral loading (compression) and unloading (extension)

been used for constant rate of strain stress path tests to failure to conduct parametric studies at a range of strain rates and temperatures just below 0 °C. Granular ice has been mixed with a representative particle size distribution from the test site according to methods developed by Arenson (2002) to represent a range of rock glacier materials. Total stress paths in deviator q and mean total stress p space (see definition in Fig. 9) have been followed in a triaxial stress path apparatus (Arenson 2002) with accurate temperature control within the sample to ±0.03 °C at different strain rates (Yamamoto and Springman 2011). The results (Fig. 10) confirm that the failure state occurs at lower deviatoric stresses, either for higher axial strain rates or greater volumetric ice contents w_i, and give credence to the concerns expressed above.

The results in axial extension are relevant for the zone under the crevasse and seem to indicate the weakest response of all. This test is the most complicated to carry out in the triaxial stress path apparatus and the results will require further investigation in the near future.

Conclusions and Future Work

The background to instabilities in alpine permafrost has been discussed in respect of past mass movements in the European Alps and future predicted climate change. Mechanisms related to degrading rock glaciers that exhibit severe cause for concern about their ongoing stability through deepening crevasses and thermokarst have been identified and discussed in general terms. The impact of the growth of these crevasses, largely attributed to climate change, on typical stress paths experienced by frozen soil has been recognised as adding a potential threat.

One rock glacier is currently being characterised through geophysical and geotechnical methods and instrumented for monitoring temperature and deformations on the surface and at depth in boreholes. Five boreholes have been drilled so far and are delivering data that shows permafrost exists within the body of this rock glacier, mainly between 0 °C and −0.5 °C. A zone of enhanced shear strain has also been detected at about 15 m depth with surface movements up to 3 m.

Two additional boreholes will be drilled to nearly 30 m in late summer 2011 in a zone along the line of F1 to F4 and halfway between F4 and the profile Q2. Surface movements of several metres a year have been measured to date by annual geodetic surveys. The extension of a preferential

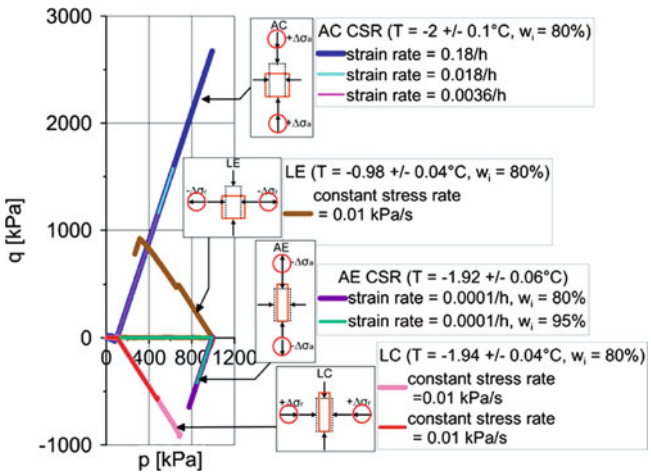

Fig. 10 Total stress paths in deviatoric (q) versus mean (p) stress (After Yamamoto and Springman 2011)

shear zone can then either be confirmed or denied as effort to expose the deformation mechanisms is progressed.

The hydrology is recognised as being significant and studies will be conducted in the active layer as well as for preferential flow on top of the active layer or through unfrozen channels in the rock glacier. Three dimensional Nuclear Magnetic Resonance surveys will be conducted to investigate whether there is any ponding of water near the thermokarst features.

Eventually thermo-hydro-mechanical modelling will be carried out, initially on soil elements loading along stress paths in compression and extension and then on the rock glacier, in order to combine prediction of the pre-failure creep and impending failure.

Acknowledgements The authors gratefully acknowledge the ETH Research Fund for supporting their Collaborative, Highly Interdisciplinary Research Project—(CHIRP1) through Grant No. CH1-01 09-3. Charly Wuilloud and Canton Valais are also thanked for supplementary technical and financial support. Without Ernst Bleiker, Marco Sperl, Thomi Keller, Lasse Rabenstein and Beat Rinderknecht, the fieldwork would not have been as successful. Professors Wolfgang Kinzelbach and Fritz Stauffer are acknowledged for their support. The authors offer their heartfelt thanks to all.

References

Arenson LU (2002) Unstable alpine permafrost: a potentially important natural hazard – variations of geotechnical behaviour with time and temperature. Doctoral thesis no. 14801, Swiss Federal Institute of Technology, Zurich

Arenson LU, Hawkins PG, Springman SM (2003) Pressuremeter tests within an active rock glacier in the Swiss Alps. In: 8th international conference on permafrost, Zurich, 21–25 July 2003, pp 33–38

Barsch D (1996) Rockglaciers: indicators for the present and former geoecology in high mountain environments. Springer, New York, 331p

Boike J, Roth K, Overduin PP (1998) Thermal and hydrologic dynamics of the active layer at a continuous permafrost site (Taymyr Peninsula, Siberia). Water Res Res 34(3):355–363

Brown RJE, Johnston GH, Mackay JR, Morgenstern NR, Shilts WW (1981) Permafrost distribution and terrain characteristics. In: Johnston GH (ed) Permafrost engineering design and construction. Wiley, New York, pp 31–77

Crosta GB, Chen H, Lee CF (2004) Replay of the 1987 Val Pola Landslide, Italian Alps. Geomorphology 60(1–2):127–146

Davies MCR, Hamaz O, Harris C (2001) The effect of rise in mean annual temperature on the stability of rock slopes containing ice-filled discontinuities. Permafrost Periglac Process 12:137–144

Delaloye R, Perruchoud E, Avian M, Kaufmann V, Bodin X, Hausmann H, Ikeda A, Kääb A, Kellerer-Pirklbauer A, Krainer K, Lambiel Ch, Mihajlovic D, Staub B, Roer I, Thibert E (2008) Recent interannual variations of rock glacier creep in the European Alps. In: 9th international conference on permafrost, Fairbanks, pp 343–348

Delaloye R, Morad S, Abbet D, Hilbich C (2010) The slump of the Grabengufer Rock Glacier (Swiss Alps). In: Third European conference on permafrost, Svalbard, 13–17 June 2010, pp 157

Giardino JR, Shroder JF, Vitek JD (1987) Rock glaciers. Allen & Unwin, Boston, 355p

Haeberli W (1990) Permafrost. In: VAW (ed) Schnee, Eis und Wasser der Alpen in einer wärmeren Atmosphäre, Mitteilungen der Versuchsanstalt für Wasserbau, Hydrologie und Glaziologie, ETH Zürich, vol 108, pp 71–88

Haeberli W (1992) Construction, environmental problems and natural hazards in periglacial mountain belts. Permafrost Periglac Process 3:111–124

Haeberli W, Hohmann R (2008) Climate, glaciers, and permafrost in the Swiss Alps 2050: scenarios, consequences, and recommendations. In: 9th international conference on permafrost, Fairbanks, pp 607–612

Haeberli W, Hoelzle M, Keller F, Schmid W, Vonder Mühll D, Wagner S (1993a) Monitoring the long-term evolution of mountain permafrost in the Swiss Alps. In: Proceedings of the 6th international conference on permafrost, Beijing, pp 214–219

Haeberli W, Wegmann M, Vonder Mühll DS (1997) Slope stability problems related to glacier shrinkage and permafrost degradation in the Alps. Eclogae Geologicae Helveticae 90(3):407–414

Haeberli W, Hallet B, Arenson L, Elconin R, Humlum O, Kääb A, Kaufmann V, Ladanyi B, Matsuoka N, Springman SM, Vonder Mühll D (2006) Permafrost creep and rock glacier dynamics. Final report of the IPA/ICSI Task Force. Permafrost Periglac Process 17(3):189–214

Hohmann R (2007) Klimaänderung und die Schweiz 2050. OcCC/ProClim, Bern

Kääb A, Frauenfelder R, Roer I (2007) On the response of the rockglacier creep to surface temperature increase. Glob Planet Change 56(1–2):172–187

King L, Akerman J (1993) Mountain permafrost in Europe. In: Proceedings of the 6th international conference on permafrost, Beijing, pp 1022–1027

Krysiecki JM, Bodin X, Schoeneich P (2008) Collapse of the Bérard Rock Glacier (Southern French Alps). In: Extended abstracts, 9th international conference on permafrost, University of Alaska, Fairbanks, USA, 29 June–3 July 2008, pp 153–154

Lachenbruch AH, Marshall BV (1986) Changing climate – geothermal evidence from permafrost in the Alaskan Arctic. Science 234(4777):689–696

Mani P (1994) Ritigraben (Mattertal), Grundlagen-Zusammenstellung und erste Interpretation, Geo7 Bericht für das Baudepartement des Kantons Wallis, 9407.01

Martin HE, Whalley WB (1987) Rock glaciers: I rock glacier morphology: classification and distribution. Progr Phys Geogr 11:261–282

Maurer H, Hauck C (2007) Geophysical imaging of alpine rock glaciers. J Glaciol 53(180):110–120

Nyenhuis M (2005) Permafrost und Sedimenthaushalt in einem alpine Geosystem. Dissertation. University Bonn

Pfister C, Hächler S (1990) Hochwasserkatastrophen im schweizerischen Alpenraum seit dem 14 Jahrhundert, Bericht Nationales Forschungsprogramm. Analyse der Hochwasser 1987

Rebetez M, Lugon R, Baeriswyl P (1997) Climatic change and debris flows in high mountain regions: the case study of the Ritigraben torrent (Swiss Alps). Clim Change 36:371–389

Rist A (2007) Hydrothermal processes within the active layer above Alpine permafrost in steep scree slopes and their influence on slope stability. Faculty of Science, University of Zurich, Zurich

Rist A, Phillips M (2005) First results of investigations on hydrothermal processes within active layer above alpine permafrost in steep terrain. Nor J Geogr 59:177–183

Roer I (2005) Rockglacier kinematics in a high mountain geosystem. Dissertation, University Bonn

Roer I, Kääb A, Dikau R (2005) Rockglacier kinematics derived from small-scale aerial photography and digital airborne pushbroom imagery. Zeitschrift Fur Geomorphologie 49(1):73–87

Roer I, Haeberli W, Avian M, Kaufmann V, Delaloye R, Lambiel C, Kääb A (2008) Observations and considerations on destabilizing active rock glaciers in the European Alps. In: 9th international conference on permafrost, Fairbanks, pp 1505–1510

Romanovsky VE, Osterkamp TE (2000) Effects of unfrozen water on heat and mass transport processes in the active layer and permafrost. Permafrost Periglac Process 11(3):219–239

Röthlisberger G (1991) Chronik der Unwetterschäden in der Schweiz. Berichte der Eidgenössischen Forschunganstalt für Wald. Schnee und Landschaft. 330, 122

Schnydrig AL (1952) Grächen, Walliser Bergdorf an der Mischabel'. Paul Haupt, Bern, 104p

Van Tatenhove F, Dikau R (1990) Past and present permafrost distribution in the Turtmanntal, Wallis Swiss Alps. Arct Alp Res 22:302–316

Vonder Mühll D, Haeberli W (1990) Thermal characteristics of the permafrost within an active rock glacier. J Glaciol 36(123):151–158

Vonder Mühll DS, Noetzli J, Roer I (2008) PERMOS: a comprehensive monitoring network of mountain permafrost in the Swiss Alps. In: 9th international conference on permafrost, Fairbanks, pp 1869–1874

Yamamoto Y, Springman SM (2011) Triaxial tests on artificial frozen soil samples at temperature close to 0 °C. Geophysical Research Abstracts, vol 13, EGU2011-3537. 2011 EGU. 3537

Zimmermann M, Haeberli W (1992) Climatic change and debris flow activity in high-mountain areas – a case study in the Swiss Alps. Catena Suppl 22:59–72

Potential Effects of Climate Change on Slope Stability in Unsaturated Pyroclastic Soils

Emilia Damiano and Paola Mercogliano

Abstract

Landslides are one of the most dangerous natural hazards since they degrade the productivity of soils, harm people, and damage property. Slope failures are caused by a combination of several factors; in unsaturated granular deposits which are often susceptible to rapid catastrophic landslides induced by rainwater infiltration, climatic conditions play a fundamental role. Therefore, global warming due to the greenhouse effect and changes in precipitation and evaporation patterns might affect future landslide hazard.

The paper reports the results of a complex investigation in a sample site, including in situ suction and precipitation monitoring, soil characterization and numerical simulations which allowed us to focus on some aspects of climate change on slope behaviour.

Keywords

Shallow landslides • Unsaturated soils • Climate change

Introduction

Rapid rainfall-induced landslides, involving slopes covered by shallow deposits of unsaturated granular soils, occur everywhere in the world. Stability of the deposits that often lie on steep slopes with inclination higher than the friction angle of the soils in saturated conditions, is ensured by the positive effect of matric suction on shear strength of the soils. The stabilizing effects of partial saturation on strength can be accounted for by a simple extension of the Mohr-Coulomb criterion (Fredlund and Rahardjo 1993):

$$\tau_{lim} = [c' + (u_a - u_w)\tan\phi_b] + (\sigma - u_a)\tan\phi' \quad (1)$$

where:

c' and ϕ' are the cohesion and the friction angle in conditions of complete saturation;

$(u_a - u_w)$ is the matric suction (difference between air pressure, u_a, and pore water pressure, u_w);

$(\sigma - u_a)$ is the net stress;

ϕ_b is the friction angle related to suction.

In this simplified approach, the strength envelope of unsaturated soil is parallel to the envelope for fully saturated conditions and the higher resistance associated to partial saturation is due to an intercept of cohesion related to suction through the term $(u_a - u_w)tg\phi_b$. In the described hypotheses, as rainwater infiltration proceeds, suction decreases and causes a reduction in the intercept of cohesion, leading to slope failure. It is worth noting that increase in the degree of saturation leads also to progressive increase in hydraulic conductivity of the soil.

E. Damiano (✉)
Department of Civil Engineering (DIC), Second University of Naples, via Roma 29, Aversa (CE), Italy

Analysis and Monitoring of Environmental Risks (AMRA), Napoli, Italy
e-mail: emilia.damiano@unina2.it

P. Mercogliano
Italian Aerospace Research Center (CIRA) – Meteo System & Instrumentation Laboratory, Capua (CE), Italy

Euro Mediterranean Centre for Climate Changes (CMCC) – Impacts on Ground and Coast (ISC) Division, Lecce, Italy

C. Margottini et al. (eds.), *Landslide Science and Practice*, Vol. 4,
DOI 10.1007/978-3-642-31337-0_2,

Depending on slope morphology, in shallow deposits a very small suction is often enough to ensure quite high safety factors. Thus, the triggering of a landslide is not a common phenomenon. Indeed, the covers often exhibit a high unsaturated hydraulic conductivity which, even during the most intense rainfall events, usually prevents the soil from approaching saturation, especially when they lie directly upon a fractured pervious bedrock. Furthermore, during the dry periods between rainfall events, the soil loses part of its water content, mainly by evaporation, favoured in many cases by the presence of vegetation: as a consequence, only intense rain storms occurring after prolonged rainy periods may lead the soil to such wet conditions as to trigger slope instability.

In general, a rational procedure to link climate forecasting to prediction of slope failure at a local scale should include: (i) identification of the climatic factors which might affect slope response; (ii) in-depth knowledge of the geomorphological context and of geotechnical and hydraulic characteristics of the soils involved; (iii) building reliable numerical models for both climatic and slope stability forecasting; (iv) prediction of landslide triggering probability based upon climate change scenarios. Despite the apparently simple described procedure, the high uncertainty in future climate parameters and the complex climate-landslide interaction (landslide is related to climate via the non-linear soil-plant-atmosphere system) make it very hard to draw general conclusions. Moreover, to complete the assessment, scenarios of other than climatic factors should be included in the approach: landslides result from interdependent spatio-temporal processes, including hydrology, vegetation surcharge (weight of vegetation), root strength, soil conditions, bedrock, topography, and human activities. However, such impacts are currently speculative and will be difficult to unravel from anthropogenic effects (Sidle 1992).

Based on such considerations the present study analyses some aspects of the interaction between climatic factors and slope behaviour through the results of 10-year in situ monitoring, an in-depth investigation of soil properties and numerical simulations of the hydrological behaviour of the sample slope of Cervinara in Campania (southern Italy), representing a typical geomorphologic context subjected to shallow landslides in unsaturated granular soils.

Climate Scenarios in the Mediterranean Area

In order to investigate the impacts that change in some climatic factors such as rainfall patterns, drought periods or evapotranspiration could induce on slope stability, the future trend of climate scenarios for the Mediterranean area was evaluated.

The analysis was performed by numerical COSMO Climate Local Model (COSMO CLM) (Rockel et al. 2008), developed by the German Weather Service and updated by the European CLM-Community. Although it can be used with a spatial resolution between 1 and 50 km, the adopted non-hydrostatic formulation of the dynamic equations without any scale assumption makes it eligible especially for use at a horizontal grid resolution of about 20 km and below (Böhm et al. 2006). These high resolutions allow a better description of the terrain orography than the global model, where there is an over- and underestimation of valley and mountain heights, leading to errors in precipitation estimation, as this is closely related to terrain height. Moreover, non-hydrostatic modelling provides a good description of the convective phenomena, which are generated by vertical movement (through transport and turbulent mixing) of energy (heat), water vapour and momentum. Convection can redistribute significant amounts of moisture, heat and mass on small temporal and spatial scales. Furthermore convection can cause severe precipitation events (i.e., a thunderstorm or cluster of thunderstorms).

The mathematical formulation of COSMO-CLM is based on the Navier–Stokes equations for a compressible flow. The atmosphere is treated as a multicomponent fluid (dry air, water vapour, liquid and solid water) for which the perfect gas equation holds, and subject to the gravity and to Coriolis forces. The model includes several parameterizations, in order to allow, at least in a statistical manner, for several phenomena that take place on unresolved scales, but that have significant effects on the meteorological scales concerned (e.g., interaction with the terrain orography).

In the present work climate predictions were obtained with COSMO-CLM (version 4.8) forced by the global model CMCC-MED (Gualdi et al. 2011). The IPCC emission scenarios used is the A1B. The simulation was performed over Italy at a spatial resolution of 8 km with 184 $\times$ 230 grid points and 40 vertical levels. The time step used for the time resolution is 50 s, while the period considered is 1965–2100.

The COSMO CLM model is widely used in Europe and has been validated in different projects and geographical areas (Rockel and Geyer 2008; Bucchignani et al. 2011) in order to analyze its capability to capture European climatic features. Comparison of predicted data and observations shows that COSMO CLM has a cold bias during the winter while it exhibits a warm bias in summer over large parts of Europe (http://climaqs.vito.be/deliverables/nonconf/Deliverable%201.1%20Nudging-ready%20version%20of%20COSMO.pdf).

For the present simulation the COSMO CLM was also validated by comparing predicted data with global satellite observations (Mitchell and Jones 2005) averaged on the period 1971–2000. The results show a quite good capability

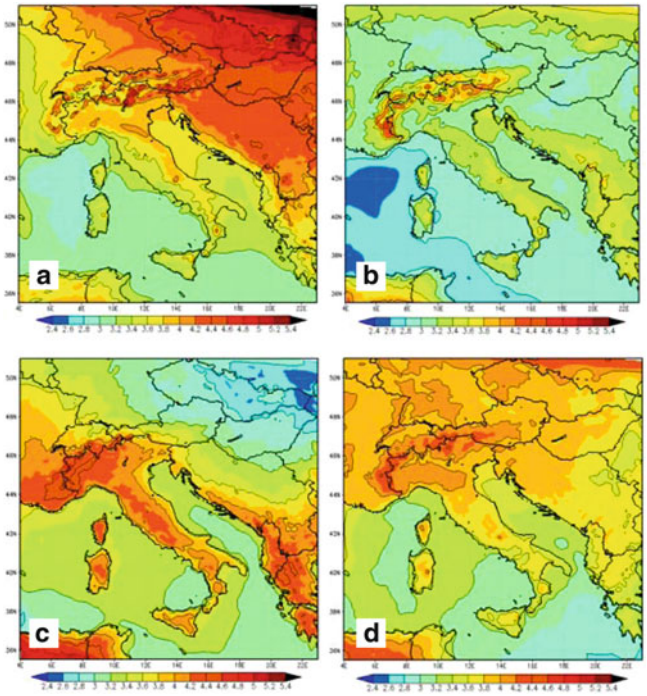

Fig. 1 COSMO CLM daily T2m mean seasonal difference between 2071–2100 and 1971–2000 CLM: (**a**) winter, (**b**) spring, (**c**) summer and (**d**) autumn

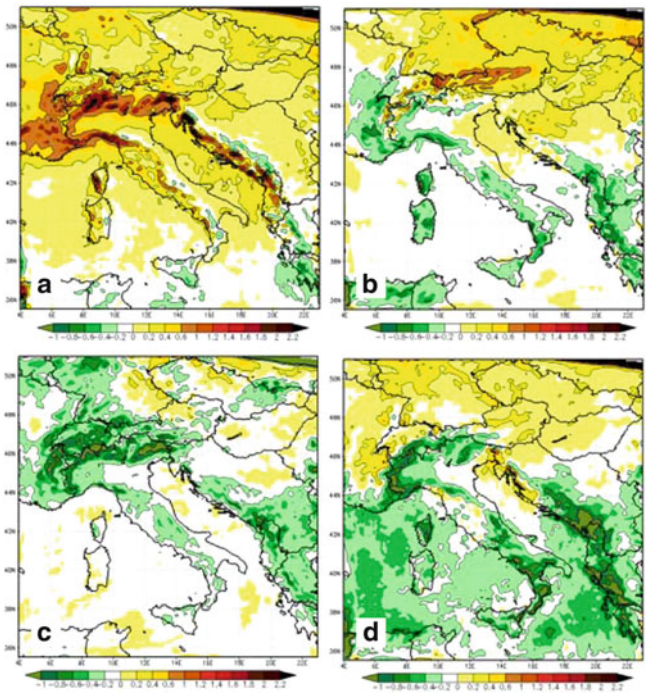

Fig. 2 COSMO CLM daily precipitation seasonal averaged difference between 2071–2100 and 1971–2000 CLM: (**a**) winter, (**b**) spring, (**c**) summer and (**d**) autumn

of the model to capture the mean features of the Italian climate (Bucchignani et al. 2011).

As regards the future predictions of the climate on Italy's land area, the simulation results are illustrated in Figs. 1 and 2 in terms of mean seasonal air temperature (at 2 m) and daily precipitation anomalies between periods 2071–2100 and 1971–2000. For the period 2071–2100 such scenarios indicate:

- an increase in the air temperature especially during the summer (Fig. 1c);
- a general decrease in terms of daily precipitation, except for the winter period when the projection indicates a slight increase (Fig. 2a).

The COSMO CLM simulations are in good agreement with the IPCC (International panel on Climate Change) reports on the Mediterranean area (Solomon et al. 2011) which indicate a general agreement among different regional climate projections on the following climate features:

- an increase in mean temperature in all seasons, with the greatest warming in summer;
- an increase in terms of intensity, duration and frequency of extreme temperature events. In particular, maximum summer temperatures are likely to increase by more than the average;
- a higher spatial variability of the seasonal precipitation; in particular a decrease is evident in most European areas, especially in summer;
- an increase in the intensity of the extreme precipitation;
- a decrease in the annual number of precipitation days;
- an increase in the risk of summer drought.

Physical Characterization of Unsaturated Granular Shallow Covers

The complexity of infiltration processes in unsaturated soils requires the use of a numerical model to predict the hydrologic slope response to rainfall. The reliability of the model has to be proven through preliminary calibration, given the variability in soil parameters, the uncertainties in the initial and boundary conditions, the simplified assumptions made, followed by validation based upon in situ monitoring data. To this aim, data from the Cervinara site were used.

In December 1999, several landslides triggered by heavy rainfall occurred in the mountainous area of Cervinara, about 40 km northeast of Naples. One of these assumed the characteristics of a flowslide, occurring along a fairly regular slope with an average inclination of 40° formed by a shallow primary deposit of unsaturated layered air-fall pyroclastites overlying fractured limestone. The slope is covered by chestnut trees which are regularly cultivated. Since that event, a complex investigation has been carried out including field suction and rainfall readings (Damiano et al. 2012) and laboratory testing about mechanical and hydraulic

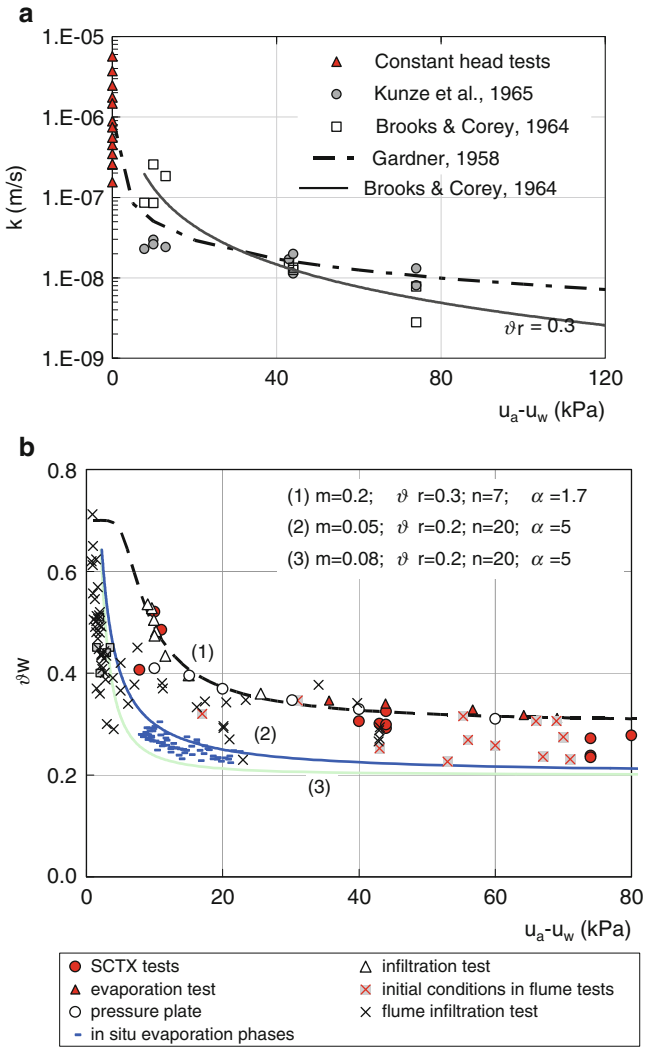

Fig. 3 Hydraulic properties of volcanic ashes: (**a**) conductivity function; (**b**) soil water retention curve (SWRC) (after Damiano and Olivares 2010)

properties of the soils (Lampitiello 2004; Olivares and Picarelli 2003; Damiano and Olivares 2010; Greco et al. 2010).

Figure 3 shows the functional relationships between hydraulic conductivity and matric suction (Fig. 3a) and volumetric water content θ_w and matric suction (Fig. 3b).

The saturated permeability of Cervinara volcanic ashes measured in constant head tests under mean effective stresses between 20 and 640 kPa ranges between $1.5E^{-7}$ and $5E^{-6}$ m/s. The unsaturated hydraulic conductivity k_{unsat} was obtained through:

- The interpretation of suction equalization stages in suction-controlled triaxial tests SCTX as described by Kunze et al. (1968);
- Applying the Brooks and Corey expression (1964) for the degrees of saturation measured in the SCTX tests, assuming as residual volumetric water content $\theta_r = 0.3$ and as saturated hydraulic conductivity $k_{sat} = 1E^{-6}$ m/s.

The results, fitted in Fig. 3a by the permeability functions derived by Gardner's expression (1958) and by Brooks and Corey's expression (1964), show that for the range of suction between 0 and 80 kPa, hydraulic conductivity decreases by about two orders of magnitude as suction increases.

Figure 3b reports the experimental data in terms of volumetric water content (θ_w) versus matric suction ($u_a - u_w$) obtained through:

- Conventional laboratory long-term tests (SCTX tests; evaporation and infiltration tests; pressure plate);
- Flume infiltration tests on small-scale slopes subjected to rainfall until failure;
- In situ monitoring during evaporation periods;

and the best fitting of the experimental data sets derived by the van Genuchten expression (1980).

The obtained soil water retention curves (SWRC) are typical of granular soils with a low air-entry value, low residual water content and a transition zone with a steep slope. However, the SWRC extracted by flume infiltration tests and in situ measurements show a different trend characterized by a lower air entry value and a steeper slope of the curve in the transition zone. This reveals the substantial influence of the procedure adopted to retrieve the SWRC. Indeed, notice that experimental data obtained through conventional tests are determined under equilibrium conditions, whereas data from both in situ monitoring and flume infiltration tests are related to transient conditions.

Modelling the Behaviour of Unsaturated Shallow Granular Covers

Exploiting the observed range of variability of hydraulic parameters, numerical sensitivity analysis (Table 1) was performed to reproduce the Cervinara in situ measurements and to stress the influence that the various hydraulic parameters have on the rainwater infiltration processes. In the following, the results are shown in terms of variability of k_{sat} (and hence of the k_{unsat} function) and ($\theta_s - \theta_r$) since the analysis highlighted that their influence on the transient regime of the groundwater flow is stronger than that of the other parameters. In the analysis θ_s was assumed equal to mean soil porosity 0.7.

The period between January 2006 and December 2007 was selected to validate the model. The reproduction of two annual measurement cycles ensures that the effects of the established initial conditions vanish.

Numerical analysis were carried out by means of the home-made finite volumes code I-MOD3D (Olivares and Tommasi 2008) under the assumption of isothermal conditions for a rigid unsaturated porous medium neglecting the flux of the

Table 1 Set of parametric analysis

Analysis	Conductivity	m	k_{sat} (m/s)	θ_r
$C_{1,2,3,4,5,6}$	$K_{unsat} = k_{sat}*S_e^{\wedge 3}$	0.05, 0.08	$1 \cdot 10^{-7}$	0.1, 0.2, 0.3
$C_{7,8,9,10,11,12}$	$K_{unsat} = k_{sat}*S_r^{\wedge 3}$			
$C_{13,14,15,16,17,18}$	$K_{unsat} = k_{sat}*S_e^{\wedge 3}$	0.05, 0.08	$1 \cdot 10^{-6}$	0.1, 0.2, 0.3
$C_{20,21,22,23,24,25}$	$K_{unsat} = k_{sat}*S_r^{\wedge 3}$			
$C_{26,27,28,29,30,31}$	$K_{unsat} = k_{sat}*S_e^{\wedge 3}$	0.05, 0.08	$5 \cdot 10^{-6}$	0.1, 0.2, 0.3
$C_{32,33,34,35,36,37}$	$K_{unsat} = k_{sat}*S_r^{\wedge 3}$			

Sr degree of saturation
Srr residual degree of saturation
Se = [(Sr − Srr)/(1 − Srr)] effective degree of saturation

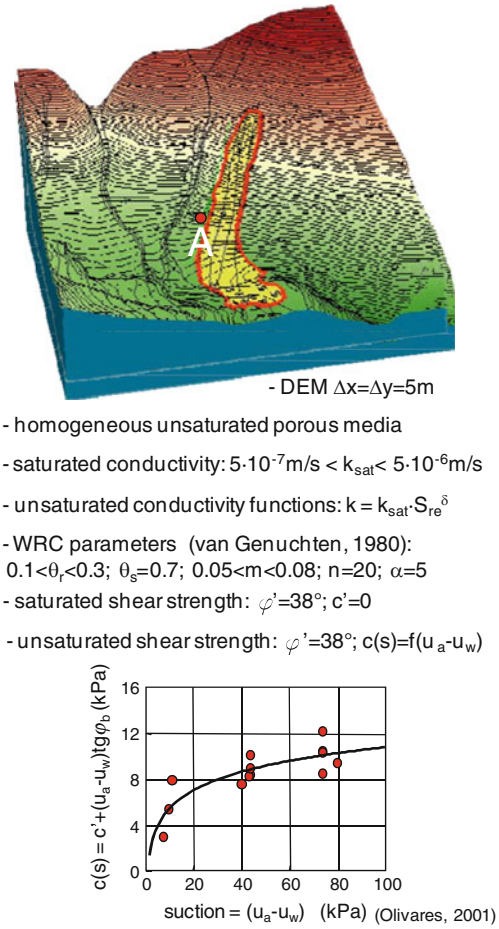

Fig. 4 Digital Terrain Model (DTM) of the Cervinara slope

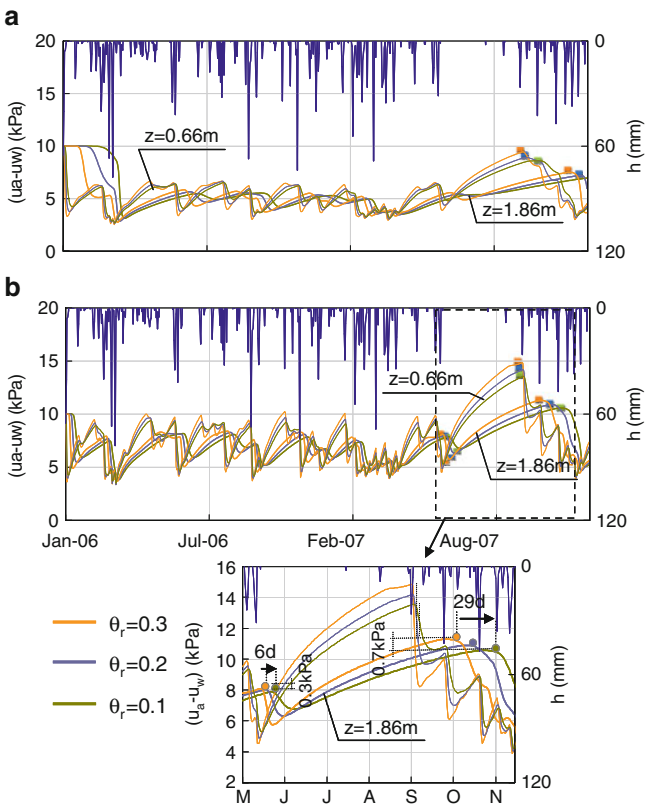

Fig. 5 Comparison of numerical simulations at various θr for: (**a**) $k_{sat} = 1 \cdot 10^{-6}$ m/s; (**b**) $k_{sat} = 5 \cdot 10^{-6}$ m/s

gas phase. The slope was schematized as a homogeneous deposit with a 3D mesh derived by DEM (with dx = dy = 0.5 m) using a dz = 0.12 m (Fig. 4). The initial condition in terms of suction was established from in situ measurements, adopting a constant suction profile equal to mean suction (10 kPa) recorded at the beginning of 2006. At the ground surface two boundary conditions were imposed: average daily rainfall intensity or evaporation flux during dry days, evaluated from in situ suction measurements and illustrated in the following section (Fig. 8b). For the lateral and base surfaces a condition of free flow was assumed.

In Fig. 5a,b the results of numerical simulations C16, C17, C18 and C29, C30, C31 performed adopting the two higher saturated hydraulic conductivities and exploiting the variability of θ_r are compared in terms of suction trends at two different depths (0.66 m reported as thin lines and 1.86 m as bold lines). In the same figure blue lines indicate the recorded daily precipitation heights (h).

As expected, conductivity influences both the time needed for the effect of initial conditions to vanish (from 12 to 62 days for $k_{sat} = 1E^{-6}$ m/s and from 1 to 10 days for $k_{sat} = 5E^{-6}$ m/s at a depth of 1.86 m) and the propagation time of wetting fronts caused by the rainfall pattern. This is revealed by the smoother shape of suction trends for the

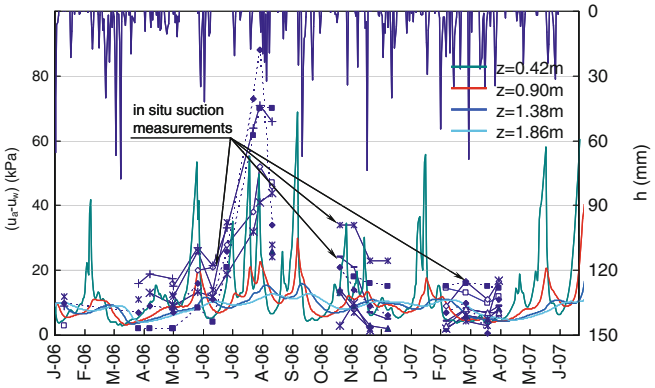

Fig. 6 Comparison between in situ measurements and numerical analysis

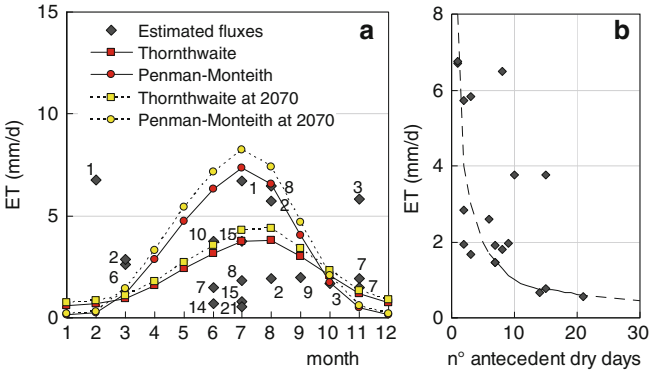

Fig. 7 (**a**) Potential and actual estimated ET fluxes; (**b**) actual ET fluxes plotted against number of antecedent dry days

adopted lower value of k_{sat}. Obviously, conductivity greatly influences the peaks of suction and the range of suction variation within two consecutive relative maxima. Indeed, under the same suction level a higher k_{sat} corresponds to a higher k_{unsat} which, in turn, corresponds to faster groundwater processes, both in infiltration and evaporation.

The enlargement of Fig. 5b for the period May–November 2007 shows the effect of $(\theta_s - \theta_r)$ on the transient regime flows. In particular, the range of suction variation decreases with increasing differences $(\theta_s - \theta_r)$ whereas the delay of the infiltration process at different depths increases. Indeed, comparing the results at 1.86 m of depth obtained with $\theta_r = 0.3$ and $\theta_r = 0.1$, at the beginning of September 2007 after a prolonged dry period (Fig. 5b), the suction peak decreases by about 6 %, while the delay is about 29 days. After a wet period, as in May 2007, owing to the higher degree of saturation, the suction minimum increases by about 3 %, while the delay is definitely lower (about 6 days). Once again this has to be linked to the values assumed by k_{unsat} which, starting from a given suction level, are lower in the case of SWRC with higher $(\theta_s - \theta_r)$. This effect becomes significant when the soil approaches low degrees of saturation, i.e. during dry periods, whereas it tends to vanish when high water contents are reached, i.e. during wet periods (differences in terms of SWRC due to different θ_r are negligible approaching complete saturation).

Figure 6 shows the output of the numerical simulation C23, which represents the best approximation of the monitoring results, compared with suction measurements performed at different depths (50–220 cm) available during the period from January 2006 to July 2007. The best fitting was obtained using the unsaturated conductivity function $k_{unsat} = k_{sat} S_r^3$ with $k_{sat} = 1E^{-6}$ m/s, and the SWRC described by $\theta_s = 0.7$, $\theta_r = 0.1$, $m = 0.08$, $n = 20$, $\alpha = 5$ van Genuchten parameters which provided the best agreement with both the trend and the peaks of matric suction although the maximum suction values recorded during the dry period could not be reproduced. However, fair agreement during wet periods was reached.

It is worth noting that the adopted hydraulic functional relationships differ from those which fit the experimental data with particular reference to SWRC determined through conventional laboratory tests. This highlights the importance of the availability of in situ measurements to validate the model since laboratory investigations on small soil samples and in conditions often different from those present at the slope scale are sometimes not representative (due to different rates of the processes, heterogeneity, presence of roots, etc.. . ..).

Impacts of Climatic Factors on Slope Response

To analyse the role of climatic factors on slope response, soil-atmosphere water exchanges were evaluated. Various formulations are available in the literature to estimate potential infiltration and evapotranspiration, but evaluation of the actual values assumed by the water exchanges at the soil-atmosphere boundary is somewhat more complicated since it depends on atmospheric conditions as well as soil properties, layering, presence of roots, vegetation, etc. However, this is a crucial point.

To this aim, some indications are provided by in situ monitoring. Suction data collected from 2001 to 2008 at different depths in Cervinara site enabled estimation of the flux of water towards the ground surface during dry periods (Damiano et al. 2012). The estimated fluxes are compared in Fig. 7a with two of the most common literature expressions for potential evapotranspiration ET, Thornthwaite (1946) and Penman-Monteith (Monteith 1965) respectively based on the mean monthly air temperature and the mean climate and vegetation characteristics using climatic data records at the Montesarchio and Trevico weather stations, about 10 and 50 km from Cervinara.

The diagram shows that both Thornthwaite and Penman-Monteith ET values are strongly related to the seasonal cycle while the measured ET rates do not show a clear trend over the year. Moreover, in contrast with the intuitive perception

the lowest ET rate (0.5 mm/day) occurred in the hot month of July, the highest (7 mm/day) in the cold month of February. However, the diagram in Fig. 7b, which reports the calculated fluxes as a function of antecedent dry days (indicated by labels in Fig.7a), suggests that actual evapotranspiration is strongly affected by top soil moisture, which decreases with time during dry days, and only indirectly by air temperature and relative humidity. In general, the higher the number of dry days, the lower is the flux rate even though a unique correlation cannot be found: however, the variable fluxes estimated after the same number of dry days suggest the important role of the initial soil moisture conditions.

Formulations from the literature can be used to evaluate the impact of future climate scenarios on the ET regime under the heavily simplified hypothesis that vegetation will not be affected by climate change. The expected temperature increase of 0.05 °C per year (Damiano 2009) over the next 60 years provides the potential ET trends reported as yellow points in Fig. 7a, causing an increase smaller than 1.0 mm/day. Thus, potential ET is expected to remain in the actual range of values. Based on this consideration, in simulating future slope behaviour the ET fluxes imposed as the boundary condition at ground surface during dry periods will be assumed equal to the trend line plotted in Fig. 7b.

At the same time, changes in the duration of dry periods are not expected to affect significantly annual cumulative evapotranspiration significantly. As shown, the ET flux is highly related to soil moisture conditions, and in the considered unsaturated granular covers, with a relatively high saturated conductivity and a low air-entry point, it rapidly decreases as a function of antecedent dry days, reducing to less than 2.0 mm/day after 7 days, since an abrupt conductivity reduction occurs. Hence, an increase in drought periods could lead to a local increase in ET fluxes, but to a substantially equal amount of cumulative ET.

In order to investigate the potential effects of climate change on the stability of steep slopes in unsaturated granular soils, we performed a series of analyses of the hydrologic behaviour of the Cervinara slope, for the duration of 1 year, and compared the results in terms of suction and safety factors with the corresponding values assumed during the reference year 2006, characterized by a slightly higher total precipitation than the 1965–2010 average (1,350 mm). In particular, to highlight the effects of expected changes in the annual precipitation regime, three different yearly hyetographs, obtained by modifying that observed during 2006, were applied as a boundary condition at ground surface:

- Scenario A1: increase in storm intensities and number of dry days, with no changes in cumulative annual precipitation;
- Scenario A2: increase in storm intensities during winter;
- Scenario A3: heavy rainfall event added at the end of winter.

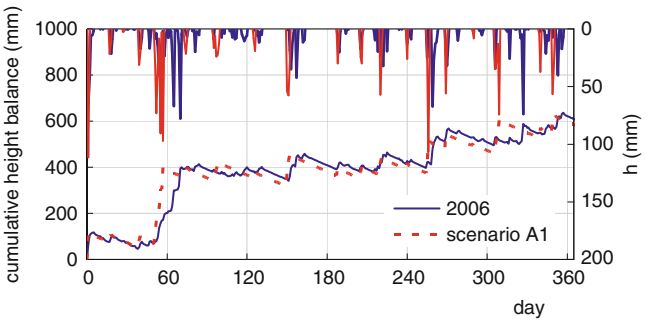

Fig. 8 Scenario A1: adopted hyetograph and cumulative in-out balance

Scenario A1 is the most representative of the COSMO CLM projection. The others (A2 and A3) focus on the predicted increase in storm intensities during winter. In particular, they allow to investigate the relationship between triggering event and antecedent rainfall.

Slope stability was analysed on the basis of the simple infinite slope hypothesis which leads to the following expression of safety factor:

$$FS = \tau_{lim}/\tau = \{[c' + (u_a - u_w)\tan\phi_b] + (\sigma_\alpha - u_a)\tan\phi'\}/(\gamma z \sin\alpha\cos\alpha) \quad (2)$$

where

τ_{lim} is the shear strength of soil along a plane parallel to the ground surface (1);

$(\sigma_\alpha - u_a)$ is the normal net stress along a plane parallel to the ground surface;

γ is the unit weight;

z is the depth from the ground surface;

α is the slope inclination angle.

The experimental relationship determined by Olivares (2001) for Cervinara volcanic ashes, plotted in Fig. 4, was used to evaluate apparent cohesion due to suction $(u_a - u_w)\tan\phi_b$.

Scenario A1

The hyetograph concerning scenario A1 was derived from the reference one by concentrating the rainfall height of three consecutive days in a single rain event, in such a way as to obtain a decrease in rainy days and an increase in rainfall intensity for each storm, without variation in annual precipitation.

Figure 8 shows the reference (year 2006) and the modified hyetograph (scenario A1) in terms of rainfall heights and cumulative in-out height balances estimated by subtracting the ET heights (calculated with the expression of Fig.7b) to the precipitation heights, neglecting surface

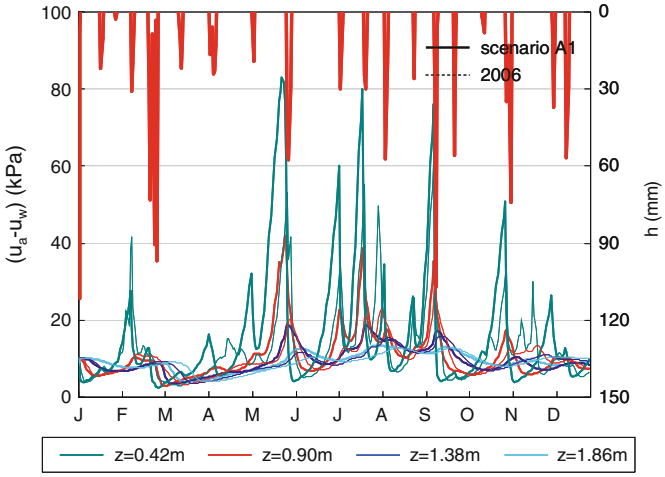

Fig. 9 Scenario A1: suction evolution at four depths compared with 2006 values

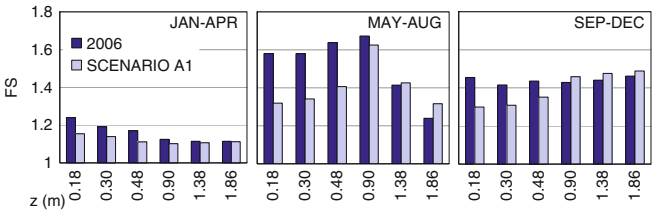

Fig. 10 Scenario A1: minimum FS values by depth compared with corresponding values for 2006

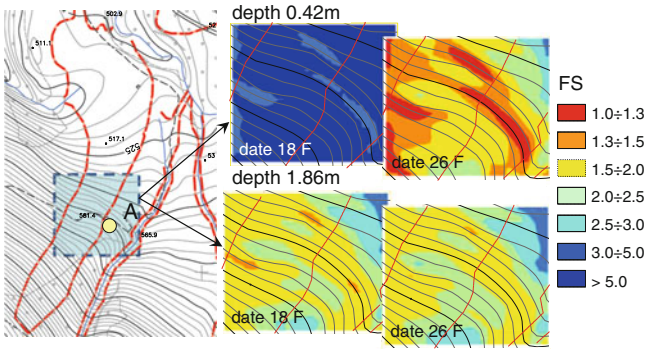

Fig. 11 Scenario A1: FS maps at two depths before and after the rainstorm of 18–26 February

runoff. The adopted procedure, in this case, led to a 44 % increase in dry days and a slight decrease in cumulative infiltration height (4 %).

The results of the analysis are reported in Fig. 9 in terms of suction at four depths evaluated at point A in Fig. 4. Comparing the simulated values with those regarding the real rainfall pattern in 2006 (dashed lines) it may be recognized that during summer and autumn the soil experiences an increase in maximum values (ranging from +2.5 % at a depth of 1.86 m to +45 % at a depth of 0.48 m) and a decrease in minimum values (−21 % at a depth of 0.48 m and −2 % at a depth of 1.86 m). The coupled effect of higher storm intensities and prolonged dry periods modifies the groundwater flow regime, inducing wider variations particularly in upper soil layers. At the end of the simulation year, characterized by a more intermittent rainfall pattern, suction assumes values similar to the initial ones even if a different vertical profile can be recognized.

Figure 10 reports the minimum values that safety factors assume at different depths during three periods of the year compared with the corresponding values for 2006. As expected, the minimum values are those corresponding to the highest depths at the end of the winter, which attain values similar to those obtained for the real hyetograph. On the contrary, the FS of the shallowest layers, up to a depth of 0.9 m, is less than the 2006 one throughout the year, with a more significant decrease (up to 50 %) during summer and autumn.

In depth the FS slightly increases from May to December owing to the different amounts of infiltrated rainfall. In fact, the effects of a given amount of rainfall falling in a shorter time remain confined in the shallowest layers. Afterwards, during dry periods, evaporation subtracts parts of the infiltrated water, thus reducing the leakage towards the deepest layers. Hence, the suction trend and, in turn, the FS in depth are influenced by the cumulative effects of rainfall events during the previous months rather than by the single storm event. Thus, the increase in storm intensities, if not accompanied by a related increase in cumulative monthly precipitation, essentially affects the superficial layers, reducing the stability only of the shallowest covers, while the main climatic factor influencing the stability of the entire underlying cover is cumulative monthly rainfall.

The distribution of FS at depths of 0.46 and 1.86 m evaluated before and after the rainstorm of 18–26 February is illustrated in Fig. 11. It suggests that rainfall patterns similar to scenario A1 would lead to an increase in the probability of very shallow landslides occurring.

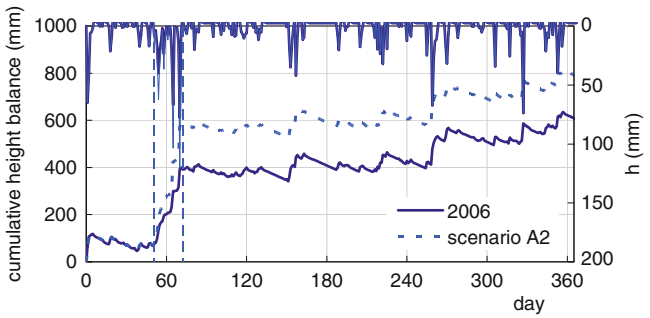

Fig. 12 Scenarios A2: adopted hyetograph and cumulative in-out balance

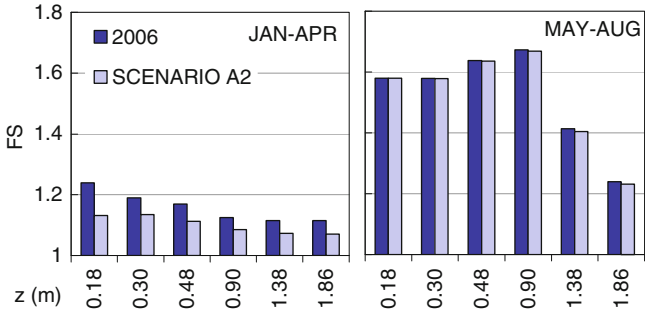

Fig. 14 Scenario A2: minimum values of FS by depth compared with values assumed during 2006

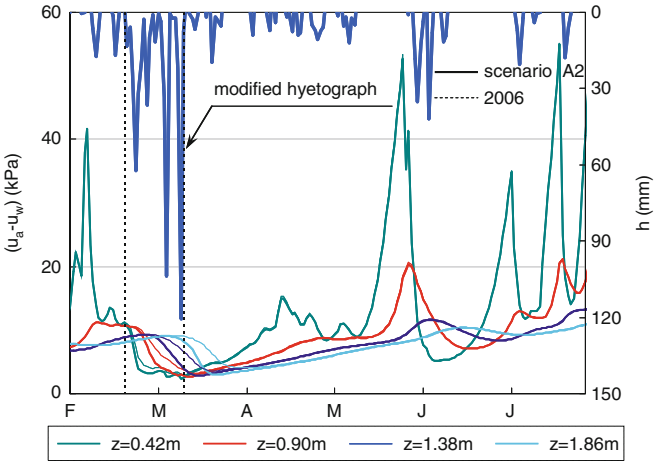

Fig. 13 Scenario A2: suction evolution at four depths compared with 2006 values

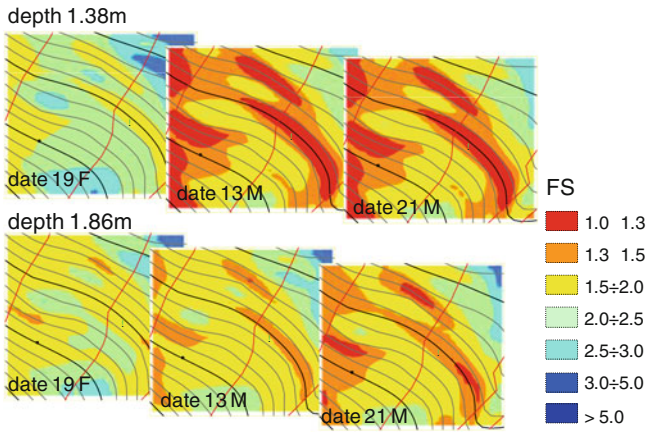

Fig. 15 Scenario A2: FS maps at two depths before, at the end of, and after the rainstorm of 20 February–13 March

Scenario A2

For scenario A2 the daily precipitation intensity of the events occurred between 20 February and 13 March 2006 was increased by 50 % (Fig. 12). This way, as for scenario A3, an annual precipitation increase of about 30 % was imposed which still remains in the range of normal variation of actual annual cumulative precipitation (ranging from 780 mm in 1988 to 1,930 mm in 2010).

The effects of scenario A2 are illustrated in Figs. 13 and 14 respectively in terms of suction trend and minimum safety factors from January to August since no significant differences, with respect to 2006, can be noted starting from 2 months after the end of the modified rainfall.

The increase in rainfall intensity determines quick response at every depth and, even if it seems to produce only a slight decrease in suction (in the order of hPa), the effects on slope stability are significant since a 35 % decrease in FS along the entire thickness occurs with a minimum value close to one (1.06 at a depth of 1.38 m). This is due to the strong non-linearity of the relationship between suction and apparent cohesion at such low stress levels.

The time evolution of FS at the critical depths of 1.38 and 1.86 m across the increased rainy period is illustrated in Fig. 15. In this case, prolonged intense rainfall significantly affects the stability of the intermediate and deep layers. Major effects are recognized at intermediate depths where the soil experiences a diffuse decrease in FS first and for longer.

Scenario A3

Scenario A3, aimed at evaluating the effect of higher concentrations of storm events at the end of the rainy season, was obtained by introducing a rainfall event, identical to the intense event of 5–12 March 2006, on April 04, when the results of numerical analysis for the reference year indicate that the minimum suction values at a depth of 2.2 m had been attained. The obtained hyetograph is reported in Fig. 16.

Unlike scenario A2, the slope hydrological response is affected for a longer period, as indicated by the significant suction decrease observed at any depth for 5 months after the event of 4–11 April (Fig. 17). In this case suction shows a greater than 50 % reduction in minimum and

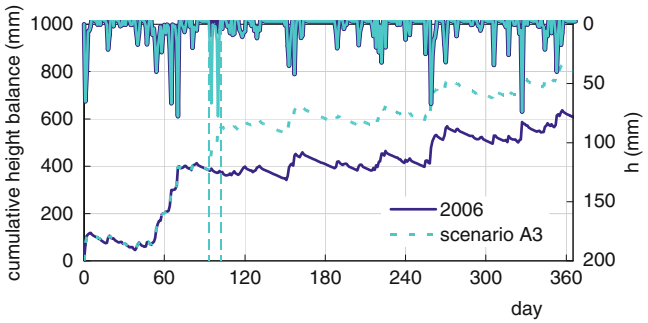

Fig. 16 Scenarios A3: adopted hyetograph and cumulative in-out balance

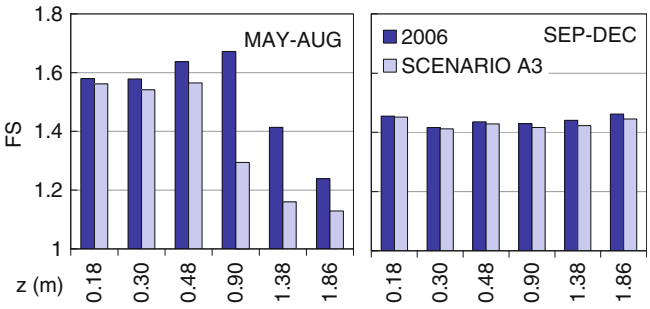

Fig. 18 Scenario A3: minimum values of FS by depth compared with values assumed during 2006

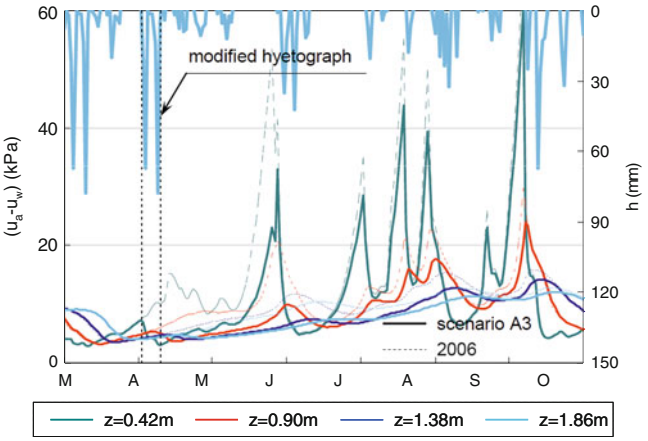

Fig. 17 Scenarios A3: suction evolution at four depths compared with 2006 values

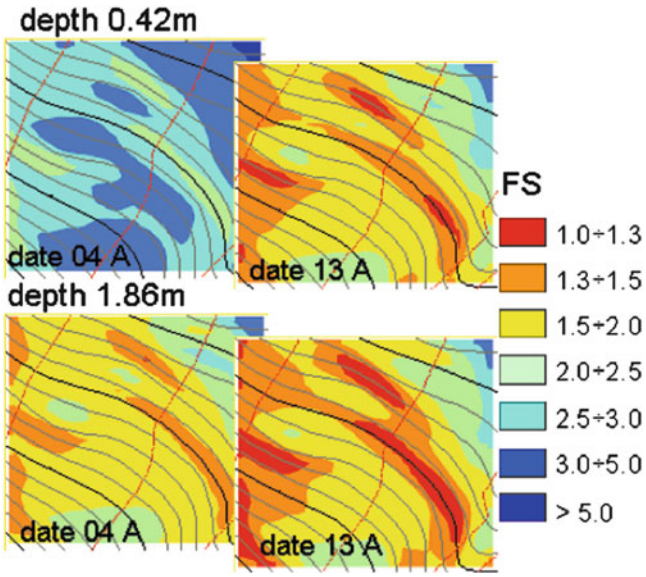

Fig. 19 Scenario A3: FS maps at two depths before and at the end of the storm event of 4–11 April

maximum values with a consequent smoothness of the shapes of suction trends.

The relatively high unsaturated conductivity profile of the cover at the beginning of rainfall causes rapid infiltration towards the deepest layers (about 20 days against about 60 days obtained in the parametric analysis C16 for $k_{sat} = 1e^{-6}$ m/s). As a consequence, even a single storm event can affect the suction trend in depth, inducing a strong reduction in FS (Fig. 18). Comparison between FS maps at the depths of 0.42 and 1.86 m before and after the rain storm (Fig. 19) highlights that the highest decrease in FS occurs in upper layers but in depth absolute minimum values are reached just at the end of the rain storm.

Slight increase in rainfall intensity could lead to slope failure affecting the entire thickness of the cover. This is probably what occurred in Campania in 1998 when at the beginning of May a series of catastrophic flowslides triggered by an intense storm involved the entire pyroclastic covers of the slopes surrounding the towns of Sarno, Quindici and Bracigliano (Cascini et al. 2000).

Conclusions

In this paper the potential effects of climate change in the Mediterranean area on the stability of steep slopes in shallow unsaturated granular covers have been investigated. Extensive experimental and mathematical investigation on pyroclastic covers indicates that in order to effectively model the mechanical and hydrological behaviour of such slopes, it is worth supplementing the usual laboratory tests with data from in situ monitoring since slope response to rainfall is affected by soil characteristics as well as by rainfall variability. By applying a simplified mathematical model validated on field data, the effects of climate changes estimated with the COSMO CLM regional climate model have been investigated. This entailed an increase in the intensity of

the extreme precipitation mainly concentrated during winter and a decrease in the number of rainy days.

The results of the analysis appear to indicate that, under the assumed simplified hypothesis:

- Increases in air temperature and in the number of dry periods are not expected to affect annual cumulative evapotranspiration significantly;
- An increase in storm intensities and dry period durations would affect the stability conditions of the shallowest layers;
- An increase in seasonal cumulative rainfall might induce instability of the entire cover especially when intense storms occur at the end of the rainy season, i.e. at high soil moisture contents.

Acknowledgments The authors wish to thank Prof. R. Greco and Prof. L. Olivares for their suggestions and constructive criticisms, Prof. L. Picarelli for his contribution in coordinating the research, Dr E. Bucchignani and Dr M. Montesarchio (CIRA) for their help in climatic simulations, prof. L. Olivares and Dr V. Savastano (STIIA) for developing the I-MOD3D program and the Region Campania Civil Protection Agency which provided precipitation data from 2001 to 2010.

The work was partially supported by the UE/FP7 SAFELAND G.A. No. 226479.

References

Böhm U, Kücken M, Ahrens W, Block A, Hauffe D, Keuler K, Rockel B, Will A (2006) CLM – the climate version of LM: brief description and long-term applications. COSMO Newsletter, 6 available on http://www.clm-community.eu/dokumente/upload/3a8e8_COSMOnewsLetter06_clm.pdf

Brooks RH, Corey AT (1964). Hydraulic properties of porous media. Hydrology Paper No. 3, Colorado State University, Fort Collins

Bucchignani E, Sanna A, Gualdi S, Castellari S, Schiano P (2011) Simulation of the climate of the XX century in the Alpine space. Nat Hazards. doi:10.1007/s11069-011-9883-8

Cascini L, Guida D, Romanzi G, Nocera N, Sorbino G (2000) A preliminary model for the landslides of May 1998 in Campania Region. In: Evangelista A, Picarelli L (eds), Proceedings of the 2nd international symposium on the geotechnics of hard soils-soft rocks, vol 3, Napoli, pp 1623–1649

Damiano E (2009) A study on climatologic aspects for forecasting of shallow landslides in pyroclastic soils due to climatic change. CMCC Technical Report

Damiano E, Olivares L (2010) The role of infiltration processes in steep slope stability of pyroclastic granular soils: laboratory and numerical investigation. Nat Hazards 52(2):329–350

Damiano E, Olivares L, Picarelli L (2012) Steep-slope monitoring in unsaturated pyroclastic soils. Eng Geol 137–138:1–12

Fredlund DG, Rahardjo H (1993) Soil mechanics for unsaturated soils. A Wiley-Interscience Publication. Wiley, Hoboken

Gardner WR (1958) Some steady state solutions of the un-saturated moisture flow equation with application to evaporation from water table. Soil Sci 85(4):228–232

Greco R, Guida A, Damiano E, Olivares L (2010) Soil water content and suction monitoring in model slopes for shallow flowslides early warning applications. Phys Chem Earth, Elsevier Ltd., 35:127–136

Gualdi S, Somot S, May W, Castellari S, Déqué M, Adani M, Artale V, Bellucci A, Breitgand JS, Carillo A,Cornes R, Dell'Aquilla A, Dubois C, Efthymiadis D, Elizalde A, Gimeno L, Goodess CM, Harzallah A,Krichak SO, Kuglitsch FG, Leckebusch GC, L'Heveder BP, Li L, Lionello P, Luterbacher J, Mariotti A, NietoR, Nissen KM, Oddo P, Ruti P, Sanna A, Sannino G, Scoccimarro1 E, Struglia MV, Toreti A, Ulbrich U, Xoplaki E (2011) Future climate projections. In: Navarra A, Tubiana L (eds) Regional assessment ofclimate change in the mediterranean. Springer, Dordrecht

Kunze RJ, Uehara G, Graham K (1968) Factors important in the calculation of hydraulic conductivity. Proc Soil Sci Soc Am 32:760–765

Lampitiello S (2004) Resistenza non drenata e suscettività alla liquefazione di ceneri vulcaniche della Regione Campania. Ph.D. Thesis, Second University of Naples

Mitchell TD, Jones PD (2005) An improved method of constructing a database of monthly climate observations and associated high resolution grids. Int J Climatol 25:693–712

Monteith JL (1965) Evaporation and the environment. Symp Soc Exp Biol 19:205–234

Olivares L (2001) Static liquefaction: an hypothesis for explaining transition from slide to flows in pyroclastic soils. Proceeding of TC11 Landslide conference on Transition from slide to flow – mechanisms and remedial measures. Trabzon, Turkey

Olivares L, Picarelli L (2003) Shallow flowslides triggered by intense rainfalls on natural slopes covered by loose unsaturated pyroclastic soils. Géotechnique 53(2):283–288

Olivares L, Tommasi P (2008) The role of suction and its changes on stability of steep slopes in unsaturated granular soils. Proceeding of 10th international symposium on landslides and engineered slopes, Xi'an, China, vol 1, pp 203–215

Rockel B, Geyer B (2008) The performance of the regional climate model CLM in different climate regions, based on the example of precipitation. Meteorol Z 17(4):487–498

Rockel B, Will A, Hense A (2008) The regional climate model COSMO-CLM (CCLM). Meteorol Z 17(4):347–348

Sidle RC (1992) A theoretical model of the effects of timber harvesting on slope stability. Wat Resour Res 28:1897–1910

Solomon S, Qin D, Manning M, Chen Z, Marquis M, Averyt KB, Tignor M, Miller HL (eds) (2011) Contribution of working group I to the Fourth Assessment Report of the Intergovernmental Panel on Climate Change. Cambridge University Press, Cambridge, UK and New York,, 996 pp, available on http://www.ipcc.ch/publications_and_data/publications_ipcc_fourth_assessment_report_wg1_report_the_physical_science_basis.htm.

Thornthwaite CW (1946) An approach toward a rational classification of climate. Trans Am Geophys Union 27(1):55–94

van Genuchten MT (1980) A closed-form equation for predicting the hydraulic conductivity of unsaturated soil. Soil Sci Soc Am J 44:615–628

Recent Mass Movements in the Tramuntana Range (Majorca, Spain)

Rosa María Mateos, Inmaculada García-Moreno, Gerardo Herrera, and Joaquín Mulas

Abstract

Between 2008 and 2010, the island of Majorca (Spain) experienced the coldest and wettest winters of the last 40 years. Accumulated rainfall was twice the average and values of intense rainfall up to 296 mm/24 h were recorded. Additionally, high precipitation coincided with anomalous, low temperatures and freezing in the highest zones of the Tramuntana range (NW sector of the island). As a result, 34 mass movements were recorded: 14 rockfalls, 1 rock avalanche, 15 landslides and 4 karstic collapses. The geological structure determines the distribution and the failure pattern of the movements. Most of the movements have taken place after antecedent rainfall over 800 mm. Intense rainfall >90 mm/24 h also caused rockfalls. Additionally, the rockfalls have also occurred after several freeze-thaw cycles, being a determining and unusual factor in this warm region. The results aim to contribute to the design of an early warning system coordinating emergency, infrastructure and meteorological centres, in a region of high risk.

Keywords

Landslides • Rockfalls • Rainfall • Freeze-thaw cycles • High risk • Early warning system

Introduction

The island of Majorca has a variety of different geomorphological domains, most prominently the Tramuntana Range (1,100 km^2) in the Northwestern part of the island (Fig. 1). The steep topography of this chain, which is linked to its geological complexity and Mediterranean climate, determines intense slope dynamics (Mateos 2002; Mateos and Azañón 2005). The main income of the island of Majorca comes from tourism (83 % of its GDP), as it welcomes 9 million visitors each year. The vast urban development that the Tramuntana region has undergone in the past 30 years has considerably increased the risk originated from mass movements.

During the hydrological years 2008–2010, Majorca experienced one of the coldest and wettest winters in living memory. Not only did the accumulated rainfall showed twice the average recorded values. This period also witnessed the highest rates of intense rainfall (up to 296 mm/24 h) since instrumental records have been available (1944). These rainy episodes have also coincided with cold periods in which several days elapsed with temperatures around 0 °C and minima at −6.8 °C, which are anomalous values in the mild Mediterranean climate. The result was that 34 mass movements were triggered, distributed along the Tramuntana Range (Fig. 1), namely 14 rockfalls, 1 rock avalanche, 15 complex landslides (earth slides- earth flows) and 4 karstic collapses.

Fortunately, there were no deaths but there were numerous cases of damage to dwellings, holiday apartment blocks, barns and power stations etc., and especially the road network in the range, most significant the numerous blockages on the

R.M. Mateos (✉) • I. García-Moreno
Research Unit of the Geological Survey of Spain in the Balearic Islands, Palma de Mallorca, Avda. Ciudad Querétaro s/n, Mallorca, Spain
e-mail: rm.mateos@igme.es

G. Herrera • J. Mulas
Hazard and Natural Risk Department, Geological Survey of Spain, Ríos Rosas, 23, Madrid, Spain

C. Margottini et al. (eds.), *Landslide Science and Practice*, Vol. 4,
DOI 10.1007/978-3-642-31337-0_3,

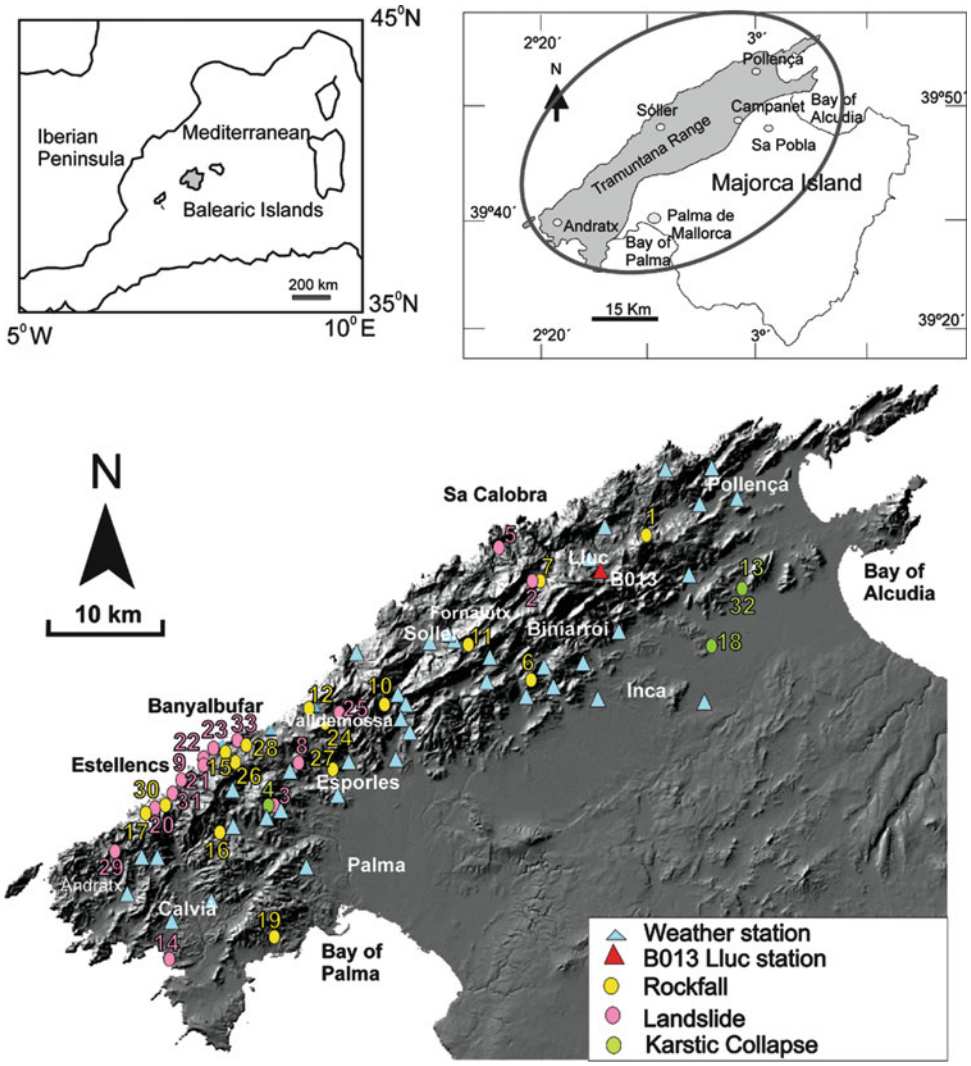

Fig. 1 Location of Majorca in the Western Mediterranean and the Tramuntana Range on the Northwest extreme of the island. The 34 mass movements registered, as well as the weather stations locations, are shown over the digital elevation model

Ma-10 road, which caused significant economic losses in the different tourist sites.

This study aims to contribute to the examination of different parameters that condition the spatial and temporal distribution of the slope movements that have taken place.

Geological Structure Controlling the Spatial Distribution of Recent Mass Movements

The structural layout of the materials that outcrop on the Tramuntana Range conditioned the distribution of the movements. The Northern face, where 23 of the 34 movements took place (68 %), is more hazardous due to the existence of steeper slopes and a higher presence of outcroppings of soft materials. Both of these factors are conditioned by the NW-overlapping thrusts and the regional tectonics (Alvaro 1987).

Rockfalls

Over the hydrological years 2008–2010, 15 rockfalls have taken place in the Tramuntana Range. Figure 2 shows the photographs of some of the most important. The distribution of these movements (Fig. 1) shows that both the Northern (ten events) and the Southern face (five events) were affected. The largest rockfall was at Son Cocó (Fig. 2-2), leaving a tongue of blocks over an area of 60,000 m^2 and 300,000 m^3 in volume, and it was classified as a rock avalanche (Mateos et al. 2010).

All the rockfalls have affected practically vertical rock scarps made up of Liassic limestone, located at altitudes between 250 and 700 m. On the northern face, the rockfalls took place through planar failures, with the predominant direction being N30 °E (thrust fronts). On the Southern face, the failure model in the rockfalls is a wedge type,

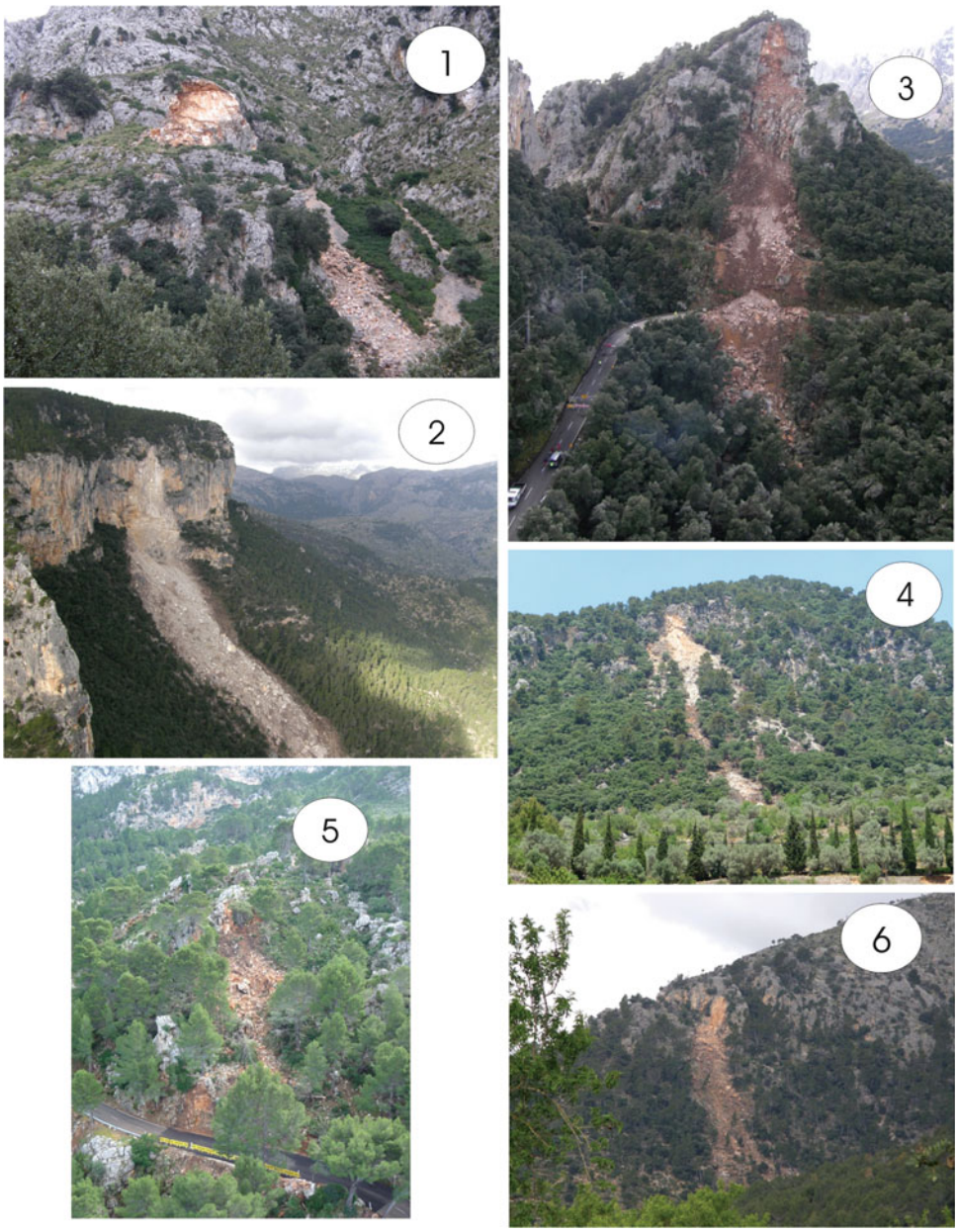

Fig. 2 Photographs of the most important dated rockfalls. (**1**) Puig Tomir (27/11/2008), (**2**) Son Cocó (19/12/2008), (**3**) Gorg Blau (31/12/2008), which cut off the Ma-10 road for 4 months (**4**) Biniforani (5/01/2009), (**5**) Estellencs (15/01/2010) and (**6**) Son Antic (17/02/2010)

with two main failure planes – N30 °E and N110 °E – that mark the fracture pattern of the mountain range on this face (Gelabert et al. 1992).

The runout of the rockfalls that took place on the Southern face was longer than those on the Northern face due to the layout of the materials on the slopes. Thus, on the Southern face, rockfalls took place on vertical rock massifs of Liassic limestone which overlie the softer materials from the Rhaetian (Upper Triassic), made up of dolomites and marls. The latter give rise to less rugged slopes with angles around 30°, which allow the loose blocks plenty of room to move and roll. However, on the northern face, the thrusts give rise to very vertical fronts that define the slope, as the blocks accumulate at the foot with a lower horizontal component to the movement.

Landslides

Landslides are small to medium-sized movements that affect clays with gypsum and volcanic rocks dating to the Late Triassic (Keuper). Keuper outcroppings are on the northern face, linked to the detaching surfaces of the thrusts. They are fine-grained soils with low to medium plasticity,

Fig. 3 The road network in the mountain range has been affected by several landslides: (**1**) Sa Calobra (3/12/2008), (**2**) Cala Tuent (15/12/2008), (**3**) Estellencs (8/3/2010), which cut off the Ma-10 road for 3 months, and (**4**) Banyalbufar (9/5/2010)

with effective cohesion values of around 4 KPa and very low permeability values of around 1.8×10^{-8} m/s (Mateos et al. 2003, 2009). All the landslides were located on the Northern face of the Tramuntana and they tend to be complex earth landslides- rotational landslides with mudflows at the bottom.

Figure 3 shows some photographs of the most important ones. They all affected the road network in the mountain range, primarily the Ma-10 road. The Estellencs landslide (Fig. 3-3) on the 8 March 2010 kept this road closed for three months, triggering numerous economic losses in the towns of Estellencs and Banyalbufar.

Triggering Factors

Majorca has a typically Mediterranean climate, with mild winters and warm-dry summers. The maximum precipitation takes place during the autumn months due to the arrival of the first high cold air masses, which contrast with the high temperature retained by the sea. This phenomenon is known as "*gota fría*" (cold rain), in which heavy storms are accompanied by intense rainfall episodes (up to 250 mm in 24 h). The orography of the range clearly controls the distribution of precipitation. The central sector (Lluc) registers average annual precipitation of 1,200 mm, which gradually drops towards the extreme SW of the range (Calviá), where average annual precipitation is no more than 300.

During the period spanning from October 2008 to May 2010, Majorca experienced two of the coldest and rainiest winters in living memory, with accumulated rainfall being almost twice the average value. On the 15th of December 2008 the highest precipitation was registered since instrumental data is available (1944). A total of 296 mm of rain fell in 24 h near Sóller. Mateos et al. (2007) carried out a statistical analysis of intense rainfall in the area, which allowed obtaining the maximum 24-h rainfall values for return periods of 5, 10, 25 and 100 years. The values obtained on the 15th of December 2008 are very similar to those calculated for the return period of 100 years, which reflects the uniqueness of this precipitation record. However, the 2008–2010 period was not only exceptionally rainy but also anomalously cold, with abundant snowfall as well as freezing in the highest zones in the range. The high precipitation and the low temperatures coincided, as the rainfall took place mainly during the winter months. As a consequence, the majority of the weather stations in the range had registered temperatures oscillating around 0 °C, with minimum values as low as −6.8 °C (500 m a.s.l).

Rockfalls

Figure 4 shows the graphs that relate the daily precipitation, accumulated rainfall and minimum temperatures recorded to the occurrence of the dated rockfalls. In order to obtain a

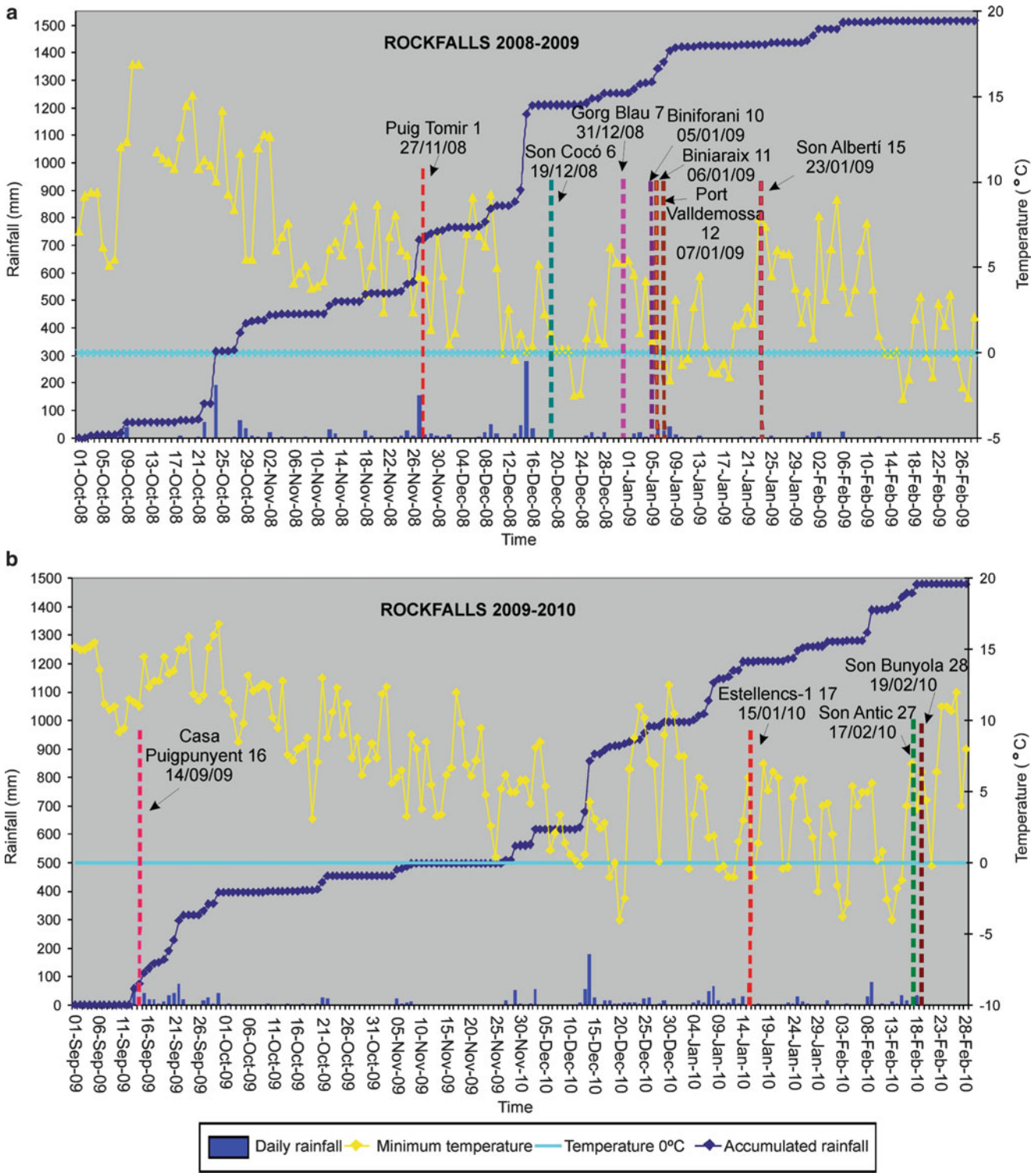

Fig. 4 Relationship between daily rainfall, accumulated rainfall and minimum temperatures (recorded at the B013 Lluc weather station) and the occurrence of rockfalls in the periods (**a**) October 2008–February 2009 (**b**) September 2009–March 2010

general picture, the reference was the meteorological data from the B013-Lluc weather station (490 m a.s.l), located in the heart of the range (Fig. 1). As a general criterion, all the rockfalls took place after intense precipitations and very clearly in the coldest periods, when the temperature hovered at around 0 °C. With the aim of carrying out a thorough analysis, Table 1 was drawn up, in which the following parameters were quantified for each rockfall, taking into

Table 1 Values of the meteorological data related to the occurrence of rockfalls. For each case, the weather stations closest to the failure point were used

Rockfall inventory No. date	Max. rainfall in 24/h (mm) (10 days prior to event)	Minimum temp. (°C) (10 days prior to event)	Accumulated rainfall (mm)	No. of freeze-thaw cycles
Puig Tomir (No. 1) 27 Nov 08	128.5 (27 Nov 2008)	1.6 (26 Nov 2008)	843.3	0
Son Cocó (No. 6) 19 Dec 08	150.2 (15 Dec 2008)	−1.6 (11 Dec 2008)	874.2	3
Gorg Blau (No. 7) 31 Dec 08	35.1 (26 Dec 2008)	−3.2 (23 Dec 2008)	1,409.2	6
Biniforani (No. 10) 5 Jan 09	33.3 (26 Dec 2008)	−3.5 (05 Dec 2009)	931.7	8
Biniaraix (No. 11) 6 Jan 09	23.5 (06 Jan 2009)	−1.1 (05 Jan 2009)	953.6	5
Port Valldemossa (No. 12) 07 Jan 09	24.3 (07 Jan 2009)	−1.3 (07 Jan 2009)	892.3	4
Son Alberti (No. 15) 23 Jan 09	6.3 (13 Jan 2009)	5.13 (18 Jan 2009)	669.7	0
Puigpunyent (No. 16) 14 Sept 09	45.3 (14 Sept 2009)	12.69 (12 Sept 2009)	87.9	0
			14 Sept 2009	Ligntning storm
Estellencs 1 (No. 17) 15 Jan 10	93.1(12 Jan 2010)	2.3 (10 Jan 2010	789.3	0
Son Antic (No. 27) 17 Feb 10	28.6 (15 Feb 2010)	−1.5 (13 Feb 2010)	874.4	2
Son Bunyola (No. 28) 19 Feb 10	36.2 (12 Feb 2010)	−1.5 (13 Feb 2010)	790.4	2

account the meteorological data from the stations closest to the failure point: (1) maximum precipitation in 24 h recorded in the ten days prior to the failure; (2) minimum temperature recorded in the 10 days prior to the failure. To get these values, the temperature at the elevation of the rockfall scarp was estimated by applying a thermal gradient of −6.5 °C for each 1,000 m (Mateos et al. 2007); (3) accumulated rainfall from the start of the rainy period until the moment of failure; and (4) number of freeze-thaw cycles that took place prior to the rockfall.

The analysis of these data reveals the following:

- Some of the rockfalls (~27 %) took place after occurrences of intense rain >90 mm/24 h, regardless of the temperature.
- Most of the rockfalls started after accumulated rain values over 800 mm, and when there were several freeze-thaw cycles in the days prior to the failure, regardless of whether the maximum daily rainfall were overly intense (around 30 mm).

Table 1 and Fig. 2 provide an overview which enables us to establish that largest rockfalls were produced on rocky scarps located above 600 m, showing a clear relationship to freeze-thaw cycles prior to the failure. Minor rockfalls were caused on lower scarps, 250–350 m, and were more closely related to episodes of moderate-intense rainfall.

Landslides

Figure 5 shows the relationships between the different meteorological parameters – daily rainfall, accumulated rainfall and minimum temperatures – and the occurrence of dated landslides. Once again B013-Lluc weather station was taken as the reference point. This overall picture reveals that the recorded landslides took place after episodes of moderate to extreme intense rainfall, with very high accumulated rainfall totals (>800 mm). Bearing in mind the same parameters as the ones used for rockfalls, Table 2 was elaborated using the information from the weather stations located the closest to the movements. Some of the landslides (five of the eight dated) were triggered after prior medium intensity rains, between 20 and 65 mm/24 h, and with very high accumulated rainfall figure (up to 1,000 mm); while others took place after very intense rainfall >120 mm/24 h, with values up to 190 mm/24 h in the case of the Sa Calobra landslide (N° 2). This threshold coincides with that of 130 mm/24 h estimated by Mateos et al. (2007) for historical landslides. However, unlike rockfalls, freeze-thaw cycles do not seem to trigger landslides and the altitude at which the movements took place is of no relevance.

Discussion and Results

In the present study, we can state that the occurrence of 34 mass movements in the Tramuntana Range recorded during the period 2008–2010 is an exceptional event in the history of the island as there is no evidence in the historical record (since the seventeenth Century) of any similar event. These movements took place as a result of a confluence of intense rainfall and low temperatures in a very rainy climatic episode.

The rockfalls recorded during the period 2008–2010 took place under the following circumstances: (1) after occurrences of intense rain >90 mm/24 h, regardless of the temperature. These circumstances occurred in many others rockfalls recorded in literature (Ferrer et al. 1997; Mateos 2002 and Mateos and Azañón 2005), and (2) they started in saturated rocky massifs (accumulated rain >800 mm) when there were several freeze-thaw cycles in the days prior to the failure, regardless of whether the maximum daily rainfall were overly

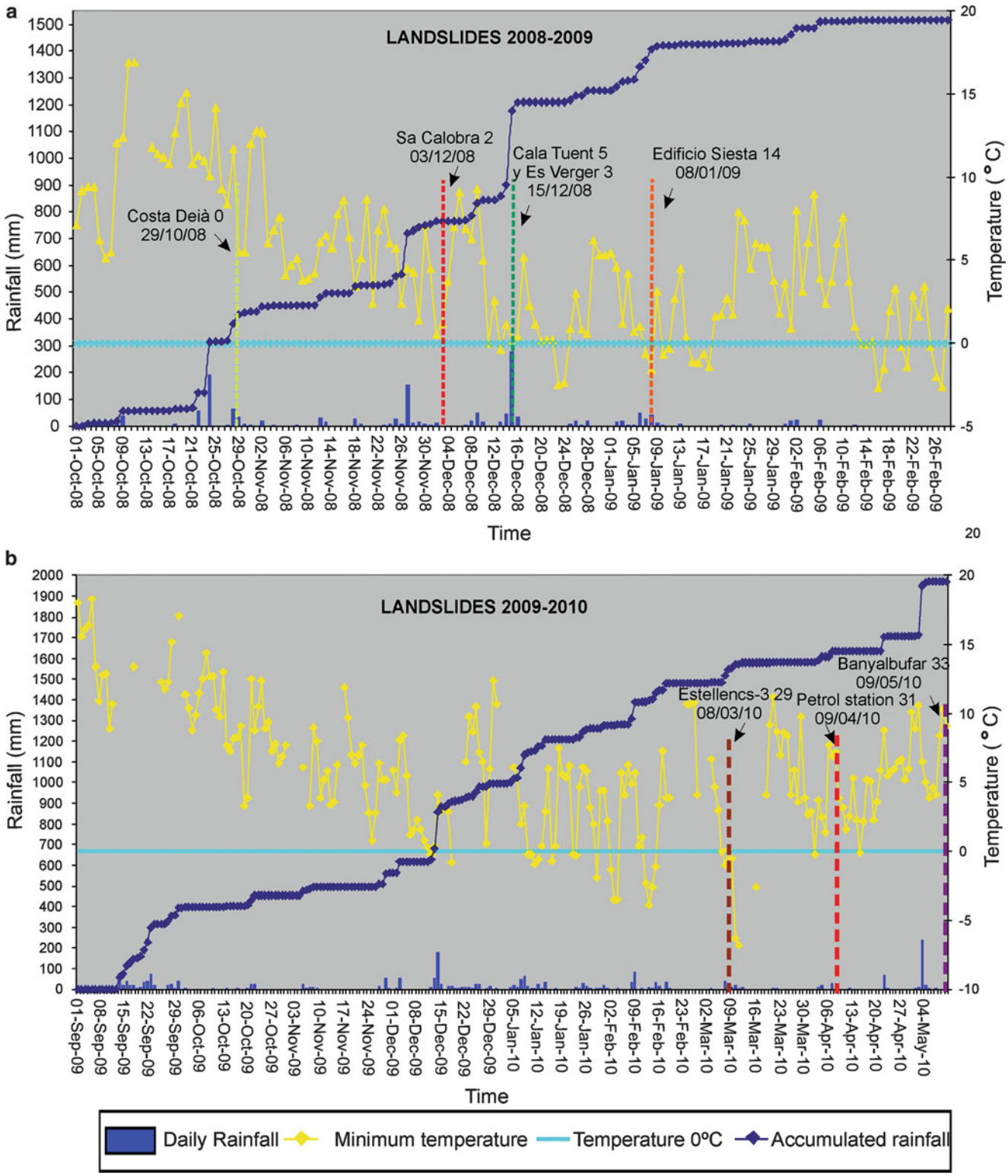

Fig. 5 Relationship between the different meteorological parameters – daily rainfall, accumulated rainfall and minimum temperatures recorded – and the occurrence of landslides, taking B013-Lluc weather station as the point of reference. The landslides recorded took place after episodes of moderately to extremely intense rainfall, with high accumulated rainfall (>850 mm)

intense (around 30 mm). The rockfalls took place because of the cumulative effect of the freeze-thaw cycles, which weaken the rock and propagate fissures. Some researchers believe that the frequency of rockfalls seems to be regulated by thermal fluctuations around 0 °C (Frayssines and Hantz 2006; Wieczorek and Jäger 1996; Shihi et al. 2004), and the

Table 2 Values of the meteorological data related to the occurrence of landslides. For each case, the weather stations closest to the failure point were used

Landslide inventory No. date	Max. rainfall in 24 h (mm) (10 days prior to event)	Minimum temp. (°C) (10 days prior to event)	Accumulated rain (mm) Since the start of the season	No. of freeze-thaw cycles (10 days prior to event)
Costa Deià (No. 0) 9 Oct 08	64 (28 Oct 2008)	10.21 (25 Oct 2008)	179.6	0
Sa Calobra (No. 2) 03 Dec 08	190.2 (27 Nov 2008)	−0.1 (02 Dec 2008)	900.3	1
Cala Tuent (No. 5) 15 Dec 08	61.7 (14 Dec 2008)	1.7 (13 Dec 2008)	1,075.2	0
Es Verger (No.3) 15 Dec 08	178.3 (15 Dec 2008)	−0.3 (01 Dec 2008)	626.4	1
Edificio Siesta (No. 14) 08 Jan 09	26.5 (06 Jan 2009)	0.8 (08 Jan 2009)	718.2	0
Estellencs (No. 29) 08 Mar 10	44.5 (07 Mar 2010)	−0.05 (07 Mar 2010)	864.5	1
Petrol station (No. 31) 09 Apr 10	20,2 (04 Apr 2010)	8,9 (08 Apr 2010)	927,6	0
Banyalbufar (No. 33) 09 May 10	120.3 (03 May 2010)	16.4 (08 May 2010)	1,220.7	0

frequency of temperature changes rises, while the absolute value of the thermal oscillation bears little influence (Orozco et al. 2002), as in the present study. Numerous authors also established a clear relationship between rockfall intensity and wet freeze-thaw cycles frequency in different European regions, when major precipitation events are recorded (Krautblatter and Moser 2009; Schneuwly and Stoffel 2008). The altitude of the scarp failure is also consistently relevant. The largest rockfalls were produced on scarps located above 600 m. Duarte and Marquinez (2002) established a relationship between a higher rockfall frecuency and a higher altitude of the scarp failures, in a region located in the N of Spain, with similar weather conditions to Majorca.

In the Mediterranean Alpine mountain ranges, several examples of rainy episodes which triggered surface landslides and mudflows are documented, which generally affect colluvial formations (Paronuzzi et al. 1998; Bolley and Oliaro 1999; Portilla et al. 2010), and where the interstitial pressure dissipates rapidly. In these cases, the preceding rainfall is almost irrelevant but it is the intensity of the rain which assumes greater importance. However, the behaviour is quite different in slopes with low permeability materials, such as the soft-material slopes in Majorca, where pre-saturation is a necessary condition for landslides. Most of the landslides recorded in this study took place on roadside slopes after preceding rains of $>$ 800 mm. In roadside slopes the critical rainfall thresholds may drop substantially compared to natural slopes (Corominas 2006). This argument is valid for some of the landslides registered, with low- moderate rainfall intensities of 20–62 mm/24 h prior to the failures, which are completely in line with those estimated by other in Spanish (Domínguez et al. 1999; Díaz de Terán et al. 1997). However, this does not hold true in other cases, where rain threshold to generate the failure was higher than 120 mm/24 h, which is closer to the threshold (130 mm/24 h) estimated by Mateos et al., (2007). These results enable us to conclude that the main triggering factor for landslides has been the high accumulated rainfall figures, in an exceptionally rainy period, with values being almost twice the average. The value of the rain intensity is less determinant.

In this study, the structural layout of the materials that outcrop in the Tramuntana Range conditioned the distribution of the movements. The Northern face is more hazardous due to the existence of steeper slopes and a higher presence of outcroppings of soft materials. Both of these factors are conditioned by the NW-overlapping thrusts and the regional tectonics. This coastal slope is also the one at the highest risk, as it is the most densely populated and urbanised. However, something that had not been noted earlier is the greater runout of the rockfalls on the Southern face, due to the stratigraphic distribution of the materials that comprise the failed massifs.

The results of this work have allowed the first steps to be taken towards the creation of an early warning system on the island. The system will be coordinated by the Emergency Service which will be put on alert by the Meteorological Service, when rain gauges record accumulated rainfall $>$ 800 mm or when forecasts predict heavy rainfall $>$ 90 mm/24 h. If, in addition to this, the forecast predicts a cold period, the alert will be higher in scale. In these situations, the road maintenance services will cut off the Ma-10 road at several sections which have already been identified as having greater susceptibility. Taking into account the fact that the island economy is based on tourism, the authorities are increasingly aware of the need to adopt preventative measures and to put safety first.

Acknowledgements This research work has been supported by the DORIS Project, n° 242212. Space Call FP7-SPACE-2009-1. We acknowledge the support of the Emergency Service of the Balearic Islands

References

Alvaro M (1987) La tectónica de cabalgamientos de la Sierra Norte de Mallorca (Islas Baleares). Boletín Geológico y Minero 98:34–41

Bolley S, Oliaro P (1999) Analisi dei debris flows in alcuni bacini campioni dell´Alta Val Susa. Geoingenieria Ambientale e Mineraria, XXXVI:69–74

Corominas J (2006) El clima y sus consecuencias sobre la actividad de los movimientos de ladera en España. Cuaternario y Geología 20 (3–4):89–113

Díaz de Terán JKR, Cendrero A, Araña V, Badiola ER (1997) In: Thomas Telford (ed) Geomorphological hazards of Europe, Elsevier, pp 429–456

Domínguez MJ, Jiménez M, Rodríguez A (1999) Press archives as temporal records of landslides in the North of Spain: relationships between rainfall and instability slope events. Geomorphology 30:125–132

Duarte RM, Marquinez J (2002) The influence of environmental and lithologic factors onrockfall at a regional scale: an evaluation using GIS. Geomorphology 43(1–2):117–136

Ferrer M, López JM, Mateos RM, Morales R, Rodríguez-Perea A (1997) Análisis de los Desprendimientos Rocosos en la Cala de Banyalbufar. Boletín Geológico y Minero 87:39–51

Frayssines M, Hantz D (2006) Failure mechanisms and triggering factors in calcareous cliffs of the Subalpine Rangers (French Alps). Engineering Geology 86(4):256–270, 25 Aug 2006

Gelabert B, Sabat F, Rodríguez-Perea A (1992) A structural outline of the Serra de Tramuntana of Mallorca (Balearic Islands). Tectonophysics 203:167–183

Krautblatter M, Moser M (2009) A non linear model coupling rockfall and rainfall intensity based on a four year measurement in a high Alpine rock wall (Reintal, German Alps). Nat Hazards Earth Syst Sci 9(4):1425–1432

Mateos RM (2002) Slope movements in the Majorca Island (Spain). Hazard analysis. In: McInnes RG, Jakeways J (eds) Instability, planning and management. Seeking sustainable solutions to ground movements problems. Thomas Telford, Ventnor

Mateos RM, Azañón JM (2005) Los movimientos de ladera en la Sierra de Tramuntana de la Isla de Mallorca: tipos, características y factores condicionantes. Revista de la Sociedad Geológica de España 18(1–2):89–99

Mateos RM, Ferrer M, González de vallejo L (2003) Los materiales rocosos de la Sierra de Tramuntana (Mallorca). Caracterización Geomecánica y Clasificación Geotécnica. Boletín Geológico y Minero 113(4):415–427

Mateos RM, Azañón M, Morales R, López-chicano M (2007) Regional prediction of landslides in the Tramuntana Range (Majorca) using probability analysis of intense rainfall. Zeitschrift fur Geomorphologie 51(3):287–306

Mateos RM, Bermejo M, Hijazo T, Rodríguiez-Franco JA, Ferrer M, González de Vallejo LI, García-Moreno I (2009) Los deslizamientos de la ladera de la margen izquierda del torrente de Fornalutx (Mallorca). Boletín Geológico y Minero 119(4):443–458

Mateos RM, García-Moreno I, Azañón JM, Tsige M (2010) La avalancha de rocas de Son Cocó (Alaró, Mallorca). Descripción y análisis del movimiento. Boletín Geológico y Minero 121(2):153–168

Orozco M, Azañón JM, Azor A, Alonso-Chaves F (2002) Geología Física. In: Paraninfo Thomson learning, 187 pp

Paronuzzi P, Coccolo A, Garlatti G (1998) Eventi meteorici critici e debris flows nei bacini montani del Friuli. L´ Acqua Sezione I Memorie, pp 39–50

Portilla M, Chevalier G, Hürlimann M (2010) Description and analisis of the debris flows occurred Turing 2008 in the Eastern Pyrenees. Nat Hazards Earth Syst Sci 10:1635–1645

Schneuwly DM, Stoffel M (2008) Tree-ring based reconstruction of the seasonal timing, major events and origin of rockfall on a case-study slope in the Swiss Alps. Nat Hazards Earth Syst Sci 8:203–211

Shihi S, Guzzetti F, Reichenbach P (2004) Rockfall hazard and risk assessment along a transportion corridor in the Nera Valley, central Italy. Environ Manag 34(2):191–208

Wieczorek GF, Jäger S (1996) Triggering mechanisms and depositional rates of postglacial slope-movement processes in the Yosemite Valley, California. Geomorphology 15(1):17–31

Climate Variability and Landslide Occurrence in Apulia (Southern Italy)

Maurizio Polemio and Teresa Lonigro

Abstract

This contribution is based on the analysis of different types of data recorded to provide monthly time series related to climate (rainfall, wet days, rainfall intensity and temperature) from 1877 to 2008, in order to verify the relationship between climate changes and landslide occurrence in Apulia region. Despite the decreasing trend of rainfall and rainfall intensity and the increasing trend of temperatures and wet days, there is an increasing trend of landslide occurrence, highlighting the negative effect of anthropogenic activities in landslide-prone areas.

Keywords

Climate change • Landslides • Apulia region

Introduction

Recent international research has underscored the evidence of climate change throughout the world, which is evident in the gradual, but constant, rise of temperatures and in the variation in the distribution of rainfall, which are concentrated in certain periods of time, often assuming exceptional intensities (EEA 2008). The consequences of these climate conditions are often droughts, depletion of water resources, desertification and/or increasing recurrence of catastrophic natural disasters.

Southern Italy, Apulia in particular, is affected by climate changes, enduring significant effects in terms of the decreasing trends of water availability (Polemio and Casarano 2008; Polemio et al. 2011). For the Apulia territory, the aim of this paper is to verify whether there are relationships between climate changes and the occurrence of damaging hydrogeological events (DHE) (Petrucci and Polemio 2003), especially landslides. For this purpose, two different databases were set up, a climate database for monthly data concerning rainfall, wet days, rainfall intensity and temperature and another database concerning damaging landslides. Thus, the trend of climate parameters and catastrophic landslides could be identified and there is a discussion of the different time series.

M. Polemio (✉) • T. Lonigro
CNR IRPI, Via Amendola 122/I, Bari, Italy
e-mail: m.polemio@ba.irpi.cnr.it

Materials and Methods

Classification of the Study Area

The Apulia region has an area of approximately 20,000 km^2, of which 54.2 % is flat, 44.4 % is hilly and only 1.4 % is mountainous. The few areas with relief are mainly concentrated in *Subappennino dauno*, where the maximum altitude reaches 1,152 m a.s.l. (Monte Cornacchia) and Gargano (Monte Calvo, 1,056 m a.s.l.) (Fig. 1). From an administrative point of view, the region is divided into six provinces (including the newly formed province BAT) and these provinces include 258 municipalities.

From east to west, it is possible to recognise three different geological domains related to Apennine orogenic phase, the foreland, the foredeep and the chain, which in Apulia are named *Avampaese Apulo, Fossa Bradanica* and the southern Apennine chain, respectively (Fig. 1).

C. Margottini et al. (eds.), *Landslide Science and Practice*, Vol. 4,
DOI 10.1007/978-3-642-31337-0_4,

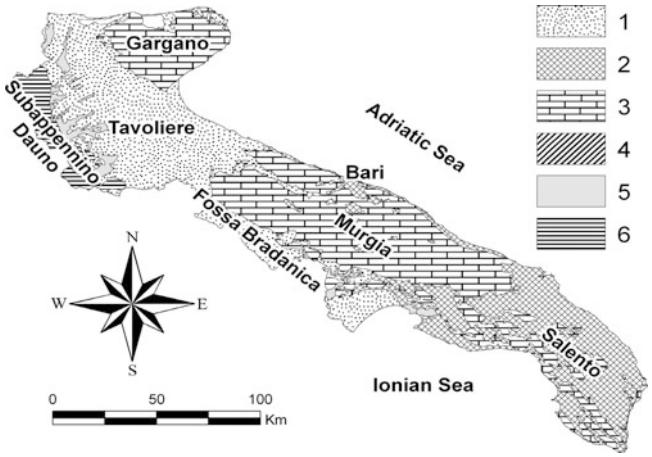

Fig. 1 Apulian geological-technical map. *1* – Sandy clay, clayey sand, sand and gravel; *2* – Sand, silt, calcareous sandstone, limestone and dolomite; *3* – Limestone and dolomite; *4* – Calcareous sandstone and sandstone; *5* – Marly clay; *6* – Flysch

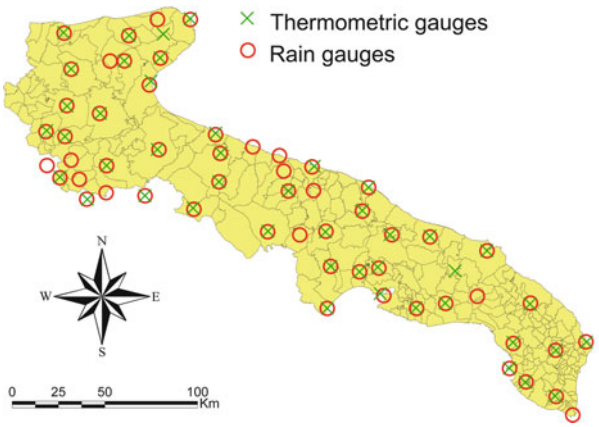

Fig. 2 Map of rain and temperature gauges and municipalities

The foreland represents the stable part of the entire orogenetic system, the area towards which all structures converge and which is made primarily of the carbonate platform sediments deposited during the Upper Jurassic – Cretaceous. The foreland is represented by Gargano, Murge and Salento (Ricchetti et al. 1988) and is composed of micritic limestones, with a fairly high fossil content. The typical landforms of karst (sinkholes, caves, etc.) are the markers of the subsequent emergence of the carbonate platform.

Moving eastward, there are Plio – Pleistocene units filling the *Fossa Bradanica*, in transgression on the carbonate platform units; the entire cycle of sedimentation includes limestones, clays, sands and conglomerates (Casnedi 1988).

In the *Subappennino dauno,* there are units belonging to the Apennine chain; they consist primarily of carbonate silicoclastic and marine deposits, which settled in different pre-orogenic sedimentary basins (D'Argenio et al. 1973). The tectonic forces then stacked these sediments, which, at present, are chaotic and strongly tectonised; they also present poor geotechnical properties, which is the reason that slope failures occur mostly in this area.

The Climate Database and Synthetic Indices

The CLIMAPULIA database was realised by collecting data on rainfall, temperature and wet days from the *Annali Idrologici* (annual publication of the national hydrological service), published from 1919 to 1996. This database has been integrated with historical data from 1877 with a series of publications edited by Prof. Eredia (1918, 1928). The most recent data (until 2008) were provided by the Centre of Functional Service of Civil Protection of Regione Puglia.

For this note, monthly data of temperature T, rainfall R and wet days WD (days in which precipitation is equal to or greater than 1 mm) were used. Since 1920, the *Annali Idrologici* defined wet days as the number of days in which rainfall is equal to or greater than 1 mm (SIMN 1919–1996). Historical data prior to 1920 considered a wet day a day during which the rainfall was greater than zero. A complex statistical treatment was performed to homogenise the data before 1920 with the data after 1920.

Sixty rainfall gauges/time series were selected, 47 of which were also thermometric. The selection was optimised by maximising time series length, minimising time series gaps and pursuing a sufficient gauge density (Fig. 2).

For each month and rain gauge, the monthly-mean rainfall intensity of wet days (following rainfall intensity or I) was calculated as the ratio between the monthly rainfall R and the monthly number of wet days WD. The following text always refers to the hydrological year, which runs from September to August.

For each of the climate parameters mentioned above (R, WD, I and T for temperature), maps of the average annual values of the entire period (1877–2008) were produced (Fig. 3)

To simplify the complexities of the spatial-temporal analysis of changes in the climate, the damaging landslide occurrences and the relationship between these variables, indices were defined by reducing the discussion to a discussion of time series (Polemio and Petrucci 2010). The index of monthly rainfall, bimonthly and . . . RI1 (z), RI2 (z), . . ., RIm (z) with m = 1, 2, . . ., 12, is defined by the relation:

$$RI_m(z) = \frac{\sum_{j=z-m}^{z} \sum_{i=1}^{n} MR_{i,j}(z)}{\sum_{j=z-m}^{z} \sum_{i=1}^{n} AMR_{i,j}(x)} 100 - 100$$

where x is the month of the average year (from 1 to 12, beginning in September), z is the position number of the month considered, beginning in September 1918, MR_i is

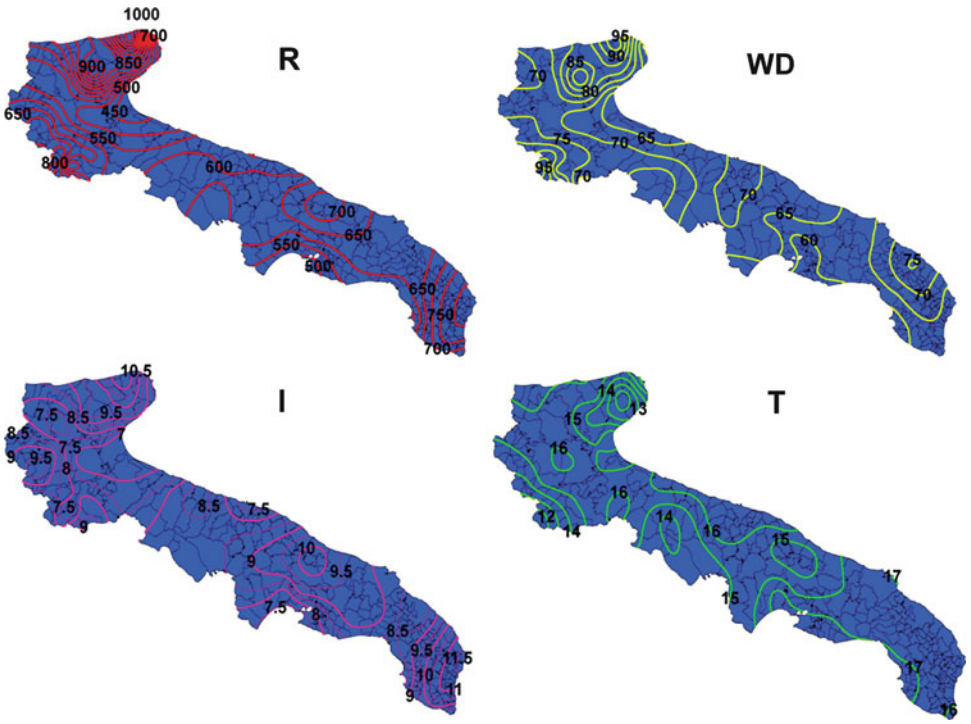

Fig. 3 Maps of average annual values (1877–2008) of: rainfall (*R*, mm), number of wet days (*WD*), rainfall intensity (*I*, mm/day) and temperature (*T*, °C)

the monthly rainfall at gauge i and AMR_i is the average monthly rainfall at gauge i, with i = 1, 2, . . ., n, where n is the number of available gauges in the month z. RI_m (z) takes into account the values of rainfall of the month m and of z−1 previous months, where m is the duration of the index considered. Using this dimensionless index, a single time series of rainfall can be considered for the entire study area. Replacing WD, I or T to R, similar indices can be obtained for the other parameters; such indicators may vary within a wide range of values, where the negative ones indicate rainfall (temperature, etc.) below the average in the entire area, while positive values indicate the opposite (a more deepened discussion of the indexes can be found in Polemio and Petrucci 2010).

For m = 12, the index becomes annual; in this case, if z is September of year y, the index is Ry, WDy, etc.

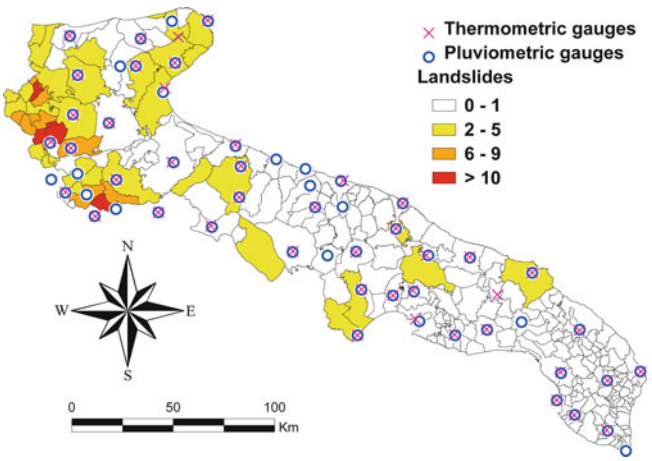

Fig. 4 Recurrence of local landslides (1918–2006)

The Landslide Database

The main source of records of damaging landslides for Apulia is the AVI database (CNR-GNDCI 1999), which is useful for the period 1918–1996. This source was integrated up to 2006 by consulting newspapers, publications and technical reports kept by the authors' Institute. In Apulia, 237 landslide events (the first recorded landslide was in 1928) were recognised. Landslide monthly time series were defined both for each municipality and for the entire region. The whole dataset was implemented in a GIS environment (Fig. 4).

As with the climate data, synthetic indices were calculated for 1–12 months and for hydrological years (Ly).

The map of the regional distribution of landslides underlines the high concentration of these events in the area of the Subappennino dauno, where geological, morphological and geotechnical features allow slope instability phenomena.

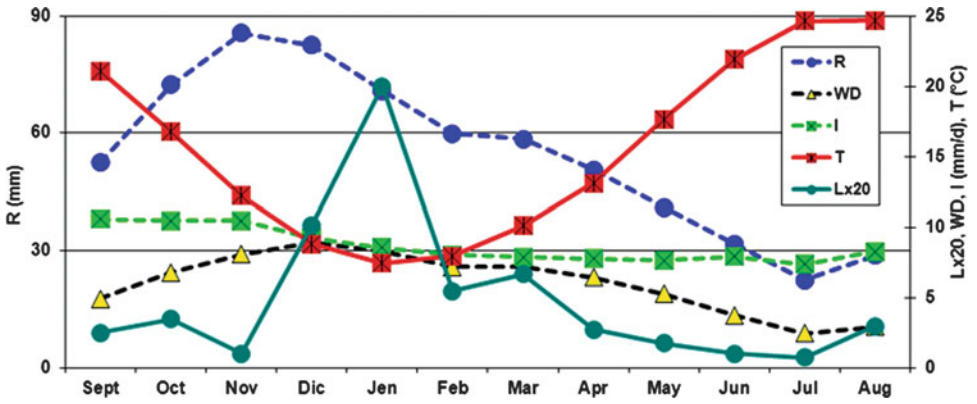

Fig. 5 Climate and landslides system. *R* rainfall, *WD* wet days, *I* rainfall intensity, *T* temperature, *L* number of landslides

Table 1 Correlation coefficient between annual indices of landslides (Ly), rainfall (Ry), wet days (WDy), rainfall intensity (Iy) and temperature (Ty)

	Ly	Ry	WDy	Iy	Ty
Ly	1.0				
Ry	0.1	1.0			
WDy	0.2	0.8	1.0		
Iy	0.0	0.6	0.1	1.0	
Ty	0.3	0.0	−0.1	0.0	1.0

Results and Discussion

The regime of climate and landslides was plotted by considering the average hydrological year (the landslide values were amplified) (Fig. 5).

The landslide peak is observed in January (0.2 events), immediately after the period of higher rainfall. Sixty-one per cent of the total number of landslides occur from December

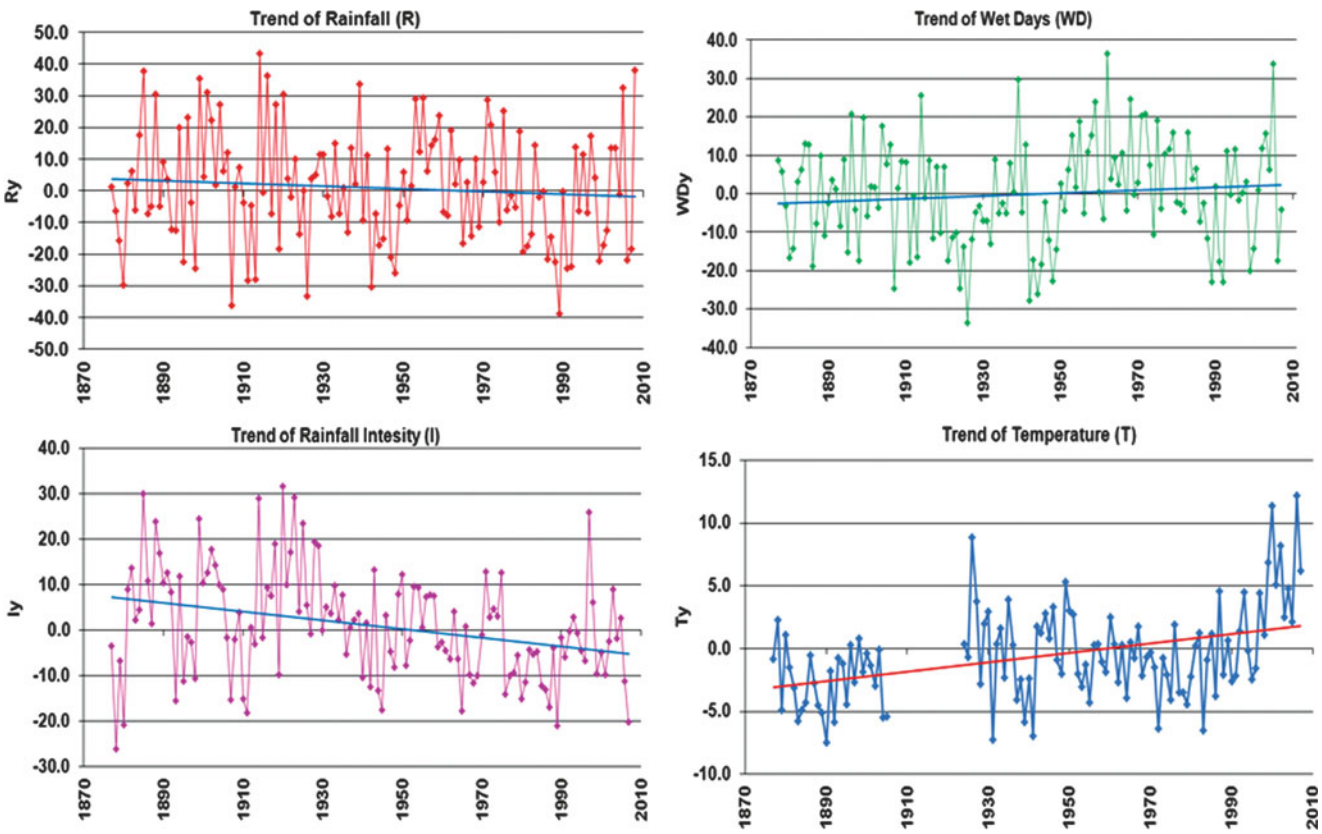

Fig. 6 Trend of Rainfall (*R*), Wet Days (*WD*), Intensity of rainfall (*I*) and Temperature (*T*)

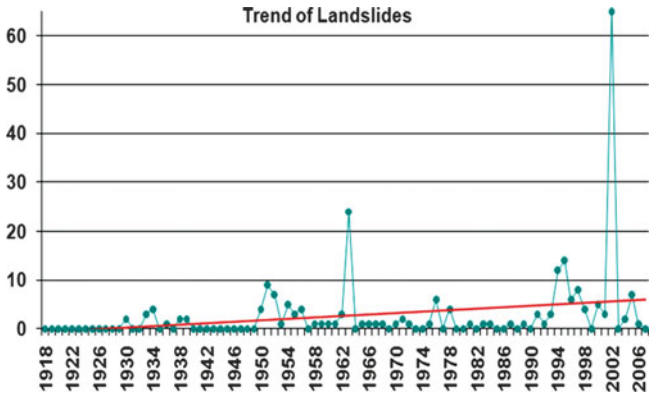

Fig. 7 Time series of annual landslide number and trend

to February, with 3 per year on average. The monthly maximum of landslides is 61, which occurred in January 2003.

The correlation analysis between annual indices underlines a direct correlation between rainfall, rainfall intensity, wet days and landslides and an indirect or inverse correlation in the case of temperature, with low values of the correlation coefficient (Table 1).

Tests were repeated for cumulative periods up to 5 years, considering again couples of cumulative annual indices: the results showed no relevant difference from the results in Table 1.

Previous research on other areas of southern Italy affected by widespread landslide occurrence showed a higher correlation between climatic indices and the occurrence of landslides (Polemio and Sdao 1996; Polemio and Petrucci 2010).

This figure can be explained by considering two different effects. The Apulia landslides are mainly concentrated in part of the region, the Subappennino dauno, while the climatic indices refer to the whole region. Secondly, the Subappennino dauno can be considered socioeconomically a marginal area and almost remote, especially in the past. For both of these reasons, the number of damaging landslides is likely to be underestimated in the beginning of the study period.

The trend analysis shows a decreasing trend of rainfall and rainfall intensity and an increasing trend of wet days and temperatures (Fig. 6), in agreement with what is known for all of southern Italy (EEA 2008; Polemio and Casarano 2008).

The climate trend, overall, does not show favourable conditions for the increase of the annual landslide number. Nevertheless, the trend of the annual number of damaging landslides is positive or increasing (Fig. 7).

These results could be explained by hypothesising an increasing use (land misuse?) of landslide prone areas.

To reduce the uncertainty in the results described above, the research is being expanded with two approaches. The climate and hydrological analysis considers peak rainfall from 1 h up to 5 days. The whole set of statistical calculations will be repeated at the regional and local scale (Subappennino dauno). The historical research on damaging landslides is improving in quality and quantity of information back to 1850. The expansion is almost complete: the preliminary results are consistent with main results of this paper.

References

Casnedi R (1988) La Fossa bradanica: origine, sedimentazione e migrazione. Mem Soc Geol It 41:439–448

CNR-GNDCI (1999) Database AVI degli eventi alluvionali occorsi su tutto il territorio nazionale dal 1930 al 1999

D'Argenio B, Pescatore T, Scandone P (1973) Schema geologico dell'Appennino meridionale (Campania e Lucania). Accademia Nazionale dei Lincei 183:49–72

EEA (2008) Impacts of Europe's changing climate – an indicator-based assessment. European Environment Agency Report, 4, http://www.eea.europa.eu/publications/eea_report_2008_4/

Ministero LL. PP (1918) Osservazioni pluviometriche raccolte a tutto l'anno 1915 dal R. Ufficio centrale di Meteorologia e ordinate a cura del Prof. FILIPPO EREDIA, Puglia

Ministero LL. PP (1928) Osservazioni pluviometriche raccolte a tutto l'anno 1915. Pubbl. n.1 del Servizio Idrografico, Appendice al volume I, Italia peninsulare e isole, ordinate a cura del Prof. Filippo Eredia

Petrucci O, Polemio M (2003) The use of historical data for the characterisation of multiple damaging hydrogeological events. Nat Hazards Earth Syst Sci 3(1/2):17–30

Polemio M, Casarano D (2008) Climate change, drought and groundwater availability in southern Italy. In: Dragoni W, Sukhija BS (eds) Climate change and groundwater, vol 288. Geological Society, London, pp 39–51, Special Publications

Polemio M, Petrucci O (2010) Occurrence of landslide events and the role of climate in the twentieth century in Calabria, southern Italy. Quart J Eng Geol Hydrogeol 43:1–14

Polemio M, Sdao F (1996) Landslide hazard and critical rainfall in southern Italy. In: Proceedings of VIIth international symposium on landslides, Balkema, Norway/Rotterdam, pp 847–852

Polemio M, Dragone V, Casarano D, Basso A, Brunetti M, Maugeri M, Nanni T, Simolo C (2011) Cambiamenti climatici e disponibilità di acque superficiali e sotterranee: trend in atto e previsioni. In: Polemio M (ed) Le modificazioni climatiche e i rischi naturali. CNR IRPI, Bari, pp 213–216

Ricchetti G, Ciaranfi N, Luperto Sinni E, Mongelli F, Pieri P (1988) Geodinamica ed evoluzione sedimentaria e tettonica dell'avampaese Apulo. Mem Soc Geol It 41:57–82

SIMN (1919–1996) Annali Idrologici – Parte I. Sezione di Bari, Ministero dei Lavori Pubblici, Roma

Geotechnical and Mineralogical Characterisation of Soils from Landslide Scars and Inferred Sliding Mechanism: Case of Limbe, SW Cameroon

Vivian Bih Che, Philippe Trefois, Matthieu Kervyn, Gerald G.J. Ernst, Eric Van Ranst, Jean-Claude Verbrugge, Christian Schroeder, Patric Jacobs, and Cheo Emmanuel Suh

Abstract

The occurrence of landslides in any area may be attributed to the geotechnical, mineralogical and chemical properties of the soils as well as to forces acting on these materials. In this paper, we investigate the role of geotechnical and mineralogical properties of soils in the occurrence of shallow translational landslides in Limbe, SW Cameroon. Laboratory results show that the soils are mainly inorganic silts of medium to high plasticity with clay fraction composed of non-swelling clay minerals. Calculated factor of safety using the infinite slope model for completely saturated soil is greater than 1.5. We therefore propose that failure is generated as a result of fracture enhanced permeability in localized zones of the superficial soils leading to rainwater accumulation and the development of a perched water table in the saprolite from which high positive pore pressure may development and result in the mobilisation of the overlying soil column.

Keywords

Sliding mechanism • Fracture permeability • Residual soil • Geotechnical • Limbe • Mt Cameroon

Introduction

The occurrence of landslides in any area may be attributed to the geotechnical (Yalcin 2007), mineralogical and chemical properties of the soils as well as forces acting on these materials. Ground conditions such as weak strength, sensitive fabric, degree of weathering, non uniform weathering and intense fracturing are some of the factors that influence slope stability. Sidle et al. (1985) observed that soil properties such as particle size and pore distribution in the soil matrix influence slope stability. These properties influence the rate of water movement in soils and the capacity of the soil to retain water. Finer soils tend to hold higher volumes of water under unsaturated conditions than their coarse textured equivalents (Sidle 1984). Other soil parameters that contribute in landslide occurrence include the rate at which water infiltrates into the soil at depth (Inganga and Ucakuwun 2001).

It is thus essential to evaluate the properties of landslide-prone soils, in order to understand the sliding mechanisms operating in a particular area. Sliding mechanisms as defined

V.B. Che (✉)
Department of Geology and Environmental Science, University of Buea, Buea, SW Cameroon

Department of Geology and Soil Science, Ghent University, Ghent, Belgium
e-mail: chevivianbih@yahoo.com

P. Trefois
Royal Museum for Central Africa, Tervuren, Belgium

M. Kervyn
Department of Geography, Vrije Universiteit Brussel, Brussel, Belgium

G.G.J. Ernst • E. Van Ranst • P. Jacobs
Department of Geology and Soil Science, Ghent University, Ghent, Belgium

J.-C. Verbrugge • C. Schroeder
Laboratoire de mécaniques des sols, Université Libre de Bruxelles, Bruxelles, Belgium

C.E. Suh
Department of Geology and Environmental Science, University of Buea, Buea, SW Cameroon

C. Margottini et al. (eds.), *Landslide Science and Practice*, Vol. 4,
DOI 10.1007/978-3-642-31337-0_5,

by Hutchinson (1988) are idealized ways through which slope material might move. Sliding mechanism depend on the geometric, physical and mechanical properties (ie the particle size, pore pressure, cohesion, effective angle of internal friction, soil thickness, slope angle, bulk density), the transient properties (natural water content, degree of saturation) and the mineralogical composition of the soils. They are also affected by external factors such as human intervention, rainfall and seismic activities.

Limbe Study Area

The Limbe area (SW Cameroon) has witnessed a number of deadly landslide occurrences in the last two decades. According to Fell's classification scheme (Fell 1994), most of these slides are extremely small to small shallow translational slides involving only the thin veneer of soil developed by in-situ weathering of bed rock (Che et al. 2011). The major rock types in this area are alkali basaltic lava flows, basaltic to picrobasaltic pyroclatic materials, mudflow deposits and alluvial deposits mostly confined to the flood plain of streams and rivers. These rock types show variable degrees of weathering. Solid basaltic rocks either lay exposed at the surface or are overlain by thick purplish to grey saprolite sequences on which are found sticky yellowish brown or reddish soils with a mean thickness of 3 m but can extent to over 10 m in some areas. Saprolite, refers to residual soils developed on crystalline rocks in which some or all of the primary minerals have been extensively transformed in situ to weathering products with the preservation of parent rock texture structure and fabric (Velbel 1985) whereas soil refer to material that has been complete degraded and all trace of the parent material lost.

Topographically, the area is characterised by a series of E-W trending ridges separated by deep valleys. These valleys are occupied by ephemeral or perennial streams and rivers that show a parallel to dendritic drainage pattern. Elevation ranges between 0 and 300 m above sea level. The climate is tropical with a 4-month dry season from November to March and an 8-month long rainy season from March to October. Most of the rainfall recorded falls between the months of June and September which coincides with periods of recorded landslides. Rainfall is intense with mean value of 4,000 mm/year. Rainfall, however, shows significant spatio-temporal variability within the area. Mean annual temperature reached 28 °C in the last 15 years.

Material and Method

In order to characterize landslide prone soils, better understand destabilization processes and propose remediation measures for the Limbe area, three slide scars were chosen

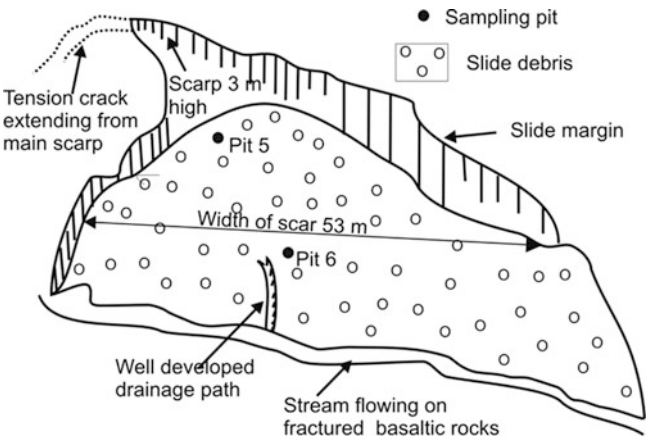

Fig. 1 Sketch of Makuka slide showing the location of sampling pits. Two samples (P5S15 and P5S16) were drawn from pit 5 and 4 samples P6S17 (Diagram not drawn to scale)

and studied in detail. Six 2.5–4 m deep rectangular (1 × 1.5 m) pits were dug into the landslide scars and their profiles described. This article however focuses only on one of these slides, located in Makuka, (Fig. 1, 53 × 55 m wide translational slide) into which two pits were dug. Only two samples were collected from pit 5 due to the presence of partially weathered rock masses that made digging impossible. Similarly, deeper soils in pit 6 were not characterised because sampling was not possible due to the presence of rock fragments as described in Fig. 2.

In situ shear tests were done by driving a Torvane meter into the sides of the pit and rotating it until failure. The corresponding torque is read off the vane meter and later converted to shear strength values, providing the in situ apparent cohesion (undrained shear strength). Soil colour characteristics were obtained from the Munsell Soil Classification Chart, natural moisture content by oven drying soils at 110 °C for 24 h and loss on ignition (LOI) by igniting samples at 550 °C in a muffle type furnace for 2 h. Sample bulk density was determined by water immersion of paraffin coated samples and particle specific gravity (particle density) with the aid of a pycnometer. Sieve and hydrometer analysis were done to determine the grain size distribution. Atterberg's (consistency) limits were also determined. At least four specimens were prepared for each sample and average values reported for each test.

Shear strength parameters (cohesion and effective angle of internal friction) and permeability were also determined by consolidated undrained triaxial tests on reconstructed samples. Here, a specific amount of water was added to air dried soil samples to mimic natural moisture conditions and then extruder in a metallic cylinder to obtained soil columns with a length width ratio of 2. Sample mass and volume are calculated in order to reconstruct in situ bulk volumic weight of the samples.

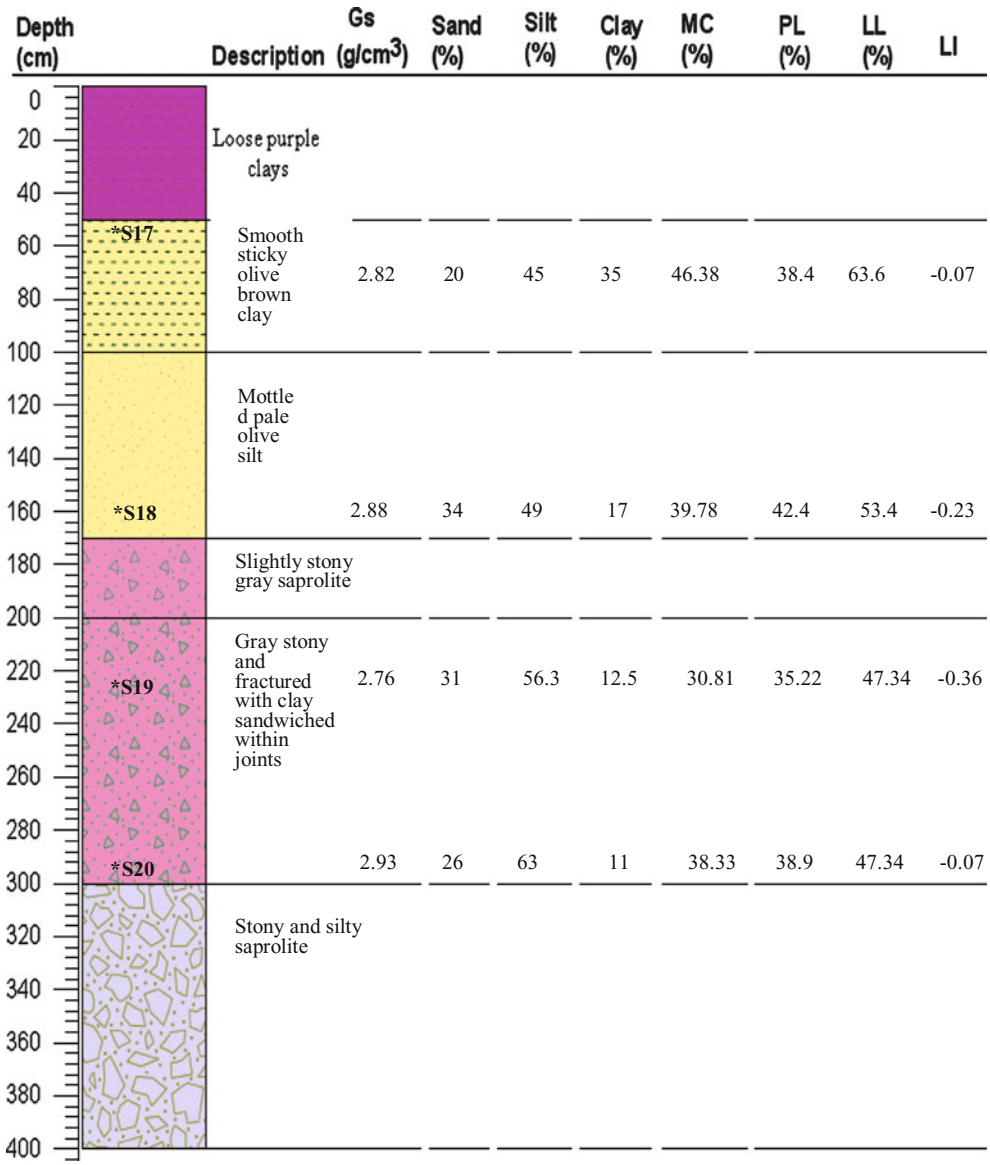

Fig. 2 Geotechnical profile of Pit 6. *Gs* particle specific gravity, *MC* natural moisture content, *PL* plastic limit, *LL* liquid limit, *LI* Liquidity index

Results

Geotechnical Properties

The natural moisture content, grain size distribution and other geotechnical properties measured in this study are presented in Table 1 and some incorporated in the geotechnical profile of Pit 6 presented in Fig. 2.

Natural moisture content ranges from 31 % to 50 % and generally show a downward decreasing trend with depth to the noticeable exception of the deepest soil sample probably due to the effect of water stored in the fractures of the underlying layer. LOI ranges from 7 % to 12 % and also show a downward decreasing trend probably due to decrease in the intensity of weathering with depth. The plastic and liquid limits range from 32 to 45 and from 47 % to 65 %, respectively. Plasticity index (PI), a measure of the range of moisture content over which the soil behaves plastically, ranges from 8 to 25 with highest values recorded in the topmost horizons. PI decreases progressively with depth suggesting that the top layers are less likely to liquefy relative to the underlying saprolites.

Particle specific gravity (Gs) sometimes referred to as the particle density of a soil is high, ranging from 2.76 to 2.98 g/cm^3 with mean values of 2.86 $\pm$ 0.06 g/cm. The average bulk density is 1.95 g/cm, ie approximately half the bulk density of the fresh rock sample. Porosity (a measure of the volume of voids in the bulk sample volume) ranges from 24 % to 36 %. It also shows variable pattern down the profile probably due to non uniform weathering with depth. All these data fit well with other results obtained

Table 1 Index and geotechnical properties of soils from landslide scars in the study area as derived from laboratory analysis. *Mc* natural moisture content, *LOI* loss on ignition, *PL* plastic limit, *LL* liquid limit, *SL* shrinkage limit, *LI* liquidity, *AC,* activity coefficient, *Gs* particle specific gravity. γd dry density, γ bulk density, *n* porosity, τ_u undrained shear strength measured with a Torvane meter

S No	P5S 14	P5S15	P6S 17	P6S 18	P6S19	P6S20
Pit No	Pit 5		Pit 6			
Depth (cm)	40	70	50	160	230	290
Texture	Clay loam	Silt loam	Silty clay loam	Loam	Silt loam	Silt loam
Sand (%)	32.0	39.0	20.0	34.0	31.0	26.0
Silt (%)	41.0	50.0	45.0	49.0	57.0	63.0
Clay (%)	27.0	11.0	35.0	17.0	13.0	11.0
Mc (%)	50.4	34.6	46.4	39.8	30.8	38.3
LOI (%)	9.0	8.2	11.8	8.4	7.4	7.1
PL (%)	45.0	31.9	38.3	42.4	35.2	38.9
LL (%)	64.7	46.7	63.6	53.4	47.4	47.3
PI (%)	19.7	14.8	25.3	11.0	12.2	8.4
SL (%)	38.8	37.4	28.8	40.7	40.6	37.4
LI	0.3	0.2	0.3	0.2	0.4	0.1
AC	0.7	1.4	0.7	0.7	1.0	0.8
Gs (g/cm)	2.9	2.8	2.8	2.9	2.8	2.93
γd (g/cm^3)	1.4	1.6	1.3	1.3	1.5	1.6
γ (g/cm^3)	2.1	2.2	2.2	1.9	1.9	2.0
n (%)	26.8	24.0	24.9	31.3	35.8	30.4
τ_u (kPa)	59.9	57.1	78.7	62.6	65.3	58.8

from studies on residual soils in tropical climates (Lohnes et al. 1971; Vaughan et al. 1988; Rahman et al. 2010).

According to the Unified Soil Classification Scheme based on soil consistency limits (Casagrande's 1948), the soils from the Makuka scar are categorised as inorganic silts of medium plasticity to high plasticity. The activity and swelling behaviour of the soils as shown in Fig. 3 indicate that the soils have a low to medium swelling potential.

Mineralogical characterisation by X-ray diffraction suggests that the dominant mineral species include non-expanding clays (dehydrated halloysite), sanidine and minor amounts of (titano) magnetite, goethite, and Illite Fig. 4. Thus accounting for the low to medium swelling potential observed in the soils.

Cohesion and effective angle of internal friction measured by consolidated undrained triaxial tests on reconstructed samples are 67.9 kPa and 34.2°, respectively. The permeability is low measuring 6.9×10^{-10} m^3/s. From the above mentioned parameters, the factor of safety for this slope calculated based on the standard infinite slope stability model for a fully saturated slope given by

$$FS = \frac{C}{H\gamma \sin\beta} + \frac{\tan\phi}{\tan\beta} - \frac{m\gamma_w \tan\phi}{\gamma \tan\beta}$$

where FS: is factor of safety; C: effective cohesion (kPa); γ: total unit weight of the soil (KN/m^3); H: thickness of the sliding mass (m); β: slope gradient; γ_w: unit weight of water (kN/m^3); m: height of water table (degree of saturation); and ϕ: the internal friction angle of the soil (°).

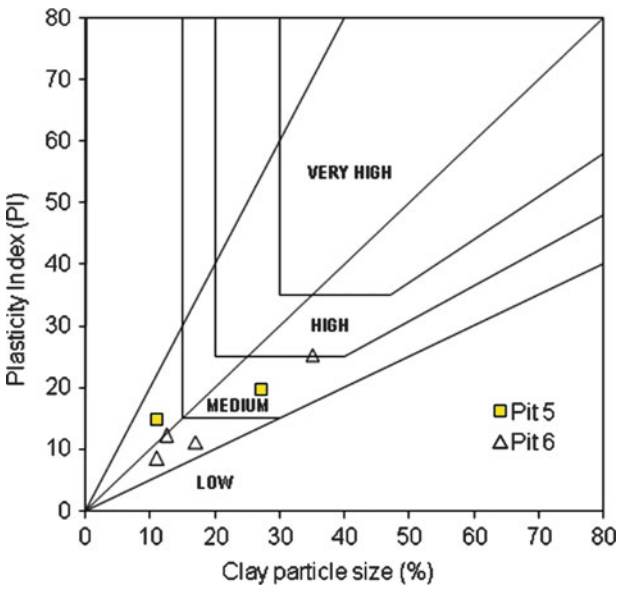

Fig. 3 Activity and swelling potential (after Williams and Donaldson 1980) of soil samples from the Makuka slide

The first term accounts for the resistance due to cohesion, and is the only one to be sensitive to variations in the thickness of the sliding layer H. The second term represents the resistance related to the internal frictional angle and the third term accounts for static effect of water saturation.

Considering that the slip surface is parallel to the ground, thickness of sliding mass is 3 m and slope gradient 30° (parameters measured in the field) the factor of safety is far

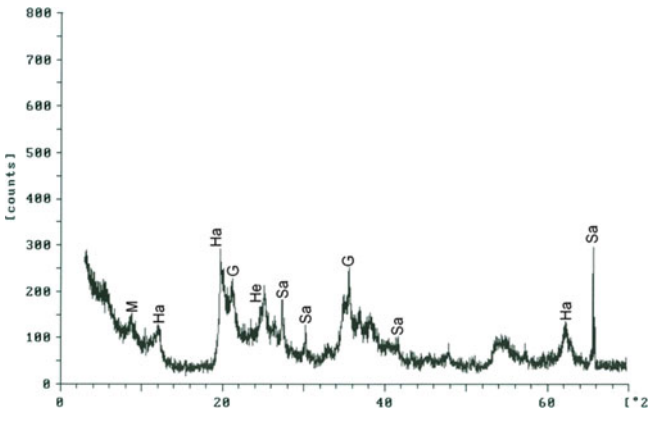

Fig. 4 X-ray diffractogram of soil from the Makuka slide scar. Note the dominance of sanidine halloysite and illite peaks

bigger than I.5. This value indicates that the slope is supposed to be stable. As slope failure is however observed, we propose an alternative model to account for the slope instability. The proposed model assumes that the infiltration of rainwater into the soil is driven by macropores and micropores. Secondly, soil saturation during and after rainfall can proceed from two fronts. Finally, the soils are less permeable than the underlying saprolite with permeability enhanced by the presence of non-uniformly distributed fractures.

During rainfall events, soil saturation proceeds from the surface down the profile due to infiltration of rainwater through the macro- and micropore network, thus resulting in the propagation of a downward wetting front. Usually, the migration of water through the macropores (fractures) is relatively fast, particularly if the fractures are interconnected. In the saprolite, downward flow is inhibited by fracture discontinuity and non uniform weathering thus facilitating lateral spread and subsequent accumulation of water resulting in a perched saturated zone in the saprolite. Intense and prolonged rainfall that characterise this area may also result in rapid changes in the regional ground water level.

The perched aquifer and change in ground water level can result in an upward wetting front that is prevented from rising freely by the presence of the overlying less permeable soil horizon thus providing a conducive environment for the generation of positive pressure at the soil/saprolite interface where a permeability boundary is encountered thus enhancing uplift and mobilization of the overlying soil column.

This model is constrained by field observations and laboratory test results. Field observations indicate that the saprolite is highly fractured basalt and that the slip surface lies at the soil/saprolite boundary rather than at the soil/ bed rock interface. In the field, water was observed oozing out at the contact between saprolites and the soil at the head scarp after rainfall events, thereby confirming the existence of temporal aquifers. Field observation also advocates that downward flow of water through the saprolite is inhibited by non-uniform weathering, non-uniform distribution of fractures and discontinuous fractures in the saprolites as observed in Fig. 5.

Eyewitnesses who observed some other slides within this area reported an increase in ground water discharges below the foundation of some houses prior to sliding, suggesting the emergence of pressurised ground water.

Furthermore, sections observed along road cuts indicate the presence of dense fracturing and non-uniform weathering in this area.

Laboratory results also point out higher porosity, silt and sand fraction and a corresponding lower clay concentration particularly at depths of 1.5–2 m depth that mark the transition from soils to saprolite. It is worth noting that unsaturated ground water movement through soil is inhibited when it encounters textural heterogeneities or permeability boundaries. These discontinuity interfaces provide a conducive environment for the development of positive pore pressure. Notwithstanding, the amount of pressure required to build up and the time it takes for it to build up was not quantified in this study

Discussions

The study of rainfall-induced landslide mechanisms is one of the most important and difficult issues in landslide research (Hengxing et al. 2003). This is because the engineering, chemical, and mineralogical properties of soils are closely related to the mechanical behaviour of soils at different moisture concentrations, stress state and stress history. Water thus play a very important role in the occurrence of landslides (Al-Homoud et al. 1997). Rainfall within the study area, represents the main source of ground water recharge. Water penetrating the topsoil may accumulate forming perched water table or result in changes in region ground water level and thus enhance the development of positive pore pressure within the profile.

Unlike reports presented by Meisina and Scarabelli (2007) for Oltrepo Pavese (Italy), the slip surface of this slide lies at the soil/saprolite boundary which is a common characteristic for slope failure triggered by high intensity/ short duration rain (Larsen and Simon 1993). The geotechnical profile shows variability with depth. As shown in Fig. 2 above, there is a decrease in the clay content and a net increase in the amount of silt as one move down the profile thus providing a permeability boundary where positive pore pressure can result.

The soils analysed in this study are characterised by high particle specific gravity, high porosity, high cohesion and angles of internal friction. These observations imply good geotechnical performance of the soils from this scar and thus low susceptibility to failure. Bearing in mind that the shear strength and permeability was measured on remoulded/

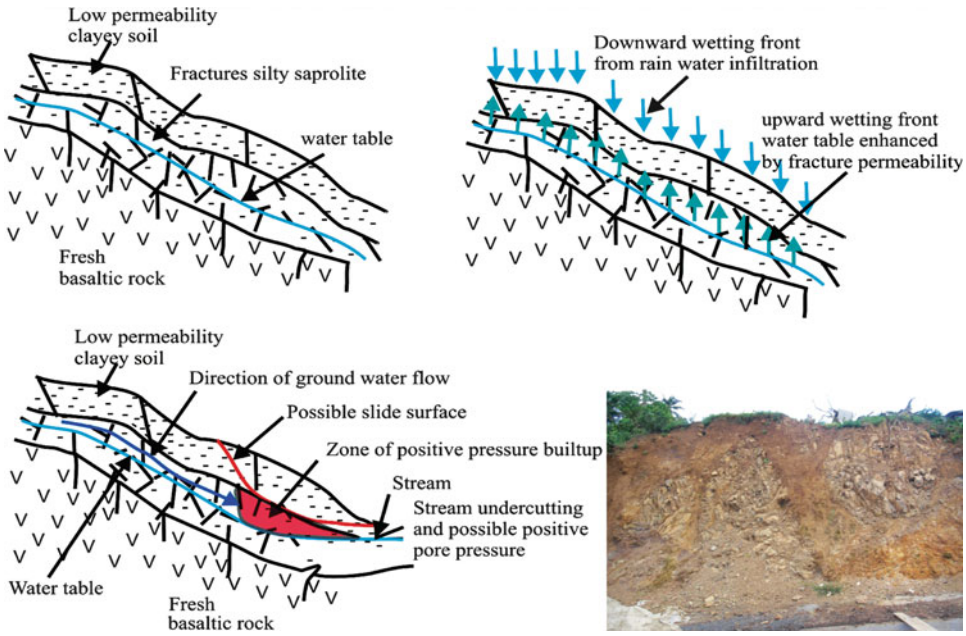

Fig. 5 Sketch of the steps and processes involved in the proposed fracture permeability sliding mechanism. Note the presence of intense fracturing and non-uniform weathering observed within the study area. Photograph depicts field evidence of intense fracturing in saprolite and non-uniform weathering at a road cut

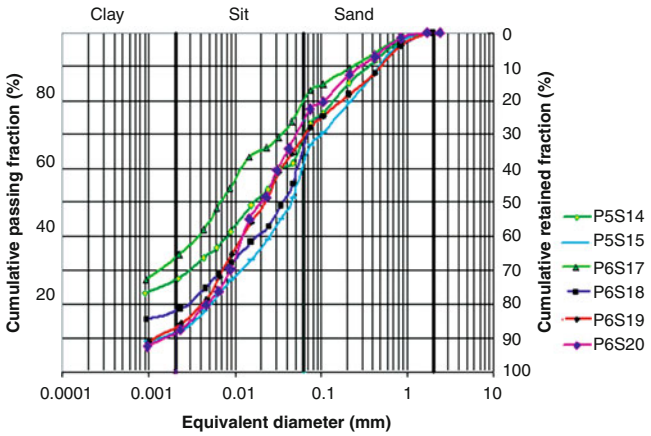

Fig. 6 Grain size distribution curve for samples collected at Makuka Pits 5 and 6. Note the abundance of the silt fraction and low clay and sand concentrations

reconstructed samples it is possible that the values are over- or underestimated; as such further analysis on undisturbed samples needs to be performed for comparison. The granulometric curves (Fig. 6) differ significantly from those of sedimentary soils: they are poorly graded (no sedimentation or selective sorting effect) and made up of a wide range of grains including sand, silt and clay in the same soil. This may result to a specific soil skeleton with a grain intrication favouring good mechanical properties if undisturbed but may completely collapse when saturated.

Particle specific gravity sometimes referred to as particle density of soils gives us an idea about the relative proportion of organic matter and mineral particles present in a soil as well as the chemical composition and structure of the soil minerals.

In this study, the high particle densities suggest low organic matter content and dominance of mineral constituents particularly (titano) magnetite, and pyroxene which are the most abundant mineral phases in the parent rock.

The average particle specific gravity of soils reported in literature is ca. 2.6 g/cm^3, but may range from 2.4 to 3.6 g/cm^3 depending on the nature of it's mineral constituents (Cernica 1995). In this study the observed Gs is generally higher than the reported mean, ranging from 2.8 to 2.93 g/cm. These higher values can be attributed to the mafic composition of the parent rock which is rich in iron and magnesium silicates (olivine, pyroxenes) and to the presence of magnetic minerals (e.g. (titano) magnetite, goethite) that are characterized by high specific gravity values and constitute the major opaque mineral phases in rocks of the Mount Cameroon region (Suh et al. 2003; Njome et al. 2008).

Atterberg's plastic and liquid limits are widely used parameters for determining the consistency of cohesive soils. They provide useful information regarding soil strength, stability, mineralogy, state of consolidation of the soil, and the classification of soils into organic or inorganic clays (Yalcin 2007, 2011). The dominance of halloysite and illite in these soils is the most likely explanation for the moderate plasticity indices observed for these soils.

The Liquidity index (LI), a measure of the behaviour of fine grained soils upon shearing or of the undrained shear behaviour of remoulded samples for all the samples is slightly above zero. Other studies have shown that for remoulded samples when LI is equal to or less than zero the soil is compact, solid and unlikely to fail by flow (Shakoor and Smithmyer 2005). In in-situ residual soils, weathering might result in a relatively strong porous soil structure that can hold

large proportions of entrapped water and air. The samples analysed in this study, therefore, will behave as brittle solids and are unlikely to fail by flow type movement unless a large amounts of water is added.

Strength parameters determined by consolidated undrained triaxial test suggest that the factor of safety for this slope is higher than 1.5 thus failure was initiated by another process than loading on the natural slope. Field observations suggest that fracture enhanced permeability contributed to the occurrence of this slide. This is most likely because the saprolite observed in Pit 6 is highly fractured and weathering is not uniform.

According to Campbell in Shakoor and Smithmyer (2005), shallow storm-induced flow type failure requires three conditions to occur: a mantle of colluvial soil, steep slopes and soil moisture equal to or greater than the liquid limit of the colluvial soil. The first two conditions were met but the third was not achievable from laboratory results thus is a possible explanation for the characteristic slide type instead of the flow type failure pattern observed at this site.

Conclusion

From the geotechnical point of view, the following conclusions may be drawn:

- Soils from the Makuka landslide scar have good geotechnical properties and will be stable under normal circumstances.
- Index and geotechnical properties of soils can be used as a fingerprint or a proxy to the sliding mechanism.
- Based on the present results, it is suggested that the Makuka slide was triggered as a result of fracture enhanced permeability in localized zones of the superficial soils leading to the development of positive pore pressure from a perched water table in the saprolite.

Acknowledgments This manuscript is a part of Vivian Bih Che's Ph.D. thesis. The research was funded by the Flemish Interuniversity Council – University Development Cooperation as an 'Own Initiative' project entitled 'Capacity building in geohazard monitoring in volcanically active areas of South-West Cameroon.

References

Al-Homoud AS, Tal AB, Taqieddin SA (1997) A comparative study of stability methods and mitigative design of a high way embankment landslide with a potential for deep seated sliding. Eng Geol 46:157–173

Casagrande A (1948) Classification and identification of soils. Trans Am Soc Civ Eng 113:901–930

Cernica JN (1995) Geotechnical engineering: soil mechanics. Wiley, USA

Che VB, Kervyn M, Ernst GGJ, Trefois P, Ayonghe S, Jacobs P, Van Ranst E, Suh CE (2011) Systematic documentation of landslide events in Limbe area (Mt Cameroon Volcano, SW Cameroon): geometry, controlling and triggering factors. Nat Hazards. doi:10.1007/s11069-011-9738-3

Fell R (1994) Landslide risk assessment and acceptable risk. Can Geotech J 31:261–272

Hengxing L, Chebghu Z, Lee CF, Sijing W, Faquan W (2003) Rainfall –induced landslide stability analysis in response to transient pore pressure. A case of natural terrain landslide in Hong Kong. Sci China Ser E Technol Sci 46:52–68

Hutchinson JN (1988) General report: morphological and geotechnical parameters of landslides in relation to geology and hydrology. In: Proceedings of 5th international symposium on landslides, vol 1, Balkema, Rotterdam, pp 3–35

Inganga S, Ucakuwun E (2001) Rate of swelling of expansive soils: a critical factor in triggering of landslides and damage to structure. Documenta Naturae 136:93–98

Larsen MC, Simon A (1993) Rainfall-threshold conditions for landslide in a humid–tropical system, Puerto Rico. Geogr Ann 75A(1–2):13–23

Lohnes RA, Fish RO, Demirel T (1971) Geotechnical properties of selected Puerto Rican soils in relation to climate and parent rock. Geol Soc Am Bull 82:2617–2624

Meisina C, Scarabelli S (2007) Acomparative analysis of terrain stability models for predicting shallow landslide in colluvial soils. Geomorphology 87:207–223

Njome MS, Suh CE, Sparks RSJ, Ayonghe SN, Fitton JG (2008) The Mount Cameroon 1959 compound lava flow field: morphology petrology and geochemistry. Swiss J Geosci 101:85–98

Rahman ZA, Hamzah U, Taha R, Ithnain NS, Almad N (2010) Influence of oil contamination on geotechnical properties of basaltic residual soil. Am J Appl Sci 7(7):954–961

Shakoor A, Smithmyer AJ (2005) An analysis of storm-induced landslides in colluvial soils overlying mudrock sequences, south eastern Ohio, USA. Eng Geol 78:257–274

Sidle RC (1984) Shallow groundwater fluctuations in unstable hill slopes of coastal Alaska. Zeitschrift für Gletscherkunde und Glazialgeoleologie 20:79–95

Sidle RC, Pearce AJ, O'loughlin CL (1985) Hill slope stability and land use. American Geophysical Union, Washington, DC, p 125

Suh CE, Sparks RSJ, Fitton JG, Ayonghe SN, Annen C, Nana R, Luckman A (2003) The 1999 and 2000 eruptions of Mount Cameroon: eruption behaviour and petrochemistry of lava. Bull Volcanol 65:267–281

Vaughan PR, Maccarinit M, Mokhtar K (1988) Indexing the engineering properties of residual soil. Quart J Eng Geol 21:69–84

Velbel MA (1985) Geochemical mass balance and weathering rates in forested water sheds of the Southern Blue ridge. Am J Sci 285:904–930

Williams AB, Donaldson GW (1980) Development relating to building on expansive soils in South Africa: 1973–1980. In: Proceedings of the 4th international conference on expansive soils, vol 2, Denver, pp 834–844

Yalcin A (2007) The effect of clay on landslides. Appl Clay Sci 38 (1–2):77–85

Yalcin A (2011) The geotechnical study on the landslides in the Trabzon Province, NE Turkey. Appl Clay Sci 52:11–19

Large Reactivated Earth Flows in the Northern Apennines (Italy): An Overview

Giovanni Bertolini and Chiara Fioroni

Abstract

This paper proposes an overview on ancient earth flows and their reactivation mechanisms. All considerations made herein are the result of direct experience and observation of actual events which have occurred in the Northern Apennines from 1994 to 2006, when many large earth flows reactivated, 17 of which have been studied and monitored by the part of technical surveys of the Emilia-Romagna regional authority. Particular attention has been paid to the analysis of the evolution of landslides, acknowledging a typical, recurring succession of events that precede the failure of the slope. In general, the observation of past events has proved to be an useful mean for understanding which are the conditions and behaviours that usually lead to the reactivation of an ancient landslide body.

Keywords

Landslides • Earth flows • Reactivation • Northern Apennines • Italy

Introduction

From 1994 to 2006 several large, ancient earth flows reactivated in the Northern Apennines causing damages and destruction of villages, hamlets and roads. Many of these landslides were object of studies and interventions by the part of the regional technical services, with the investment of a great amount of public money for investigation, monitoring, reconstruction and consolidation works. In few cases they were the subject of scientific papers and communications in thematic conferences, but the majority remained confined in mere technical papers, internal reports, even simple discussions among experts. The aim of this paper is to collect all these experiences and to draw, in a synthetic way, all the possible elements of knowledge that may be useful in the future to forecast similar scenarios in analogous cases.

All considerations made herein are the result of studies performed by the technical surveys of the Emilia-Romagna regional authority by direct experience and observation of these events. Particular attention has been paid to the survey of field evidences and cinematic indicators observable on the terrain or by means of field instrumentation. Since 20 years, 100 inclinometers have been placed by the administration on tens of these landslide bodies, allowing us to follow closely the transition between dormancy and activity on many of them and often acknowledging a typical, recurring succession of events that precede the new failure of the slope.

Location

The study area (Emilia Apennines) corresponds to the northern flank of the chain, under the administration of the Emilia-Romagna Regional Authority (Fig. 1).

G. Bertolini (✉)
Emilia-Romagna Regional Authority, Po River Basin Technical Survey, Reggio Emilia, Italy
e-mail: gbertolini@regione.emilia-romagna.it

C. Fioroni
Department of Earth Sciences, Modena and Reggio Emilia University, L.go S.Eufemia, 19, Modena 41100, Italy
e-mail: chiara.fioroni@unimore.it

C. Margottini et al. (eds.), *Landslide Science and Practice*, Vol. 4,
DOI 10.1007/978-3-642-31337-0_6,

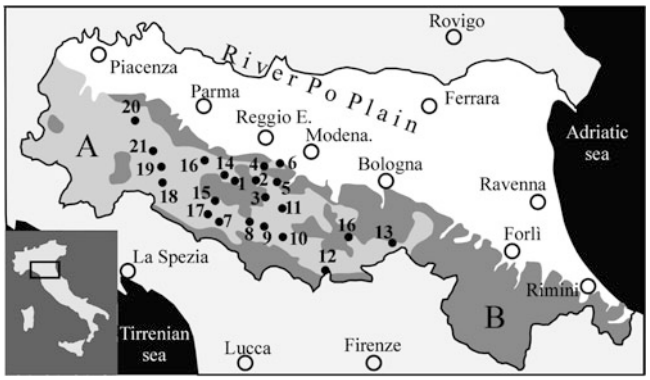

Fig. 1 Location map of the Emilia-Romagna region, with landslides cited in the text and geology sketch. *1* Cavola, *2* Magliatica, *3* Cà Lita, *4* Casoletta¸ *5* S. Romano, *6* Monte Evangelo, *7* Sologno, *8* Morsiano, *9* Boschi di Valoria, *10* Lezza Nuova, *11* Morano, *12* Marano, *13* Cà di Sotto, *14* Lavina di Roncovetro, *15* Groppo, *16* Silla, *17* Cervarezza, *18* Corniglio, *19* Costa di Casaselvatica, *20* Casa Ravera, *21* Case Pennetta. *A Argille Scagliose* prevailing (Emilia sector); *B* Arenites and marls prevailing (Romagna sector)

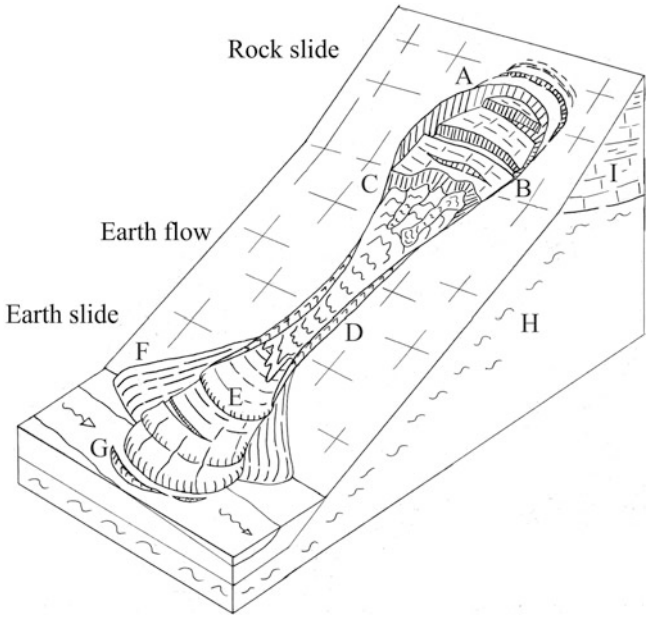

Fig. 2 This sketch summarises, in a simplified way, the main features that are visible in the field. *A* Main scarp, *B* tension cracks and trench, *C* Minor scarp, *D* Lateral levee; *E* Listric imbricate thrust faults cutting the reactivated foot; *F* Portion of the ancient foot that remains inactive, *G* Uplifting of clay breccias as first symptom at the early stage of the foot reactivation, *H Argille Scagliose, I* Helmintoid Flysch. Terminology from Cruden and Varnes, 1996

Geology and Landslide Susceptibility

The Cretaceous *Argille Scagliose* – consisting of tectonic and sedimentary melanges (i.e. "olistostromes")- due to their clay content and bimrock structure, here represent the main source of landslides. As for Helmintoid Flysch (Cretaceous-Eocene in age), despite its well-preserved stratified structure, the high content of shale and clay makes it very susceptible to weathering processes, producing thick colluvial deposits where erosion and landslides easily occur. According to the regional 1:25000 Landslide Susceptibility Map (Bertolini et al. 2002), the *Argille Scagliose*'s Landslide Density Index (ratio between the sum of landslide areas affecting these geological units and their total mapped surface) is varying from 20 % to 40 %. Usually, earth flows originate on the the lower part of the slopes, where *Argille Scagliose* prevail, and gradually migrate upslope, by retrogression (see also Fig. 2), inside the Helmintoid Flysches.

The majority of landslides are concentrated in areas where the slope gradient ranges from 8° to 11°, which is the usual slope angle of *Argille Scagliose* and similar formations, whereas they are very rare in slopes whose gradients exceed 25°, thanks to the presence of a stronger bedrock.

Features of Ancient Earth Flows

In most cases, from plan view, these landslides show a typical "hourglass" shape: a large crown, a relatively narrower middle "channel" – corresponding to the area of flow – and a wide basal fan reaching the valley floor, with a modest or null slope inclination (Figs. 2 and 3). Table 1 summarizes the main landslide characteristics of the earth flows recently reactivated, derived by literature or direct observation. Thanks to their simple morphology, these landslides are easily identifiable through geomorphological analysis. In most cases, the landslide toe protrudes on the main valley floor and interfingers with alluvial sediments and/or forms a sort of wide fluvial meander.

Calculations based on 46 different landslides, whose movements are monitored by 190 inclinometers, show that the majority of them (52 %) reaches a depth ranging from 10 to 30 m and about 12 % of them exceeds 40 m. The depth has seldom reached a magnitude of 80–100 m, as in the Corniglio and in the Cervarezza case.

Their present shape was built along the time and – in consequence – the internal structure is formed by several portions originated at different periods in the past and from different parts of the slope. Thus, the lithology is extremely variable, as it features the different geological units forming the slope, with a prevalence of clay matrix produced by the softening of shaly units.

As for shear strength properties, in very general terms, Φ' shows a range of variability from 20° to 25°, while cohesion peak values, in most cases, are lower than 30 kPa.

Minimum shear strength values are found in argillaceous materials with montmorillonite minerals. In this extreme cases (e.g. the Casoletta landslide) Φ' may range from 6° to 20°, while cohesion values – including peak – are usually less than 20 kPa.

Fig. 3 The Large Morsiano landslide represents at the best the typical features of large earth flows; despite its age (a wood sample found inside it dates back to 13,500 Cal. years BP) the landslide is still active in several portions, threatening and damaging the village; according to historical records, reactivations occurred in 1631 (partial), 1651 (total), 1880 and 1959 (partial). (Photo by G. Bertolini, 2007–2008)

The Reactivation of Ancient Earth Flows

In the majority of the reactivations of ancient earth flows occurred within the 1994–2006 period, a recurring behaviour was evident. In many documented or observed events the movement initiates in the source area, causing a retrogression of the main scarp, which is the most unstable part of the slope. Instability often produces the displacement of a sliding portion of rock, which is rapidly affected by a progressive differentiate subsidence and disjointed by tensional cracks, normal faults and gravitational tranches. A minor scarp forms downslope (Fig. 2) and from there the displaced material approaches the liquid state, thus producing earth flows moving downward as far as the landslide body's mid-section. The undrained surcharge triggers a series of listric and imbricate thrust faults inside the underlying main landslide body. They come to light as steep, curve scarps dipping upslope, whose dip (of the fault plane) becomes shallower with increased depth (Fig. 4a). They are transversely interrupted by long vertical straight-slip fault, directed downslope. This pattern migrates valleyward (Fig. 4b), propagating the progressive failure along the base of the ancient landslide (Fig. 4c), which may entirely reactivate by sliding (Fig. 4d). This sequence of events with many variations and sometimes only partially achieved, was observed in many cases during the 1994–2006 period and was reported in literature in many other cases. The complete reactivation of the entire landslide body was achieved in the cases of Corniglio (both in 1902 and in 1994 events; Larini et al. 2001a); Cà Lita (2002; Borgatti et al. 2005); Costa di Casaselvatica (1994; Larini et al. 2001b); Casa Ravera (1997; Danini et al. 2001); Lavina di Roncovetro (1994; Bertolini and Gorgoni 2001); Casoletta (1995; Bertolini 2001b); Sologno (1996; Bertolini and Sartini 2001); Cà di Sotto (1994; Carboni et al. 2001); Cervarezza (in 1472, 1560, 1697 and partially 1936 events; Bertolini 2010); Lezza Nuova (1998; Leuratti et al. 2007); for other references.

Also other landslides (see Table 1) suffered complete reactivation and their evolution was the object of direct observation and internal reports.

In few cases the multiplication of slip surfaces inside the main landslide body led to a complete disorder of the mass (e.g.: Cà Lita, Lavina di Roncovetro, Cà di Sotto) allowing the waters to easily permeate inside it. Seldom the clay matrix reached the limit of moderate to high plasticity, thus contributing to the appearance of a general flowing movement, as occurred in the Cà Lita case in 2003–2004.

Usually, during the propagation of the progressive failure, the activation of new thrusts downhill triggers the relative deactivation of those uphill, which will be rapidly obliterated by swelling processes and by the arrival of the earth flow from above (Fig. 4).

In general, from the moment it is triggered, the time required for a full reactivation of a landslide can vary between a few days (e.g. Morano) to to a few years (e.g. Corniglio). In the great majority of cases, the movement comes to a stop in a few months.

The Corniglio and Cà Lita cases are an exception: they returned to dormancy, respectively, after about 6 and 4 years of activity. Boschi di Valoria was fully active for 4 years and still shows movements in the source area. Although in absence of quantitative data, we may say that, at the end of the reactivation event, the volume of advancement of the foot is similar to the material displaced from the crown. In this way the limit equilibrium of the landslide is restored. As for the new main scarp, after the reactivation, weathering processes initiate the decaying of the newly exposed rock masses. This process will take several decades to completely develop and to start a new earth flow from the scarp, thus

Table 1 Some characteristics of the cited landslides. For location see Fig. 1. (A) Velocity of superficial earth flows coming from the crown and seldom extended to the mid-lower sector; (B) Velocity of the main earth sliding mass, usually corresponding to the mid-lower sector; Normal block = average value usually measured by benchmarks; **Bold** = peak values; *Italics* = instrumental values (usually inclinometers); (?) = estimated (by direct observation or by morphology). Data of landslides Nr. 3, 4, 9, 10, 12, 13, 14, 15, 16, 18, 19, 20 derive from literature (see text); Nr. 1, 2, 5, 6, 7, 8, 11, 17, 21 from direct observation

	Latest reactivation	Province	Average slope angle(°)	Diff. in altitude (m)	Crown altitude (m.a.l.s)	Max length (m)	Max width (m)	Max depth (m)	Volume (10^6 m^3)	(A) Velocity (mm/s)	(B) Velocity (mm/s)	Reference in Fig. 1
Earth flows completely reactivated in the 1994–2006 period												
Magliatica	2000	RE	7	300	600	2,500	400	33	19			2
Cà Lita	2002	RE	8 ÷ 10	410	640	2,700	1,500	43	42	$4 \cdot 10^{-4}$	~0.1	3
Casoletta	Oct 1995	RE	13	140	360	1,000	150	18	1.0	**0.09**	$2 \cdot 10^{-6}$	4
San Romano	~1995	RE	9	190	380	1,132	130	~8(?)	0.8(?)			5
Monte Evangelo	Oct 2005	RE	16	210	360	1,100	120	~10(?)	1.0(?)			6
Sologno	Feb 1996	RE	10	350	900	2,500	450	40	20	0.01	0.005	7
Boschi di Valoria	Dec 2000	MO	13	815	1,335	3,300	587	~20	13	**~2.7**		9
Lezza Nuova	1998	MO	11	770	1,390	4,000	1,000	50	40	**~0.34**		10
Morano	Feb 1994	MO	7	160	440	1,219	170	~8	0.9		~0.01	11
Marano	Mar 2006	BO	10	128	392	714	135	22	5.3	1.0		12
Cà di Sotto	Jun 1994	BO	11	350	820	1,815	333	28	5	**~8,0**		13
Lavina di Roncovetro	Apr 1994	RE	11 ÷ 17	373	693	2,500	300	18	3	~0.1		14
Groppo	Jan 1996	RE	13	310	780	1,800	250	~24	3.6	0.01	**1.4**	15
Corniglio	Nov 1994	PR	10	600	1,150	3,100	1,120	~80	110	**0.6**	0,27	18
Costa di Casaselvatica	Dec 1994	PR	6 ÷ 18	330	940	610	380	55	24		~0.01	19
Case Ravera	Jan 1997	PR	10	260	650	1,650	500	18	12.6	~0.01		20
Other earth flows cited in the text												
Cavola	Apr 1960	RE	10	514	850	4,600	1,102	~50	115		*0.001*	1
Morsiano		RE	10	510	1,130	2,900	980	>24	~60			8
Cervarezza	2000	RE	12	750	1,250	3,500	1,150	>80(?)	90			17
Case Pennetta		PR	14	400	650	1,700	252	n/a	n/a			21
Silla	Nov 1994	BO	9	360	725	2,300	500	33	7.9	**~0.06**	***1 · 10*$^{-5}$**	16

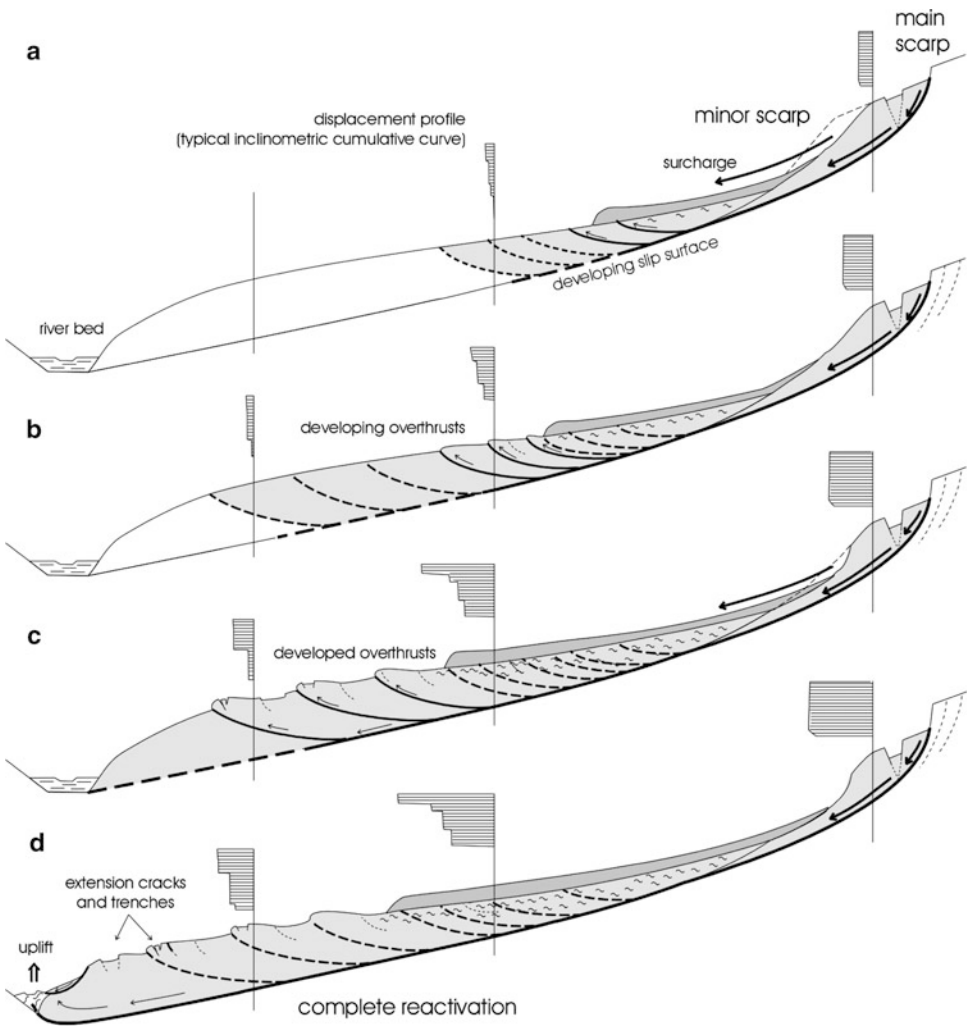

Fig. 4 Reactivation often occurs through a recurring behaviour. This sketch shows the typical time-space evolution of reactivation as observed in several cases (e.g. Corniglio, Boschi di Valoria, Morano, Cà Lita etc.). For details see text From Bertolini 2002, modified

beginning a new cycle of the landslide life. Getting into the details, other recurring features and behaviours may be observed:

- Despite the block-in-matrix internal structure of the landslide, a layer evidently enriched in highly plastic clay (the term "soap layer" seems appropriate) appears on the main shear surfaces, showing a grain-size selection that is clearly shifted towards finer fraction, due to mechanical action and squeezing of clay in confined conditions. This almost impermeable layer, some 1–2 cm thick, helps to retain water inside the landslide. The layer may be evident in the crown area during the movement, while, if exposed to external elements, it is rapidly weathered after a few days.
- According to Skempton (1964) and Calabresi and Scarpelli (1985), this layer shows an "anomalous" natural water content (Wn): In the Casoletta case laboratory tests measured a Wn higher than 30 % with respect to landslide material (Bertolini 2001b).
- Accordingly to Baum et al. (2003), the reduced shear strength of this clay layer "helps to perpetuate movements" on surprisingly gentle slopes.
- Again in accordance with the aforementioned authors, observations of active events demonstrate that even where (and when) landslide material reaches a sufficiently degraded state of consistency as to produce a complete earth flow, the prevailing type of movement nonetheless remains a sliding advancement along the basal and lateral surfaces, which appears notably striated.
- The internal deformation is produced by a multiplicity of pervasive shear surfaces but accounts for a small fraction of the movement; elongated ridges (or "levees" in Baum et al. 2003) tend to form along both flanks of the earth flow, ascribable to alternating rates of movement, with slowing, dilation and relevant accumulation of material, followed by an intensification of movement within a narrower "channel".
- The first symptom of the landslide foot reactivation may be the extrusion of clay breccias along the toe line. If this

Table 2 The three most recent and largest events: Boschi di Valoria, Corniglio and Cà Lita in comparison

	Boschi di Valoria event (2000)	Corniglio event (1994)	Cà Lita event (2002)
Date of reactivation	November 2000	15 November 1994	December 2002
Activity period	2000-Present	Nov. 1994–1999	Dec. 2002–2006
Prevailing mechanism, from the crown to the toe	Roto-translational rock slide/earth flow/translational earth slide	Earth flow/roto - translational earth slide	Roto translational rock slide/earth flow
Total displacements (mid sector/toe)	> 100/~10(?) m	185 m/28 m	430/>330 m
Max thickness	~20 m[a/b]	80 m[b]	43 m[a] ;~30 m[b]
Reactivation cause	Pore pressure – rainfall/snowmelt	Pore pressure – rainfall	Pore pressure – rainfall/ snow melt (2003–2004)
Previous complete Rectivations (as documented in literature)	1951	Sixteenth century, 1612, 1740, 1770, 1902	1928, 1940
Time elapsed between the beginning (crown) and total reactive. (toe)	5 month	15 month	16 month
Annual average precipitation (aap)	1,300 mm	1,500 mm	1,100 mm
Cumulated rainfall prior to the initial reactivation			
30-days	300 mm (23 %)[c]	450 mm (30 %)[c]	120 mm (11 %)[c]
60-days	450 mm (34 %)	750 mm (50 %)	180 mm (16 %)
90-days	490 mm (37 %)	1,450 mm (96 %)	240 mm (21 %)
120-days	525 mm (40 %)	1,500 mm (100 %)	240 mm (21 %)

[a]Source area
[b]Mid-lower sector
[c]Percentage of aap

one is buried by alluvial sediments, the emergence of clay from the middle of the river bed, accompanied by simultaneous uplift of the latter, may occur (Figs 2 and 4). Long protruding clay ridges have been observed in the middle of the stream in almost two cases (Morsiano, Lavina di Roncovetro; Bertolini and Gorgoni 2001). The finely disaggregated cataclasite-like internal structure of this material suggests that these ridges may be a product of squeezing effect from below the advancing foot.

Pattern and Intensity of Displacements

Among the many observed events, in only few cases the movement led to a significant advancement of the toe (e.g.10, 28, 56 and 330 m respectively in the Boschi di Valoria, Corniglio, Cerrè Sologno and Cà Lita cases. In Tables 1 and 2 some examples of velocities, measured by instruments or by benchmarks displacements, are reported. As evident, the scale of deformations and displacement velocities decrease moving from the source sector in the direction of the toe, which, as already stated, is generally the last section of the landslide to reactivate.

In the majority of cases, if the earth flow coming from the main scarp covers hundreds of metres, the deformation of the ancient basal fan is limited to several or tens of metres. The usual maximal velocity is up to few decimetres per day.

On the other hand, a slope with a complex geometry, gradient changes and counter-sloping forms may produce local and temporary variations of the rate of displacement, with sudden accelerations.

Unusual velocities may be caused by the rapid melting of the snow cover (the tip of the Groppo landslide reached the rate of 60 m in 12 h; Bertolini 2001a).

Causes of Reactivation

The usual relationship between precipitation and movement seems inadequate to justify the particular distribution in time and space of these reactivation events, characterised by many almost synchronous events in a wide territory, alternated to long-lasting periods of quiet.

Obviously, prolonged precipitations ("ultimate" and "antecedent" together) play a major role as a triggering factors in reactivating these landslide bodies, "shifting the landslide body from a marginally stable to the unstable state" (definition given by Dai et al. 2002).

On the other hand the preparatory agents -those placing the slope in a marginally stable condition- may be related to a more subtle factor (or mix of factors), whose function is difficult to demonstrate or quantify, like climatic variations, morphology changes and active tectonics.

One thing remains certain: once the activity phase is ended, these landslides reach a sort of equilibrium state, assuring the stability for a long-time (usually decades).

The role of seismic shocks is statistically non-influential and confined to limited areas where strong earthquakes historically occurred (Romagna sector and Reggio Emilia watershed ridge).

Nevertheless, experience suggests that the instability is often prepared, months and years in advance, by the

overburden on the original landslide body, due to the gradual superimposition of new earth flows. Because of that, when the limit equilibrium is reached, few precipitations may produce apparently disproportionate effects.

Alternatively, instability may be facilitated by drag effects on the landslide flanks by other coalescing, moving landslides, as in the Casoletta case. Riverbank erosion on the landslide toe usually generates local instabilities, as in the Morsiano and Morano cases, but is hardly able, alone, to trigger the reactivation of the above landside.

In conclusion, as the Cà Lita earth flow demonstrates (see Table 2), exceptional levels of precipitation are not always necessary to trigger reactivation if the landslide body is already in condition of limit equilibrium, due to the progressive accumulation of material in the mid to upper sector.

Monitoring and Stabilization Measures

During the last 25 years, many landslide bodies were monitored by regional services by means of manual inclinometers, ground-water gauges and, less frequently, by more sophisticated unmanned gauges as robotic total stations, wire extensometers and GPS antennas with tele-transmission of data via GSM (e.g. Casoletta, Corniglio, Poviglio, Boschi di Valoria).

The number of monitored landslides has now increased to about a 100. The total amount of inclinometers in Emilia-Romagna may now be quantified in the order of several hundreds. Both monitoring and stabilisation measures are performed almost always by regional services. The strategy of stabilisation of reactivated earth flow has deeply changed during the last 10 years, shifting from traditional drainage systems (e.g. drainage trenches dug up to a depth of 12 m in the case of Corniglio), to retaining structures (e.g. concrete walls sustained by large-diameter foundation piles and reinforced by sub-horizontal anchors) coupled with nets of deep large-diameter drainage wells (e.g. Cà Lita).

Usually, these costly works are performed in the source area, from where the reactivation often starts. They can be carried out only when the landslide body has lost the great part of its energy and displacements are residual. In the "Boschi di Valoria" case, in order to restore the functionality of a provincial road, bridging was considered to be the most suitable solution.

Final Remarks

Experience teaches us that the instability is often prepared, months and years in advance, by the overburden on the original landslide body, due to the gradual superimposition of new earth flows.

Exceptional levels of precipitation are not always necessary to trigger reactivation if the landslide body is already in condition of limit equilibrium, due to the progressive accumulation of material in the mid-upper sector. In fact, when the limit equilibrium is reached, few precipitations may produce apparently disproportionate effects.

In general, the observation of past events has proved to be an useful mean for understanding which are the conditions and behaviours that usually lead to the reactivation of an ancient landslide body. This knowledge plays a fundamental role in all the activities aimed to the management of risk, like territorial planning, the strategies for the assessment of their dangerousness, the implementation of preventive or after-event consolidation works. Above all, the main usefulness of this experience is its contribution to the scenario predictability of future events.

References

Baum RL, Savage WS, Wasowski J (2003) Mechanics of earth flows. In: Proceedings of the international conference FLOWS 2003, Sorrento

Bertolini G (2010) Large earth flows in Emilia-Romagna (Northern Apennines, Italy): origin, reactivation and possible hazard assessment strategies. Zeitschrift der Deutschen Gesellschaft fur Geowissenschaften 161(2):139–162. doi:10.1127/1860-1804/2010/0161-0139, Stuttgart

Bertolini G, Gorgoni C (2001) La lavina di Roncovetro (Vedriano, Comune di Canossa, Provincia di Reggio Emilia). Quad Geol Appl 8(2):1–23, Bologna (Pitagora)

Bertolini G, Sartini G (2001) La Frana del Rio di Sologno: l'evento del febbraio 1996 e il rinvenimento dell'Albero di Sologno" (Comune di Villaminozzo, Provincia di Reggio Emilia). Quad Geol Appl 8(2):23–31, Bologna (Pitagora)

Bertolini G, Canuti P, Casagli N, De Nardo MT, Egidi D, Mainetti M, Pignone R, Pizziolo M (2002) Landslide Susceptibility Map of the Emilia-Romagna Region, Italy (1:25.000). SystemCart, Rome

Borgatti L, Corsini A, Barbieri M, Sartini G, Truffelli G, Caputo G, Pugliesi C (2005) Large reactivated landslides in weak rock masses: a case study from the Northern Apennines (Italy). Landslides 3(2):115–124. doi:10.1007/s10346-005-0033-9

Bertolini G (2001a) La Frana di Groppo (Comune di Vetto, Provincia di Reggio Emilia). Quad Geol Appl 8(1):183–195, Bologna (Pitagora)

Bertolini G (2001b) Modalità di riattivazione, interventi, caratteri geotecnici e mineralogici di una frana di argilla a struttura caotica ("Argille Scagliose" Auctt): la frana di Casoletta (Comune di Vezzano, Provincia di Reggio Emilia). Quad Geol Appl 8(1): 163–183, Bologna (Pitagora)

Calabresi G, Scarpelli G (1985) Argille sovraconsolidate e fessurate: fenomeni franosi. Geol Appl Idrogeol 20(2):93–126

Cruden DM, Varnes DJ (1996) Landslide types and processes. In: Turner AK, Shuster RL (eds) Landslides: investigation and mitigation. Transportation Research Board, National Research Council, Special Report 247, National Academy Press, Washington, DC, pp 36–75

Carboni R, Casagli N, Iotti A, Monti L, Tarchiani U (2001) La frana di Cà di Sotto (San Benedetto Val di Sambro, Bologna): caratteri geomorfologici, analisi geotecniche ed interventi di mitigazione del rischio. Quad Geol Appl, 8(1):93–104, Bologna (Pitagora)

Dai FC, Lee CF, Nhai YY (2002) Landslide risk assessment and management: an overview. Eng Geol 64:65–87

Danini S, Larini G, Malaguti C (2001) La frana di Casa Ravera (Comune di Pellegrino Parmense, Provincia di Parma). Quad Geol Appl 8(2):45–59, Bologna (Pitagora)

Larini G, Malaguti C, Pellegrini M, Tellini C (2001a) "La Lama" di Corniglio (Appennino Parmense), riattivata negli anni 1994–1999. Quad Geol Appl 8(2):59–114, Bologna (Pitagora)

Larini G, Malaguti C, Tellini C (2001b) La frana di Costa di Casaselvatica (Comune di Berceto, Provincia di Parma). Quad Geol Appl, 8(2):31–44, Bologna (Pitagora)

Leuratti E, Lucente CC, Medda E, Manzi V, Corsini A, Tosatti G, Ronchetti F, Guerra M (2007) Primi interventi di consolidamento sulle frane dei Boschi di Valoria, di Tolara e Lezza Nuova (Val Dolo e Val Dragone, Appennino modenese). Giornale di Geologia Applicata (AIGAA) 7:17–30. doi:10.1474/GGA.2007-07.0-02.0183

Skempton AW (1964) Long-term stability of clay slopes. Geotechnique 14(2):75–101

The Impact of Climatic Changes on the Behaviour of Active Landslides in Clay

Luca Comegna, Paolo Tommasi, Luciano Picarelli, Edoardo Bucchignani, and Paola Mercogliano

Abstract

Forecasting the effects of forthcoming climate changes on natural hazards is a new frontier of the research. The problem is crucial for landslide hazard but available data are still doubtful, thus only some hypotheses can be drawn. The paper examines the potential effects of climate during next 50 years on two active landslides in clay. Considerations are based on data regarding local rainfall history, available climatic scenarios, monitoring and results of simple geotechnical analyses.

Keywords

Active landslide • Clay • Climate change • Scenario

Foreword

Significant parts of the Italian territory are covered by fine-grained deposits subject to slow active translational movements which interact with urban settlements, infrastructures and lifelines. Pore pressure fluctuations govern the shear stress level and the displacement rate. The risk is generally low, but long-term cumulative displacements often damage man made works reducing performance or compromising serviceability (Picarelli and Russo 2004; Mansour et al. 2011). This is a major concern for whoever is called to face such a challenge and establish programmes for societal adaption and land management.

L. Comegna (✉) • L. Picarelli
Dipartimento di Ingegneria Civile, Seconda Università di Napoli, Aversa, Italy

Analisi e Monitoraggio del Rischio Ambientale (AMRA), Naples, Italy
e-mail: luca.comegna@unina2.it

P. Tommasi
Consiglio Nazionale delle Ricerche, Istituto di Geologia Ambientale e Geoingegneria, Rome, Italy

E. Bucchignani • P. Mercogliano
Impacts On Ground And Coast (ISC) Division, Euro Mediterranean Centre For Climate Changes (CMCC), Lecce, Italy

Meteo System and Instrumentation Laboratory, Italian Aerospace Research Center (CIRA), Capua (CE), Italy

The Influence of Weather on Slope Movement

Since slow active slides in clay are generally translational, the overall state of stress does not significantly change during movement. Periodical accelerations are due to the fluctuation of pore pressures, that affect the stress level at the base of the slide and in turn the operational shear strength. In general, movements are slow since the stress–strain behaviour of the slip surface is ductile and any acceleration due to even unusual pore pressures increases is balanced by the consequent increase in the shear strength due to soil viscosity (Ledesma et al. 2009). Even though this consideration is not completely supported by laboratory tests, that sometimes provide contradictory results (Kenney 1967; Skempton 1985), a clear link between pore pressure regime, operative shear strength of the soil and movement acceleration is definitely shown by monitoring data (Bertini et al. 1984; Picarelli et al. 1999). This link encourages the prediction of slope movements once a relationship between pore pressure and meteorological parameters has been established. In fact, pore pressure change depends on change in infiltrating water, which in turn is a complex function of hydraulic soil

C. Margottini et al. (eds.), *Landslide Science and Practice*, Vol. 4,
DOI 10.1007/978-3-642-31337-0_7,

properties and of duration and intensity of precipitations, air humidity/temperature, wind speed, radiation and transpiration for vegetated soils. All these factors are modified by long-term climatic changes whose influence on the hydrological response and the stability of sloping lands can be quantitatively estimated on the basis of geotechnical analysis coupled to climatic scenarios (Schiano et al. 2009).

Climate Scenarios in Italy in the Next Century

A large amount of data coming from different sources suggest that the Earth is being subjected to climatic changes whose magnitude and distribution are not yet completely clear. However, the present knowledge enables to depict credible scenarios. In order to forecast the effects of such changes on landslide hazard, analysis of local conditions is mandatory especially in areas having a topography that is so complex as to strongly affects regional and local climate. For this purpose Regional Climate Models (RCM) can be adopted, such as the COSMO-CLM (Rockel et al. 2008) which provides high-resolution climate change projections on a spatial scale of about 10 km. Conversely, Global Climate Models (GCM) are unsuitable due to their poor resolution (generally coarser than 100 km).

Figure 1 reports some results of a simulation over the Italian peninsula for the period 1965–2100 employing the IPCC-A1B emission scenario and the boundary conditions provided by the global climate model CMCC-MED (Scoccimarro et al. 2010). The model precipitation has been validated over the period 1971–2000 (Bucchignani et al. 2011) through a comparison with the Climate Research Unit (CRU) data set (Mitchell and Jones 2005).

Based on such simulations, by the end of the twenty-first century precipitations should decrease over the entire peninsula; only in Alps they should slightly increase. However, some data seem to indicate that the decrease in the number of rainy days should be accompanied with an increase in the intensity of single storms. According to the same simulation, the temperature growth should be 2–3° degrees during fall and winter; similar increments should occur also in spring and summer in the Alpine area.

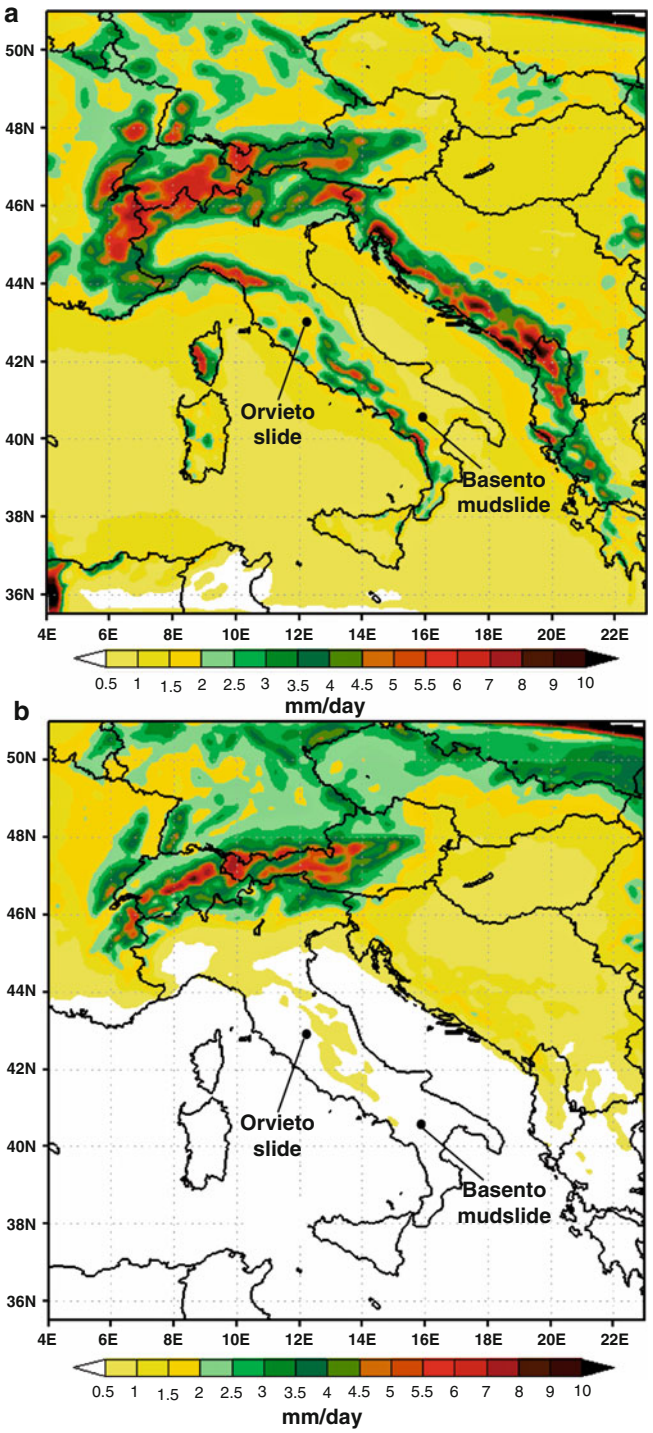

Fig. 1 Averaged total precipitation distribution in winter (**a**) and summer (**b**) over the time period 2071–2100

Two Case Studies of Landslides in Clay

Two cases of slow slope movements have been considered: (1) a slide involving the overconsolidated Orvieto clays (Central Italy) and (2) a mudslide in tectonized clay shales outcropping in the Basento valley (Southern Italy) (Fig. 1). The approaches adopted for the assessment of their future behaviour are fairly different, thus the two cases are examined separately.

The Orvieto Slide

Orvieto is a medieval town located 105 km North to Rome, on top of a 50 m thick tuff slab (Fig. 2) overlying an overconsolidated clay formation. Landslides on the clay slope are documented since historical times (Manfredini et al. 1980); the largest involved the northern slope of the

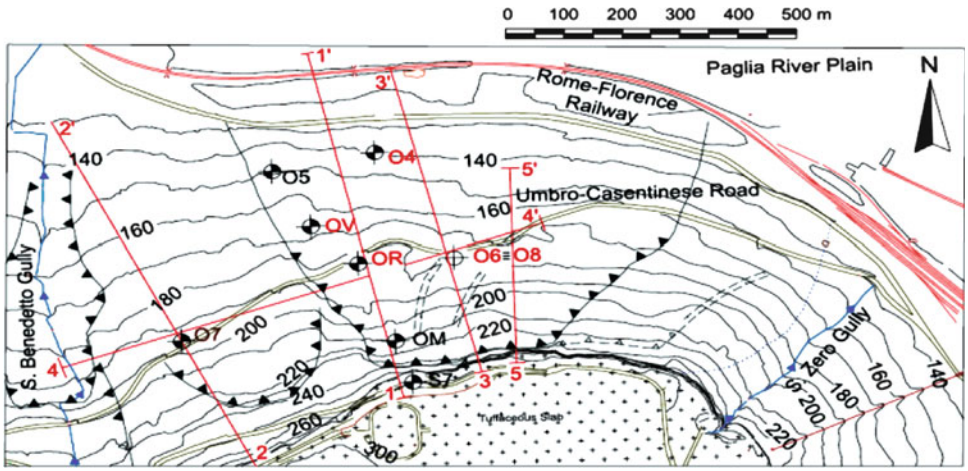

Fig. 2 Northern side of the Orvieto hill (Tommasi et al. 2006)

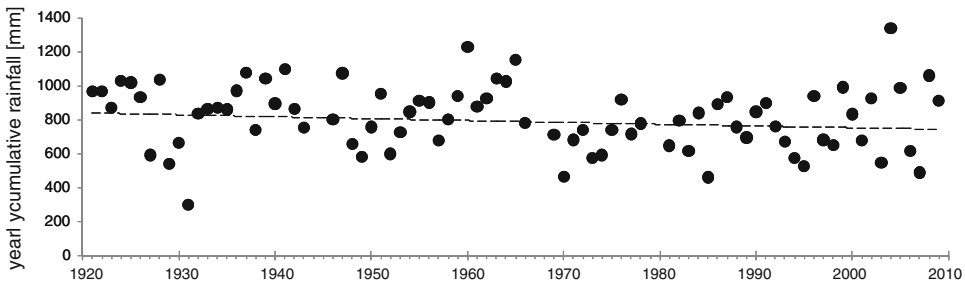

Fig. 3 Yearly cumulative rainfall in Orvieto

hill, dipping at 11.5° for a length of 550 m long. A slide debris blanket up to 17.5 m deep, consisting of volcanic materials and remoulded clay, overlies the clay formation, which is fissured and softened at the top (down to a maximum depth of 27.5 m) whereas is stiff and intact at depth. The fine-grained component of the uppermost debris is a medium-plasticity clay (CF = 56 %; w_L = 53 %). Similar properties characterize the underlying softened and stiff clays (CF = 50 %; w_L = 50 %). The hydraulic conductivity of these materials, measured through in situ falling head tests, decreases with depth: its average value passes from about 10^{-9} m/s in the debris and decreases to 10^{-10} m/s in the softened clay and to 10^{-11} in stiff clay.

Daily rainfall data are available since 1921 thanks to a rainfall gauge installed by the State Hydrographic Survey on top of the hill. A number of Casagrande piezometers and inclinometer tubes have been installed since 1982 in the slope (Tommasi et al. 2006). Precipitations are mainly concentrated in November and usually display a further increase in February. The dry season lasts from the second half of June to the first half of August. The general trend of yearly cumulative rainfalls in the last century presents a clear decrease in the order of about 1.3 % per decade (Fig. 3): its average value was 884 mm in the Twenties of previous century dropping to 839 mm in the last decade.

The fluctuation of piezometer levels in the debris usually ranges between 2 and 4 m. The highest level is generally attained between January and March, while the lowest one is reached in September. Pore pressure changes are delayed with respect to precipitations: a good correlation has been found between pore pressures and rainfall accumulated over 2 months (Tommasi et al. 2006). Fluctuations of water levels in the softened and stiff clay are smaller, respectively in the order of 1 and 0.5 m. They correlate quite well with rainfall accumulated over 3 months. This means that influence of single rainstorms on groundwater levels is negligible when compared to that of rainfalls accumulated over long time intervals.

The shallow slides on the northern slope of the hill involve only the debris cover and display an average displacement rate of 10–60 mm/year and more than one acceleration phase. The deep slides occur along sliding surfaces located in the softened clay layer, at an average displacement rate of 1–6 mm/year with only one acceleration phase per year.

The influence of weather on the groundwater regime has been investigated through simple numerical simulations on an active slide located on the northern slope, used as reference case (Fig. 4). Its sliding surface is located at a depth of 18 m, at the contact between the softened and the stiff clay (inclinometer O7, Fig. 4). The inclinometer is coupled to a borehole equipped with three Casagrande cells, two of which are placed at depths of 6 and 15 m, within the debris and the softened clay respectively, which were read monthly between May 1998 and June 2000.

The analyses were performed under 2D flow conditions through the SEEP/W FEM code (Krahn 2004).

The following hydraulic boundary conditions have been adopted: ingress flow at the ground surface governed by the

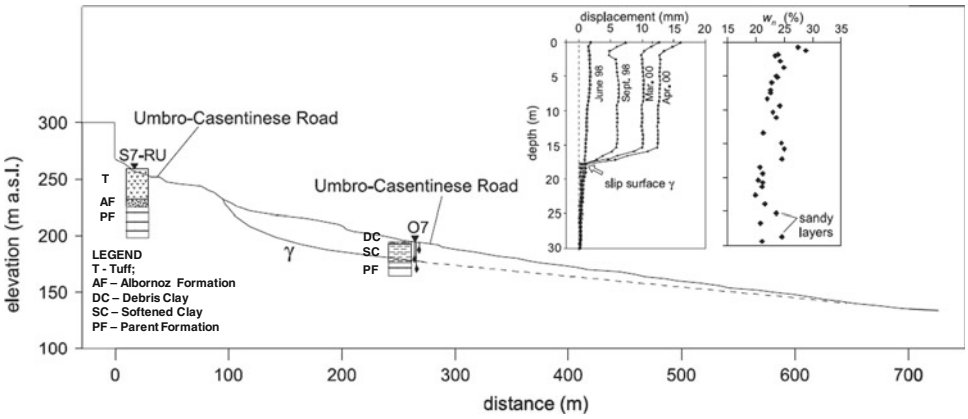

Fig. 4 The investigated slide (section 2-2' in Fig. 2) (Tommasi et al. 2006)

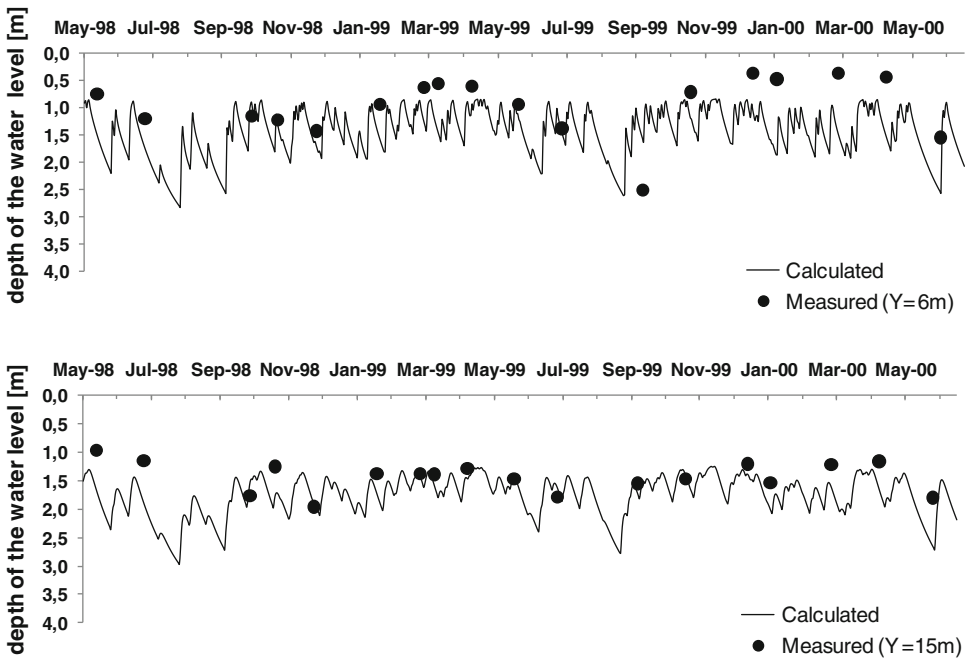

Fig. 5 Orvieto slide: calculated and measured piezometric levels at depths 6 and 15 m (borehole O7)

rainfall history; constant zero pore pressure at the tuff-clay contact; impervious surface along the top the parent formation (stiff clay); impervious vertical upslope lateral boundary; hydrostatic pore pressure distribution along the vertical downslope lateral boundary. The soil has been characterised by constant saturated hydraulic conductivity, $k_{w,s}$, and volumetric compressibility, $m_{w,s}$: the best matching between calculated and measured piezometric levels (Fig. 5) has been obtained putting $k_{w,s} = 10^{-7}$ m/s for the clay debris and 10^{-8} m/s for the softened clay; $m_{w,s} = 10^{-5}$ m^2/kN has been adopted for both soils. Adopted hydraulic conductivities are two orders of magnitude higher than the measured values, suggesting that the actual hydraulic behaviour of the soil is governed by sets of fissures and joints. Their contribution is not captured in the laboratory and is underestimated by the piezometer tests due to their prevailing vertical extension.

Based on such data, the following empirical function has been adopted to relate the displacement rate along the slip surface, v, and the difference, $\tau - \tau_0$, between the driving shear stress and the shear strength along the slip surface (Vulliet 1986)

$$v = \frac{A}{\left(\frac{\tau}{\tau - \tau_0}\right)^x} \tag{1}$$

In such a relationship, A and x are material parameters. Being the denominator directly related to the depth of the water level, h, the following simplest power law has been adopted:

$$v = \frac{a}{h^b} \tag{2}$$

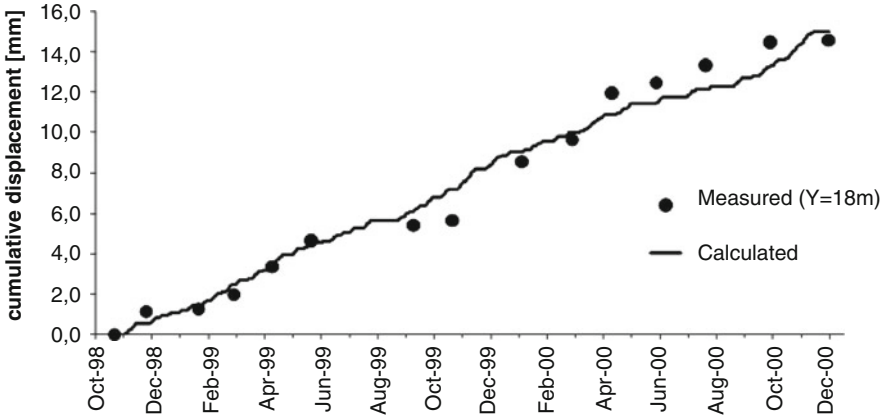

Fig. 6 Orvieto slide: calculated and measured displacement along the 18 m deep sliding surface (inclinometer O7)

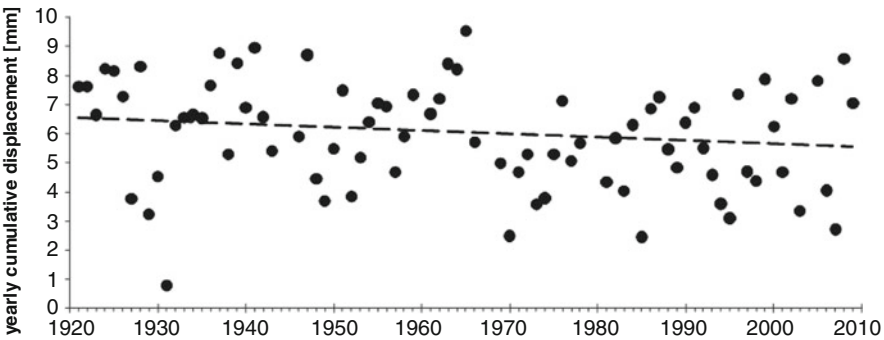

Fig. 7 Orvieto slide: estimated yearly displacement since 1921

The displacement rate has been expressed in mm/day and the depth of the water level in metres. The empirical material parameters have been obtained after a calibration of the expression (2) for the period October 1998 – December 2000 (Foglia 2011). The best correlation (Fig. 6) has been obtained using $a = 0.078$ mm/day and $b = 1$ and 10 respectively, for groundwater rising and lowering. Such a result suggests a hysteretic slope response which was observed in similar cases (Bertini et al. 1984).

Based on such a correlation, the pore pressure regime was estimated for the entire period covered by daily rainfall data (i.e. since 1921 today) imposing on the ground surface the measured daily rainfalls. Then, the displacement rate was estimated introducing in (2) the calculated water levels, h, for the section where the borehole O7 is located (Fig. 7): the velocity of the landslide shows a decreasing trend of about 0.11 mm/decade per decade. Imposing the present trend of the yearly cumulative rainfall over the next 50 years, the future cumulative displacement can be evaluated in about 26 cm.

The Basento Mudslide

The Basento valley mudslide involves highly fissured clay shales, which extensively outcrop in the Southern Apennines chain. Mudslides are the most usual landslide type in these deposits. The very first phase of these movements is generally characterised by sliding, but this soon turns into a flow-like style. In this phase the landslide can reach a peak velocity in the order of metres per hour (Picarelli et al. 2005). Then the velocity progressively decreases, dropping in some months to metres per year. The very last phase of movement is once again characterised by a slide style with displacement rates of centimetres per year, unless a reactivation occurs due to renewed alimentation from the main scarp.

The investigated mudslide is located on the right bank of the river (Fig. 8) within a corridor characterised by a number of relict, quiescent and active mudslides. Its length and average slope are respectively 1,100 m and 10° (Di Maio et al. 2010). The accumulation zone is located in the alluvial plain. The subsoil consists of a very thick deposit of highly fissured clay shales covered by a thin top soil. Clay shales present a clay fraction very close to 50 % and a liquidity limit in the range 60 ÷ 80 %. The residual friction angle is 10°.

Two weather stations are located respectively at 4 and 5 km from the site. Available data include daily rainfall readings since 1916, maximum, minimum and average daily temperature since 1924 and air temperature and humidity measured every 20 min, since 2005. The mudslide is instrumented with some Casagrande piezometers and inclinometer tubes (Vassallo and Di Maio 2008).

As in the Orvieto site, more than 60 % of the total yearly precipitation falls during autumn and winter. The peak

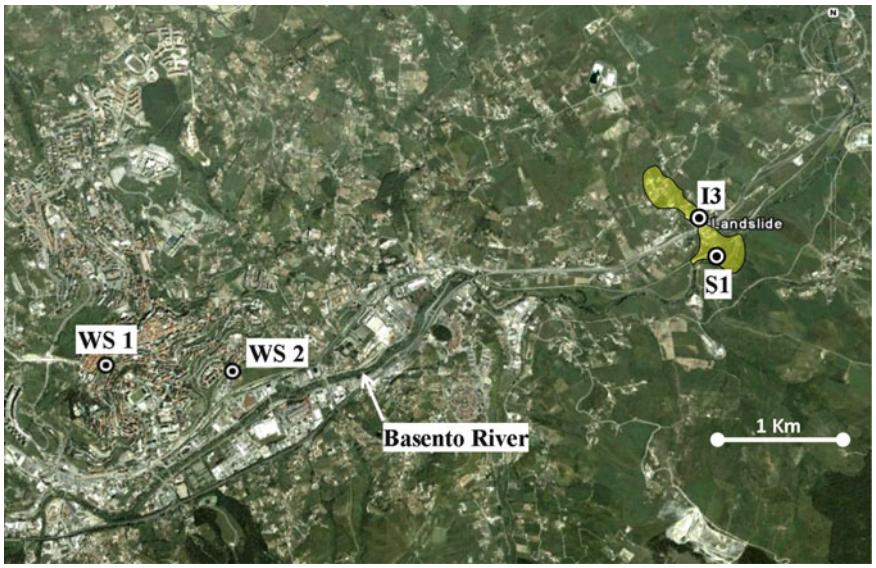

Fig. 8 The Basento mudslide

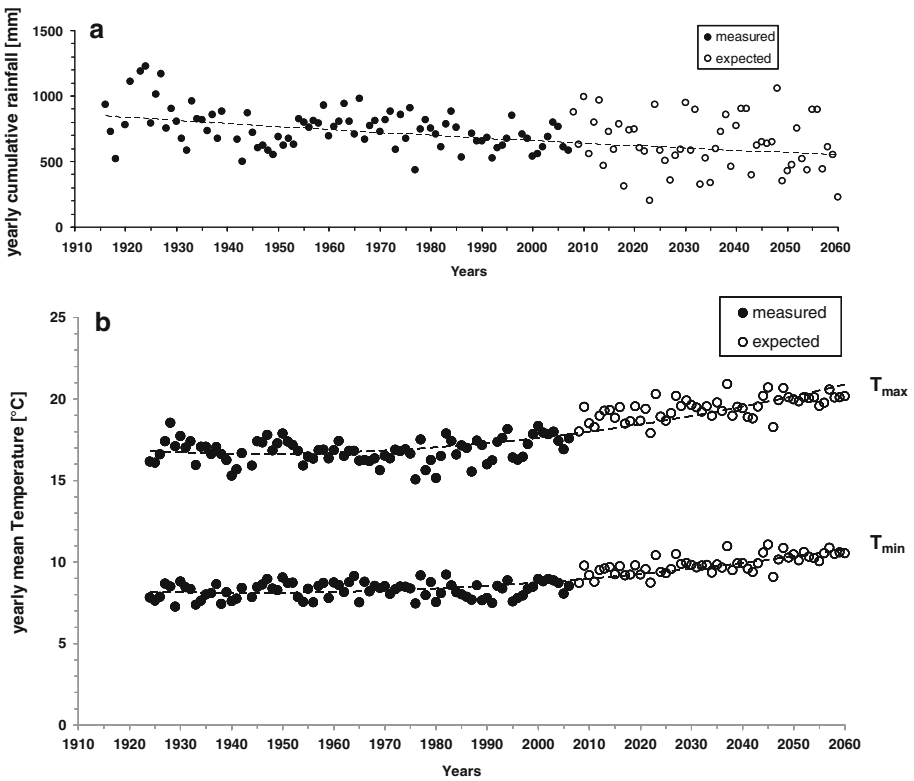

Fig. 9 Measured and expected yearly cumulative rainfall (**a**) and (**b**) average temperature in the Basento valley (Comegna et al. 2012)

temperature can exceed 30 °C during summer, dropping below 0 °C in winter. The minimum daily relative humidity, RH, is around 40 %, while the maximum value trespasses 90 %. Figure 9 reports the yearly rainfall and maximum and minimum temperature since 1921; it includes expected values until 2060 based on COSMO-CLM. A decrease in cumulative rainfall and an increase in temperature in the last century are evident; climatic scenarios forecast an even steeper gradient of temperature in the next years.

Readings at piezometer S1, located at the depth of 15 m (Fig. 8), show that pore pressure fluctuations trespass 10 m at depth of 15 m and are generally less than 1 m at depth of 34 m. The displacement rate at depth of 10 m (inclinometer I3) is quite constantly around 20 mm/year, and is governed by cumulative rainfall over a time interval of about 3 months (Di Rosario 2008). Once again pore pressures are scarcely affected by single rainfall events. The mobilised shear strength is close to residual. In this case the analysis of the groundwater regime has been carried out accounting for both infiltration during wet periods and evaporation (driven by external temperature and humidity) during dry periods. The analysis has been carried out through the VADOSE/W FEM

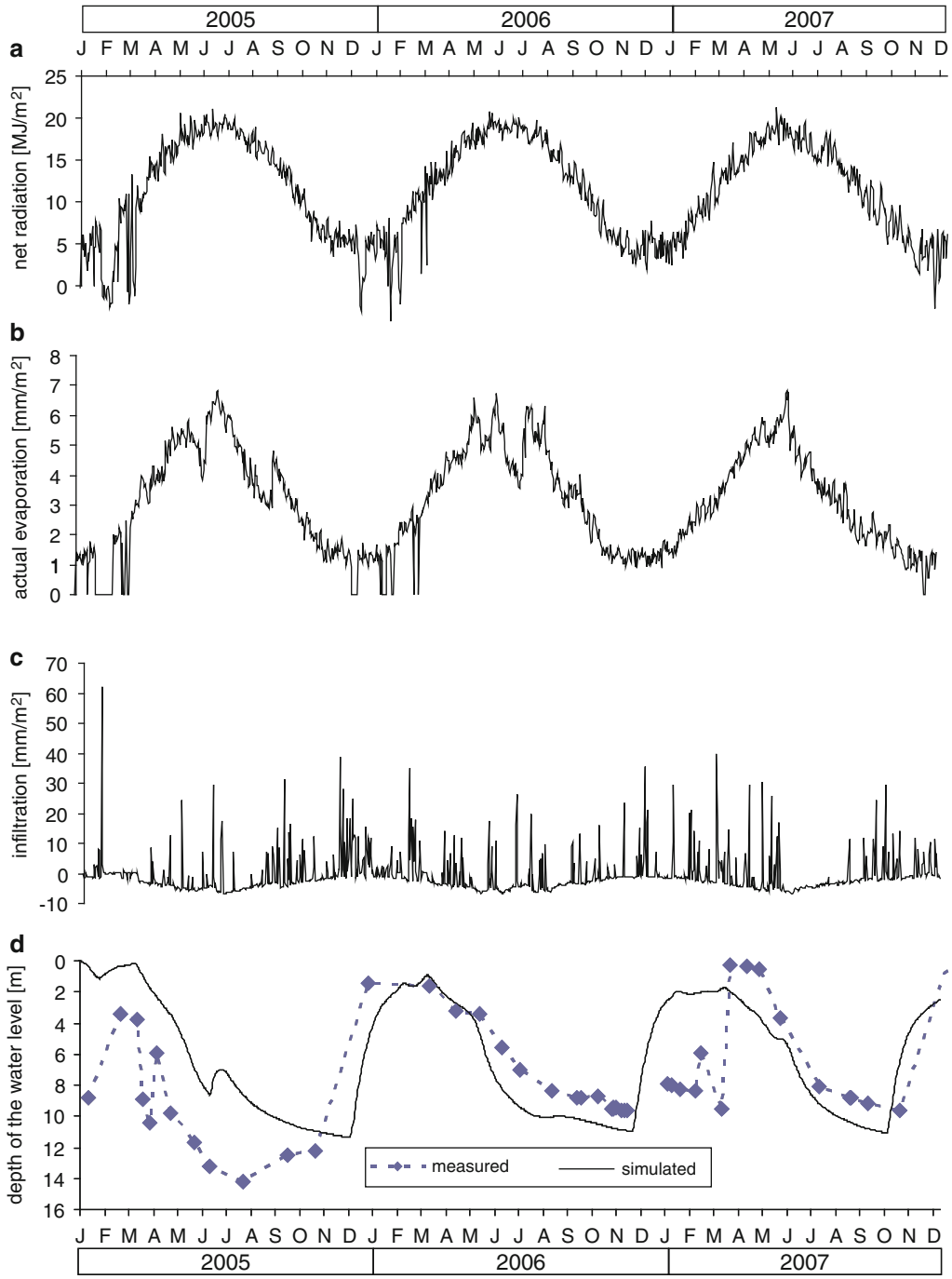

Fig. 10 Basento mudslide: net radiation (**a**), evaporation (**b**) and amount of infiltration (**c**) calculated at the ground surface; (**d**) computed and measured piezometric level at depth of 15 m (Comegna et al. 2012)

code (Krahn 2004). Transpiration has been neglected due to absence of a significant vegetative cover. In order to reduce computational time without significantly changing the seepage pattern in the slope, 1D flow conditions have been adopted. A 1 m thick top soil resting on semi-infinite clay deposit has been considered. The variation of permeability with matric suction, $u_a - u_w$, was introduced through the Mualem's expression (1976) adopting the saturated permeability obtained by field tests (Di Rosario 2008). Comegna et al. (2012) discuss the procedures adopted in the analysis that led to the best fitting between calculated and measured piezometric levels at S1 piezometer (15 m deep). The results of the calibration, which covered the time interval 2005–2007, are reported in Fig. 10. This compares measured and calculated values of the water level.

Once again, the expression (2) has been used to calculate the displacement rate. In this case, a is equal to 0.01 mm/day and b is equal to 0.2 and 0.62 for the phases of groundwater

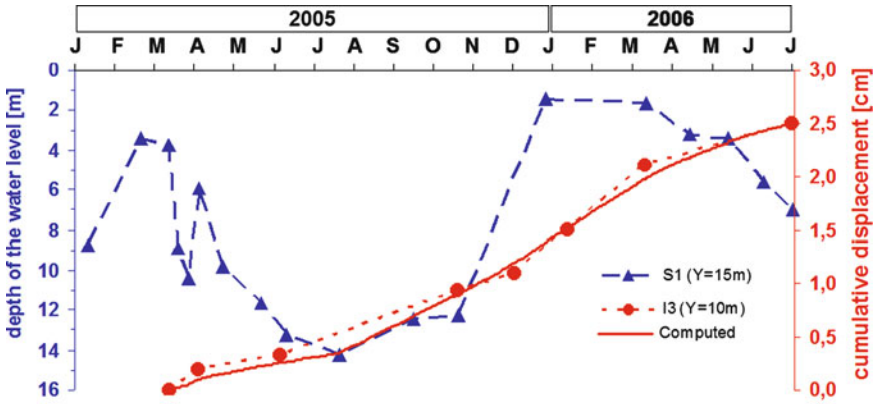

Fig. 11 Basento mudslide: calibration of the water level-cumulative displacement relationship (Comegna et al. 2012)

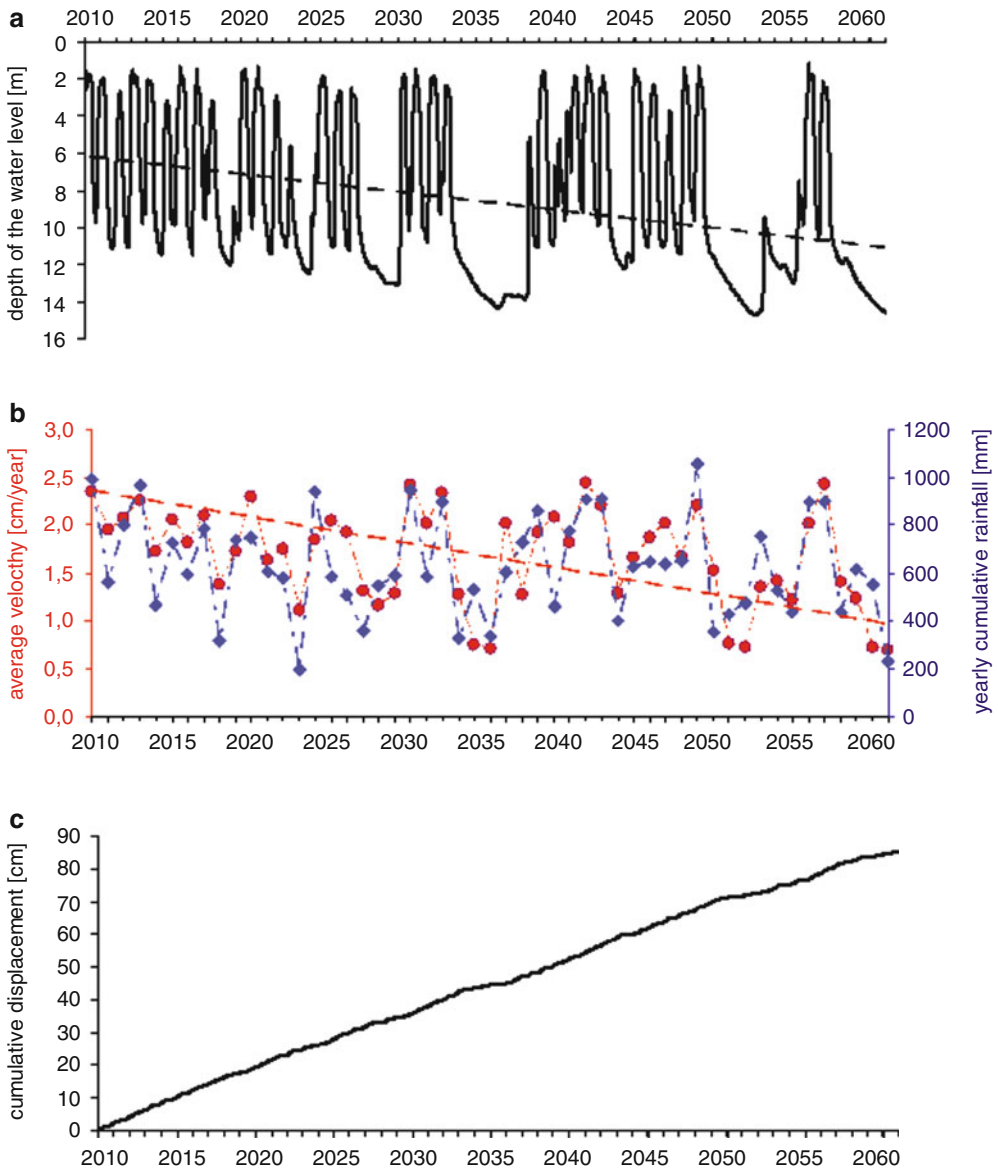

Fig. 12 Basento mudslide: effects of climatic scenarios for the time interval 2010–2060 on yearly average water levels (**a**) cumulative rainfall and rate of movement (**b**) and cumulative displacement (**c**) (Comegna et al. 2012)

rising and lowering respectively (Fig. 11). Further analyses allowed to assess the influence of the distribution over the year of the assumed total rainfall value. The following cases were considered (Comegna et al. 2012): (a) 70 % of the total yearly rainfall concentrated in the first half year; (b) 70 % of the rainfall concentrated in the second half; (c) the average distribution in the century. The analysis shows no remarkable differences in the annual trend of calculated pore pressures. The range of displacements in the next 50 years has been calculated using the 1920 and 2004 pluviometric distributions: the first one corresponds to case (b) while the second one more or less corresponds to case (c).

Figure 12 reports the scenario of water levels, rates of displacement and cumulative movement assuming the annual rainfall distribution as in 2004 (case c). Due to the expected climate changes (increase in temperature and decrease in precipitations with practically constant relative humidity), the future piezometric levels should present a slow progressive reduction in the order of 8 mm per decade (Fig. 12a). Combining pore pressures and mudslide velocity, the future displacement rate should decrease of 3 mm/decade per decade (Fig. 12b). The cumulative displacement from 2010 to 2060 should attain a value of 86 cm (Fig. 12c).

Conclusions

In principle, the consequences on landslide activity of the weather conditions associated with climate changes should not be uniform, depending on properties of soil/rock masses. In particular, the interaction between expected rainfalls and global hydraulic conductivity of the subsoil should play a significant role: in spite of potential increasing intensity of single rainstorms, it should imply a decrease in the displacement rate of slow-moving slides in clay, at least in the Apennines context. This paper provides a contribution based on data from monitoring of two active landslides, on extrapolation to future of recorded precipitations in the last century or on available climatic scenarios and on geotechnical analyses.

Acknowledgments Present work is being carried with the support of the project SafeLand under Grant Agreement No. 226479 in the 7th Framework Programme of the European Commission.

References

Bertini T, Cugusi F, Esu F, Rossi-Doria M (1984) Climatic conditions and slow movements of colluvial covers in Central Italy. In: Proceedings of the 4th ISL, vol 1, Toronto, pp 367–376

Bucchignani E, Sanna A, Gualdi S, Castellari S, Schiano P (2011) Simulation of the climate of the XX century in the Alpine space. Nat Hazards. doi:10.1007/s11069-011-9883-8

Comegna L, Picarelli L, Bucchignani E., Mercogliano P (2012) Potential effects of incoming climatic changes on the behaviour of slow active landslides in clay. Landslides, published online 14 June 2012, doi:10.1007/s10346-012-0339-3

Di Maio C, Vassallo R, Vallario M, Pascale S, Sdao F (2010) Structure and kinematics of a landslide in a complex clayey formation of the Italian Southern Apennines. Eng Geol 116:311–322

Di Rosario F (2008) Comportamento di grandi frane in argilla. Ph.D. thesis, Università degli Studi di Roma La Sapienza, Italy

Foglia C (2011) Effetti del regime pluviometrico sui movimenti di un versante nel Comune di Orvieto. MS thesis, Seconda Università di Napoli, Aversa

Kenney TC (1967) The influence of mineral composition on the residual strength of natural soils. In: Proceedings of the geotechnical conference, vol 1, Oslo, pp 123–129

Krahn J (2004) Vadose zone modeling with VADOSE /W – an engineering methodology. GEO-SLOPE International Ltd., Calgary

Ledesma A, Corominas J, Gonzales DA, Ferrari A (2009) Modelling slow moving landslide controlled by rainfall. In: Picarelli L, Tommasi P, Urciuoli G, Versace P (eds) Proceedings of the 1st IWL rainfall-induced landslides: mechanisms, monitoring techniques and nowcasting models for early warning systems, Naples, 8–10 June 2009, vol 1, pp 196–205

Manfredini M, Martinetti S, Ribacchi R, Sciotti M (1980) Problemi di stabilità della rupe di Orvieto. In: Proceedings of the XIV Covegno Nazionale di Geotecnica, vol 1, Firenze, 28–31 Oct 1980, pp 231–246

Mansour MF, Morgenstern NR, Martin DD (2011) Expected damage from displacement of slow-moving slides. Landslides 8(1):117–132

Mitchell TD, Jones PD (2005) An improved method of constructing a database of monthly climate observations and associated high-resolution grids. Int J Climatol 25:693–712

Mualem Y (1976) A new model predicting the hydraulic conductivity of unsaturated porous media. Water Resour Res 12:513–522

Picarelli L, Russo C (2004) Mechanics of slow active landslides and interaction with man-made works. In: Proceedings of 9th international symposium on landslides, vol 2, Rio de Janeiro, 28 June – 2 July 2004, pp 1141–1176

Picarelli L, Russo C, Mandolini A (1999) Long-term movements of an earthflow in tectonised clay shales. In: Proceedings of the international symposium on slope stability engineering, vol 2, Matsuyama, pp 1151–1158

Picarelli L, Urciuoli G, Ramondini M, Comegna L (2005) Main features of mudslides in tectonized highly fissured clay shales. Landslides 2(1):15–30

Picarelli L, Tommasi P, Urciuoli G, Versace P (eds) (2009) Proceedings of the 1st IWL Rainfall-Induced Landslides: mechanisms, monitoring techniques and nowcasting models for early warning systems. Naples, 8–10 June 2009

Rockel B, Will A, Hense A (2008) The regional climate model COSMO-CLM (CCLM). Meteorologische Zeitschrift 17(4):347–348

Schiano P, Mercogliano, Comegna L (2009) Simulation chains for the forecasting and prevention for landslide induced by intensive rainfall. vol 1, pp 232–237

Scoccimarro E, Gualdi S, Bellucci A, Sanna A, Fogli PG, Manzini E, Vichi M, Oddo P, Navarra A (2010) Effects of tropical cyclones on ocean heat transport in a high resolution coupled general circulation model. J Clim 24:4368–4384

Skempton AW (1985) Residual strength of clays in landslides, folded strata and the laboratory. Géotechnique 35(1):3–18

Tommasi P, Pellegrini P, Boldini D, Ribacchi R (2006) Influence of rainfall regime on hydraulic conditions and movement rates in the overconsolidated clayey slope of the Orvieto hill (central Italy). Can Geotech J 43:70–86

Vassallo R, Di Maio C (2008) Misure di spostamenti superficiali e profondi in un versante argilloso in frana. Incontro Annuale dei Ricercatori di Geotecnica, Catania, 15–17 Sept 2008

Vulliet L (1986) Modélisation des pentes naturelles en mouvement. Ph.D. thesis, École Politéchnique Fédérale de Lausanne, Switzerland

Research on Chuni Landslide Geological Evolution Process

Junfeng Wu, Yunsheng Wang, and Simeng Dong

Abstract

According to limited research in the past, Chuni landslide is a giant rock landslide located on the right bank of the Daduhe River, Luding County, Sichuan Province. The detailed geological survey reveals that Chuni landslide developed in the Kangding complex strata. The combination of steep rock mass structural planes which affected by the Luding fault and Jinping fault was the controlling factor which leads to the formation of landslide, and the strong earthquake in the history was the triggering factor. By the ESR time dating of samples from the lake sand in the dammed reservoir of the landslide, Chuni landslide was formed in 20.2 ± 2 ka B.P. Moreover, due to the "gully piracy" of North gully in 7.1 ± 2 ka B.P, the landscape of Chuni landslide has changed a lot. The ancient geological environment in the landslide area can be reconstructed effectively by our study on its complicated evolution process. And since the landslide position is in the Yingliangbao hydropower station reservoir, which is under the construction, it is worth making an analysis on the causes of landslide as well as its stability.

Keywords

Landslide • Evolution process • ESR time dating • Ancient geological environment

Introduction

Based on limited researches in the past, Chuni landslide is a giant rock landslide developed on the right bank of the Daduhe River, Luding County, Sichuan Province. And the shape of landslide looks like a round stage (Ding et al. 2007). The landslide accumulation is composed of completely discomposed aggregated massive-block stone, debris and soil or huge and non-disaggregated heavy weathering block. Since the formation of the landslide, its landform has changed: the south part has been cut by flood, an alluvial–pluvial fan occur in the gully, a new landslide is developed on the left bank of the gully, which provides clues to reconstruct the ancient geological environment. Each evolution stage of landslide could be ascertained from ESR dating of the lake sand. Since Chuni landslide is located in the Yingliangbao hydropower station reservoir, the research of the landslide turns out to be necessary for the safety during construction process.

Background of Chuni Landslide

Chuni ancient landslide is a giant rock landslide which locates on the right bank of Daduhe River, apart from Luding country about 9.5 km, with the volume over 400 million cubic meters. Such huge landslide was once blocked Daduhe River and formed a huge reservoir with the end reached the mouth of Wasigou. And the length of temporary reservoir is about 35 km.

J. Wu (✉) • Y. Wang
State key Lab of Geohazard Prevention and Geoenvironment Protection, Chengdu University of Technology, Chengdu, China
e-mail: viris@126.com

S. Dong
Graduate School of Engineering, Kyushu University, Fukuoka 819-0395, Japan

C. Margottini et al. (eds.), *Landslide Science and Practice*, Vol. 4,
DOI 10.1007/978-3-642-31337-0_8,

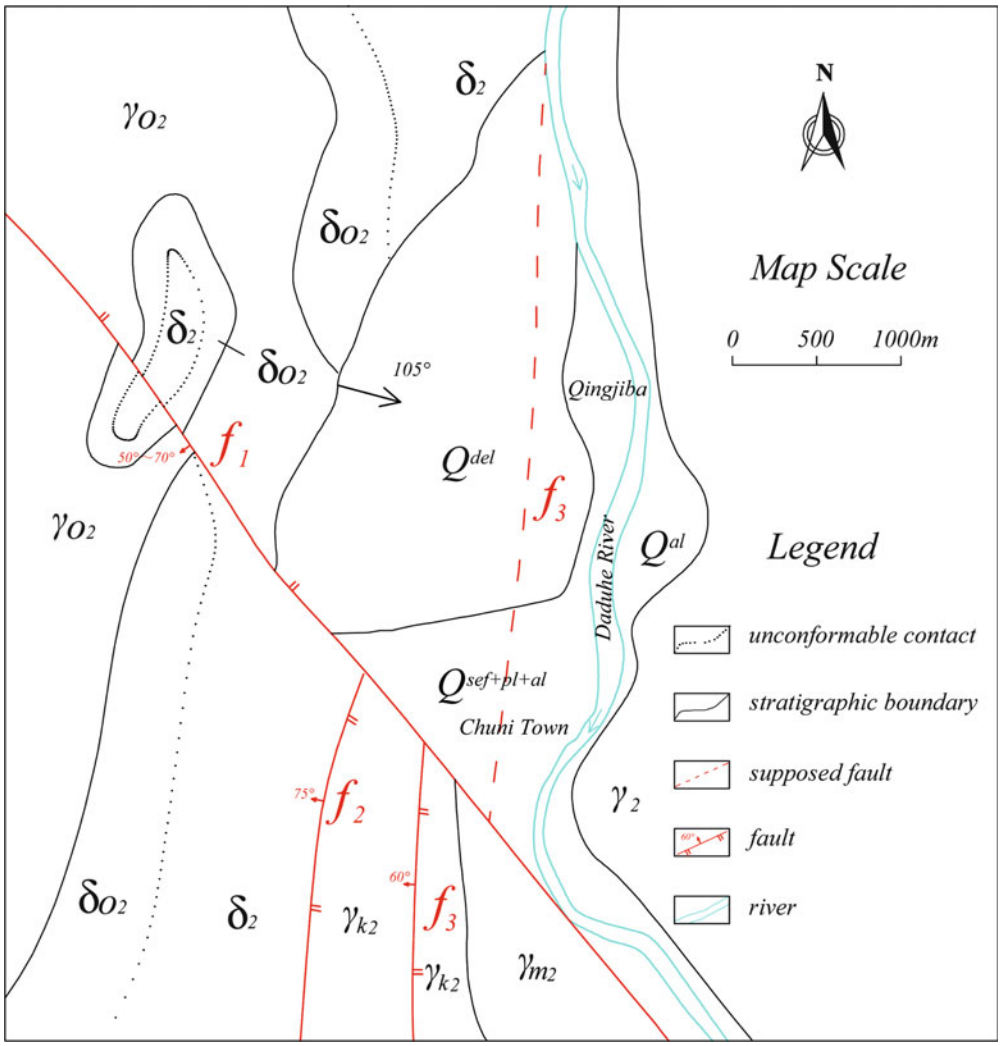

Fig. 1 The geological map of Chuni landslide. f_1 – Jinping fault, f_2 – Detuo fault, f_3 – Luding fault, δ_{O2} – quartz diorite, δ_2 – diorite, γ_{O2} – plagioclase granite, γ_2 – Proterozoic granite, γ_{m2} – mixed granite, γ_{k2} – moyite, Q^{del} – landslide accumulation, Q^{al} – alluvium, $Q^{sef+pl+al}$ – mixed with debris flow and fluvial deposits

Geological Setting of Landslide

Chuni Landslide located in the conjunction of Chuandian SN-strike structural belt and NE-strike Longmenshan structural belt. The main fractures in the region are Xianshuihe fracture, Daduhe fracture and Longmenshan fracture. earthquakes occur intensely (Deng et al. 2007; Liu et al. 2010). According to the historical earthquake records, the Moxi earthquake happened in 1786 with the magnitude Ms7.7 (Wang and Pei 1988).

There are three faults in the region (Fig. 1), they are Jinping fault, Detuo fault and Luding fault, which belong to the secondary faults of the Daduhe Fracture. The Detuo fault becomes less observed after the Jinping faults interrupted the Detuo fault and Luding fault. Luding fault stretched to the north along the toe of Chuni landslide. These

Fig. 2 The landform of Chuni landslide (Camera toward west). *1* south gully, *2* north gully, *3* secondly landslide, *4* alluvial fan

faults become less active after late Pleistocene according to seismic research (Deng et al. 2007). In the landslide area, the horizontal PGA (Peak Ground Acceleration) is 0.3 g for 10 % probabilities of exceedance in 50 years (State bureau of quality and technical supervision 2001).

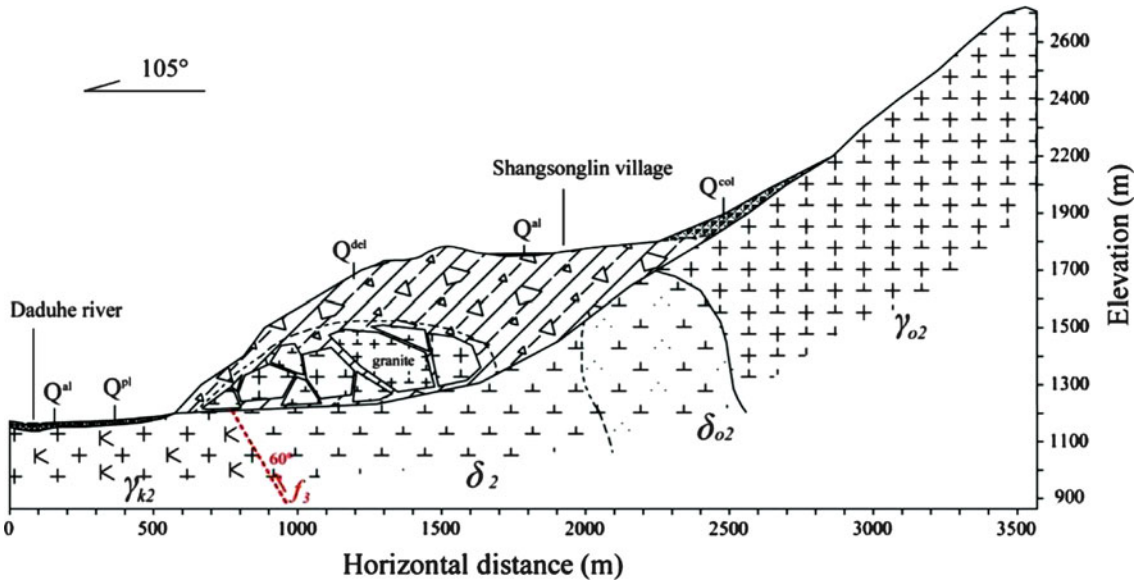

Fig. 3 The cross section of Chuni landslide. f_3 – Luding Fracture, δ_{O2} – quartz diorite, δ_2 – diorite, γ_{O2} – plagioclase granite, γ_{k2} – moyite, Q^{del} – landslide accumulation, Q^{al} – alluvium, Q^{pl} – fluvial deposits, Q^{col} – coluvial

The Characteristics of Chuni Landslide

The landslide appears in a typical circle-chair terrain shape (Fig. 2). Main sliding direction is 105°. Lateral gullies and Daduhe River are the boundaries of north and south, east part of the zone, respectively. The landslide is about 1,640 m in length, 2,920 m in width alone the Daduhe River. The front part is a steep slope with the average slope angle of 40°, the height ranges from 1,290 m at the toe to 1,800 m at the back edge. There is a gully in the middle part of the body which divides the landslide into two parts. And a platform in the position of 1,882 m high of the accumulation body and there is slight depression in the middle with obvious erosion trace. The maximum depth of the groove is 50 m. This landslide owns obvious terrain characteristics: the bottom of the accumulation body is rather close to the river erosion surface nowadays and the thickness of landslide body is about 540 m and its volume is 4.0×10^8 m^3.

The Chuni landslide developed in the Kangding complex strata of Pre-Sinian system, including diorite and granite, etc. The accumulation is composed of block stone, debris and soil, some non-disaggregated massive-block stone (Fig. 3). The stone block is mainly found at the foot and in the middle of the slope. The platform at the top is the Shangsonglin village, which attributes a lot of human activity influences. Most of the surface of the platform has been turned into plough land. Thickness of the soil layer is around 0.5–3 m with large massive rocks scattered on the plough land and the border. The types of these block stones are mainly composed of diorite and quartz diorite, etc. The roundness of block stones are from angular to sub-angular shapes. The grain diameter of stone block is usually from 20 to 40 cm with a maximum of 7 m and the grain diameter of debris is generally 2–10 cm. With a long-developing history of its formation, the accumulation is well cemented and compacted, but there could be also some local aerial phenomenon (Fig. 4).

Analysis on Genetic Mechanism and Evolution Process of Chuni Landslide

Genetic Mechanism of Chuni Landslide

Chuni town is on the junction of the SN strike Luding *fault* and NW strike Jinping fault, the SN strike texture plane and NW strike fracture are well developed. The Daduhe River flows from the north to the south, the free surface dipping to the east on the right bank of Daduhe River as well as the high intensity make it possible for the granite slope to form a huge landslide.

Therefore, the movement process can be concluded as the strong unloading rockmass was in lower safety, triggering by strong earthquake and the landform amplified effect (Wang et al. 2009; Huang et al. 2008; Okura et al. 2003; Celebi 1987).

The Evolution Process of Chuni Landslide

By researching the characteristics of ancient geological environment, conclusions can be drawn as: After the formation of Chuni Landslide, the exogenic forces become the

the accumulation section is will cemented and compacted *local aerial phenomenon in accumulation section*

Fig. 4 The texture of Chuni landslide

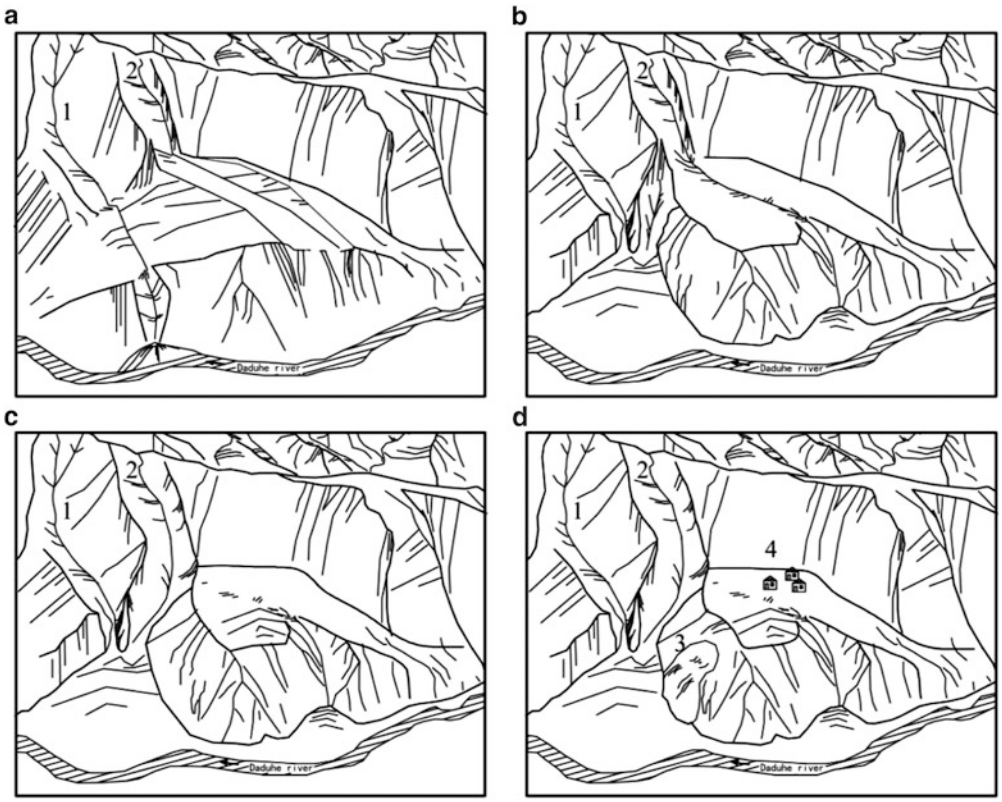

Fig. 5 The evolution process of the landslide. *1* south gully, *2* north gully, *3* secondly landslide, *4* Shangsonglin village

controlling factors to reconstruct it, such as weathering, rainfall erosion, landslide, etc. The authors divided the evolution process into four parts, which is shown in Fig. 5.

(a) Formation (20.2 ± 2 ka B.P.)

By ESR measure of the lake sand in the dammed reservoir of the landslide, the formation time of the landslide is 20.2 ± 2 ka B.P., i.e. the late Pleistocene. In early period of the formation, Chuni landslide was a wide platform, center part had high altitudes compared to the border parts, and two small scale gullies (south gully and north gully) developed on the central part of landslide which was heading to the downstream.

(b) Heavy erosion on south gully

South gully locates along the downstream on the border of landslide. The accumulation is composed of loss materials and silt sand, it can be concluded that the erosion heavier is stronger than the north gully. On the mouth of the gully, a debris pluvial fan is well developed, it take one third of the

area on the landslide platform, Another small gully is well developed by eroded heading to the north gully direction on the top of the fan.

(c) Gully piracy (7,000 years ago)

A small gully on the top of the fan erodes till 1,960 m altitude and replaced the north gully ("gully piracy"). By ESR measuring on the sand samples in north gully, it shows such event occur in 7.1 ± 2 ka B.P. (the Holocene).

(d) Small scale landslide developed along the downstream

As the north gully piracy, the south gully had strong erosions, and the south part of the Chuni landslide was cut heavily, and small landslide was formed on the left bank for slope foot erosion. A large fluvial fan occurs in the mouth of the gully.

Conclusions

1. Chuni landslide is a giant ancient rock landslide which is triggered by earthquake.
2. During the 20,000 years geological time, heavy reconstruction occurred in Chuni landslide, almost one third of the landslide has been eroded to become a pluvial fan, accompanied by the phenomena of north gully piracy, regional collapses.
3. There is no significant deformation on Chuni landslide so far, it is stable on the whole.
4. Due to the water force become stronger in the south gully, the erosion become more serious on the slope foot. The stability of the small scale landslide become worse. The only entrance of Shangsonglin village is located on the landslide, the stability becomes smaller by the process of erosion. Suggestion has been given to make countermeasures on the slope.

Acknowledgments The research has been supported by National Natural Science Foundation of China (NSFC), (Grant No.2008CB425801, 41072231), and by the China Geological Survey Bureau (Grant No.1212010914010). We are particularly thankful to Hailiang Li, Jianlin Zhao, Yi Zhou for field researches.

References

Celebi M (1987) Topographic and geological amplification determined from strong-motion and aftershock records of 3 March 1985 Chile earthquake. Bull Seismol Soc Am 77:1107–1147

Deng JH, Chen F, Yin H (2007) Geological origin and stability evaluation of Siwancun landslide in Luding country. Chin J Rock Mech Eng 26(10):1945–1950

Ding J, Yan Y, Yue CT (2007) Analysis of the geological hazards' distribution and development trend in Dadu River Catchments of Sichuan Province. Chin J Geol Hazard Control 18(2):22–25

Huang RQ, Pei XJ, Li TB (2008) Basic characteristics and formation mechanism of the largest scale landslide at DaGuangBao occurred during the Wenchuan earthquake. J Eng Geol 16 (6):730–741

Liu YC, Wu DC, Wang DY (2010) Research on the deformation characteristics of the Luding fault belt in west Sichuan, China. J Chengdu Univers Technol (Sci Technol Edition) 37(3):262–267

Okura Y, Kitahara H, Kawanami A, Kurokawa U (2003) Topoguaphy and volume effects on travel distance of surface failure. Eng Geol 67:243–254

State Bureau of Quality and Technical Supervision (2001) Seismic ground motion parameter zonation map of China (GB18306-2001). Standards Press of China, Beijing

Wang XM, Pei XY (1988) Some new points of view on the 1786 earthquake (M = 7.7) occurring in the area between Kandding and Moxi, Luding country, Sichuan province. Earthq Res China 4 (1):108–115

Wang YS, Luo YH, Xu HB (2009) A study on the genetic mechanism and movement mode and process of earthquake high slope landslides. Chin J Rock Mech Eng 28(11):2360–2368

A Geotechnical Explanation for the Transition from Creep to Slides in the Alpine Foreland

Philip Leopold, Erich Draganits, Gerhard Heiss, and Ede Kovacs

Abstract

A 5 years continuing study of the regional distribution of mass movements in the eastern Styrian Basin in the Austrian alpine foreland indicates that fast mass movements develop preferably on slopes that showed creep processes before. The geotechnical explanation for this observation is that slopes, which experienced deformation by creep over a long period of time, already show a reduced safety factor for the displaced slope material. Therefore slope areas that have experienced deformation by creep are much more vulnerable to heavy precipitation events and evolve into fast moving slides and flows more common than slopes that have not experienced creep before.

Keywords

Creep • Slide • Shear strength • Boundary of creep • Styrian basin • Alpine foreland

Introduction and Investigated Area

Since 2005 an ongoing study of the regional distribution of mass movements in the eastern Styrian Basin has been performed. The investigated area is located in the eastern alpine foreland in Austria (Fig. 1). The area covers the districts of Jennersdorf, Güssing and Oberwart in the south of the province of Burgenland. The geology of the area is characterised by Neogene and Quarternary sediments mainly comprising clay, silt, sand and gravel, commonly interbedded. In many cases the clay material is overconsolidated. This setup makes the area particular vulnerable to form mass movements. Nevertheless, only very view authors (e.g.: Alker et al. 1969) have investigated mass movements in this area before.

P. Leopold (✉)
Health and Environment Department, AIT – Austrian Institute of Technology GmbH, Donau-City-Straße 1, Vienna 1220, Austria

Department of Geodynamics and Sedimentology, University of Vienna, Vienna, Austria
e-mail: philip.leopold@ait.ac.at

E. Draganits
Department of Geodynamics and Sedimentology, University of Vienna, Vienna, Austria

G. Heiss • E. Kovacs
Health and Environment Department, AIT – Austrian Institute of Technology GmbH, Donau-City-Straße 1, Vienna 1220, Austria

Inventory: Creep and Fast Moving Slides

During this investigation more than 200 areas showing creep deformation have been located and characterized in the investigated area by remote sensing, geomorphological field mapping and engineering geological measurements. An example of the typical local morphology of a slope affected by deep-seated creep processes is shown in Fig. 2. In the center of the slope, a depression with increased soil moisture is indicated by a more intense green colour of the vegetation. Downslope of the depression follows a zone of flattening (red arrow in Fig. 2) and further downwards a convex accumulation zone is visible. All this morphological patterns are interpreted as the results of a creep process acting slowly over a very long period of time.

C. Margottini et al. (eds.), *Landslide Science and Practice*, Vol. 4,
DOI 10.1007/978-3-642-31337-0_9,

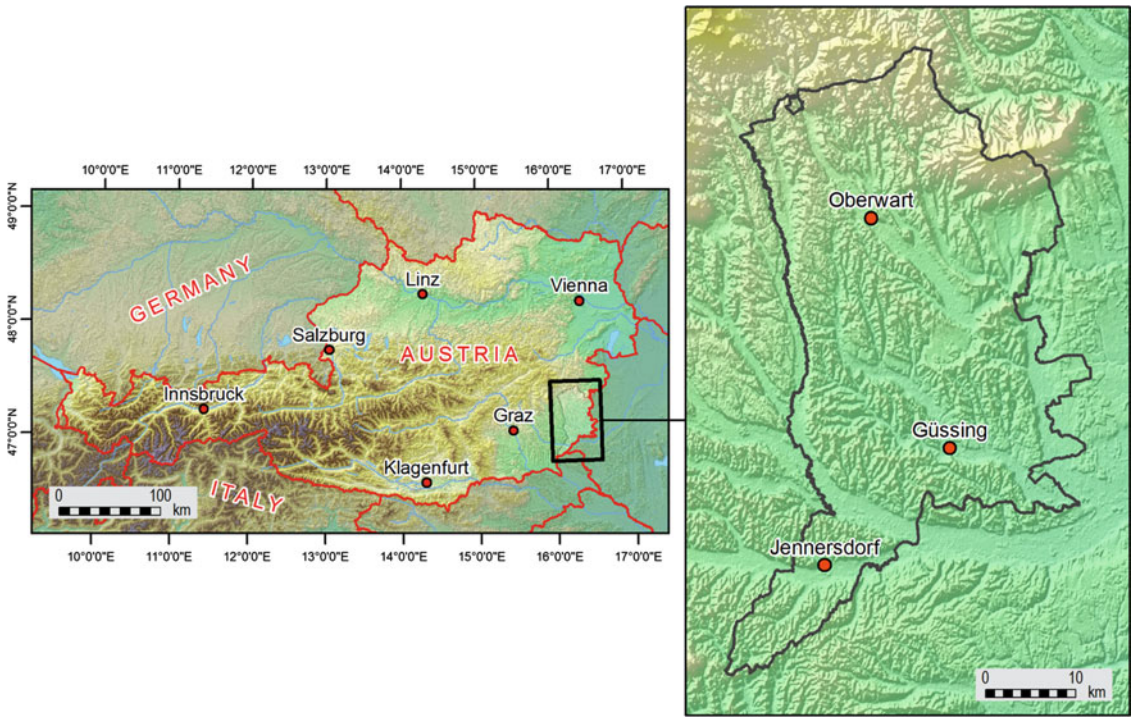

Fig. 1 Investigated area in the eastern alpine foreland in Austria, districts of Jennersdorf, Güssing and Oberwart in the south of the province of Burgenland

Fig. 2 Example of a slope that is affected by a deep seated creep process. Zones of depression, flattening (*red arrow*) and convex soil accumulation are visible. District of Jennersdorf

Fig. 3 Example of a rotational slide formed during the 2009 event. The former terrain of the slide is already partly reconstructed, but the mass movement scarp is still clearly visible. District of Jennersdorf

In June 2009 the Styrian Basin was seriously affected by the heaviest rainfall event since the beginning of weather chronicles in Austria in the year 1800 (Auer et al. 2007). The pluviometric measurement showed that the amount of rain during a single day reached values of the monthly average precipitation (Godina and Müller 2009), i.e. more than 100 l of rain per square meter in 24 h. This exceptional rain triggered many fast moving mass movements like slides and flows causing a number of damages to infrastructure.

In addition to the previously mapped areas of creep 102 fast moving mass movements from the 2009 event could be located and characterized. An example of a rotational slide formed during the 2009 event is shown in Fig. 3. The former terrain of the slide is already partly reconstructed, including the tree in the middle of the displaced slope material. However, the scarp of the rotational slide is still clearly visible.

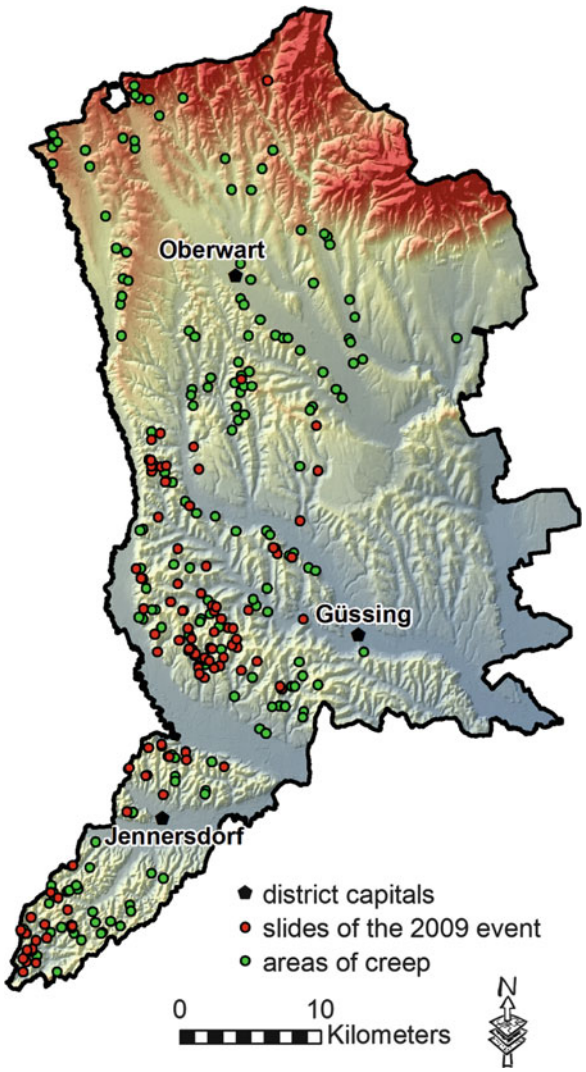

Fig. 4 The distribution of areas of creep and slides of the 2009 event within the investigation area. Due to different spatial extensions of the movements, they are all marked as *dots* using the balance point of the area. The overlap of areas of creep and slide is therefore not always visible

Results: Correlation Between Creep and Slides

Based on the investigation of the fast moving landslides from the 2009 event it can be calculated, that 59 % of them are located in areas that have already been affected by creep before. This spatial relationship is computed by using a buffer zone of 500 m around previously outlined areas with creep, because of the difficulties to discern the exact boundaries of areas of creep in fieldwork as also described in Highland and Bobrowsky (2008). The distribution of areas of creep and slides of the 2009 event inside the investigation area is shown in Fig. 4.

For the understanding of possible triggers for the transition from slow mass movements, such as creep, to fast ones, including slides and flows, it is essential to distinguish between these two types of deformation processes. According to Highland and Bobrowsky (2008) creep is a very slow type of mass movement that occurs typically on slopes with gradients between 10° and 35°. The deformation velocity is very low, usually not more than 1 m per decade. In comparison, the deformation velocity of slides ranges between meters per month and much faster (Highland and Bobrowsky 2008).

It is important to notice, that in contrast to slides, creep doesn't necessarily develop a rupture surface (Terzaghi 1950). Creep is a land forming process that may act at constant rates over a very long period of time (decades or centuries).

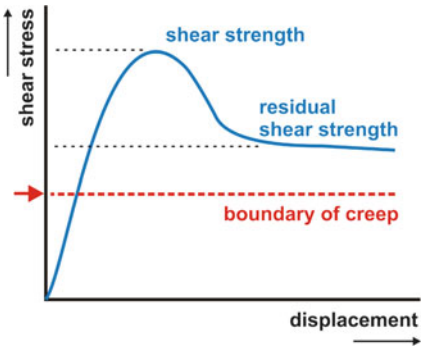

Fig. 5 Typical shear stress/displacement relationship after Waltham (2009) for soils with high amounts of clay and silt or overconsolidated clay. Creep already occurs at much lower values of shear stress than the actual shear strength of the soil material, the so called boundary of creep. Creep deformation leads to a reduction of the shear strength of the displaced slope material up to the residual shear strength of the former unaffected mass

Discussion: Geotechnical Reasons for the Correlation

Already Haefeli (1967) realized that creep occurs at much lower values of shear stress than the actual shear strength of the soil material. The shear stress where creep starts to occur is called critical shear stress or boundary of creep (Prinz and Strauß 2006). If the critical shear stress impacts the slope material over a long period of time (decades or centuries) the displaced slope material will react by reducing its (peak) shear strength. That causes the original shear strength in the displaced mass to be reduced up to the residual shear strength of the former unaffected mass. This phenomenon is exemplified in Fig. 5 using a typical shear stress/displacement relationship after Waltham (2009) for soils with high amounts of clay and silt or overconsolidated clay.

Prinz (1991) and Prinz and Strauß (2006) call this lowering of the shear strength in conjunction with creep progressive failure, which occurs in soils mentioned above. It starts with a local exceeding of the shear strength causing very

small and local zones of slide inside the area of creep. In consequence of occurring overstress of close ranges those weak zones swell and increasingly large areas develop, in which the shear strength shelves to the residual shear strength. Once these areas gain critical magnitude, rupture can occur and a large scale slide may develop.

Conclusions

Due to the phenomenon of the described progressive failure, the safety factor of the displaced slope material is lowered compared to slope material unaffected by creep. During heavy precipitation water acts as an additional weight-component in the displaced mass and increases the pore pressure. This decreases the safety factor of slopes affected by creep further and can cause it to drop below 1.

Consequently the high amount of precipitation in June 2009 (Godina and Müller 2009) in the investigation area generally increased the susceptibility to develop fast moving landslides. Field data and geotechnical considerations showed, that slope areas which experienced deformation by creep before are much more vulnerable to form fast moving slides and flows than those which did not experience creep before.

Acknowledgments This study was co-funded by the provincial government of Burgenland.

References

Alker A, Haas H, Homann A (1969) Hangbewegungen in der Steiermark. Mitteilungen des Museums für Bergbau, Geologie und Technik am Landesmuseum "Joanneum" Graz 30:2–35

Auer I, Böhm R, Jurkovic A, Lipa W, Orlik A, Potzmann R, Schöner W, Ungersböck M, Matulla C, Brunetti M, Nanni T, Maugeri M, Mercalli L, Briffa K, Jones P, Efthymiadis D, Mestre O, Moisselin J, Begert M, Müller-Westermeier G, Kveton V, Bochnicek O, Stastny P, Lapin M, Nieplova E, Cegnar T, Dolinar M, Gajic-Capka M, Zaninovic K, Majstorovic Z, Szalai S, Szentimrey T (2007) HISTALP – Historical instrumental climatological surfacetime series of the greater alpine region 1760–2003. Int J Climatol 27:17–46

Godina R, Müller G (2009) Das Hochwasser in Österreich vom 22. bis 30. Juni 2009. Bundesministerium für Land- und Forstwirtschaft, Umwelt und Wasserwirtschaft, Abt. VII/3 – Wasserhaushalt, p 21

Haefeli R (1967) Kriechen und progressiver Bruch im Schnee, Boden, Fels und Eis. Schweizerische Bauzeitung 85(1):1–9

Highland LM, Bobrowsky P (2008) The landslide handbook – a guide to understanding landslides, vol 1325. U.S. Geological Survey Circular, Reston, p 129

Prinz H (1991) Abriss der Ingenieurgeologie, 2nd edn. F. Enke, Stuttgart, p 466. ISBN 3432923325

Prinz H, Strauß R (2006) Abriss der Ingenieurgeologie, 4th edn. Spektrum Akademischer Verlag – Elsevier, München, p 671. ISBN 978–3432923338

Terzaghi K (1950) Mechanism of Landslides. In: Paige S (ed) Application of geology to engineering practice. Berkey volume. Geological Society of America, Boulder/New York, pp 83–123

Waltham T (2009) Foundations of engineering geology, 3rd edn. Spon Press, London/New York, p 98. ISBN 0-7514-0071-8

Pore Pressure Fluctuations Within Quasi-Stable Slopes in South-Western Estonia and Their Influence on Slope Stability

Marko Kohv and Tiit Hang

Abstract

Pore pressure fluctuations within slopes are widely considered as one of the most common landslide triggers. Ten automatic piezometers were installed within two quasi-stable slopes in south-western Estonia in order to record fluctuating pore pressures during a 2-year period. Pore pressure values and meteorological and hydrological data were studied by non-parametric correlation and cluster analyses in order to quantify the influence of external parameters. Data from 51 groundwater monitoring wells, covering the period from 1960 to 2009, were analysed in order to evaluate long-term changes in the underlying artesian aquifer. The development, refilling and movement of the groundwater depression were recorded. The pore pressure field was modelled with the finite element model and used as an input for slope stability analyses. Significant changes in slope stability were revealed. The influence of the ongoing climate change on slope stability is discussed.

Keywords

Landslide • Groundwater • Varved clay • Baltic • Climate change

Introduction

Rising pore pressures are known as one of the most common triggers of landslides all around the world (Picarelli et al. 2004). Therefore the knowledge about pore pressure dynamics and its response to the changing climate is considered as one with utmost importance in landslide science (Van Asch et al. 2007; Simoni et al. 2004). Low altitude (<20 m asl) areas at the eastern coasts of the Baltic Sea are smoothed to even topography by deposits of proglacial lakes and the Baltic Sea. In such a conditions landslide hazards are usually considered to be a rare occurrence (Miidel and Raukas 2005). However, in recent years the number of landslides in the area has grown considerably (Kohv et al. 2009). Detailed analysis of the individual slides point to the importance of the changing pore pressures but concrete measurements were lacking. The aim of the current study is: (1) to monitor actual pore pressures within quasi-stable slopes, (2) to quantify climatic and hydrological influence to the pore pressures; (3) to model slope stability fluctuactions caused by the changing pore pressures.

Regional Background

The studied river valleys lay within an area of ca 200 km^2 around Pärnu Bay, on the eastern Baltic Sea coast, Estonia, between N 58° 20′ to 58° 27′ and E 24° 15′ to 24° 40′ (Fig. 1). The Pärnu region is the most landslide prone area in Estonia (Kohv et al. 2010). It is a coastal plain with altitudes varying between 2 and 15 m, diversified by dunes, raised bogs and river valleys. River valleys, eroded into the lacustrine-marine plain, are up to 15 m deep.

The uppermost part of the sedimentary cover in the Pärnu area includes Silurian limestone or Devonian sandstone. Paleozoic rocks are covered by Quaternary sediments in the following upward order: Late-Weichselian till,

M. Kohv (✉) • T. Hang
Department of Geology, University of Tartu, Ravila 14a, Tartu, Estonia
e-mail: marko.kohv@gmail.com

C. Margottini et al. (eds.), *Landslide Science and Practice*, Vol. 4,
DOI 10.1007/978-3-642-31337-0_10,

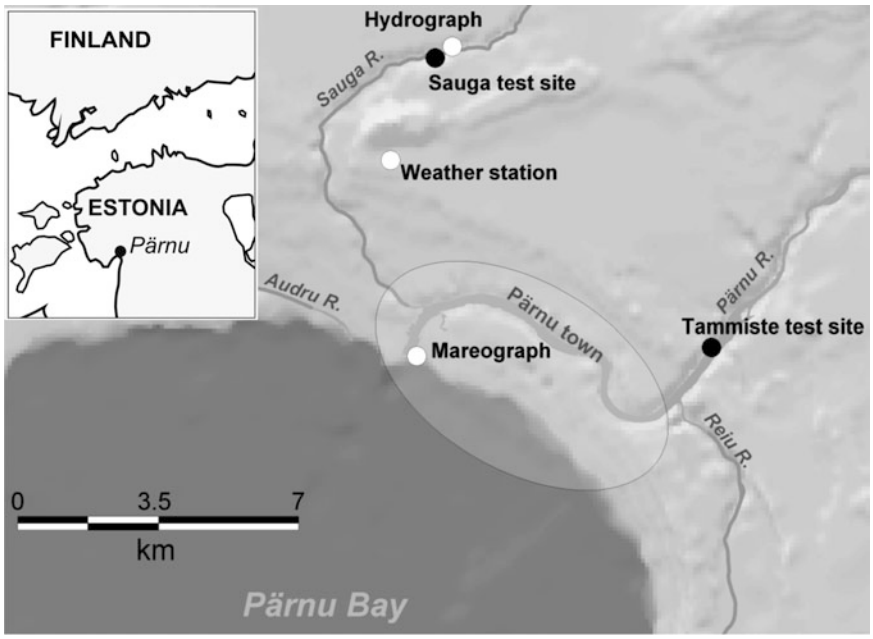

Fig. 1 Location of the test sites and measuring stations

glaciolacustrine varved clay and marine silt or sand. The Holocene marine cover may be locally absent.

Two groundwater aquifers occur in the Quaternary sediments in the Pärnu area. The upper, unconfined aquifer is bound to marine sands; it is used only by individual households. Lower, artesian groundwater below the varved clays, is bound to glacial till and uppermost bedrock layers and is used as one of the water sources for Pärnu town. Glaciolacustrine clay acts as an aquiclude between the two groundwater aquifers.

The climate in the area is temperate marine. Temperatures vary between −30 °C and 35 °C, with an annual average of 5.8 °C. Mean precipitation is ca. 700 mm/year and potential evaporation from 400 to 500 mm/year during the ice-free season. Snow cover typically lasts around 100 (max. 140) days and melts in March, causing high water levels both in the ground and rivers (Jaagus 1999).

Methods

In order to analyse long-term changes in the pressurized groundwater level, monitoring data from 51 groundwater monitoring wells (opening Quaternary, Devonian and/or Silurian aquifers) operated by the Estonian Geological Survey or the company of IPT Projektijuhtimine OÜ were used. The datasets covering the period from 1960 to 2009 were cleaned of measurement errors, computed to yearly averages and organized as a GIS-database. Interpolated groundwater surfaces with the grid size of 300 × 300 m were generated for selected years with the kriging interpolator within software package Surfer v 9.0 (Golden Software Inc.).

Pore pressures were measured at two test sites (Fig. 1) with automatic piezometers (pressure hysteresis <0.1 % and linearity error <0.15 %) manufactured by BAT Geosystems AB, Sweden. The bonded resistance strain gage piezometers were installed in vertical cluster configuration at two test sites: six piezometers at the Sauga and four at the Tammiste test site (Fig. 3). The Tammiste test site was set up between the abundant marks of single rotational landslides in the Pärnu River valley. The Sauga test site was set up in the middle of one of the most landslide prone areas in the Pärnu region (Kohv et al. 2009), right at the top of the retrogressive Sauga landslide complex. Standard metal water pipes and couples were used to install porous polyethylene plastic filters (filter height 35 or 20 mm) to the desired depth. The pore pressure and temperature were measured with an 1 h interval during the period from 01 May 2009 to 01 May 2011. The meteorological and hydrological data were obtained from the Sauga meteorological station and the hydrological posts operated by the Estonian Meteorological and Hydrological Institute (Fig. 1).

Spearmans rank order correlation method was used for statistical analysis as Shapiro-Wilk test proved non-normal data distribution. Tree cluster analysis with Ward linkage method was used for classification of the datasets. Good overview of the used statistical methods is written by Davis (2002). Significance level $p = 0.05$ was used in all analysis.

Slope stability calculations were done with the software package Slide v 5.0, which couples steady state finite element groundwater model (2,500 triangular elements) with slope stability analysis. Rigorous method, Spencers calculation scheme (Spencer 1967) was used for slope stability analysis. Strength and hydraulic parameters and slope

Table 1 Soil parameters used in the stability model

Test site	Soil type	Y kN/m^3	c′, kPa	ϕ′, °	k, m/s Horizontal/vertical
Sauga	Silt	19	10	20	$\mathbf{10^{-7}}$
	Desiccated clay	19	46[a]	0	$\mathbf{10^{-8}/10^{-4}}$
	Upper clay	16	0	17[b]	$\mathbf{10^{-10}/10^{-8}}$
	Lower clay	17	0	30[b]	$\mathbf{10^{-9}/10^{-7}}$
	Till	Bedrock			$\mathbf{10^{-5}}$
Tammiste	Sand	19	10	30	$\mathbf{10^{-5}}$
	Varved clay	17	8	21	$\mathbf{10^{-9}/10^{-7}}$
	Till	Bedrock			$\mathbf{10^{-5}}$

[a]Undrained strength.
[b]Fully softened strength.

profiles used in the modelling are obtained from Kohv et al. (2009, 2010) and presented in Table 1. Varved clay has anisotropic hydraulic conductivity due to alternating thin layers of silt and clay that form a varved clay complex and fissure system at the desiccated crust. In total 441 (20 × 20 grid) slip surface centres above the slope were used in the model. Eleven evenly spaced circular slip surfaces were calculated for each centre. The software calculated in total 4,851 slip surfaces for each pore pressure set-up.

Results

Long-Term Changes of the Groundwater Level

The groundwater depression during the 1960s was located in the old town and its center was at an altitude of −8 m. Depression gradually deepened and widened due to increased pumping and reached its maximum in the late 1980s. In 1986 the centre, located at the centre of the old town, was lowered to an altitude of −12 m. (Fig. 3).

The groundwater depression was partly refilled during the period 1990–2000 when the observation data show a mean 5 m (max 12 m) rise in the piezometric level within the town. The refilling was mainly caused by decreasing water consumption due to collapse of the Soviet era industry and rising water prices. The centre of the depression also moved eastwards due to extensive opening of new groundwater wells outside Pärnu, with corresponding lessening of water pumping from the wells located within the town. The piezometric level of pressurized groundwater in Pärnu town has been stable since the year 2001, at an altitude between 0 and 1.5 m. The main problem complicating analysis is the inconsistency of the spatiotemporal distribution of data. However, the general development and evolution of the groundwater depression caused by water withdrawal for Pärnu town are still observable. We can elicit from Fig. 2 that the artesian groundwater level in 1986 was about 4 m lower than in 2001 at the Tammiste test site and 2 m lower at the Sauga test site.

Seasonal Fluctuations of the Pore Pressures

Pore pressures fluctuated at the Tammiste test site within 1 m (Fig. 3). Although the difference of the installation depth of piezometers was 7 m, the difference in pore pressures was only 2–2.5 m. This indicates general downward groundwater flow as hydrostatic pressure increases at a lower rate than depth. Pore pressures from various depths and geological strata fluctuated relatively coherently. Spearman's rank order correlation analysis between pore pressure datasets gave the lowest R = 0.56.

Cluster analysis divides pore pressure datasets into two first order groups but none of them forms first or second-order group with meteorological or hydrological data. The latter forms the second cluster, which is relatively weakly linked with the pore pressure group.

At the Sauga test site pore pressure distribution loosely follows the hydrostatic distribution, with mild downward gradient (Fig. 3). Seasonal variations are greatest (up to 2.6 m) and almost synchronous within the capping desiccated clay and the upper part of the varved clay layer. Almost total unison (R = 0.99) in pore pressure fluctuations with a ca 5-6 h time lag within the upper 4 m of sediment points to a water-conducting fissure system in the upper desiccated clay layer, similar system has been described in French Alp glaciolacustrine clays (Van Asch et al. 1996). Pore pressures in the lower part of the varved clay were very stable during the measuring period. Pore pressure variations in till are relatively large (ca 1.5 m) but changes are much slower than close to the ground surface. Cluster analysis divides pore pressure datasets into three first-order groups, mixed with external parameters. Both correlation and cluster analysis confirm the river water level as a very good indicator for pore pressures at the upper part of the clay slope and close (<40 m) to the river channel.

Due to enhanced evapotranspiration, temperature ($R > -0.60$) has good correlation with pore pressures during the snow-free period at the Tammiste test site (Table 2). Precipitation has generally little effect on pore pressures

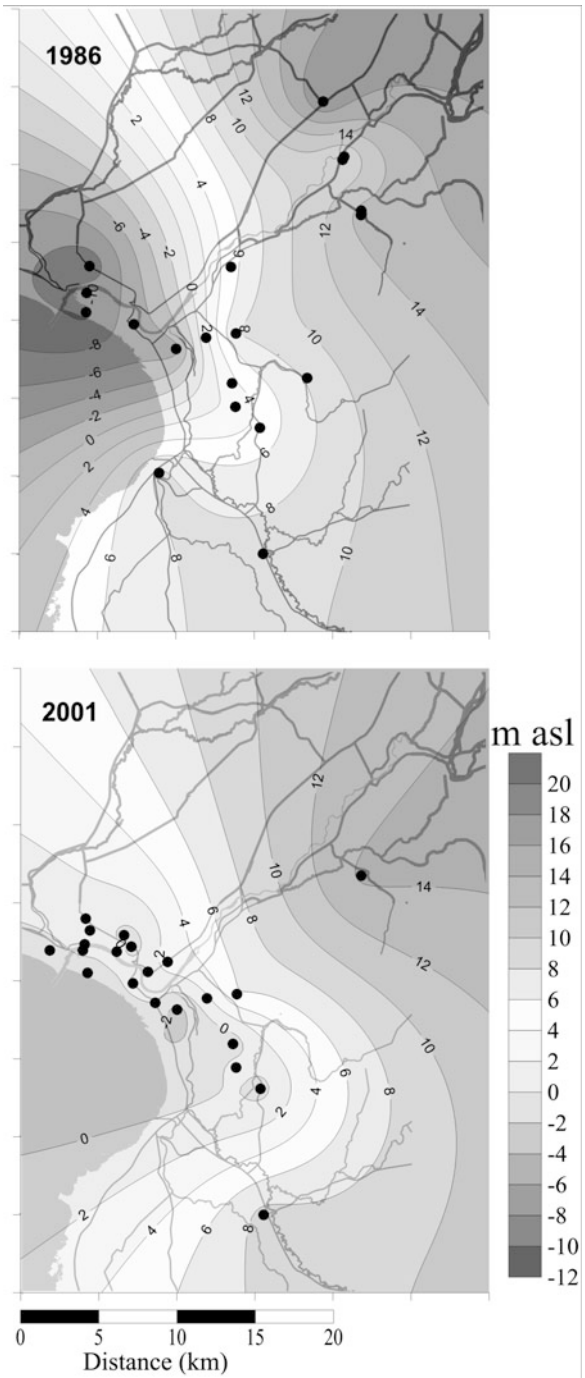

Fig. 2 Artesian groundwater level around Pärnu town during the lowstand in 1986 and after refilling in 2001. *Black dots* mark monitoring wells

during the snow-free period. Even relatively rainy August (123 mm) and following September (99 mm) of 2010 did not raise pore pressures notably. The precipitation starts to influence the slope more profoundly when the 14-day average temperature drops below 5 °C and at least 4 mm of average daily precipitation in the form of rain is needed within a 14-day period to cause a rise in the pore pressures. Spring thaw is the second period of rapid pore pressure rise. Pore pressures gradually lower between those high-stand periods due to seepage and evapotranspiration

Relations are somewhat different at the Sauga test site (Table 3). During the snow-free period the first piezometer subgroup (3428, 3423, 3425) has strong positive correlation with water level in the Sauga River and strong negative correlation with temperature. Precipitation has only mild correlation with pore pressures. The second subgroup (3441 and 3452) shows inverted correlations with temperature, the Sauga River and precipitation compared to the data from the upper piezometers. The correlations are generally weak, but still statistically significant. Those differences between subgroups probably indicate considerable, smoothing time lag between external input and response of the deeper pore pressures but longer data series are needed to confirm this suggestion. The third subgroup (3453) has only very weak or statistically insignificant correlations with all analysed parameters.

Good correlation between sea level, Sauga River water level and pore pressures during the winter is not most likely casual as those parameters were simply very stable in the presence of the snow cover. The thickness of the snow correlates pretty well with the pore pressures, being again inversely correlated with the second subgroup.

The pore pressures measured at two test sites show a different distribution and response dynamics to the same meteorological and hydrological changes (Tables 2 and 3). Pore pressures in the clayey slope at the Sauga test site have a much larger seasonal variability than the sandy slope in Tammiste. For example, pore pressures, expressed as water column height in the upper part of the clayey Sauga slope rose 1.4 m in 2 days in response to the autumn rains in 2009, while it took 25 days for pore pressure to raise 0.7 m rise at the sandy Tammiste site. On the other hand, the influence of the rainy autumn in 2009 is evident even in the deepest pore pressure measurements at Tammiste, while varved clays shielded completely its effect at the Sauga site. Extended periods (probably years) of increased precipitation are needed to raise pore pressure in the whole slope at Sauga, whereas slope as a whole at the Tammiste site is more sensitive to single extreme rainstorms or shorter rainy periods (weeks).

Fluctuations in the Slope Stability

Rise in pore pressures reduces effective normal stress within the slope and causes therefore reduction of the frictional component of the soil strength (Iverson et al. 1997). This mechanism, in turn, destabilizes slopes and therefore the factor of safety (FoS) of the slope fluctuates together with pore pressures. Those changes at both test sites are displayed

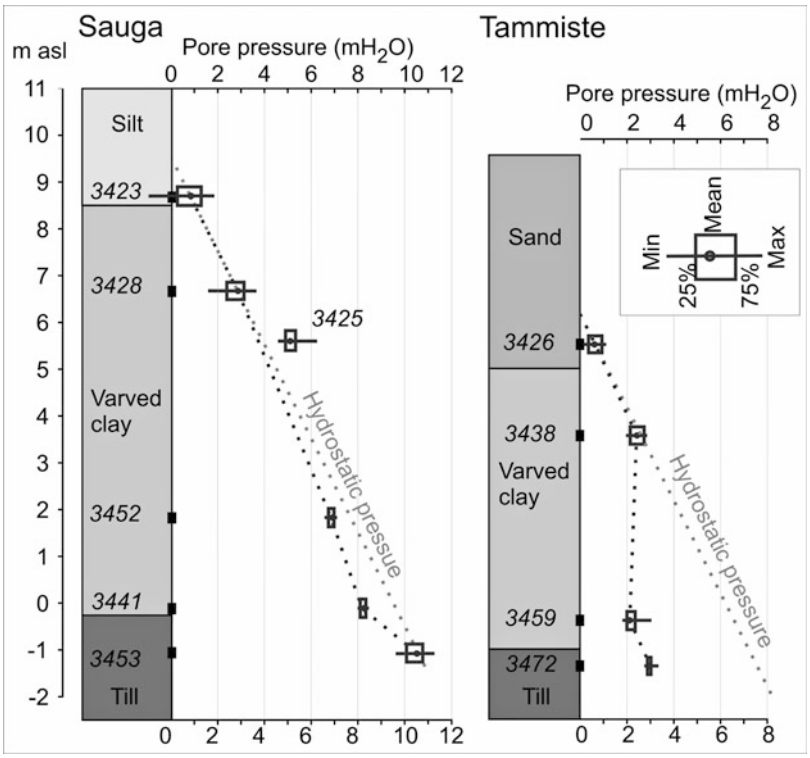

Fig. 3 Piesometers set-up and pore pressures distrbution, variance and mean at the Sauga and Tammiste test sites during the 2-year period

Table 2 Correlation coefficients between the pore pressure datasets and selected external parameters at the Tammiste test site. Bold number mark statistically significant correlations

	Snow free period			
Piezometer	Precipitat. 14 day. m. a.	Temp. 14 day. m. a.	Sea l.	Snow
Tammiste 3426	**−0.15**	**−0.69**	**−0.34**	–
Tammiste 3438	**−0.24**	**−0.64**	**−0.40**	–
Tammiste 3459	**−0.10**	**−0.60**	**−0.27**	–
Tammiste 3472	**0.18**	**−0.68**	0.10	–
	Snow period			
Tammiste 3426	**0.3**	0.05	0.01	**−0.40**
Tammiste 3438	**0.47**	−0.07	0.00	−0.08
Tammiste 3459	**0.50**	**−0.18**	0.07	**0.15**
Tammiste 3472	**0.61**	**0.24**	**0.43**	0.04

in Fig. 4. The highest and lowest pore pressure situations from the 2-year pore pressure monitoring period were chosen for the modelling. Concurrent water level in the river was also used in the model. The low-stand (Fig. 2) and hypothetical rise in the artesian groundwater aquifer level were modelled as well; in this case the level of the artesian aquifer was changed in otherwise highest or lowest pore pressure model set-up. Measured pore pressure values were ascribed to the corresponding nodes in the groundwater model and the model calculated the whole pore pressure field within the slope. Corresponding six slope stability situations are presented at the lower part of the Fig. 4. The entire analysed slope is divided into bins, 2 m (Fig. 4a) or 4 m (Fig. 4b) wide. Their location on the slope profiles is given in the upper part of Fig. 4. All the analysed slip surfaces are allocated between the bins according to the intersection points between the individual slip and ground surface. The FoS of the weakest slip surface within each bin is plotted in the lower part of Fig. 4. Four FoS curves along the slope characterize both seasonal fluctuations and long-term changes in slope stability at the Tammiste and Sauga test sites. Seasonal slope stability variations at the Tammiste test site (Fig. 4a) are far smaller than at the Sauga test site (Fig. 4b). Median seasonal variation of the FoS is only 0.08 at the Tammiste site and the largest changes occur close to the Pärnu River channel, indicating the importance of the

Table 3 Correlation coefficients between the pore pressure datasets and selected external parameters at the Sauga test site. Bold number mark statistically significant correlations

		Snow free period			
Piezometer	Sauga R.	Precipitat. 14 day. m. a.	Temp. 14 day. m. a.	Sea l.	Snow
Sauga 3423	**0.86**	**0.30**	**−0.84**	0.08	–
Sauga 3428	**0.86**	**0.18**	**−0.87**	0.06	–
Sauga 3452	**−0.22**	**−0.33**	**0.30**	**−0.25**	–
Sauga 3441	−0.02	**−0.35**	**0.10**	**−0.25**	–
Sauga 3453	**0.13**	0.02	−0.05	**0.12**	–
Sauga 3425	**0.78**	0.07	**−0.76**	**−0.13**	–
		Snow period			
Sauga 3423	**0.89**	**0.17**	**0.83**	**0.68**	**−0.42**
Sauga 3428	**0.89**	**0.43**	**0.74**	0.69	**−0.25**
Sauga 3452	−0.13	**−0.58**	−0.03	**−0.08**	**0.43**
Sauga 3441	**0.21**	**−0.43**	0.10	**0.10**	**0.44**
Sauga 3453	**−0.63**	**−0.41**	**−0.35**	**−0.37**	**−0.22**
Sauga 3425	**0.89**	**0.23**	**0.70**	0.68	−0.09

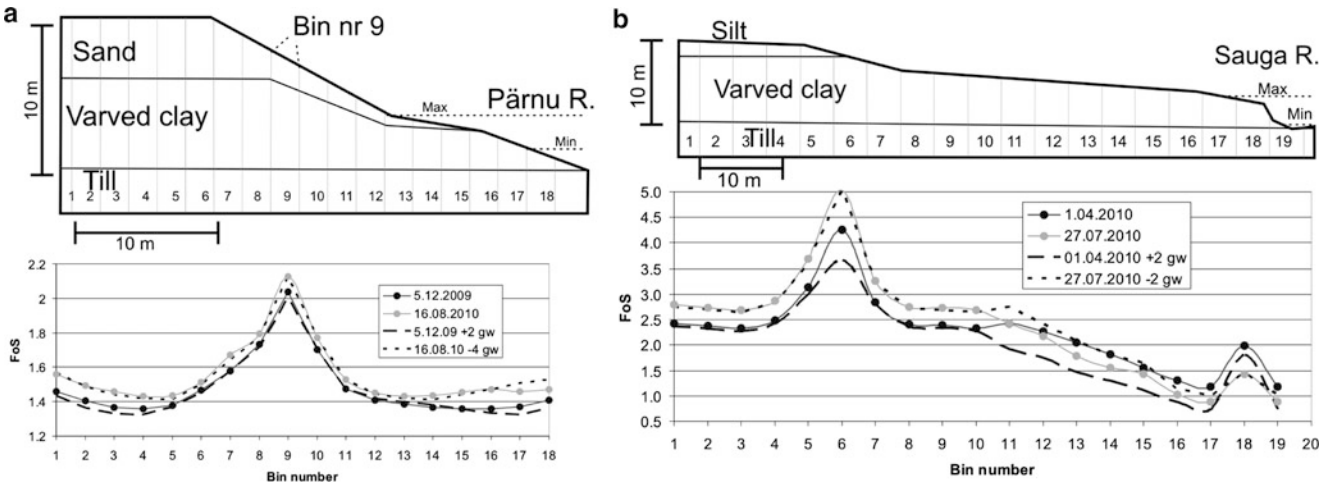

Fig. 4 Slope stability changes due to pore pressure fluctuations at the Tammiste (**a**) and Sauga (**b**) test site together with the corresponding slope profile. Gw-artesian groundwater level, FoS-factor of safety. For location of the test site see Fig. 1

river water level. The two lowermost points of the FoS curve, within bins 4 and 16 in Fig. 4a, mark intersections between the global minimum slip surface (FoS = 1.3) and the ground surface. The piezometric level of the underlying artesian aquifer has also a small effect on the slope stability at the Tammiste test site. The slope was only marginally more stable during the low-stand during the 1980s (Fig. 2); then the piezometric level was about 4 m lower than now. Hypothetical increase in the piezometric level (+ 2 m) has also a minor effect on slope stability. The pore pressures generally little affect the slope stability at the Tammiste test site. The slope failures near the Tammiste site are mainly controlled by the river undercutting and water level in the channel.

Seasonal changes in the FoS at the Sauga test site can be as large as 0.77, the median being around 0.34 (Fig. 4b). A similar fluctuation range was calculated for Canadian clay slopes by Kenney and Lau (1984). The largest fluctuations occur in the upper part of the slope, together with the most variable pore pressures (Fig. 3). The water level in the Sauga River influences the slope from bin 10 to 19 where the high-stand FoS curve (01 April 2010) crosses the low-stand one (27 July 2010). This equals the distance of up to 40 m upslope from the river channel. The Sauga River bank is unstable (FoS > 1) during the low-stand of the river up to 15 m upslope from the channel. The ongoing slope failures reported by Kohv et al. (2010) support this statement. The modelled slope configuration is, however, stable during the high-stand of the Sauga River (01 April 2010), even if it is concurrent with elevated pore pressures (Fig. 4b). The turning point occurs when the river level falls below 2.5 m asl.

The underlying pressurized aquifer influences slope stability up to 40 m upslope from the Sauga River (bin 10 in Fig. 4b). The lower part of the Sauga slope had a 0.2–0.3 higher FoS than now during the aquifer low-stand in the 1980s (Fig. 2), but the upper part of the slope was not affected at all. Hypothetical rise in the piezometric level by 2 m would also influence mostly

the lower part of the slope. Its FoS would decrease as much as 0.4–0.6. This phenomenon would cause larger landslide complexes as clay slopes near Pärnu are known to fail in a retrogressive manner (Kohv et al. 2009).

Ongoing climate change manifests itself in Estonia mostly by rising temperatures and increasing precipitation during spring and winter (Jaagus 2003). Both trends are also predicted to continue (Graham et al. 2008). Thus mild, snowy winters, followed by early spring with warm, rainy westerly cyclones, will probably be more common in the future. Spring storms that bring rain and strong warm wind will melt snowpack most effectively. An up to 25 % increase in infiltration rates was measured by Harr (1981) in Oregon during the snow on rain events. Elevated spring runoff will also lead to more intense river bank undercutting, which is the most prominent destabilizing geological process nowadays. On the other hand, rising temperatures cause increase in evapotranspiration, which may almost completely compensate the effect of increasing precipitation on pore pressures (Persson 2008). Still, evapotranspiration is highest during the vegetation period, clearly evident in Figs. 13 and 16 as a steady drop in the pore pressures at the upper parts of the slopes during the summers of 2009 and 2010. Pore pressures during high-stand periods, early spring and late autumn, are less influenced as temperatures are usually below 5 °C and therefore evapotranspiration is inhibited. Combined effect to of the above-mentioned climatic trends and increasing human activities on slope activity has not yet investigated but is most likely destabilizing.

Acknowledgments The study was funded by Estonian Science Foundation Grant 6992, Estonian State Target Funding Project SF0180048s08, and by Estonian Environmental Investment Centre.

References

Davis JC (2002) Statistics and data analysis in geology, 3rd edn. Wiley, New Jersy, p 656. ISBN 978-0-471-17275-8

Graham LP, Chen D, Christensen OB, Kjellström E, Krysanova V, Meier HEM, Radziejewski M, Räisänen J, Rockel B, Ruosteenoja K (2008) Projections of future anthropogenic climate change. In: BACC Author Team (ed) Assessment of climate change for the Baltic Sea Basin, Regional climate studies. Springer, Berlin, pp 133–219

Harr RD (1981) Some characteristics and consequences of snowmelt during rainfall in western Oregon. J Hydrol 53:277–304

Iverson RM, Reid ME, LaHusen RG (1997) Debris-flow mobilization from landslides. Annu Rev Earth Planet Sci 25:85–138

Jaagus J (1999) Uusi andmeid Eesti kliimast. Publicationes Instituti Geographici Universitatis Tartuensis 85:28–38 (In Estonian)

Jaagus J (2003) Uusi andmeid Eesti kliimast. Publicationes Instituti Geographici Universitatis Tartuensis 93:78–101 (In Estonian)

Kenney TC, Lau KC (1984) Temporal changes of groundwater pressure in a natural slope of nonfissured clay. Can Geotech J 20:138–146

Kohv M, Talviste P, Hang T, Kalm V, Rosentau A (2009) Slope stability and landslides in proglacial varved clays of western Estonia. Geomorphology 106:315–323

Kohv M, Talviste P, Hang T, Kalm V (2010) Slope failure in glaciolacustrine clay: Sauga landslide, Western Estonia. Geomorphology 124(3–4):229–237

Miidel A, Raukas A (2005) Slope processes at the North Estonian Klint. Proc Estonian Acad Sci Geol 54(4):209–224

Persson H (2008) Estimation of pore pressure levels in slope stability calculations: analyses and modelling of groundwater level fluctuations in confined aquifers along the Swedish west coast. Licentiate thesis, Chalmers University of Technology, Göteburg

Picarelli L, Urciuoli G, Russo C (2004) Effect of groundwater regime on the behaviour of clayey slopes. Can Geotech J 41:467–484

Simoni A, Berti M, Generali M, Elmi C, Ghirotti M (2004) Preliminary result from pore pressure monitoring on an unstable clay slope. Eng Geol 73:117–128

Spencer E (1967) A method for analysis of the stability of embankments assuming parallel interslice forces. Géotechnique 17(1):11–26

Van Asch TWJ, Hendriks MR, Hessel R, Rappange FE (1996) Hydrological triggering conditions of landslides in varved clays in the French Alps. Eng Geol 42:239–251

Van Asch TWJ, Malet J-P, Beek LPH, Amitrano D (2007) Techniques, issues and advances in numerical modelling of landslide hazard. Bulletin de la Societe Geologique de France 178(2):65–88

Triggering Factors of Landslides and Determination of Rainfall Threshold: A Case Study from North East India

Kuntala Bhusan and Dulal C. Goswami

Abstract

The North Eastern Region of India because of its relatively immature topography, fragile geologic base and active tectonics is vulnerable to landslide activities and the scenario is further accentuated due to various developmental activities. Almost one fifth of India's landslide prone areas are located in this region. Guwahati, a major city in North East India is one such fast developing city that falls under medium to high category of the Global Landslide Susceptibility Map. The hills of the city have slopes between 15° and 25° where numbers of landslide affected sites are scattered. Almost 50 % of the soil samples analyzed from landslide affected sites showed low strength of the soils. Compared to the global threshold, Guwahati needs less intensity of rainfall (I = 28.7 D-0.890) for landsliding. Moreover, change in land use over a period of 30 years shows correlation between hill slope alteration and increment in landslide incidences.

Keywords

Guwahati • Rainfall threshold • Plastic limit • Liquid limit • Land use

Introduction

North Eastern Region (NER) of India is a part of Extra-Peninsular region. The mountainous ranges exhibit oldest gneissic rocks (Archaean) to youngest boulder beds (Late Tertiary). The plain areas bordering the mountains, consists of fresh water and estuarine deposits of Mio-Pliocene age derived largely from the erosion of the rising Himalayas and recent alluvial deposits. Structurally, this region is marked by complex folds, reverse faults, overthrusts and nappes of large dimension along with numerous localized macro- and micro- structures (Krishnan 1982). This area is still active in terms of geological activities and all these make the region unique in terms of topography/physiography, geology, natural resources, as well as vulnerable to natural disasters. Global Landslide Susceptibility Map classified hilly regions of NER into medium to high and high category with few hotspot areas along the Himalayan foothills (Kirschbaum et al. 2009).

Landslides are of no concern if it takes place in uninhabited areas or if the related damage and casualties are less. But with increasing population, accelerated developmental activities, deforestation and related phenomena, many areas once considered to be safe are now becoming hazardous. Guwahati, the capital of Assam and a major city in NER is one such fast developing city. It is the gateway to the north-east of India and ranks 44 among the 5,230 urban centers of India. During the last three decades incidences of landslides in Guwahati city have increased alarmingly. However, it is also not possible to restrict developmental activities in hilly terrains. Proper understanding about causative and triggering factors of landslides in an area and their scientific management can only help in controlled hill slope development. The case study, illustrated in this paper is an integrated approach

K. Bhusan (✉)
Department of Space, North Eastern Space Applications Centre, Government of India, Umiam, Meghalaya 793103, India
e-mail: kuntalabhusan@yahoo.com

D.C. Goswami
Department of Environmental Science, Gauhati University, Guwahati 781014, India

C. Margottini et al. (eds.), *Landslide Science and Practice*, Vol. 4,
DOI 10.1007/978-3-642-31337-0_11,

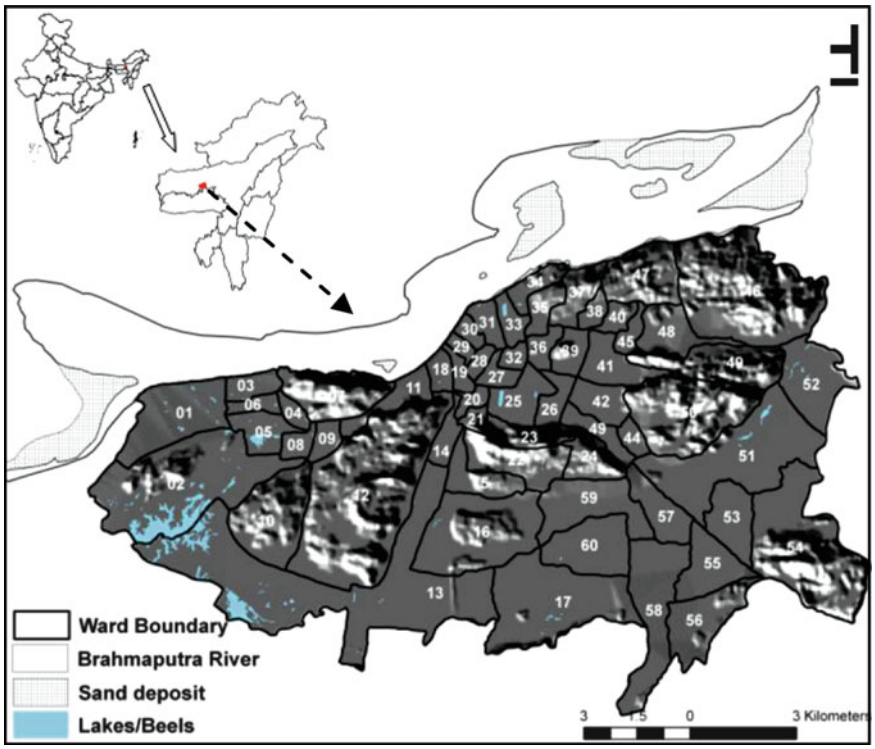

Fig. 1 Location map of the Guwahati city showing wards within municipal area

adopted to understand especially the triggering factors of landslide in Guwahati city. This will help in formulating a "working methodology" for landslide risk reduction in future.

Study Area Environment

The city is bounded by 26° 05′ N to 26° 10′ N latitude and 91° 30′ E to 91° 50′ E longitudes and is situated on the southern bank of the River Brahmaputra. The Guwahati Municipal Corporation (GMC) covers an area of 216.7 km^2 with 60 numbers of wards out of which 21 are either partially or fully hilly region (Fig. 1). Guwahati city is covered with recent alluvium with Archaean hillocks exposed at places (Nath et al. 2008). Physiographically, the area is divisible into three units consisting of low to moderately high denudational hill ranges, alluvial plains with few inselbergs and areas of negative topography represented by swampy or marshy lands and beels. The important hills of Guwahati city are, (1) Nabagraha-Sunsali hill series situated in extreme north eastern corner (2) Japorigog hill situated in the extreme east, (3) Sonaighuli-Jutikuchi situated in the south, (4) Narakashur hill in the east central (5) Kamakshya/Nilachal hill situated in west central, (6) Fatasil hill situated in south-west and (7) Jalukbari hill in the extreme south western corner of the city. The general trend of most of the hill ranges is E-W with slope amount varying between 15° and 25°. The dominant rock unit is Quartzo Feldspathic Gneiss (QFG) represented by granite gneiss and migmatite (Sarma and Maswood 1998), followed by Grey Porphyritic Granite which occur as massive boulders on the hill tops and slopes. Both QFG and porphyritic granites are highly jointed and four sets of joints trend in NE-SW, E-W, N-S, NW-SE directions. The joints dip at an angle from around 6° to almost vertical. In the study area every where some visible sign of rock weathering is seen and in general, weathering of porphyritic granite is very low compared to QFG. QFG is highly weathered and in many places already converted to lateritic soil.

Methodology

Under similar conditions of environmental set up, the spatial distribution of past (relict) and recent slope failures are the keys for predicting slope movements in future (Carrara et al. 1995). With this understanding, the study initiated with preparation of landslide inventory partly through the interpretation of high resolution remotely sensed data and partly in the field with the aid of GPS in consultation with history of landslide occurrences. The inventory reveals that hills are dotted with debris and complex slides which involve mainly overburden and top soils. Our preliminary investigation shows no valid correlation of earthquake incidences in triggering landslides. In fact, most of the landslides are triggered by rainfall. With this background present study aimed to carry out relevant geo-technical investigations of the soil samples collected from landslide areas to assess their inherent character and to establish rainfall threshold in

triggering landslide. The study also quantifies the land use changes over a period of 30 years.

Laboratory investigations of the soil samples were carried out following Indian Standard Methods of Test for Soils (IS: 2720, Part 5 1985; Casagrande 1958), to determine Liquid limits (W_L) and Plastic limit (P_L) and finally, Plasticity index (I_P) was calculated. Soil samples were collected from all the landslide affected areas to have a good coverage of the severely landslide affected hills and were subjected to pretreatment before laboratory investigations.

Good number of researches has been carried out to establish rainfall thresholds for landslides either on empirical or physical basis. The minimum or maximum level of some quantity needed for a process to take place or a state to change is generally defined as a threshold (White et al. 1996; Reichenbach et al. 1998). In the case of landslides and rainfall, however, the minimum intensity or duration of rainfall necessary to cause a landslide of shallow soil slips, debris flows, debris slides or slumps is known as the rainfall threshold for landsliding (Varnes 1978). Wieczorek (1996) defined rainfall threshold as rainfall intensity that facilitate slope instability for a given region. The main objective of the study is to identify the empirical triggering thresholds for the Guwahati city and for this study; debris slides and complex slides are considered not the rock falls. The method used in calculating rainfall thresholds is similar to that described by Caine (1980). Crozier (1997), however, pointed out that Caine's dataset did not include climatic events that did not trigger landslides, which is equally important (Larsen and Simon 1993; Deganutti et al. 2000). In this study also it is considered to be one of the limitations.

To estimate the land use changes particularly on hill tops and slopes two sets of land use/land cover maps were prepared, one set from SOI topographical maps of (78 N/12 and 78 N/16) of 1967 and 1968 reprinted in 1970 and the other set from remotely sensed data of IRS LISS IV MX of 27th December 2006 and 10th January 2007. Extents of hills and land use classes are demarcated from SOI toposheets and this map was then superimposed on satellite imageries followed by demarcation of modified areas. Accordingly change detection was carried out and area statistics were calculated.

Results and Discussion

Determination of Consistency Limits of Soil Samples

Soil, in an engineering sense is the relatively loose mass of mineral and organic material and sediments found above the bed rock, which can be easily broken down in to its constituent minerals or organic particles (Singh 2004). The laboratory investigation of soil samples was carried out to classify them based on their engineering properties and to establish a correlation between liquid limit and reported landslide incidences. The consistency limits (Liquid limit and Plastic limit) are useful for soil identification and classification and depends on both the type and amount of clay. Almost 50 % of the analyzed soil samples showed non plastic behaviour or had low values suggesting low strength of the soils of Guwahati city. This would mean an easy erodability of the soils under the action of flowing water and hence generation of debris.

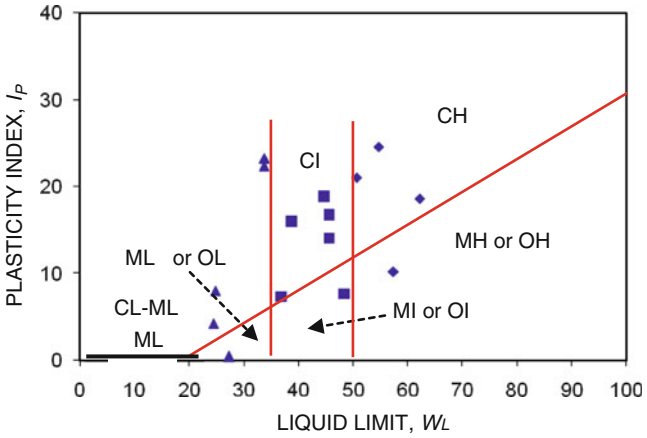

Fig. 2 Plasticity chart for fine-grained soil

Soil Classification

Various engineering classification of soils have been adopted throughout the world. The Indian Soil Classification (ISC) System adopted by the Indian Standards Institution (IS: 1498, 1970) is essentially the Unified Soil Classification (USC) system with modification in the classification of the fine grained soils only. The plasticity chart for fine-grained soil (Fig. 2) for Guwahati City, excluding the above mentioned non-plastic soils show scattered distribution thus indicating their variable composition from clays and mud of low plasticity to clays and mud of high plasticity.

Rainfall Threshold for Landsliding

In the present study, threshold was calculated based on empirical model, for that relationship between intensity-duration and antecedent and critical rainfall were analyzed, however relationship could be establish only in case of intensity-duration.

Intensity-Duration Relationship

Guwahati City has very poor database of landslide events as recorded, out of 31 landslide events, only 26 landslides were identified with respect to rainfall duration. Using the rainfall data corresponding to these a threshold relationship between

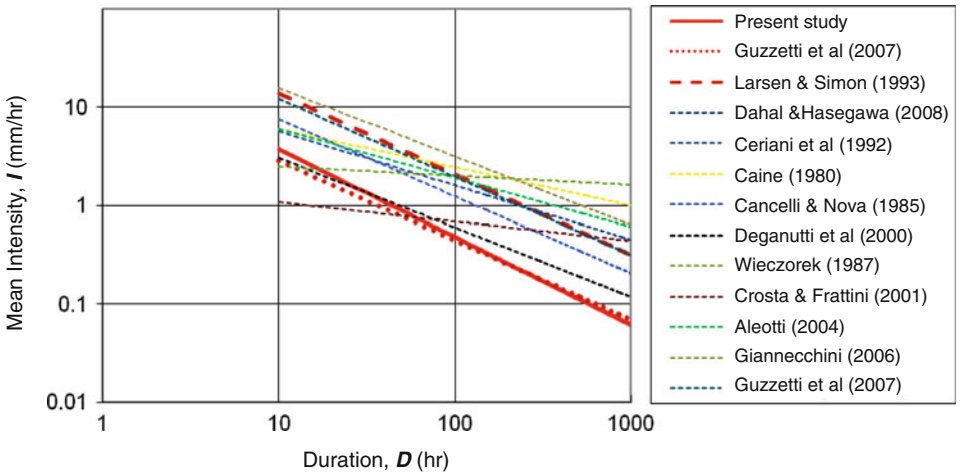

Fig. 3 Comparison of the landslide triggering rainfall intensity-duration threshold

rainfall intensity and duration for landsliding was established and is expressed as:

$$I = 28.7\ \mathrm{D}^{-0.89} \quad (1)$$

Where I is hourly rainfall intensity in millimeters (mm h^{-1}) and D is duration in hours. The (1) has a coefficient of determination of 0.7174.

According to this threshold relation for rainfall events of shorter duration such as < 10 h, a rainfall intensity of 6.0 mm h^{-1} is necessary to trigger landslides, while an average precipitation of less than 2 mm h^{-1} appears sufficient to cause landslide if continued for more than 100 h. Moreover, for continuous rainfall of more than 1 month, landslides may be triggered even by an average rainfall of less than 1 mm h^{-1} and this is quite possible during monsoon periods. When the calculated threshold is compared with some of these relations available in the literature (Fig. 3), it resembles that proposed by Larsen and Simon (1993) for humid tropical Puerto Rico but with a lower threshold value and similar curve inclination. Moreover, compared to the global threshold, Guwahati needs less intensity rainfall for landsliding; with increasing duration required rainfall intensity becomes much lesser than that of the global threshold. This may be attributed due to the geomorphological difference of the study areas. Guzzetti et al. (2007) reveal that inclination of the threshold lines generally depends on the climatic environment of the region. Guwahati is a tropical region with 1,620 mm average annual rainfall. Previous researchers point out that the thresholds defined by various researchers for mid-latitude (approximately 30°–60° north or south of the equator) climates are steeper (power value of D in between −0.70 and −0.81) than the thresholds obtained for the mountains and cold climates (power value of D in between −0.48 and −0.64). This observation also holds true for the calculated threshold in Guwahati, which lies in the tropical zone (26° 05′ N to 26° 10′ N latitude) and power of the obtained D is −0.89.

Table 1 Aerial distances of the hills from the rain gauge station

Name of the hill	Aerial distance from the rain gauge station (App. In Km.)
Kamakshya hill	14
Fatasil hill	13
Narakasur hill	19
Japorigog hill	24
Nabagraha hill	23
Sunsali hill	26

The major constrain in establishing rainfall threshold is the non availability of dense network of rain gauge stations near the landslide affected areas. Unfortunately, the study area has only one rain gauge station run by India Meteorological Department (IMD) Regional Office. Aleotti (2004) evaluated the importance of the distance of rain gauges. According to him a direct relation exists between the maximum difference in rainfall values and the distance between rain gauges, which is greater for distances lower than 10–15 kms and decreases for larger distances. For the present study this distance varies between 13 and 26 km. (Table 1).

Relationship Between Rainfall and Liquid Limit of the Soils

An attempt has been made to investigate the relation between rainfall and liquid limit of soils from the slide area. According to Campbell (1975), shallow storm- induced landslides require three conditions,

- A mantle of colluvial soil
- A steep slope, and
- Soil moisture equal to or greater than the liquid limit of the soil.

Table 2 Change in land use land cover over a period of 30 years

	Area of LULC classes			
	LULC during 1970		LULC during 2006	
Name of the hill	Settlements (%)	Quary (%)	Settlements (%)	Quary (%)
Kamakshya hill	22.82	0	49.72	0
Fatasil hill	0.2	0	47.07975	2.11
Narakasur hill	16.7	0	68.13	0
Japorigog hill	4.26	0	66.27	0.3
Nabagraha hill	31.91	0	87.21	0
Sunsali hill	0.68	0	48.05	0
Sonaighuli hill	0	0	83.78	0
Jutikuchi hill	6	0	9.3	69
Jalukbari hill (E)	13.67	0	20.96.	0
Jalukbari hill (W)	0	4.9	0	0

Hence keeping in view of the third condition cited by Campbell (1975), a relationship between rainfall and liquid limit was evaluated. For this two bivarient graphs were plotted- (1) Intensity of rainfall versus liquid limit of soils, and (2) Critical rainfall versus liquid limit of soils. Out of these two, intensity of rainfall versus liquid limit plot showed no correlation, while the cross plot between critical rainfall and liquid limit shows some correlation. But the correlation coefficient was only 0.45 hence, this result was not considered as convincing.

Changes in Land Use Pattern

The way how a community uses land at a given time could be defined as "Land use" and usage of particular land parcel is categorized by the socio-economic description or functional dimension of the land. In most cases the usage of land is decided by the owner considering its suitability for a particular utilization, convenience of the user, as well as social, economic and environmental factors. However, certain land uses can increase the possibility of landslide events while others can amplify the effect of triggering mechanism. In the study area also major changes in land use pattern is noticed over the period of 30 years which is again directly related to population growth in the city. According to 2001 census the Guwahati municipal area covering 216.09 km^2 area has a population of 8,09,895. Urbanization and economic growth has given rise to rapid migration of people to the city leading to an increased demand for free space. The houses are coming up even on the hill tops and slopes and also in the marshy lands surrounding beels. Previous studies shows that, 73 % of the Guwahati city area claimed by residential land use followed by public and semi-public land use 9.35 %, in industrial 4 %, commercial 5.3 %, recreational 0.4 % and mixed built up land 0.7 % (Goswami 1993). In the present study, area statistics of hill slopes which are modified due to various developmental as well as constructional activities and quarrying was calculated and a comparison was made to estimate the changes. It is found that almost every hill is altered during last three decades or so due to change in land use/land cover (LULC) practices. This change or alteration has taken place mainly due to construction activities (Table 2). A direct correlation between hill slope alteration and increment in landslide incidences are observed when compared with landslide inventory data since 1972.

Conclusion

This study is first of its kind to address triggering factors of landslides in Guwahati City. The soil analysis showed low strength of the soils which causes an easy erodability of the soils under the action of flowing water and hence generation of debris. The threshold value obtained from the Intensity-Duration relation indicates that compared to the global threshold, Guwahati needs less intensity of rainfall for landsliding; moreover with increasing duration required rainfall intensity becomes much lesser than that of the global threshold. However, threshold value was obtained with few limitations, for example, non availability of dense rain gauge network near the landslide affected areas, systematically recorded landslide information in terms of date and time and corresponding rainfall data etc. Change in land use/land cover of Guwahati city was also quantified. Approximately, 47 %, 55 %, 62 %, 83 %, 51 %, 26 %, 47 % and 7 % increase in settlement on hill tops or on slopes are observed for Sunsali, Nabagraha, Japorigog, Sonaighuli, Narakashur, Kamakshya, Fatasil and Jalukbari hills respectively for the period of 30 years. These data when correlated with number of landslide incidences reported from various hills of Guwahati since 1972, sharp increase in frequency of landslide occurrences in those hills are observed. During 1970s only one such incidence was reported from Nabagraha hill, while during 1980s and as well as in 1990s landslide incidences were reported

eight times in each decade. From 2000 onwards till 2008 landslide incidences reportedly increased 15 times. The city has recorded population growth of 51.36 % in the year 1971, 78.83 % in 1981, 29.51 % in 1991 and 38.79 % in 2001. Therefore, a combined effect of land use change resulting in hill slope alteration, thus exposing already low strength soil to rainfall triggers debris slide in the Guwahati city. Careful development and land use planning on hill slopes can reduce economic and social losses due to slope failures and also ensure sustainable development.

Acknowledgement Thanks are due to Dr S Sudhakar, Director, North Eastern Space Applications Centre, Umiam, Meghalaya, India for allowing us to publish this paper. Thanks are also due to Dr. J.J. Laskar, Asst. Prof. Dept. of Geological Sciences, Gauhati University, India for his guidance during sample collection and geo-technical analysis.

References

Aleotti P (2004) A warning system of rainfall-induced shallow failure. Eng Geol 73:247–265

Caine N (1980) The rainfall intensity-duration control of shallow landslides and debris flows. Geogr Ann 62(A):23–27

Campbell RH (1975) Soil Slips, Debris Flows, and Rainstorms in the Santa Monica Mountains and Vicinity, Southern California. Geological Survey Professional Paper 851, U.S. Government Printing Office, Washington, pp 1–20

Carrara A, Cardinali M, Guzzetti F, Reichenbach P (1995) GIS technology in mapping landslide hazard. In: Carrara A, Guzzetti F (eds) Geographical information systems in assessing natural hazards. Kluwer, Dordrecht, pp 135–175

Casagrande A (1958) Notes on the design of the liquid limit device. Geotechnique, London 8(2):84–91

Crozier MJ (1997) The climate-landslide couple: a southern hemisphere perspective. In: Matthews JA, Brunsden D, Frenzel B, Glaeser B, Weiss MM (eds) Rapid mass movement as a source of climatic evidence for the Holocene. Gustav Fischer Verlag, Stuttgart, pp 333–354

Deganutti AM, Marchi M, Arattano M (2000) Rainfall and debris flow occurrence in the Moscardo basin (Italian Alps). In: Wieczorek GF, Naeser ND (eds) Proceedings 2nd international conference on debris- flow hazards mitigation: mechanics, prediction, and assessment. American Society of Civil Engineers, Taipei, Taiwan, 67–72 Edition, Chapman and Hall, London, p 616

Goswami DC (1993) Assam's land resources- a satellite based ARSAC survey. Assam Science Society, Guwahati, pp 23–27

Guzzetti F, Peruccacci S, Rossi M, Stark CP (2007) Rainfall thresholds for the initiation of landslides in central and southern Europe. Meterology and Atmospheric Physics online first version. DOI 10.1007/sO0703-O07 -0262- 7. Accessed 7 Aug 2007

IS: 1498 (1970) Classification and identification of soils for general engineering purposes. ISI, New Delhi

IS: 2720 (Part 5) (1985) Methods of test for soils. Determination of liquid limit and plastic limit. ISI, New Delhi

Kirschbaum D, Adler R, Hong Y, Lerner-Lam A (2009) Evaluation of a preliminary satellite-based landslide hazard algorithm using global landslide inventories. Nat Hazard Earth Syst Sci 9:673–686

Krishnan MS (ed) (1982) Geology of India and Burma. CBS Publishers and Distributors, Delhi, p 536. ISBN 81-239-0012-0

Larsen MC, Simon A (1993) A rainfall intensity-duration threshold for landslides in a humid-tropical environment, Puerto Rico. Geogr Ann 75:13–23

Nath SK, Thingbaijam SKK, Raj A (2008) Earthquake hazard in Northeast India- a seismic microzonation approach with typical case studies from Sikkim Himalaya and Guwahati city. J Earth Syst Sci 117(S2):809–831

Reichenbach P, Cardinali M, De Vita P, Guzzetti F (1998) Regional hydrological thresholds for landslides and floods in the Tiber River Basin (central Italy). Environ Geol 35:146–159

Sarma KP, Maswood M (1998) Structure controlled mode of emplacement of pegmattite around Guwahati, Kamrup District, Assam. Indian J Geochem 13:25–32, ISSN 09709088

Singh A (2004) Modern geotechnical engineering, 3rd edn. CBS Publishers and Distributers, New Delhi/Bangalore, p 846. ISBN 81-239-0121-6

Varnes DJ (1978) Slope movement types and processes. In: Schuster RL, Krizek RJ (eds) Landslides, analysis and control, vol 176, Transportation Research Board special report. National Academy of Sciences, Washington, DC, pp 11–33

White ID, Mottershead DN, Harrison JJ (1996) Environmental systems, 2nd edn. Chapman and Hall, London, 616

Wieczorek GF (1996) Landslide triggering mechanisms. In: Turner AK, Schuster RL (eds) Landslides: investigation and mitigation, vol 247, Transportation Research Board, special report. National Research Council, Washington, pp 76–79

Changing Patterns in Climate-Driven Landslide Hazard: An Alpine Test Site

Audrey Bailles, Rosalie Vandromme, Nicolas Desramaut, Olivier Sedan-Miegemolle, and Gilles Grandjean

Abstract

The aim of this work is to develop a methodology for integrating climate change scenarios into quantitative hazard assessment and especially their precipitation component. The effects of climate change will be different depending on both the location of the site and the type of landslide considered. Indeed, mass movements can be triggered by different factors. This paper describes a methodology to address this issue and shows an application on an alpine test site.

The proposed approach is based on coupling a hydrological model (GARDENIA®) with a slope stability model (ALICE®), estimating safety factors spatially. From a DEM, land-cover map, geology, geotechnical data and so forth the program classifies hazard zones depending on geotechnics and different hydrological contexts varying in time. The methodology is applied to the Ubaye valley (France) using present and past climate conditions.

Keywords

Hazard • Landslide • Climate change • Hydrology

Introduction

In the next century climate change will lead to a modification of various meteorological parameters. The modifications of precipitation quantities and the variations in the spatial and temporal distributions of extreme events are some of the probable changes that should have an important impact on rainfall-induced landslides. However, development plans and mitigation measures are often designed for estimated impacts from hazard assessments based on past data and existing contexts, neglecting potential influences due to global change. These changes should be incorporated in the decision making process so that measures and plans will have longer validity.

In order to estimate the changing pattern of landslide activity, we present in the following a combination of models used to integrate these rainfall scenarios into quantitative landslide hazard assessments.

Models and Method

Models

GARDÉNIA

The GARDÉNIA® v.7.0 software package has been developed by BRGM for lumped hydrological modelling of rainfall–runoff and aquifer level (Thiéry 2003). The GARDÉNIA® model simulates the water cycle from rainfall received by the soil surface until the outlet, either as the discharge rate or as the aquifer level at a given point. The hydrological system is modelled by a system of three or four tanks (top tens of centimetres of soil, where evapotranspiration occurs; an intermediate level, where runoff occurs; and one or two aquifer zones, with delayed flows) (Fig. 1).

A. Bailles (✉) • R. Vandromme • N. Desramaut • O. Sedan-Miegemolle • G. Grandjean
BRGM, Risks division, 3 avenue Claude Guillemin, BP36009, 45060 Orléans Cedex 2, France
e-mail: a.bailles@brgm.fr

C. Margottini et al. (eds.), *Landslide Science and Practice*, Vol. 4,
DOI 10.1007/978-3-642-31337-0_12,

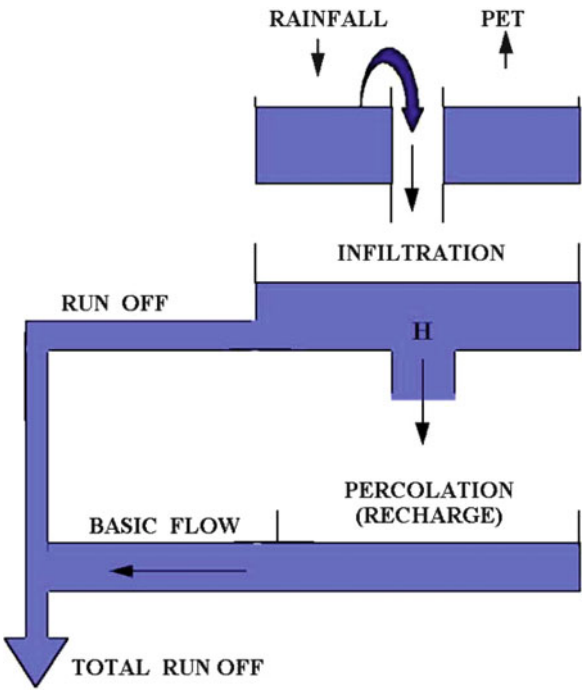

Fig. 1 Schematic representation of GARDÉNIA®'s operating principle

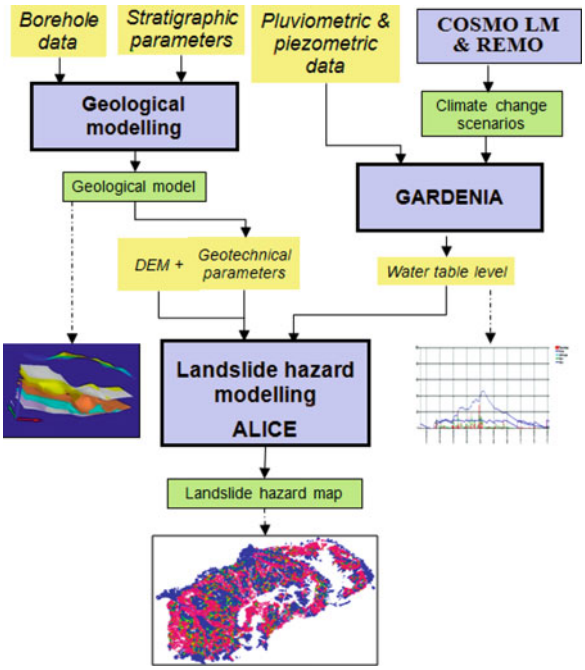

Fig. 2 Chain of the methodology for coupling the hazard assessment tool with the hydrological model

Hence, it allows the simulation of the relationships between series of:

- Discharge data of a spring or stream and rainfall amounts received by the corresponding basin; and
- Piezometric levels in an aquifer and amounts of rainfall received by the corresponding basin.

This modelling involves 4–6 lump parameters (soil and atmospheric characteristics). These parameters have to be calibrated using rainfall and water level data from past records.

ALICE®, Assessment of Landslides Induced by Climatic Events

ALICE® (Sedan 2011) is a software developed by BRGM whose main function is to produce landslide hazard maps, based on slope stability analysis, at various scales, from the single slope to hundreds of square kilometres. It was conceived as a tool within quantitative landslide risk assessment, which could be applied homogeneously on the whole French territory. Its principal components are:

- A finite slope stability model using the method of Morgenstern and Price (1967) applied at regular intervals of the 2D topographic profiles;
- A geographical Information System (GIS) since the software operates spatially; and
- The management of the variability and uncertainties of geotechnical parameters (through probability distributions).

The results are expressed either as a safety factor or a probability that this safety factor is below unity (instability).

A more detailed description of the software can be found in (Olivier et al. 2011, this issue).

In ALICE®, water in soil influences pore pressure. For the moment, the water component is simply introduced through the level of the saturated layer.

Method

The methodology proposed in this work is based on the coupling of both tools described above (Fig. 2).

1. GARDENIA converts meteorological inputs (either from past observations, current predictions or climate change models) into filling ratios of the different tanks.
2. The filling ratio of the intermediate tank is then converted to the level of the saturated layer into ALICE® using minimum and maximum piezometric maps. These maps are established thanks to piezometric data and SIG hydrological calculations weighted by experts.
3. ALICE® computes probabilistic distributions of the safety factor for each profile.
4. Susceptibility (equal to the probability of the safety factor being below unity) is mapped.

Hence, after a calibration phase for both tools, based on available observations of rainfall events, water table levels and historical landslides, this methodology computes an estimate of the susceptibility for rainfall-induced landslides that could occur at the regional scale. Meteorological events gather all information from forecasts for near-future events

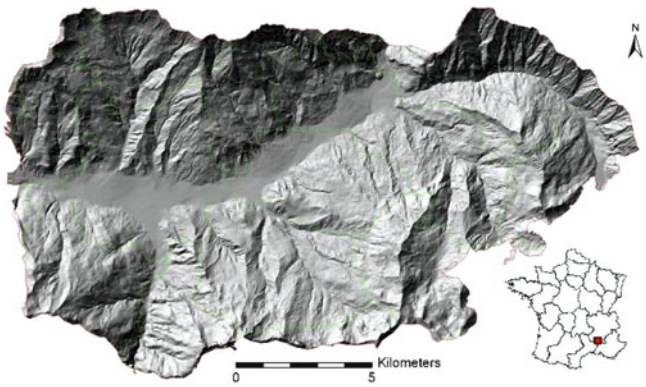

Fig. 3 Study area location

to scenarios from climate change models for further periods. This is particularly useful in evaluating changing patterns of landslide activities due to climate change.

Application to an Alpine Site: The Ubaye Valley

Site Presentation

The studied site is a 350 km zone, situated in the south of France in the département Alpes de Haute Provence around the municipality of Barcelonnette. It is located in a mountainous area, reaching altitudes of approximately 3,100 m, with an average altitude of 1,100 m, and it is crossed by the Ubaye River.

The Barcelonnette Basin is characterized by a asymmetric valley. The north-facing slope is characterized by allochtonous sandstones outcrops and autochthonous marls. Dominated by black marls covered by moraine deposits (2–20 m), its gentle slopes (10–30°) present an irregular topography with steep convex, planar and hummocky slopes. On the other side, the south-facing slope presents the steepest slopes (35–75°) which associated bar rocks on the upper part (45–75°), and screes on the lower part (35–50°). The lower slopes associates convex and hummocky slopes (15–30°) and are covered by moraine deposits (Malet 2003).

The landslide hazard is high in this area, the slopes being notably affected by severe gullying and both shallow and deep-seated large landslides (for example La Valette and Super-Sauze). Currently, many factors tend to make slopes unstable such as a dry and mountainous Mediterranean climate, with strong inter-annual rainfall variability (Fig. 3).

Data

Climate Data

The regional climate model REMO (Jacob 2001) provides basic information on possible future changes in the European climate until the end of the twenty-first century at a spatial scale of 25 km. These simulations have been carried out under the SRES emission scenario A1B within the European ENSEMBLES project. They have been used as boundary conditions of dedicated REMO simulations at a very high resolution of 10 × 10 km for the period 1950–2050 in the area of the Alps.

The second phase of the study consists in applying the non-hydrostatic COSMO Lokal Modell with a resolution of 3.8 × 3.8 km to the results of the REMO simulations. In this way, a physically consistent simulation of small scale climatic features, e.g., local precipitation extremes and other landslide triggering events, is possible and can be linked to geo-mechanical models used for high resolution case studies.

Geotechnical Data

A simplified geological model has been established from an engineering soil map (Thiéry 2007). For the first ALICE® runs, it has been decided to divide the area in ten different geotechnical zones. Each zone is represented by a soil column made of three layers called soil units (the lower one is bedrock). Each soil unit is characterized by its thickness and several geotechnical parameters such as friction angle, dry density and cohesion. Because laboratory tests do not always supply large-scale parameters some of them have been determined thanks to expert judgement. In a first step, constant values have been used (Fig. 4).

First Modelling Scenario

Before being able to use climate change data (COSMO Lokal Modell simulations were still running when the study began), the methodology was tested using three different water table scenarios. These scenarios cover the two extreme cases: the minimum water level (filling ratio = 0), corresponding to a drought period and the maximal one (filling ratio = 1), corresponding to period of heavy and lasting rainfall; and an average situation (filling ratio = 0.5). The safety factor calculation also needs the landslide type (rotational or translational) and its length. These parameters were defined for the whole studied area and, for now, only 50 m-rotational slides were considered.

Results

The whole chain was run with the three different filling ratios, providing three maps of safety factors (Fig. 5). These preliminary results show that, as expected, an increase of the water content of the soil (e.g. in our case due to a long period of rainfall) induces a reduction in the safety factor, and a decrease in the water level makes the slopes more stable. These changes are not uniform over the area. Effects of water-table changes are more pronounced on profiles with steepest slopes.

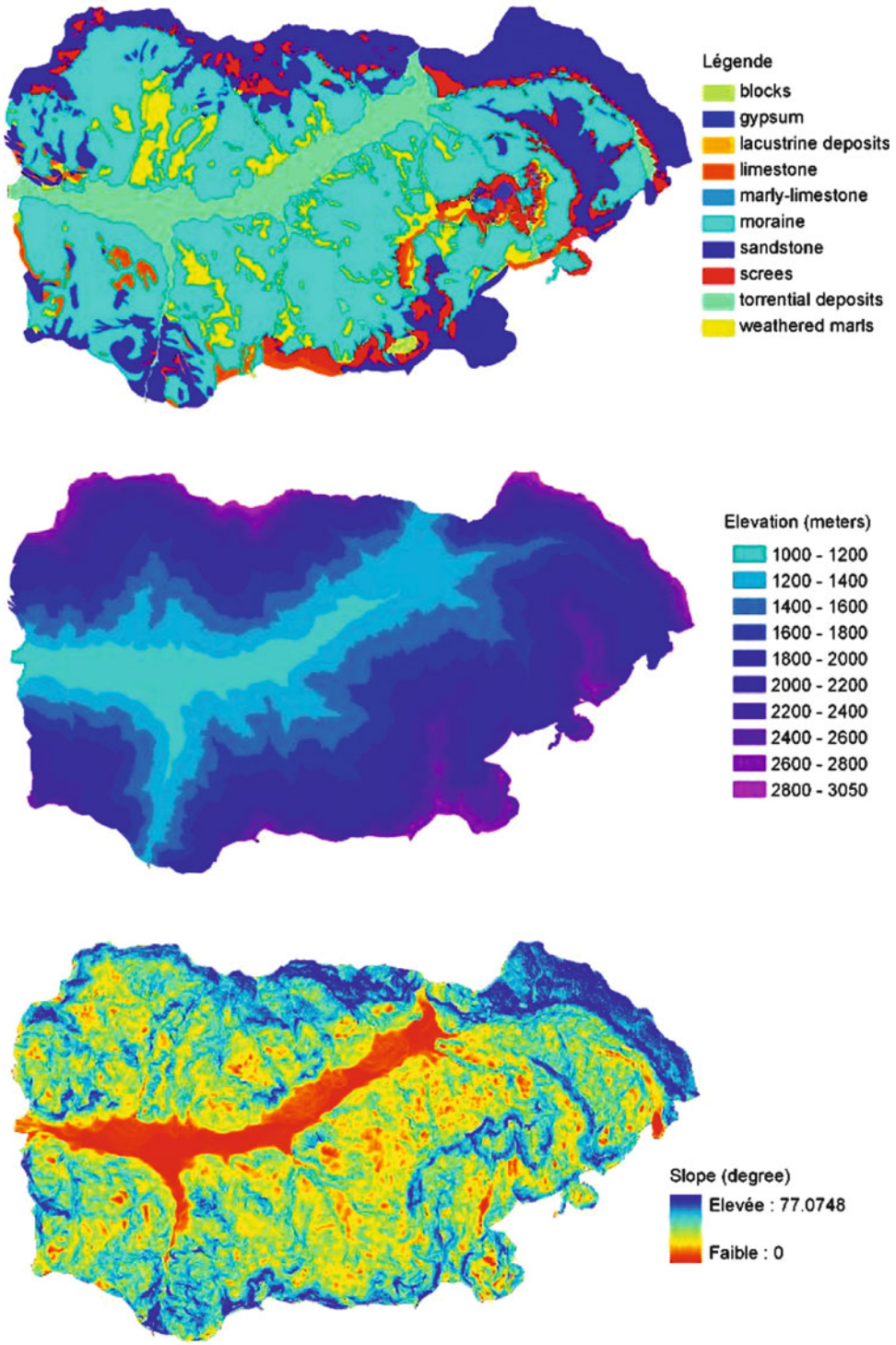

Fig. 4 Main data used in the model: geotechnical zones, elevation model (resolution: 10 m) and slope map (resolution: 10 m)

Conclusion and Perspectives

Dealing with risks requires an evaluation of what the future could be. Thus, changes in triggering factors have to be taken into account in hazard assessment, and not only qualitatively, but also quantitatively. In order to cope with this issue, a method was proposed here.

A hydrological model (GARDENIA®) is combined with a quantitative landslide assessment model (ALICE®) to allow the integration of climatic scenarios into landslide susceptibility mapping.

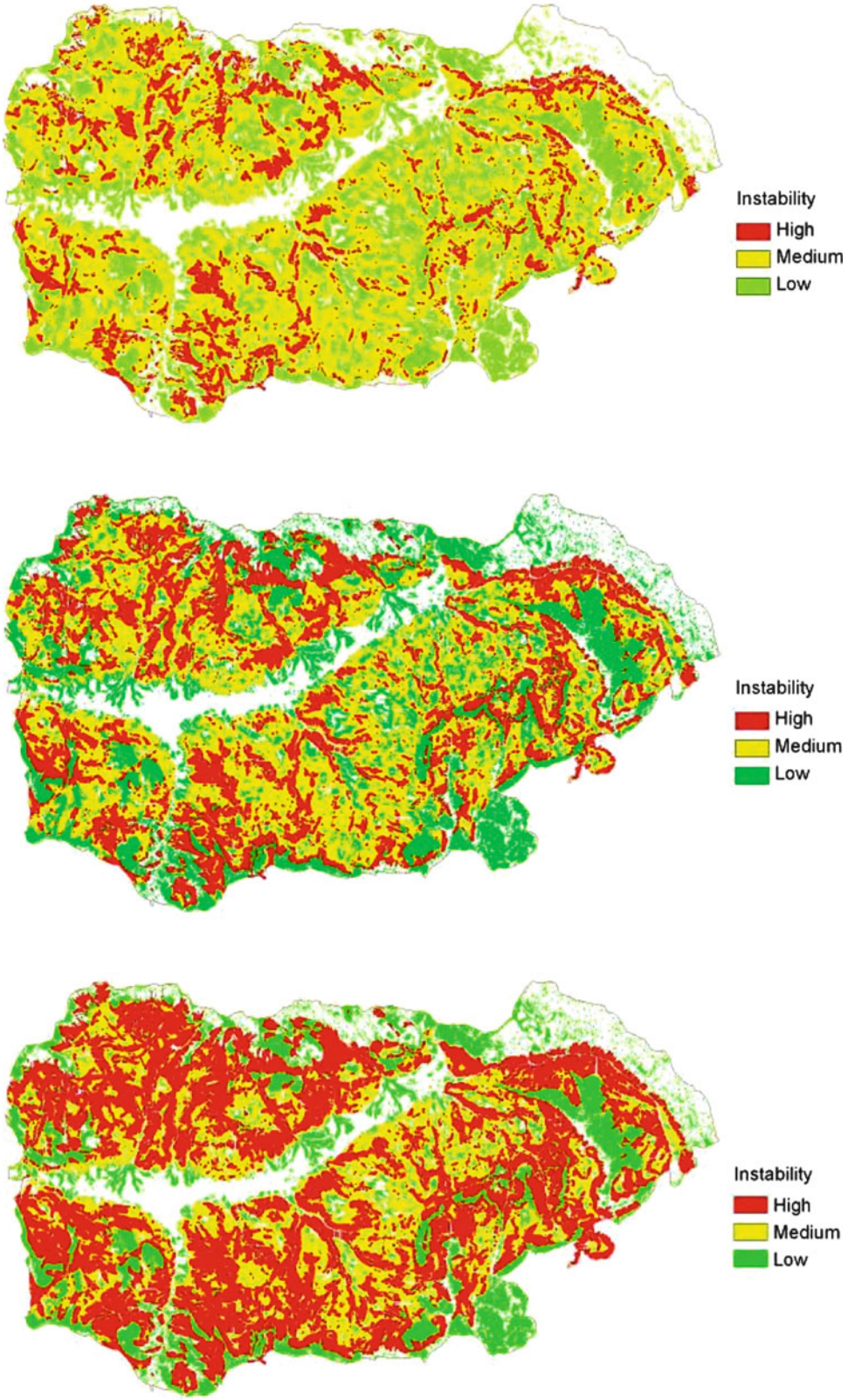

Fig. 5 Representation of instability resulting from the simulations using the three different filling ratios. The ratio is 0 (*top*), 0.5 (*middle*) and 1 (*bottom*)

The results presented here are only preliminary results and were shown to demonstrate the feasibility of the method. In the near future, the following developments will be presented.

- Uncertainties and variability of the geotechnical parameters would be quantified thanks to probabilistic distributions.
- Monte Carlo simulations will be performed to provide probabilistic information on safety factors.
- The hydrogeological model will be completed, taking into account the unsaturated part of soils.
- Analysis will be done for the different types and lengths of landslides, which occur in the area.
- Geotechnical models will be refined.
- Climate change data will be used to evaluate changing patterns of landslide activity.

Acknowledgments The geotechnical data were provided by Jean-Philippe Malet from CNRS, France, and climatic data were provided Pasquale Schiano from CMCC- Centro Euro-Mediterraneo per I Cambiamenti Climatici s.c.a.r.l, Italy, in collaboration with MPG – Max Planck Gesellschaft zur Förderung der Wissenschaften e.V., Germany. The SafeLand project is co-funded by BRGM and the European Commission under the 7th Framework Programme for Research and Technological Development, Area "Environment", Activity 1.3.3.1 "Prediction of triggering and risk assessment for landslides".

References

Jacob D (2001) A note to the simulation of the annual and interannual variability of the water budget over the Baltic Sea drainage basin. Meteorol Atmos Phys 58(1–4):61–74

Malet JP (2003) Les 'glissements de type écoulement' dans les marnes noires des Alpes du Sud. Morphologie, fonctionnement et modélisation hydro-mécanique. Ph.D. thesis, Université Louis Pasteur, Strasbourg

Morgenstern NR, Price VE (1967) A numerical method for solving the equations of stability of general slip surfaces. Comput J 9:388–393

Olivier M, Sedan O, Monod B (2011) Contribution of physical modeling to landslide hazard mapping: case of the French Basque coast. In: Proceedings of the 2nd world landslide forum, Rome, Italy, 3 Oct 2011 (this issue)

Sedan O (2011) Logiciel ALICE version 7 – Guide Utilisateur. BRGM report. RP-60004-FR. 31 p

Thiéry D (2003) Logiciel GARDÉNIA version 6.0 – Guide d'utilisation. BRGM report. RP-52832-FR. 104 p

Thiéry Y (2007) Susceptibilité du Bassin de Barcelonnette (Alpes du sud, France) aux 'mouvements de versant': cartographie morphodynamique, analyse spatiale et modélisation probabiliste. Ph.D. thesis, Université de Caen, Caen

Recent Landslides with Economical and Human Losses in Medellin City (Colombia)

Edilma Gómez and Manuel Villarraga

Abstract

Medellin has shown in recent years extraordinary weather conditions that triggered various slope instability processes. These processes resulted in economic and numerous human casualties. This document describes the most relevant processes analyzed by INTEINSA for public entities. The causes of processes and their relationship to uncontrolled human intervention in the city are presented.

Keywords

Alluvial deposit • Antrophogenic interventions • Complex conditions • Landslide deposits and anthropic (manmade) fills

Introduction

There have been several landslides during rainy seasons of recent years in Medellin, which left significant economic losses and a number of deaths and missing persons.

Local entities like "Empresas Públicas de Medellín", "Secretaría de Obras Públicas de Medellín" and "Sistema Municipal para Prevención y Atención de Desastres" hired INTEINSA to assess the causes related to each instability process and to design mitigation and stabilization works.

Studies made by INTEINSA established that anthropogenic interventions have been the most important triggering factor (INTEINSA 2008a–c, 2011). There are complex geotechnical, geological and hydrological conditions, in addition to the recent extraordinary climatic conditions, specifically the highest rain intensity of the last 60 years. However, human intervention via fill construction on small creeks and adjacent drainage areas, construction of fills on hillsides and steep slopes, and an inadequate geometry of cut slopes have been decisive aspects in generating numerous landslides in Medellin.

This paper presents a brief description of some of the most important landslides occurred within the past 3 years in Medellin and studied by INTEINSA. General descriptions and particular causes are presented along with the stabilization remedies recommended and designed by INTEINSA. Finally, an analysis of the causes of landslides is presented, in which we emphasize the urgent need of a more orderly and controlled intervention in the city, and the execution of technical studies in accordance with the complex natural conditions of the city.

General Conditions of Medellin

Medellin is the capital of the state of Antioquia, located on the northwest region of Colombia. The continental territory of the Republic of Colombia is located on the northwest corner of South America, on the equator, and in a tropical environment.

Medellin and the municipalities of Caldas, La Estrella, Sabaneta, Envigado, Itagüí, Bello, Copacabana, Girardota and Barbosa make the Metropolitan Area of the Aburra Valley (Fig. 1) (Alcaldia De Medellin 2006).

E. Gómez (✉) • M. Villarraga
Ingeniería, Tecnología e Instrumentación S.A. (INTEINSA), Calle 8B No. 65-131, Medellín, Colombia
e-mail: inteinsa@inteinsa.com

C. Margottini et al. (eds.), *Landslide Science and Practice*, Vol. 4,
DOI 10.1007/978-3-642-31337-0_13,

Fig. 1 The Aburra valley

The Aburra Valley covers an elongated depression with and area of 1,154 km and is surrounded by a system of high mountains. The valley narrows to the south, it extends at the center in Medellin widening to about 7 km, and narrows again to the north in Copacabana. Elevation variations are important, and while the valley is at an average elevation of 1,538 m above sea level, the top of the mountains surrounding the valley can reach up to 3,000 m in the highlands of San Miguel, Padre Amaya and Boqueron.

The valley has a wide variety of lithologies, ranging from Paleozoic rocks to Quaternary deposits. In relation to the origin and composition, there are metamorphic rocks, such as schists, amphibolites, migmatites and gneisses; igneous rocks, such as granodiorites, dunites, gabbros and basalts; volcanic sedimentary rocks; alluvial deposits and landslide deposits, in addition to manmade fills. Rock units, alluvial deposits and landslides deposits created complex weathering profiles that include residual soils of varying thickness with individual characteristics, weathered rock and bedrock.

Medellin was originally sited on the valley, which corresponds to very flat surfaces dominated by alluvial deposits and lacking problems related to geomorphological conditions. City development brought high urbanization rates within the valley and forced many people to live on areas where geomorphological conditions are unacceptable. Such conditions range from steep natural slopes to presence of weak materials (landslides deposits and poorly engineered fills).

Medellin River enters the valley at "Alto San Miguel", municipality of Caldas, at about elevation 2,700 m, and crosses the Central Mountain Range to join the Riogrande River. At this point it is called Porce River and continues north to join the Nechi River. Finally, it arrives to the Cauca River. The length of Medellin River is 100 km from its source until it merges with Porce River. Medellin River receives water from about 200 direct tributaries and through them, more than 352 creeks which constitute the Medellin River basin.

Fig. 2 Landslide at El Socorro neighbourhood

Recent Landslides

Landslide of Manmade Fill Located at El Socorro Neighborhood

This landslide occurred on May 31, 2008, in the neighborhood known as El Socorro.

The area affected by the movement corresponds to a depression of land used illegally to accumulate construction debris. The landslide occurred during the first rainy season of 2008, following a rainfall of 83 mm in 2½ h. Movement started as rotational landslide, but later became a debris flow (Fig. 2). It traveled a distance of 180 m and the involved a volume of nearly 50,000 m^3. The first movement was directed towards the bottom of the slope and then continued in a horizontal curve. The landslide process involved exclusively the construction debris of manmade fill, which suggests that the foundation material was not part of the problem.

Geological, geotechnical and hydrologic assessment of the area allowed us to find the following causes of the landslide: construction of the fill on an old drainage basin, lack of stripping and drainage works, high precipitations and run-off contributions reaching the old basin.

The solution recommended by INTEINSA was to change the geometry of the fill by implementing a template of 10 m height and 2.0 H:1.0 V slopes. In addition, lowering of the water table by constructing a filter/drainage layer, a series of subhorizontal drains, and ditches on each berm. A reinforced earth wall was recommended to contain the construction debris at the toe. Soil nailing with a minimum length of 23 m was advised to stabilize the head scarp. Finally, run off water was managed by a system of surface drains.

Fig. 3 Landslide at Alto Verde condominium

Landslide on Slope of Alto Verde Condominium

This landslide occurred in November 2008, during one of the heaviest rainy seasons in recent years. It happened on an engineered slope designed to fit the Alto Verde Condominium, which is located in one of the most exclusive neighbourhoods in Medellin.

Mobilized material shown in Fig. 3 comprised a volume of 15,000 m^3, leaving a balance of six houses destroyed and 12 deaths. Each house had a built area of 200 m and was properly engineered with good specifications, formed with frameworks and unreinforced masonry, and supported on deep pile foundations.

The landslide occurred in an area where geological, geomorphological and hydrological conditions have generated controversy in recent years. The area corresponds to hillsides with medium steep to very steep slopes, developed on landslide deposits (with low shear resistance) and has numerous drainage tributaries to the Medellin River. However, the area has been affected by uncontrolled urban development without adequate pre-treatments. In various cases, presence of underground flows covered by landslide deposits creates serious problems for urban development.

The geological assessment was crucial because it showed that landslide occurred on residual soils derived from weathering of breccia and not on the landslide deposits (mud flows and debris). Hence, the initial hypothesis of the presence of underground flows was ruled out.

The landslide was a local problem and it was mainly associated with a slope of inadequate geometry. Run off infiltration and the accidental overflow from a water storage tank at the top of Alto Verde Condominium favored the gradual deterioration of materials until failure occurred. Low permeability materials caused infiltrated water to be held in the soil mass for long periods of time, and encouraged saturation while reducing the shear strength. The dispersive nature of the soil also contributed to the failure.

The recommended solution was to construct a concrete wall supported by 20 m long piles and changing the geometry of the slope in the area behind the wall. Additionally, ditches and channels discharging into natural water sources were recommended. It was also recommended not to rebuild the tank at the top of the failed slope.

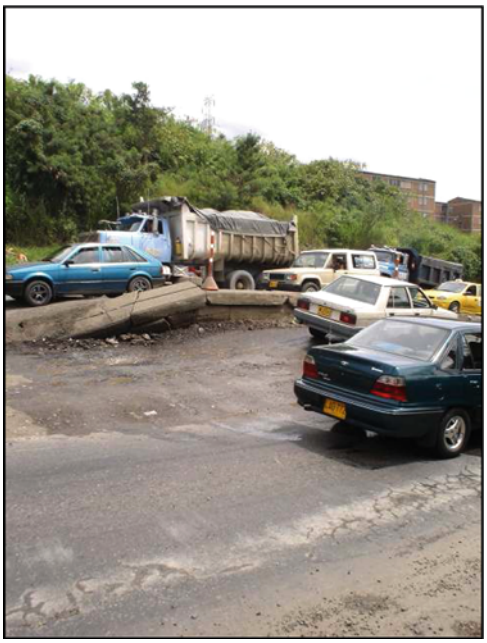

Fig. 4 Landslide in manmade fill of Northern Freeway

Landslide in Manmade Fill of Northern Freeway

This landslide occurred in 2008 in a manmade fill (of construction debris) placed near the Northern Freeway, which connects Medellin with the capital of Colombia (Bogota). The study determined that it was a 12 m thick fill on top and 4 m at the toe, founded on a sloped deposit with very low shear strength characteristics.

Field observations and slope stability analyses revealed that this process corresponds to a landslide with rotational failure involving the fill and foundation material (Fig. 4).

The volume involved was 25,000 m^3. The movement produced severe damage to 100 m of road, seriously affecting its safety and operation. A traffic accident caused by the sudden lifting of the road left three deaths and damages in water and sewage pipes running through the base of the fill.

The fill was constructed on a foundation with low shear strength, obstructing the drainage located south of the site and without a proper drainage system. These factors and high precipitation occurred during the first half of 2008 produced loads that exceeded the residual soil strength which in turns triggered the landslide.

The recommended solution was change in geometry of fill, lowering the water table with filters/drains and gutters at the top of the slope and a retaining structure together with a filter system at the toe.

Landslides at La Heliodora Creek

These landslides occurred at La Heliodora creek between the neighbourhoods of Bosques de San Rafael and Mediterranean Condominium, both in Envigado. Since 2009 there has been a recurrent destabilization process affecting nearby houses and sewer pipes running along the left bank of the creek. The area of study has approximately 50 morphodynamic processes, including small movements that mobilized less than 1,000 m^3, to much larger movements that mobilized up to 10,000 m^3.

Morphodynamic processes correspond to landslides caused by human intervention through fills, creek bed occupancy by houses reducing the hydraulic section, discharges from new developments and buildings that changed the hydrological and hydraulic conditions of the area, as well as lateral and bottom scour on the creek. Landslides are produced by loss of passive load due to scour in the channel, and increasing active loads with manmade fills on the banks of the channel.

Occupation of the channel reflects an uncontrolled population growth, which today presents formal housing development via special permits, and informal structures corresponding to illegal occupation of the creek banks. Regardless of the type of occupation, they generally contribute to instability processes.

A longitudinal analysis was conducted for the study of these landslides along the creek. A staged study was carried out by overlapping area maps from different years (70s and 90s) with topographic information from 2010. By comparing the maps of several years, the population growth on the banks of "La Heliodora" creek became evident (Fig. 5). This growth often resulted on the invasion and disappearance of existing drains, factor by which the fills are saturated and cause landslides in the area. Also, manmade fills and a change on the hydrological conditions of the creek have deepened the channel and generated strong variations in its natural path, promoting instability problems involving a parallel collector pipe.

Figure 6 shows some of manmade fills constructed on the banks of La Heliodora creek. Fills and houses, and clogged drains cause strangulation of the stream and accelerate downstream scour processes (Fig. 7). The scouring triggers additional morphodynamic processes.

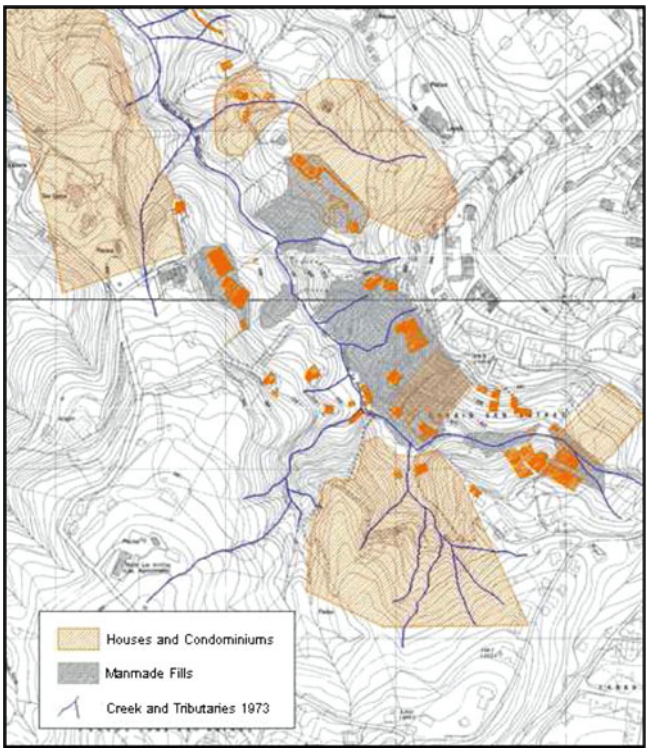

Fig. 5 Multitemporal analysis on La Heliodora creek

Fig. 6 Manmade fills in La Heliodora creek

Analysis of Causes

Recent landslides in Medellin originated on a very complex technical environment, involving convoluted geological, geomorphological and hydrological aspects.

From the geological point of view, the variety of lithologies creates a very intricate environment comprised of complex residual soils and landslides and alluvial deposits with heterogeneous characteristics. These characteristics make field and laboratory identification and characterization, and reliable modelling of processes a very challenging task.

An example of the complexity of residual soils can be seen in the landslide of Alto Verde Condominium. Figure 8 shows the values friction angle and cohesion obtained from samples taken on the failed slope. Particularly striking is the

Fig. 7 Scour in La Heliodora creek

Fig. 9 Discontinuities in La Palencia creek

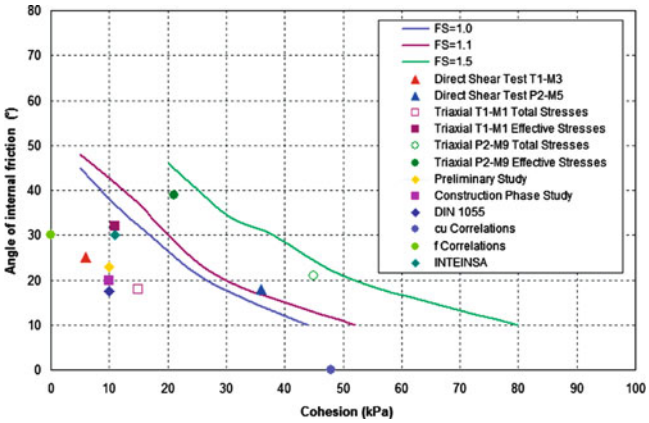

Fig. 8 Static slope stability analyses for the landslide at Alto Verde condominium

Fig. 10 Discontinuities in La Blanquizala creek

wide variation in both cohesion and the friction parameters, even though it is the same material with the same degree of weathering. The main question in cases like this is how many shear strength tests and of what type should be executed to obtain truly representative parameters of the material. To solve this problem, in addition to a significant number of trials, we recommend the use of graphics as shown in Fig. 8. It shows the variation of the factor of safety to different combinations of cohesion and friction angles. In this case, these plots helped to determine that the majority of cohesion and friction angle combinations measured resulted in poor safety factors. This approach also provides the engineers with ranges of values to solve the geotechnical problems, instead of a unique set of values.

Also from the geological point of view, the presence of discontinuities in weathered and non-weathered materials can precipitate different failure mechanisms of many slopes. When this factor combines with the hydrologic circumstances (consisting in the presence of many natural drainages restricting the available areas for urban development) the situation is worsened. Figures 9 and 10 show this problem in two creeks located to the east of Medellin. Landslides on the right bank of the creeks occurred due to loss of passive support, the presence of unfavorably oriented discontinuities in the direction of water flow and scouring of the creek bed. In the case of the La Palencia creek the problem was in the bedrock while La Blanquizala creek presented problems in saprolite. This indicates that scouring is not exclusive to weak materials.

From the geomorphological point of view, many landslide deposits are located in areas of medium to low slope, attractive for urban development, with poor conditions of

Fig. 11 Invasion of La Carevieja creek with manmade fills

Fig. 12 Scour at La Blanquizala creek

stability (metastable conditions), and are generally comprised of materials with very low shear strength. The high rate of urbanization of the valley forced many people to live on these hazardous areas. This situation is triggering landslides and increasing the impact of natural disasters.

On the other hand, the rainfall conditions in recent years in the Aburra Valley have been the most dramatic of the last 60 years.

As indicated above, there are very complex natural conditions. Unfortunately, an inappropriate human intervention has also brought unintended consequences.

Detailed analysis of Medellin River shows a chaotic situation: clogged and polluted drains and buffer areas occupied by recent home developments. The landslides at El Socorro neighborhood, at the Northern Freeway and along La Heliodora creek are examples of consequences generated by the construction of fills which clog drains with inadequate pre-treatment. Another examples are the landslides on the banks of La Carevieja creek (Fig. 11) caused by the construction of fills on the creek banks.

The landslide at La Blanquizala creek shown in Fig. 12, was aggravated by a box culvert strongly scouring the outlet. In these cases, the energy of the water creates lateral and bottom scour problems and usually generates significant instability processes.

Similarly, the inadequate soil exploration, in type and amounts, as well as a lack of absolute respect for technical studies has lead to disasters. The landslide at Alto Verde Condominium is an example of this. The slope was built improperly using a material not meeting the minimum required shear strength to obtain a safe final template.

The discussed complexity of the soils in Medellin is especially important because the city is located in a developing country where investments for development infrastructure are very limited. In addition, social problems have led to a very disorganized development of the city, especially on hillside areas where the problems are much more dramatic.

Conclusions

The root causes of the recent landslides in Medellin are diverse. The city has very complex geological, geomorphological and hydrological conditions, and rainfalls have become heavier in recent years. However, human intervention is not coping well with this complexity and has aggravated and generated massive landslides. Consequently, the city has incurred in extra costs, lost lives, and continues to find proper solutions to these problems.

On the other hand, considering the occurrence of large-scale rainfall in recent years, engineers should see that climate changes and its effects are testing infrastructure built in recent years. The damage to the waste water system along La Heliodora creek is an example of this. For this reason, engineers should think about the needs for more demanding technical studies. For instance, engineers should question the return period to be considered for designs given such complex conditions. Should the design criteria be considered similar to much more demanding projects (e.g. nuclear power plants, dams, etc.)? Are state entities willing to modify construction criteria for new projects, adapted to the changes we are experiencing?

The professionals responsible for technical studies cannot overlook the poor practices of some urban developers, and cannot become careless of local problems. Though many efforts are being made for drastic and definitive solutions by municipalities and universities in the city, efforts must be made to work together to reach more interdisciplinary and complete final solutions. “Good practice” assumes that the following aspects are always covered:

Geological: This aspect should cover lithology, tectonics, hydrogeology, structure and geochemistry.

Geotechnical: Exploration of the subsoil must be suitable, and an adequate material characterization should be carried out by appropriate and sufficient field and laboratory tests. Continuum mechanics should be considered. Discontinuities analysis and modeling with adequate methods should be used. Several tools of easy application should be implemented in areas affected by previous human interventions: longitudinal analysis (consisting of overlapping surveys of previous processes to the existing area maps) to help determine causes of landslides, anthropogenic interventions and blocked or diverted drains, among others.

Building: The most appropriate methods and those currently available should be considered in the solutions. Risk management should also be taken into account (Grupo de Sismologia de Medellin, 1988). Procurement laws and the issue of insurance claims should be considered within the assessments to be made.

Acknowledgments The authors wish to express their gratitude to all involved government agencies: "Empresas Públicas de Medellín", "Secretaría de Obras Públicas de Medellín", and "Sistema Municipal para Prevención y Atención de Desastres" for commissioning INTEINSA to develop the analysis of the most controversial landslides in recent years in Medellin.

References

Alcaldia De Medellin (2006) Plan de Ordenamiento Territorial de Medellín. Acuerdo 46 de 2006

Grupo de Sismologia de Medellin (1988) Microzonificacion Sısmica del Valle de Aburrá

INTEINSA (2008a) Informe Final Estudio Deslizamiento Urbanizacio´n Alto Verde. Noviembre de 2008

INTEINSA (2008b) Informe Final Estudio Deslizamiento Botadero Barrio El Socorro. Noviembre de 2008

INTEINSA (2008c) Informe Final Estudio Deslizamiento Autopista Norte. Noviembre de 2008

INTEINSA (2011) Informe Final Problema´tica Quebrada La Heliodora. Mayo de 2011

Informe Final Estudio Deslizamiento Urbanización Alto Verde. INTEINSA. Noviembre de 2008

Informe Final Estudio Deslizamiento Botadero Barrio El Socorro. INTEINSA. Noviembre de 2008

Informe Final Estudio Deslizamiento Autopista Norte. INTEINSA. Noviembre de 2008

Informe Final Problemática Quebrada La Heliodora. INTEINSA. Mayo de 2011

Plan de Ordenamiento Territorial de Medellín. ALCALDÍA DE MEDELLÍN. Acuerdo 46 de 2006

Analysis of the Rainfall Preceding the Activation of the Large Maierato Landslide in 2010

Angelo Doglioni, Annalisa Galeandro, Alessandro Guerricchio, Gerardo Fortunato, Elena Guglielmo, Maurizio Ponte, and Vincenzo Simeone

Abstract

This work focuses on the impact of the antecedent rainfall as triggering factor of the large landslide occurred in Maierato (south Italy) on February 15, 2010. According to previous studies by Guerricchio et al. (Tecniche per la difesa dall'inquinamento – 31° Corso di aggiornamento, pp 661–706, 2010) the predisposing factor of the landslide is an ancient deep-seated gravitational slope deformation that significantly affected landforms, drainage networks and infiltration processes of the whole slope where Maierato is located. Here after a brief introduction of the landslide according to the aforementioned study, a hydrological analysis of the rainfall preceding the landslide is presented. The analysis aims at evaluating the exceptionality and some peculiar characters of rainfall, which may be considered among the triggering factors of the landslide.

Keywords

Rainfall and landslide • Hydrological analysis for landslide • Maierato landslide • Large landslide • Calabria region

Introduction

A large landslide occurred on February 15th 2010, close to the town of Maierato, Calabria, south-west of Italy (Figs. 1 and 2). The landslide was preceded by a long sequence of deformations at its toe. When the landslide occurred, the area was surveyed and a really impressive video showing the evolution of the landslide was taken (Tg24.sky 2010), which attracted the attention of a lot of researchers (Guerricchio et al. 2010; Scesi and Gattinoni 2010; Comerci and Di Manna 2010; Antronico et al. 2010). According to the previous study by Guerricchio et al. (2010), the site was characterised by landslide predisposing factors related to an ancient deep-seated gravitational slope deformations (DSGSD) and old landslides partially due to the severe 1783 earthquake, affecting the surface hydrology and the geomorphology of the investigated area (Cotecchia et al. 1986).

The landslide occurred after a period of abundant rainfalls, which may constitute the triggering factor, also because 2009–2010 winter was very rainy, as well as the previous one. Here the analysis of the antecedent rainfall events is undertaken using specific hydrological techniques, in order to show the exceptionality and some peculiar charters of the rainfall before the landslide as triggering factors. The analysis was developed on the base of the daily rainfall data from Vibo Valentia raingauge station, where daily rainfall data are available since 1920.

A. Doglioni (✉) • A. Galeandro • V. Simeone
Engineering Faculty of Taranto, Technical University of Bari, viale del Turismo 8, Taranto, Italy
e-mail: a.doglioni@poliba.it

A. Guerricchio • G. Fortunato • E. Guglielmo
Soil Defense Department, University of Calabria, Ponte Pietro Bucci, Arcavacata di Rende (Cosenza), Italy

M. Ponte
Earth Science Department, University of Calabria, Ponte Pietro Bucci, Arcavacata di Rende (Cosenza), Italy

C. Margottini et al. (eds.), *Landslide Science and Practice*, Vol. 4,
DOI 10.1007/978-3-642-31337-0_14,

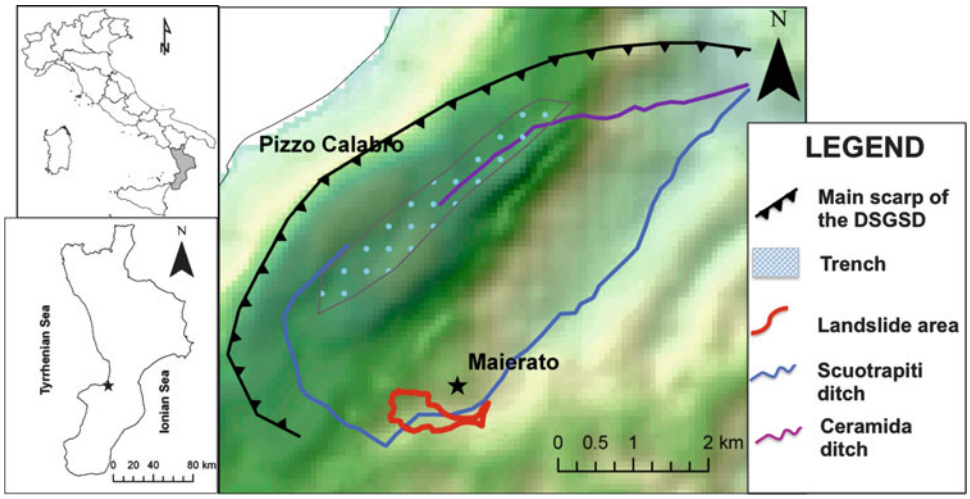

Fig. 1 Overview of the site of the landslide

Fig. 2 Overview of Maierato landslide (Picture by Doglioni 2010)

Geological Description of the Site of Maierato

According to the Calabria geological map Cassa per il Mezzogiorno (1971), the stratigraphic sequence of Maierato area is characterized by the Palaeozoic metamorphic bedrock. Upon this bedrock, there is a sequence of middle Miocene coarse sands, clays, silty-clays and silts directly transgressive on the crystalline base. Upon these rocks, there is a unit of upper-middle Miocene yellowish-white evaporitic limestones, with some calcarenites, up to 45 m thick, interlayered by narrow silts and silty clays. Upon the limestones, a lower-middle Pliocene layer of silty-clays and silts, locally interlayered by coarse sands exists and Pleistocene continental deposits, mostly made by gravel and pebbles, top the stratigraphic sequence.

Due to the tectonic uplift, a complex of direct faults, mainly oriented NE-SW, originated the asymmetric horst, which separates the Tyrrhenic steep side of Pizzo Calabro, from Maierato side (Fig. 1). This is gently sloping and affected by several landslides (Regione Calabria 2001). According to Guerricchio et al. (2010), the slope is disturbed by a huge ancient DSGSD affecting the morphology of the area and pushing the activation of several landslides in the area. The DSGSD is characterized by a relevant movement of large masses from NW to SE, where the main break goes NE-SW and creates the trench associated with the upper part of Ceramida and Scuotrapiti ditches (Fig. 1). Scuotrapiti ditch shows a particular flow path, which surrounds the large DSGSD and Maierato town and then flows at the toe of Maierato slope toward north. The contact between Miocene evaporitic limestone and the underlying sands, clays, silty-clays and silts, is disturbed by this ancient DSGSD and large landslides (Guerricchio et al. 2010).

On the south-west side of Maierato, where the landslide occurred, limestones host an aquifer fed by the upstream trench (Fig. 1) and down confined by the metamorphic bedrock and by Miocene clays. The groundwater flows through the evaporitic limestones, due to the porosity and particularly to the long karst cracks and fractures (Figs. 3 and 4). At the base of the slope, the aquifer locally flows under pressure as consequence of the interlayers and the mix of Miocenic silty clayey level and limestone strata, due to the disturbance of the ancient DSGSD. Therefore groundwater flow was partially dammed at the base of the collapsed slope originating several small springs supplied by this aquifer under pressure at the base of the slope (Giardino site).

Maierato Landslide

Maierato landslide, see Figs. 1 and 2, occurred on February 15th 2010. Despite there were reactivated masses partially dislocated by past gravitational movements, it can be classified as a first-time slide.

Fig. 3 Particular of the tubular channels along the vertical crack of the evaporitic limestones (Picture by Doglioni 2010)

Fig. 4 Particular of the cracks and fracture on the upper north side of the landslide (Picture by Doglioni 2010)

The main body of the landslide is constituted by evaporitic Miocene limestones, with the overlying Pliocene sandy clays and silts and Pleistocene gravels. According to Guerricchio et al. (2010) the failure occurred at the contact of the evaporitic limestone with the underlying Miocene silty clayey level (not outcropping in the area). This contact is severely disturbed by the deformation induced by the DSGSD and large landslides, thus determining the conditions that led to the activation of Maierato large landslide.

The movement developed like a sort of huge regressive multiple slides, characterized by 1.1 km long front and 40 m thick. The landslide evolves into a "flow" of large blocks of Miocene evaporitic limestone and calcarenites, Pliocene sandstones and sands, in a disjointed mass of muddy fluid calcareous-clays (Fig. 2).

The velocity of the diastrophic phase of the event, as it appears from the TV images (Tg24.sky 2010), suggests (Guerricchio et al. 2010) that the movement occurred on a substratum of plasticized material: the Miocene clay and silts overlaid by relatively more rigid materials, evaporitic limestones. This situation fostered the disjoining of limestones, which shaped into blocks of few cubic meters originating a large flow of blocks and mud material, which dammed Scuotrapiti ditch for a length of 600–700 m.

When severe rainfalls occur, at the base of the slope groundwater can flow under pressure through evaporitic limestones. Groundwater cannot be fully drained by the spring at the base of the slope, originating high pore pressure and a decrease of effective stress. The high pore pressure can originate a plastic behaviour of the clay level and is consistent with the deformations observed since few days before the landslide at the lower zone of the slope (Giardino). In fact, the landslide started with severe local deformations of the toe of the slope probably due just to the increase of pore pressure. These deformations evolved backward up to the collapse of the whole slope.

After the loss of strength at the base of the slope, the movement likely propagate upward, as consequence of the decompression of upstream rock masses, thus causing a series of breaks and detachments up to delineate the upper limit of the rupture zone. These outlined the conditions for the collapse of evaporitic limestone and the overlying soils in a multiple rotational slide, followed by deep "disarticulation" of the landslide body itself. This can be considered a "debris and rock block flow" with the morphology of the landslide body similar to a "wave" (Guerricchio et al. 2010), see Fig. 2.

The Rainfall Preceding the Event

The latest two winters before the landslide were much more rainy than the standard and characterized by well time-distributed rain events but never extreme in terms of intensity. Well-distributed rainfall normally favours the infiltration rather than the runoff (Mls 1980; Doglioni et al. 2011). Although long and well-distributed rainfall cannot be considered "exceptional" hydrological events, they are indeed unusual or "singular". Therefore, the particular rainy winters 2009 and 2010 maybe fostered high infiltration thus feeding groundwater. The high amount of groundwater supply combined with the described particular stratigraphic structure

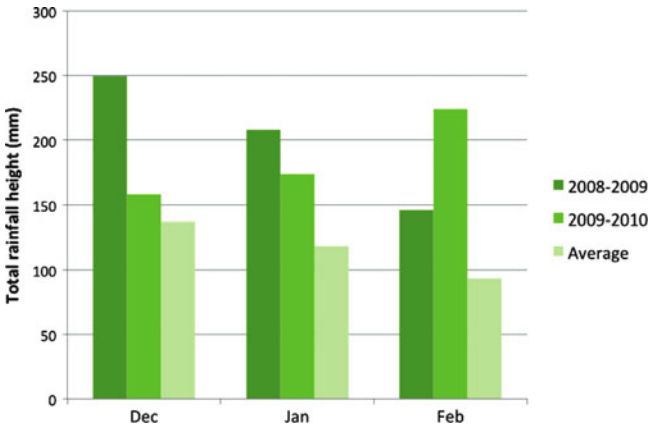

Fig. 5 Average (1919–2010) monthly rainfall and rainfall heights of the 3 months before the landslide for the last two winters before the event

likely increased pore pressure, thus triggering the collapse of the slope.

A hydrological analysis of the daily rainfall is here undertaken to show some peculiar characters of the rainfall antecedent to the landslide, as triggering factor. Daily rainfall values are taken from the data base of the raingauge of Vibo Valentia, which is close to the site of the landslide, about 8 km. Data are available as continuous daily measurements since 1919.

In particular, the rainfalls preceding the event are accounted, as well as the precipitations, which characterized the two winters before the landslide. Looking at the rainfall of the winter period (December, January and February) the last two winters (Fig. 5) were much more rainy of the standard of that period accounted from 1919 to 2010. Similarly to Doglioni et al. (2011), Fig. 6 shows the evolution of total cumulative rainfall since the beginning of the hydrological year: September 2009 up to the landslide compared with the average (1919–2010) cumulative values of the same periods and its standard deviation. It is noteworthy that during 2009–2010 winter, rainfall was really abundant, always exceeding the mean value and in a large part of the autumn and winter period over the mean plus standard deviation value. The rainfall was also quite uniformly distributed because of the absence of knickpoints or high steps in the cumulative rainfall curve. In particular, during the 20 days before the landslide, rain was continuous, whereas no single hydrologically extraordinary event, in term of rainfall amount, was observed (Fig. 7). Such prolonged rainfall period fostered a continuous infiltration. Analysing in details the value of total cumulative rainfall since September to February 15th, it is 900.8 mm, while the average value (1919–2010) of cumulative rainfall on the aforementioned period is 614.1 mm, whereas the standard deviation is 133 mm. This means that the cumulative rainfall for the winter 2009–2010 is 1.2 times the mean value plus the standard deviation.

It is envisaged that the highest value of total daily rain since December was experienced on the 14th of February, i.e. the day before the landslide and was 35 mm, which is not a severely rainy day.

The Hydrological Analysis of the Rainfall Preceding the Event

The presented preliminary analysis of rainfall preceding the event evidences that landslide occurred after two consecutive winters, characterized by a total rainfall volume higher than the average and a large amount of rainfall before the landslide. So cumulative rainfall preceding the event seems to be one of the triggering variables. Here a statistical evaluation of hydrological exceptionality of cumulative rainfall values preceding the landslide is presented. In particular, 5, 10, 15, 20, 30, 45, 60 days cumulative rainfall heights before the landslide are studied. These values are estimated as moving sum of the daily rainfall on the period January 1919 – February 2010, extracting the annual maxima for each cumulative interval. The results are seven timeseries, of the annual maxima for each interval. The annual maxima are then processed in order to find the probability distribution, which better fits the samples, to evaluate the return period of the cumulative rainfall and then the magnitude of events. Manifold probability distribution functions for extreme events were used to fit the values: Gumbel, Gamma and Lognormal. For each of the seven cumulative rainfall series h Gamma probability distribution, (1), better fits data. Thus, Gamma probability distribution function is preferred to the others. The parameters a and b of the distribution were estimated using the maximum likelihood estimate (Benjamin and Cornell 1960). Equations (1) and (2) show in the order the expressions of gamma probability density function and gamma function.

$$p(h) = \frac{1}{b^a \Gamma(a)} h^{a-1} e^{\frac{-x}{b}} \tag{1}$$

$$\Gamma(a) = \int_0^{+\infty} e^{-t} t^{a-1} dt \tag{2}$$

Looking at the results of the statistical processing (Fig. 8), it is noteworthy that the maximum value of 60 days cumulative rainfall of 2010 is 467.6 mm, corresponding to a return period of 6.1 years. The maximum value of 60 days cumulative value of 2009 is 475.2 mm, corresponding to a return period of 6.83 years. These values are characterized by the highest values of return times for the last 20 years. Similarly,

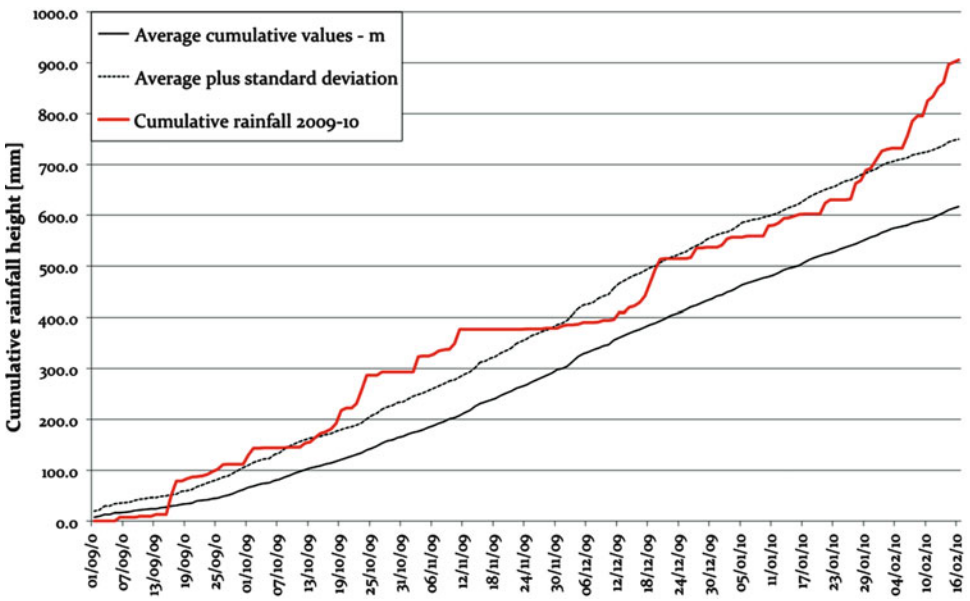

Fig. 6 Trend of cumulative rainfall heights during the period September 2009–15 February 2010, compared with the average values and average values plus standard deviation

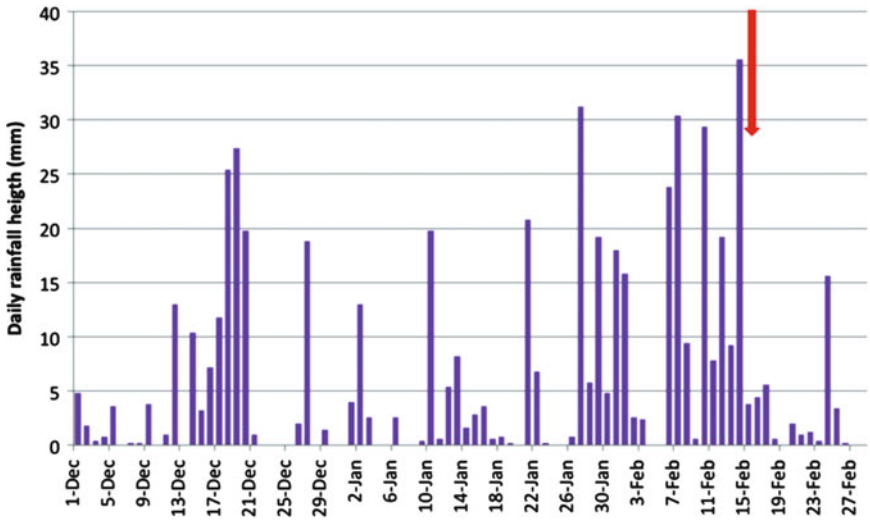

Fig. 7 Daily rainfall heights of the period December 2009 to February 2010. The *red arrow* points on the day of the landslide

looking at 20-days cumulative values, the highest value for 2010 is 269 mm, corresponding to the value of the day just before the landslide. This value is the highest of the last 20 years before the landslide, corresponding to a return period of 9.24 years. The other cumulative intervals show for 2009 and 2010 low return time values, all lower than 5 years.

These values prove that the rainfall scenario was severe but not extreme according to a classic hydrological analysis.

It is assumed that rainfall can trigger landslide, if it can infiltrate increasing groundwater levels and pore pressure lowering the strength. Infiltration processes are conditioned by several variables. Rainfall intensity is one of the more relevant, also for structured soils (Mancarella and Simeone 2007; Galeandro et al. 2011). Low intensity rainfall events have higher probability to contribute at infiltration processes. While intense rainfall events are likely deputed to produce severe run-off that is not relevant for landslide triggering. Therefore, it is not always possible a direct correlation between the hydrological exceptionality of a rainfall and its exceptionality as rainfall triggering factor (Galeandro and Simeone 2010; Mancarella et al. 2012; Mancarella and Simeone 2012).

Then, the presented hydrological analysis is repeated assuming filtered daily rain values according to the procedure introduced by Cotecchia and Simeone (1996). According to that procedure daily rainfall data are cut-off assuming a filter value of 25 mm/day. When daily rainfall

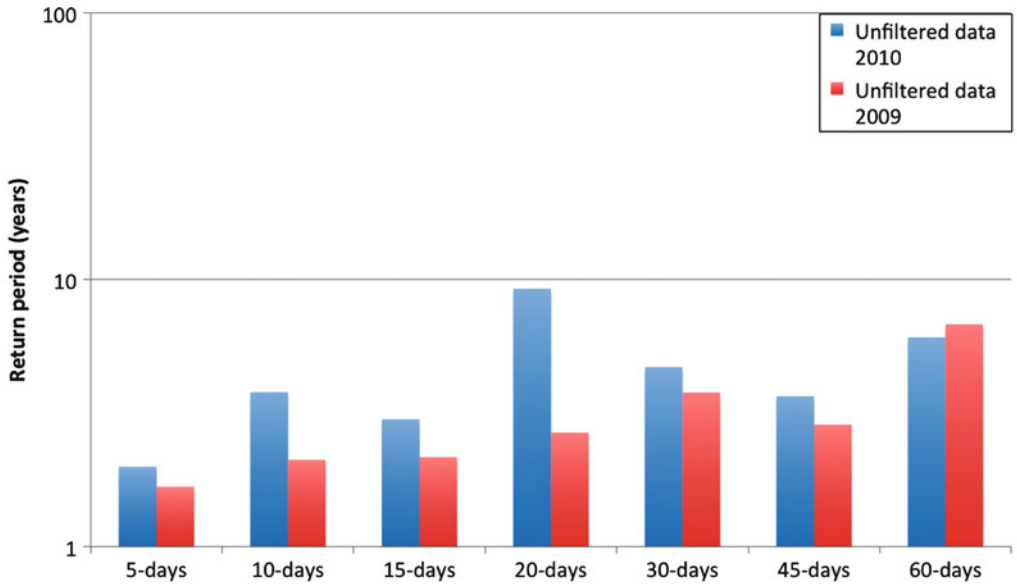

Fig. 8 Return periods of the maximum cumulative rainfall values of 2009 and 2010, for unfiltered data

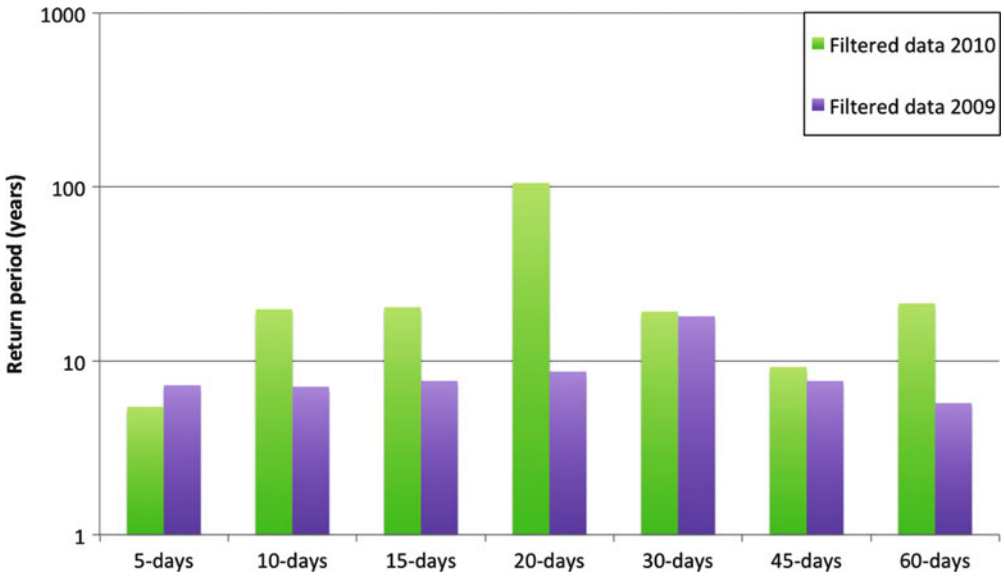

Fig. 9 Return periods of the maximum cumulative rainfall values of 2009 and 2010, for cut-off data

amount exceeds 25 mm/day, it is fixed to 25 mm/day. Then the daily rainfall amount exceeding 25 mm/day is filtered. This approach makes it possible to emphasize rainfall period characterized by well distributed also if not exceptional rainfall volumes.

The threshold value of 25 mm/day appears somehow arbitrary. However, it was chosen according to Cotecchia and Simeone (1996), since it corresponds to the maximum value of infiltration where medium permeability soil outcrops (Linsley and Franzini 1978).

This rainfall processing procedure (Cotecchia and Simeone 1996) is an indirect approach at the evaluation of the effectiveness of a rainfall at infiltrating and an indirect way to evaluate the exceptionality of rainfall as landslide triggering factor in particular for medium permeability soils. Independently from the chosen threshold value, it allows for showing how different approaches to this analysis can return different results.

Indeed, looking at the events preceding the landslide, there are no values of daily rain higher than 35.6 mm/h, then all the rainfall events before the landslide likely seriously infiltrated. The outcome of the statistical processing of filtered data is quite interesting because it returns results quite different than the previous ones (see Figs. 8 and 9). The 10-days highest cumulative height of filtered data of 2010 is 148.8 mm, corresponding to a return periods of

19.9 years, the highest value of the 60 years before the landslide. Similarly, the 20-days filtered cumulative value showed 242.4 mm as the maximum of 201o, corresponding to a return period of 105 years. In addition, maxima of cumulative values for 30, 45 and 60 days of 2010 have high return periods. This implies that probably the percentage of rainfall that actually infiltrated was quite huge during 2010. Therefore in these terms, 2010 rainfall events, even if not hydrologically exceptional, were quite peculiar. It can be considered as "singular" rainfall event, becoming quite exceptional in terms of infiltration processes and therefore crucial for the activation of the large landslide of Maierato.

Figures 8 and 9 clearly shows the sharp difference between unfiltered and filtered data, as well as the clear superiority, in terms of return period, of the 20-days filtered value. It is interesting to observe (Fig. 9) that the maxima of 2009 of filtered data did not show very high values as 2010.

Conclusions

This work presents a hydrological analysis of the rainfall antecedent to the large landslide of Maierato, occurred on February 15th 2010. Although the landslide was severely conditioned by an ancient DSGSD as predisposing factor, the event was triggered by rainfall. However, looking at the single rainfall events, these never show extreme values. Moreover, looking at the cumulative rainfall values, there are no values characterized by high return periods. Anyway the whole sequence of events is quite peculiar so that it can be considered "singular", since a really long period of continuous but not intense rainfall occurred. In fact, assuming a cut-off threshold of the daily rainfall values at 25 mm, whereas rainfall exceeding this value is not considered contributing to the infiltration, interesting results are returned in terms of hydrological analysis. In particular, it is proved that the cumulative rainfall heights of filtered values were extraordinary, showing some of the highest return times of the whole series. Moreover, the maximum value of 20-days cumulative filtered rainfall of 2010 has a return period of more than 100 years. The activation of a landslide in that specific context is likely due to the singularity of the rainfall event that favored infiltration processes and groundwater supply by the trench of the large DSGSD. Moreover, also anthropic work or land modifications may have concurred to increase infiltration processes and the negative influence of the particular rainfall event.

In conclusion it is possible to argue that the large landslide of Maierato has the geomorphological scenario of the zone as predisposing factor but was triggered by the particular rainfall preceding the landslide event. In fact, the long period of rainfall preceding the landslide can be assumed not exceptional from the hydrological point of view, but singular in terms of rainfall distribution. This likely produced severe infiltration, in particular through the fractures and cracks due to the DSGSD.

References

Antronico L, Borrelli L, Gullà G, Sorriso Valvo GM (2010) La frana di Maierato (Calabria, Italia meridionale) del febbraio 2010: caratteristiche geomorfologiche ed evoluzione – Maierato landslide (Calabria, Southern Italy) of February 2010: geomorphological features and evolution GEAM. Geoingegneria Ambientale e Mineraria 2:15–26

Benjamin JR, Cornell CA (1960) Probability, statistics and decisions for civil engineering. McGraw-Hill Ryerson, New York, p 684. ISBN 0070045496

Cassa per il Mezzogiorno (1971) Carta Geologica della Calabria – Geological Map of Calabria, Scale 1:25000 – Sheet 241 IISO and 241 IIISE

Comerci V, Di Manna P (2010) Secondo verbale di sopralluogo sulla frana di Maierato (VV) – Second survey report on Maierato (VV) landslide. ISPRA Dip. Difesa del Suolo, Serv Geol D'Italia, Rapporto Tecnico RT/SUO-RIS 18/2010

Cotecchia V, Simeone V (1996) Studio dell'incidenza degli eventi di pioggia sulla grande frana di Ancona del 13.12.82. – Analysis of the rainfall effects on the large landslide of Ancona of 13.12.1982. In: International conference on the prevention of hydrogeological disasters: the contribute of scientific research, vol 1, Alba, 5–7 Nov 1996, pp 19–29

Cotecchia V, Guerricchio A, Melidoro G (1986) The morphogenetic crisis triggered by the 1783 earthquake in Calabria (Southern Italy). Geol Appl e Idrogeol., XXI, Bari

Doglioni A, Fiorillo F, Guadagno FM, Simeone V (2011) Evolutionary polynomial regression to alert rainfall-triggered landslide reactivation, Landslide (in press). DOI: 10.1007/s10346-011-0274-8

Galeandro A, Simeone V (2010) Un modello dual-porosity per l'analisi dell'infiltrazione in mezzi porosi rigonfianti con reticoli di fratture. Eng Hydro Environ Geol 13:71–85

Galeandro A, Simunek J, Simeone V (2011) Analysis of infiltration processes into fractured and swelling soils as triggering factors of landslides. In: Proceedings of II World Landslide forum, Rome, 3–7 Oct 2011

Guerricchio A, Fortunato G, Guglielmo EA, Ponte M, Simeone V (2010) Condizionamenti idrologici e da DGPV nell'attivazione della grande frana di Maierato (VV) del 2010 – Hydrogeological conditioning and deep-seated gravitational slope deformations effects on the activation of the large landslide of Maierato in 2010. In: Tecniche per la difesa dall'inquinamento – 31° Corso di aggiornamento, pp 661–706, June 2010

Linsley RK, Franzini JB (1978) Water resources engineering. McGraw Hill, New York, p 688. ISBN 0070380104

Mancarella D, Simeone V (2007) Analysis of capillary barrier effects in the activation of debris avalanches in pyroclastic cover. In: Proceedings of 4th debris flow hazard and management conference, Chengdu, Sept 2007

Macarella D, Simeone V (2012) Capillary barrier effects in unsaturated layered soils, with special reference to the pyroclastic veneer of the Pizzo d'Alvano, Campania, Italy. Bull Eng Geol Environ 71 (4):791–801. doi:10.1007/s10064-012-0419-6

Mancarella D, Doglioni A, Simeone V (2012) On capillary barrier effects and debris slide triggering in unsaturated layered covers. Eng Geol 147–148:14–27. doi:10.1016/j.enggeo.2012.07.003

Mls J (1980) Effective rainfall estimation. J Hydrol 45(3–4):305–311

Regione Calabria (2001) Carta inventario delle frane (Map of the landslides), Piano stralcio per l'Assetto Idrogeologico – PAI (Plan for the Hydrogeological layout)

Scesi L, Gattinoni P (2010) Studio geologico-tecnico del movimento franoso verificatosi nel Comune di Maierato il 15 febbraio 2010: ricostruzione del modello concettuale e predisposizione di un cronoprogramma degli interventi (Geological and technical investigation on the landslide of Maierato occurred on February 15th 2010: reconstruction of the event and policy of remediation), Politecnico di Milano – D.I.I.A.R

Tg24.sky (2010) http://tg24.sky.it/tg24/cronaca/2010/02/15/frana_montagna_video_choc_vibo_valentia.html. Accessed 24 June 2011

Quick Clay Landslides, Landscape Evolution, and Climate Change: A Perspective from British Columbia

Marten Geertsema

Abstract

I examine prehistoric and historic quick clay landslide scars in two valleys in northwestern British Columbia, and test the evidence against Bjerrum's and Levebvre's landscape evolution models. Streams in the Terrace-Kitimat valley are still incising deep glaciomarine sediments and appear to be in the early and intermediate stages of valley formation, thus large landslides are still occurring and more are expected. In contrast, streams in the Nass Valley are incised into bedrock, in the late stages of valley formation. Early evidence suggests most of the landslides are old, and more large landslides are not expected to be triggered by bank erosion. Rapid incision in the Nass valley may have overwhelmed climatic influences, however in the Terrace-Kitimat valley identified wetter climate regimes seem to correspond to higher earth flow activity. Here, a future warmer and wetter climate, as predicted by most global circulation models, will likely lead to increased landsliding.

Keywords

Quick clay • Landslide • Glaciomarine sediment • Fjord • British Columbia

Introduction

In this paper I examine two large fjordal valleys riddled with quick clay landslide scars. The Terrace-Kitimat and Nass River valleys (Geertsema and Schwab 1997) are about 100 km apart in north coastal British Columbia (Fig. 1). I consider the spatial and temporal pattern of landslides both from landscape evolution and climate perspectives, and specalute on future hazard regimes for the two areas.

Setting

The glacially gouged, fjord-dissected, glacioisostatically uplifted coast of British Columbia is similar to that of Norway. Broad flat valley bottoms flanked by precipitous slopes are common in both regions, as are sensitive glaciomarine clays.

There are also many similarities between Terrace-Kitimat and Nass valleys (Fig. 1). Both valleys are broad, contain glaciomarine sediments, and are considerably uplifted above present-day sea level. Deltas in the Terrace-Kitimat area are graded to a marine limit of about 200 m (Clague 1984) and to a marine limit of 230 m in the lower Nass River valley (McCuaig 1997).

The bedrock geology in the two areas is different. Granodiorite is the most common bedrock near Terrace and Kitimat, while the Nass valley contains softer mud and silt stones – and this has impacted stream incision. Streams in the Terrace-Kitimat area are still down-cutting through glaciomarine mud, while streams in the Nass River area are incised into soft bedrock (Fig. 2).

The region has cold, wet winters and cool summers due to the influence of Polar Maritime air. Mean annual precipitation ranges from 150 to 350 cm, with higher mountain peaks

M. Geertsema (✉)
Ministry of Forests, Lands, and Natural Resource Operations, Prince George, BC, Canada
e-mail: Marten.geertsema@gov.bc.ca

C. Margottini et al. (eds.), *Landslide Science and Practice*, Vol. 4,
DOI 10.1007/978-3-642-31337-0_15,

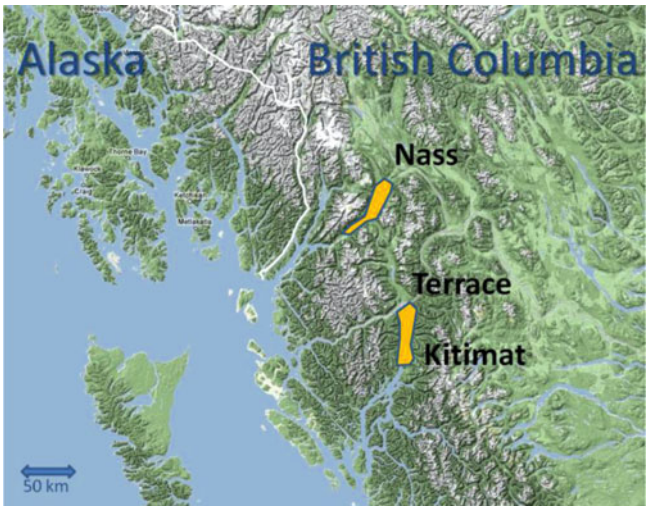

Fig. 1 Map of the study area. *Orange-shaded areas* near Terrace and Nass River have abundant quick clay landslides

Fig. 2 Nass River is incised into soft, slightly metamorphosed, sedimentary rock

receiving most precipitation, primarily in the form of snow (Farley 1979). January temperatures average between 0° and −15 °C, while July temperatures average 14–16 °C in the valleys and less than 14 °C in the mountains.

Fig. 3 An example of prehistoric flowslide scars (scarps outlined by *dashes*) along Nass River

Landslides

General Characteristics

Old landslide scars are common in both the Nass River and Terrace-Kitimat areas. Most of the landslides are characterized by steep short scarps and wide, gently sloping zones of depletion. Both wide and narrow outlets are common (see Figs. 3 and 4).

Ribbed morphology, commonly preserved in eastern Canada, is absent from the BC landslides (except in a portion of the Mink Creek landslide (Fig 5) (Geertsema et al. 2006)). Although translational ridges, that give earth spreads their ribbed appearance, degrade rapidly and substantially, it is likely that some subdued surface expression would remain (Geertsema and Schwab 1996). Therefore I suspect that the absence of residual ribbed morphology may indicate the ease of the removal of displaced material from the zones of depletion, and suggests that most of the landslides were flows, rather than spreads.

Landslide Ages

Sixteen landslides were dated by radiocarbon methods in the Terrace area, and one in the Nass valley. All, except one were from basal peats developed in landslide scars (Fig. 6). More than 75 % of the Terrace landslide ages were younger than 4,000 calibrated years before present. More than one third of the dates plot between 2,000 and 3,300 BP – more on this later. The sole Nass River date was 6,890 ± 100 BP

Fig. 4 An example of a prehistoric "*bottleneck*" earth flow in the Terrace-Kitimat area

Fig. 5 The 1993/1994 Mink Creek landslide near Terrace, 1,200 m from crown to tip, covers some 43 ha and remobilized 6,000 year old landslide material as well as previously undisturbed quick clay

(GSC-6328) (McNeely 2005) and calibrates to a median date of 7,740 BP.

No significant modern flowslides have occured in the Nass valley, but three large landslides did occur in the Terrace area. Two were triggered by higheway construction in 1962 (Geertsema and Schwab 1997), and another (the Mink Creek landslide) happened in the winter of 1993/94 (Geertsema et al. 2006). The Mink Creek landslide in part remobilized the debris of a 6,000 year old landslide.

Landscape Evolution Models

Stream erosion is the most common trigger of retrogressive landslides in marine sediments (Bjerrum et al. 1969; Lebuis et al. 1983; Viberg 1983). Both Bjerrum et al. (1969) in Norway, and Lefebvre (1986) in Quebec used a landscape evolution approach to map zones of earth flow potential in sensitive clay areas. They were interested in stream incision.

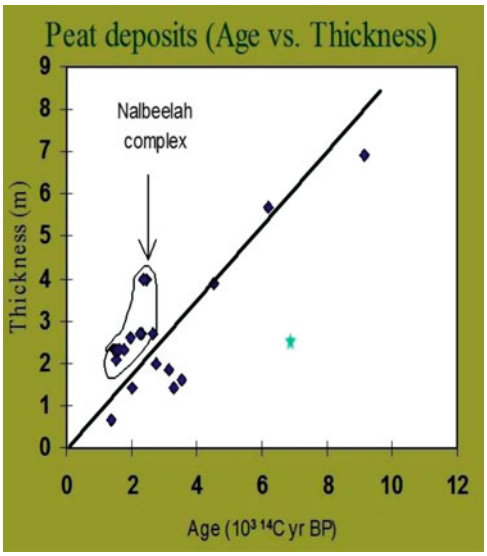

Fig. 6 Scatter graph showing landslide ages (from basal peats): *diamonds*, Terrace landslides; *star*, Nass landslide

Bjerrum

Bjerrum et al. (1969), working on the premise that stream bank erosion was the main trigger of quick clay slides, determined equilibrium gradients for streams from which it was possible to predict future erosion. They defined three zones of erosion for streams.

1. A lower zone, no longer actively downcutting, is characterized by old slide scars, and localized bank failures in stream bends. This is a mature zone and the danger of quick clay landslides is small.
2. An intermediate zone exists where streams are flowing almost exclusively on displaced landslide deposits, and in general, the streams are eroding back to their old levels. As long as streams are cutting through old landslide deposits, Bjerrum et al. (1969) argue that earth flows will be restricted to that material, and the risk of quick clay landslides triggered by erosion is low.
3. An upper zone is identified as the original horizontal plateau where streams are cutting into undisturbed clay.

It is at the boundary between these latter two zones that the risk of retrogression was found to be the greatest. They called this boundary the "front of aggression". Every time an earth flow happened the intermediate zone would be extended, moving the front of aggression upstream.

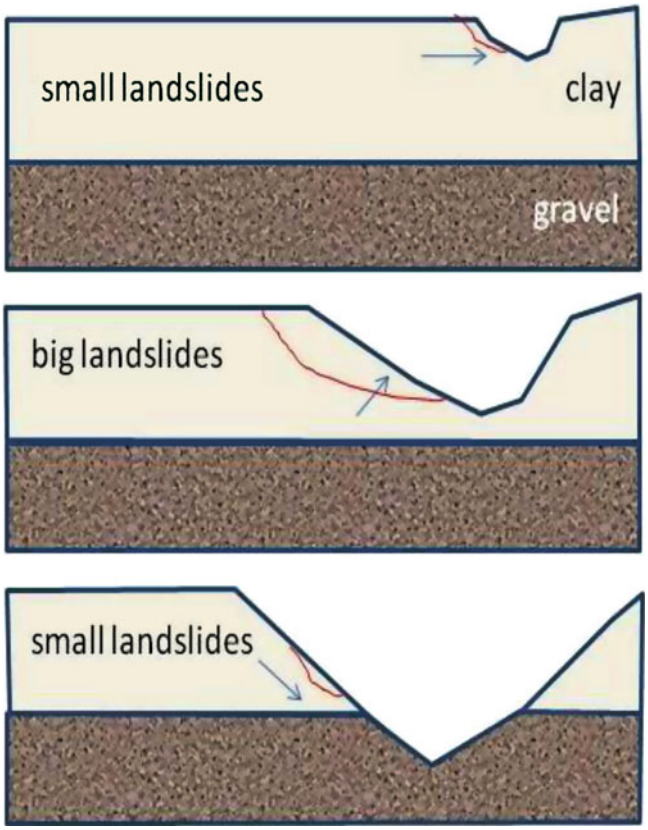

Fig. 7 Stages of valley formation (Modified from Lafleur and Lefebvre (1980) and Lefebvre (1986)). Conditions are most unstable when groundwater flow (*blue arrows*) is *upward*, or artesian, and large landslides (*red lines*) tend to occur. Once the river erodes into the more pervious gravels, groundwater flow is *downward*, and the landslide threat diminishes

Lefebvre

Lefebvre (1986, 1996) proposed a zonation based on phases of valley formation modified from Lafleur and Lefebvre (1980) using a groundwater flow regime approach (Fig. 7). An early phase involves relatively shallow stream incision into deep mud deposits where groundwater flow is not influenced by lower pervious gravels (gravelly till in his case). An intermediate phase of valley formation is characterized by strong artesian pressures and favours large, retrogressive landslides. A late phase occurs when streams have incised through the lower pervious till (if it exists) resulting in downward flows. Only small landslides are expected during the early and late phases of valley formation.

Whose Model Fits Northern BC?

While the zones proposed by Bjerrum et al. (1969) do not relate directly to Lefebvre's (1986, 1996) phases of valley formation, in both approaches the intermediate zones present the greatest hazards for retrogressive flowsliding.

There is some evidence against Bjerrum's front of aggression approach in the Terrace area, because large landslides are already well distributed throughout the valley, and large landslides are occurring in areas with previous retrogressive failures – rather than at the "front of aggression". For example, the 43 ha Mink Creek landslide (Fig. 5), near Terrace, involved material from a 6,000 year old landslide (Geertsema et al. 2006). Moreover, in eastern Canada the Saint-Jean-Vianney slide (Tavenas et al. 1971; Potvin et al. 2002) also remobilized old landslide deposits.

It appears that Lefebvre's valley formation approach is more applicable to the Terrace-Kitimat and Nass River areas than the front of aggression approach of Bjerrum. Lefebvre's phases of stream incision are different between the two areas. Streams in the Terrace area are still incising deep glaciomarine sediments (Geertsema 1998) and appear to be in the early and intermediate stages of valley formation, thus large landslides are still occurring and more are expected. In contrast, the Nass River and it's tributaries went through the three phases of valley formation very rapidly – and the streams are now incised in bedrock. The 7.7 thousand year old landslide (albeit a single data point) and lack of historic flowslides fit with a period of enhanced landslide activity, coinciding with an intermediate phase of valley formation, sometime in the early Holocene.

Climate and Landslides

Prehistoric Climate

Paleoclimatic records are scant in the Terrace and Nass River areas. However, Clague and Mathews (1996) obtained a proxy climate record from a site near Berendon Glacier, about 200 km northwest of the Terrace. They identified a cool, wet period between 3,300 and 1,900 years ago. More than 1/3 of the Terrace-Kitimat landslide ages fall within this period and most of the dates are younger than 4,000 years old. Thus there may have been greater flowsliding activity during Neoglacial time (the last 5,000 years) than during the warmer and drier Hypsithermal (5,000–8,000 years ago – Pielou 1991), suggesting the possibility of climatic controls on the overall incidence of landslide activity.

Historic Climate

The 1993/94 Mink Creek landslide near Terrace was well documented by Geertsema et al. (2006). They show that a decade of increasing precipitation (cumulative deviation from the mean) and a decade of increasing temperature

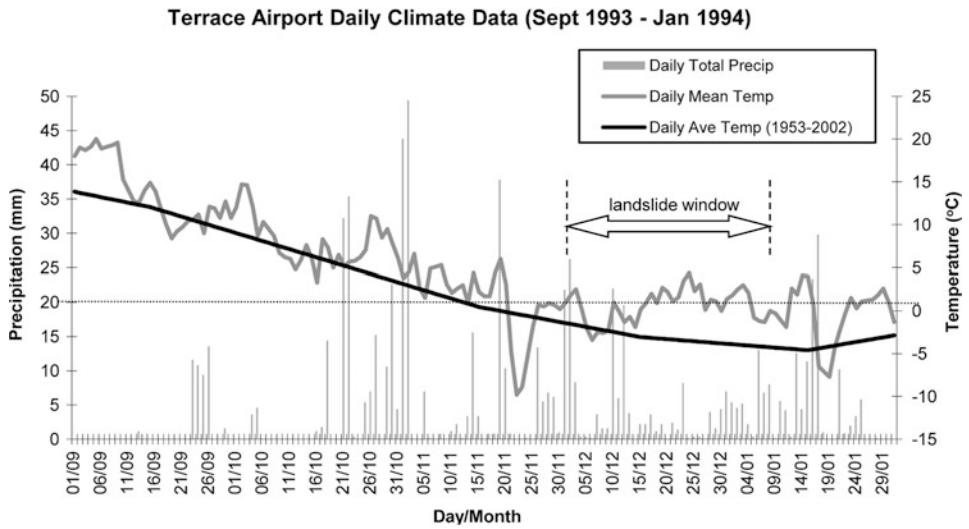

Fig. 8 Terrace airport daily precipitation and temperature data for the period September 1993 to January 1994 for the Mink Creek landslide (Fig. 5). Note that this period experienced warmer than average temperatures. Most of the precipitation was rain. The landslide also occurred after a decade of warmer and wetter conditions (not shown) (Modified from Geertsema et al. 2006)

(important for snowmelt) preceded the landslide. Figure 8 shows temperature and precipitation for the period September 1993 to end January 1994. This was a period of above average temperatures and most precipitation fell as rain. Water levels in wells were higher than normal Geertsema et al. (2006). The combination of climate data and water level observations indicate that the time of the landslide coincided with the culmination of 8 years of increasing precipitation, 9 years of increased warming, and a warmer than average fall and early winter. These hydroclimatic conditions likely contributed to high ground water and stream levels, setting up the preconditions for the Mink Creek landslide.

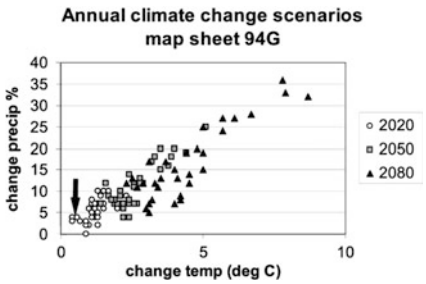

Fig. 9 Annual climate change scenarios for 2020, 2050, and 2080 for Terrace, British Columbia, with respect to a 1961–1990 global climate model baseline. The *points* represent the results of 58 different global circulation models, predicting a progressively warmer and wetter climate. The data was obtained from the Canadian Institute for Climate Studies website (http://www.cics.uvic.ca)

Future Climate

In British Columbia, studies of landslide–climate relationships have largely been restricted to shallow debris slides and flows in steep mountainous terrain (Schwab 1983; Church and Miles 1987; Evans 1989; Hogan and Schwab 1991; Jakob and Weatherly 2003). However Bovis and Jones (1992) have shown how large deep seated earth flow activity in Southern British Columbia corresponded to wet climatic periods in the Holocene. Almost invariably all the models predict warmer and wetter conditions. Almost a decade of increasing precipitation and temperature, plus a mild wet fall and early winter (Fig. 8) led up to the landslide at Mink Creek (Geertsema et al. 2006). Figure 9 shows climate change plots scenarios for Terrace for 2020, 2050 and 2080 from 58 global circulation models (Canadian Institute for Climate Studies: http://www.cics.uvic.ca). Thus we can expect similar conditions that led up to the landslide in the decades ahead.

Conclusions

There are abundant prehistoric landslides in the Terrace-Kitimat and Nass River areas. As the most common trigger for large earth flows is bank erosion, these movements may have occurred during a period when rivers eroded slopes below these landslides. Landscape evolution from landsliding is better supported here by Lebvevre's valley formation model than by Bjerrum's "front of aggression" approach. This is because landslides occur in areas of previous landslides – thus not only at the front of aggression. According to Lebevre's model large landslide hazard should be eliminated from the Nass valley (late stage of valley formation), but be high for

the Terrace-Kitimat area in the intermediate phase of valley formation. Preliminary evidence supports this. Bank-erosion triggers are unlikely in the Nass area, but that this must have played an important role earlier in the Holocene. Streams in the Terrace area are still in the early to intermediate phases of valley formation – a condition that favours triggering of new large landslides – evidenced by recent flowslides.

There are three interesting points to be made about climate. (1) About one third of the dated prehistoric landslides occurred during a wet climatic period. (2) Almost a decade of increasing precipitation and temperature and a wet and warm fall and early winter preceded the landslide at Mink Creek (Fig. 5). (3) Climate change scenarios predict a wetter and warmer future climate for Terrace.

Given the phases of valley formation, the history of previous landsliding, and the link between climate and landslides, the climate change scenarios for (Fig. 8) should alert us to the increased likelihood of future large landslides in the Terrace-Kitimat area, but not necessarily for the Nass valley.

References

Bjerrum L, Løken T, Heiberg S, Foster R (1969) A field study of factors responsible for quick clay slides. In: Proceedings of 7th ICSMFE, vol 2, Mexico, pp 531–540

Bovis MJ, Jones P (1992) Holocene history of earthflow mass movements in south-central British Columbia: the influence of hydroclimatic changes. Can J Earth Sci 29:1746–1755

Church M, MJ Miles (1987) Meteorological antecedents to debris flow in southwestern British Columbia; some case studies. Geol Soc Am Rev Eng Geol 7:63–79

Clague JJ (1984) Quaternary geology and geomorphology, Smithers-Terrace-Prince Rupert area, British Columbia. Geological Survey of Canada, Memoir 413, 71 pp

Clague JJ, Mathewes RW (1996) Neoglaciation, glacier-dammed lakes, and vegetation change in northwestern British Columbia, Canada. Arctic Alpine Res 28:10–24

Evans SG (1989) Rain-induced landslides in the Canadian Cordillera, July 1988. Geosci Can 16:193–200

Farley AL (1979) Atlas of British Columbia, people, environment and resource use. University of British Columbia Press, Vancouver, 136 p

Geertsema M (1998) Flowslides in waterlain muds of northwestern British Columbia, Canada. In: Moore DP, Hungr O (eds) Proceedings of 8th IAEG Congress, vol III, Vancouver, pp 1913–1921

Geertsema M, Schwab JW (1996) A photographic overview and record of the Mink Creek Earthflow, Terrace, British Columbia. B.C. Min. For., Victoria, B.C. Res. Rep. 08

Geertsema M, Schwab JW (1997) Retrogressive flowslides in the Terrace-Kitimat, British Columbia area: from early post-deglaciation to present – and implications for future slides. In: Proceedings of the 11th Vancouver Geotechnical Society Symposium (pp. 115–133). Vancouver BC

Geertsema M, Cruden DK, Schwab JW (2006) A large, rapid landslide in sensitive glaciomarine sediments at Mink Creek, northwestern British Columbia, Canada. Eng Geol 83:36–63

Hogan DL, Schwab JW (1991) Meteorological conditions associated with hillslope failures on the Queen Charlotte Islands. Land management report 73, BC Ministry of forests, 36 pp

Jakob M, Weatherly H (2003) A hydroclimatic threshold for landslide initiation on the North Shore Mountains of Vancouver, British Columbia. Geomorphology 54:137–156

Lafleur J, Lefebvre G (1980) Groundwater regime associated with slope stability in Champlain clay deposits. Can Geotech J 17:44–53

Lebuis JJ, Robert M, Rissmann P (1983) Regional mapping of landslide hazard in Quebec. In: Bergren B, Lindgren J (eds) Symposium on slopes on soft clays, Swedish Geotechnical Institute report No. 17, Linkoping, pp 205–262

Lefebvre G (1986) Slope instability and valley formation in Canadian soft clay deposits. Can Geotech J 23:261–270

Lefebvre G (1996) Soft sensitive clays. In: Turner AK, Shuster RL (eds) Special report 247: landslides investigation and mitigation. TRB, National Research Council, Washington, DC, pp 607–619

McCuaig SJ (1997) Quaternary geology of the Nass River region, British Columbia. Current research 1997-A. Geological Survey of Canada, Ottawa, ON, Canada, pp 183–189.

McNeely R (2005) Geological Survey of Canada radiocarbon dates XXXIV; Geological Survey of Canada current research, Ottawa, ON, Canada, 113 p

Pielou EC (1991) After the ice age: the return of life to glaciated North America. The University of Chicago Press, Chicago and London

Potvin EC, Pellerin F, Demers D, Robitaille D, La Rochelle P, Chagnon J-Y (2002) Revue et investigation complementaire du site du glissement de Saint-Jean-Vianney. In: Proceedings of an Earth Odyssey 2001, Canadian Geotechnical Society, Laval, PQ, Canada, pp 792–800

Schwab JW (1983) Mass wasting: October–November 1978 storm, Rennell Sound, Queen Charlotte Islands, British Columbia. Research Note 91. BC Ministry of Forests, Victoria, BC, Canada, p 23

Tavenas F, Chagnon J-Y, La Rochelle P (1971) The Saint-Jean-Vianney landslide: observations and eyewitnesses accounts. Can Geotech J 8:463–478

Viberg L (1983) Experiences of mapping and classification of stability conditions. In: Bergren B, Lindgren J (eds) Symposium on slopes on soft clays, Swedish Geotechnical Institute Report No. 17, Linkoping, pp 455–461

Short Term Weather Forecasting for Shallow Landslide Prediction

Paola Mercogliano, Nicola Casagli, Filippo Catani, Emilia Damiano, Lucio Olivares, Luciano Picarelli, Guglielmo Rossi, Pasquale Schiano, Samuele Segoni, Bogdan Sikorski, and Veronica Tofani

Abstract

The paper describes the activities developed within the work package 4.1 of the UE/FP7 SAFELAND Project. The first scope of this research activity is to define and to implement a warning system for shallow landslide prediction, at large and slope scale, based on the forecast precipitation. The warning system is based on different numerical tools and simulation models: stability analysis model at slope and regional scale and numerical weather prediction models (global and regional) and downscaling algorithms.

Keywords

Early warning • Landslide risk • Weather forecast

Motivation and Scope

The activities under development have the goal to design and to develop simulation models able to produce regional and detailed warning maps for shallow landslides triggered by meteorological events. The interests for this topic comes from the experience that severe rain can trigger rapid shallow landslides in a very brief time with severe soil impacts as life and properties loss especially in the most vulnerable areas. Some expected effects of the climate changes, as the modification in the precipitation patterns (increasing of extreme rain events), the snow melting and the increasing of ground temperatures (IPCC 2007) can modify the slope stability conditions and trigger more landslides. The scope of this research is to define a warning system, in the short range, for shallow landslide prediction, at large or basin scale. The prediction in the short range time (from 0 to 3 days before potential landslide triggering) is based on the forecast of meteorological variables as precipitation and also atmospherical parameters at the soil level by NWP (numerical weather prediction model). NWP forecast will be used to initialize landslide triggering model at regional and slope scale. These last simulation models will have as output warning map for shallow landslide risk to make possible the launch of the warning to the competent authorities. The integrated model use statistic tool together with state of art landslide triggering models and NWP model (see Fig. 1). Mediterranean Centre for climate change (www.cmcc.it) is to develop the tool implementing the downscaling techniques for the coupling of different simulation models; in collaboration with the COSMO consortium, CMCC is developing the atmospherical regional model COSMO LM (www.cosmo-model.org).

The goal of AMRA is to implement and test the simulation code for evaluation of the infiltration processes induced by rainfall and assessment of the stability conditions of sloping deposits at local and basin scale. Finally, UNIFI works on the development and testing of a simulation

P. Mercogliano (✉) • P. Schiano • B. Sikorski
Impacts on Ground and Coast (ISC) Division, Euro Mediterranean Centre for Climate Changes (CMCC), Lecce, Italy

Meteo System and Instrumentation Laboratory, Italian Aerospace Research Center (CIRA), Capua (CE), Italy
e-mail: p.mercogliano@cira.it

N. Casagli • F. Catani • G. Rossi • S. Segoni • V. Tofani
Department of Earth Sciences, University of Firenze (UNIFI), Florence, Italy

E. Damiano • L. Olivares • L. Picarelli
Analisi E Monitoraggio Del Rischio Ambientale (AMRA), Napoli, Italy

Seconda Università di Napoli, Aversa, Italy

C. Margottini et al. (eds.), *Landslide Science and Practice*, Vol. 4,
DOI 10.1007/978-3-642-31337-0_16,

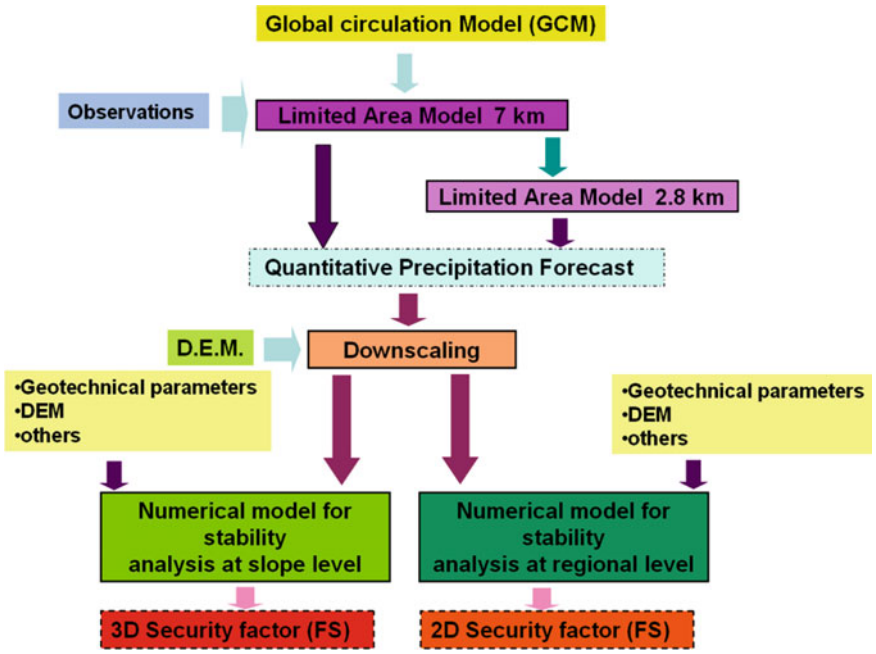

Fig. 1 Flow chart of numerical simulations chain in the short time range

model at regional scale that is a combination of the infinite slope stability analysis and a transient, analytic solution for pore pressure response to rainfall infiltration.

Integrated Model Features

Atmospherical Models

The first simulation models adopted in the "simulation chain" are represented by NWP models. Two different kinds of NWP models are used. The first one is IFS global by ECMWF (2004) is employed to forecast the weather synoptic on the globe with a horizontal resolution of about 20 Km, but, due the low resolution, it is not able to carefully describe mesoscale phenomena, as orographic and convective rain that often are the cause of the intensive rainfall. Such a global model is hence coupled to the limited area model COSMO-LM (by COSMO Consortium) (Doms et al. 1998) providing the initial and the boundary conditions. In The COSMO-LM model, used for this application, different numerical schemes and physical parameterization are implemented, so the same code can run with different configurations. Currently there are two versions: the first one with a horizontal resolution of 7 km and a temporal forecast range up to 72 h and a second one with 2.8 km of horizontal resolution and a forecast range up to 24 h. In the following test cases the "simulation chain" has been implemented by the version 4.11 of COSMO LM model and the data assimilation tool has been used for COSMO LM 7 km.

Downscaling Techniques for Improving Coupling of Meteorological and Landslide Models

The hydrological-stability models and the atmospherical one are coupled in the integrated model through the precipitation forecast. This is a very discontinuous meteorological variable, whose distribution strongly depends on the orography and on the soil properties. The three step nesting adopted for the NWP model (global model, COSMO LM 7 km and COSMO LM 2.8 km) to produce high resolution precipitation forecast, is not sufficient for the hydrological-stability models due to the very different resolutions required by the two models. In order to avoid inconsistencies proper downscaling techniques are necessary. Up to now, different interpolation methods have been analyzed based on a digital model. Starting from the precipitation data provided by COSMO LM model, they create in the examined area, a regular grid with a resolution up to 100 × 100 m. As a result of such downscaling procedures precipitation data with a resolution much larger than the one of the output of NWP model are then available. Evaluations on statistical basis (correlations between observed and foreseen values) indicate that the best interpolation method, on the whole, is MRI (physical disaggregation of precipitation with topographical variables) and the residual one is interpolated with RBF (radial basis function) method. This is a deterministic interpolation method creating surfaces from measured points, based on the degree of smoothing (Hardy 1971). The topographic variables utilized for MRI disaggregation are: elevation, slope and aspect. CMCC has also developed an interface software tool in GIS (Geographic Information System) environment.

Taking forecast data (mainly precipitation) from COSMO-LM 7 km and 2.8 km, it can automatically generate downscaled data of precipitation with MRI giving the input for the hydrological-stability models software. This software can manage precipitation data coming from: radar, satellite and other atmospherical models (global or on limited area) producing an output with a format readable by GIS software

A Landslide Triggering Model for Early Prediction of Rapid Landslides at Slope Scale

AMRA developed a landslide triggering model (geotechnical model) whose goal is the prediction of rapid precipitation-induced debris flows and flowslides. Such a model is integrated in the "simulation chain" using as hydraulic boundary condition the precipitation forecast produced by the downscaling module. The model consists of a 3D finite volume model (I-MOD3D) and of a slope stability module which have respectively the goal of analyzing the rainfall-induced infiltration process and assessing the slope stability conditions. These two parts are integrated through an interface able to automatically define a finite volume discretization of soil starting from a Digital Terrain Model (DTM), and to capture the forecasted rain from the downscaling module. I-MOD3D has developed as a Visual Basic Application (VBA) for ARC-GIS 9.2 in an uncoupled formulation for unsaturated porous medium in isothermal condition neglecting the flux of the gas phase. The water retention curve, WRC, which describes the relationship between matric suction and volumetric water content, is described by the Van Genuchten expression (1980). The permeability function of soil, which depends on the matric suction or on the volumetric water content, is expressed by the Gardner (1958) or by the Brooks and Corey (1964) relationships. It is worth mentioning that the user can directly use experimental data. The stability module computes for each point of the subsoil the local safety factor under the assumption of infinite slope; the shear strength of soil along planes parallel to the ground surface is calculated by the extension of the Mohr-Coulomb criterion for unsaturated soils (Fredlund and Rahardjo 1993) which is supplied by the values of suction which are calculated by I-MOD3D. The code contains an integrated post processor displaying, for each integration time and for different depths, contour maps of the volumetric water content, matric suction and local safety factor.

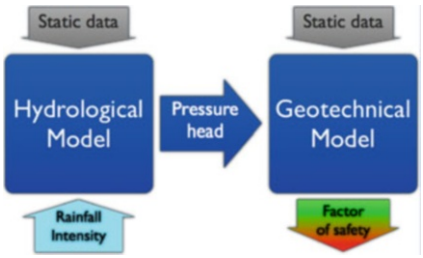

Fig. 2 A scheme of HIRESSS code for the analysis of stability at regional level

A Landslide Triggering Model for Prediction of Rapid Landslides at Regional Level

The model developed by UNIFI, HIRESSS, is a combination of an infinite slope stability calculation with a transient, analytic solution for pore pressure response to steady state and transient rainfall infiltration (Rossi et al. 2013). A complex operative chain was devised and setup based on radar rainfall measurements, a soil saturation hydrological model and a simple infinite-slope stability code. Recently further advancements are made by the introduction of a more sophisticated two-stage geotechnical model coupling an explicit saturation scheme and a slope stability model with cohesion terms and variable depth of detachment surface. Furthermore under development is the attempt at perfecting the deterministic model with the add-on of a probabilistic definition of the parameters with high spatial variability. In Fig. 2 is reported a scheme of the landslide triggering model.

Concerning the Hydrological model, some assumptions are needed to obtain the analytical solution for the Richards equation that governs the unsteady and variably saturated Darcinian flow of groundwater in response to rainfall. These assumptions include nearly saturated soil and relatively isotropic, homogeneous hydrologic properties. The first assumption allows simplifying the Richards equation by neglecting the effect of groundwater flow in unsaturated soils. Like suggested by Baum (Baum et al. 2002, 2005), the saturated soil assumption is usually satisfied during the winter rainy season in many areas characterized by quite wet climatic conditions but even after the occurrence of prolonged rainfall in areas usually characterized by dry conditions (Salciarini et al. 2006). A peculiarity of the proposed model is that during the slope stability analysis it takes into account for the increase in strength and cohesion due to matrix suction in unsaturated soil, that is where the pressure head is negative (Tsai et al. 2007). The geotechnical stability module is based on a infinity slope model and calculates the

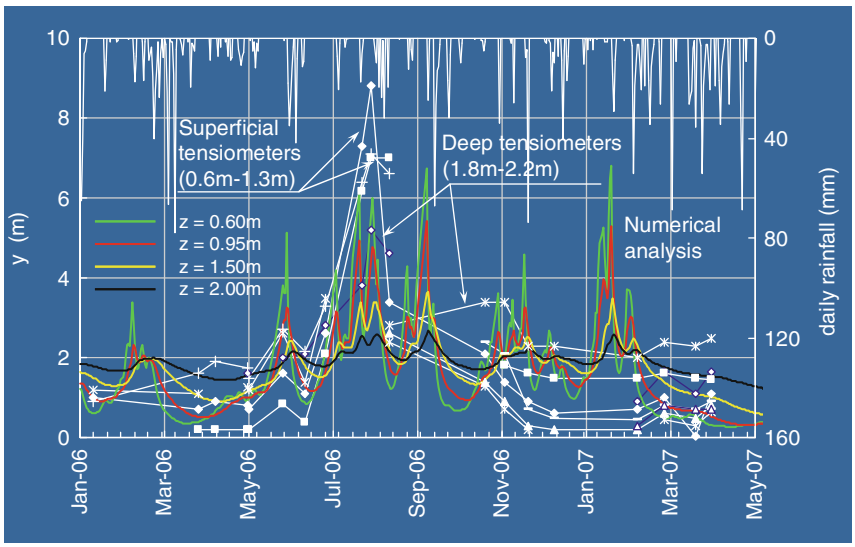

Fig. 3 Comparison of experimental (*white color*) and simulated data (*colors*), by IMOD-3D in terms of capillary height at four different depths

ratio of resisting forces versus destabilizing forces: this ratio is called the safety factor (FS), it is a dimensionless parameter, that assumes unit value when destabilizing forces they equal the resistant forces; the FS value 1 shows the beginning of the instability condition. The model input data are constituted by DEM, geotechnical parameters and soil thickness (Rossi et al. 2013). The last one is a fundamental parameter in shallow-landsliding initiation. A model has been developed to determine this parameter, based on geomorphometric and geological parameters easily measurable in the field or through remote sensing (Catani et al. 2010). Furthermore the model makes use of forecasted rainfall intensity derived from the COSMO-LM model.

Evaluation of the Integrated Simulation Model

The performance of the integrated model has been tested in some typical geomorphologic contexts of Mediterranean area. The test cases has been adopted to check the reliability of the proposed model in the evaluation of landslide triggering at regional or at slope level comparing field observations with results of numerical simulations.

Cervinara Test Case

The Cervinara site has been selected as a representative test case at slope scale. The selected area is characterised by fairly regular steep slopes consisting of layered unsaturated air-fall pyroclastic cover overlying fractured limestone. Results of in situ and laboratory investigations provide detailed data on stratigraphy and soil properties (Lampitiello 2004; Picarelli et al. 2006). The slope angle is around 40° and the average thickness of the pyroclastic cover, is slightly less than 2.5 m. First, the geotechnical model for the analysis of infiltration has been calibrated through numerical simulations, based on the values of suction measured in 2006 and 2007 (Fig. 3). The boundary conditions at the ground surface consisted in: (1) the average measured daily rainfall intensity in wet seasons, or (2) the evaporation flux during dry days estimated from suction measurements (Damiano et al. 2012). For the lateral and basal boundaries, a condition of free flow has been adopted. The best fitting of observed data has been obtained through a set of parametric analyses carried out using the soil parameters measured in the laboratory by comparing the computed and measured values of suction in 2006–2007 (Fig. 3). Finally, a general validation of the integrated model has been pursued by substituting a sequence of 1 h downscaled forecast rainfalls, from COSMO LM 2.8 km, for a range of 48/106 h (depending from rain event duration) to the measured rainfall. Tests have been carried out during three different time periods in which the area experienced moderate rainfalls (Mercogliano et al. 2011): 6–10 February 2007, 6–7 March 2007 and 3–4 April 2007.

In all tests the simulation chain has been successful in providing reliable quantitative information on the link between forecasted rainfall and slope response (Mercogliano et al. 2011). These numerical simulations have been performed adopting:

1. For the water retention curves the van Genuchten (1980) expression with $s = 0.7$, $r = 0.1$, $m = 0.05$, $n = 20$, $\alpha = 5$;
2. For the unsaturated hydraulic conductivity functions the Brooks and Corey (1964) expression ($k = ksat(Sr)\delta$) considering for the saturated conductivity the mean value obtained in the laboratory test ($ksat = 1E{-}6$ m/s) and a nil value of the residual degree of saturation Srr and an empirical constant $\delta = 3$ (Fig. 4).

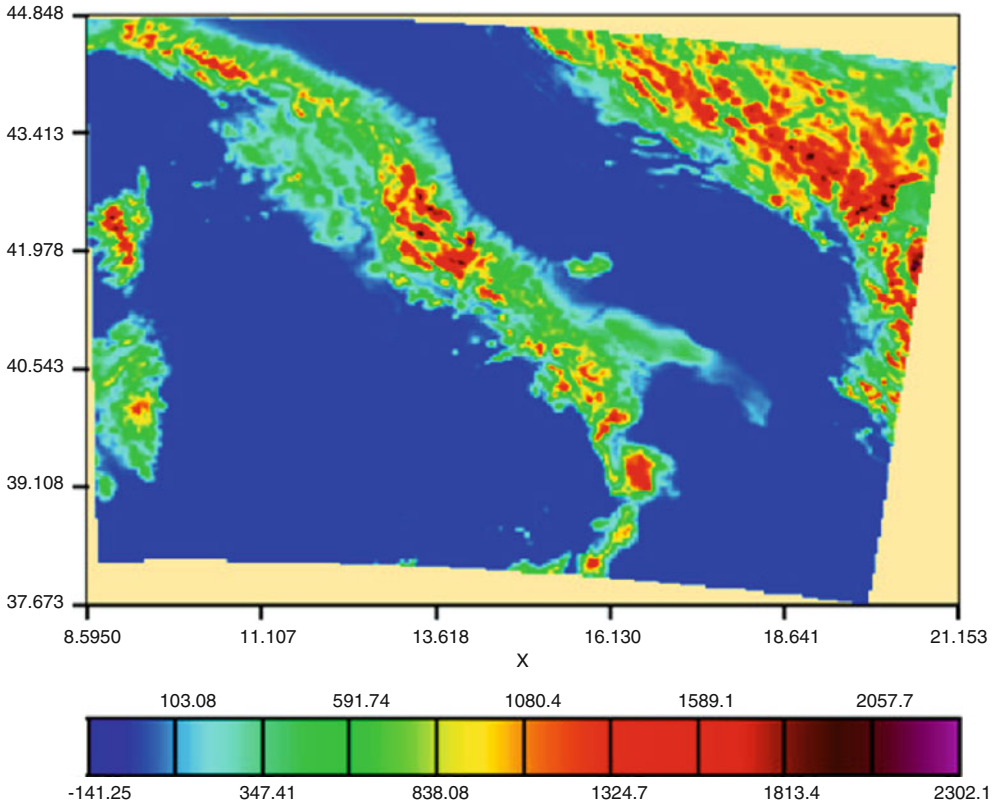

Fig. 4 COSMO LM 2.8 km geographical domain for Cervinara test cases. In the picture the domain and the model orography in meters. Each COSMO LM simulation is initialized at 00:00 UTC running for 24 h

Figure 5 reports the rainfall intensity (a) and height (b), the variation of the safety factor with depth during the event (c) and the areal distribution of the safety factor at three different depth (d) in the highlighted zone indicated in Fig. 5e. As expected in the considered short time interval (as short as about 120 h) the effects of the forecasted rainfall are significant for depths comprised between the ground surface and 50 cm. At higher depths the effects are practically negligible

Apennine Test Cases

The study area which is located in Northern Tuscany and includes the provinces of Pistoia, Prato and Lucca shows two different geological settings in the east and west sectors respectively. The Northern Apennines is a complex thrust-belt system made up by the juxtaposition of several tectonic units, piled during the Tertiary under a compressive regime that was followed by extensional tectonics from the Upper Tortonian. The latter phase produced a sequence of horst-graben structures with an alignment NW-SE that resulted in the emplacement of Neogene sedimentary basins, mainly of marine (to the West) and fluvio-lacustrine (to the East) origin (Martini and Vai 2001). Today, the morphology is dictated by the presence of NW-SE trending ridges where Mesozoic and Tertiary flysch and calcareous units outcrop, separated by Pliocene-Quaternary basins. The provinces area of Pistoia, Lucca and Prato has been elected for a large fieldwork campaign o f measurements (34 field measurements) specifically planned for the SafeLand project. In December 2009 the area was hit by a severe rainstorm which triggered during Christmas period around 300 shallow landslides. The results of the slope stability analysis of this 2009 test case were deeply affected by the errors due to snow melting phenomena. The simulations performed largely underestimate the slope failure probability of events that triggered hundreds of landslides, even if not all of them were shallows slope failure: in fact, HIRESSS physics engine contains approximation that allows only the shallows landslide triggering analysis. The results from the analysis of 24–25 December shows some critical areas diffused mainly over Lucca province but is not possible a clear spatial individuation of slope movement triggering. We can conclude that the simulating chain was able to catch a generalized state of instability probability, at least in the 25 December simulation and in Lucca province, which is confirmed by the large number of landslides reported and almost spatially distributed over all the area. The east part of that area does not show any critical situation despite the large number of

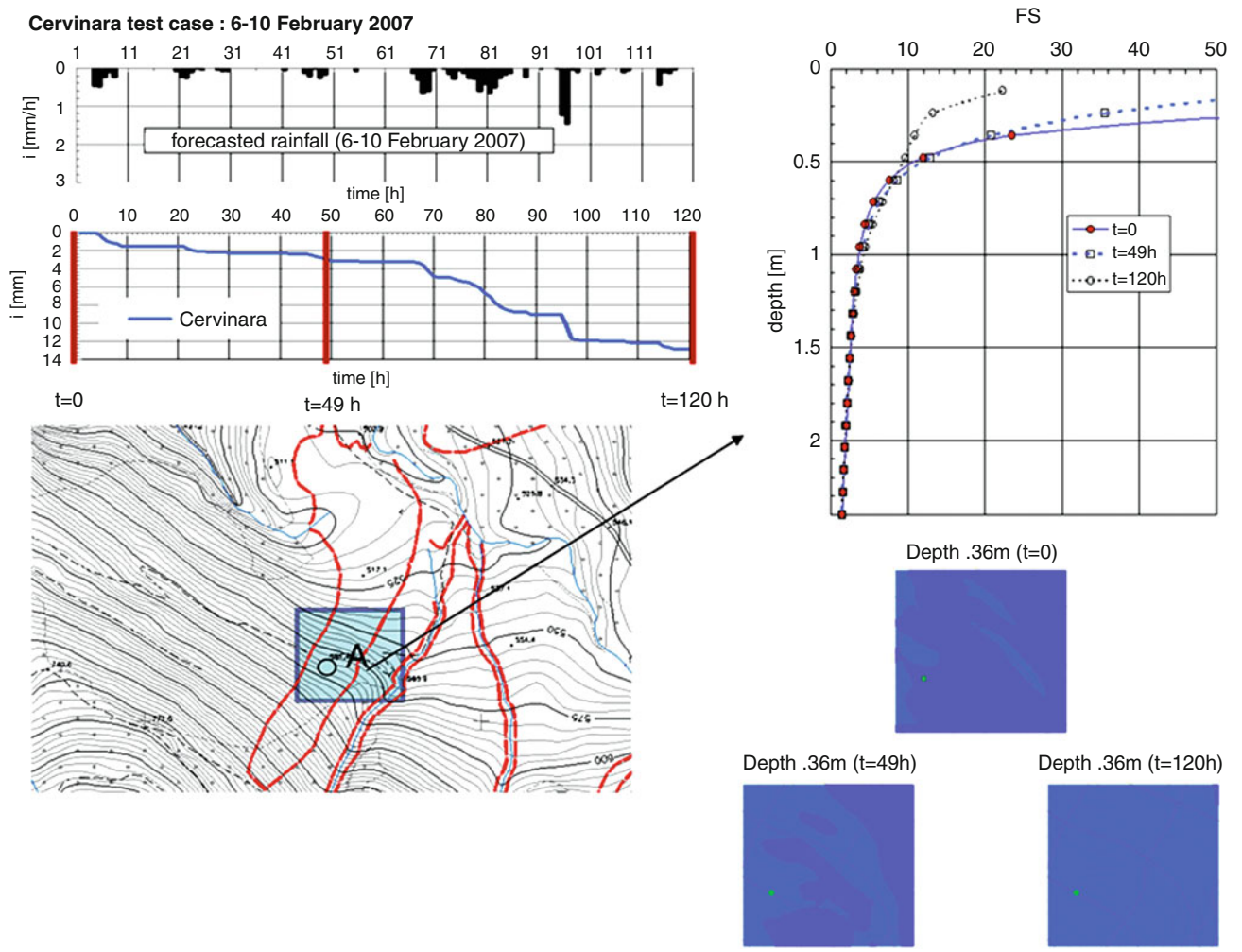

Fig. 5 Slope stability analysis for a Cervinara test case

landslides reported in that area. This test case has shown a weakness of the simulation chain that is not to able to manage the contribution of the snow at the slope instability mechanism, even if the general critical condition can be detected. The second test case event performed from data of the end of October 2003 was not affected by snow melting phenomena like those of December 2009 and was characterized by heavy rainfall. The stability analysis simulation of the 2003 event shows a better teaming between HIRESSS and the COSMO-LM forecasted rainfall intensity. The event is not affected by meteorological phenomena not implemented in the simulating chain, like snow melting encountered in 2009 event simulation, and the results has a better accordance with the historic landslides reports. The simulations do not detect a heavy critical slope condition at the North West of the area but only some localized spot. The landslides reports are numerous in this area but we cannot discriminate between shallow landslides or other soil movement types due to lack in description. Obviously the slope stability simulator cannot recognize other type of landslides due to its physics engine that can detect only shallows landslides triggering condition (Fig. 6).

The east part of test area appears affected by an overestimation of the slope failure probability considering the number and the position of triggered landslides. This zone even in 2009 event simulation was indicated like the most unstable without have a proportional number of reported soil movements. A possible partial explanation is a lack of reporting because the area is a non populated mountainous region: usually the larger number of reporting regarding landslides that involve infrastructure and water stream. Anyway the results of the two simulations suggest a more accurate investigation of this area to verify a possible inaccuracy of geotechnical and morphometric parameters characterization.

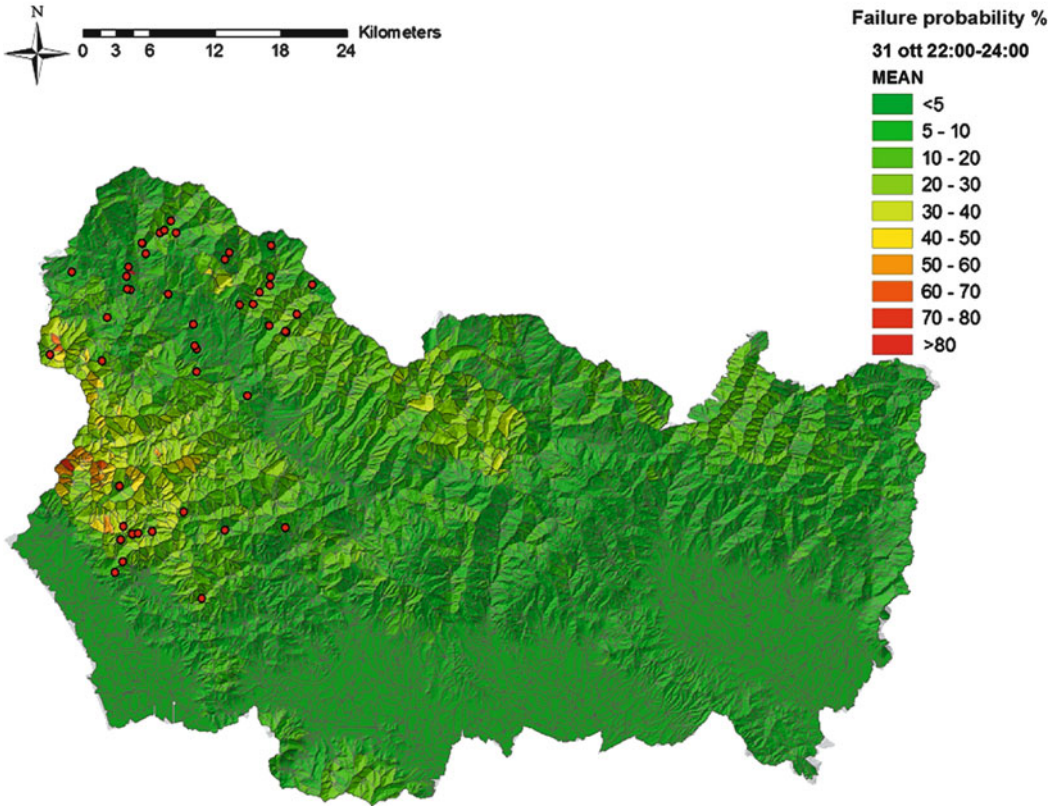

Fig. 6 The simulated slope failure probability of the Lucca, Pistoia and Prato province area during the 31 October 2003 event in a shorter timeframe analysis. Map shows the average of 3 h timeframe (22:00–24:00 of 31/10/2003). Landslides reported in the 2003 event are represented by *red dots*

Ischia Test Case

The island of Ischia is located in the southern part of the Tyrrhenian Sea, between 40°44′ North latitude and 13°56′ East longitude, 33 km from Naples. This island is 7 km wide from North to South and 10 km from East to West. The coastline is 39 km long and the total surface is 46 km^2. On Ischia prior to 2006, very few shallow landslides information is available. These events certainly have occurred in the past, as the geologic and geomorphologic settings of the territory are very similar to other areas in Campania, namely volcanic soils overlying steep massifs, where landslides have occurred frequently and with catastrophic effects. Moreover, many debris flows deposits have been found within the volcanic succession the same as geomorphologic evidences of deep landslide especially in the western side of the island and near Monte Vezzi (De Vita et al. 2006). However, as no precise documentation exists regarding earlier events it is not possible to create a comprehensive landslide inventory. The chosen test case concerns a convective rainfall event occurred on April 30, 2006. The precipitation triggered four small soil slips on the slopes of Mt. Vezzi (about 400 m on the sea level (Fig. 7)).

Fig. 7 Monte Vezzi landslides triggered by a heavy rainstorm in the morning of April 30, 2006

The slope stability analysis performed with HIRESSS using the measured radar rainfall dataset shows a progressive increase of slope failure probability that peaks in the time slot when the landslides has triggered. Throughout the day of 30 April the area gains stability and returns to a normalized condition before the end of the day. The

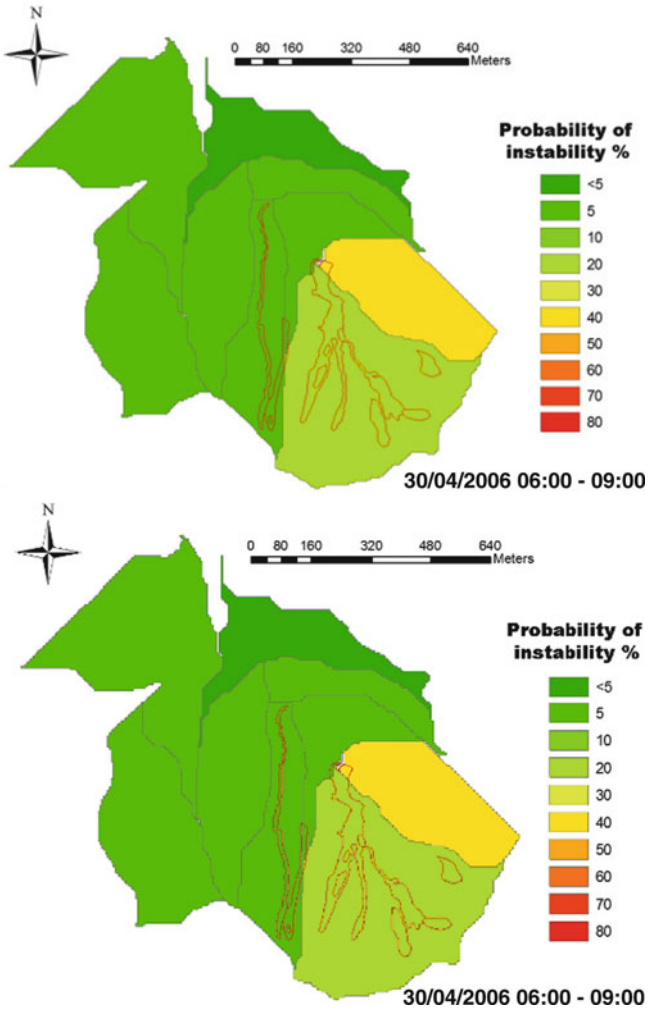

Fig. 8 The average probability of slope instability of Monte Vezzi area computed between 6:00 and 9:00 of 30 April 2006 using forecasted rainfall data (*top*) and radar measurements (*bottom figure*). Monte Vezzi landslides occurred between 6:30 and 8:00. The landslides contours are drawn in *red*

HIRESSS simulation provides realistic and satisfying results in this area coupled with radar measurement, but we do not have a complete landslide inventory of those days to perform a complete validation. Throughout the day of 30 April the area gains stability and returns to a normalized condition before the end of the day. The HIRESSS simulation provides realistic and satisfying results in this area coupled with radar measurement, but we do not have a complete landslide inventory of those days to perform a complete validation. The simulation performed with the hybrid measured-forecasted dataset, that will be the typical operative method proposed in this deliverable, shows unsurprisingly incorrect results. As mentioned, the meteorological event is recognized by COSMO-LM simulation, but the real intensity of the phenomena is not rendered. The case study suggests focalizing efforts on improving forecast of localized convective event (Fig. 8).

Conclusions

This paper present a tool for the systematic prediction of shallow landslide, triggered by intense rainfall, using as input rainfall forecast by NWP models. In particular, the COSMO LM model, a limited area model for numerical weather prediction (NWP) in the short range time (from 0 up to 3 days before the event occurrence) is used. The realized simulation chain permits to have warning map on big areas or detailed stability analysis (if well documented data about the soil structure and properties and observed rainfall are available on long period), on a particular site, with the possibility of fast upgrade. The simulation chain developed in this research activity has some very important features:

1. The time required producing regional warning map and warning information on particular test site could be available, beginning from the instant on which output or atmospherical model is obtainable, in 2–3 h. This is possible thanks to the opportunity to run HIRESSS on supercomputer, or, for IMOD-3D, to his capability to produce safety factor map in a particular site in few minutes using a normal laptop.
2. The RMI module (the tool for precipitation forecast downscaling) manages the output of an operative atmospherical model (COSMO LM) in automatic way.

This choice to use an operative atmospherical model to initialize the stability analysis will gives the opportunity to test each day the performances of the developed tools. The daily validation is the first step to decide on operative implementation of the tool but also to know and manage the forecast uncertainty and to resolve the possible systematic errors present.

Acknowledgments Thanks to ARPA Emilia Romagna, COSMO Consortium and to Centro funzionale per la Previsione Meteorologica e il Monitoraggio Meteo-Pluvio-IDrometrico e delle frane, Protezione Civile -Regione Campania. The work was (partially) supported by the UE/FP7 SAFELAND G.A. No. 226479. This support is gratefully acknowledged.

References

Baum RL, Savage WZ, Godt RW (2002) TRIGRS – a fortran program for transient rainfall infiltration and grid-based regional slope-stability analysis, U.S. Geological Survey Open- File Report, 2002-424. http://pubs.usgs.gov/of/2002/424/

Baum RL, McKenna JP, Godt JW, Harp EL, McMullen SR (2005) Hydrologic monitoring of landslide-prone coastal bluffs near Edmonds and Everett, Washington, 2001–2004, U.S. Geological Survey open-file report 2005-1063. http://pubs.usgs.gov/of/2005/1063/

Brooks RH, Corey AT (1964) Hydraulic properties of porous media, Hydrology paper 3, 27 pp. Colorado State University, Fort Collins, 1964

Catani F, Segoni S, Falorni G (2010) An empirical geomorphology-based approach to the spatial prediction of soil thickness at catchment scale. Water Resour Res 46:W05508. doi:10.1029/2008WR007450

Damiano E, Olivares L, Picarelli L (2012) Steep-slope monitoring in unsaturated soils. Eng Geol 137–138:1–12

De Vita S, Sansivero F, Orsi G, Marotta E (2006) Cyclical slope instability and volcanism related to volcano-tectonism in resurgent calderas: the Ischia island (Italy) case study. Eng Geol 86:148–165

Doms G, Schättler U, Steppeler J, Wicker L (1998) Development of the Nonhydrostatic Regional Model LM at DWD. Research Activities in Atmospheric and Oceanic Modelling, No. 27, WMO/TD-No. 865, pp 5.17–5.18 <tel:5.17-5.18%201998>

ECMWF (2004) ECMWF, Part VII: ECMWF Wave-model documentation, in IFS documentation CY28r1, available at http://www.ecmwf.int/research/ifsdocs/CY28r1/index.html, edited (2004)

Fredlund DG, Rahardjo H (1993) Soil mechanics for unsaturated soils. Wiley, New York

Gardner WR (1958) Some steady state solutions of unsaturated moisture flow equations with applications to evaporation from a water table. Soil Sci 85(4):228–232

Hardy LR (1971) Multiquadric equations of topography and other irregular surfaces. J Geophys Res 76:1905–1915

IPCC (2007) Climate change 2007: the physical science basis. In: Solomon S, Qin D, Manning M, Chen Z, Marquis M, Averyt KB, Tignor M, Miller HL (eds) Contribution of working Group I to the fourth assessment report of the intergovernmental panel on climate change. Cambridge University Press, Cambridge, UK and New York

Lampitiello S (2004) Resistenza non drenata e suscettività alla liquefazione di ceneri vulcaniche della Regione Campania. Ph.D. thesis, Seconda Università di Napoli, Aversa

Martini IP, Vai GB (eds) (2001) Anatomy of an orogen: the Apennines and adjacent Mediterranean Basins. Kluwer, Dordrecht, 632 pp

Mercogliano P, Damiano E, Bucchignani E, Olivares L (2011) Prediction of shallow landslides in pyroclastic soils due to climatic changes in the Mediterranean area. G.R.A Open Access Publication of the Earth, Planetary and Space Sciences – ISSN: 1607–7962 – vol 13, EGU2011-7789-1

Picarelli L, Evangelista A, Rolandi G, Paone A, Nicotera MV, Olivares L, Scotto di Santolo A, Lampitiello S, Rolandi M (2006) Mechanical properties of pyroclastic soils in Campania Region. In: Invited paper, 2nd international workshop on characterisation and engineering properties of natural soils, Singapore

Rossi G, Catani F, Leoni L, Segoni S, Tofani V (2013) HIRESSS: a physically based slope stability simulator for HPC applications. Nat Hazards Earth Syst Sci 13:151–166

Salciarini D, Godt JW, Savage WZ, Conversini P, Baum RL, Michael JA (2006) Modelling regional initiation of rainfall induced shallow landslides in the eastern Umbria Region of central Italy. Landslides 3:181–194

Tsai T, Chen H, Yang J (2007) Numerical modelling of rainstorm-induced shallow landslides in saturated and un-saturated soils. Environmental Geology 55(6):1269–1277. doi:10.1007/s00254-007-1075-1

Van Genuchten MT (1980) A closed-form equation for predicting the hydraulic conductivity of unsaturated soils. Soil Sci Soc Am J 44:892–898

Variation in the Occurrence of Rainfall Events Triggering Landslides

Mario Floris, Andrea D'Alpaos, Anna De Agostini, Giulia Tessari, Giovanni Stevan, and Rinaldo Genevois

Abstract

We analyze the climatic features of the Vicenza Province (NE Italy) and the characteristics of the exceptional rainfall event that hit the area in November 2010, triggering a huge number of landslides. Our analysis aims at identifying the hydrological variable related to the triggering of the recorded instabilities and the recent variation in the occurrence of rainfall events inducing landslides.

During the period 1920–2009, a negative trend in the annual rainfall and a marked positive trend of the mean annual temperature have been observed in the study area. Rainfall has become more concentrated during autumnal season (October–December) and the greatest increase in temperature has been registered in winter (January–March) and summer (June–August). As a consequence, the quantity of meteoric water available for infiltration and run off processes has increased in autumn, which has typically been the season with the maximum number of landslides. Moreover, the statistical analysis of annual rainfall maxima for durations of 1, 3, 6, 12 and 24 h, and 1, 2, 5, 10, 30, 60, 90, and 120 days, allowed us to highlight that the occurrence of intense rainfall events has increased in the last 20 years.

Our results show that the degree of rainfall-induced landslide hazard has increased in the study area, possibly due to recent climate changes. In the near future, such results should be taken into account for landslide forecasting, monitoring and mitigation.

Keywords

Rainfall • Landslides • Climate changes • NE Italy

Introduction

The characterization of the climatic settings of areas affected by landslides and the identification of the hydrological variables related to landslide triggering are the basic steps to investigate the relationships between rainfall and landslides. In the last decade, several authors suggested that a rapid increase in the frequency and intensity of heavy rainfall, possibly due to climate changes, occurred. Moreover, the frequency of rainfall-related phenomena, such as floods and landslides, increased as well together with the related economic losses and social implications, thus increasing the attention of scientists to these issuses (Gong and Wang 2000; Easterling et al. 2000; Fauchereau et al. 2003; Jomelli et al. 2007; Pelfini and Santilli 2008; Sillmann and Roeckner 2008; Floris et al. 2010; de Luis et al. 2011).

In this work we analyze the exceptional rainfall event that hit the Vicenza Province (north-eastern Italy) on November 2010, triggering a huge number of landslides. Our goal is to identify the hydrological variable (e.g. cumulative rainfall over n minutes, hours, days, or over the entire rainfall event)

M. Floris (✉) • A. D'Alpaos • A. De Agostini • R. Genevois
Department of Geosciences, University of Padua, via Gradenigo, 6, Padua, Italy
e-mail: mario.floris@unipd.it

G. Tessari • G. Stevan
Vicenza Province, Soil Protection Division, Italy

C. Margottini et al. (eds.), *Landslide Science and Practice*, Vol. 4,
DOI 10.1007/978-3-642-31337-0_17,

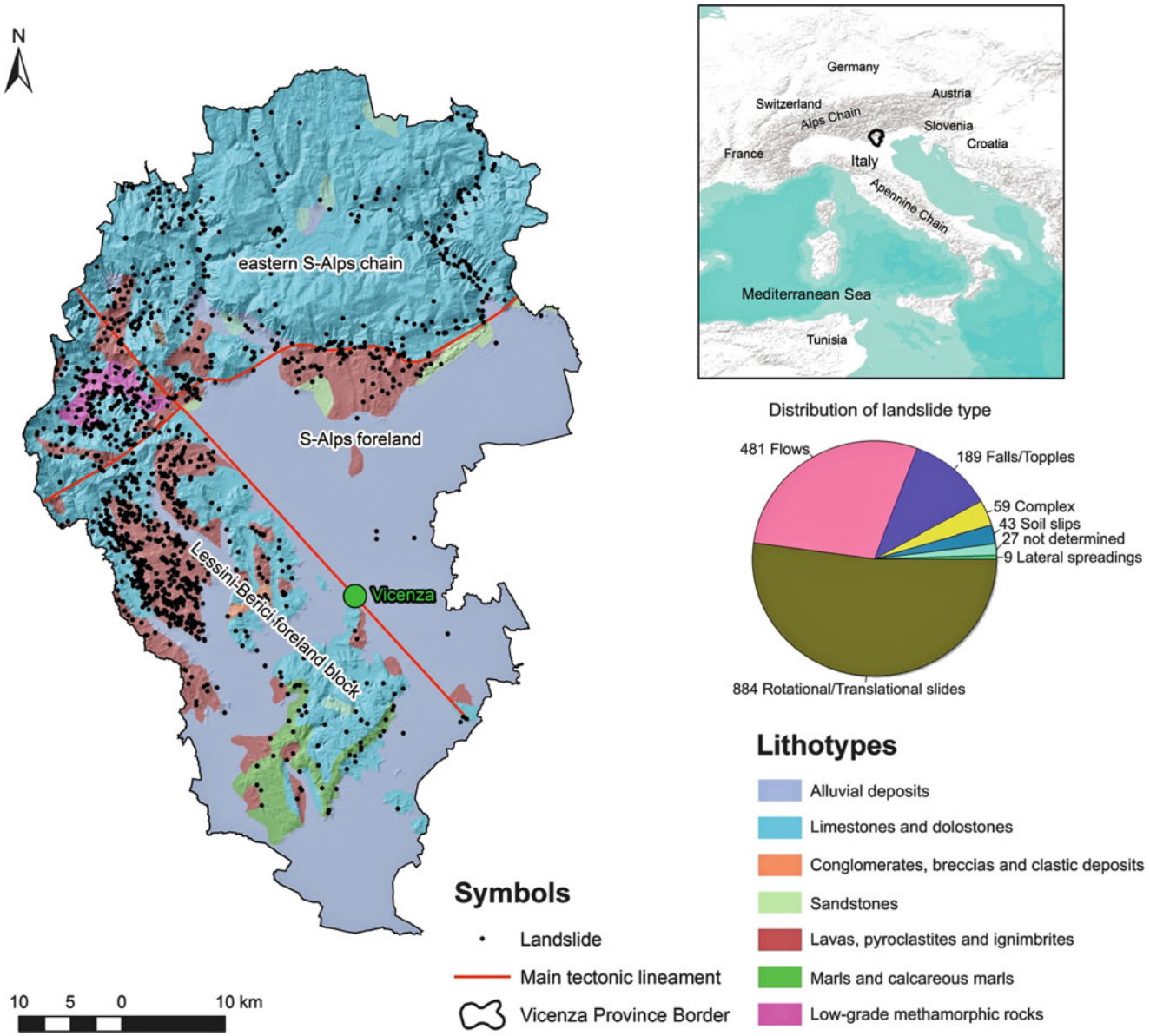

Fig. 1 Geological sketch of the Vicenza Province and location and distribution of landslides

that can be related to the triggering of these phenomena. The recent variations in the climate and in the occurrence of rainfall events triggering landslides is also analysed and discussed.

Study Area

The investigated area is located in the Vicenza Province, which can be sub-divided into two main geological and geomorphological domains separated by the main tectonic lineaments (Fig. 1).

One domain is characterized by elevations up to 700 m a.s.l. and low slope angles, and by the outcropping of volcanic deposits (lavas, pyroclastites, and ignimbrites) overlain by varying thicknesses of eluvial and colluvial deposits. This domain is mainly affected by shallow soil slips, flows and rotational and translational slides which represent more than 80 % of landslides in the Vicenza Province.

The other domain is characterized by elevations up to 1,900 m a.s.l. and medium to high slope angles, and by the outcropping of limestone and dolostone rocks, which are affected by falls, topples, deep and complex mass movements which represent less than 20 % of landslides in the study area.

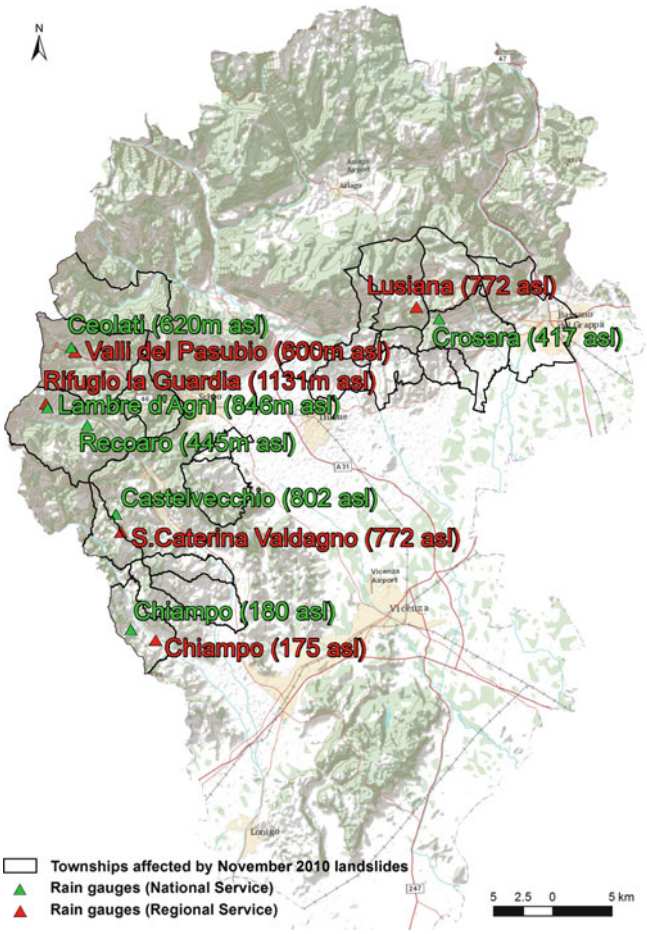

Fig. 2 Location of meteorological stations considered in the study and of the townships affected by November 2010 landslides

Climate

We analyze data collected by 11 meteorological stations of the national and regional measurement networks in the area affected by the November 2010 rainfall event (Fig. 2). The available data sets consist of: minimum and maximum daily temperature from 1949 to 2004, daily rainfall from 1920 to 1989, and 5 min rainfall from 1990 to 2010.

The climate of the study area is typical of the pre-Alps sectors in NE Italy, but some different conditions between the north-western and the south-western/north-eastern parts can be noted. The NW sector is characterised by a mean annual rainfall between 1,900 and 2,400 mm (Fig. 3a, b), and a mean annual temperature between 10 °C and 12 °C (Fig. 4a). In the other two sectors the mean annual rainfall is between 1,300 and 1,600 mm (Fig. 3c–e), whereas the mean annual temperature is between 11 °C and 14 °C (Fig. 4 b).

The distribution of rainfall (Fig. 5) and temperature (Fig. 6) during the year are similar over the entire area. Rainfall is concentrated in spring (April, May) and autumn (October, November) with a minimum in summer (July, August). The maximum temperature occurs in summer (August) and the minimum in winter (January).

The November 2010 Rainfall Event

From October 31 to November 2, 2010, an exceptional rainfall event hit the Vicenza Province with a maximum cumulative rainfall of about 500 mm and a mean of 336 mm over the area. This event represents one of the most intense and catastrophic historical floods of the last 100 years, together with the November 1966 and October 1992 floods.

The intense rainfall triggered a huge number of mass movements in the Northern and Western parts of the Province. Recorded landslides consist mainly of small to medium shallow movements involving debris cover and affecting the road network. The total estimated cost for remediation works is about 80 million euros. In the alluvial plain area the main rivers (e.g., Bacchiglione, Astico and Retrone rivers) overflowed their banks causing damages of about a billion euros to infrastructures, industrial activities, and private buildings.

In this paper, measurements of rainfall depths registered at the rain gauge located at Valli del Pasubio municipality (Ceolati rainfall station, Fig. 2) in 2010 are analyzed to investigate the November 2010 rainfall event.

The rainfall event started during the night of October 31st and finished on November 2nd at 2:00 pm and the maximum intensity was reached on November 1st (Fig. 7). To investigate which hydrological variable can be related to the triggering of landslides, we considered maximum cumulative rainfall over 1, 3, 6, 12, and 24 h during the event and cumulative rainfall over 1, 2, 5, 10, 30, 60, 90, and 120 days. We evaluated the degree of exceptionality of the mentioned hydrological variable based on the assumption that the more exceptional the rainfall event is, the stronger is the cause-effect relationship between rainfall and landslide triggering.

The Extreme Value Type I or Gumbel distribution has been fitted to the annual rainfall maxima of the extreme value series for the period 1925–1975 and to the extreme value series for the period 1990–2009, by using the method of moments for durations of 1, 3, 6, 12, and 24 h. Subsequently, the estimated parameters of the Gumbel distribution have been modelled as a function of duration to determine the DDF curves of Fig. 8, using the method of least squares. Rainfall depths measured during the November 2010 storm are also shown, to investigate the degree of exceptionality of the different variables. Rainfall Depth-Duration-Frequency (DDF) curves, in fact, allow one to determine rainfall depth

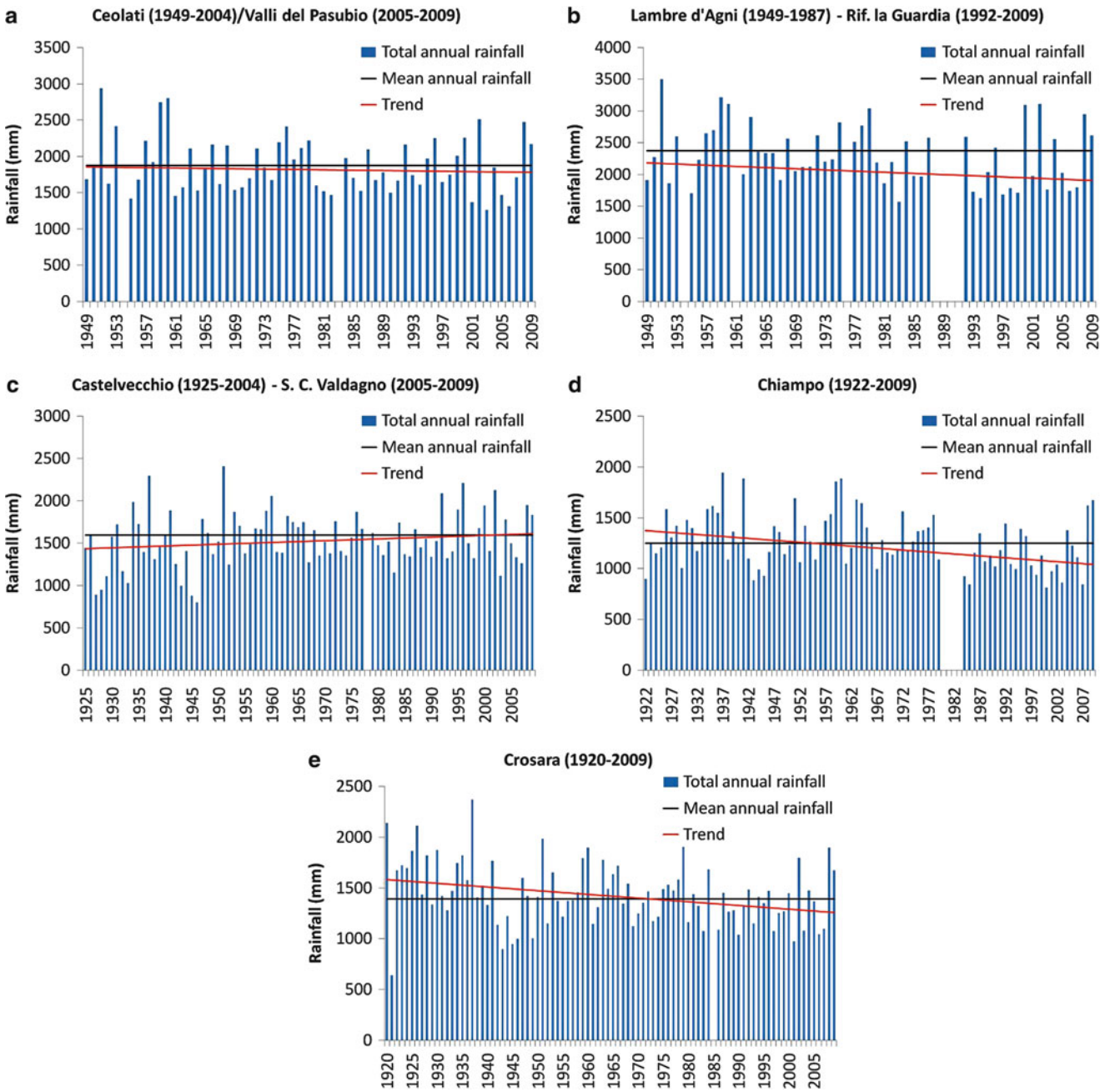

Fig. 3 Total annual rainfall at different rain gauges

(or intensity) as a function of duration for given return periods or probabilities of exceedance (frequencies).

Both the graphs of Fig. 8 show that the cumulative rainfall depths related to short durations do not intersect the lower DDF curves, displaying a value lower than the one obtained for a return period of 5 years. As the duration increases, the cumulative rainfall depths reach the DDF curves for increasing return periods. In Fig. 8a, where the DDF curves are plotted for the period 1925–1975, we show that the cumulated rainfall over 12 h reaches the DDF curve with a return period of 100 years, while the cumulated rainfall over 24 h exceeds a return period of 200 years. Similar observations emerge also from the analysis of Fig. 8b where the DDF curves were obtained using extreme value series for the period 1990–2009. The cumulative rainfall for different durations intersect the DDF curves with lower return periods compared with the previous case. However, the DDF curve with a return period of 50 years is almost reached for cumulated rainfall of 24 h.

In Fig. 9 we show the DDF curves for cumulative rainfall over 1–120 days, which has been chosen as the period that potentially influences the soil water content before the flood and, thus, the infiltration, seepage and accumulation processes inducing instability conditions. In this case the

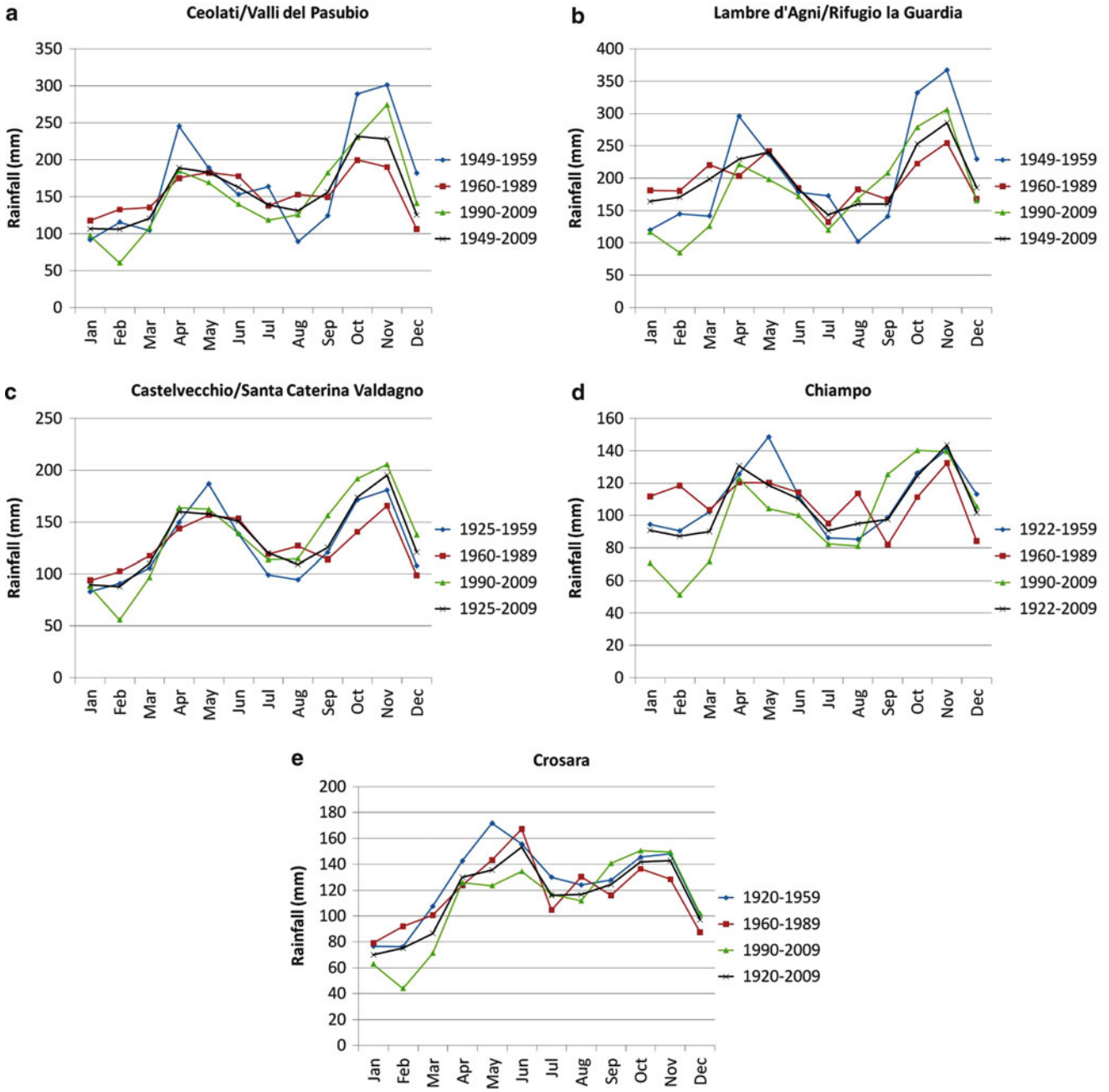

Fig. 4 Mean monthly rainfall for different periods

Extreme Value Type I or Gumbel distribution is fitted to the annual rainfall maxima (belonging to the extreme value series for the period 1949–2004) by using the method of moments for durations of 1, 2, 5, 10, 30, 60, 90, and 120 days. Subsequently, the estimated parameters of the Gumbel distribution have been modelled as a function of duration to construct DDF curves, using the method of least squares. Cumulative rainfall depths obtained for the most intense floods of the last 100 years are plotted together with DDF curves to compare rainfall depths occurred during the November 2010 event with those occurred in November 1966 and October 1992.

Results

In all the sectors of the study area a general negative trend in the annual rainfall (Fig. 3) and a marked positive trend of the mean annual temperature (Fig. 4) is observed. In particular, the mean annual temperature increased up to 2 °C in the period 1955–2004.

The distribution of mean monthly rainfall changed during the observation period (Fig. 5). Rainfall has become more concentrated in autumn (from September to November) and mean monthly rainfall of January, February, April and May

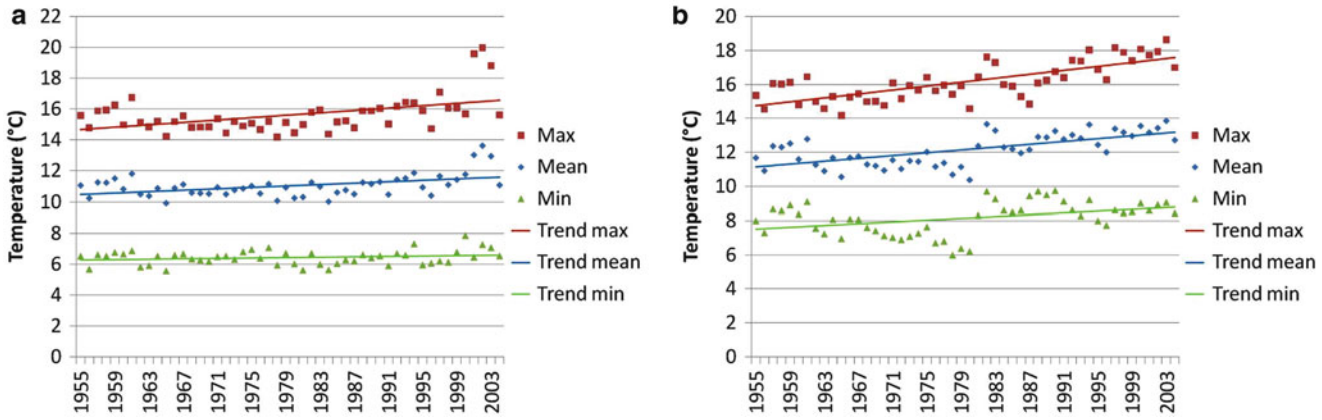

Fig. 5 Annual temperature measured at Recoaro (**a**) and Crosara (**b**) meteorological stations during 1955–2004

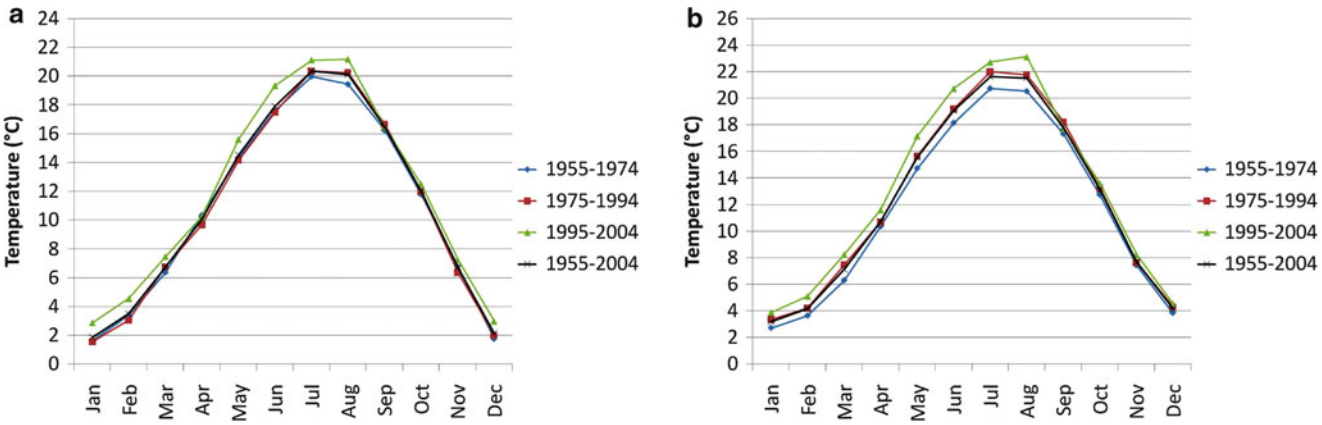

Fig. 6 Recoaro (**a**) and Crosara (**b**) mean monthly temperature for different periods

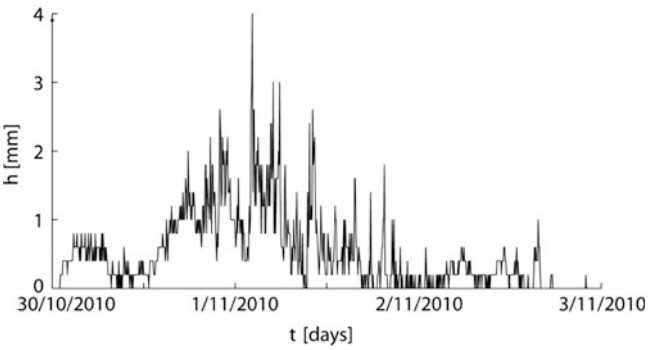

Fig. 7 Five minutes rainfall depths measured at Ceolati station during the flood event

is markedly decreased. The distribution of mean monthly temperature calculated in different periods has not changed, but in the last two decades a marked increase in the mean monthly temperature of January, February, July and August emerges (Fig. 6).

The comparison of the DDF curves for different periods (Fig. 8), suggest that annual rainfall maxima have increased in the last 20 years. In fact, as reported in the previous paragraph a given rainfall depth emerges to be more exceptional in the period 1925–1975 than the period 1990–2009.

Regarding the November 2010 rainfall event, the hydrological variable related to the triggering of landslides is the cumulative rainfall over *n* days. Rainfall depth of the 3 days of the event is more exceptional than the maximum cumulative rainfall over 1, 3, 6, 12 and 24 h during the event (Figs. 8 and 9).

Finally, the comparison of the cumulated rainfall curves among the main floods of the last 100 years (1966, 1992 and 2010 floods), shows that the 2010 event is the most relevant, particularly in terms of the cumulative rainfall depths for the first 10 days of each event (Fig. 9). It also emerges that the 1966 event was the less intense and exceptional being characterized by a return period of 5 years for the cumulative rainfall over the 2 days of the flood.

Conclusions

The November 2010 rainfall event is the most intense that occurred in the Vicenza Province in the last 100 years. Also the induced damages are the greatest, but this clearly depends on the increasing vulnerability of the territory rather than the intensity of the event.

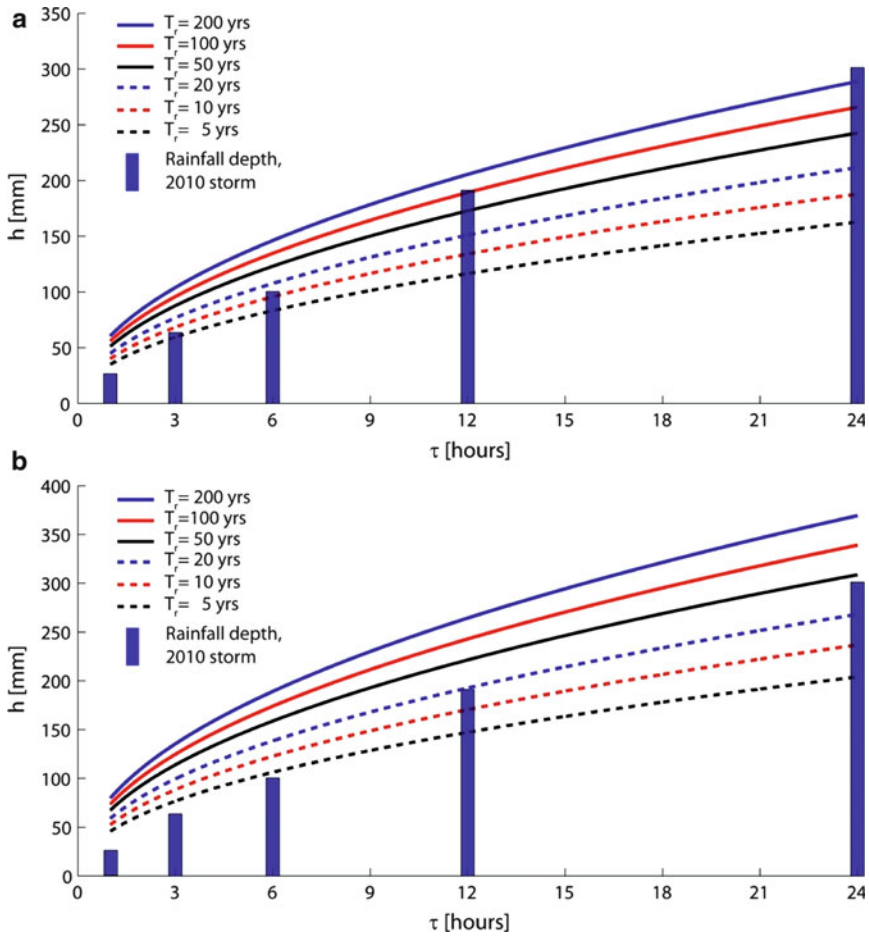

Fig. 8 Rainfall Depth-Duration-Frequency (DDF) curves calculated using 1925–1975 (**a**) and 1990–2009 (**b**) data series. *Blue bars* indicate the maximum cumulative rainfall over 1, 3, 6, 12 and 24 h during the November 2010 rainfall event

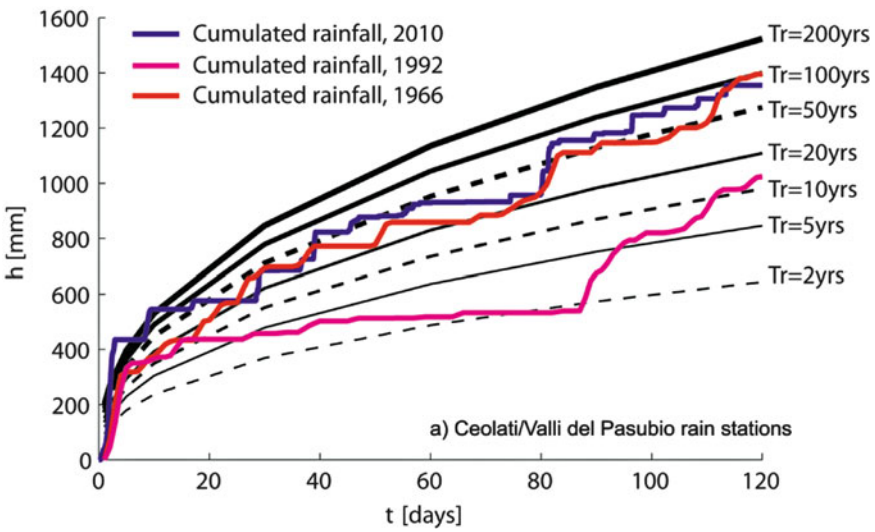

Fig. 9 Rainfall DDF curves for the most intense floods of the last 100 years cumulative rainfall over 1–120 days

Our results suggest that in the future an increase in the frequency and intensity of flood events can be expected in the study area. Something is changing in the climate in the last 20 years, possibly due to global climate changes. Because of the changes in the distribution of rainfall and temperature during the year, the quantity of meteoric water available for infiltration, seepage and run off processes has increased in autumn, which has always been the season with the maximum number of landslides. On the other hand, in winter and spring seasons the marked decrease in the rainfall and the increase in temperature suggest that in these periods the

availability of meteoric water for instability processes has become limited. Furthermore, as highlighted by the rainfall extreme value analysis, the occurrence of intense rainfall events has increased. As a consequence, the level of rainfall-induced landslide hazard has become higher.

The observed changes in the climate and the inventory of the areas affected by landslides can help in landslide forecasting, monitoring, and risk mitigation planning. The obtained results not only show which is the most hazardous period for landslide, but also indicate the hydrological variable related to the occurred instabilities as the cumulative rainfall over n days. In fact, the November 2010 rainfall occurred in a hydrological context which already presented critical characters due to the rainfall during the months before the event. Possibly this is the reason for the huge number, about 500s, of instability phenomena. Even if more in depth studies on the physical phenomena inducing landslide are necessary, the Depth-Duration-Frequency (DDF) curves implemented in this study can be used to forecast new floods and to set an alert system for rainfall-induced landslides in the Vicenza Province. The comparison among the DDF curves and the cumulated rainfall depths of the last century flood events points out that the 1966 rainfall event could be considered as the minimum threshold for floods and landslides over large areas, and the corresponding DDF curve with a return period of 5 years can be considered as the minimum alert threshold. Higher threshold alerts can be assigned taking into account the increase in the degree of exceptionality in correspondence of the DDF curves for different return periods.

Acknowledgments This research was financially supported by the University of Padova, research projects CPDA085240 (Principal investigator: Mario Floris, Department of Geosciences) and GEORISKS (Principal investigator: Rinaldo Genevois, Department of Geosciences). The authors thank the Vicenza Province and ARPAV (Agenzia Regionale per la Prevenzione e Protezione Ambientale del Veneto, Agency for Environmental Prevention and Protection in the Veneto Region) for their collaboration.

References

de Luis M, Gonzalez-Hidalgo JC, Brunetti M, Longares LA (2011) Precipitation concentration changes in Spain 1946–2005. Nat Hazards Earth Syst Sci 11:1259–1265

Easterling DR, Evans JL, Groisman PY, Karl TR, Kunkel KE, Ambenje P (2000) Observed variability and trends in extreme climate events: a brief review. Bull Am Meteor Soc 81:417–425

Fauchereau N, Trzaska S, Rouault M, Richard Y (2003) Rainfall variability and changes in Southern Africa during the 20th century in the global warming contex. Nat Hazards 29:139–154

Floris M, D'Alpaos A, Squarzoni C, Genevois R, Marani M (2010) Recent changes in rainfall characteristics and their influence on thresholds for debris flow triggering in the Dolomitic area of Cortina d'Ampezzo, north-eastern Italian Alps. Nat Hazards Earth Syst Sci 10:571–580

Gong DY, Wang SW (2000) Severe summer rainfall in China associated with enhanced global warming. Clim Res 16:51–59

Jomelli V, Brunstein D, Grancher D, Pech P (2007) Is the response of hill slope debris flows to recent climate change univocal? A case study in the Massif des Ecrins (French Alps). Clim Chang 85:119–137

Pelfini M, Santilli M (2008) Frequency of debris flows and their relation with precipitation: a case study in the Central Alps, Italy. Geomorphology 101:721–730

Sillmann J, Roeckner E (2008) Indices for extreme events in projections of anthropogenic climate change. Clim Chang 86:83–104

Part II

Landslides, land-use systems and food security

Introduction by Thomas Hofer

Watershed Management and Mountains – Forestry Department,
UN Food and Agriculture Organization, Viale delle Terme di Caracalla,
Rome I-00153, Italy

The Food and Agriculture Organization of the United Nations (FAO) convened Session L02 on "Landslides, Land-Use Systems and Food Security" which provided an opportunity to explore new grounds of landslide research and to make first steps towards moving beyond its traditional focus. Besides understanding of the earth movements in terms of volume, slope angle and geological structure among others, the session offered a venue at which the human dimension related to landslides hazards was highlighted and gained particular focus. It turned out to be a relevant platform to discuss and give voice to the importance of livelihoods in disaster risk reduction/disaster risk management approaches, in line with the WLF-II slogan "*putting science into practice*".

The workshop was attended by a small but very active group of participants that enriched the discussion by sharing their perspectives, experiences and expertise in natural risks mitigation. The geographical scope of the session was well sorted and presentations covered different areas of the world, namely Uganda, Honduras, Ecuador, Pakistan, India and Nepal.

The session was introduced by a presentation of FAO vision on the prevention and mitigation of adverse effects of natural hazards to provide timely and reliable hazard forecast. The introduction to FAO's approach on disaster risk management gave a conceptual framework to start the debate which followed the presentations of the case studies collected in this chapter.

On the whole, each presentation emphasized how landslides depend and, in turn, affect a number of interacting components and need to be read in the broader context of livelihoods and food security. Participants voiced the importance of reflecting landslides, and in general natural hazards, under a landscape and multi-hazard approach. In fact, the inter-connectivity of landslide processes with overall natural resources management practices, economic conditions and social factors is perceived as a major challenge to focus on.

Furthermore, the need to take action at a political level in the context of disaster risk reduction was raised in each speech. Land tenure rights and secure access to local resources are considered fundamental to enhance people's interest in managing land in a sustainable way which can, in turn, decrease the occurrence of natural hazards. In particular, a relevant trade-off emerged as regards the construction of roads, since they provide accessibility but can be damaging and trigger landslides. Special attention was also given to role of forests in term of protection against natural disasters.

Also, most presentations bought attention on and advocated the importance to look not only at the big and spectacular landslides but also at "invisible disasters": the summing up of many small and unspectacular earth movements which can have disastrous livelihood consequences.

Integrated Watershed Management was recognized as a very appropriate approach for landslide risk mitigation and overall disaster risk reduction/disaster risk management, capable of taking into account different components that can potentially contribute to unsustainable human-led activities and resulting natural hazards. The essential role of indigenous experience and local knowledge gain particular attention in this approach.

Under the slogan “putting science into practice” the session on Landslide, Land-Use Systems and Food Security underlined the need to implement landslide research with a landscape approach which considers different perspectives, includes livelihood aspects, and involves different disciplines such as social sciences. In this context, the overall concept of “science” has to be expanded when addressing disaster risk reduction/management. To do so, researchers have to translate science into products which can be understood by practitioners and decision makers and which allow science to inform/advance through field evidence and practice.

Landslides, Land-Use Systems and Food Security

Thomas Hofer

The Problem

Landslides pose considerable risks to the environment. They threaten the lives of people and livestock and destroy land-use systems and agricultural production. This has heavy impacts on the livelihoods of affected people, their economic situation and food security. It is a stark fact that it is often the poorest and hungriest people who are the most seriously hit by these dramatic events. In developing countries, poor and marginalized people are often forced to settle and to cultivate land in hazard-prone areas due to population pressure and, accordingly, the effects of landslides on lives and assets can be disastrous.

People and their land-use systems, on the other hand, can influence the occurrence of landslides. Besides the physical causes and triggers of landslides such as geological failures, erosion processes and heavy rainfall events, activities such as forest harvesting, road construction, mining, unsustainable agricultural practices and overgrazing have been found to have an impact on shallow landslides. Their influence on deep-rooted landslides is, however, minimal.

Recent developments such as population growth and the expansion of commercial agriculture have reduced the availability of arable land. Impoverished farmers are increasingly forced to clear marginal lands on steep slopes and reduce needed fallow periods. More and more animals graze on mountain pastures and in forested land. Such inappropriate farming practices and the destruction of forests aggravate the pressure on the natural resources and increase the likelihood for landslides. Ground cover is destroyed, soils get compacted and erosion rates accelerate – all processes that increase the potential for natural hazards.

A vicious circle arises: Poverty increases the likelihood for settlement and cultivation in hazard-prone areas and can lead to unsustainable use of natural resources. As a result, poor people are more often and more seriously hit by the occurrence of landslides which has heavy impacts on food security.

Most of the current approaches in landslide risk reduction follow a mainly technical path and neglect the human factor. Integrated approaches that take into account people and all aspects of local livelihoods, including socio-economic issues, agriculture, pasture, forestry and hydrology are needed in order to address this complex problem.

The Solution

Integrated disaster risk management (DRM) addresses all types of measures for natural disaster reduction. Such an approach includes measures to reduce the vulnerability of a given setting, measures limiting the extent of damage just after the occurrence of an event as well as provision for efficient rehabilitation and reconstruction. It is the systematic action in a cycle of prevention, response and recovery.

To organize spatially the different land-uses and promote the implementation of suitable practices, one ideal planning unit is the **watershed**. It allows addressing upstream-downstream linkages, such as landslides, and provides a framework for sound land use planning. Based on risk and hazard assessment the landscape is divided into different risk zones. By taking into account the risk level of a certain area, a specific land-use (e.g. forestry, agriculture, settlement etc.) can be identified. **Adapted land-use systems** and adequate **natural resource management** can reduce the potential for landslides and, especially, mitigate the processes leading to increased landslide hazards, such as gully erosion.

T. Hofer (✉)
Watershed Management and Mountains – Forestry Department, UN Food and Agriculture Organization, Viale delle Terme di Caracalla, Rome I-00153, Italy
e-mail: Thomas.Hofer@fao.org

C. Margottini et al. (eds.), *Landslide Science and Practice*, Vol. 4,
DOI 10.1007/978-3-642-31337-0_18,

Every land-use system has its different problems and poses particular challenges for its sustainable management. For example:

- **Protection forests** which are a well-adapted and cost-effective solution for steep, high risk zones have to be managed sustainably considering tree species, age repartition, stand density, stand health, stability etc. Particular attention is necessary during forest harvesting operations and when constructing access roads.
- **Pasture** management: In order to avoid overgrazing, the number of animals a certain area can sustain has to be carefully assessed and respected; rotational grazing should be applied.
- **Agriculture:** Conservation agriculture and soil and water conservation measures such as zero tillage, agroforestry and mulching have to be encouraged. Such measures aim at stabilizing the slope, increase water infiltration and soil strength, reduce erosion and, hence, contribute to the reduction of landslide risks.

Thus, land-use systems play different roles. They provide food, wood and habitat to local livelihoods and should, at the same time, reduce the risk for and increase the resilience to natural hazards. Land-use systems always involve people. **Integrated approaches that also take into account socio-economic issues** are required in order to assure the sustainable management of different land-use systems. Experience shows that often the underlying causes of unsustainable land-use are social or economic and that sustainable land-use practices are not adopted because they are socially not acceptable and/or economically not viable. Alternative income-generating activities can provide farmers with an additional income source which, in turn, can divert the pressure on land resources and contribute to its sustainable management. **Diversification** of livelihoods, vegetation cover types and crop species – the mixing of different land uses in general – increases the resilience of local farmers and may improve the way natural resources and corresponding livelihoods can be rehabilitated after landslide events. Further, the sustainable management of natural resources and the diversification of livelihoods increase people's food security and have positive effects on water resources.

Land-use and disaster risk management require the **participation of different stakeholders**, such as politicians, technicians, local farmers, foresters etc. The practices and points of view of local people have to be taken into account in the search for sustainable solutions. Gathering all stakeholders in a given setting enables more informed decision making on landslide risk mitigation. Furthermore, action has to be taken at the **political level**. Policies and laws are needed that regulate the use of the natural resources. A particular problem, especially in developing countries, is the absence of official land tenure rights for local farmers. When given secure access to local resources, farmers have a greater interest in managing them sustainably which, in turn, contributes to landslide risk reduction.

By applying such integrated approaches the vicious circle mentioned previously can be interrupted: Due to risk and hazard assessment, people do not settle nor cultivate in high risk areas. Therefore the risk for landslides can be reduced by diverting the pressure on the natural resources and applying sustainable land-use practices. This reduces people's exposure to and the risk of occurrence of landslides which, in turn, improves the situation of local livelihoods also with regard to food security.

In this framework, FAO recognizes the need for a more holistic disaster risk management (DRM) approach that integrates risk reduction (pre-disaster preparedness, prevention and mitigation) with emergency response and post-disaster transition strategies, while working in close collaboration with various partners and stakeholders on regional initiatives.

When implementing post-emergency rehabilitation projects, The Food and Agriculture Organization of the United Nations (FAO) promotes an approach that goes from relief to rehabilitation and puts special emphasis on the long-term planning for sustainable development. Risk and hazard assessment and mapping and subsequent spatial planning are an integral part of this approach. Particularly in developing countries, where this important aspect is often neglected, it is indispensable that also these steps receive adequate attention in order to avert or at least mitigate future disasters. This, in turn, contributes to the stabilization and overall sustainable development of affected regions.

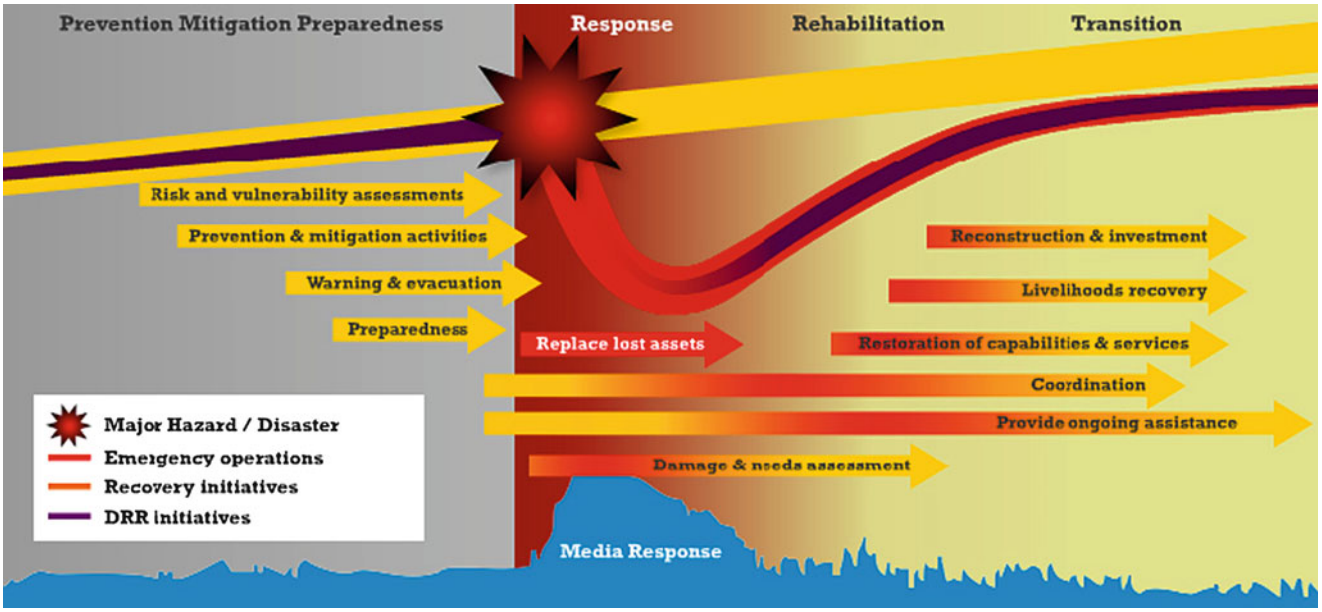

FAO. 2011. Introduction to disaster risk management (e-learning module) (Adapted from TorQaid)

Landslides in Bududa, Eastern Uganda: Preliminary Assessment and Proposed Solutions

Yuri Gorokhovich, Shannon Doocy, Felix Walyawula, Andrew Muwanga, and Fernando Nardi

Abstract

Severe rains at the beginning of March in eastern Uganda caused fatal landslide in village Nametsi, district Bududa. On March 1st 300 people were missing or dead as the result of this event. More than 8,000 people from nearby villages were evacuated in UN funded temporary camp in Bulucheke. Results of preliminary assessment of the landslide situation showed development of new scarp within 300 m from the head of the Nametsi landslide. Absence of drainage systems, steep slopes and changes of the land cover exacerbate the potential for new landslides and will lead to new disasters in the future. Bududa area is known for Arabica coffee plantations that provide cash and jobs to local residents. Establishment of a simple monitoring system and education of local population regarding mitigation measures will reduce the risk of future disasters and provide better and safe environment for the coffee production. This will also lead to the reduction of poverty in the area and creating a potential for the future economic growth.

Keywords

Landslides • Bududa • Uganda • Assessment

Introduction

Bududa district has a long record of landslide activity. The district is located at an average elevation of 1,800 m above sea level (a.s.l.) on the western slope of Mt. Elgon, former volcano active during the Miocene epoch (early-middle Neogene). Weathering and erosion of volcanic material created steep slopes up to 60–70° covered by colluvial deposits prone to mudflows. The Bagisu tribe people living in the area remember occurrences of landslides in the early 1930s, 1954, 1983, 1997 and 2006/2007 with fatal accidents.

Human settlements in the forested slopes in Bududa are noted since fourteenth century. Two resettlement programs in 1983 and 1990 restricted cultivation areas outside of the Mt. Elgon National Park. Cultivation is the main activity for 92 % of population. Main food crops are maize, potatoes, millet, beans, onions, bananas. Main cash crops are Arabica coffee, cotton and cashew nuts.

According to Sayer (2002) the most famous Arabica coffee (Bugisu) in Uganda comes from Bududa where

Y. Gorokhovich (✉)
Department of Environmental, Geographic and Geological Sciences, Lehman College, City University of New York, 250 Bedford Park Blvd West, Bronx, NY 10468, USA
e-mail: yuri.gorokhovich@lehman.cuny.edu

S. Doocy
Center for Refugee and Disaster Response, Johns Hopkins Bloomberg School of Public Health, 615 N, Wolfe Street, Baltimore, MD 21205, USA

F. Walyawula
Makerere University, P.O. Box 6023, Kampala, Uganda
e-mail: felixwaa@hotmail.com

A. Muwanga
Department of Geology and Petroleum Studies, Makerere University, P.O. Box 7062Kampala, Uganda
e-mail: amuwanga@sci.mak.ac.ug

F. Nardi
Honors Center of Italian Universities (H2CU), Sapienza University of Rome, Via Eudossiana 18, Rome 00100, Italy
e-mail: fernando.nardi@uniroma1.it

C. Margottini et al. (eds.), *Landslide Science and Practice*, Vol. 4,
DOI 10.1007/978-3-642-31337-0_19,

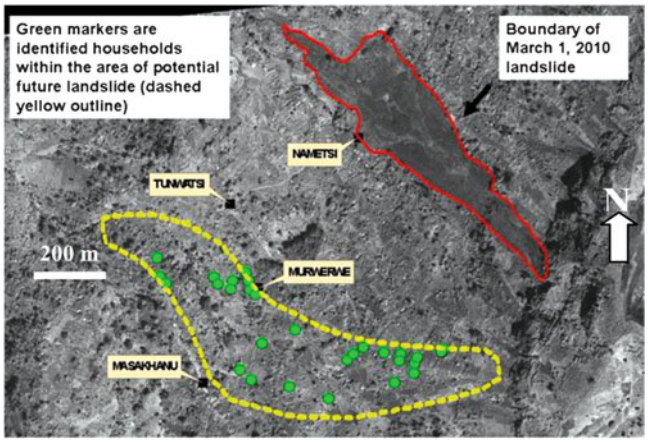

Fig. 1 Location of March 1, 2010 landslide and boundary of potential future landslide (*dashed yellow line*) identified from elevation data and field survey (by newly developing scarp) (Images were obtained from eMap Inc.)

it was introduced in 1912. Coffee plantations can be cultivated up to 2,300 m elevation. Rainy seasons in October–November and March–June provide two harvests; however the best Arabica growing at higher altitudes has only single crop (Sayer 2002). Coffee then exported via several organizations including Sucafina, Volcafe, Ecom and local Bugisu Cooperative Union (BCU).

Average production of arabica is estimated to be 750–3,000 kg/ha (Masiga and Ruhweza 2007; Sayer 2002). Considering coffee price of 1,050 Ugandan shillings per kilogram (in 2002) and total area of Arabica coffee 33,985 ha (Sayer 2002), the total minimum potential of this industry for one crop is roughly $1{,}050 \times 750 \times 33{,}985 = 26{,}763{,}187{,}500$ Ugandan shillings or 9,930,681 USD. This is considerable economic asset for Uganda and especially for local people in Bududa district.

Economic losses do not come only from the fluctuating prices on the global market or political changes in Ugandan society. Landslides (Kitutu et al. 2011) are one of the main factors in the loss of income and land for local farmers in Bududa, Bulucheke, Bushika and Bubita districts. Losses of human life are not considerable (the maximum is 300 people missing or dead on March 1, 2010), however the displacement of population reaches thousands.

Recent landslide in Nametsi village that occurred on March 1, 2010 became the most fatal one for the past 50 years. More than 4,000 people from surrounding villages were displaced temporarily in UN sponsored camp. By July 2010 Bulucheke camp population grew to the staggering 8,170 people who arrived from 13 villages surrounding Nametsi because of the fear of future landslides.

Among people who left landslide prone areas and settled in UN camp, many come back on a daily basis to tend to their gardens and crop fields. Still many people remain in their villages, hoping that landslides will not occur again. Meantime, new scarp is being developed above village

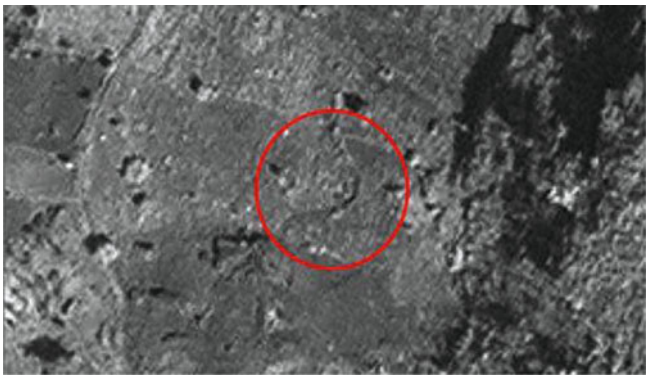

Fig. 2 Newly developing scarp above village Murwerwe (World View 1 image was obtained from eMap Inc.)

Murwerwe, next to Nametsi village (Fig. 1). Absence of geologic monitoring program, slope stabilization measures and land use planning increase risk of future landslides and potential human losses.

Presented paper is an attempt to summarize findings of the field assessment conducted in July 2010 by interdisciplinary team from the John Hopkins University, Lehman College and Makerere University and provide simple recommendations that can be implemented by local communities.

Materials and Methods

In July 2010, a geologic field survey and mapping of the March 1, 2010 Nametsi landslide and surrounding areas was conducted using GPS equipment (Trimble ProXH receiver and Nomad data logger). Additionally, images from World View 1 and QuickBird satellites with resolution 0.5–0.6 m. were used to identify landslide area before and after March 1 event (Fig. 1). Field survey included visual analysis of the terrain, measuring topographic profiles along and across the landslide area, and identification of geomorphologic characteristics related to the landslide processes.

Survey of affected population was conducted by four groups of students from Makerere University. Groups were introduced to survey sheets with questions about family status, health conditions, living characteristics, etc. Groups of students visited displaced population families in Bulucheke camp and also collected data on population still living in villages near Nametsi (i.e. people who refused to be relocated and felt safe).

Field and Satellite Image Assessment

Mapping of the slope area above the adjacent village of Murwerwe revealed a newly developed scarp or crack 0.5–2.0 m high, 25 m long and 9 m wide at the apex (Fig. 2). The apex, located at 2,076 m, is at the same elevation as the apex of the fatal March 1, 2010 Nametsi

Fig. 3 Rock exposure shows dipping layers, almost parallel to the slope (Photo is taken on flat surface near the top of the hill)

Fig. 4 Water tank releases water into the ground and causes erosion

landslide. The distance between the two is approximately 300 m along the convex slope which is completely covered with crop fields.

Along the bottom of the scarp, a newly developed crack 10–15 cm wide is visible for at least 100 m. By overlaying field survey data and elevation model from ASTER GDEM data we found that the apex of the scarp is in the upper-middle part of the concave slope which is a common geomorphologic form that favors landslides. Considering the very high slopes (up to 60°) in the area, the location of the scarp signifies a critical situation where an excess of rainfall could trigger another massive landslide.

Using high resolution (0.5 m) satellite imagery of the Nametsi area, we estimated that at least 29 households are in eminent danger if a new landslide develops (Fig. 1). Each household was identified from the image by characteristic reflection from the metal roof and its rectangular/square shape. Assuming that the geologic structure of the slope above Murwerwe is similar to nearby Nametsi, the potential landslide will affect not only Murwerwe village but also nearby Masakhanu.

Field survey of the Nametsi and surrounding area showed that:

1. In many locations carbonate rocks of the substrate exhibit a dip almost parallel to the hill slope (Fig. 3).
2. Landslide in Nametsi and newly developing scarp are located within concave slope areas.
3. Water supply to villages is not maintained properly and leaking water faucets and mains increase water content in soils and cause slope erosion (Fig. 4).
4. Houses are build on dug-in terraces that lack drainage and lateral support (Fig. 5).
5. Land cover changed considerably on most slopes surrounding area (Fig. 5) from native vegetation to agricultural species.
6. Settlements and plantations are located on steep slopes ranging from 40° to 70°.

Assessment of Relocated Population

Much of the surviving population in Nametsi as well as 13 other surrounding at risk villages were resettled to nearby Bulucheke Camp. Our assessment of Bulucheke Camp was limited to key informant interviews because Makerere University recently completed a larger evaluation of the camp population and living conditions. The overcrowded camp

Fig. 5 Artifical terrace on steep slope without drainage system and lateral support. In the *lower left corner* of the photo (where tree fell) can be seen a shallow landslide and developing scarp

was originally planned as a temporary settlement for a population of 4,000; however, the current camp population exceeds 8,170, more than double the planned capacity.

The camp was scheduled to be closed in May 2010, however, identifying permanent resettlement options for the population has been problematic and the camp remains open without an anticipated closure date. As a result of the planned camp closure, many UN agencies and international NGOs phased out of the camp. Currently the Red Cross is the lead agency in the camp and food rations are provided by the Office of the Prime Minister (OPM); Transcultural Pyschosocial Organization (TPO) has remained in the camp to address psychosocial needs.

Because the camp is overcrowded, new residents are not allowed into the camp and populations in high risk villages have no resettlement options. Additional landslides have occurred as recently as June, and new cracks and scarps continue developing in the ground above the neighboring villages such as Murwerwe, which suggests a need for temporary resettlement options for populations that remain in high risk landslide areas.

Living conditions in Bulucheke camp are challenging and indicate that additional support for the displaced population is needed. Many families live in shared communal tents which house as many as 30–40 individuals; in addition, there is a shortage of tarps and mud is a problem in tents which do not have floors. Rations, provided by OPM, consist of 4.5 kg/person/week of maize flour and beans; no sugar, cooking oil, or other commodities are provided.

The camp primary school, initially supported by Save the Children, is overcrowded with an estimated 2,100 students; with only 15 teachers it is grossly understaffed, with a teacher to student ratio of approximately 140:1 learning is nearly impossible. Secondary school age children attend schools in the surrounding community which has also resulted in overcrowding. The camp health facility is understaffed, which leads to wait times sometimes in excess of 5 h. Drug stocks are limited and referrals, either to Bulecheke health center or Bududa hospital are problematic because patients are carried by hand; obstetric cases are a particular challenge and several babies died in en route since the departure of the Red Cross ambulance in April. Camp water supplies are reportedly adequate; however, hygiene and sanitation are major concerns. Approximately half of the 70 initially constructed latrines are no longer in service because they are full; more latrines and permanent structures are urgently needed in the camp.

The local government does not have the resources to adequately support the Bulucheke camp population and the remaining NGOs do not have the capacity to address all of the issues in the camp. Additional resources are required to meet the needs of the camp population, and long term resettlement strategies for affected populations in both the camp and the at-risk communities should be developed and implemented since geologic conditions of the area indicate high possibility of the next fatal landslide event during the coming rainfall season.

Conclusions and Recommendations

Geological structure of the area consists of red colored soils, products of weathering of fenitised basement rocks of alkaline volcanic complex known as Bukigai (Kitutu et al. 2009). The immediate location of Nametsi landlside contains compacted silty clay with debris of colluvial material. Recent soil engineering study by Mugagga et al. (2011) described Nametsi soils as vertisol, highly expandable (by water content) soil type.

Combination of steep slopes, highly expandable (by water content) soils, concave areas of slopes, dip of substrate rocks parallel to slopes and human practices of uncontrolled terraces, expanding plantations, mismanagement of water supply provide critical conditions for landslide occurrence. These factors were summarized in previous studies by Claessens et al. (2007) and Knapen et al. (2006) and provide a solid basis for the modelling with Geographic Information System.

Displacement of population due to the landslides is a difficult task for both, people and the government. It requires funding and produces internal conflicts, causes degradation of environmental and health conditions, especially for children, women and elders. Displacement also reduces available work force for agriculture, especially if landslides occur during the period of harvest.

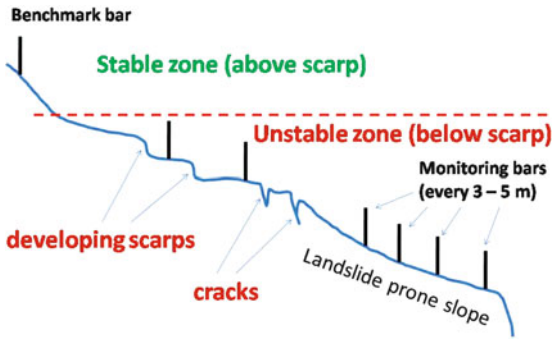

Fig. 6 Landslide monitoring scheme

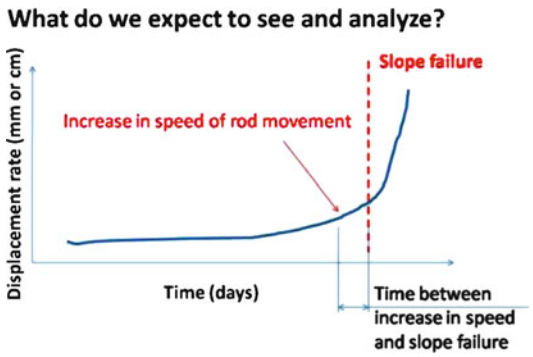

Fig. 7 Expected landslide behavior derived from monitoring data

Recommendations

While it is impossible to prevent landslides in the area, it is possible to mitigate landslide effects and reduce the risk of the landslide occurrence by implementing simple monitoring and management measures. Establishment of the landslide monitoring is particularly urgent for the area above Murwerwe where new scarp is developing (Figs. 1 and 2). The proposed monitoring scheme (Fig. 6) is simple and inexpensive and could consist of series of vertical bars (metal or wooden) placed in rows along and across the slope, both above and below the scarp area. The only equipment for this task would consist of optical theodolite and surveying rod.

The benchmark bar can be used for the theodolite position. Monitoring bars below scarp zone will provide targets for measurement of angles and distances from the main benchmark. The subsequent bi-weekly or monthly mapping will reveal any slight movements of bars which can be used to identify the presence and speed of slope deformations. Monitoring frequency should increase in the rainy season and if there are considerable increases in the speed of deformations. Any increase in the speed of deformations should be considered a serious warning of an impending landslide and the local population should be evacuated.

In addition to the theodolite survey we propose to establish three rain gauges that can be monitored by local school children under the supervision of the teacher. Landslide research always points to the tight relationship between rains and landslide events. However, in each geographic region this relationship might be different.

Combined data on slope movement and rainfall should provide data (in long-term) for the early warning of local residents. Early warning will be associated with time period between increase in speed movement of the slope and slope failure (Fig. 7).

In addition to monitoring system the awareness program for local residents should be also implemented. This program will include sign postings in local dialects and landslide education in local schools.

Acknowledgments Special thanks to faculty at Makerere University School of Public Health, including Drs. William Bazeyo, Roy Mayega, and Juliet Kiguli who helped to facilitate the study. We are also most grateful for the support of our Ugandan field team, including Moses Mande, Barbie Basiimwa, Pande Gerald, Mercy Mutuwa, Eva Nalwanga, Lillian Nabafu, Felix Walyawula, John Bosco Isunju, Ben Mooya, Lubunde Edward along with our US based collaborators Daniela Lewy, Evan Russell and Tajib Rahman.

This research was funded by the National Science Foundation (grant #0624106).

References

Claessens L, Knapen A, Kitutu MG, Poesen J, Deckers JA (2007) Modelling landslide hazard, soil redistribution and sediment yield of landslides on the Ugandan footslopes of Mount Elgon. Geomorphology 90:23–35

Kitutu MG, Muwanga A, Poesen J, Deckers JA (2009) Influence of soil properties on landslide occurrences in Bududa district, eastern Uganda. Afr J Agric Res 4(7):611–620

Kitutu MG, Muwanga A, Poesen J, Deckers JA (2011) Farmer's perception of landslide occurences in Bududa district, eastern Uganda. Afr J Agric Res 6(1):7–18

Knapen A, Kitutu MG, Poesen J, Breugelmans W, Deckers J, Muwanga A (2006) Landslides in a densely populated county at the footslopes of Mount Elgon (Uganda): characteristics and causal factors. Geomorphology 73:149–165

Masiga M, Ruhweza A (2007) Commodity revenue management: coffee and cotton in Uganda. International Institute for Sustainable Development (IISD), 26 p. http://www.iisd.org/pdf/2007/trade_price_case_coffee_cotton.pdf

Mugagga F, Kakembo V, Buyinza M (2011) A characterization of the physical properties of soil and the implications for landslide occurrence on the slopes of Mount Elgon, eastern Uganda. Nat Hazards, Online First™, 12 July 2011

Sayer G (2002) Coffee futures: the impact of falling world prices on livelihoods in Uganda. Uganda Coffee Report, 121 p

Landslides, Land Use Systems and Food Security

Saralavandanam Sattenpalli and Surya Parkash

Abstract

Generally the land divided on usage categories like cultivation, human settlements, pastures, fallow lands, arable lands, canals, hillocks etc. During ancient times, only tribal people used to settle in hilly terrains but now-a-days urban agglomerations are also found on hill slopes. People prefer to live in these areas even much hinter-lands, due to scope for growth in vertical/horizontal way. Priority to settle on slopes is due to hike in land cost, hype of real estate, change in land use, role of land mafia, urban pressures, proximity to work places, livelihood and social and economic compulsions. Change in land use is the utmost important factor for settlement of people in landslide prone areas. Majority of land alienated to software and other allied industries, SEZS, Corporate educational institutions, corporate hospitals, golf courses, real estate firms run by private companies, transfer to para-statal agencies, tourism developmental activities, infrastructure developments such as Metro rails, air ports, highways, flyovers, utilities and services etc. People living there are vulnerable to normal life such as no connectivity for food chain, water, transport, communication, no access to health, education and good hygienic conditions, all became hindrances to their social and economic life. Heavy rains, sudden fast draw-down from water reservoirs and water leakage from utilities causes landslides in hill slopes particularly in monsoon period. Due to increasing in population density and landslide damage, the urban areas suffer heavy damages and losses.

In high altitude areas people live near to landslide prone zones facing peculiar problem of inaccessibility to communication, transportation and food security. The control of damage in fire accidents, reduction of casualties is not feasible as only manual linkage is accessible for immediate relief. Governance is complicating in creation of infrastructure while providing amenities, accessibility to livelihoods affected on linkage of welfare programs results set back to developmental plans, vulnerability reduction is difficult in case of increasing population density. Abundant gap in permissions and taxation and immediate relief in exigencies exist in the government system. Land use planning by creating fool proof mechanism in water usage utilities, control blasting operations/debris in nearby areas, creation of better alternative living environment in proximity to work places. In core areas 20 % land reserved for this people, through legislation of 'slum identification, redevelopment, rehabilitation and prevention Act', covered security of tenure with a reserved quota to the people living on

S. Sattenpalli (✉)
Revenue, Collector and District Magistrate Office, Hyderabad,
Andhra Pradesh, India
e-mail: saralareddy007@gmail.com

S. Parkash
National Institute of Disaster Management, New Delhi 110002, India
e-mail: suryanidm@gmail.com

C. Margottini et al. (eds.), *Landslide Science and Practice*, Vol. 4,
DOI 10.1007/978-3-642-31337-0_20,

landslides areas and solid waste landfill sites, and other hazardous areas like canal bunds, tank beds, road margins, burial grounds etc. shall be covered under JNNURM, RAY, IAY, ACDP programs in phased manner. Permissions for settlement and expansions should be discouraged by ULBs. Mentioning the people living in landslide prone areas as special category in UNIQUE ID Card, not in a manner of HUCKO ID Cards of China, may provide flexibility to settle in better livelihood places by giving top priority, by reserving land in SEZS for the people. Segregate accommodation to be provided for families to avoid destruction in social life unlike dormitories. Equal priority for food security will be given to these people in issuing of smart cards such as chronic hungers like children, pregnant women, old persons, disabled and homeless in supply of essential commodities with a comprehensive approach for implementing of Food security Act. Providing incentives and subsidies to go downs in protected areas near to landslides for PDS and kept buffer stocks for immediate relief in emergency seasons. Separate calamity fund are available for ULBs to meet exigencies against incessant heavy rains, fire accidents and other hazards. Training on mitigation and skill development along with NSDC and MEPMA for better livelihoods would be good option.

Keywords
Land use • Landslide • Food Security • Government • Management

Introduction

People generally prefer to live in urban plain areas and not inclined to go for settlements at hilly terrains / landslide prone areas due to its vulnerability to natural disasters, comparatively weak infrastructure and hardships in living conditions. Much demand arrived to the plain areas suitable for habitation in all nations around the world. Even barren lands will also get its importance to give dignity and honour for the people holding large chunks of land. Land use in core areas as well as in peripheral areas become as an investment zone for business people in view of globalization and economic reforms, in shape of SEZs, Software and allied industries, Corporate Hospitals, Corporate Education Institutions, Real Estate Firms, Golf Courses, Hotels and other allied Tourism Developmental activities, Resorts, Theme Parks etc. For the smooth development of these above economic investment zones, it is mandatory to the Governments to create infrastructure facilities such as MMTS, Metro Rails, Air Ports, High Ways, Flyovers, Outer Ring Road and Inner Ring Road Projects, Utility services etc. Hence land use and its expansion in usage is extended to hilly terrains, canal bunds, river beds, sea shores, passage roads, polluted areas, low lying areas and unhygienic areas, leaving these small bits of lands at different places for poor migrating people. Majority of land in urban areas are secured in the hands of Government or by the higher caste people (rich people) who are in power from centuries. The rich people protect the lands for their sustainable economic growth, increase in position of power and to expand their economic growth in different fields of income generating activities and they live in good conditioned houses, secluded areas meant for rich people, or in middle class localities.

The Poor People belongs to downtrodden communities and vulnerable sections generally cultivators, illiterates and low skilled labour and economically weaker section are from centuries old have no shelter, in core areas of urban places or in or in urban agglomerations from their ancestors to present era As in the prevailing conditions of non-availability of land in urban plain areas pose survival problems to the people; thereby forcing millions of people to settle in landslide prone areas in the hilly terrains.

People migrated to urban areas in conditions such as no minimum supporting price to their crop and hike in expenses for cultivation, very small extents in their possession are not sufficient for eking their livelihood, no irrigation facility to get high and sustainable yields for creation of better living opportunities. [1]Mahathma Gandhi National Rural Employment Guarantee Scheme (MGNREGS) supported with a legal Act providing rural employment guarantee for 100 days in a year to a family, is not supporting total food security and failed in giving sustainable economic growth to the rural people in stopping their migration to urban areas. By dire necessity, in desperate conditions, for better opportunities and Change in living style of rural people is also a cause behind migration to urban areas.

In case of Vijayawada Municipal Corporation with 2 million population in state of Andhra Pradesh, India, majority of vulnerable section are forced to live/settle on hill slopes at Vidyadhara Puram, Undavalli, Gunnadala, Mogulrajapuram, in addition to settling on banks of three rivers in the city. Here the lands in peripheral areas are highly fertile and were available to the purchasers only on higher rates. The migrated people and unaffordable poor people starting to settle on hilly slope areas in heart of the town and at that time not much resistance arrived from either Government or from the vested interested people and land mafia. The other reasons are their livelihood areas such as small, medium and major industries were much nearer to these land slide areas. Moreover Railway station, Bus stations, potential work places were very nearer to these hilly areas.

State Intervention in Settling of People on Hillocks/Landslide Prone Areas

The available government land at the time of colonial rule and after independence (1947) is meant for allotment of public purpose only. Under circumstances of non availability of suitable government lands for public purpose such as for establishing Government Offices, Government employees quarters, Government Educational Institutions, public sector industries, bunds, culverts, internal roads, drainage systems, PWS schemes (Protected Water Supply Schemes), house sites for weaker sections and for down trodden Communities etc., the land is acquired under the provisions of the [2]Land Acquisition Act 1894. Now the Government's vision on developmental aspect has changed and acquisition and alienation of land has been initiated for establishing industries and other income generating activities run by private persons in core areas as well as in peripheral areas through Industrial Infrastructure Corporations instead other welfare programmes.

In agglomerations. Government transfer lands to urban development authorities/ para-statal agencies intern to develop parks, shopping Complexes, recreation clubs, housing schemes to affordable people. It is the prevailing policy in all over the country. These para-statal agencies put the lands into auction for their governance in the guise of providing infrastructure facilities and civic amenities to the

urban population and stating that the protection of Government lands from land grabbers is becoming a big problem. The state intervention to provide affordable housing with all infrastructure facilities is not up to desirable level on par with rapid migration level.

It is most contradictory whether it is legal or illegal, but a necessity to the Government to provide all civic amenities to the people living in land slide prone areas due to high demand arrived from settlers and state's failure in creating affordable housing. It is an unavoidable factor behind sanctioning permissions by the Government. For instance in Visakhapatnam and in Vijayawada, Municipal Corporations settlements are increased in last 30 years, from 2 % to 5 % in vulnerable areas. In those habitations, 30 % population has been provided with individual needs of civic amenities such as drinking water, sanitation, electricity, accessibility to public distribution system etc. In addition community needs of roads, communication facilities, public health,

transportation facilities, Education are also provided to them. On demand arrived from slum dwellers, the State is granting even security of tenure to them.

Government is lagging behind to rehabilitate these people in new settlements in considerable extent due to several reasons. People living in these areas are not willing to shift to the new settlements in majority cases especially in case of street vendors, hard labourers, construction labour, domestic workers, unskilled workers and the labour working in small, marginal and medium Industries in and around core areas and these workers usually come back daily to their settlements from work places with their professional tools and articles. The alternative facilities provided by the Government were not nearer to their livelihood zones in the new settlements is the common hurdle. In reality for instance, the houses sanctioned under JNNURM were 78,746 in Hyderabad, A.P. State. Out of that 52,065 houses construction were completed in 106 Colonies. But lacunae in creating infrastructure facilities like drinking water, drainage, roads, electricity and far away to their livelihood places, only 26,126 families were joined in those houses because, the rehabilitation and resettlement should not be done in potential work places. In this instance, almost Rs.400 crores investment become useless. Due to this hard reality, poor people compelled to live in landslide prone areas even much hinter land is available for their settlements. Even in the ULBs (Urban Local Bodies) with no natural barriers in and around and there is every chance for expansion, it is necessary to these people to settle at landslide prone areas for their livelihood, social and economic compulsions.

The slums notified under [3]Slum Improvement Act, 1956 are on high side for creating civic amenities and security to the people living there. In addition to that, in the year 1994, Government of Andhra Pradesh State, India, issued GO.Ms. No: 508 for regularization of dwelling houses occupied by the people below poverty line. In Vijayawada alone 20,734 poor people get rights on their occupation by getting house site ownership. But it is not on desirable level, that the development is a continuous process and people are uninterruptedly migrating to these areas for better livelihood opportunities.

Majority of Corporate sector is not providing independent shelter to their employees and very limited firms were providing dormitories, which lead to destruction in social life. Duty of the state to look after the welfare of employees in providing good shelter with all civic amenities at work places of private sector Industries SEZs (Special Economic Zones), Corporate Educational Institutions, Corporate Hospitals, Real Estates firms, Developers, Software and other allied Industries, power stations etc. is the major cause for settlement of unorganized sector workers in vulnerable areas. In addition failure of state in control of land grabbers, land mafia and occupation of government lands by real estate firms is another factor. In view of the reasons stated above, the lands available in urban areas for the settlement of the poor migrated people are only on vulnerable places i.e. prone to landslides, river banks that are frequently attacked by floods, polluted areas, and unhygienic areas.

Living Conditions of People Settled at Landslide Prone Areas

The persons living in plain areas are facing general hurdles like accessibility for good constructed intact houses, ration cards, electricity, transportation, Free Education, health, nearest safe drinking water supply etc. By fulfilling these general needs, people can lead good social and economic life, whereas in case of people living in hillocks / landslide prone areas, they are vulnerable to their normal life such as no chance to connectivity to proper food chain, public distribution system, lack of transportation etc. The P.D.S (Public Distribution System) is only accessible to those people having door number, electricity connection, water connection etc. The ULBs are not in a position to sanction permissions to the dwellers as they are living in hazardous places. Through continuous struggle and persuasion with the help of local political leaders, nongovernmental organizations, permissions are granting to these people after a long time (takes more than 3–5 years) in comparison to the people living in plain areas.

Creating safe drinking water facilities, or connectivity to P.W.S. (Protected Water Supply Scheme) or drilling of bore wells is a hazardous task, either to the settlers or to the state. P.W.S scheme pipelines are generally prone to leakage problems both in normal areas and in high altitudes. This leakage leads to slow draw down of earth, and its bad effect gradually decrease the strength of walls of the dwellings and increasing the damaging effects in comparison to plain areas. Available Polluted drinking water causes frequent epidemic in habitations to the people.

Providing road facility or connectivity to transportation is sometimes not possible in majority areas. In possibility cases budget requirement is more than in plain areas. As there is no transportation facility, the people living there must daily walk a distance of minimum 100 m height on hazardous slopes to reach normal areas for going to their destinations. Getting Essential commodities from market places is only on manual but not on vehicles. This continuous hard labour spoils the health of the people residing in these areas. It's bad effect on bones and muscular system of human beings leads to decrease of their life span. In so many places, construction of steps from higher level to lower level and its accessibility to roads were attained by the people through agitations lead by public representatives because they are big vote bank to them.

Electricity connectivity to house holds is also very much difficult to erect the polls in slope areas. Communication connectivity to other plain areas is a Hercules task. Digging of pits for providing sanitation facilities is very difficult as the majority of area is with rocky sheets or with loose debris, it causes damage to dwellings on blasting in digging of pits or draw-down arises from that. Its adverse effect on the strength of neighboring settlements is very high than in plain areas.

Providing education to the children living these areas is difficult to the government. Permanent construction of buildings for schools is not possible because of vulnerability on land slopes. Parents are not in a position to afford the educational expenses in distant places.

In monsoon seasons, the people living on high altitudes are not affected due to floods unlike in low lying areas. But, the falling of loose soil from high altitudes causes heavy damages to dwellings and sometimes death toll is higher than in floods. In majority incidents at the time of hazards, deployment of machines for relief operations to affected areas is not possible due to lack of transport connectivity. Increasing death toll cannot be controlled by manual assistance, using machinery for floods such as victims in plain areas. The control of damage in fire accident is not easy and its bad impact is very high as the fire engines cannot reach near by places with their relief equipment. Reducing casualties is not possible because the transportation mainly depends on manual labor. Reaching Ambulances with emergency health equipment is also not feasible and shifting the injured people to near by hospitals consumes long time which increases casualty rate. The only connectivity to food chain and other relief materials at the time of hazards is through manual labour and it consumes more time.

A peculiar problem of non connectivity arises to neighbouring habitations other than those not residing in land slide prone areas on fall of landslides at roads and other communication facilities. The link to the main stream has cut to these areas for months together in rainy seasons in majority of states in India. In Jammu & Kashmir, Himachal Pradesh, north eastern states like Assam, Nagaland, Sikkim, Arunachal Pradesh, it is a recurring problem every year. The machinery using for road clearance is not sufficient to their needs. Every year, the road maintenance agency is struggling with this problem. Food security to the people is badly affected, in case no buffer stock available in their houses for their personal needs. The people living in these areas are generally exploited by the business people, who demanding higher prices for essential commodities in the needy situations.

In rainy seasons, the sudden release of excess water from up land irrigation projects into low level projects, prone to falling landslides in shape of mud. It is continuing for hours to days until the water comes to FRL (Full Reservoir Level). Every year at Srisailam dam, Andhra Pradesh State, the Hydro power station is submerging due to release of excess water from Tungabhadra dam in neighbouring Karnataka state. The damage ranges between two and three million dollars in shape of machinery damage due to mud and water flow and on stoppage of the production at peak time's i.e. water available at its higher level.

Government Intervention in Control of Landslides

The government has to discourage people to settle at landslide prone areas in the initial stage. If not possible, at least control further expansion of settlements on landslide prone areas by notifying these areas as prohibited zones or red zones or green belt. ULBS deploy security around those areas not to allow people to settle in these areas. Erect fencing in those areas is another solution.

Evacuation of people from old settlements by selecting better alternative areas near to potential livelihood areas. Extend the benefits under [6]Rehabilitation and Resettlement policy meant for the people effected on land acquisition evacuees by providing immediate placements in unorganised sector with a guarantee of minimum employment prospects at new settlements. In case of failure in showing placements by the Government under R&R package, these families will be supported with Rs. 2,000/- stipend every month up to (20) years as announced by Rural Development Minister, GOI in draft Bill on Integrated National Land Acquisition Rehabilitation and Resettlement Bill 2011, covered under calamities quota on par with Land Acquisition for larger Industries etc.,

On the evacuation all the people evacuated must be covered under [7]'Rajeev Awas Yojana' and 'Indira Awas Yojana' with majority of unit cost supported by Government covering under JNNURM housing aided by World Bank. Government announcing new programme in 250 ULBs providing houses to slum dwellers with 50 % assistance of GOI (Government of India) and 50 % share of states with institutional finance will be applicable to these vulnerable sections as a special case. The Housing should be taken up with the money arrived through 20–25 % land reserved to the poor people in Government lands putting for auction according to the norms in RAY. Ensure of following National Building Code in construction of houses under the guidelines of [8]RBI (Reserve Bank of India). Evacuation will be taken up after completion of construction of housing with all civic amenities.

In addition to governments' assistance in housing, providing good shelter to the employees working under private sector by their employers' is ensured with a new mandatory law by the Government. Strictly follow the norms in Article 25 of International Human Rights Agreement, clearly

instructed to construct new Housing Colonies with a share of LIG 40 %, MIG 40 % and HIG 20 %. Segregate accommodation will be provided for families unlike dormitories to avoid destruction of social life at SEZs, other major industries and ensuing coming manufacturing zones.

In addition to that, under urban reconstruction programme, a special reservation has to be maintained to the people living in the hazardous areas by providing houses in newly constructed development projects by Developers in core areas and peripheral areas with livelihood assurances in 20 % of land reserved in lieu of permissions for their projects under [9]"Slum identification, redevelopment, rehabilitation and prevention Act". Institutional lending support shall be provided by a policy decision of government as in case of supporting lending activities to the farmers in rural areas for cultivation by fixing targets through [10]NABARD.

Evacuee people are provided with skill development training under [11]National Skill Development Policy through MEPMA, Rajeev Education and Employment Mission in addition to all National Financial corporation's of GOI. Training should be in their existing profession and support it with tools of their profession. People opt for new training skills in the profession other than their old profession will be given utmost importance and they must be assured to job guarantee in new places.

Behavioural training to cope up with new environment should be part and parcel in the training to come out from general behavioural problems arrived at new settlements. The proactive reaction to those stigmas will be utmost important factor for fruitful settlement of an individual. Some of the new habitations must be selected as pilot projects and field visit to those pilot projects by the new incumbents / evacuees must be in training curriculum. Timing schedule for skill development training must be according to their present work schedule and not becoming an hindrance to their present livelihood activity. This vulnerable section shall be given importance in the new 'Manufacturing Policy" announced by Commerce and Industry Ministry, GOI to achieve objectives by creating potential employment in skill labour in National investment manufacturing zones by not easing the labour laws.

Next utmost important assistance provided by the government to the people living in landslide prone areas or evacuees resettled in new places is accessibility to public distribution system. The people must be enrolled in Public food delivery services provided by the government fall under three major programmes;

1. Distribution of rice or wheat for below poverty line people every month in shape of 25 kg food grains, 2 kg sugar and 5–8 l kerosene and cooking LPG Gas on subsidized prices. In case of retail prices at higher stage, the government will start distributing other millets, tamarind, salt, edible oils according to the demand. To the old and needy destitutes a separate food grain distribution system called AAY (Anthyodaya Anna Yojana) is also a part in public distribution system for maintaining food security. The AAY is supporting the poorest people in addition to the regular Ration.

   Food materials received through the public distribution system is not sufficient to the entire family but it balancing the purchasing power parity of people for keeping the retail prices at an affordable level to a family. Hence, PDS coverage to these people is more than general quota treating them as a special case in similar to 'Antyodaya Annayojana' beneficiaries, covering all scheduled essential commodities. It should be as equal to the 35 kgs ensured for a family in forth coming Draft [12]"Food Security Act".
2. Coverage in Midday meals to the school going children every day at schools will be applicable to these vulnerable sections.
3. The Anganwadi Centers (Nutritional centres) to feed below 5 years age children in urban areas under [13]ICDS programme must be covered to these children. At present 35 % of urban population under below poverty line in the country covered under this public services food security programme. A concise plan of action has to be started to cover all these people living in landslide areas in 85 % coverage of food security as stated in the coming National Food Security Act.

These people shall be covered under the other government assistance programme of providing financial assistance every month through India's National Old Age Pension Scheme meant for Old Age people, widow & destitute women and physically handicapped people. Introduce Brazil's Bolsa Familia and Mexicos opportunidadis which can be used to create social protection system for achievement of an initiative under Nation's Social Protection Floor.

Providing public health is a major hazardous snag in the landslide prone areas. Establishing of new urban health centres or construction of new clinics is not feasible in the landslide prone areas. In view of such hazardous environment, the local literate persons are to be trained under the new program of Government on Health to the Slum dwellers in ULB's with an ambitious budget of Rs. 30,000/- crores in 7 years by setting up 4214 public Urban Health centres, providing outreach services, referral services and emergency medical services through [14]National Urban Health Mission (NUHM). General emergency medicines will always be available with them. Issue a special health card to all the people live in landslide areas on top priority under NUHM. In addition to that covered under Rajeev Arogyasree Programme providing treatment to ailments in corporate hospitals to the people under below poverty line with the assistance of government through insurance companies

practised in A.P. State. For the children living in land side prone areas aster health check up must be done for every 3 months by issuing Health Cards under Rajiv Vidya Mission. Because lower poverty levels with better health care facilities lead to better health outcomes, despite their lower purchasing power parity and low calorie food consumption.

If in case of non possibility of evacuation of the people living in landslide prone areas, the ULBS have to strictly confine to land use planning. Fool proof mechanism has to be adopted especially in water usage. Dumping of wastage in these areas shall not to be entertained. Control blasting activities in nearby affected areas and not grant permissions for blasting in future. Reserve these areas in prohibitory order book of mining department, revenue department and in ULBS. If precious metals are available in nearby areas, examine the sanction of blasting in near by habitations as a special case by a committee constituted with all experts including sociological field to consider the evacuation of the people living in these affected areas. The evacuee must be rehabilitated and resettled as per the norms in the new comprehensive LA Act.

Under JNNURM, develop trenches to divert the flow of water coming from upland areas without obstruction via uninhabited areas to maintain good drainage system. Good technological devices will be erected for stoppage of landslides with the help of financial institutions and other NBFIs (Non-Banking Finance Institutions) and Foreign Aid agencies under PPP.

These people shall be covered by infrastructure facilities and civic amenities under BSUP (Basic services to the urban poor) of JNNURM. The benefits must reach to these hazardous people under a separate internal reservation category in similar to grounding of welfare programmes of GOI. In total budget allocations of JNNURM, out of 40 % budget earmarked for implementation of BSUP, the allocation must be according to their population of the 2011 census with well prepared analytical data.

People living in landslide prone areas must given utmost importance in issuing UNIQUE ID cards treated them as special category under vulnerable groups on par with chronic hungers such as children, pregnant women, old persons, disabled and homeless persons. At present, Government is issuing UNIQUE ID cards to the people living in coastal areas treated them as special category for assisting in fishing, rehabilitation in case of Tsunamis, cyclones, floods and to control extremist invasion from sea areas by assisting marine police. In such a way they will also given a special category ID number useful to accessibility to all benefits arrived from Government in addition to the people living in other hazardous areas abutting to canal bunds, tank beds, road margins, graveyards, dumping yards etc. for rehabilitation and resettlement. ID Cards issued should be useful to get livelihood opportunities at any place in the country unlike HUCKO Cards prevailing in China. This facility must be loaded in Central Data Repository of [15]UNIDAI (Unique Identification Authority of India), and must be transferrable and used at any place in such as smart cards issued for Social Security pensions and NREGS beneficiaries.

Education to the children will be provided with free boarding and lodging facilities – give a special quota in government residential schools. Appoint 'Vidya Volunteers' of the same habitation to educate dropout children as per the provisions in [16]"Right to Education Act".

Government has to extend its help to these people by providing employment through urban employment guarantee scheme in similar to MGNREGS prevailing in rural areas, especially for cleaning and greening operations to supplement the job opportunities for the unskilled workers and to empower the ULBs. A separate administrative setup formulized like District rural development agency (DRDA) converging with all departments under the control of MA&UD. Representatives from MEPMA, JNNURM, Rajiv Swagruha, DLBC (District Level Bankers Committee), RVM, Women & Child Welfare, Medical & Health, MA&UD(Municipal Administration and Urban Development) and Public Representatives must play their role in that administrative setup with District Relief Commissioner as Chairman for convergence with all the government departments as well as private sector units in allocation of special calamity funds and assistance at the time of disasters. There must be an abundant share to the people living in landslide prone areas in the aid of world bank @ Rs. 1,158 crores to the country for the implementation of disaster mitigation through [17]NDMA (under NCRM programme).

The future landslides mitigation plan is also prepared in identifying nearest rehabilitation centres emergency contact addresses and list of like minded organizations for their assistance in emergency. It establishes inventory data of resources like machines used in relief operations such as excavators, cranes used in the disasters to reduce damage/risk at the time of hazards. In addition, it includes training as well as capacity building on mitigation and participation in rescue operations to all the people living in hazardous areas as well as neighbours such as nearby interested people to rescue their neighbours. In so many incidents, any rescue team from government side or NGOs side arrived to the affected places after neighbour's first response. Establish fire stations close to vulnerable habitations with suitable equipment meant for hillock areas. People living in these areas insure their houses and other belongings and their life's compulsorily. The government has to link insurance to its welfare schemes under Building and other construction workers (RE & COS) Act 1996, and RSBY (Restriya Swasthaya Bheema Yojana) to get benefits.

Public Participation

People themselves should be in a position to acquire food security on their own is an important task. It will be achieved by formation of self help groups with strength of 10–20 members formed as a single group having common interests to achieve self sufficiency. The group formation concept is to enlighten them on poverty reduction, women empowerment and promoting them towards thrift and other financial inclusion parameters. These groups after a prescribed short period get financial assistance through banks with government guarantee in addition to their thrift regularly deposited in banks. With that capital, the SHGS purchase the grains directly from cultivators at harvesting time and other essential commodities by retail, when rates are in down stage and procure them with the help of the government. Their procurement is giving minimum support price to the poor cultivators. In West Godavari District, A.P. State alone, the SHG Groups purchase Rs. 110 crores grain with bank guarantee in this season. GOI also extending the SHGs strength in creating necessary storage capacity of present 633.62 lakh metric tonnes to 150 lakh metric tonnes of space by 2012 under the private entrepreneur guarantee scheme under National Rural Livelihood Mission.

Providing food security to the people is not a mere extension of benefits through public distribution system i.e. supply of essential commodities on subsidies. Food security will be arrived through security of tenure, education, health, sanitation & access to livelihood for the community. Hence in addition to the Food security, the SHG groups got lending support from Banks and other NBFIs for their livelihood activities to assist their group members according to their needs and capacities. The members in SHGs achieve sustainable economic growth by revolving those funds. In rural areas the government's role in formation of SHGs restricted to a facilitator under the guidance of SERP (Society for Elimination of Poverty in Rural areas), an autonomous body in A.P. State run by civil servants and well educated committed community coordinators at village level under APRPRP (Andhra Pradesh Rural Poverty Reduction Project). [18]Mr. Jayesh Ranjan, an All India Civil Servant, one of the SERP Executive in its beginning stage has got good results in economic sustainability in Poorest of the Poor as Project head in Chittoor District and an executive consultant at state level. It is one of the most successful supported programme assisted by the government in rural areas. The depressed class people and the population in tribal areas once attracted towards left wing extremism come into main stream with this SHG women movment. The banks finance to SHGs also reach Rs 7,092 crores out of target of 7,263 crores for the financial year 2010–2011 in Andhra Pradesh State. This SHG concept can achieve community empowerment through social mobilisation by creating income generating resources to the poor.

Under women empowerment initiative, SHG groups were also assisted with capacity building on maintenance of accounts, non entrepreneurial skills etc. for their economic viability. The trainings can address the wide spread complexities in urban areas such as poor infrastructure in slums, lack of employment, unskilled in existing employment, cost increase in standards of living and unremitting ill health problems. Instead of revival of urban consumer co – operation societies in slum areas/landslide prone areas, the SHG management system will be better and the group members feel it is for the welfare of their families as if, their small investments involved in the capital.

Notes

1. MGNREGS Act 2005 aims at enhancing the livelihood security of people in rural areas by guaranteeing 100 days wage employment in a financial year to a rural household to do unskilled manual work. See www.nrega.nic.in.
2. Land Acquisition Act, 1894 – Private lands acquired by the government for public purpose under this act.
3. Slum Improvement Act, 1956 – an act to provide for the improvement and clearance of slum areas in states for protection of tenants in such areas from eviction.
4. JNNURM – is a programme aided by World Bank implementing in ULBs and Municipal Corporations all over the country to attain sustainable infrastructure development linked with reforms. See www.jnnurm.nic.in.
5. MEMPA – to improve the quality of life of poorest of poor in urban areas by accessing services from all organizations through their own strong self reliant and self managed institutions. See www.ap.mempa.gov.in
6. Rehabilitation & Resettlement Policy- It's a World Bank policy to the displaced people under any project to resettle them with land , housing , infrastructure and other compensation like creation of livelihood activities etc., In India, it is practiced sector wide and for specific projects. See www.his.com.
7. Rajiv Awas Yojana is a housing scheme to provide 15 lakh houses to the urban slum dwellers by 2018 in all over the country under JNNURM. Indira Awas Yojana is a scheme started in 1985 to construct independent houses to the rural poor with total unit cost assistance of GOI. See www.jnnurm.nic.in
8. RBI- Reserve Bank of India is Indias central bank and monitory authority in supervising nations financial system. See www.rbi.org.in
9. AP Slum (Identification, Redevelopment, Rehabilitation and Prevention Act, 2010 for comprehensive reconstruction of the existing slums in the state in terms of housing and infrastructure facilities by assisting property rights to the slum dwellers and envisages the prevention of formation of new slums.

10. NABARD- National Bank for Agricultural Development is the apex institution, accredited with all matters concerning policy, planning and operations in the field of credit for agriculture and economic activities in rural India. See www.nabard.org
11. National Skill Development Policy- Facilitate or catalyse skill development initiatives in organized and unorganized sector under PPP (public private partnership) model by providing viability gap funding to reduce the existing gap between demand and supply skills. See www.nsdcindia.org
12. Draft Food Security Act – It is a proposed law guaranteeing nutritional security to all implemented by states and local governments with the support of GOI. See www.nac.nic.in
13. ICDS- Integrated Child Development Service Programme is a GOI sponsored one, to Pre- school children in an integrated manner in rural, tribal and slum areas. See www.icds.gov.in
14. NUHM- National Urban Health Mission started in 2005 , aimed on segments of nutrition , sanitation , hygiene and safe drinking water to the poor women and children. See http://mohfw.nic.in
15. UNIDAI- It is a authenticated body to issue Identity Cards to all citizens in India in the goal of shifting India from a limited access to an open access economy and it uses in implementation of a universal micropayments solution. See www.uidai. gov.in
16. Right to Education Act- It envisages compulsory education to 6 to 14 years children. See www.indg.in
17. NDMA- Apex disaster management agency in India. . ..
18. Mr. Jayesh Ranjan- All India Administrative Service topper in the year 1992, working in A.P. State for past 19 years and worked in a number of grass roots projects in AP relating to Tribal Development, Drought prone area development management and Poverty Alleviation Projects. See www.jayesh_ranjan@hotmail.com

Anthropogenic Activity Triggering Landslides in Densely Populated Mountain Areas

Veerle Vanacker, Vincent Balthazar, and Armando Molina

Abstract

Flooding, landsliding and accelerated erosion are common hazards in tropical mountainous regions around the world. The aim of this study is to analyse the triggering factors of landslides in densely populated areas with different land cover dynamics. Landslide inventories and land cover data were derived from optical remote sensing data for different periods in time. Our results indicate that human activities significantly increased the landslide hazard. We observed an increase in the occurrence of landslides after deforestation and road construction. The financial and environmental losses that are associated with these landslides might induce some negative feedback mechanisms leading to a deceleration of deforestation rates.

Keywords

Human activity • Land use change • Landslides • Tropical Andes • Remote sensing • Landslide inventory

Introduction

Flooding, landsliding and accelerated erosion are common hazards in tropical mountainous regions around the world. Not only considerable financial costs are suffered, but also major ecological and environmental problems often arise in a larger geographical area. Land cover modification and conversion have clear impacts on natural disaster risks. Increasing population pressure, together with socio-economic development are forcing more people to move to unstable hillside areas, thereby changing the impacts of natural disasters (Vanacker et al. 2003).

Assessing the rate and spatial patterns of landslides is challenging given the ruggedness and the inaccessibility of mountain areas. Satellite data offer an inexpensive means of deriving complete spatial coverage of land attributes such as land use and natural disasters in a consistent manner that may be updated regularly. Therefore, remote sensing techniques are a privileged tool, even if they suffer from methodological challenges which have to be resolved by appropriate pre-processing techniques (Lu et al. 2008; Vicente-Serrano et al. 2008; Richter 2009; Balthazar et al. 2012).

The aim of this study is to evaluate the efficiency of high spatial resolution satellite sensors with relatively high spectral and temporal resolution to create regional landslide inventories. Time series of land use and landslide data allowed us to analyse the impact of anthropogenic vs. natural controlling variables of landslides in this mountainous terrain.

V. Vanacker (✉) • V. Balthazar
Earth and Life Institute, Georges Lemaître Centre for Earth and Climate Research, Université de Louvain, Place Louis Pasteur 3, Louvain-la-Neuve 1348, Belgium
e-mail: veerle.vanacker@uclouvain.be

A. Molina
Department of Earth and Environmental Sciences, Katholieke Universiteit Leuven, Celestijnenlaan 200E, Leuven, Belgium

C. Margottini et al. (eds.), *Landslide Science and Practice*, Vol. 4,
DOI 10.1007/978-3-642-31337-0_21,

Fig. 1 Photograph of the study area, with localisation of the Pangor catchment. Land use in the Pangor basin is highly heterogeneous (Picture: M. Guns)

Materials and Methods

Study Area

The Ecuadorian Andes are selected as a preliminary test site, as this region is facing rapid land use changes. Land cover in the Central Ecuadorian Andes is highly heterogeneous, and mainly composed of paramo and subparamo, natural forests, plantation forest, grassland, pasture and cultivated land.

The intense rainfall on steep slopes is causing major environmental treats in the region. Landsliding and accelerated erosion are common hazards (Molina et al. 2008; Vanacker et al. 2003; Fig. 1). Episodic slope movements comprise shallow failures in slope and regolith material involving rotational and translational slides and some flows of debris and soil material (Guns and Vanacker 2012).

Landslide Inventory

Detecting and mapping landslides over extensive areas is of great importance and cannot be accomplished by time consuming methods like point-based field measurements or aerial photographs analysis. High spatial resolution satellite sensors with relatively high spectral and temporal resolutions might be considered for regional scale landslide inventories. However, the use of such data in steep terrain is highly constrained by topographical and shadowing effects that require appropriate and advanced pre-processing techniques.

Preprocessing of remote sensing data commonly addresses atmospheric and geometric corrections, but rarely incorporates topographic corrections even though they are recognized as a major problem for quantitative analysis. To account for the effects of shadowing in steep terrain, we applied three levels of pre-processing techniques (Fig. 2)

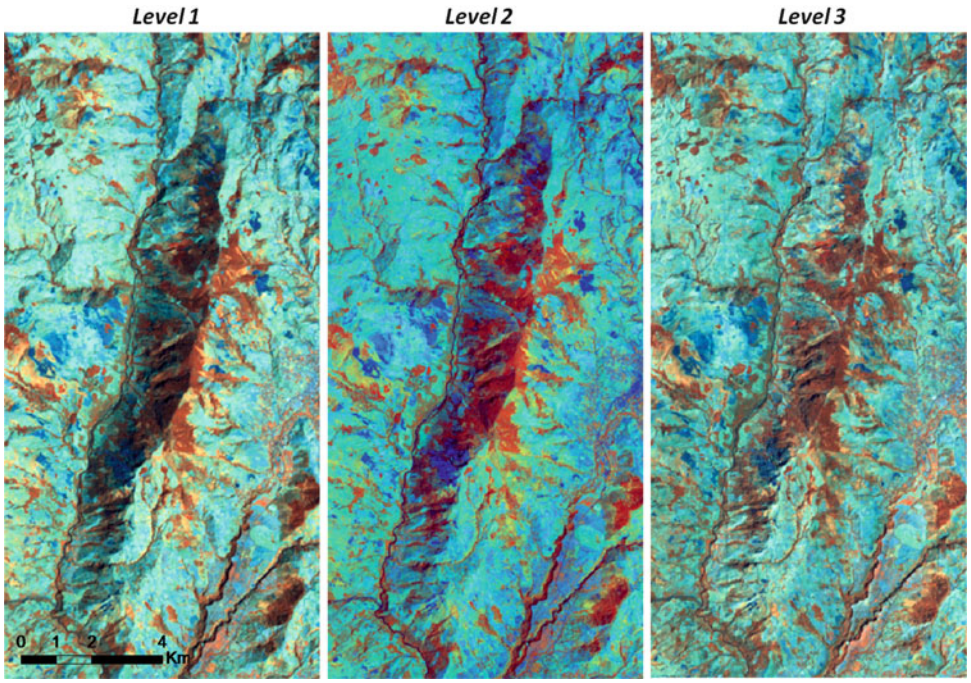

Fig. 2 Landsat ETM+ false color composite (RGB 457) after the application of empirical (*level 1*), semi-empirical (*level 2*) and physically-based (*level 3*) correction techniques for topographic effects (Path 10/Row 61, 3/11/2001, Source: USGS)

with different degrees of complexity and time investment, namely empirical, semi-empirical and physically-based correction methods. While the empirical correction techniques do not require auxiliary data, the semi-empirical and physically-based techniques reconstruct the illumination conditions of a particular satellite scene based on a high-resolution Digital Elevation Model (DEM).

A landslide inventory was established based on high-resolution remote sensing data and ancillary datasets in order to add information on landscape characteristics. Multi-spectral images have proven to be particularly effective for mass movement mapping, improving the 2D shape recognition of features, particularly with processing techniques such as color composites, vegetation indexes, pan-sharpening, band arithmetic or principal component analysis. Along with the importance of spatial resolution, spectral characteristics of remotely sensed data play a major role in detecting landslides. For instance, the ASTER sensor covers a part of the electromagnetic spectrum that enables to highlight more efficiently geological features in comparison to other data of similar spatial resolution such as a pan-sharpened LANDSAT ETM + image.

Along with these techniques, we analyzed the effect of the three topographic correction levels on landslide detection accuracy. Semi-automated procedures were developed based on the ASTER and LANDSAT ETM + spectral signatures, and topographic and geomorphic landscape characteristics derived from a DEM. The landslide inventories that are established based on semi-automated procedures have been validated with the help of very-high resolution remote sensing imagery and field campaigns for ground-truthing.

Table 1 Land use in the Pangor catchment between 1991 and 2009

Land use (%)	1991	2001	2009
Natural forest	13.7	12.7	11.8
Agricultural land	45.1	46.5	47.4
Paramo	40.7	37.4	35.8
Pine plantation	0.4	3.3	5.1

Human Activities and Land Use Change

Anthropogenic impact in the Rio Pangor catchment results in a highly heterogeneous landscape. In 2009, crops and pastures represented about half of the total area in the basin (Table 1) while paramo, natural forest and pine plantations together constitute the remainder 50 %. The increasing demand for agricultural land leads to cultivation of marginal sloping lands. In the Pangor area, about 44 % of agricultural areas are located on slopes higher than 25°.

The catchment is also facing intense and rapid land-use dynamics through time (Table 1). Both natural vegetation types in the catchment are progressively replaced by agricultural lands and pine plantations. Most of the pine plantations are occurring in areas originally covered by natural forest but rather in high elevations that are naturally covered by paramo vegetation.

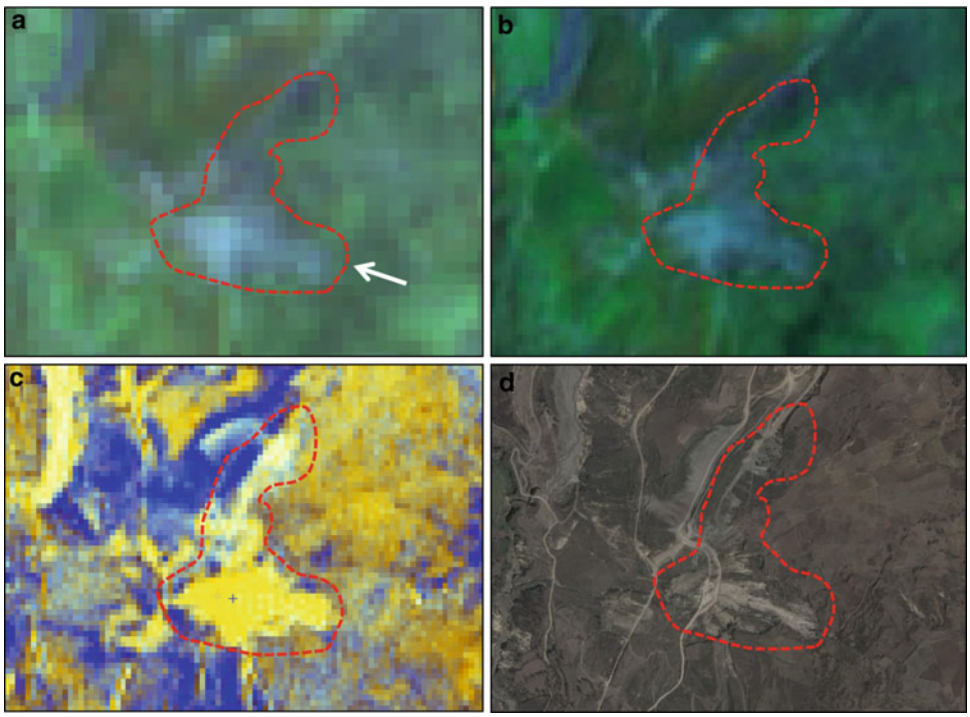

Fig. 3 Comparison of landslide detection accuracy for HR sensors LANDSAT ETM+ (**a** and **b**) and ASTER (**c**) in confrontation to a VHR Quickbird image (**d**). (**a**) RGB 457, (**b**) RGB 457 with PAN-sharpening, (**c**) RGB PCA1/PCA2/PCA3, (**d**) True colors RGB

Results and Discussion

Landslide Mapping

In areas of low vegetation cover, ASTER images are performing better results for the detection of translational and rotational slides than those captured from the Landsat sensor (Fig. 3). Even if ASTER images have the same spatial resolution than the panchromatic layer of the Enhanced Thematic Mapper, the nine spectral bands of the Aster sensor (in the VNIR and SWIR regions) can clearly distinguish fresh rock and sediments from landslides and/or enhanced sediment transport in rivers. In this case study, the use of a Principal Component Analysis on the different spectral bands of the ASTER images (PCA, Fig. 3c) enables to detect accurately landslides.

In areas of high vegetation cover that are covered essentially by dense tropical forests, the Normalized Difference Vegetation Index (NDVI) is able to highlight mass movements in natural forested areas. However, because of strong topographical effects, the detection accuracy of landslides, mostly debris flows, is compromised. The alternation of shaded and sunlit slopes makes the feature recognition difficult, and confusions between reflectance abnormality due to topography and slope movement are common (Fig. 4a). The topographic correction of the satellite data makes the information from the scene more homogeneous and independent of illumination effects. The semi-empirical correction of the satellite data has clearly an important impact on the accuracy of the landslide inventories (Fig. 4b).

Anthropogenic Impact on Landslide Occurrence

Based on landslide inventories, land-use and soil maps, as well as field data, we have calibrated and validated a simple slope stability model (Vanacker et al. 2003). This slope stability model was used to predict the potential landslide hazard for different land use change scenarios. The scenarios were developed based on the land use history derived from satellite images from 1991 to 2010.

Following this procedure, we created a dynamic and spatial indicator of mass movement regulation.

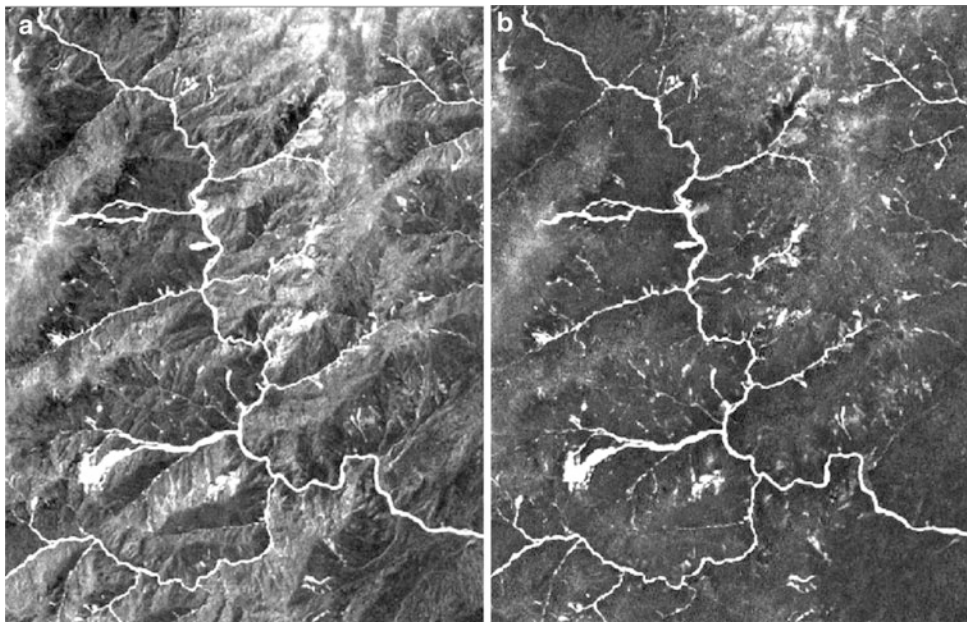

Fig. 4 Detection of landslides based on the vegetation index (NDVI) in a forested areas based on a LANDSAT ETM+ imagery without (**a**) and with topographic correction (**b**) (Path 10/Row 61, 3/11/2001, Source: USGS)

Conclusions

Our study indicated that topographic correction was an important step before the use of enhancements techniques for mass movement detection because of the strong variations that exist between sunlit and shaded slopes in high mountain environments. Semi-empirical methods give the best results for correction of these effects.

We have also applied different detection techniques for which the efficiency was depending on the type of mass movement and on its surrounding area. But in most cases, the landslide detection was significantly improved by the use of topographic corrections.

The landslide inventories were used for calibration and validation of a slope stability model. In a dynamic landscape facing important land-use changes on short time scales, scenarios of future land cover change were used to assess the human impact on mass movement occurrence.

Acknowledgments Funding for this research was provided by the Belgian Federal Science Policy Programme BELSPO through the StereoII SR/00/133 project, and the CUD-PIC project '*Strengthening the scientific and technological capacities to implement spatially integrated land and water management schemes adapted to local socio-economic and physical settings*' between the Faculty of Agricultural Engineering at the Universidad de Cuenca (Ecuador), the University of Louvain, the KULeuven and the FUNDP (Belgium).

References

Balthazar V, Vanacker V, Lambin EF (2012) Evaluation and parameterization of ATCOR3 topographic correction method for forest cover mapping in mountain areas. Int J Appl Earth Obs Geoinf 18:436–450

Guns M, Vanacker V (2012) Logistic regression applied to natural hazards: rare event logistic regression with replications. Nat Hazards Earth Syst Sci 12:1937–1947

Lu DS, Ge HL, He SZ, Xu AJ, Zhou GM, Du HQ (2008) Pixel-based Minnaert correction method for reducing topographic effects on a Landsat 7 ETM+ image. Photogramm Eng Rem Sens 74:1343–1350

Molina A, Govers G, Poesen J, Van Hemelryck H, De Bievre B, Vanacker V (2008) Environmental factors controlling spatial variation in sediment yield in a central Andean mountain area. Geomorphology 98:176–186

Richter R (2009) Atmospheric/topographic correction for satellite imagery. Report DLR-IB 565-01/09, available online at: ftp://ftp.dfd.dlr.de/put/richter/ATCOR/

Vanacker V, Vanderschaeghe M, Govers G, Willems E, Poesen J, Deckers J, De Bievre B (2003) Linking hydrological, infinite slope stability and land-use change models through GIS for assessing the impact of deforestation on slope stability in high Andean watersheds. Geomorphology 52:299–315

Vicente-Serrano SM, Pérez-Cabello F, Lasanta T (2008) Assessment of radiometric correction techniques in analysing vegetation variability and change using time series of Landsat images. Remote Sens Environ 112:3916–3934

A Neglected Disaster: Landslides and Livelihoods in Central-Eastern Nepal

K. Sudmeier-Rieux, S. Jaquet, G.K. Basyal, M. Derron, S. Devkota, M. Jaboyedoff, and S. Shrestha

Abstract

Landslides have an underestimated impact on rural livelihoods and food security in Nepal, with little attention received from government, the international community, or researchers. Landslides are the leading natural hazard after epidemics, killing over 100 persons per year and are predicted to increase with more intense monsoon rains (Ministry of Home Affairs (MoHA), Government of Nepal and Disaster Preparedness Network (DPNet) (2009) Nepal Disaster Report 2009: The Hazardscape and Vulnerability, Kathmandu). This paper explores current landslide trends in Nepal and impacts on rural development. Six communities in Central-Eastern Nepal were studied; four of landslide-affected rural communities, and for comparison's sake, two are flood-affected urban areas. The research links geological knowledge about landslides with a social analysis of affected populations. The study's methods are interdisciplinary, combining a geological assessment of landslides, with participatory social science research methods. Results show that landslides are very costly for households, often obliging them to convert or abandon rice fields, reconstruct their houses, or migrate abroad, considerably affecting food security. The goal of this research is to contribute to the literature on integrated approaches to landslide risk reduction.

Keywords

Landslides • Rural development • Livelihoods • Food security • Coping strategies

Introduction

Nepal is one of the most disaster-prone countries in world causing huge impacts in terms of mortality, injury and property losses (MoHA 2009). Hazard events now account for 25 % of all deaths in Nepal, or 900 per year, 84 % of affected people and 76 % of economic losses (MoHA 2009). In 2007, over 1,000 people were killed by landslides in the Himalaya, representing almost 35 % of the global total (Petley et al. 2007).

It is thus widely recognized that disasters contribute significantly to poor food security, out-migration and marginalization of vulnerable groups, caught in a typical negative poverty spiral with few rights and opportunities (UNDP 2004). However, landslides have a considerable underestimated impact on rural livelihoods in Nepal, with little attention received from government, the international community, NGOs or scientists. They are the leading natural hazard after epidemics, killing over 100 persons per year, compared to 77 for flooding and 29 for fire according to official statistics (MoHA 2009). However reporting on landslides is often difficult as many occur in

K. Sudmeier-Rieux (✉) • S. Jaquet • M. Derron • M. Jaboyedoff
Faculty of Geosciences and Geomatics, University of Lausanne, Institute of Geomatics and Risk Analysis, Lausanne, Switzerland
e-mail: karen.sudmeier-rieux@unil.ch

G.K. Basyal
National Society for Earthquake Technology – Nepal (NSET), Kathmandu, Nepal

S. Devkota
FEED (P) Ltd, Kathmandu, Nepal

S. Shrestha
Mercy Corps, Kathmandu, Nepal

C. Margottini et al. (eds.), *Landslide Science and Practice*, Vol. 4,
DOI 10.1007/978-3-642-31337-0_22,

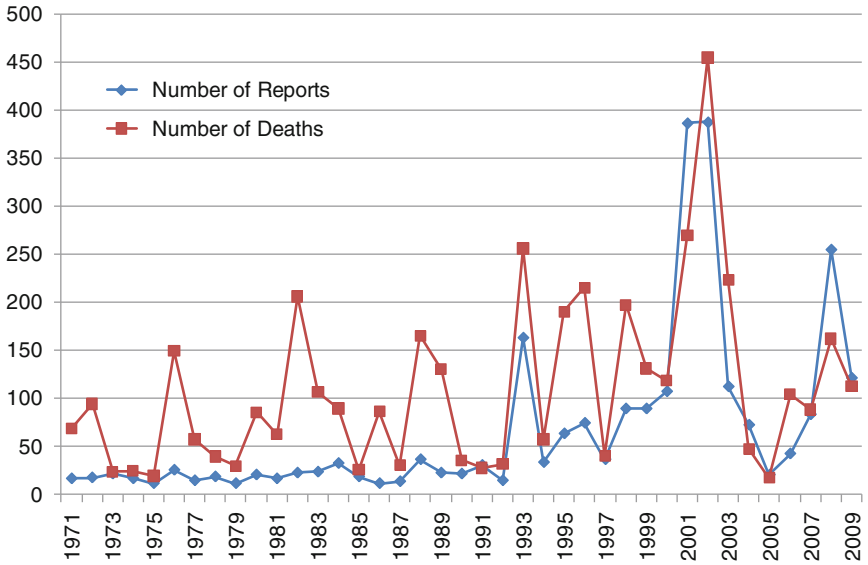

Fig. 1 Number of landslide reports and associated deaths due to landslides in Nepal 1970–2009, www.desinventar.net

remote mountain areas, and until now were included in official hazard statistics with flooding (MoHA 2009). These statistics are very similar to those posted by DesInventar Database of Nepal (Desinventar 2011), an independent source of hazard data (Fig. 1). Shallow landslides (<1 m deep) are the most common type of landslide with the greatest impact on rural livelihoods in the Middle Hills region, which supports a majority of its population (CBS 2009; Gerrard and Gardner 2002).

Climate change impacts are predicted to aggravate this vicious cycle with more intense rainfall patterns, the most common triggering factors of both shallow and deep-seated landslides in Nepal (Petley et al. 2007; Li and Zeng 2003). In parallel, several trends are currently shaping rural Nepal: increased mobility and connectivity, a shift toward cash crops and out-migration, all influencing livelihoods, food security and landslide occurrence. Decentralization of budgets to local authorities and emphasis on infrastructure development have led to a doubling of the road network 1998–2007 from 4,740 to 9,399 km (DoR 2010). Easier transportation and access to information about market prices has encouraged the shift toward cash crops. A steep rise in rural emigration is being shaped by push factors: mainly food insecurity and pull factors: a construction boom in Gulf State countries and greater ease of transportation.

The aim of this research is to highlight how landslides, this neglected disaster, is affecting livelihoods and food security. Six communities in Central-Eastern Nepal were studied in detail in three districts with different geographical, socio-economic and livelihood characteristics from Dolakha (Mountain/Hill), Sunsari (Hill/Terai) and Tehrathum (Hill) districts, with four of landslide affected communities, and for comparison, two are flood affected urban areas (Fig. 2). Moreover these areas were selected to contrast different types of landslide communities with different demographic compositions and different risk situations. The study's methods are interdisciplinary, combining a geological assessment of landslides, with participatory social science research methods: participatory risk- and resources mapping, focus group discussions, transect walks and semi-structured household interviews.

Landslide and Rural Development Trends in Nepal

Geologically, Nepal is situated in a region with high seismic activity due to the collision of Indian and Eurasian plates, which continuously create uplift for the young Himalayan range (Sharma 1991). With just 200 km separating the lowland Terai plains and the highest mountains on earth, most of Nepal's terrain consists of steep, rugged terrain, which populations have transformed over centuries into productive fields. Despite the rugged topography, the population density of Nepal is 194 people per km2 (projected for 2011) and the growth rate is 2.13 % per annum (projected for 2011) (CBS 2009). Although it has made major improvements in education, is Nepal is ranked 138th out of 169 countries in the UNDP 2009 Human Development Index (UNDP 2009). Main causal factors of Nepal's poverty are proneness to natural hazards, unequal distribution of quality of land, lack of access to education and basic health facilities, low level of infrastructure development and low employment opportunities (CBS 2009). In 2001, Nepal's land use was divided as follows: agricultural land (21 %), non-cultivated land (7 %), forest (29 %), shrub (11 %) grass/pastureland (12 %) water/lake (2 %) and other (18 %), including snow areas, barren land, rocky areas and eroded areas (CBS 2008).

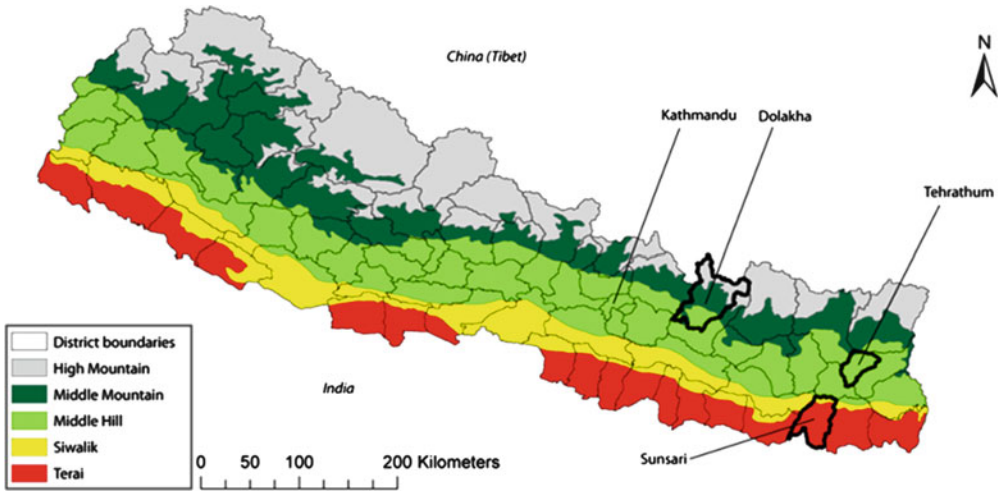

Fig. 2 Physiographic map of Nepal. Highlighted districts where research took place. (Map developed by Jaquet, based on MENRIS/ICIMOD data, 2011)

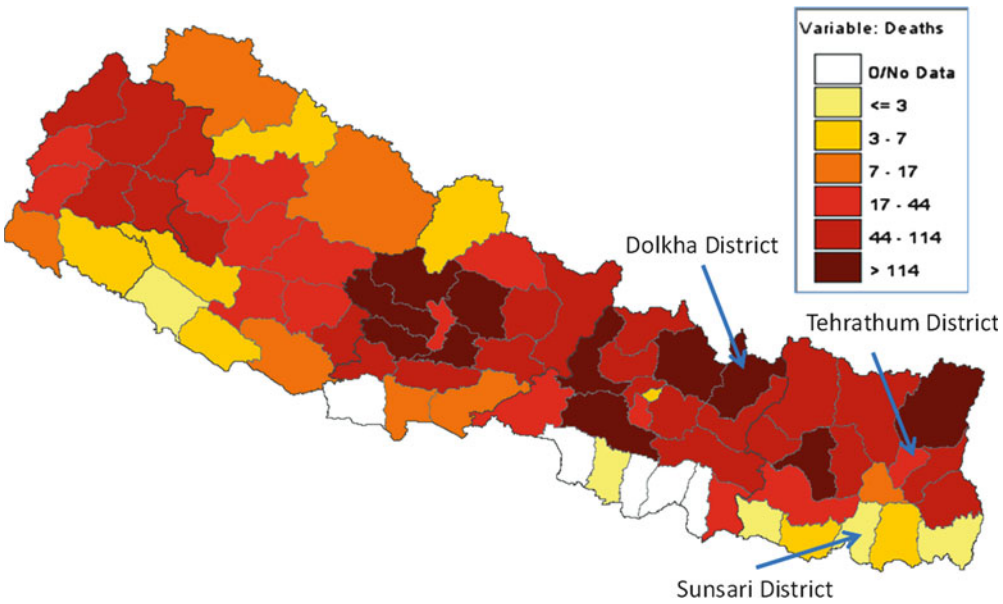

Fig. 3 Mortality due to landslides in Nepal 1971–2009. (www.desinventar.net/nepal)

Thus the combination of high population density, high population growth rate, low income and steep terrain means that the country is vulnerable to the effects of landslides (Petley et al. 2007). These are especially pronounced in the Middle Hills regions, which combine high rainfall, lithology susceptible to landslides and relatively high population density (Petley et al. 2007) (Fig. 3).

In order to examine linkages between landslides and livelihoods, it is important to have a good understanding of both human and natural landslide causes. In addition to gravity, two categories of forces cause landslides: triggers and preparatory factors (Caine and Mool 1982; Crozier and Glade 2004; Petley et al. 2007). Both types of factors can be natural or human-induced and controlled by topography, lithology, geology and hydrology. Human-induced activities, such as deforestation, grazing, road building and mining can disturb the inherent force of a slope, causing it to move under pressure from gravity under heavy rainfall or earthquake activity (Crozier and Glade 2004). Landslides are dispersed and less easily reached by authorities and NGOs with considerably less media attention than floods, which often occur in highly concentrated population areas. In contrast to floods, landslides cause more long-lasting damage to livelihoods as lost terraces or irrigation systems may not be recoverable or take years to reconvert to productive lands.

There is increasing evidence that shallow landslides are shifting from mainly highly degraded areas along waterways and gully erosion, largely caused by grazing, toward landslides along roads (Jaquet et al. submitted). The hypothesis is that two decades of community forestry has had a large influence on increasing forest cover in selected areas, due to improved grazing practices and sustainable forestry with a positive influence on the occurrence of shallow landslides.

Landslide and Impacts on Livelihoods and Food Security

The exact impact of landslides on food security in Nepal is difficult to estimate, however we can make some indirect estimates based on land use and household income data and results from this research. Most studies agree that the most common larger and damaging landslides (>10 m^3) in agricultural lands occur primarily on rainfed terraces (*bari*), followed by those occurring on irrigated (*khet*) terraces, abandoned fields and old landslide areas (Caine and Mool 1982; Gerrard and Gardner 2002). *Khet* landslides are likely the most frequent but small in nature (>2 m^3) (Gerrard and Gardner 2002) and due to water mismanagement. Small landslides that can be repaired cost significant time and labor for farmers, estimated at 14 days for repairing *khet* failures (Gerrard and Gardner 2002), in addition to lost yields. Another underreported cost are the resources required for relocating housing due to landslides, often within the same village but requiring time and money that could be used for income generating activities.

Over the past two decades, Nepal has changed from a net exporter to a net importer of food and the trend is toward increasing food insecurity (Bohle and Adhikari 1998). According to CBS data (2009), arable land per 100 persons has declined in Nepal between 1990 and 2007 from 9.4 to 8.5 hectares (ha). The proportion of the population living in rural areas remains high, 83 % in 2008, a decline from 91 % in 1990, with a total population of 23.1 million (CBS 2009). According to an interagency assessment report, 41 % of the population is undernourished, whilst the 31 % are under the poverty line (Govt of Nepal et al. 2008). The most poverty affected region is the Middle and High Mountains with 56 % of residents living in poverty and the mid- and western regions, where local food production sometimes only covers 3 months of the annual household requirements (Govt of Nepal et al. 2008).

Reasons for this food insecurity are multiple: unequal access to land, rising food and commodity prices, heavy dependence on food and oil imports, high transportation costs and inaccessibility of remote mountains and Western Nepal, declining long term trend in public investment, agricultural support services and outreach (Govt of Nepal et al. 2008), to which we add lost agricultural land and income due to natural hazards, especially drought, landslides and flooding. According to the NLSS 2003–2004 study the average Nepali household spends on average 59 % of their total expenditure on food, the poorest quintile of the population spends as much as 73 % (CBS 2004).

Methodology

Our methodology combines "bottom-up" qualitative and quantitative participatory approaches with "top-down" quantitative geological assessments, remote sensing and a geographic information system (GIS) database. The study used well-tested participatory qualitative methodologies, typically used in Vulnerability and Capacity Analyses (VCA), such as stakeholder consultations, transect walks, participatory risk and resource mapping to understand how the communities function, relations between groups, coping strategies, and to identify vulnerable households and dangerous areas (Kafle and Murshed 2004). The participatory risk mapping exercises especially provided a means for improved communications about risk between community members and scientists.

The scale of the study is at the community and household level. As part of the participatory process of this research, communities were selected in consultation with partner organizations to reflect as much as possible a diversity of risk situations incorporating local experiences on: proneness to landslide and flooding, ethnic composition, migration status, economic status, rural and urban. The studies were conducted between October 2008 and October 2010 with a team of researchers, at minimum, two geologists and two social scientists of which two were native Nepali speakers. In total, approximately 1 week was spent in each village.

The study is based on 160 semi-structured household surveys, circa 50 % of representation of each village, focus group discussions and risk mapping exercises. Results were tabulated in excel tables and open ended questions were analyzed manually. In addition to being subject to higher risk, women are known to have different perceptions and responses to risk than men. Therefore, separate focus groups were held for women and men with a total of ca. 60 persons participating in focus group discussions. Sessions were recorded and translated into English and a manual content analysis was conducted to detect main trends. Secondly, men and women were separated into groups of 8–10 persons to conduct a modified SWOT analysis or "social mapping"

Table 1 Geographic data

Geographic data	Sabra	Thang thang	Khariswara	Katahare	Punarbas Ward 3	Dharan Ward 4
District	Tehrathum	Dolakha	Dolakha	Sunsari	Sunsari	Sunsari
VDC	Basantapur	Suspa	Gairimudi	Bishnupaduka	Barahachhetra	Dharan Municipal
Population	110	120	130	210	500;10,000 total	3,384; 100,000 total
Altitude m.a.s.l.	2,300	1,500–1,800	950–1,300	400–750	100	400–500
Physiographic zones	Middle Hills	Middle Hills	Middle Hills	Siwalik	Terai/Siwalik	Terai/Siwalik
Climatic zones	Temperate	Temperate	Tropical/ Temperate	Tropical	Tropical	Tropical
Ave. annual rainfall (mm)	2,000	2,000	1,600	2,000	2,300	2,300

of their resources and main threats and priorities, as a self-assessment of risks, resources and threats. Finally, a household survey was conducted, with a purposeful sampling of households to ensure than households within a high risk (<100 m) and low risk (>100 m) perimeter from the landslides (as source of hazard) were questioned. Proxy questions on literacy rates, consumer durables, livestock, landholdings, average spending (household expenditure) per month were used to obtain a measure of household income as direct questions on income were considered too sensitive. The methodology was designed to cover a number of physical and socio-economic aspects of the communities with regard to landslide and flood risks, however this article mainly focuses on those aspects related to livelihoods, food security, coping strategies, risk perceptions and disaster losses.

Results

Geographic Situation

The study sites are representative of a variety of geographic locations, across the Terai, Siwalik and Middle Hills areas, from the semi-tropical climatic zone at 100 m.a.s.l in Punarbas to temperate at 2,300 m.a.s.l (Table 1). The four landslide areas selected are in rural areas in proximity to roads, except for Katahare, 1 h walk from the nearest road and Khariswara, 1.5 h walk during the monsoon period. All the landslide areas are situated in high risk areas as estimated by the team of geologists (Jaboyedoff, Derron, Devkota), as all are situated in areas with geological formations with low soil cohesion. Dharan Ward 4 is at high risk for flash flooding and chronic flooding, due to the high exposure of the population to Khare Khola stream (torrential stream), which runs right through the city and floods it annually. Flooding was chronic in the semi-urban town of Punarbas (pop. 10,000) until a series of dykes were erected in 2008 and displacing the flood waters towards forests. One neighborhood, where the secondary school is located, is still subject to occasional flash flooding. All of these areas are very susceptible to high rainfall events, which could easily cause casualties and loss of land.

Demographic and Economic Data

Table 2 details substantial differences between communities, with a close correlation between ethnic status, average landholdings and food stocks. Differences between urban and rural areas are not surprisingly marked by different levels of sectorial activity: the rural areas are dominated by agriculture and semi–skilled labor, with a high number of retired persons and wage earners in Khariswara, Punarbas and Dharan, of which most are unemployed. Rural respondents did not report unemployment if they were engaged in some type of agricultural activity, even if they were also seeking supplementary employment, somewhat skewing this figure. The areas with the highest number of government employees are Sabra, Punarbas and Khariswara and are also primarily constituted by so-called high caste groups with higher literacy rates, higher landholdings per household, more livestock per household, receiving more remittances, owning more mobile telephones, electricity and with more months of food stocks. Monthly expenditures for the urban respondents are not surprisingly higher, as households are more dependent on purchasing food, mirrored by the few respondents in Dharan with landholdings and livestock. Sabra has relatively high numbers of livestock due to the terrain, which is largely grasslands, in addition to the good economic situation of this village.

In- migration has played an important role for several communities, especially Katahare, Punarbas and Dharan, communities situated in the Terai plains or foothills, confirming the continuing trend of out-migration from the Middle Hills. Reasons for the migration are mainly economic, followed by

Table 2 Demographic data

Demographics	Sabra n = 11	Thang/thang n = 13	Khariswara n = 13	Katahare n = 30	Punarbas n = 42	Dharan n = 59
Occupation%						
Agriculture	80	92	38	83	21	0
Semi-skilled labour	0	8	7	10	21	62
Retired/unemployed/out-migrated	0	0	23	0	40	33
Government/salaried	20	0	16.5	7	16	4
Literate %	63	7	61	23	40	61
Disadvantaged ethnic group %[a]	0	100	0	100	18	65
Remittances %	18	8	38	20	27	3
Average landholding (ha)	1.3	0.2	0.6	0.35	0.2	0.0
Food stocks (months)	4.5	3.8	6.8	3.2	3.4	n/a
Average number of livestock per household[b]	4.6	1.7	2.5	2.3	1.7	0.7

[a]Based on NDFIN (2011)
[b]CBS 2004

Table 3 Landslide losses and livelihood impacts

Landslide losses and livelihood impacts	Sabra	Thang/thang	Khariswara	Katahare
Average landholding (ha)	1.28	0.16	0.58	0.35
Average landholding (ha)	0.70[a]	0.34[b]	0.50[a]	0.70[b]
Mean household income for region (000 NPR)	89.9	89.9	89.9	73.5
Est household income (000 NPR)	161.8	42.2	107.9	36.7
Food stocks (months)	4.5	3.8	6.8	3.2
House lost or damaged %	63	38	31	70
Percent of *khet* lost or converted to *bari*	0.30	0.50	0.75	0.45
Average rice yield kg/ha[c]	2,500	2,500	2,678	3,125
Lost annual rice production (kg)	960	200	1,164	169
Cost of lost annual rice production (000 NPR)	38	8	46,5	7
Min. cost of house construction over 10 years (000 NPR)	10	8	10	5
Average annual loss due to landslides (000 NPR)	48	16	56	12
Percent of mean household income affected by landslides %	29	38	52	32

[a]CBS 2004
[b]Dolakha VDC profile data 2007
[c]Govt of Nepal 2008

landslides or flooding elsewhere, which caused respondents to relocate. Punarbas was actually created by the government to relocate settlements affected by numerous floods caused by nearby Koshi river. The Dharan settlements that were surveyed are mainly illegal settlements, with large numbers of in-migrants. The upper part of Katahare was settled without legal registration after a large landslide in 1966 destroyed 13 houses (no casualties) and families over the years laid claim to the landslide-prone abandoned land.

Impact of Landslides on Livelihoods and Food Security

The impact of landslides on livelihoods is extremely high for communities surveyed, in terms of lost income, land, irrigation canals and the need to reconstruct and repair houses. Faced with landslides, most common strategies were to convert irrigated fields with valuable rice crops to lesser valued millet or wheat, as landslides damage irrigation or render a slope unsuitable for rice paddies. This has resulted in lost income, conversion to crops with lower nutritional and economic value and a need to purchase rice. In Sabra, there were fewer *khet* terraces due to the higher elevation, instead farmers had invested in cash crops, such as cabbage, cauliflower, cardamom and livestock. For all communities, outmigration is another common strategy and migrants from wealthier communities tended to send home greater sums of remittances.

Table 3 was developed using both our primary data and secondary data, mainly from the NLSS 2004 survey and the Nepal Food Monitoring Survey (WFP 2011). We estimated mean household income using average landholding per our surveys compared to data on average landholdings, giving us

a ratio either above or below the average. We include data on food stocks and percent of *khet* converted to *bari* based on our survey data. The cost of lost rice production was then estimated based on an average sale price of 40NPR per kilo. Considering that most households surveyed rebuilt their houses once or twice over 20 years, the cost of reconstruction for each location was spread out over 10 years. We then obtained the average losses per community due to landslides. By these estimates, landslides cause considerable economic damage, in the order of 29–52 % of annual household income, affecting both high and low income communities. This is a significant drain on household resources that could be used for other purposes such as improvement in agricultural productivity, education, purchase of new land, etc. This figure is of course a rough estimate as are other costs that have not been included, such as the cost of reconstructing irrigation canals, roads, trails that may have been destroyed by landslides.

Discussion

One of the most important findings of this comparative study is that losses due to landslides are extremely high with a high negative impact households. Landslides create more permanent loss of land with a longer rehabilitation period as compared to flooding. This is also due to the remote nature of many communities in the Middle Hills, where most landslides occur and where transportation costs are higher. Losses of due to landslides are similar among poor and rich communities as measured by landholdings per household, literacy rates, livestock, consumer durables and expenditures. However, poorer communities are affected more proportionally and richer communities demonstrate higher capacities to cope, by diversifying livelihoods, seeking external assistance, ability to spend more on repairs, purchasing food, greater technical knowledge and outmigration for higher skilled positions.

Due to space limitations, data on coping strategies were not presented in detail here. Overall, the amount of preventive measures, monitoring and evacuation preparedness is extremely low due to limited resources and knowledge about mitigation for prevention as well as nowhere to go in case of an emergency. Also, for the poorest communities, food security was the main concern, followed by education and landslide mitigation. The other communities were mainly concerned with access to roads, or better roads, in spite of high landslide risk. According to respondents, roads bring the possibility of investing in more cash crops due to ease of transportation, they end isolation and enhance social status. This priority also reflects the current road building focus of the government.

Where this survey fell short is in documenting how households financed house reconstruction, whether using savings or taking out loans and the extent to which landslides have reduced food security as calculated in reduced months of food stocks. More research documenting direct impacts of landslides on food security deserve further research.

Conclusions

Lessons from this study are that landslides have a large impact on livelihoods and food security, forcing households to spend sparse resources on purchasing food, rebuilding or repairing homes, terraces and irrigation systems. Landslides greatly affect livelihoods in rural areas and are grossly underreported by official statistics and DesInventar data, by an order of two according to our estimates. By focusing a large portion of local and national budgets on building roads, without proper mitigation, roads have become one of the main human causes of landslides, versus deforestation or grazing, which have been curtailed in areas with well-managed community forests (Jaquet et al. submitted). Communities are understandably yearning for increased connectivity and the opportunities that roads bring. However, investing in improved agricultural outreach and farming techniques that include technical advice on landslide mitigation, monitoring and emergency preparedness may be a wiser investment of public funds and foreign grants in order to address Nepal's chronic food security problems. In the high risk context of rural Nepal, integrated approaches are required that combine both development and DRR components. It is about time that more attention be paid to landslides, Nepal's neglected disaster.

Acknowledgements This research was entirely funded by the Swiss National Science Foundation (grant 26083591) during the period 2009–2011, for which we are extremely grateful.

References

Bohle H-G, Adhikari J (1998) Rural livelihoods at risk how nepalese farmers cope with food insecurity. Mt Res Dev 18(4):321–332

Caine N, Mool PK (1982) Landslides in the Kolpu khola drainage, middle mountains, Nepal. Mount Res Develop 2(2):157–173

CBS (2008) Environmental statistics of Nepal 2008. Central Bureau of Statistics, Govt of Nepal National Planning Commission Secretariat, Kathmandu

CBS (2009) Statistical year book of Nepal 2009. Govt of Nepal National Planning Commission Secretariat, Kathmandu

CBS (Central Bureau of Statistics) (2004) Nepal living standards survey 2003/04, statistical report volume 1 and 2. Govt of Nepal National Planning Commission Secretariat, Kathmandu

Crozier M, Glade T (2004) Landslide hazard and risk: issues concepts and approach. In: Glade TMA, Crozier M (eds) Landslide hazard and risk. Wiley, Sussex

DesInventar Dabase, Disaster Inventory/Information Management System for Nepal, online Disaster Database for Nepal maintained by National Society for Earthquake Technology - Nepal (NSET), http://www.desinventar.net/nepal. Accessed 16 May 2011

Dolakha VDC Profile Data Report (2007) Department of Survey, Government of Nepal

DoR (Department of Roads) (2010) Government of Nepal, Ministry of Physical Planning and Work www.dor.gov.np. Accessed 16 May 2011

Gerrard AJ, Gardner R (2002) Relationships between landsliding and land use in the Likhu Khola drainage basin, middle hills, Nepal. Mt Res Dev 22(1):48–55

Government of Nepal, FAO, WFP, IFAD, Asia Development Bank, World Bank (2008) Nepal initiative on soaring food prices, Draft Report of Mission Findings and Recommendations, Kathmandu, 21–31 July 2008

Jaquet J, Sudmeier-Rieux K, Jaboyedoff M, Derron M-H (2013 in print) Forest trends, landslides community and forests in Dolakha district, Central Nepal. In: Renaud F, Estrella M, Sudmeier-Rieux K (eds) The role of ecosystems for disaster risk reduction. United Nations University Press, Bonn

Kafle SK, Murshed Z (2004) Community-based disaster risk management for local authorities. Asian Disaster Preparedness Center, Bangkok

Li J, Zeng Q (2003) A new monsoon index and the geographical distribution of the global monsoons. Adv Atmos Sci 20:299–302

Ministry of Home Affairs (MoHA), Government of Nepal and Disaster Preparedness Network (DPNet) (2009) Nepal Disaster Report 2009: The Hazardscape and Vulnerability, Kathmandu

NFDIN (2011) Categories of Indigenous Nationalities of Nepal. http://www.nfdin.gov.np/index.php?option=com_k2&view=item&id=27:categories-of-indigenous-nationalities-of-nepal, National Foundation for Development of Indigenous Nationalities, Kathmandu, Nepal. Accessed 1 Mar 2011.

Petley D, Hearn G, Hart A, Rosser N, Dunning S, Oven K, Mitchell W (2007) Trends in landslide occurrence in Nepal. Nat Hazards 43:23–44

Sharma CK (1991) Engineering challenges in Nepal Himalaya. Printing support Pvt. Ltd., Kathmandu

UNDP (2004) Reducing disaster risk: a challenge for development. A global report. UNDP – Bureau for Crisis Prevention and Recovery, New York

UNDP (2009) Nepal human development report 2009. UNDP, Kathmandu

WFP (2011) Nepal- Food Security Monitoring System. sites.google.com/site/nefoodsec/home. Accessed 16 May 2011

Strategies and Options to Address Land Degradation Due to Landslides: Bhutanese Scenarios

Phuntsho Gyeltshen and Chencho Norbu

Abstract

Occurrence of landslides poses a very serious threat to Bhutan. It causes serious socio-economic and environmental impacts. Therefore, this phenomenon necessitates appropriate interventions. Recently, the government of Bhutan has been making continued efforts in mitigating landslides; through introduction of bio-technical slope protection measures and installation of retaining structures at the toe of landslides. Besides, attempts were also made to reduce the ill effects of poor water management practices from irrigation, drinking water and roadside drains. Hitherto, the results indicate that bio-technical slope protection measures are generally efficient in stabilizing the slopes with stable geology. For hedgerows, certain technical adjustments are necessary to make it acceptable for farming communities. It was also realized that for a landform characterized by steep slopes, it is crucial to mitigate the upslope physical land degradation processes viz. sheet, rill and gully erosions. Furthermore, the stage of landslide initiation and other bio-geophysical factors play significant role in landslide stabilization.

Keywords

Landslides • Bio-technical • Bio-geophysical • Land degradation • Bhutan

Introduction

In Bhutan, approximately 69 % of the population practice subsistence farming on 2.95–8 % of the total area (36,800 km^2), which is considered to be cultivable (NSSC 2010). This indicates that Bhutan has inherently limited resources for productive land (Norbu et al. 2003).

Due to the geo-morphological and climatic conditions, most of the landscape is "quasi-stable" (Norbu et al. 2003). Only a small trigger is necessary to destabilise it and for the surface materials to slip down and eventually be washed away. Norbu et al. (2003) mention that those soils derived from gneiss rock types erodes less in contrast to soils from other rocks such as schists and phyllites. As a result, occurrence of landslides is widespread particularly in Eastern, Central and Southern parts of Bhutan (NSSC 2009), since these regions are underlain by less stable geology such as schists and phyllites. This is of great concern for Bhutan.

The impacts of landslide disasters are observed in a unique way. At the source, it changes the characteristics of landform (Hancox et al. 2005; Restrepo and Alvarez 2006) and water regimes in the catchments (Narayana 1987). Farmers lose substantial portion of arable land, thus posing threat to their livelihoods. Along its pathway, the landslides destroy infrastructure and impact transport and service industries. The sediments pollute water systems and impacts hydropower, since the landslides are a major source of sediments in the mountain environments (Narayana 1987; Burton et al. 1998; Korup et al. 2004). In the downstream areas, i.e. once it leaves the catchment, landslides cause flooding, bringing misery to the lives of people. The occurrences of landslides entail huge

P. Gyeltshen (✉)
National Soil Services Centre, P.O. Box 907, Thimphu, Bhutan
e-mail: p.gyeltshenn@gmail.com

C. Norbu
Department of Agriculture, Ministry of Agriculture and Forests, Thimphu, Bhutan

C. Margottini et al. (eds.), *Landslide Science and Practice*, Vol. 4,
DOI 10.1007/978-3-642-31337-0_23,

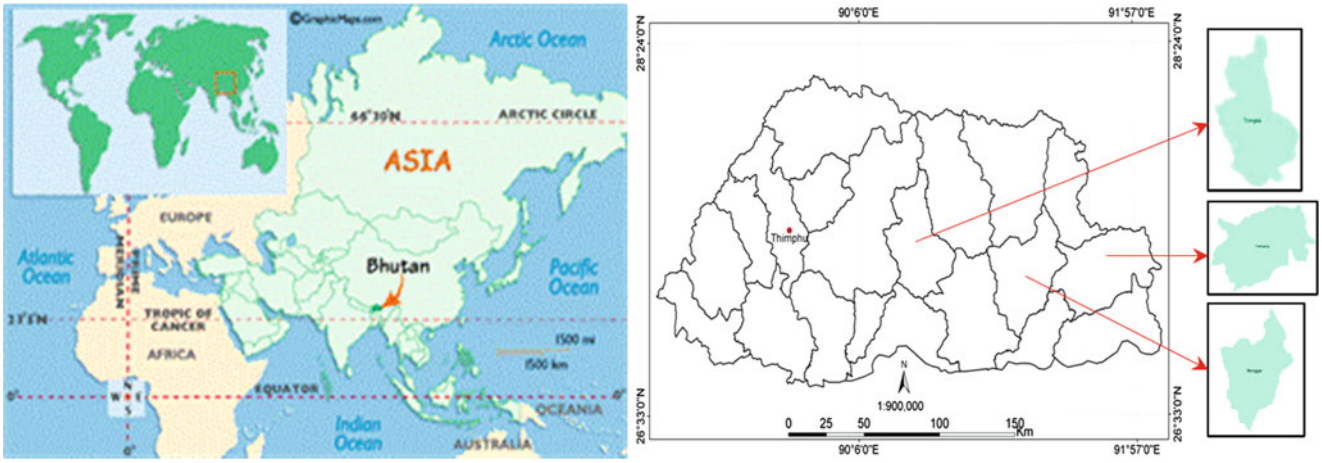

Fig. 1 Bhutan in world context (*right*) and location of land management campaign sites in Eastern and Central Bhutan

economic losses. Ngechu and Mathu (1990) rightly mention that the enormous economic loss due to landslides becomes unquantifiable. As a result, the resource stricken countries take long time to recover from these events. Furthermore, the landslides have other impacts too. The events influence mountain ecosystems both in qualitative and quantitative manner (Restrepo and Alvarez 2006).

In recent years, occurrence of increasing landslides has been reported from across Bhutan (NSSC 2006). As reported by researchers, this may be because of contributing factors such as increasing population (Dai et al. 2002; Restrepo and Alvarez 2006) and due to impacts of climate change which is observed through uncharacteristic patterns of weather changes (UNEP 2001; Bürki et al. 2003; NSSC 2006). Other researchers in the region also indicate that landslide causes serious problems. For instance, Chamlagain and Suwal (2010) report that landslide is the major natural disaster responsible for the loss of life, property and damages to infrastructure in Nepal, Patley et al. (2010) report that the 8th October 2005 earthquake induced landslides in Pakistan caused third highest landslide disaster recorded in the history (26,500 fatalities including 300 in India) and Dai et al. (2002) mention that landslides have become so widespread in the mountain areas of China that people living there consider it part of their daily lives. Visual observation of Fig. 3 (Left) also indicates that some communities in Bhutan may be experiencing the similar fate.

There are many strategies to address landslides depending upon its scale and magnitude. This can be a simple reforestation in the degraded forest areas. Other measures include introduction of low cost bio-technical measures such as check-dams, re-vegetation, construction of revetments, drainage ditches and benching (Tianchi 1990; NSSC 2005a), or more complicated engineering measures such as correction of unstable underlying slopes, use of retaining structures and internal slope reinforcements, and so on (Dai et al. 2002). The latter requires detailed geo-technical information.

The ensuing sections focuses on: the general setting of this study, methodology adopted for disseminating landslide mitigation works, results realised so far, discussions and a brief conclusion.

Study Regions

Bhutan is geographically located in South Asia, between India and China at 27° 30′ to 27°50′ N and 89° 20′ to 91° 10′ E (Fig. 1). It has a very complex geo-morphology with very steep slopes incised with deep valleys, and with altitudes stretching from 100 t0 7,500 m above sea level (asl) (Baillie and Norbu 2004).

Geologically, the country is divided into three geological zones (Gansser, 1983- cited in Kuenza et al. 2010). Parts of the country in the Southern belts (Lower Himalayas) experiences tropical weather conditions, cool winters and hot summer in the central valleys (Lesser Himalayas), and severe winters and cool summers in the northern parts (Greater Himalayas). Each zone consists of different rock types.

- Lower Himalayas: Unconsolidated sandstones, shale, mudstone and conglomerates
- Lesser Himalayas: There are two categories of rocks- (a) relatively soft rocks on gentle slopes with deep soils, and (b) relatively hard rocks on steep slopes with shallow soils. The former consists of the common rock types such as granitic gneisses, limestone and quartzites, whereas, the latter is composed of rocks such as quartizites, phyllites, dolomites and schists
- Higher Himalayas: Consists of gneisses, granitic rocks, schists and dolomites

This paper makes a strong focus on the landslide management activities that was carried out in the mode of Land Management Campaigns (LMC). The LMC was first executed in Trashigang Dzongkhag (District) in Eastern Bhutan in 2005. In the following year, the same activity was replicated in Mongar (East) and Trongsa Dzongkhags in the Central region (Fig. 1- left). The LMC sites are located in the Inner Himalayas. Similar activities [of smaller scales] were also executed in the Southern parts of the country, where occurrence of ladnslides is more frequent (NSSC 2009). It would be an over exaggeration to mention the precipitation figure of any activity site for two reasons: firstly, due to an occurrence of localised precipitations because of high relief, and secondly there are no weather stations that will record the daily atmospheric conditions at the LMC sites. However, some southern regions in Bhutan receives rainfall as high as 5,500 mm per year, whereas, some regions in the north receives rainfall as low as 300 mm per year.

Methods

This section consists of three parts: an approach adopted to mitigate landslides and other physical land degradation processes, mode of communication of landslide mitigation works, risks and hazards, and the types of technologies adopted for the purpose.

Approach

Government Initiatives

Prior to 2005, management of landslides along the roads and in the mining areas gained special focus. It is rather pertinent to point out that the landslides in and around the agricultural fields are left either to the mercy of the nature, or in the hands of the farmers with limited technical knowledge to carry out mitigation works. Therefore, the Government of Bhutan through its concerned agencies (Particularly Ministry of Agriculture and Forests- MoAF) made special effort to make it a central program to address landslides within and in the vicinity of agricultural fields. For this, top-down approach was adopted to disseminate bio-technical know-how to the farmers. This was continued for few years.

Empowering the Local Communities

In later years, a rather different strategy; empowering local communities in making the decisions to manage landslides in their regions was adopted. With guidance from extension agents, the communities make an annual work plan on land management. The necessary financial and technical support was provided by the government. This allows communities to make their own decisions on mitigating the prevailing land degradation processes such as landslides and accordingly manage the land resources sustainably. This strategy is also important in leveraging the horizontal spread of the sustainable land management activities.

Communication of Landslide Hazards

It is very crucial that the stakeholders understand about the hazards and risks associated with the landslides. Likewise, the stakeholders should also know about the various technologies available to mitigate the process. Different methodologies were adopted to achieve this; the foremost method was an employment of media to disseminate and educate the stakeholders. Secondly, practical demonstrations on technology implementation were also done for the stakeholders to educate them about the intervening technologies in the field. This was particularly carried out by the National Soil Services Centre (NSSC), together with extension agents, from various departments, under MoFA.

Bio-technical Measures

Mitigation of the Precursors of Landslides

Firstly, interventions to mitigate the upslope land degradation processes were executed. These upslope processes include degradation attributes such as sheet, surface, rill and gully erosions. The main bio-technical interventions include establishment of hedgerows in the arable fields, constructions of check dams (both stone and log check dams) in the gully floors, plantation of grass slips along the gully sides slopes, plantation of multi-purpose tree seedlings, etc. were carried out. In addition, physical measures such as stone bunding and terracing were also introduced.

Mitigation of Landslides

Low cost bio-technical measures to mitigate landslides were introduced. These includes plantation of multi-purpose tree seedlings, banana and bamboo rhizomes, plantation of fast growing live cuttings and grass slips, edge trimming on the slide edges, brush layering, etc. On the other hand, physical structures such as stone walling at the toe of landslides were done. In areas where it is too risky to carry out any interventions, seeding grass of fast growing tree species was also done.

Results

The mitigation works to reduce physical land degradation has, so far, shown mixed results. Few selected results are reported below.

Fig. 2 Most of the agricultural activities are on the steep slopes (*right*) – in some cases on slopes up to 40°. And in some regions the communities are impacted by landslides very badly (Photo NSSC 2006)

Mitigation for Precursors of Landslide (Upslope)

Hedgerows: These are established in the arable field to mitigate the processes such as surface, sheet and rill erosions. The results have indicated that this technique is generally efficient in containing the sediment that were brought down from upslope. True to its theoritical stance, it was also observed that hedgerows acts as barriers in reducing the flow velocity of discharge during high intensity rainfalls. However, this measure is without its problem. Strictly following the technical guidelines while running A-frame along the contours impede farmers while preparing field during cultivation using drought animals. This is mainly because as the slope increases, the distance between the two hedgerows decreases significantly (NSSC 2005a). This limits the use of local tools for cultivation. Therefore, technical adjustments have to be made for the farming communities to accept this technology.

Check dams: In places where the geology is stable, the check dams are found to be very effective in stabilizing the gullies. It not only contains the sediment flow in its banks, but also reduces the velocity of water flow considerably. Series of well spaced log and stone check dams along the gully does all the trick in retaining the sediments onsite (Fig. 2b). The reduction of the flow velocity of water prevents further scouring and detachment and hence it reduces overall sediment load leaving a particular micro-catchment. However, results from most of the LMC sites were rather different. It was found that in places with geology comprising of schists and phyllites, the soils are generally silty textured. These coupled with steep slopes render both stone and log check dams ineffective, suggesting that the rate of erosion is too high in such areas.

Plantations: The plantation were done to stabilise the slopes through revegetation . The results indicate that this technique is generally sound in providing the ground cover and minimising the runoff. Nevertheless, the effectiveness of this technology unstable slopes with extensive mosaic of cracks is questionable. This may be partly because the slopes are in constant downward movement.

Mitigation of Landslides

Plantation in the old landslide scars are found to be very effective in quick stabilization of the slopes. However, any aspiration to mitigate the recent and/or fresh landslides could be a big asking. Keeping aside the low cost bio-technical measures, in extreme cases, even the stone walling at the toe of landslides doesn't have a remote chance when landslide events continue to occur. This suggest an existence of very strong interplay of implicit geo-morphological and environmental factors in triggering the landslides. On the other hand, seed boradcasting on landslides where it is too risky to place any other mitigation measures were found to be ineffective. This raises two concerns; firstly, about the the quality of the seeds, and secondly about the suitibility of seeds in question in a given environment.

Discussions

With over two third of the total population deriving their livelihoods by agricultural farming on less that 8 % of the total land that is cultivable, there are daunting challenges posed by land degradation due to landslides. The socio-economic impacts of landslides are immense. As pointed out by Tianchi (1990) and Dai et al. (2002), this may only become worse as the population increases annually and more people put pressure on finite natural resources and cultivate on marginal lands (Fig. 3- right). The impact of anthropogenic actions and environmental factors in triggering landslides may only increase either due to greater pressure on resources (Restrepo and Alvarez 2006; NSSC 2009), or due to an increasing effect of climate change, since the mountain areas are more sensitive to such changes (Bürki et al. 2003), or both (Chang and Slaymaker 2001). Some researchers have particular blame towards human actions as a sole responsible factor. For instance, Ngechu and Mathu (1999) goes further in saying that majority of the landslides are triggered by diverse human activities.

Fig. 3 Bio-technical measures for landslide mitigation – (**a**) Hedgerows introduced to reduce, surface, sheet and rill erosion, (**b**) Log check dams to mitigate gully erosion, which is completely filled with erodeddebris from upslope, (**c**) Brush layering on landslides, and (**d**) Communities carrying out plantation in the landslide areas, part of the maize field washed away (Photo NSSC 2005a)

Addressing the landslide problems within, and in the vicinity of the agricultural fields gained greater importance of late. This may be primarily to protect the arable lands from being washed away. Other reason could be because, as stated by Jakob (1999), the landslides in the natural forests are generally smaller as opposed to the ones where there is some kind of human influence on nature. Jakob (1999) also found that occurrence of landslides in areas with certain human activity, for instance, deforestation, is eight times more than in the nature areas. This finding is in agreement with the general observations made across Bhutan where there are landslide problems particularly concentrated in areas with human activities (NSSC 2005b). Therefore, it emerges that the landslides close to settlements demand prior attentions.

The landslides occurring on a landform which is characterized by steep slopes are generally located down-slope, and are associated with the up-slope land degradation processes. Therefore, the seriousness [and extent] of up-slope processes determines the scale and magnitude of landslides. This is a situation in Bhutan. In light of this, and knowing that landslides have wide range of consequences, both at the site of the slope and further afield (Burton et al. 1998), there are some decisions to be made. It may be logical to mitigate the precursors of landslides by adopting low cost bio-technical measures to reduce the scale of down-slope events. In Bhutanese situation, this may be an amicable option, but not an absolute remedy.

One truth which is simply being overlooked is that there are landslides that can hardly be mitigated, for instance, a landslide occurring on steep slopes where the landform is geologically unstable. In such situations, it would be vital to consider the effectiveness of placing mitigating technologies and the resulting economics, since the measure may be vulnerable to overtopping by either high velocity landslide debris or accumulated deposits from repeated events (Dai et al. 2002). This was also realised from the LMC experiences. Proper technical assessment may be crucial to reduce the risks and hazards. It is worth mentioning that today; Bhutan is relatively inexperienced in dealing with the landslides. It would be vital to learn from the experiences of other countries in the region.

What is more? Currently, there is an institutional void in the system. Each agency makes its own [or sector-specific] approaches to address land degradation. In essence, this overlooks the bigger picture that solving landslide issues requires cross-sectoral approach. In the current set up, there are three key Ministries making sector-specific attempts in mitigating landslides. These includes; the MoFA, mostly concentrating within and around the arable land, the Ministry of Economic Affairs (MEA)- focusing in the mining areas and Ministry of Works and Human Settlements (MoWHS)- focusing along the roads. This is a disjointed approach for a common problem and needs integration. Taking the current path would be too risky, since the Government has adopted ambitious developmental strategies (EDP 2010). In working towards realisation of the economic goals, there would be increased activities on a fragile landscape that would exacerbate occurrence of landslides. Arguably, this may hinder the development of other sectors; say for instance the hydro-power, which is currently the biggest revenue generator for Bhutan. Therefore, there is immense need of a propellant; a common national policy, that would bring all the concerned sectors and agencies onto one platform and steer them to make an integrated approach in addressing the problems associated with the landslides.

Conclusion

Land degradation due to landslides has been one of the most common problems in Bhutan for a long time. It took considerable time to get the necessary attention of the government. However, recently the issue of land degradation became one of the prime focuses. It is justifiable to say that landslides still require greater attention for many obvious reasons.

- There are many threats posed by landslides. It causes immense socio-economic impacts. Occurrence of landslides is likely to exacerbate due to increasing population and increasing effects of climate change.
- There are different measures to mitigate landslides. But in view of the technical capabilities and the financial constraints, it is best to opt for the low cost bio-technical measures to address landslide problems.
- Considering the geo-morphology, topography and reliefs in Bhutan, it looks worthy to first mitigate the up-slope land degradation processes to reduce the scale and magnitude of landslides occurring down-slopes.
- Hitherto, different sectors make their own approach in mitigating landslides. Formulation of common policy is crucial to ensure an integrated approach in mitigating landslides.

References

Baillie I, Norbu C (2004) Climate and other factors in the development of river and interfluves profile in Bhutan. J Asian Earth Sci 22:539–553

Bürki R, Elsasser H, Abegg B (2003) Climate change- impacts on tourism industry in mountain areas. In: Proceedings of 1st international conference on climate change and tourism, Djerba/Tunisia

Burton A, Arkell TJ, Bathurst JC (1998) Field variability of landslide model parameters. Environ Geol 35(2–3):100–114

Chamlagain D, Suwal S (2010) Overview of landslide hazard in Nepal Himalaya. In: Proceedings of AARC workshop on landslide risk management in South Asia, Thimphu, pp 91–105, 11–12 May 2010

Chang J, Slaymaker O (2001) Frequency and spatial distribution of landslides in a mountainous drainage basin: Western Foothills, Taiwan. Catena 46:285–307

Dai FC, Lee CF, Ngai YY (2002) Landslide risk assessment and management an overview. Eng geol 64:65–87

EDP (2010) Economic Development Policy of the Kingdom of Bhutan, Thimphu

Hancox GT, McSaveney MJ, Manville VR (2005) The October 1999 Mt Adams rock avalanche and subsequent landslide dam-break flood and effects in Poerua River, Westland, New Zealand. N Z J Geol Geophys 48:683–705

Havenith HB, Torgoev I, Meleshko A, Alioshin Y, Dannels G (2006) Landslides in the Mailuu-Suu valley, Kyrgzstan- hazards and impacts. Landslides 3:137–147

Jakob M (1999) The impacts of logging on landslide activity at Clayoquot Sound, British Columbia. Catena 38:279–300

Koi T, Hotta N, Ishigaki I, Matuzaki N, Uchiyama Y, Suzuki M (2008) Prolonged impacts of earthquake-induced landslides on sediment yield in a mountain watershed: the Tanzawa region, Japan. Geomorphology 101:692–702

Korup O, McSaveney MJ, Davis TRH (2004) Sediment generation and delivery from large historic landslides in the Southern Alps, New Zealand. Geomorphology 61:189–207

Kuenza K, Dorji Y, Wangda D (2010) Landslides in Bhutan. In: Proceedings of SAARC workshop on landslide risk management in South Asia, Thimphu, pp 73–80, 11–12 May 2010

Lin S, Shaw D, Ho M-C (2008) Why flood and landslide victims less willing to take mitigation measures than public? Nat Hazards 44:305–314

Narayana VVD (1987) Down-stream impacts of soil erosion in the Himalayan region. Mt Res Dev 7(3):287–298

Ngechu WM, Mathu EM (1999) The El Nino triggered landslides and their socio-economic impacts on Kenya. Department of Geology, University of Nairobi, Kenya, pp 284–288

Norbu C, Baillie I, Dema K, Tamang HB, Turkelboom F (2003) Types of land degradation in Bhutan. J Bhutan Stud 8:88–114

NSSC (2005a) Soil erosion manuel. Ministry of Agriculture and Forests, Royal Government of Bhutan, Thimphu

NSSC (2005b) Assessment of land degradation in Bhutan. Ministry of Agriculture and Forests, Royal Government of Bhutan, Thimphu

NSSC (2006) Implementation of united nations conventions to combat desertification in Bhutan. National Report, Ministry of Agriculture and Forests. Royal Government of Bhutan, Thimphu

NSSC (2009) National action program to combat land degradation (Draft). Ministry of Agriculture and Forests, Royal Government of Bhutan, Thimphu

NSSC (2010) Land cover assessment map of Bhutan. Ministry of Agriculture and Forests, Royal Government of Bhutan, Thimphu

Petley D, Dunning S, Rosser N, Kausar AB (2010) Incipient landslides in the Jhelum Valley, Pakistan, following the 8th October 2005 Earthquake. In: Proceedings of SAARC workshop on landslide risk management in South Asia, Thimphu, 11–12 May 2010, pp 106–116

Restrepo C, Alvarez N (2006) Landslides and their contribution to the land-cover change in the mountains of Mexico and Central America. Biotropica 38(4):446–457

Tianchi Li (1990) Landslide management in the mountain areas of China. ICIMOD Occasional Paper No. 15, Kathmandu

UNEP (2001) Bhutan: state of the environment: available at www.rrcap.unep.org/. Accessed 30 May 2011

Rainfall Variability, Landslides and Food Security in Himalaya

Prakash C. Tiwari and Bhagwati Joshi

Abstract

In Himalaya, increasing rainfall variability has accelerated landslide activity damaging cultivated land and devastating agricultural infrastructure. Paper aims to analyze rainfall variability and interpret its linkages with landslides and food security with an example of Kumaon Himalaya. Food security in the region depends on local agricultural production, food purchasing power, and road connectivity. Study revealed that both number of rainy days as well as amount of rainfall reduced respectively by 18 % and 25 % during last 10 years, but incidences of high intensity rainfall, cloud bursts and flash floods have increased. This has triggered landside activity devastating 4.83 ha cultivated land, 800 m canals length and 3,891 m road network ever year. Consequently, food production has declined by 15 % rendering 45 % families highly vulnerable to food insecurity. Adaptive agricultural land use planning and diversification and improvement of rural livelihood could reduce vulnerability of mountain communities to climate change and food insecurity.

Keywords

Tectonically alive • Subsistence agriculture • Slope instability • Erratic rainfall • Food deficit • Marginalized people • Adaptive management

Introduction

Himalaya represents one of the youngest, tectonically alive, ecologically fragile, socially marginalized, economically underdeveloped, and the most densely populated mountain ecosystems on the planet (Sharma and Pant 2004). The nature of terrain and climate impose severe limitations on scale of resource productivity as well as on efficiency of infrastructural facilities. As a result, biomass based subsistence agriculture constitutes main source of rural food and livelihood even though the availability of arable land is severely limited and agricultural productivity is low (Tiwari 2008, Tiwari and Joshi 2011a). During the recent past, a variety of changes have emerged in the traditional resource use structure mainly in response to increasing pressure of population and resultant increased demand of natural resources in Himalaya (Tiwari and Joshi 2005). Besides, the fast expansion of road linkages has facilitated the rapid urbanization, emergence and growth of rural service centers and increased access to markets. A large proportion of arable land is being encroached upon by the process of rapid urbanization and expansion of infrastructure, services and economic activities in the region, every year (Tiwari and Joshi 2005, 2011b). As a result, critical natural resources, such as, land, water and forests have deteriorated and depleted steadily and significantly leading to their conversion into degraded and non-productive lands, during the last 20–30 years.

Moreover, changing climatic conditions have stressed local agricultural and food systems through, higher mean

P.C. Tiwari (✉)
Department of Geography, Kumaun University, Nainital, Uttarakhand, India
e-mail: pctiwari@yahoo.com

B. Joshi
Department of Geography, Government Post Graduate College, Rudrapur, Uttarakhand, India

C. Margottini et al. (eds.), *Landslide Science and Practice*, Vol. 4,
DOI 10.1007/978-3-642-31337-0_24,

annual temperatures and melting of glaciers and snow, altered precipitation patterns, and more frequent and extreme weather events (IPCC 2007; ICIMOD 2007). During recent years, pattern of Indian monsoon has shown sweeping changes resulting into erratic rainfall and increased incidences of cloud bursts and flash floods and causing hydrological disruptions and slope instability across the Himalayan Mountains (Rawat et al. 2011). Himalaya being geotectonically active and environmentally sensitive is highly vulnerable to these changes in precipitation pattern and hydrological system which have increased severity, frequency and intensity of landslides in these young and fragile mountains (ICIMOD 2007). The increasing incidences of slope failure and landslides are not only damaging the productive agricultural land and disrupting natural drainage and conventional irrigation system, but are also disrupting road network which constitutes the only means of transportation, distribution and supply of food to the villages located in remote and fragile mountains as the local agricultural productivity is considerably low (Rawat et al. 2004). Long-term impacts of these changes are likely to increase vulnerability of regional population to food insecurity through substantial decrease in production, availability and access to food (Cline 2008; Aase et al. 2009).

Objective and Research Methods

The main objective of the paper is to (1) analyse the trends of changes in rainfall pattern, (2) assess its impact on slope instability and landslides, and (3) interpret the linkages between landslides and food security with a case illustration of Lake Region in Kumaon Himalaya, India. In order to attain the objectives of the study following methodological procedure has been adopted:

- Numbers of rainy days, amount of annual rainfall and incidences of cloud bursts and flash floods have been taken into account for observing the changes in monsoon pattern, and these parameters were analyzed through the interpretation of long-term meteorological data collected from local weather stations.
- Detailed mapping and interpretation of landslides hazards and assessment of their impacts on agricultural land, natural drainage, irrigation system and road network were carried out through the digital interpretation of high resolution satellite data and field mapping techniques and consulting the available published literature, reports and maps.
- The parameters of production, availability and access to food have been analyzed by conducting comprehensive socio-economic surveys in selected villages using exclusively designed interview schedules.
- In order to analyze the linkages between rainfall variability, landslides and food security digital maps of landslides hazards, rainfall, agricultural land, road network, drainage and irrigation system have been integrated using Geographic Information System (GIS).

The Study Region

The Lake Region consisting of the micro-watersheds of six perennial lakes and part of Balia River micro-watershed, in the Lesser Himalayan Ranges and *Siwalik* Mountains in Kumaon Himalaya in India was taken up as the area of study for the present investigation (Fig. 1). The region encompasses a geographical land surface of 94.04 km^2 with an average altitude ranging between 700 and 2,600 m above the mean sea level. The region is situated along the Main Boundary Thrust (MBT) – the major tectonic juncture between the Lesser Himalayan Ranges in the north and the *Siwaliks* Mountains in the south and is transversed by several other faults. The entire area is therefore tectonically alive and highly vulnerable to large-scale tectonic movements, landslides and processes of surface removal. These complexities of structure and terrain are manifest not only in characteristic geomorphic processes and the resultant landform types but also in ecological diversities (Sharma and Pant 2004). Climatically, the region extends from sub-tropical to cool temperate climatic regimes, and it is a critical zone, in as much as, it lies within the belt of maximum precipitation (298.60 cm). Consequently, the entire area is tectonically instable and environmentally sensitive. The region represents one of the densely populated mountainous parts of Kumaon Himalaya. The total population of Lake Region was 27,840 persons in 2010, which was inhabited in 41 villages excluding the urban population of three towns – Nainital, Bhowali and Bhimtal – situated in the region. Nearly 78 % of total rural population depends on traditional agriculture for its food and livelihood.

Results and Discussion

Food security is defined as "a situation that exists when all people, at all times, have physical, social and economic access to sufficient, safe and nutritious food that meets their dietary needs and food preference for an active and healthy life" (FAO 2003). In developing and underdeveloped countries the food security situation has been continuously deteriorating for the last several years mainly because of increasing world population and resultant increasing gap in supply and demand of food, increasing demand of food in emerging economies, changing food habits, use of

Fig. 1 The study region

food-grains in bio-fuel production, and encroachment of productive agricultural land by rapid urbanization and industrialization, rapid depletion of agricultural resources and climate change (Fullbrook 2010; Roberts 2009; World Commission on Environment and Development 1987). Mountains are particularly susceptible to food insecurity mainly because of their subsistence economies, constraints of terrain and climate and resultant physical isolation and low productivity, vulnerability to natural risks, poor infrastructure, limited access to markets and higher cost of production. Consequently, a large proportion of food insecure population now live in mountain regions of the world, and nearly 245 million rural population living in world-mountains was vulnerable to food insecurity (Hauenstein et al. 2010; Huddleston et al. 2003; FAO 2008).

As in other parts of Himalaya, forest based subsistence agriculture constitutes the major source of rural food in Lake Region (Adhikari and Bohle 1999; Tiwari and Joshi 2005). But, more than 90 % operational land holdings are of less than one hectare and the availability of per capita cultivated land is merely 0.17 ha. Owing to the constraints of subsistence agricultural economy a large proportion of adult male migrates out of the region in search of livelihood and employment. Despite the increasing trend of rural out-migration the population has shown rapid growth putting increased biotic stress on land, forests, water and other

critical natural resources in the region (Tiwari and Joshi 2011b; Tiwari 2008). However, the study clearly indicated that the productivity of agriculture has declined by nearly 15 % during the last 10 years mainly due to depletion of natural resources, such as, land, water and forests and consequent loss of ecosystem services. Furthermore, the impacts of climate change have already stressed the traditional agricultural and food systems in the region. The region registered considerable decline in per capita food production during the last 30 years in the region.

Currently, the region is facing an annual food deficit of 65 % which is balanced by food import from other parts of the country. In view of this, the food security in the region mainly depends on (1) availability of food from local agricultural production, (2) purchasing power of local people to buy food from the market, and (3) the level of road connectivity for the efficient import and distribution of food in remote mountains (Tiwari and Joshi 2011a; Barrett 2010). These parameters put together determine the availability of and access to food, and therefore constitute the critical parameters of food security in the region. Marginal and small farmers, landless households which mainly include socially backward communities and families with marginal or very small income constitute the highly food insecure sections of rural community in the region.

The altitude of Lake Region ranges between 700 and 2,600 m from the mean sea level. The entire region has been classified into four altitudinal zones for studying the altitudinal distribution of agricultural land. The agricultural land in the region is spatially distributed along the altitudinal transact ranging from below 1,000 m to more than 2,500 m from the mean sea level. Table 1 reveals that in general the cultivated land increases with the increase in altitude up to an elevation of 2,000 m. The maximum concentration of cultivated land (43.25 %) has been observed in altitude ranging between 1,500 and 2,000 followed by 2,000–2,500 (27.43 %) which put together account for more 70 % of the total arable land of Lake Region (Table 1). Interestingly, the areas lying in altitudinal range of above 2,500 are also under cultivation. However, the agricultural land at lower elevation of below 1,000 m is merely 12.66 % as the hill slopes below 1,500 m altitude are characterized by dissected slopes, and the availability of cultivated land is only confined to river terraces, colluvial fans and cones with gentle slope (Table 1).

Slope is one the most important physical characteristics that not only determines the availability, distribution, utilization productivity of arable land, but also fix its vulnerability to natural risk in mountain ecosystem. Slope and altitude put together give rise to wide variations in terrain features, distributional pattern of rainfall and temperatures, physical and chemical properties of soils, resource utilization structure, land use pattern and stability of mountain slopes to landslides and other processes of mass movements. In order to analyze the slope characteristics of agricultural land the entire region was divided into four slope categories ranging from below 15°, 15–30°, 30–45° and above 45° (Table 2). It was observed that the distributional pattern of cultivated land in the region is directly controlled by the surface slope. The maximum concentration of cultivated land was found in areas characterized by surface slope between 15° and 30° (Table 2). More than 80 % of the total cultivated land in the region is marked with slope between 15° and 45°. However, only 13.29 % agricultural land of the region is located in areas having slope more than 45°. Similarly, only 6.54 % of the total arable land of the Lake Region has surface slope below 15° (Table 2).

Table 1 Distribution of agricultural in different altitudinal zones

Relief categories	Agricultural land (in Km^2)	% of total agricultural land
Below 1,000	00.60	12.66
1,000–1,500	00.50	10.54
1,500–2,000	02.05	43.25
2,000–2,500	01.30	27.43
Above 2,500	00.29	06.12
Total	04.74	100.00

Table 2 Distribution of agricultural land in different slope categories

Slope categories	Agricultural land (in Km^2)	% of total agricultural land
Below 15°	00.31	06.54
15–30°	02.25	47.47
30–45°	01.55	32.70
Above 45°	00.63	13.29
Total	04.74	100.00

The interpretation of the terrain characteristics of agricultural land in the region brings out the fact clearly that most of the cultivated land in the region is characterized by medium to high relief and moderate to steep slope, and therefore highly vulnerable to landslides and slope failure. The integration of land use and landslide hazard maps revealed that more than 50 % of the total agricultural land of the region is located in the areas delineated as moderate to high landslide hazard zones. Obviously, a large proportion of existing cultivated land is highly susceptible to the risks of slope failure, mass movement and landslides even without the incidences of high intensity rainfall and extreme weather events, such as, clod bursts and flesh floods in the entire region.

The Lake Region recorded nearly 3,000 mm average annual rainfall during 1951 and 2000. As much as 70 % of the total annual rainfall occurs during monsoon season from roughly from 15 June to 15 September, 25 % in April, May and June and the region receives only 5 % of its total annual rainfall during winter season extending from October to

Table 3 Observed rainfall variability and landslide occurrence

Years	Rainfall (in mm)	Number of rainy days	Days of high intensity rainfall	Incidences of cloud bursts	Incidences of flash floods	Occurrence of landslides
2001	2,400	61	04	02	21	14
2002	2,125	55	04	00	11	11
2003	2,010	51	03	01	11	27
2004	2,200	50	07	05	09	31
2005	1,915	50	09	09	10	35
2006	1,870	51	11	09	17	55
2007	1,700	52	14	11	24	55
2008	2,970	51	15	17	27	61
2009	1,635	55	14	21	35	65
2010	3,570	61	17	27	47	77
Average	2,240	53	10	10	21	43

Table 4 Loss of agricultural land, irrigation channels, road network and food production due to landslides

Years	Loss of agricultural land (ha)	Irrigation channels disrupted (m)	Decline in agricultural production (%)	Decline in agricultural production (%)	Road network damaged	Food import decreased (%)
2001	03.66	710	11	11	3,400	15
2002	03.50	700	14	14	3,475	17
2003	03.79	770	14	14	3,525	17
2004	04.25	690	07	07	3,020	12
2005	04.80	690	08	08	3,000	11
2006	04.75	711	17	17	3,700	19
2007	04.90	750	16	16	4,150	23
2008	05.00	800	18	18	4,300	17
2009	06.10	825	21	21	4,770	21
2010	07.55	980	25	25	5,570	37
Total	48.30	7,626	15	15	38,910	19

March. However, the region received an annual average annual rainfall of only about 2,240 mm during 2001 and 2010 with very high spatial as well as seasonal variability in its distributional pattern. The region enjoyed approximately 65 rainy days in a year during 1951 and 2000. The study revealed that both the number of rainy days as well the amount of annual average rainfall reduced respectively by 18 % and 25 % during the last 10 years (2001 and 2010). It was observed that the amount of annual rainfall declined consistently between 2001 and 2010 except in the years 2004, 2008 and 2010. Similarly the number of rainy days also indicated a declining trend during the last 10 years except in the year 2009. Whereas, the incidences of high intensity rainfall, cloud bursts and flash floods have registered an increasing rate in the region during 2001 and 2010 (Table 3).

These changes in rainfall pattern, particularly the increasing frequency of high intensity rainfall, cloud bursts and flash floods have disrupted geo-hydrological regime and destabilize slope stability in the entire region. Consequently, the geo-tectonically active and anthropogenic-ally modified slopes, such as, cultivated areas, roads and irrigation channels have now become highly vulnerable of to increased slope instability. More than 48 ha agricultural land has been devastated by landslides during 2001 and 2010 with an overall average damage of 4.83 ha per year (Table 4). This is indeed a massive and direct loss affecting adversely the socio-economic sustainability as the availability of agricultural land is merely 4.74 km^2 or 5.16 % of the total land resource of the region. Out of the total cultivated land of Lake Region (4.74 km^2) only 11 % is irrigated and the remaining agricultural land (89 %) is never irrigated due to non-availability of water. The tiny mountain gravity canals (locally known as *guls)* which take water from streams and natural springs are the prime source of irrigating the small proportion of cultivated land. Nevertheless, landslides have damaged 7,626 m length of canals each year since 2001 with an average annual destruction of about 800 m, and the level of this disruption is increasing with each passing year mainly due to erratic rainfall. As a result, the proportion of irrigated land has reduced nearly by 7 % mainly due to disruption of water sources and irrigation systems by frequent landslides posing serious threat to the sustainability of subsistence agricultural economy and quality of life of rural population in the area. As a result, the production of food crops has been decreasing steadily in region since 2001 with an overall

decline of as much as 15 % during 1991 and 2010 (Table 4). Consequently, the entire Lake Region faced a food deficit of 65 % in 2010 compared to 45 % in the year 2000, thus increasing consistently the gap between local production and demand of food.

As mentioned in the preceding section, high level of road connectivity is therefore indispensable not only for importing food commodities from other parts of the country, but also for their efficient distribution in the entire region to balance the increasing food deficit. Table 4 makes it clear that escalating frequency of landslides in the region has caused a damage of 38,910 m of road network between 2001 and 2010 with an average road destruction of 3,891 m per year. The distraction of road network, particularly during monsoon months (June to September) disrupts the transportation of essential food items and causes bottleneck in the supply of food in the markets for a long period of time. The region could not receive 19 % of its required food supplies during the last 10 years mainly owing to disruption of road transport caused by frequent landslides decreasing the availability of food for local population in the markets (Table 4). Furthermore, approximately 35 % population living in 19 villages in region has no or very limited access to imported food during monsoon season of four months due to extensive damage of road network. Further, it would be difficult to fill the food deficit gap in near future as the local income level and purchasing power have declined due loss of employment opportunities and recent economic recession and the increasing food-prices.

The study revealed that 45 % families of 21 villages were highly vulnerable to food insecurity in the region. The households identified most vulnerable to food insecurity in the region mainly include marginal and small farmers with land holding size less than 1 ha (45 %), landless households mainly include lower caste communities (5 %), households with marginal income from other sources (41 %), households with no income from other sources (9 %), and households with most of the cultivated land rain-fed and with scarce family labour. This will have long-term impacts in food security of the region in terms of quantity, quality and nutritional value of the food affecting particularly the poor and socially marginalized people which constitute nearly 75 % of the total population.

Conclusion

As much as, more than 75 % population depends on subsistence agriculture even though the availability of arable land is severely limited and food production is low. The food security in the region therefore, primarily depends of local production of food and procurement from market. Most of the agricultural land is located at higher elevations marked with moderate to steep slopes which are highly vulnerable to terrain instability and landslides as the region is located in tectonically active zone. The observed changes in rainfall pattern, particularly the increasing incidences of high intensity rainfall, flash floods and cloud bursts have not only damaged the cultivated land, but also disrupted the irrigation and transport system during the last 10 years. These changes have further declined the agricultural productivity and adversely affected the import of essential food commodities threatening the food security of poor and marginalized population in the region. It is therefore highly imperative to evolve a framework for adaptive management of agricultural resources and improving road transport taking into account the terrain characteristics and landslide hazard status of the region. Further, it would be essential to enhance the income level of rural communities through the diversification and improvement of livelihood in off-farm sectors. This would not only help in decreasing the dependency of local population on subsistence agriculture which is does not seem resilient to long term impacts of climate change, but would also increase the food purchasing power of rural population and thus reduce their vulnerability to food insecurity. The finding of the study and its recommendations could be translated across the socio-economically marginalized and environmentally sensitive mountain ecosystems to enable them to cope efficiently with rapidly changing climatic conditions.

Acknowledgement The Authors are grateful to Indian Space Research Organization (IRSO), Government of India, Bangalore and the University Grants Commission (UGC), New Delhi, India for providing generous financial support for carrying out the study.

References

Aase TH, Chaudhary RP, Vetaas OR (2009) Farming flexibility and food security under climatic uncertainty: Manang, Nepal Himalaya, AREA. Roy Geogr Soc 42(2):228–238. doi:10.1111/j.1475-4762.2009.00911.x (with the Institute of British Geographers)

Adhikari J, Bohle HG (1999) Food crisis in Nepal: how mountain farmers cope? Adroit Publications, New Delhi

Barrett CB (2010) Measuring food insecurity. Science 327 (5967):825–828. http://www.sciencemag.org/cgi/content/abstract/327/5967/825

Cline WR (2008) Global warming and agriculture: impact estimates by country. Centre for Global Development. Peterson Institute for International Economics, Washington, DC, p 186

Food and Agricultural Organization (2003) Agriculture, food and water. Chapter 2, FAO, Rome. http://www.fao.org/DOCREP/006/Y4683E/y4683e06.htm

Food and Agricultural Organization (2008) Food security in mountains – high time for action. Brochure of the International Mountain Day

2008. http://www.mountaineering.ie/documentbank/uploads/IMD08%20brochure.pdf
Fullbrook D (2010) Food as security. Food Secur 2:5–20. doi:10.1007/s12571-009-0050-y
Hauenstein S, Hadley SS, Cichon B (2010) Crisis behind closed doors: global food crisis and local hunger. J Agrar Change 10(1):107–118. http://dx.doi.org/10.1111/j.1471-0366.2009.00252.x
Huddleston B, Ataman E, d'Ostlanl LF (2003) Towards a GIS-based analysis of mountain environments and populations. Food Agric Organ, Rome
International Centre for Integrated Mountain Development (2007) Melting himalayas: regional challenges and local impacts of climate change on mountain ecosystems and livelihoods. Technical Paper, pp 11–24
Intergovernmental Panel on Climate Change (2007) Climate change 2007: impacts, adaption and vulnerability. Contribution of Working Group II to the *Fourth Assessment Report*. http://www.ipcc.ch/ipccreports/ar4-wg2.htm
Rawat PK, Tiwari PC, Pant CC, Sharma AK, Pant PD (2011) Climate change and its geo-hydrological impacts on mountainous terrain: a case study through remote sensing and GIS modeling. E-Int Sci Res J 3(1):51–69, ISSN: 2094-1749
Roberts P (2009) The end of food. Houghton Mifflin Harcourt, New York
Rawat JS, Tiwari PC, Gupta V (2004) Landslides in didihat and its environ. Status Report, Department of Science & Technology, Government of India, New Delhi, pp 20–24
Sharma AK, Pant CC (2004) Landslide hazard evaluation and zonation in North Western Nainital hills, Lesser Himalaya. In: Pant CC (ed) Aspect of geology and environment of the Himalaya. Gayandaya Prakshan, Nainital, pp 169–186
Tiwari PC (2008) Land use changes in Himalaya and their impacts on environment, society and economy: a study of the Lake region in Kumaon Himalaya, India. Adv Atmos Sci 25(6):1029–1042, an international journal of Chinese Academy of Sciences, Beijing
Tiwari PC, Joshi B (2011a) Environmental changes and sustainable development of water resources in the Himalayan headwaters of India. Water Resour Manag. doi:10.1007/s11269-011-9825-y
Tiwari PC, Joshi B (2011b) Urban growth and food security in Himalaya, international working paper series, urbanization & global environmental change (UGEC) view point. Int Hum Dimens Progr (IHDP) 1(5):20–23p
Tiwari PC, Joshi B (2005) Environmental changes and status of water resources in Kumaon Himalaya. In: Libor J et al (eds) Sustainable management of headwater resources: research from Africa and Asia. United Nations University, Tokyo, pp 109–112
World Commission on Environment and Development (1987) Our common future. Oxford University Press, Oxford

Watershed Management: An Approach for Landslide Risk Reduction Through Integrated Landuse Planning

Thomas Hofer, Gérard Marquis, Claudia Veith, and Paolo Ceci

Abstract

Landslides pose considerable risks to the environment. They threaten the lives of people and livestock and destroy land-use systems and agricultural production. This has heavy impacts on the livelihoods of affected people, their economic situation and food security. In developing countries, poor and marginalized people are often forced to settle and to cultivate land in hazard-prone areas due to population pressure and, accordingly, the effects of landslides on lives and assets can be disastrous. People and their land-use systems, on the other hand, can influence the occurrence of landslides. Besides the physical causes and triggers of landslides such as geological failures, erosion processes and heavy rainfall events, activities such as forest harvesting, road construction, mining, unsustainable agricultural practices and overgrazing have been found to have an impact on shallow landslides. Their influence on deep-rooted landslides is, however, minimal.

Most of the current approaches in landslide risk reduction follow a mainly technical path and neglect the human factor. Integrated approaches that take into account people and all aspects of local livelihoods, including socio-economic issues, agriculture, pasture, forestry and hydrology are needed in order to address this complex problem. To organize spatially the different land-uses and promote the implementation of suitable practices, one ideal approach is watershed management. It allows addressing upstream-downstream linkages, such as landslides, and provides a framework for sound land use planning. Adapted land-use systems and adequate natural resource management can reduce the potential for landslides and, especially, mitigate the processes leading to increased landslide hazards, such as gully erosion. Experience shows that often the underlying causes of unsustainable land-use are social or economic and that sustainable land-use practices are not adopted because they are socially not acceptable and/or economically not viable. Diversification of livelihoods, vegetation cover types and crop species – the mixing of different land uses in general – increases the resilience of local farmers and may improve the way natural resources and corresponding livelihoods can be rehabilitated after landslide events. Further, the sustainable management of natural resources and the diversification of livelihoods increase people's food security and have positive effects on water resources.

T. Hofer (✉) • G. Marquis • C. Veith
Forestry Department, Team leader Watershed Management and Mountains, UN Food and Agriculture Organization, Viale delle Terme di Caracalla, Rome I-00153, Italy
e-mail: Thomas.Hofer@fao.org

P. Ceci
Forestry Department, UN Food and Agriculture Organization, Viale delle Terme di Caracalla, Rome I-00153, Italy

C. Margottini et al. (eds.), *Landslide Science and Practice*, Vol. 4,
DOI 10.1007/978-3-642-31337-0_25,

Keywords
Watershed management • Landscape approach • Land-use systems • Livelihood

Watershed as Planning Unit for Disaster Risk Reduction

Watersheds are familiar landscapes created by mountain ranges as they slope down to valleys, with creeks and torrents flowing downstream. They are the zones from which rain or melting snow drains into a river, lake, dam, estuary, wetland, sea or ocean. They may vary in terms of scale: smaller watersheds (sub-watersheds) are nearly always part of larger basins. Powered by the force of gravity that generates extra energy to be exploited by human beings, watershed are dynamic environments. They are often shaped by human activities, as they offer multiple services to human society, such as water supply for domestic, agricultural and industrial uses. Moreover, well managed watersheds regulate water flows and reduce the risk of floods and droughts in the nearby downstream areas. Thanks to surface run off, watersheds provide fertile sediments to the lowlands.

At a watershed level landslides pose considerable risks to the environment. Human beings and livestock are threatened by such natural hazards which can destroy land-use systems and agricultural production. Landslides have in fact heavy impacts on livelihoods of affected people, their economic assets and food security. Unfortunately, it is often the poor and hungry who are the most seriously hit by these dramatic events.

In turn, the occurrence of landslides is influenced by people and their land-use systems. Besides the physical causes and triggers of landslides such as geological failures, erosion processes and heavy rainfall events, activities such as forest harvesting, road construction, mining, unsustainable agricultural practices and overgrazing have an impact on shallow landslides. In developing countries, poor and marginalized people are often forced to settle and to cultivate in hazard-prone land due to population pressure. Recent population growth and the expansion of commercial agriculture have drastically reduced the availability of arable land, forcing impoverished farmers to clear marginal lands on steep slopes and reduce needed fallow periods. These developments lead to loss of ground cover, accelerate soil compaction and erosion, aggravate the pressure on natural resources, with consequent increased likelihood for landslides. Thus, landslides depend and, in turn, affect a number of interacting components and, for this reason, need to be read in the broader context of livelihoods and food security, in order to reflect them under a landscape and multi-hazard approach.

In order to address such complexity and interactions, integrated approaches are needed. Watershed management considers the specificity of hydrological, ecological and socio-economic processes, including people and all aspects of local livelihoods such as agriculture, pasture and forestry. It allows to address upstream-downstream linkages and provides a framework to organize spatially the different land-uses and to promote the implementation of suitable practices. Adapted land-use systems and adequate natural resource management can reduce the potential for landslides and mitigate the processes leading to increased landslide hazards.

Natural resource and disaster risk management require the participation of different stakeholders, such as politicians, technicians, local farmers, foresters etc. The practices and points of view of local people have to be included in the search for sustainable solutions. All stakeholders in a given setting must inform decision making in landslide risk mitigation. Further, action has to be taken at the political level. In this context, policies regulating the use of natural resources become particularly important. Especially in developing countries the absence of official land tenure rights for local farmers increase land misuses. Therefore, secure access to local resources has to be given to farmers in order to enhance their interest in managing land in a sustainable way which, consequently, contributes to landslide risk reduction.

Integrated watershed management is a holistic and multi-sectoral approach able to take into account the different components that can potentially contribute to unsustainable economic activities and resulting natural hazards. Watershed management plans and projects reduce the pressure on natural resources and apply sustainable land-use practices. This decreases people's exposure to the occurrence of landslides and contributes to achieving food security and improved local livelihoods (FAO 2006; Hofer and Warren 2007).

The following section provides readers with a concrete example of the implementation of this framework in the context of rehabilitation plans, recovery and disaster risk reduction initiatives.

Putting Watershed Management into Practice: The Pakistan Project

On 8 October 2005, a disastrous earthquake struck parts of Khyber Pakhtoonkhwa (KPK) and Pakistan-Administered Kashmir (AJK) in the northeast of Pakistan. Some three to four million people were affected, and the estimated death toll exceeds 80,000. The earthquake caused significant land destabilization and damage to the natural capital assets of rural people. Seismic shifts resulted in major landslides and

Fig. 1 Example of a landslide in the Shohall Mazullah Watershed, Mansehra District, KPK, which was triggered by the earthquake on 8 October 2005 (Photographer: Paolo Ceci, FAO)

Fig. 2 Meeting of the Watershed Management Committee of Danna Galli Watershed, Muzaffarabad District, AJK (Photographer: Thomas Hofer, FAO)

thousands of landslips, affecting about 10 % of hillside arable land, forests and rangelands (Fig. 1). In downstream areas, major water channels, roads and paths were blocked by rocks and debris. Flash floods and mudslides destroyed agricultural land and fruit tree plantations. Many natural springs feeding irrigation and rural water supply schemes dried up as a result of landslides. In downstream areas, major water channels, roads and paths were blocked by rocks and debris thrown down by the earthquake. In the area, livelihoods had already been seriously affected by soil erosion following decades of deforestation and overgrazing.

A massive relief effort was mounted to respond to the dramatic situation. The Government of Pakistan established the Earthquake Reconstruction and Rehabilitation Authority (ERRA) to coordinate the rehabilitation efforts. The Food and Agriculture Organization of the United Nations (FAO) supported the development of a livelihood component for ERRA's post-emergency rehabilitation plan. From March 2007 to June 2011, with funding from the Swedish International Development Agency (SIDA), ERRA and FAO executed a multi-sectoral project for the implementation of this livelihood rehabilitation strategy.

The medium-term outcomes of the project were:

- At least restoring the livelihoods of earthquake-affected people to pre-earthquake levels, through a community-based development approach that is gender-sensitive and environmentally friendly;
- Sustaining the implementing partners' rural support services beyond the 3-year lifetime of ERRA; and
- Demonstrating how a collaborative watershed management approach can protect the environment and strengthen households' natural capital assets in steeply sloping areas.

The control of hydro geological hazards through collaborative watershed management at the village level was one key project component. It was implemented in 17 watersheds across the earthquake affected areas in close collaboration with the District Forest Offices and the Kathmandu-based International Centre for Integrated Mountain Development (ICIMOD).

The Project Activities

The project was implemented in all watersheds according to the following steps:

- Mapping of the damage caused by the earthquake or by post-earthquake processes (landslides, landslips, erosion, damaged irrigation channels, etc.);
- Participatory Rural Appraisal and institutional analysis;
- Establishment of a Watershed Management Committee (Fig. 2);
- Development of a participatory watershed management plan;
- Implementation of prioritized activities;
- On the job capacity building and training.

Specifically, forestry activities received priority attention during project implementation:

- Bioengineering interventions (waddling, brush-layering, palisades) were introduced and tested by using bushes and tree species to stabilize landslides.
- Forest regeneration was promoted through afforestation of degraded slopes, fencing off of existing, but overgrazed mountain forests, and introduction of controlled grazing.
- Tree nurseries and fruit tree orchards were established to support the afforestation and slope stabilization efforts as well as to improve the income situation of the local communities.

In addition to the practical field interventions, institutional innovations were introduced and tested. Traditionally, the District Forest Offices carried out the planning and field

implementation of forestry-related interventions. Through the creation of the Watershed Management Committees it is now the communities which plan and prioritize their activities. The District Forest Offices continue to be involved, but in the capacity to provide technical support to the communities for the implementation of their prioritized activities.

In order to provide readers with an in depth overview of the implementation of the project, two pilot watersheds will be described in the following section.

Two Pilot Watersheds: Gulmera Batora and Lamnian

The Lamnian Watershed

The Lamnian watershed is located about 21 km South East of Hattian, on the right bank of River Jehlum, in Muzaffarabad District. Two villages, including 27 hamlets, are located in the watershed. The recovery and reconstruction activities after the earthquake focused on the rebuilding of houses and infrastructure, while agriculture and livestock production was not yet restored to pre-earthquake levels. Maize was basically the only crop grown. After 2 years from the beginning of the rehabilitation activities, the drinking water supply schemes were not yet repaired or were in bad shape. Moreover, post-earthquake hazards (landslips, rock falls, and ravines) continued to threaten the safety and livelihoods of the population. Due to high population density, the pressure on land and natural resources in this very fragile and dynamic ecosystem was still very high. In order to supplement the domestic economy, men migrated for work outside the watershed during the winter months even before the earthquake. In many cases houses were reconstructed in dangerous places, where further landslips and debris flows are likely to occur in the event of heavy rains. Some houses were even rebuilt immediately below the rubble of the main landslide, which is unstable and too big to be stabilized through retaining walls.

The Watershed Management Committee, which was established through the SIDA-FAO project, developed integrative community-based activities to manage these natural disaster risks, improve the use of livelihood natural capital assets. An early warning system was hence established with the communities to cope with natural disaster risks. With the technical support from ICIMOD, physical interventions were implemented to stabilize landslips, gullies and cracks. These included loose stone retaining walls, check dams and bio-engineering works, such as palisades (Fig. 3) and wattling. Controlled rotational grazing was practiced in the hillsides, where trees were planted for soil conservation, fixing gullies and protecting against riverbank erosion with the support of the Forestry Department. The Watershed Management Committee provided the staff of the project with useful inputs to address the issues above and to broaden the scope of activities in order to comply with a sound, integrated watershed management approach. Upon conclusion of the project, the approach revealed to be appropriate and effective, and ensured a successful achievement of the intended objectives.

Fig. 3 Palisade – a successful bio-engineering technique for landslide stabilization introduced and field-tested by the project (Photographer: Paolo Ceci, FAO)

The Gulmera Batora Watershed

The Gulmera Batora watershed is located about 40 Km from Mansehra City, East of Balakot, near Kaghan Valley. Eight hamlets are counted within the watershed boundaries. Traditionally, the major activities of the communities living in the watershed are farming, livestock rearing and, for men, labouring outside the watershed. After the implementation of the recovery activities, the majority of families relied on kitchen gardens for vegetables and a few fruit trees. Women-headed households were common as many men migrated to earn a living. Women participated in agriculture, looked after the animals (buffaloes, cows and goats for milk production), poultry and kitchen gardens. They gathered firewood and fodder for the animals, fetched water and took care of maintenance of the household.

The adoption of an integrated watershed management approach through the SIDA-FAO project provided a framework for sound land use planning and supported the use of livelihood and natural capital assets. Through collaborative gender sensitive activities, the representation of women was strengthened at all levels in the Watershed Management Committee. Physical interventions were implemented for the stabilization of a big landslide located in a medium risk area, which threatened the main river running down the

watershed, where significant volumes of debris had already been deposited. These interventions included retaining walls, check dams, sealing cracks, wattling, palisades, pasture protection as well as plantations of *robinia* and other tree species suitable for slope stabilization. In the watershed, activities carried out by the community included terracing, field leveling and construction of ponds for perennial stream or roof water harvesting. A seasonal calendar for livestock vaccination was planned and put into practice. This successful multi-sectoral approach had a focus on social inclusion, and allowed vulnerable groups, such as women and men with handicaps, to develop a number of initiatives for self-consumption and the market, including kitchen gardens, flower gardens and tree nurseries with the support of the Forestry Department.

These achievements are the result of a policy of self-reliance promoted by the project's Watershed Management Team, which supported the community to escape from a culture of dependency on external aid. The project staff provided agriculture training and promoted marketing agreements for crops with downstream demand such as flowers. The Team also encouraged the development of agriculture and livestock strategies that recognize their mutual interdependency. Project livelihoods specialists were involved in the planning and organizational processes to ensure that an integrated livelihoods strategy was actually put in place, and post-harvesting, processing (fruits and vegetables) and marketing requirements were sufficiently in-built.

Lessons Learned

The SIDA-FAO project has demonstrated the value of the integrated watershed management approach and the crucial role of forests and trees in the medium-term rehabilitation efforts in steeply sloping areas, where livelihoods were seriously affected by soil erosion, landslides and landslips caused by the October 2005 earthquake. The activities undertaken in the two watersheds show how the challenge of rehabilitating livelihoods and triggering economic growth, in a system highly dependent on the natural resource base, necessitates a significant broadening up of the scope of concrete interventions. Watershed management highlights the need to shift from purely physical activities for landslide stabilization to a more strategic integrated and holistic approach, in which all aspects of livelihoods are in-built. The potential of the watershed as a geographical area where the livelihoods approach can be realized was fully caught.

The forestry-related activities were very successful and the bioengineering methods for the stabilization of landslides proved to be particularly effective. There is promising evidence of replication of these technologies and experiences beyond the project watersheds.

The Forestry Department endorsed the participatory approach of the project and considers it as key to success for projects aimed at the restoration of natural resources and livelihoods.

The flood of July 2010 has again created significant damage in AJK and KPK. However, there is evidence that those communities, which were supported by the project, were well prepared to cope with this new disaster. In addition, the flood damage in the project watersheds was comparatively low because of the protective function of the introduced forests and trees.

Through the participatory approach, the project has generated significant community ownership, capacity and confidence. The communities have gained confidence in their own ideas and skills, and feel ownership of the positive changes in their environment and livelihoods. Through the Watershed Management Committees, they are now organized and have a voice to request technical assistance and support from state line agencies and donors.

References

Food and Agriculture Organization of the United Nations (FAO) (2006) The new generation of watershed management programmes and projects, vol 150, FAO forestry paper. Food and Agriculture Organization of the United Nations, Rome. ISBN 978-92-5-105551-9

Hofer T, Warren P (2007) Why invest in watershed management? FAO, Rome. ISBN 978-92-5-305805-1

Part III

Wildfires and Slope Instability

Introduction by Jerome De Graff[1], Susan Cannon[2], Pieter Van Lierop[3], and Mario Parise[4]

1) USDA Forest Service, Clovis, CA, USA
2) US Geological Survey, Denver, CO, USA
3) Food and Agriculture Organization of the United Nations, Rome, Italy
4) IRPI-CNR, Bari, Italy

Many natural hazards such as earthquakes and cyclonic storms have distinct damaging effects and can serve as a trigger to landslide occurrence. The occurrence of damaging effects and landslides take place, more or less, contemporaneously. Wildfires are a natural hazard that causes an immediate damage by burning vegetation and flammable parts of the built environment. Rather than directly triggering landslides, wildfires alter the short-term susceptibility of slopes to gravity-related phenomena making debris flows more likely during later storm events.

The papers presented in the "Wildfires and Slope Instability" session centered on two themes reflecting the difference in how and when slope instability is altered by wildfire occurrence. The first theme was assessing wildfire effects to forecast the likelihood of landslides, especially debris flows. The keynote address, "Characterizing the immediate and subsequent hazards caused by wildfire occurrence" examined recent advances in wildfire suppression and forecasting of debris flows. Wildfire suppression has improved through earlier detection using aerial and satellite-based systems and modeling which identifies times of greater wildfire likelihood and how active wildfires will advance. Similar advances exist for wildfire-related debris flows, especially the use of modeling to forecast debris flow potential, likely volumes to occur and probable paths where damage would occur. Another paper on this theme was "Remote sensing and geospatial support to burned area emergency response (BAER) teams in assessing wildfire effects to hillslopes". The rapid identification of the varied impact of a wildfire to vegetation across the burned landscape is a key tool for determining potential secondary impacts including debris flow occurrence. Soil burn severity maps are quickly created through interpretation of spectral reflectance in satellite imagery and on-the-ground examination of soil in representative locations. The resulting GIS-based product is readily integrated with other geospatial data and models used to assess wildfire effects.

The second theme was how to quickly counter wildfire-induced debris flows where they pose a threat to transportation systems and similar infrastructure. The paper "Flexible debris flow barriers in fire-burned areas" looked at the technological intricacies of using fixed net barriers to prevent debris flow from impacting roads or other high-value structures. Examining the design and testing used in developing these flexible barriers highlighted the importance of careful site planning where these barriers are to be placed. A second paper, "Rockfall and debris flow hazards after summer wildfires in Cerreto Sannita, Benevento, Italy" provided session participants with an example of how flexible barrier can be used to counter wildfire-induced slope instability. Practical considerations ranging from site information important to their design to the logistical problems of their installation were explored.

Limiting the Immediate and Subsequent Hazards Associated with Wildfires

Jerome V. DeGraff, Susan H. Cannon, and Mario Parise

Abstract

Wildfire is a unique natural hazard because it poses immediate threats to life and property as well as creating conditions that can lead to subsequent debris flows. In recent years, the immediate destructive force of wildfires has been decreased through better understanding of fire behavior. Lightning detection networks now identify the number and locations of this common ignition source. Measurements of wind speed, temperature, slope, fuel types and fire boundaries are routinely incorporated into models for fire spread, permitting real-time adjustments to fire-fighting strategies, thus increasing fire-fighting effectiveness.

Similarly, our capability to limit impacts from post-fire debris flows is improving. Empirical models for estimating the probability of debris-flow occurrence, the volume of such an event, and mapping the inundated area, linked with improved definitions of the rainfall conditions that trigger debris flows, can be used to provide critical information for post-fire hazard mitigation and emergency-response planning.

Keywords

Wildfire • Fire behaviour • Debris flow • Hazard mitigation

Introduction

Wildfire is a natural component of many ecosystems around the world (Sugihara et al. 2006). Certain vegetative communities are dependent on periodic wildfires to renew their vitality by clearing decadent stands or triggering the release and germination of seeds which have lain dormant. Natural wildfires are ignited primarily by lightning strikes (Van Wagtendonk 2006). However, humans can also be responsible for igniting wildfires. This can be intentional as part of agricultural practices, hunting techniques or even arson, or unintentional as a result of myriad human activities ranging from camp fires to sparks from various mechanical and electrical processes. The global nature of wildfire occurrence can be seen through the Moderate Resolution Imaging Spectroradiometer (MODIS) that flies onboard NASA's Aqua and Terra satellites as part of the NASA-centered international Earth Observing System (NASA 2011a). Figure 1 is an example of a MODIS image. These images show concentrations of wildfires changing seasonally as weather increases the likelihood of lightning-associated storms or traditional agricultural burning is initiated (NASA, 2010).

Increased population around the world has resulted in more buildings, infrastructure, and related features being placed in areas where wildfire occurs naturally. Human activities in these ever expanding areas make the occurrence of human-initiated fires a far greater likelihood than in the past. Consequently, wildfires pose a far greater threat to people, property and their livelihoods around the world

J.V. DeGraff (✉)
US Forest Service, Sierra National Forest, 1600 Tollhouse Road, Clovis 93611, CA, USA
e-mail: jdegraff@fs.fed.us

S.H. Cannon
US Geological Survey, Landslide Hazards Program, DFC, MS 966, Box 25046, Denver, CO 80225, USA

M. Parise
National Research Council, Institute of Research for Hydrogeological Protection, Via Amendola, 122-I, Bari 70126, Italy

C. Margottini et al. (eds.), *Landslide Science and Practice*, Vol. 4,
DOI 10.1007/978-3-642-31337-0_26,

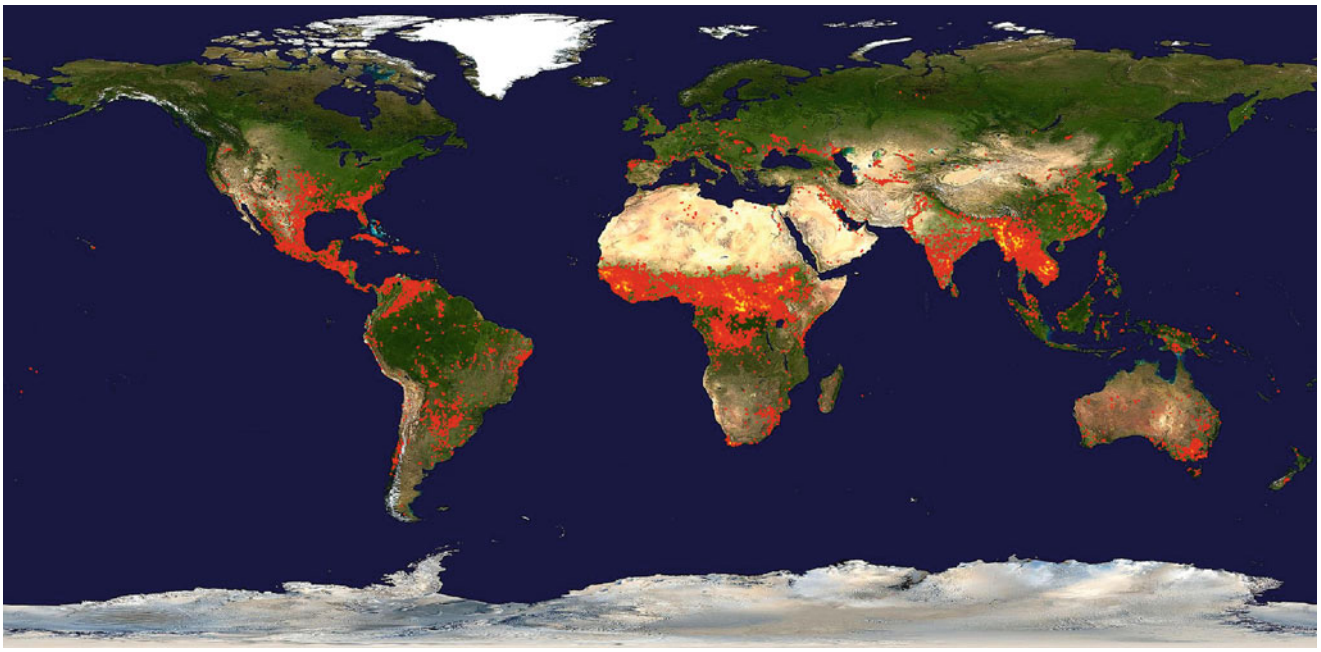

Fig. 1 Map of the world showing fires detected between 2 March and 11 March 2011 by the Moderate Resolution Imaging Spectroradiometers (MODIS) onboard the Aqua and Terra satellites operated by the National Aeronautics and Space Administration (NASA). A single fire is represented by a *colored dot*. *Red* represents where only a few fires were detected during this 10-day period and *yellow* represents were many fires were detected. http://rapidfire.sci.gsfc.nasa.gov/firemaps/?2011061-2011070

than they did only a few decades ago (Cannon and DeGraff 2009).

No one who has ever seen an advancing fire front doubts the immediate danger a wildfire poses to people and property. The combination of radiant heat, roaring noise and leaping flames assaults the senses in a manner which can bring to mind being face-to-face with a malevolent force. During the first decade of the twenty-first Century, major urban areas in the western United States have experienced or been threatened by wildfires burning in nearby wildlands, including Boulder, CO, Los Alamos, NM, Flagstaff, AZ, and San Diego, San Bernardino and Santa Barbara in southern California. Countries affected by recent large wildfires near populated areas include Spain, Portugal, Greece, Russia, Australia, and Israel. The Fourmile Canyon wildfire near Boulder, Colorado illustrates the immediate impacts of wildfire. During a 10-day period in September 2010, this wildfire burned over 2,501 ha and destroyed 169 homes. In addition to being responsible for one fatality, the wildfire resulted in USD$ 314 million in overall losses of which only USD$ 210 were insured (Munich 2011).

Given the immediate threat posed during a wildfire, people near the affected area are understandably relieved when the fire is finally controlled. However, communities that escape the immediate threat of the wildfire may be exposed to a subsequent threat from debris flows. Debris flows are a consequence of rainfall on hillslopes with wildfire-consumed vegetation and heated near-surface soils. Even rainfall from common storm events may result in increased runoff and erosion sufficient to generate debris flows. This subsequent hazard due to wildfires is particularly dangerous and destructive because: (1) debris flows are fast-moving landslides, (2) they can travel significant distances from their origin including beyond the limits of the burned area, and (3) their physical characteristics can cause damage by drag, buoyancy, lateral impact or burial (DeGraff et al. 2007; Cannon and DeGraff 2009). In August and September 2009, the Station wildfire burned 64,975 ha within the San Gabriel Mountains to become the largest wildfire in Los Angeles County history (Fig. 2). The actual loss of 58 homes within the San Gabriel Mountains was small compared to the more than 12,000 homes initially threatened along the mountain front. However, these same mountain front communities, including two neighborhoods of the City of Los Angeles and the communities of Altadena, Littlerock, La Crescenta, Acton, Glendale and La Cañada Flintridge were then potentially in the path of any debris flows generated by storms over the burned area (Cannon et al. 2009). Starting in October, 2009, several storms impacted the area, and in late January and early February 2010 heavy rainfall over several days produced damaging debris flows affecting homes and streets in the neighborhoods adjacent to the burned area in the community of La Cañada Flintridge. Debris basins designed and managed by the Los Angeles County Department of Public Works were quickly filled with debris-flow material in many locations. The events surrounding the Station wildfire demonstrate how those who may escape the immediate threat from fire can suffer

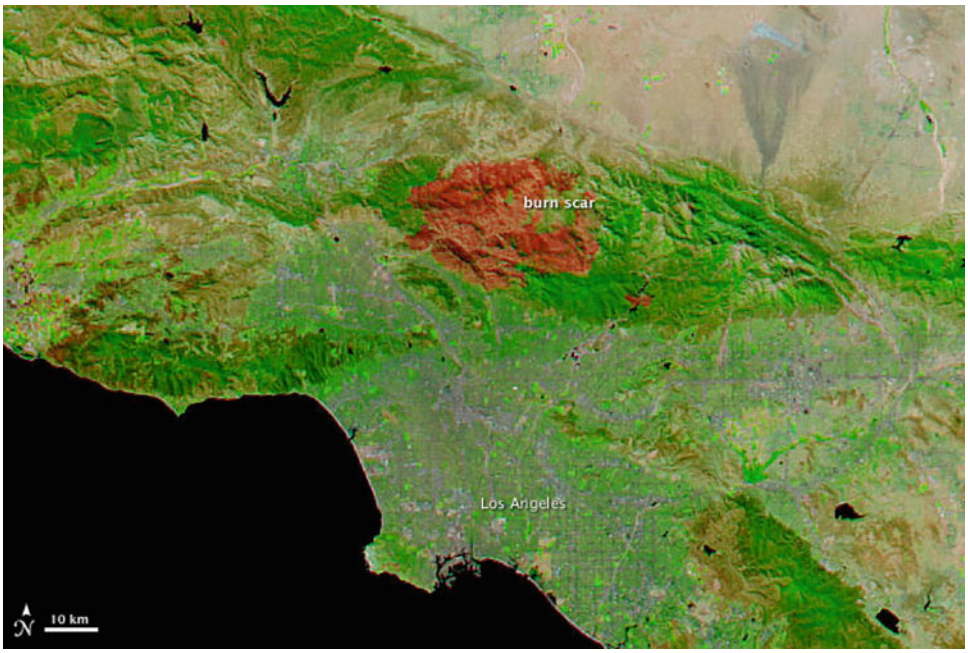

Fig. 2 A false-color image of the Station fire captured on September 16, 2009 by MODIS on an Aqua satellite operated by NASA. This wildfire in the San Gabriel Mountains north of Los Angeles, California was ignited 22 days earlier and burned about 650 km^2. The fire scar is revealed by using a combination of infrared and visible light to increase the contrast between burned and vegetated land. http://earthobservatory.nasa.gov/NaturalHazards/view.php?id=40245

from the subsequent threat from debris flows only a few months later.

Over the last 40 years, the ability to locate and suppress wildfires has advanced significantly. This is a direct result of deploying new technology, developing and managing databases on various aspects of past wildfires and contributing factors, and employing computer models to guide the tactics being used in firefighting. This has improved the effectiveness of wildland firefighting to counter the immediate threat posed by the fire. During the last 10 years, technology and modeling has been developed and applied to the post-wildfire threat from debris flows. This paper will examine the similar and sometimes interrelated technological and research-based advances in addressing the immediate and subsequent threats from wildfires.

Immediate Wildfire Hazards

The immediate hazard posed by wildfire results from combustion that destroys or damages both resources and property and intense heat that causes injuries or fatalities to people. Not all wildfire is undesirable or poses a hazard (San Miguel-Ayanz et al. 2005). Many ecosystems depend on periodic wildfire to sustain vigor by removing older, decadent vegetation or accumulated dead organic material or by providing the means for seeds to be released or germinated. Periodic fire can be useful to forest and agricultural management by limiting fuel build up in forests that would otherwise lead to large, stand-replacing wildfires. Fire is used in many parts of the world to eliminate agricultural residues and prepare fields for planting. The hazard arises when wildfires encroach on populated areas, exceed the boundaries of the managed area, or take place when weather conditions would enable a fire to reach a size or intensity harmful to the ecosystem.

To better understand how a wildfire could be suppressed, it is necessary to understand the nature of the combustion process. At its simplest, combustion is a physical process of rapid oxidation. The requirements for combustion are the application of heat to a suitable fuel that is in the presence of oxygen (Van Wagtendonk 2006). In the absence of any of these three components, any fire (including a wildfire) will not take place. As noted previously, the heat igniting a wildfire is commonly from lightning strikes. In a few rare cases, other natural processes such as underground coal fires can cause wildfires (Stracher 2007; Mariner et al. 2008). Human-caused ignition may be intentional such as the use of torches or unintentional due to sparks from welding, fireworks or explosives discharge or heat from overheating engines and spontaneous combustion of fodder placed in confined storage.

If sufficient fuels are available at an ignition source, a wildfire can grow across an area from the point of ignition. There is a diverse range of fuel types from fine-grasses to brush communities to stands of trees in a forest. The availability of fuel for a wildfire will vary due to the ecology of these vegetative communities. For example, some brush communities found in a Mediterranean climate are considered to be part of a fire-adjusted ecosystem. A Mediterranean climate is characterized by hot, dry summers and cool, wet winters (Van Wagtendonk 2006). Organisms that break down dead vegetation are not as efficient within this climate because optimal temperature and moisture conditions rarely

exist simultaneously. Consequently, the amount of deposited organic material exceeds the ability of these organisms to break it down and it accumulates as potential fuel. A lightning strike that ignites vegetation where sufficient accumulated fuel is present will start a fire that can be readily carried beyond that point of ignition. In a forested area, a fire ignited in accumulated organic debris may spread only within this material on the forest floor. In some instances, it will ignite lower lying underbrush enabling the fire to climb into the lower tree limbs and eventually reach the crown of the forest trees. This results in a crown fire.

Once ignited, weather, topography and fuel conditions control how a fire spreads. Fire suppression to counter its spread includes denying the fuel necessary for the fire to continue to burn (K. Palmer, Fire Mgt. Officer Sierra NF, Pers. Comm., March 24, 2011). By clearing swaths of bare ground (termed firelines) around the fire, it can eventually be contained. Enclosing a fire with firelines extended along its flanks to eventually pinch the fire off at its head continues to be the general strategy to fighting a wildfire. A direct attack in the face of an advancing fire is frequently unsafe and ineffective. Areas naturally deficient in fuel such as rocky areas, bodies of water, and roads are often incorporated into the developing firelines. In terrain that is difficult to reach or unsafe to use human crews for fireline construction, aerial placing of fire retardant may be needed. Winds can blow fire brands or embers beyond firelines to cause spot fires. Unless spot fires are quickly put out or encircled, the wildfire may push past an established fireline. Consequently, building of firelines is often done in conjunction with backfiring. Backfiring is the practice of setting fire inside the firelines to burn the fuel between the fireline and the advancing fire front. This is done during periods when the spread rate is low and wind conditions are favorable to moving the backfire away from the fireline.

Advances in Fire Suppression

Early Ignition Detection

The immediate hazards due to wildfire are limited if fire suppression is done quickly before the fire can grow in size. Additionally, early fire suppression is less costly in time and manpower and exposes fewer firefighters to danger than does fighting a well-developed fire. San Miguel-Ayanz et al. (2005) state that the fire suppression community in Europe considers 15 minutes to be the maximum time for early detection of a fire start. Early detection of ignition points potentially contributes to this rapid suppression of fires when they are small (Martin et al. 1999; San Miguel-Ayanz et al. 2005; Laneve 2006). In North America, this approach was the reason for building and staffing lookout towers in many mountainous areas of the west. Similarly, fixed manned towers are used for fire detection in the European part of the Mediterranean Basin (Martin et al. 1999). The detection ability of human observers is being supplemented and, in some places, replaced by automated ground detection systems utilizing visual and infrared cameras (San Miguel-Ayanz et al. 2005).

Because lightning is one of the most common sources of wildfire ignition, improvements in detection methods for areas affected by lightning have benefitted fire suppression efforts. Checking the landscape with human observers after thunderstorms have passed through is the traditional method for early detection of lightning-caused fires. Technological changes enable a more focused and effective use of human observers and eliminate the need for many fixed human observation points at lookout towers in the western U.S. This approach uses an automated lightning detection system to identify points where lightning strikes are reaching the ground. Then ground-based patrols and airborne spotters survey the vicinity of this intense activity in the days immediately after the storm event looking for possible ignitions. Knowing the distribution of cloud-to-ground lightning strikes within an area is possible in North America using the U.S. National Lightning Detection Network (NLDN) and the Canadian Lightning Detection Network (CLDN). The NLDN was fully deployed by 1989, and the CLDN was operational beginning in 1998 (Orville et al. 2002; Orville 2008). The NLDN and CLDN systems deploy 106 and 81 sensors, respectively, which instantaneously detect the electromagnetic signals generated when lightning strikes the ground (Orville 2008). Using a satellite-based communications system, the detected signals are transmitted to a central location where processing determines location, time, polarity, and amplitude of each strike (NASA 2011b). The information is distributed to the many users of this type of information including those involved with wildland fire management.

Tracking Fire Spread with Thermal Imaging

Once a wildfire is started and the decision to suppress it has been made, the success of suppression efforts depends on knowledge of the location of fire fronts and spot fires. This information can be difficult to obtain by direct observations when smoke or terrain obscures the burning area. However, thermal imaging is recognized as an approach for improving early detection of wildfire ignition and for monitoring subsequent fire growth (Martin et al. 1999; San Miguel-Ayanz et al. 2005). Development and application of thermal imaging technology for fighting wildfires involves detectors on ground-based, airborne and satellite platforms. A number of different detectors have been used with some being

specifically designed for fire detection and other adaptations of multi-purpose detectors. Different algorithms have been tried to ensure accurate identification and limit the number of false positive identifications of fires.

Ground-based thermal imaging can be deployed at look out points previously used by human observers. These systems can utilize existing towers as well as any buildings and masts that provide good visibility of the terrain of interest (San Miguel-Ayanz et al. 2005). While these systems provide the advantage of maintaining a constant surveillance for fire starts, autonomous systems for detection of hot spots have the disadvantage of generating false alarms due to a variety of common features and effects within the observed landscape. In some systems, the problem of false alarms is remedied by the alarm initially sending of the image to a control center where detection can be validated before an alert is transmitted to the firefighting organization (San Miguel-Ayanz et al. 2005). While ground-based thermal imaging systems can be effective components in early detection of fire starts, they have the same disadvantage as human observers for information on the location of fire fronts and spot fires. Their position on the ground may not be optimal for seeing the affected terrain.

Airborne- and satellite-based thermal imaging systems have the advantage of providing observations from above that are not blocked by terrain. Wright et al. (2004) demonstrated how a thermal imaging system can be combined with Global Positioning System (GPS) technology to detect fire hotspots in the forests of Canada. This fire detection system is designed to accurately show both the position and size of the fire. On an experimental scale, their effort was successful. Airborne thermal imaging systems for early fire detection have not yet replaced airborne human observers. However, their use in suppression activities on large area wildfires is more common (Ambrosia et al. 1998, 2003). For a specific fire suppression operation, the information on the fire front and spot fire locations must be sufficiently detailed and up-to-date as possible to be valuable in planning tactics for fighting the fire. There is a continuing need to transmit the information in near real-time and to ensure the geo-referencing of the images is accurate. Otherwise, the tactics initiated based on these observations will be ineffective. Ambrosia et al. (1998) demonstrated an airborne system that achieved these criteria. As large-scale wildfires have become more frequent in the United States, the ability to provide these observation in real-time during a fire faces another technical problem; how to economically deploy sufficient resources to sustain the need for this information? Melding the imaging technology to Uninhabited Aerial Vehicles (UAVs) with the ability to fly over the fire for sustained time periods is potentially a good solution (Ambrosia et al. 2003).

Satellites offer a means to acquire fire front and spot fire information for a low cost and on a reasonably frequent basis. The different satellites, available sensors, and processing algorithms offer a number of advantages and disadvantages which make optimum selection dependent on particular user needs. This variability reflects the fact that none of the present array of satellites and their sensors is specifically designed for wildfire detection and monitoring. Approaches for identifying an optimal system are found in papers by Martin et al. (1999), San Miguel-Ayanz et al. (2005), and Laneve (2006). A system of satellites dedicated to detecting and monitoring wildfires has been envisioned for a number of years (Martin-Rico et al. 2001; Escorial et al. 2003). Currently, the Australians operate a system for detecting wildfires called the Sentinel Bushfire Monitoring System (http://sentinel.ga.gov.au/acres/sentinel/), while in the U.S., http://rapidfire.sci.gsfc.nasa.gov/firemaps/#FireLocationData is used. These systems both acquire data from the NASA Earth Observation satellites Terra and Aqua. Locations of high temperatures that are identified after processing the image are placed in a spatial database and made available at a dedicated website (Fig. 3).

Modelling Fire Danger

Effective fire fighting requires two significant components: (1) preparation for the fire conditions on any given day, and (2) knowledge of how an active fire is spreading. Currently, fire behavior models are used to establish fire danger ratings to identify changing fire conditions (Fig. 4). Fire behavior models also are employed during suppression actions to predict the direction and rate of fire spread. These models are based on known relationships between various fire-related physical and chemical processes that affect fire behavior (Rothermel 1972, 1983; Anderson 1982; Weber 1991; Weise and Biging 1997). Perry (1998) points out that the complexity of natural fuel beds as well as the interactions of topography and local climatic conditions are not sufficiently understood to allow development of a comprehensive model of wildland fire behavior. Various fire behavior models developed and implemented to date have limitations. For example, some models are fundamentally statistical characterizations of wildland fires without a clear link to the physical mechanisms driving the process. Other models are based on analysis of small-scale or laboratory fires, with results up-scaled to presumably represent large-scale events (Perry 1998). In the absence of a comprehensive model of wildland fire behavior, research will continue in an effort to improve characterization of the physical and chemical processes involved (Martins-Fernandez 2001; Dimitrakopoulos 2002; Nelson 2002).

The National Fire Danger Rating System (NFDRS) used in the United States uses fuels, topography and weather factors to model the upper limit of possible fire behavior

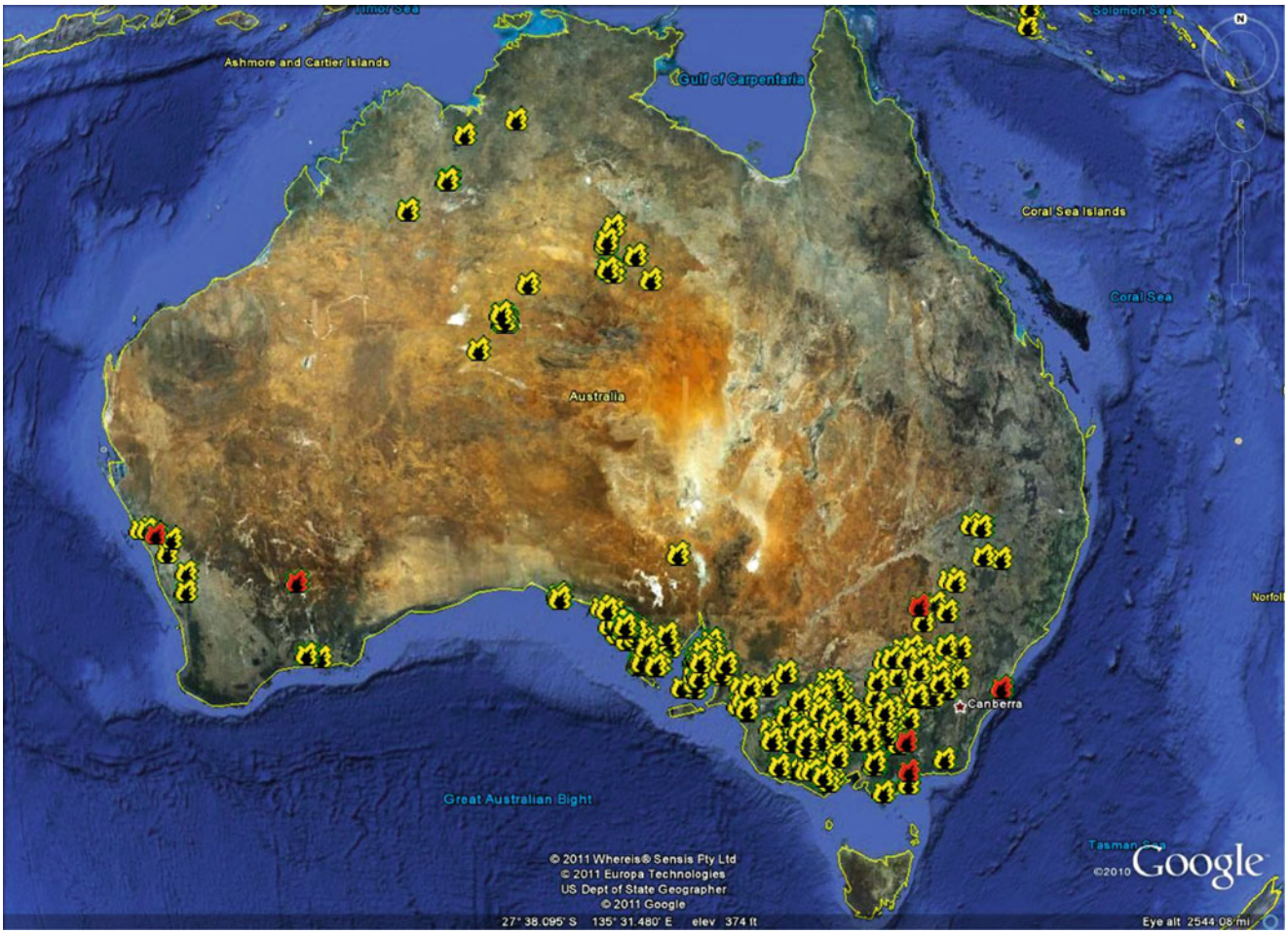

Fig. 3 Wildfires detected in Australia on March 30, 2011 by the Sentinel Brushfire Monitoring System. The fire symbols represent fires detected within the last 1–12 h (*red*) and 12–24 h (*yellow*) and are represented within 1.5 km of their actual location. The symbols represent only detected fire location, not individual fire size. http://sentinel.ga.gov.au/acres/sentinel/

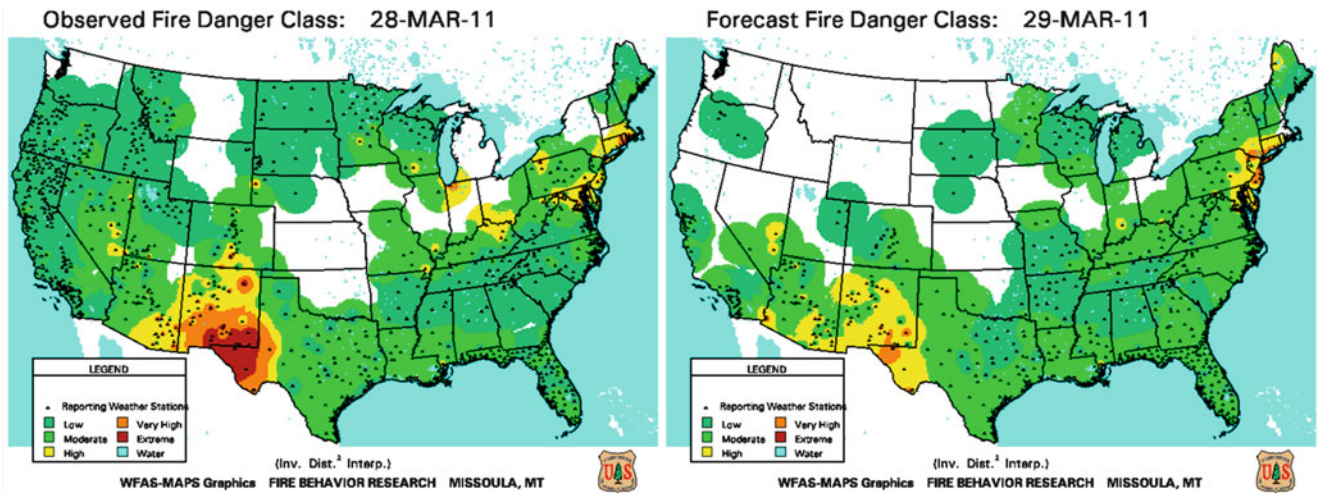

Fig. 4 Observed (*left*) and predicted (*right*) fire danger rating maps for the United States generated on 28 March 2011. These maps are a composite of fire danger ratings from numerous small areas, and are used to advise local fire fighting organizations of their local fire danger

during the next 24-h period (Fig. 4). The modeling results are used to generate relative ratings of the potential growth and behavior of any wildfire. The purpose of the ratings is to permit any organization involved with wildland fire fighting to adjust their readiness levels or execute pre-planned fire suppression actions during the coming day.

The present-day structure of the NFDRS is adapted from Deeming et al. (1977) and Burgan (1988) (NWCG 2002). Input includes site characteristics, observations of weather parameters and fuel conditions and 24-h weather factors. The model uses this input to calculate three factors: (1) the ignition component, (2) the spread component, and (3) the energy release component. The ignition component value represents the likelihood that a fire would result from an ignition source being introduced into the fine fuels present.

The spread component integrates the effects of wind and slope with the fuel bed properties and generates forward rate of spread at the head of the fire. The energy release component computes the potential available energy per square foot of flaming fire that would be at the head of the fire. These calculated values are used to define the upper limit of possible fire behavior during the next 24-h period and define a specific fire danger over the area (NWCG 2002).

The National Oceanographic and Atmospheric Administration (NOAA) issues fire danger maps and local area-specific forecasts based on the NFDRS (Fig. 4). Australia, South Africa and New Zealand have used some of the same basic research for the NFDRS and additional input to develop their fire danger rating systems (Perry 1998). The Canadian forest fire danger rating system is based on an empirical model (Perry 1998; Stocks et al. 1989). More recently, fire danger ratings systems for Indonesia and Malaysia were developed primarily based on the Canadian research model adapted to local conditions (de Groot et al. 2006).

Advances in Mapping Post-Fire Debris-Flow Hazards

Empirical Models to Predict Debris-Flow Probability, Volume and Inundation Area

As discussed previously, the recent Station fire in southern Californa (Fig. 2) posed significant postfire debris-flow hazards to life and property (Cannon et al. 2009, 2010a). Emergency-response and public-safety agencies were faced with making evacuation decisions and deploying staff and emergency-response equipment well in advance of each coming winter storm as well as during actual storms themselves. Information critical to the decision process included: (1) detailed precipitation forecasts of the timing and potential storm rainfall intensities provided by NOAA's National Weather Service; (2) definition of potential debris-flow magnitudes resulting from storms that are likely in the San Gabriel Mountains; (3) linking this information to emergency-response actions routinely implemented by fire department and incident command centers.

The association between debris flows and wildfires is well established in the San Gabriel Mountains. When the fires that consume vegetation in the steep, rugged terrain are followed by high-intensity rain storms, destructive debris flows are a frequent result (e.g., Eaton 1936; Troxell and Peterson 1937; Scott and Williams 1978; McPhee 1989). Field observations from recently burned basins throughout Southern California indicate that the majority of debris flows that occur within the first 2–3 years following wildfires are generated through the process of progressive entrainment of material eroded from hillslopes and channels by surface runoff, rather than by infiltration-triggered landsliding, as is common in unburned settings (Cannon et al. 2009, 2010a, b).

Cannon et al. (2010b) developed an approach for characterizing post-fire debris-flow hazards from these runoff-generated debris flows based on identifying the combinations of conditions within drainage basins that most strongly control debris-flow susceptibility for the first two to three rainy seasons following a wildfire. The approach identifies the probability that given drainage basins will produce debris flows, and estimates the potential volume of the debris flows at the basin outlet. By developing probability and volume models specific to southern California, the approach has been modified to be appropriate for this setting. The approach has also been advanced by modifying the method used for mapping lahar inundation developed by Iverson et al. (1998), by developing relations specific to recently-burned, southern California steeplands. The requisite regression equations that relate debris-flow volume to cross-sectional and planimetric inundation areas were derived from field measurements of 22 postfire debris-flow deposits in southern California (Bernard 2007). Thus, for a given storm event, the approach now addresses three of the fundamental questions in debris-flow hazard assessments: where might debris flows occur, how big they might be, and what may they impact (Fig. 5).

Rainfall Intensity-Duration Thresholds for Emergency-Response Planning

Empirically derived rainfall intensity-duration or rainfall accumulation-duration thresholds have been widely used to identify rainfall conditions that will lead to the generation of debris flows (see a world-wide compilation of rainfall thresholds at http://rainfallthresholds.irpi.cnr.it). This approach is based on the principle that debris-flow triggering

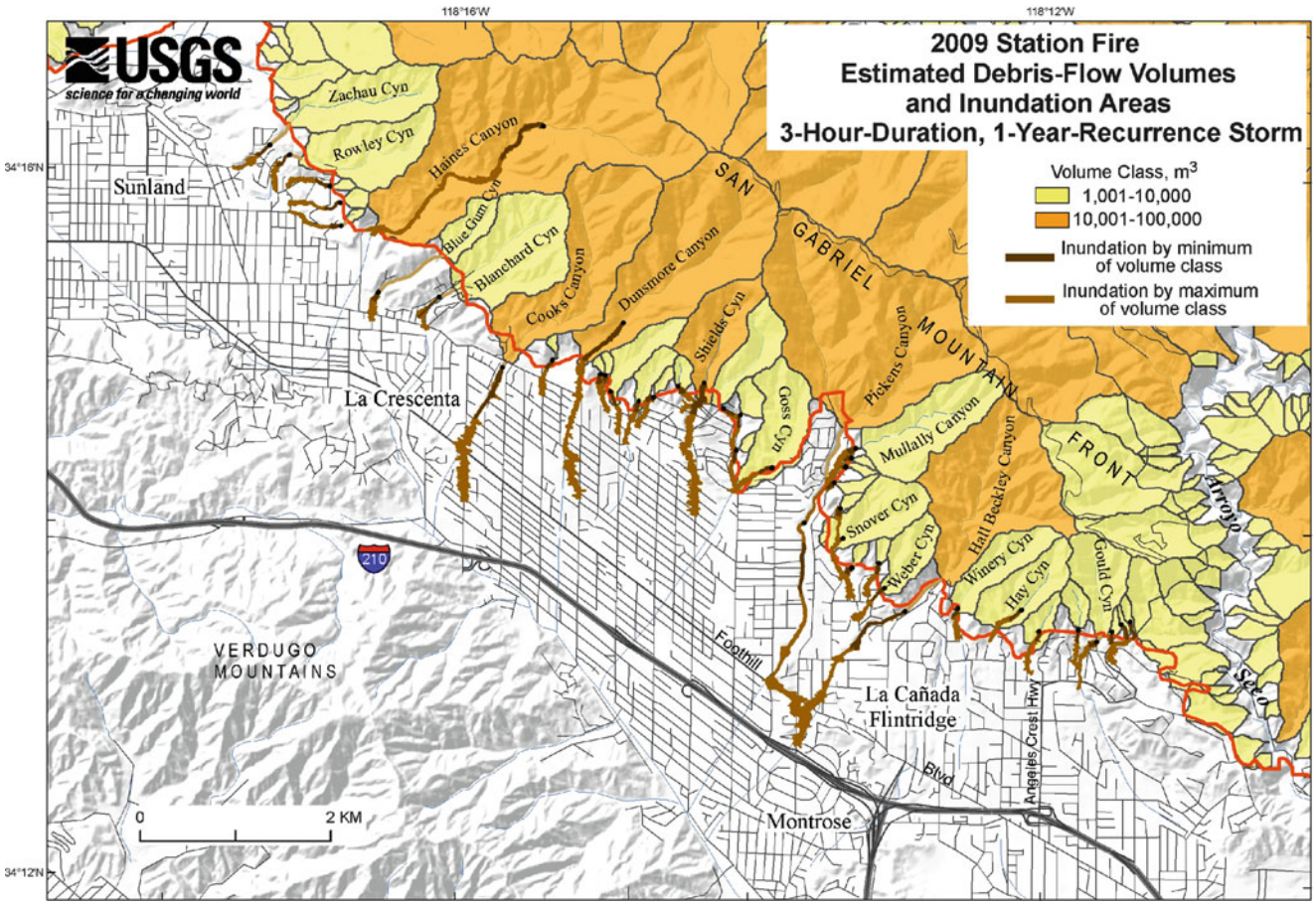

Fig. 5 Map showing areas that may be inundated by debris-flow deposits generated from basins burned by the 2009 Station fire in response to a widespread, 1-h-duration, 2-year-recurrence storm when sediment-retention basins overtop, or basin drains, spillways or outflow channels experience blockages or failures (Modified from Cannon et al. 2009)

conditions cannot be defined by a total depth of rainfall, or by instantaneous rainfall intensity, but are more accurately characterized as a function of either of these two measures and the time period over which they occur (Caine 1980). In addition, triggering rainfall conditions are best represented by a range of intensities and durations (or rainfall depths and durations) that are specific to particular settings (e.g., Caine 1980; Larsen and Simon 1993; Godt et al. 2006; Cannon et al. 2008; Guzzetti et al. 2008).

Rainfall intensity-duration thresholds have been defined for the generation of postfire debris flows for three southern California regions, including the San Gabriel, San Bernardino, and San Jacinto Mountains (Cannon et al. 2008). These regional thresholds are thought to generally reflect the rainfall conditions associated with the occurrence of debris flows in the first two to three winters following fires, but do not address the conditions that will produce events with varying magnitudes. In addition, debris-flow triggering rainfall will vary with burn severity, basin sizes and gradients, and material properties (Cannon et al. 2010b), as well as with local rainfall regimes (Moody and Martin 2009). These fire-specific and local effects are not accounted for in the regional rainfall intensity-duration thresholds.

In response to the information demands of the emergency response to the Station fire, Cannon et al. (2010a) moved from the existing regional definition of storm rainfall conditions that may lead to debris flows from recently burned southern California steeplands to develop information that is specifically relevant to conditions in the San Gabriel Mountains and takes into account the potential magnitudes of debris-flow events (Fig. 6). By linking local rainfall information with debris-flow magnitude documentation, they were able to define the rainfall conditions that may lead to debris flows of different magnitudes from recently burned areas. Cannon et al. (2010a) also developed an emergency response decision chart that can be used to determine potential event magnitudes and identify possible evacuation and resource-deployment levels based on either individual storm forecasts or measured precipitation during storms. Although this work is of particular relevance for agencies

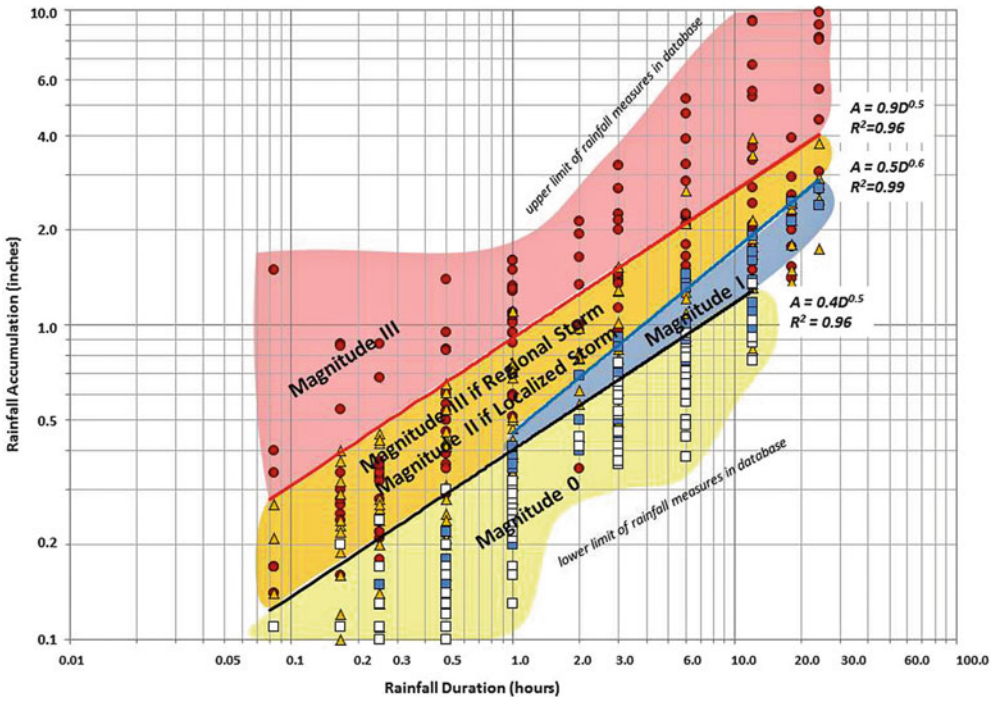

Fig. 6 Rainfall accumulation-duration thresholds that may lead to debris flow and floods of different magnitudes from recently burned areas in the San Gabriel Mountains of southern California. Threshold lines are the power law relation through the upper rainfall value at each duration within each assigned magnitude class (From Cannon et al. 2010a)

tasked with postfire emergency planning and response in the San Gabriel Mountains, the approach developed by this study can be implemented in other settings.

Summary and Conclusions

Wildfire is a unique natural hazard because it creates different hazards during and following the fire. Wildfires can pose immediate threats to life and property in that they may rapidly spread and affect a significant area until brought under containment and control. In the aftermath of fires, vegetative cover and soil surface conditions within the burned area are changed. These landscape changes are responsible for the subsequent hazards due to wildfire which can include erosion, flooding and debris flows.

During the last few decades, our ability to limit the immediate destructive force of wildfires has increased, and our understanding of fire behavior and its controlling factors has improved. Lightning detection networks now identify possible ignition points by recording the number, location and types of this common ignition source. Measurements of wind speed, temperature, slope, fuel types and fire boundaries are routinely incorporated into models of fire spread. Use of these models is enhanced by deployment of remote reporting weather stations within fire affected areas. Aerial deployment of thermal detectors to map the smoke-obscured boundaries of the advancing fire is also available. These improvements in real-time prediction of fire activity increase the effectiveness of the full range of firefighting tactics and methods. Our improved predictive ability also plays a role in determining vegetation management strategies to reduce the likelihood of catastrophic fire events. This is a particularly important factor as climatic conditions appear to favor larger and more frequent wildfires in parts of the world that include expanding urban areas.

Similarly, our capability to identify potential impacts from the wildfire-induced slope instabilities, specifically debris flows, is improving. Processing of satellite imagery from before and immediately after a wildfire enables rapid mapping of areas where vegetative changes are greatest. How changes in the landscape due to wildfire influence the hydrologic response to storm rainfall that results in slope-instability processes are better understood. This increased understanding has enabled the development of models for estimating the probability of debris-flow occurrence, the likely volume of such an event, and for mapping the area that may be impacted by that volume of material. These models provide critical information for the design and location of protective measures. Improved definition of the rainfall conditions that trigger debris flows after wildfires enables emergency-response agencies to identify possible evacuation and resource-deployment levels, and for weather networks to better provide early warning of debris-flow triggering storms. Ongoing work is focused on refining the temporal and spatial predictive

capabilities of debris flow models and quantifying the effects of post-fire vegetative recovery and changes in sediment supply.

References

Ambrosia VG, Buechel SW, Brass JA, Peterson JR, Davies RH, Kane RJ, Spain S (1998) An integration of remote sensing, GIS, and information distribution for wildfire detection and management. Photogramm Eng Remote Sens 64(10):977–985

Ambrosia VG, Wegener SS, Sullivan DV, Buechel SW, Dunagan SE, Brass JA, Stoneburner J, Schoenung SM (2003) Demonstrating UAV-acquired real-time thermal data over fires. Photogramm Eng Remote Sens 69(4):391–402

Anderson HE (1982) Aids to determining fuel models for estimating fire behavior. General Technical Report INT-122, USDA Forest Service, Intermountain Forest and Range Experimental Station, 22 p

Bernard D (2007) Estimation of inundation areas of post-wildfire debris flows. Golden, Colorado School of Mines, unpublished Master's thesis, Department of Geology and Geological Engineering, 77 p

Burgan RE (1988) 1988 revisions to the 1978 National fire-danger rating system. Research Paper SE-273, U.S. Department of Agriculture, forest Service, Southeastern Forest Experiment Station, 144 p

Caine N (1980) The rainfall intensity-duration control of shallow landslides and debris flows. Geogr Ann 62A:23–27

Cannon SH, Gartner JE, Wilson RC, Bowers JC, Laber JL (2008) Storm rainfall conditions for floods and debris flows from recently burned areas in southwestern Colorado and southern California. Geomorphology 96:250–269

Cannon SH, DeGraff J (2009) Incorporating spatial, temporal, and climate variability into tools for assessing post wildfire debris-flow hazards. In: Sassa K, Canuti P (eds) Landslides: disaster risk reduction. Springer, Berlin, pp 177–190

Cannon SH, Gartner JE, Rupert MG, Michael JA, Staley DM, Worstell BB (2009) Emergency assessment of postfire debris-flow hazards for the 2009 Station Fire, San Gabriel Mountains, Southern California. U.S. Geological Survey Open-File Report OF 09-1227, 26 p

Cannon SH, Boldt EM, Kean JW, Laber JL, Staley DM (2010a) Relations between rainfall and postfire debris-flow and flood magnitudes for emergency-response planning, San Gabriel Mountains, Southern California. Nat Hazards. doi:10.1007/s11069-011-9747-2

Cannon SH, Gartner JE, Rupert MG, Michael JA, Rea AH, Parrett C (2010b) Predicting the probability and volume of postwildfire debris flows in the intermountain western United States. Geol Soc Am Bull 122(1/2):127–144

de Groot WJ, Field RD, Brady MA, Roswintiarti O, Mohamad M (2006) Development of the Indonesian and Malaysian fire danger rating systems. Mitig Adapt Strateg Glob Change 12:165–180

Deeming JE, Burgan RE, Cohen JD (1977) The National fire-danger rating system. U.S. Department of Agriculture, Forest Service, Intermountain forest and Range Experiment Station, General Technical Report INT-39, 66 p

DeGraff JV, Cannon SH, Gallegos AJ (2007) Reducing post-wildfire debris flow risk through the Burned Area Emergency Response (BAER). In: Schaefer VR, Schuster RL Turner AK (eds) AEG Special Publication No. 23, pp 1440–1447

Dimitrakopoulos AP (2002) Mediterranean fuel models and potential fire behavior in Greece. Int J Wildland Fire 11:127–130

Eaton EC (1936) Flood and erosion control problems and their solution. Proc Am Soc Civil Eng 62:1302–1362

Escorial D, Tourne IF, Reina FJ (2003) FUEGO: a dedicated constellation of small satellites to detect and monitor forest fires. Acta Astronaut 52(9–12):765–775

Godt JW, Baum RL, Chleborad AF (2006) Rainfall characteristics for shallow landsliding in Seattle, Washington, USA. Earth Surf Proc Land 31:97–110

Guzzetti F, Peruccacci S, Rossi M, Stark CP (2008) The rainfall intensity-duration control of shallow landslides and debris flows—an update. Landslides 5:3–7

Iverson RM, Schilling SP, Vallance JW (1998) Objective delineation of lahar-inundation hazard zones. Geol Soc Am Bull 110:972–984

Laneve G (2006) Continuous monitoring of forest fires in the Mediterranean area using MSG. IEEE Trans Geosci Remote Sens 44 (10):2761–2768

Larsen MC, Simon A (1993) Rainfall intensity-duration threshold for landslides in a humid-tropical environment, Puerto Rico. Geogr Ann 75A:13–23

Mariner RH, Minor SA, King AP, Boles JR, Kellogg KS, Evans WC, Landis GA, Hunt AG, Till CB (2008) A landslide in tertiary marine shale with superheated fumaroles, Coast Ranges, California. Geology 36(12):959–962

Martin MP, Flasse S, Downey I, Ceccato P (1999) Fire detection and fire growth monitoring using satellite data. In: Chuvieco E (ed) Remote sensing of large widlfires. Springer, Berlin, pp 101–122

Martin-Rico C, Gonzalo J, Mariani A, Leibrandt W (2001) The FUEGO system concept. Acta Astronaut 48(1):45–56

Martins Fernandes PA (2001) Fire spread prediction in shrub fuels in Portugal. For Ecol Manage 144:67–74

McPhee JA (1989) The control of nature. Farrar, Strauss, and Giroux, New York, p 272

Moody JA, Martin DA (2009) Synthesis of sediment yields after wildland fire in different rainfall regimes in the western United States. Int J Wildland Fire 18:94–115

Munich RE (2011) 2010 Natural catastrophe year in review. http://www.munichreamerica.com/webinars/2011_01_natcatreview/munich_re_2010_natcat_review.pdf. Last accessed 22 Mar 2011

NASA (2010) Fire archives for 2010 natural hazards. http://earthobservatory.nasa.gov/NaturalHazards/quarterly.php?cat_id=8. Last accessed 23 Mar 2011

NASA (2011a) MODIS rapid response system. http://rapidfire.sci.gsfc.nasa.gov/. Last accessed 22 Mar 2011

NASA (2011b) The U.S. National Lightning Detection Network Database (NLDN). HTTP://gcmd.nasa.gov/records/GCMD_NLDN.html. Last accessed 24 Mar 2011

Nelson RM Jr (2002) An effective wind speed for models of fire spread. Int J Wildland Fire 11:153–161

NWCG (2002) Gaining an understanding of the National Fire Danger Rating System. PMS 932 (NFES 2665) National Wildfire Coordinating Group. http://www.nwcg.gov/pms/pubs/MasterGaining.pdf. Last accessed 28 Mar 2011

Orville RE (2008) Development of the national lightning detection network. Bull Am Meteorol Soc 89:180–190

Orville RE, Huffines GR, Burrows WR, Holle RL, Cummins KL (2002) The North American lightning detection network (NALDN)-first results: 1998–2000. Mon Weather Rev 130:2098–2109

Perry GLW (1998) Current approaches to modeling the spread of wildland fire: a review. Prog Phys Geog 22(2):222–245

Rothermel RC (1972) A mathematical model for predicting fire spread in wildland fuels. Research Paper INT-115, USDA Forest Service, Intermountain Forest and Range Experimental Station, 40 p

Rothermel RC (1983) How to predict the spread and intensity of forest and range fires. General Technical Report INT-143. USDA Forest

Service, Intermountain Forest and Range Experimental Station, 161 p
San Miguel-Ayanz J, Ravail N, Kelha V, Ollero A (2005) Active fire detection for fire emergency management: potential and limitations for the operational use of remote sensing. Nat Hazards 35:361–376
Scott KM, Williams RP (1978) Erosion and sediment yields in the Transverse Ranges, southern California. US Geological Survey Professional Paper 1030, 38 p
Stocks BJ, Lawson BD, Alexander ME, Van Wagner CE, McAlpine RD, Lynham TJ, Dubé DE (1989) The Canadian forest fire danger rating system: an overview. Forest Chron 65:450–457
Stracher GB (ed) (2007) Geology of coal fires: case studies from around the world. Rev Eng Geol XVIII, Geological Society of America, Boulder, 283 p
Sugihara NG, van Wagtendonk JW, Fite-Kaufman J (2006) Fire as an ecological process. In: Sugihara NG, van Wagtendonk JW, Shaffer KE, Fites-Kaufman J, Thode AE (eds) Fire in California's ecosystems. University of California Press, Berkeley and Los Angeles, pp 58–74
Troxell HC, Peterson JQ (1937) Flood in La Canada Valley, California. US Geological Survey Water-Supply Paper 796-C, pp 53–98
Van Wagtendonk JW (2006) Fire as a physical process. In: Sugihara NG, Van Wagtendonk JW, Shaffer KE, Fites-Kaufman J, Thode AE (eds) Fire in California's ecosystems. University of California Press, Berkeley and Los Angeles, pp 38–57
Weber RO (1991) Modelling fire spread through fuel beds. Prog Energ Combust Sci 17:67–82
Weise DR, Biging GS (1997) A qualitative comparison of fire spread models incorporating wind and slope effects. For Sci 43(2):170–180
Wright DB, Yotsumata T, El-Sheimy N (2004) Real time identification and location of forest fire hotspots from geo-referenced thermal images. In: Proceedings of international society photogrammetry remote sensing (ISPRS) 2004 congress, commission I, Istanbul/Turkey, 15–22 July 2004, pp 3–8

Remote Sensing and Geospatial Support to Burned Area Emergency Response (BAER) Teams in Assessing Wildfire Effects to Hillslopes

Jess Clark

Abstract

Burned Area Emergency Response (BAER) teams are dispatched to fires in the United States to make an immediate post-fire assessment of the potential danger to various values due to wildfire. The U.S. Forest Service Remote Sensing Applications Center assists in the assessment by providing remote sensing and geospatial support to teams. The remote sensing support includes creation of a preliminary burn severity map called the Burned Area Reflectance Classification, or BARC. This data layer is field validated or adjusted to match ground conditions and then used in subsequent modeling to predict the hydrologic response to watersheds.

Keywords

Burned Area Emergency Response • BAER • Remote sensing • Landsat • dNBR • Burned Area Reflectance Classification • BARC

Introduction

A major concern of land managers in the United States is the reaction of watersheds to weather events after a wildfire. With an ever-expanding wildland-urban interface (WUI), land managers have to be continually cognizant of potential damage to private property and other values at risk due to the fire effects. In the Forest Service, each fire greater than 120 ha must be assessed to determine whether a BAER, or Burned Area Emergency Response, team will be deployed. A BAER team's purpose is to make an emergency assessment of the burnt lands for erosion and runoff potential due, in many cases, to the loss of vegetative cover. The BAER team's objective is only emergency stabilization, not long-term restoration of the landscape after a fire. BAER teams make assessments that direct possible treatments in an effort to protect life and property and prevent additional damage to resources. These treatments can include things such as seeding with grasses, mulching to provide ground cover, contour felling, log erosion barriers, and efforts to protect transportation corridors, such as enlargement of culverts or installing a debris fence to capture the increased debris runoff. BAER treatments are meant to be implemented within 1 year of the fire, although the timing of the fire may determine the timing of the treatments.

In addition to emergency stabilization efforts, longer-term rehabilitation efforts are considered in areas where lands are unlikely to recover naturally from the fire effects. This long-term rehabilitation effort is not done by BAER teams and is not funded out of emergency stabilization funds. In addition, long-term rehabilitation efforts must be (1) consistent with long-term goals and approved land use plans, (2) based on sound analyses of the project's potential consequences, (3) developed with interagency cooperation where necessary, (4) consistent with the objective to protect life, property, or critical cultural resources, and (5) done within the fire perimeter. This paper will focus on the process and geospatial technology used to assess the emergency stabilization needs after a wildfire.

J. Clark (✉)
United States Department of Agriculture, Forest Service, Remote Sensing Applications Center, Salt Lake City, UT, USA
e-mail: jtclark@fs.fed.us

C. Margottini et al. (eds.), *Landslide Science and Practice*, Vol. 4,
DOI 10.1007/978-3-642-31337-0_27,

Fig. 1 BAER team member hand-mapping severity (Photo courtesy of Brad Quayle, USFS)

BAER Mapping Objective

An early step in the BAER assessment process is the creation of a soil burn severity map. This map is a major component in determining treatment locations and intensity. Soil burn severity mapping does not require the use of remote sensing or geographic information systems (GIS); however, both technologies are commonly used on large wildfires. Depending on availability of resources, access, size, and time frame, some fires are mapped fastest by hand. For example, a 500-ha fire with sufficient access may be a good candidate for ground (Fig. 1) and aerial observations as part of the post-fire assessment. At times, waiting for satellite overpasses to image a fire may jeopardize a BAER team's ability to complete their assessment quickly.

For larger and more inaccessible fires, remote sensing and GIS provide means that greatly improve the speed, precision, and accuracy of post-fire mapping efforts. Soil burn severity mapping, however, should never be done solely through the use of remote sensing classifications without proper field verification (Parsons and Orlemann 2002; Hudak et al. 2004). Ecosystems and fire behavior provide sufficient variation such that field observations and refinement of the remote sensing classifications are required. Once the initial image classification has been done, a soil scientist or other specialist must verify the soil conditions in the field prior to the entire team using the map.

Remote Sensing Support

The United States Forest Service (USFS) Remote Sensing Applications Center (RSAC) and United States Geological Survey (USGS) Earth Resources Observation and Science (EROS) Center provide operational remote sensing support to BAER teams by analyzing pre- and immediate post-fire imagery of burned areas. The Centers create a GIS-ready layer that is essentially a generalized index of environmental change particularly sensitive to vegetation and soil surface changes due to fire.

Support History

The two Centers have been providing geospatial support to BAER teams for over a decade. In years prior, many forests used aerial photography to map the severity but it was a costly and time-consuming effort. After a successful pilot in 2001 where the Centers mapped 20 fires using sensors such as Landsat 5, Landsat 7, and SPOT, this effort became an operational project in 2002 (Orlemann et al. 2002). During that year alone, numerous 40,000+ hectare fires burned, including Hayman (56,000 ha), McNally (60,000 ha), Rodeo-Chediski (189,000 ha), and Biscuit (202,000 ha). The Centers have now mapped over 11.5 million hectares while supporting more than 900 BAER teams.

International Support

While this support is primarily to wildfires that burn in the United States, the Centers have also assisted international efforts. Through the United States Agency for International Development (USAID) Office of Foreign Disaster Assistance (OFDA), the Centers have mapped wildfires in Honduras (2005), Greece (2007), Australia (2009), Canada (2009), and most recently Israel (2010 – Fig. 2). Countries with significant wildfire events could potentially do this work on their own using similar techniques employed by the United States over the last 10 years.

Burned Area Reflectance Classification (BARC)

Among the products typically provided to BAER teams by RSAC and EROS are pre- and post-fire satellite images of the burned area and a preliminary classification representing landscape change. This product is referred to as the Burned Area Reflectance Classification (BARC) (Clark and Bobbe 2007).

Creation of the BARC

The BARC is derived from an image transformation algorithm known as the Normalized Burn Ratio (NBR). The NBR uses the near infrared (NIR) and short-wave infrared

Fig. 2 SPOT 5 image acquired December 8, 2010, of the Mt. Carmel Fire (*dark red*) near Haifa, Israel

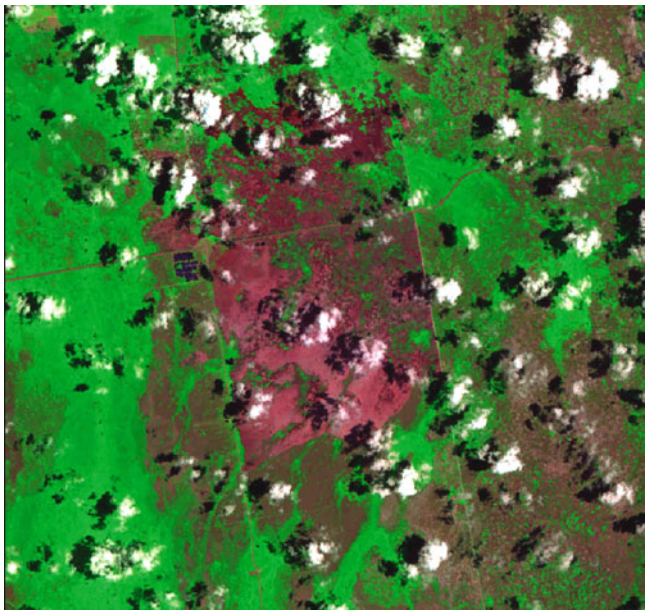

Fig. 3 Clouds often make it difficult to get a clear picture of a burn scar. Landsat Thematic Mapper (TM) 5 image acquired on May 3, 2009, over the Deep Fire in Florida, USA

(SWIR) bands (4 and 7, respectively) from the two Landsat satellite sensors. The algorithm is as follows:

$$\mathrm{NBR} = (\mathrm{NIR} - \mathrm{SWIR})/(\mathrm{NIR} + \mathrm{SWIR})$$

Healthy green vegetation reflects NIR energy. Conversely, NIR response decreases where there is little vegetation. SWIR energy is largely reflected by rock and bare soil, meaning that SWIR band values will be very high in bare, rocky areas with little vegetation and low in areas of healthy green vegetation. Imagery collected over a forest in a pre-fire condition will have very high NIR band values and very low SWIR band values, while imagery collected over a forest after a fire will have very low NIR band values and very high SWIR band values.

Many researchers have used a single-scene NBR approach (López-Garcia and Caselles 1991) as well as a change detection approach based on the NBR, the differenced Normalized Burn Ratio (often referred to as the dNBR), (van Wagtendonk et al. 2004) in burn mapping projects. The dNBR is simply an image differencing between the pre- and post-fire NBR layers, which are typically 1-year apart for vegetation and atmospheric consistency:

$$\mathrm{dNBR} = \mathrm{NBR}_{\text{pre-fire}} - \mathrm{NBR}_{\text{post-fire}}$$

In general, the dNBR has been shown to be a useful and accurate tool for burn severity mapping (Brewer et al. 2005; Cocke et al. 2005; Miller and Yool 2002). Nearly all BARC layers delivered to BAER teams are created from the dNBR. Occasionally, other algorithms are used simply due to availability of spectral bands in the post-fire satellite or airborne imagery used for the assessment.

Using the BARC

The BARC is not considered a soil burn severity map – the map product needed by BAER teams – until it has been field verified, and if necessary, refined to better represent actual soil and ground conditions. By nature, satellite images and derived products such as the BARC are reflective of the vegetative condition because that is the uppermost layer, or what the satellite "sees." Adjustments to the BARC classes are necessary to produce a map product that is reflective of the soil conditions. BAER teams can refer to a General Technical Report (GTR) written by specialists outlining the process of mapping soil burn severity for BAER teams. This document is available online in PDF format at http://treesearch.fs.fed.us/pubs/36236 (Parsons et al. 2010). The BARC begins as a continuous raster GIS layer that is classified into four colors representing the four burn severity classes (unburned-dark green, low-light blue, moderate-yellow, and high-red). BARC values are scaled 0–255 with low values indicating the least burned areas and values increase as burn severity increases. Some users may find the BARC thresholds that were applied to the delivered product to be a good fit for their wildfire. In areas of densely

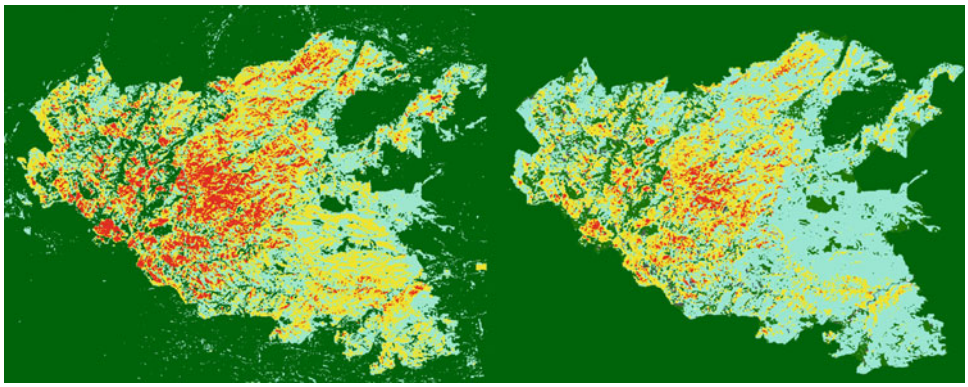

Fig. 4 The Derby Fire burned approximately 81,000 ha in 2006. The BARC (*left*) was edited by the BAER team to better reflect ground conditions. The original BARC overestimated high and moderate severities so the team made both systematic and localized edits to create their final soil burn severity map (*right*)

forested ecosystems where variation in vegetation type and density are minimal, the BARC can be very accurate. When no edits are needed as determined by field verification, the BARC may be renamed the "soil burn severity map."

On occasions, however, the thresholds applied to the delivered BARC may not be a perfect fit to the observed soil and ground conditions after the wildfire. Plotting the field observations of soil and ground conditions using GPS coordinates as a data layer overlaid on the BARC allows the user to see how closely the BARC classes match independent and unbiased field observations. Many BAER team members with basic GIS skills can adjust the BARC to quickly create a map that represents their observed soil and ground conditions by making simple adjustments to the BARC threshold values. This is referred to as "systematic" editing of the BARC – changing the thresholds across the entire fire. Systematic editing works well in situations where vegetation and other site factors produce a fairly predictable distribution of soil burn severity patterns across the landscape. To make systematic changes to the BARC in ArcMap (Environmental Systems Research Institute, Inc. [ESRI], Redlands, CA), team members can simply open the symbology tab within the properties of the BARC layer and adjust the thresholds between the various severity classes.

Other situations may require edits to localized areas because the imagery used to create the BARC may not be ideal which can cause classification confusion. Clouds (Fig. 3), snow, smoke from surrounding fires, or large water bodies within the burn scar are all things that create inconsistencies in the BARC. There may also be cases where the geology-soils-vegetation-topography interactions are so complex that systematic adjustments do not work well for the entire burned area. In these complex areas, BAER team members are required to make soil burn severity adjustments through aerial or ground observations and then integrate those observations into the BARC using GIS.

Another useful GIS technique that can be used to refine the BARC is to create an overlay with the pre-fire vegetation classes. This can help account for pre-fire vegetation densities and types that can affect the BARC classification. An overlay of timber sales or cut blocks may also be useful for changing some areas of the BARC from high to moderate or low soil burn severity. In this case, BAER team members can use GIS layers and a pre-fire vegetation classification to reclassify areas of high burn severity on the BARC into whatever is appropriate based on the soil and ground condition data gathered.

It is important for BAER team members to consider the dates of the satellite imagery used to create the BARC. While analysts at both Centers try to use image pairs (pre- and post-fire) that phenologically match each other well (i.e. ideally 1-year apart, similar dates), sometimes these image pairs may span multiple years. If there have been management activities on the landscape between the dates of the imagery used, some of those activities may influence the severity mapping results. For example, logging activities that occur between the pre- and post-fire images used to create a BARC will likely be classified as high severity. The BARC will assume that the fire in the area of the logging activity was a stand-replacing event when in reality the forest structure changed due to management activities prior to the fire event. The BARC assumes all things are equal on the landscape between pre- and post-fire imagery with the exception of the wildfire. BAER teams need to be aware of these potentially misclassified areas in the BARC.

Application of Severity Maps

Adjustments to the BARC severity classes, if necessary, are generally based upon ancillary information such as field sample points/ground truth, ocular aerial or ground observations, and local expert opinion (Fig. 4). Once the BARC classification is finalized it becomes the soil burn severity map used for further modeling. Along with other environmental and terrain variables, the burn severity information is a critical input to subsequent GIS modeling scenarios used to predict potential fire effects such as increased surface water runoff, debris flows, and erosion. These map products help BAER teams focus their limited time to the areas of most concern, such as slopes that have become unstable due to wildfire and the values at risk below.

A useful online resource for BAER team members and other interested parties is the "Burned Area Emergency Response Tools" website (http://forest.moscowfsl.wsu.edu/BAERTOOLS/) This website hosts links to documents and tools used by a variety of specialists on BAER teams, including economists, soil scientists, hydrologists, and GIS specialists.

Acknowledgements Thanks to Jennifer Lecker for her review of this paper and Brad Quayle, Rapid Disturbance Assessment and Services program leader at the USFS RSAC, for his guidance of the USFS BAER support program.

References

Brewer CK, Winne JC, Redmond RL, Opitz DW, Mangrich MV (2005) Classifying and mapping wildfire severity: a comparison of methods. Photogramm Eng Rem Sens 71:1311–1320

Clark J, Bobbe T (2007) Using remote sensing to map and monitor fire damage in forest ecosystems. In: Wulder MA, Franklin SE (eds) Ch. 5; Understanding forest disturbance and spatial patterns: remote sensing and GIS approaches. Taylor & Francis, London, p 246

Cocke AE, Fule PZ, Crouse JE (2005) Comparison of burn severity assessments using Differenced Normalized Burn Ratio and ground data. Int J Wildland Fire 14:189–198

Hudak AT, Robichaud P, Evans J, Clark J, Lannom K, Morgan P, Stone C (2004) Field validation of Burned Area Reflectance Classification (BARC) products for post-fire assessment. In: Proceedings of the tenth biennial forest service remote sensing applications conference, (CD-ROM), U.S. Department of Agriculture, Forest Service, Remote Sensing Applications Center, Salt Lake City

López-Garcia MJ, Caselles V (1991) Mapping burns and natural reforestation using thematic mapper data. Geocarto Int 6(1):31–37

Miller JD, Yool SR (2002) Mapping forest post-fire canopy consumption in several overstory types using multi-temporal Landsat TM and ETM data. Remote Sens Environ 82:481–496

Orlemann A, Saurer M, Parsons A, Jarvis B (2002) Rapid delivery of satellite imagery for burned area emergency response (BAER). In: Proceedings of the ninth biennial Forest Service remote sensing applications conference, (CD-ROM), U.S. Department of Agriculture, Forest Service, Remote Sensing Applications Center, Salt Lake City

Parsons A, Orlemann A (2002) Mapping post-wildfire burn severity using remote sensing and GIS. In: Proceedings of the 22nd annual ESRI international user conference (CD-ROM), ESRI, San Diego, 8–12 July 2002

Parsons A, Robichaud P, Lewis S, Napper C, Clark J (2010) Field guide for mapping post-fire soil burn severity, General technical report RMRS-GTR-243. U.S. Department of Agriculture, Forest Service, Rocky Mountain Research Station, Fort Collins, p 49

van Wagtendonk JW, Root RR, Key CH (2004) Comparison of AVIRIS and Landsat ETM + detection capabilities for burn severity. Remote Sens Environ 92:397–408

Rockfall and Debris Flow Hazards After Summer Wildfires in Cerreto Sannita, Benevento, Italy

Guido U. Guasti, Alberto Caprinali, and Lucia Majorca

Abstract

Wildfires transform large areas on highly dangerous slopes and create unsustainable risks where roads, railroads, or buildings are at the foot of such slopes. The casual relationship between summer wildfires and rockfall and the efforts to mitigate the resulting hazards was carried out. In order to minimize these hazards a stabilization system was put in place along a main road in the Province of Benevento, Southern Italy, connecting Cerreto Sannita to Cusano Mutri.

After summer wildfires, it became apparent that continuous rockfall from the slopes was becoming increasingly dangerous. This rockfall frequency was brought about by the lack of vegetation in the form of medium to tall trees acting as natural barriers and of surface grass serving to control erosion.

Sections of slopes were left bare after the fires meaning that the roots of the former vegetation could no longer help to maintain soil in place.

As such, a variety of factors could easily have triggered the frequently jointed limestone outcropping to collapse, including seismic forces, heavy rain, wind, wild animals, evolving from simple rockfalls to debris flow along main gullies, from the crest of the cliff to the road underneath.

Furthermore, it is likely that the high temperatures reached in the fires induced a change of stress state itself, increasing the likelihood of single blocks falling.

The adopted solution to restoring conditions of basic safety along the road was implemented in two different steps.

Firstly, climbers walked all along the slope marking and counting all the unstable rocky boulders, and cleaning any block bigger than 0.30 m. During this step, road traffic was periodically stopped. Larger blocks in inaccessible areas were treated with high resistance steel mesh and rock anchors, with the aim of actively reinforcing the surface.

In a second step, in areas where the joints were so frequent that the drilling was a danger to the workers themselves, a passive protection measure was adopted consisting of highly specialised and well performing rockfall barriers.

Once safety was ensured by means of the above solutions, further potential points of instability were directly treated with standard techniques, with environmental impact given

G.U. Guasti (✉) • A. Caprinali
Geobrugg Italia s.r.l. – 42, Via C.Jannozzi – I-20097 San Donato Milanese
e-mail: guido.guasti@geobrugg.com; alberto.caprinali@geobrugg.com

L. Majorca
Geobrugg Italia s.r.l. – Contrada Spalla, Traversa Bowling – I-96010 Melilli – Siracusa
e-mail: lucia.majorca@geobrugg.com

C. Margottini et al. (eds.), *Landslide Science and Practice*, Vol. 4,
DOI 10.1007/978-3-642-31337-0_28,

constant consideration. For instance, allowing vegetation growth alongside the aesthetic perspective from the vantage point of the road.

Consequences of further wildfires were considered when choosing the type of coating designed to prevent the corrosion of the adopted measures' steel components. In the future, new fires in the cliffs are not expected to lead to further rockfall hazard in the sites where the project has been implemented.

Keywords
Wildfires • Campania Italy • Rockfall • Slope Stabilization • Rockfall kits • ETAG 27 Standards

Introduction

Along the portion of Strada Provinciale *Monte Cigno* connecting the small villages of Cerreto Sannita to Cusano Mutri, between Ponte Risecco and Madonna del Carmine, in Benevento Province, Southern Italy, rockfall and debris flow activity have been occurring for many years in several episodes (Figs. 1 and 2).

Basically, as it happens everywhere, rockfall occurred after severe or long lasting rain fall. But it became unsustainable to the local road authority after the dramatic summers 2006 and 2007, noteable for the many wildfires that hit the hilly areas for hours in spite of the brave work of firemen and the air helicopter hard fight against them.

As reported by Rorem (2004, 2005) fires leave the slopes and natural draining barren of trees and ground cover, exposing soil to erosion. A consequence of such a heavy exposure to erosion *latu sensu* at Benevento was the high risk for travellers driving at the bottom of the slopes. As a matter of fact, some car accidents and slight injuries have been reported after rockfall, luckily without fatalities.

Framework of the Area

The area is well known from a gravitational phenomena point of view, because of fall of single rocks and, as we see later, small debris flows along the main gullies.

The hill has terracing from the toe to the top of the slopes. These were installed in order to slow the path of rocks and as a matter of fact have been the only risk mitigation measure built in the ancient times (Fig. 3).

In the 1950s, the area has been subjected to reforestation with the aim to prevent rockfall, as natural barrier, onto the main road where commercial and touristic traffic was increasing year by year. This measure has been on one hand successful, but in the other hand exposed the areas to wild fires.

Fig. 1 View of the stiff rocky slope, over the Strada Provinciale Monte Cigno

More recently, some steel rockfall barriers has been built but the frequent rockfall severely damaged those barriers or even broke them down.

Given the above situation, after a huge wildfire occurred on Summer 2007 which caused several rockfall, the Amministrazione Provinciale's Road Authority wanted to characterize the current situation of the large burned area. To achieve this goal, it instructed a specialized company to describe the whole area by means of direct surveys (basically with alpine techniques), topographic surveys and laser scanner of the main cliffs. These steps actually were part of the first approach to the problem, with the aim to have a clearer idea of the situation and to determine, after a preliminary design of modern risk assessment techniques, the funds necessary to the risk mitigation to an acceptable level (Fig. 4).

Survey Results

The results of this analysis enabled the defining of different danger levels, among a large area included between contour level 380 m (max altitude of the road) and 600 m (peak of the main hill). The area has been divided into several sub-zones,

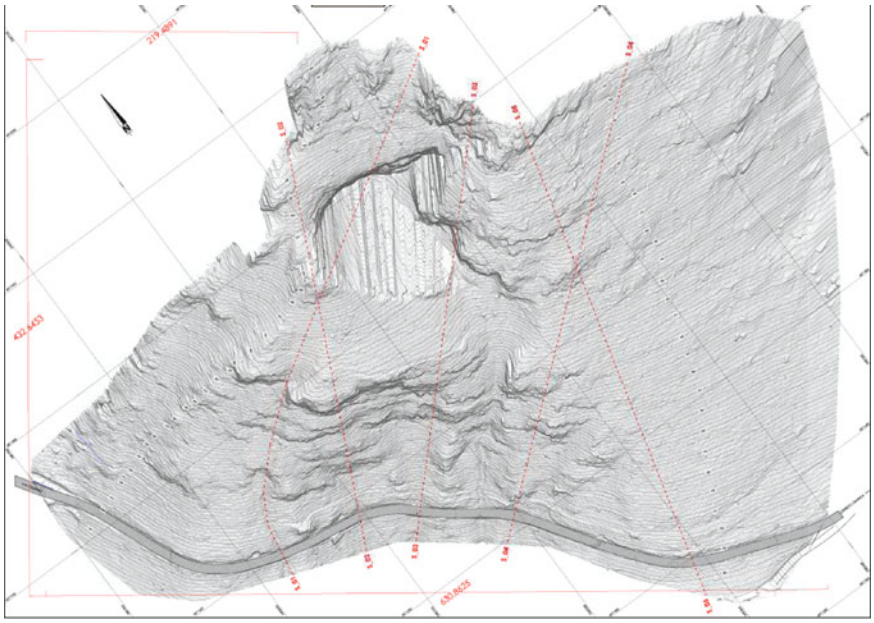

Fig. 2 Laser scanner topography

Fig. 3 Panoramic view of the area

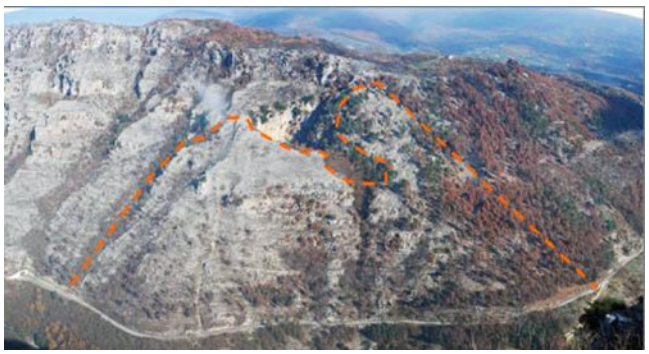

Fig. 4 Overview of the whole investigated area

either from the geomorphological or geometrical aspects, resulting basically in a risk priority scale.

All the cliffs are interrupted by shallow gullies which after the previously mentioned wild fire showed debris flows phenomena. However, the gullies more often are preferential paths for directing rocks or boulders to the road underneath. Because the area is in the southern Italy, rainfalls are not usually heavy.

The geological and structural set up of the rocky cliffs is controlled by stratificated layers dipping gently into the slope (Fig. 5).

Other joint sets are frequent as it is usual in massive limestone and marls, basically found in K1 and K2 quasi-

Fig. 5 Typical slope's stratification layer

Fig. 6 Deep collapsed area as a result of intense karst activity

Fig. 7 Superficial karst activity on limestones

perpendicular to the strata. Persistence and aperture of the main joints are fair, as it is for the other parameters describing rock mass quality, according ISRM (1978) and Bieniawsky (1989).

Important karst features are visible on different scale, either macro-scale or micro-scale (Figs. 6 and 7).

Another important aspect is the tectonic evidences of "recent" events. It is well to remember that the area is part of the Appennines, a young (from the geological point of view) mountain chain running along Italy from North to South, and that in the 1980 a severe earthquake (M = 6,9° Richter) hit the near province of Avellino (Fig. 8).

As results of the above survey, sub-zones from A to F were defined: each sub-zone has been carefully studied in order to find out the main features, the probable evolution, to evaluate the current risk and finally to identify the countermeasures to reduce or minimize such a risk.

Mechanisms of failures of blocks and masses have been investigated by means of the common techniques and a simulation of rockfall along the slopes has been performed with the program Rocfall by Hoek (Figs. 9 and 10).

Of special interest were the findings in sub-zone E. There, several lines of rockfall barriers have been built in the past, but due to the daily rockfall from the wildfires, the barriers are severely damaged and no longer useful (Figs. 11 and 12).

Besides that, one has to say that those barriers were built before any established standards existed so that any manufacturer relied on its own experience, skills or tests but actually without any certification that the barrier was suitable for such a purpose. Today things have changed, specific and stringent European standards have been in force since February 2008. So both local administrators and contractors are strictly required to install only certificated barrier according that standard (ETAG 27) issued by EOTA Organisation, Bruxelles (EOTA 2008).

It is interesting also to appreciate the behavior of a barrier like the one damaged at Cerreto Sannita involved in wild fires. The plastic box where the heart of the braking elements are located can easily melt, causing the inefficiency of the whole system (Fig. 13).

In a technical report commissioned by the National Roads Authority (ANAS – Ente Nazionale per le Strade) the authors of this paper (Guasti 2002) describe the damages that occurred within the same type of barriers and their residual efficiency after wildfires. Designed to stop boulders with 1,750 kJ of kinetic energy, it could be said that such barriers have an energy absorption limit far below that figure, due to reduced performance of brakes shown in the following picture (Fig. 14).

As conclusion of the first phase it was pointed out that most of the areas had and still have poor to medium geomechanical characteristics and that a large number of rock boulders, even up to several cubic meters in volume were about to fall.

Jointed rock outcrops, rather that rock debris accumulated on morphological obstacles are frequent to find, in a way that due to seismic waves, human activity (mining), fauna's movements or heavy rain periods would easily trigger new slides and flows, which would not encounter significant obstacles or, worse, would not find anything but barren rock since the soil and vegetation have been burned away.

Furthermore, the abandoned lands maintenance by farmers adds new reasons for landslides to fall.

The high instability conditions of the slopes, become more dramatic by the wildfires, and the total absence of controls and maintenance for the protective infrastructures installed over the last years, were considered the main cause of the described situation of widespread hazard of the *Monte Cigno* road users.

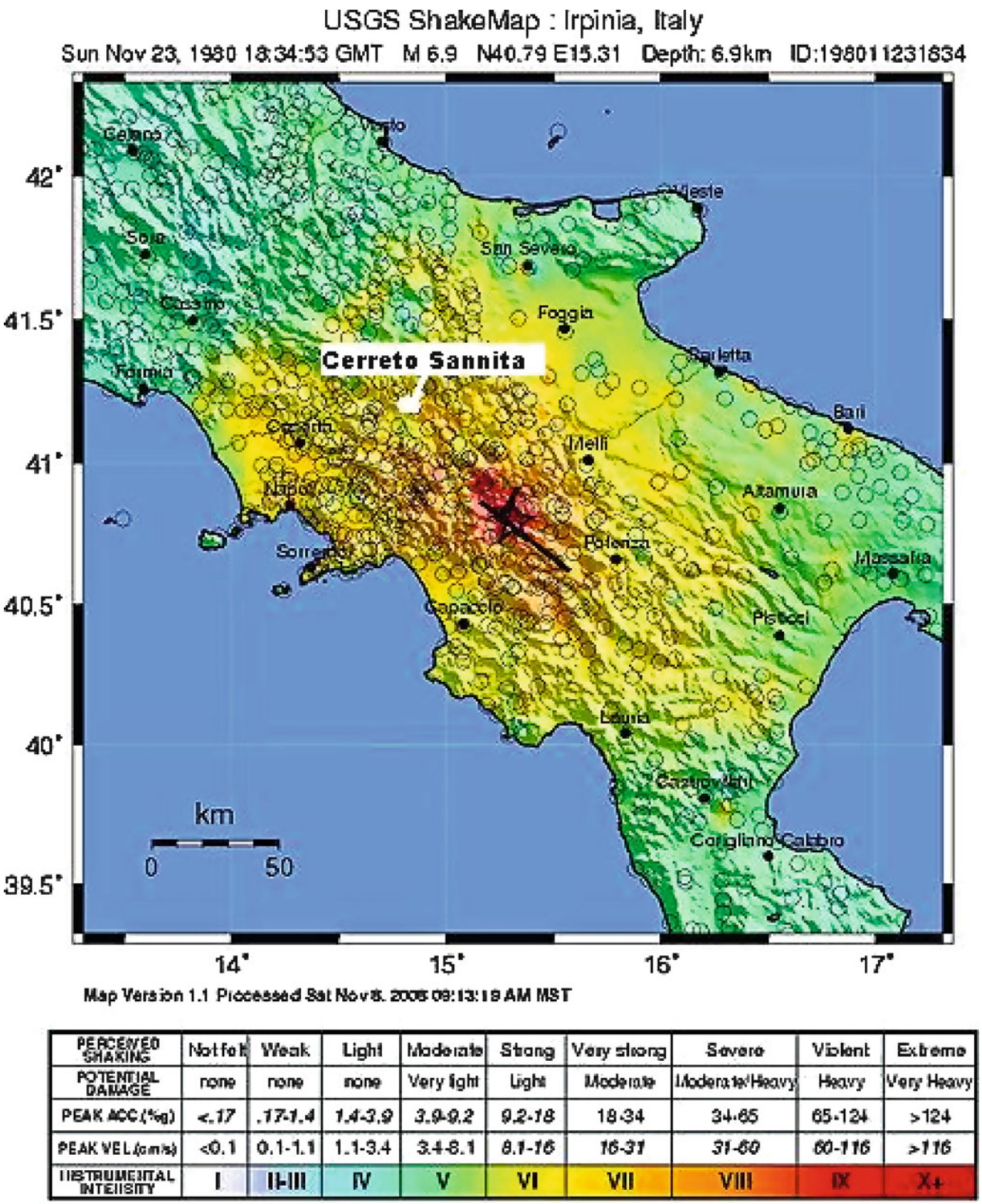

PERCEIVED SHAKING	Not felt	Weak	Light	Moderate	Strong	Very strong	Severe	Violent	Extreme
POTENTIAL DAMAGE	none	none	none	Very light	Light	Moderate	Moderate/Heavy	Heavy	Very Heavy
PEAK ACC.(%g)	<.17	.17-1.4	1.4-3.9	3.9-9.2	9.2-18	18-34	34-65	65-124	>124
PEAK VEL.(cm/s)	<0.1	0.1-1.1	1.1-3.4	3.4-8.1	8.1-16	16-31	31-60	60-116	>116
INSTRUMENTAL INTENSITY	I	II-III	IV	V	VI	VII	VIII	IX	X+

Fig. 8 Shake map of Irpinia earthquake, Italy 1980 (From USGS)

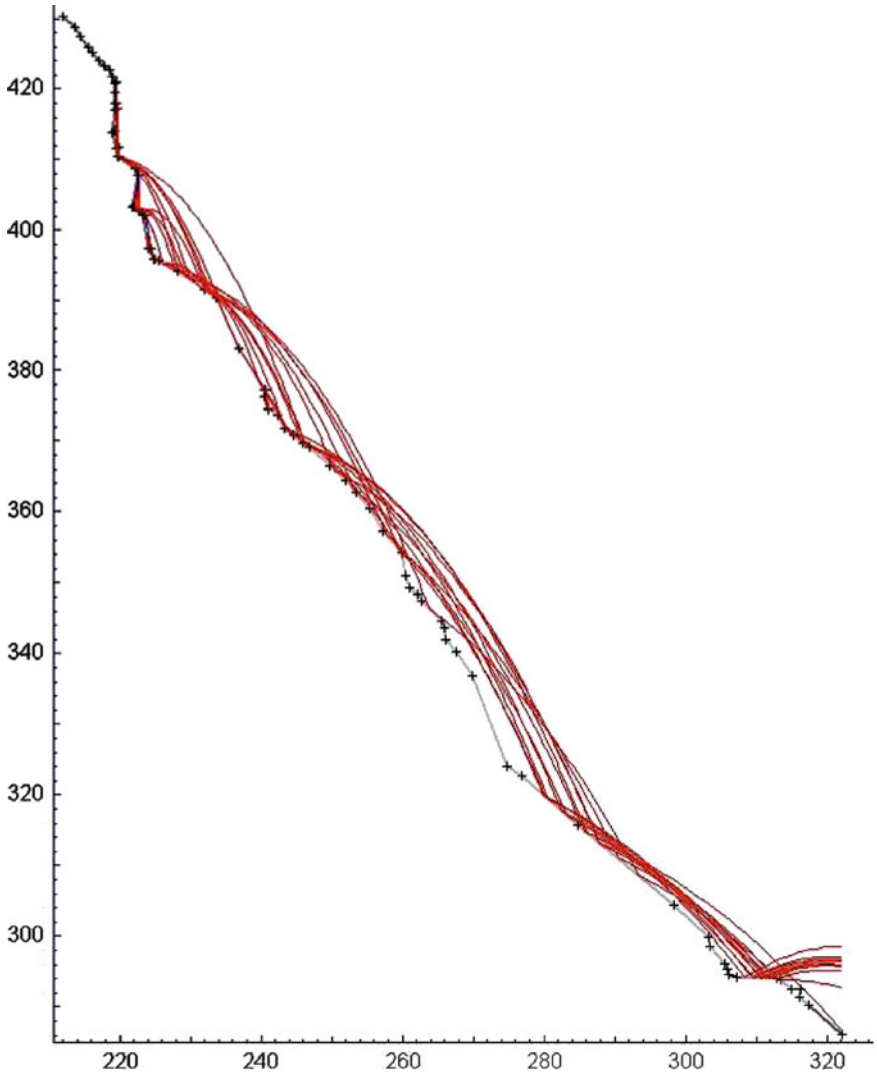

Fig. 9 Simulation of rockfall paths along the slopes – Rocfall Software – Prof. Hoek (*Hoek Evert - Rocfall simulation program, version 2.0 – www.rocscience.com*)

All these notes lead the Road Authority to better plan the different steps of works according to the funds it could get by National Government.

Countermeasures

After letting the Amministrazione Provinciale fully understood the report, the second phase has started. This involved the design of all the countermeasures needed to minimize the risk.

Concerning slope instability, zones included between 440 m above s.l. showed the highest danger level. Due to highly jointed rocky outcrops, it was subject to rockfall events with unforeseeable bouncing paths and also debris flow from the top of the area to the road during large rain falls.

Below 440 m, where the slope is mainly vertical, there was a medium to high danger level. In the lateral slope, i.e. the South-Eastern part overhanging the road within the fire damaged areas, it was noticed a medium danger level, resulted from the high rockfall probability and conditions related to severe deforestation and scouring.

Another problem, certainly not less important, was represented by the northernmost of the two most important discharge gullies, one which runs above the road tunnel and the otherinear the entrance. There, the protection infrastructure built near the tunnel is represented by an old-fashioned rockfall protection systems, installed in several lines with obvious inadequate defensive ability; two of these fences laying at ground almost eradicated, and some other barriers presenting untensioned ropes.

Generally speaking, without difference among the subzones, the countermeasures were:

- Slope's surficial survey with the localization of possible falling rocks, fallen stones and debris with important dimensions.
- Slopes cleaning and rocks demolition by levers and high pressurized outfits, like hydraulic jack and reamers (Figs. 15 and 16).

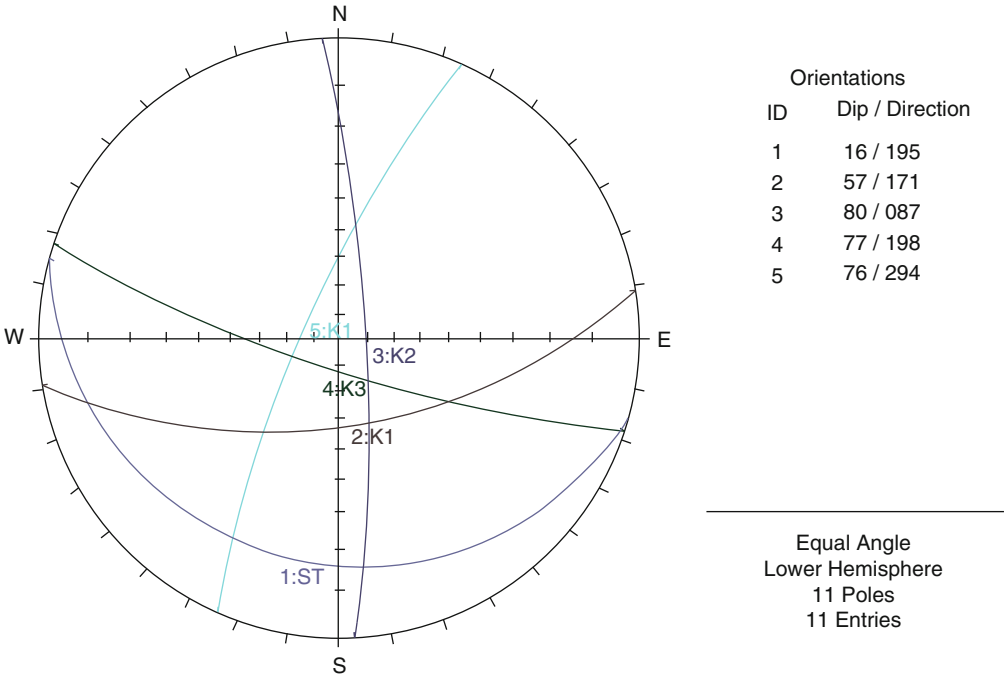

Fig. 10 Geomechanical studies of rock stability

Fig. 11 Boulders passing underneath old-concept rockfall barrier

Fig. 12 Crashed barrier after rockfall event

Rock volumes bigger than 0,30 m^3 have been cleared, when possible by chemical expansive with disrupting effects mortar (Power Bristar®) poured by gravity in holes drilled with hand equipment. At the end, the road was eventually cleaned to allow the usual traffic keeps its routine.

The two steps have been managed by high specialized crew (climbers) moving along the slopes with alpine techniques, with the support of an helicopter for stuff and outfits carriage on site.

The phase of cleaning and demolition on unstable masses has a fundamental importance for worker safety and works durability. Every instable rock or soil portion has to be removed before approaching the slopes because workers cannot see what's happening above their head. The way workers engaged in activities allows no escape way, thus the cleaning must be done very carefully and with attention to details. After the finishing of works, all the structures are meant to last as long as possible, waiting for the event for which they are installed . the cleaning limits daily debris or small slides which could affect their efficiency in the long term.

In areas where the detailed cleaning made no sense because of the large number of big boulders and where it was not possible remove them to decrease the rockfall hazards, steel nails and high resistance steel nets were

Fig. 13 Braking elements burned by wildfires

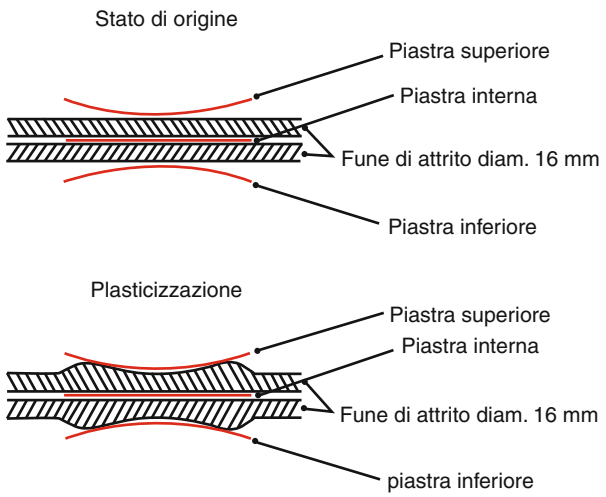

Fig. 14 Reduction of performance of brake elements

installed. For the active stabilization of the stiff rocky slopes SPIDER® S4 system was installed, produced by GEOBRUGG SA (Romanshorn, CH), with a secondary mesh, for a total covered surface of 140 m (Fig. 17).

Fig. 15 Boulders on the road after slopes cleaning

Fig. 16 Dimensions of bigger boulders removed during cleaning

Fig. 17 Active stabilization of stiff rocky slopes with SPIDER® S4

Fig. 18 Rockfall barrier GEOBRUGG RXI-050 on the top of the cliff

Meshes, galvanized by GEOBRUGG SUPERCOATING® technology, which is Zinc-Aluminum alloy for increasing the resistance against chemical etching, were anchored to the slope by passive GEWI steel nails, set with an almost regular 3 × 3 m grid and with a diameter of 25 mm.

In some areas where it was actually dangerous even for workers to directly approach the slope surface because of high rockfall hazard, a passive defensive system has been built. This is a rockfall barriers GEOBRUGG RXI-050 (500 kJ), which are set with ROCCO® ring nets, with a length of 50 m and height 3.

The design energy had been defined after rockfall path simulations developed by a the contractor's specialized consultant.

At that time, the above mentioned ETAG 27 standard were not into force, thus the Administration wanted in any case the maximum quality available in the market. So, the decision of the engineer went to rockfall barriers tested and certified according the Swiss standards, issued on 2001 and still valid in Switzerland being that country out of the EC – European Community (Fig. 18).

Works were carried out between 28/11/2007 and 7/12/2007 in a first phase and between 16/01/2008 and 01/03/2008 in a second phase, more than 1 month earlier with respect to the agreed date.

Conclusions

A portion of the Monte Cigno road were affected by severe rockfall risk, increased recently by a number of reasons, included the wild fires hitting large wooded areas. After long and detailed survey of the slopes, a detailed design has been carried out according the willing of the Amministrazione Provinciale di Benevento, road maintenance department.

Protection measure consisted in a deep cleaning of the main areas, both manually and mechanically, and afterwards in both active and passive protection systems. For its proven quality and long term reliability, the systems have been indicated by the engineer among the production of a specialized manufacturers, Geobrugg AG of Switzerland. Spider S4 systems and rockfall barrier RXI-050 were installed by a specialized contractor with alpine techniques, in short time and safety.

Acknowledgments The authors wish to thank the Amministrazione Provinciale di Benevento, and SLOPE Consultants (Trento) for their cooperation and collection of data.

References

Bieniawski ZT (1989) Engineering rock mass classifications. Wiley, New York

ETAG 27 GUIDELINE FOR EUROPEAN TECHNICAL APPROVAL of FALLING ROCK PROTECTION KITS Edition 2008 - 02 - 01 - EOTA, B-1040 Brussels

Guasti GU (2002) Indagine di accertamento della servibilità residua delle strutture di protezione dalla caduta massi tra il km 221 + 529 ed il km 222 + 280 lungo la strada statale 18 "Tirrena Inferiore" a seguito di incendi

ISRM (1978) Suggested methods for the quantitative description of discontinuities in rock masses. Int J Rock Mech Min Sci Geomech Abstr 15(6):319–368

Rorem EJ (2004) Debris flow remediation. In: 55th annual highway geology symposium, Kansas City

Rorem EJ (2005) Flexible debris flow barriers performance in fire burned areas, State Route 18, San Bernardino County, CA. In: 56th annual highway geology symposium, Wilmington

Flexible Debris Flow Barriers in Fire Burned Areas

Erik Rorem, Corinna Wendeler, and Andrea Roth

Abstract

A design model for debris flow barriers (based on a finite element software program, but not included in the paper) has been calibrated and verified by real-scale field-testing, under supervision/involvement of the Swiss Federal Institute for Forest Snow and Landscape (WSL) and is the only known valid model for properly dimensioning a corresponding tested ring net barrier type in debris flow applications (Volkwein et al. Proceedings of 5th DFHM conference, Padua, 2011). In California, this concept has been applied to several project cases involving debris flow sites along sections of highway where wildfires have denuded the adjacent slopes of natural vegetation, making them very vulnerable to debris flow. These barriers have been installed and impacted by actual debris flows, have been cleaned out, and have been impacted by multiple subsequent debris flows. The performance of these barriers has successfully prevented loss of the roadways by preventing scouring and washout, as compared to similar areas with no such protection.

Keywords

Debris flow • Barrier • Wildfires

Introduction

Following widespread wildfires in late 2003 near San Bernardino, CA and subsequent debris flows resulting from heavy rains, The California Department of Transportation (Caltrans) undertook efforts to prevent further debris flow damage to roads in the area. Much of the prior debris flow damage that occurred on a section of State Route 18 referred to as "The Narrows" was a result of debris clogging culverts, allowing water to then run over the roadway. The further erosion process of debris flow in burned areas with poor vegetation cover overtopping the road and eroding the lower part of the slope can be seen in (Fig. 1).

After repairing the road damage, various measures were taken to prevent future clogging of culverts. One such measure was the installation of so-called VX/UX flexible debris flow barriers in ten debris flow channels intersecting the road along this section (Rorem 2004).

The VX/UX barriers are an adaption of the ROCCO® ring net rockfall barrier, with variations to account for the significantly different loading characteristics of debris flow compared to rockfall. Using a unique barrier computer simulation program, a concept has been developed to predict the loading characteristics from debris flows. For this project, Caltrans personnel collected the required field data for each debris flow channel including such variables as expected debris volumes and velocities, flow composition and channel gradient, allowing the determination of debris flow loading conditions for each site using early versions of this model. Using this information, barriers were then designed to accommodate the expected loading conditions at each site.

E. Rorem (✉)
Geobrugg North America, LLC, 22 Centro Algodones, Algodones 87001, USA
e-mail: Erik.rorem@geobrugg.com

C. Wendeler • A. Roth
Geobrugg AG – Protection Systems, Aachstrasse 11, Romanshorn CH-8590, Switzerland

C. Margottini et al. (eds.), *Landslide Science and Practice*, Vol. 4,
DOI 10.1007/978-3-642-31337-0_29,

Fig. 1 Slope denuded of vegetation from wildfire and subsequent erosion (Courtesy Duffy)

Research

The first known 1:1 testing of flexible barriers in the USA to determine loading characteristics from debris flow impacts was conducted in 1996 at the USGS debris flow flume research facility in Blue River, Oregon (Duffy 1998). During six tests conducted at this site, various instrumentation was used to record flow velocities, forces on various barrier elements, and debris flow character and barrier response in a general way. The most important finding from these tests from a design standpoint was the fact that despite the relatively large openings of ring nets, they can be very effective for purposes of retaining even fine-grained mudflows. Additionally, the tests demonstrated that ring nets perform better than woven wire rope nets due to the higher flexibility, higher energy absorption capacity, better load distribution to the support infrastructure, less need for repair, and better adaptability to the irregular terrain that can be expected in debris flow channels.

Another test series was conducted in Lobental, Germany by the Technical University of Munich to test the performance of flexible barriers to impacts from torrents laden with woody debris (Rimböck 2003). In these tests, a barrier was subjected to impacts from torrents laden with timber and other woody debris, allowing water to pass but restraining the debris. Copious loading data was collected from various instrumentation in the support infrastructure. Results from this project and the Oregon tests enabled and formed the initial basis for describing expected barrier loading from debris flows.

The early tests led to a more comprehensive full-scale test series at the Ilgraben debris flow observation station in the Canton of Valais, Switzerland, leading to more accurate modeling of debris flow loads. Flexible ring net barriers were installed in this channel, and were fully instrumented to collect data such as flow velocity, flow density, loading to various elements of the barriers and so forth. Data collection then was executed upon impacts from naturally occurring debris flows. A computer program called FARO developed as part of a Swiss Commission for Technology and Innovation project to simulate the response of ring net barriers to dynamic loading was used to verify and validate a new barrier dimensioning concept based on flow pressures acting on flexible barriers (Wendeler et al. 2008).

Barrier Systems

The barriers at The Narrows in California were installed in early summer of 2004. A total of ten such barriers were installed in expected debris flow channels, close to the roadway on the upslope side of the road. Design heights ranged from 3.0 to 8.0 m, widths ranged from 9.3 to 22.0 m, and expected flow volumes ranged from 100 to 500 m^3. For barriers less than 12 m wide, no posts were required (VX barriers). For barriers somewhat wider than 12 m, one post was placed as additional span support (UX barriers). Some barriers required more than one post due to the large channel widths (UX barriers). All ROCCO® ring nets were backed with a 25 mm mesh size chainlink, or comparable hexagonal wire mesh in order to prevent passage of material smaller than the openings of the 300 mm diameter rings in the ring nets.

Performance

Several events subsequent to installation of these barriers provided very quick validation of the concept and an opportunity to evaluate performance.

October 2004 Storms

In mid October, four successive days of rain produced 21.6 cm of precipitation in the area, with rain measuring 8.9 cm in one of those days. This resulted in widespread debris flows in the area, including at all ten of the VX/UX barrier sites; the first true test of the concept on a reasonable scale. In all, the ten barriers successfully contained approximately 1,000 m^3 of debris. In the interest of brevity, results from the three most notable sites will be summarized. It should be noted that data collected after the events were estimates done in the interest of being able to compare to predicted estimate values. The actual events were not observed as they occurred, so data such as actual velocity was not available. This was not a pure research or laboratory project involving precisely controlled procedure, measurement and detailed analysis. Rather, this was an actual

Fig. 2 Site 1 immediately after install (Courtesy Duffy)

Fig. 3 Site 1 October 2004 debris (Courtesy Duffy)

mitigation project putting the concepts into practical use, that enabled collection of field observations and general validation of the concept in real field conditions.

Site 1: UX Barrier (Fig. 2).
Design debris volume – 360 m^3
Approximate slope angle – 48°
Predicted flow velocity – 5.1 m/s
Barrier height – 5.0 m
Barrier width at top support rope – 17.0 m
Event debris volume – 161 m^3
Event debris depth at barrier – 2.3 m
Event debris composition – soil 35 %, rocks/boulders 40 %, vegetation 25 %

No debris passed the barrier, and there was no barrier damage (Fig. 3). Some braking element engagement was observed however, including complete engagement on one of the post tieback ropes.

Site 2: UX Barrier (Fig. 4).
Design debris volume – 315 m^3
Approximate slope angle – 48°
Predicted flow velocity – 4.4 m/s
Barrier height – 5.0 m
Barrier width at top support rope – 22.0 m
Event debris volume – 263 m^3
Event debris depth at barrier – 3.2 m
Event debris composition – soil 35 %, rocks/boulders 40 %, vegetation 25 %, but also with very large boulders, and four trees trunks of ~1 m. diameter × 9 m. long.

A small amount of debris did pass the barrier due to rupture of the bottom support ropes (Fig. 5). It appeared that a direct impact to this rope by one of the large tree trunks was the probable cause of the breakage. Some braking element engagement observed.

Fig. 4 Site 2 after installation

Site 7: VX Barrier (Fig. 6).
Design debris volume – 100 m^3
Approximate slope angle – 60°
Predicted flow velocity – 4.9 m/s
Barrier height – 8.0 m
Barrier width at top support rope – 10.0 m
Event debris volume – 33 m^3 (Fig. 7).
Event debris depth at barrier – 2.75 m
Event debris composition – soil 70 %, rocks 30 %, vegetation 0 %

No barrier damage or significant braking element engagement was observed at any of the other seven sites. For all practical purposes, with the exception of site 2, all debris was contained other than insignificant amounts of sand passing. None of the barriers were overtopped, and no debris passed around the sides. In summary, overall performance was a great success, with remaining capacity in most of the

Fig. 5 Site 2 October 2004 debris (Courtesy Duffy)

Fig. 6 Site 7 after install

Fig. 7 Site 7 October 2004 debris (Courtesy Duffy)

Fig. 8 Site 7 December 2010 debris (Courtesy Duffy)

barriers, even before cleanout. Cleanout was undertaken nevertheless to maximize capacity for future events.

Winter 2004/2005 Storms

The amount of rainfall produced by the winter storms of 2004/2005 had been unprecedented. The barriers installed at The Narrows were thus tested to the extreme by multiple events during that winter. Several of the barriers were completely filled with debris, and some were even overtopped. Such volumes and frequency could not have been reasonably anticipated. Normally, the susceptibility of fire burned slopes to debris flow diminishes after a few years. These barriers were primarily intended to provide protection during such a time period, assuming normal or somewhat above normal precipitation. The fact that there were unprecedented rainfall events during such a time period is astonishing.

December 2010 Storms

The barriers at The Narrows along State Route 18 are impacted continually during the rainy season, year after year. But heavy rains in December 2010 resulted in another series of significant impacts (Fig. 8). Because the barriers have performed well year after year, proving the value, cleanout and minor maintenance have become routine and

Fig. 9 Braking element ring completely closed in upslope tieback rope (Courtesy Duffy)

Fig. 10 Fine material and organic matter retained by nets and mesh (Courtesy Duffy)

thus data on these later individual events was no longer collected. Nevertheless, these most recent events further validate the concept and give opportunity to point out other observations such as braking element performance and retention of fine material.

We know that some of the debris impacts were extreme, as evidenced by complete engagement of braking elements in some areas. Brake ring elements are force dissipating devices acting as a sort of mechanical fuse in the support ropes and upslope tieback ropes. When new, these brake rings have a diameter of approximately 0.5 m. When fully activated, this ring completely closes (Fig. 9).

Observation of the debris contained in the nets showed retention of significant organic matter and fine material. Some fine material did pass underneath the nets, due to the small gap between the bottom support rope and the ground which is allowed in order to permit normal runoff to pass and not accumulate in the nets. As a possible solution method for this problem see the following section "observations". But very little of this fine material actually passed through the nets (Fig. 10). Because these more recent events occurred years after the fires burned all vegetation, some vegetation has had an opportunity to return and was contained by the finer chainlink backing on the nets.

During this storm event, no sections of State Route 18 protected by these barriers were damaged, allowing the road to remain open. Sections of nearby route 330 which was not protected with this type of debris flow barrier however were washed out, necessitating closure of that road and a detour via route 18. Estimating the economic impact to local communities of such closures, though surely significant, is beyond the scope of this paper. Furthermore, the savings from not having to perform road repair surely justifies the initial investment in protective barriers plus barrier maintenance costs.

Observations

Though much of the needed cleanout and repairs were completed after the October events, not all required maintenance was completed prior to these back-to-back and continuous winter events. Further barrier damage was observed from these winter events, as it was not anticipated that the barriers would be subjected to such relentless and unusually extreme events. Consequently, barriers at some of the locations were removed, while others were repaired. Regardless, the barriers did contain large volumes of debris and did perform as intended for the expected events, and certainly prevented extensive roadway damage, road closures, and significant costs associated with roadway maintenance.

Much has been learned from these many events, and this information has been extremely useful in fine tuning future designs. Facilitation of barrier cleanout after significant events has also been improved as a result of these observations. For barriers that are not of great height, cleanout can be largely done with backhoes, as was done at The Narrows. The seam rope used for connecting net panels together and to the side ropes (instead of the normal shackling) also proved to be helpful. Modifications to the seaming have been made on subsequent installations to improve barrier performance and to better facilitate cleanout, including stronger seam ropes and seaming orientation. Additionally, modifications were made in the shackling connections that are still used for connecting the nets to the top support rope, because nets that are extremely loaded put the top rope in significant tension making removal of the shackles difficult.

Further investigations were performed for so-called shallow landslide barriers which were tested with artificially released mudflows containing more or less fine materials. Subsequently, a so-called "erosion control apron" was

Fig. 11 Big Sur flexible barrier

developed to avoid lifting up the lower support ropes and avoid passing of finer material underneath the barrier (Bugnion and Wendeler 2010).

Other California Installations

After the installations at The Narrows, Caltrans installed flexible debris flow barriers at several other post-fire locations, including at Gaviota Pass along coastal highway 101 in southern California, and along coastal highway 1 in the central California Big Sur region (Fig. 11).

Barriers of various heights, configurations and ring net sizes were installed depending on local conditions and modeling results. Some barriers were equipped with large than normal rings (1–1.5 m diameter) to trap only the largest of debris that might clog large culverts, and to allow smaller debris to pass. While the barriers at Gaviota Pass have been filled with debris and cleanout out many times since being installed in 2005, the barriers installed at Big Sur have yet to be impacted by debris flow since being installed in 2008.

Additionally, flexible barriers were installed on the island of Catalina by private owners for temporary debris flow protection in a post-fire location, none of which have been impacted to date.

Conclusions and Outlook

Invaluable information has been gained and lessons learned from this most extensive application of debris flow barriers to date anywhere in the world. Anticipating volumes and the nature of expected debris flows can be very difficult. Time and effort spent to determine critical dimensioning parameters is time well spent, and is very important. Reasonable probabilities must nevertheless be employed, to maximize benefit versus costs, meaning that unusually extreme events may overwhelm the designed barriers. There are limitations, and repair may be necessary. Chainlink or finer mesh may or may not be beneficial. In cases of the barriers protecting culverts from clogging with debris, fines and water should be allowed to pass. Some situations may justify retaining more of the fine material.

These flexible ring net barriers and the associated dimensioning modeling represent the state of the art for such applications and are superior to many other available options including check dams, large concrete structures, or other imposing structures. Larger volumes can be achieved by so-called "multi-level applications" wherein a series of barriers is installed up the channel, as explained in Wendeler et al. 2008 and Speerli et al. 2010. The first successful filling event of such a multilevel flexible barrier application happened in 2010 in Spain and retained with eight barriers around 25,000 m^3 of material (Raimat et al. 2010). Like the California sites, the slope at this Spain site is only sparsely covered by vegetation, so the erosion process in this torrent is more or less similar to burned areas.

References

Bugnion L, Wendeler C (2010) Shallow landslide full-scale experiments in combination with testing of flexible barriers. In: Debris flow conference 2010, Milano

Duffy JD (1998) Case studies on debris and mudslide barrier systems in California. In: Proceedings of one day seminar on planning design load Implementation of debris flow and rockfall hazards mitigation methods, Hong Kong, pp 77–90

Duffy J (2005) Personal communication

Duffy J (2005) Fire related debris flow mitigation in San Bernardino county, California. In: Presented to 84th annual meeting transportation research board

Raimat C, Luis R, Wendeler C, (2010) Technical documentation on behaviour of VX barriers and initial results from the pioneer monitoring station in Erill & Portainé/Spain

Rimböck A (2003) Schemmholzrückhalt in Wildbächen. Ph.d. thesis, Technical University of Munich, Germany

Rorem E (2004) Debris flow remediation. In: Proceedings of the 55th highway geology symposium, Kansas City

Speerli J, Hersperger R, Wendeler C, Roth A (2010) Physical modeling of debris flows over flexible ring-net barriers. In: Proceedings of IGPMG 2010 conference, Zurich

Wendeler C, Volkwein A, Roth A, Denk M, Wartmann S (2008) Field measurements used for numerical modeling of flexible debris flow barriers. In: Proceedings of international symposium interpraevent. Dornbirn

Part IV

Landslides and Extreme Weather

Introduction by Hiroshi Fukuoka[1] and Gabriele Scarascia Mugnozza[2]

1) Research Centre on Landslides, Kyoto University, Uji, Japan
2) University of Rome "La Sapienza", Department of Earth Sciences, Rome, Italy

Most landslides are associated with heavy rainstorms, while the frequency of extraordinary severe rainfall events associated with numerous landslides are apparently increasing in most countries for these decades. This session was devoted to introduce recent advances in early warning, mapping, hazard assessment, and mechanism of landslides induced by extreme weather conditions. Nine papers were accepted and seven papers were presented at the oral session. Most of the papers focused on the precipitation data and tried to establish models to predict shallow landslides through empirical, probabilistic or hydrological approaches. Others are introduction of recent extreme rainfall-induced landslide events, and geotechnical approach to find mechanism of shallow landslides.

Among the papers devoted to developing landslide prediction models, Nawagamuwa et al. collected rainfall data of asian countries which induced landslides, and proposed an approach considering normalized cumulative rainfall from 6 days beyond a certain landslide till the day of occurrence. Segoni et al. introduced statistics of past more than 2,000 landslide cases and recent implementation of web GIS for issueing early warning of landslides using distributed raingauges based on 72 h meteorological rainfall forecasts and indivisual thresholds of critical cumulative rainfall for 25 small zones of Tuscany region. Peres et al. tried to define rainfall thresholds for early warning of rainfall-triggered landslides: the case of North-East Sicily using FLaIR model and hourly rain gauge data. Montrasio et al. introduced GIS-based shallow landslide slope stability calculation by application of water infiltration model in Italy and showed the possibility of establishing nation-wide early warning system. Morey et al. introduced application of open-source GIS-based to estimate volume of debris-mud flows.

As the number of networked rain gauges is increasing and hourly precipitation data are available online in the developed countries, the societal needs to develop effective and reliable landslide early warning system is serious and urgent. The reliability of the presented system and thresholds was discussed most in detail.

Among the papers which was devoted to geotechnical approach, Avelar et al. inroduced January 2011 landslide disaster in Rio de Janeiro, Brazil which was induced by extreme rainfall and killed about 1,500 residents. They showed geological analysis and correlation between soil properties and geotechnical behavior through direct shear test results of the saprolite soils, which they assumed as the key material in the landslide prone slope. Dok et al. introduced the tertiary creep behaviors reproduced in their ring shear apparatus at the final accelerating stage of the landslides, and showed that the two parameters that Fukuzono found in 1985 are no longer independent and had a linear relation each other.

The freqency of the extreme rainfalls are obviously increasing in most countries possibly as the global warming and climate change is progressing. Although numerous approaches from empirical, statistical, probabilistic have been proposed and evaluated intensely, while traditional geological, geomorphological, geotechnical, and hydrological approached have been conducted separately and independently. In the upcoming decades, effective and reliable integrated model of rainfall monitoring with hydrological and geotechnical parameters should be proposed and evaluated.

Recommending Regional Rainfall Threshold Values for Early Warning of Landslides in the Asian Region

Udeni P. Nawagamuwa, Rajinder K. Bhasin, Oddvar Kjekstad, and N.M.S.I. Arambepola

Abstract

Regional landslide hazard prediction and warning are still difficult targets to be achieved and a hot topic in the research of landslide hazards. It is necessary to investigate the possibility of interpreting landslide events in terms of the rainfall patterns immediately preceding the slide event. This can be further enhanced by taking the lithological conditions in to account. Rainfall threshold values vary from region to region due to differences in exiting soil characteristics and climatological patterns in different areas. This paper addresses the needs mentioned above and it includes the data and methods for recommending threshold values adopted by countries, such as Bhutan, Bangladesh, China, India, Indonesia, Nepal, Pakistan, Philippines, Sri Lanka, Thailand and Vietnam. A new approach is proposed considering normalized cumulative rainfall from 6 days beyond a certain landslide till the day of occurrence. Data from several countries such as Sri Lanka, India etc. have shown very promising outputs as per the application of the proposed methodology. However, it is clearly evident that the extreme rainfalls in a shorter duration could trigger disastrous landslides. This is confirmed by the data from countries such as Nepal, Bangladesh, etc. when the rainfall collected 3 days preceding the event till the landslide occurrences is considered.

Keywords

Landslides • Early warning • Rainfall threshold values

Introduction

In recent times landslides have increased both in frequency and intensity and have assumed catastrophic and disastrous proportions, causing extensive damage to life and property and posing great problems and serious challenges to man and his development process. This increase has been triggered by a combination of several attributes (geological, morphometric, climatic and anthropogenetic) that directly or indirectly cause slope instability, most of which (if not all) are either man-made or man-accelerated (Singh 2010).

Regional landslide hazard prediction and warning is still a difficult target to be achieved and a hot topic in the research of landslide hazards. In the past decade, the researchers mainly focused on the analysis of the combination of rainfall and geological environment. However, still the main focus in the developing countries is to develop such a model for regional uses despite knowing the benefits of advanced technologies enjoyed by well developed countries for early warning.

A review of available literature emphasizes the role of precipitation as an important control on the initiation of slope failures and provides evidence that landslides are

U.P. Nawagamuwa (✉)
Department of Civil Engineering, University of Moratuwa, Moratuwa, Sri Lanka
e-mail: udeni@uom.lk

R.K. Bhasin • O. Kjekstad
Norwegian Geotechnical Institute, Oslo, Norway

N. Arambepola
Asian Disaster Preparedness Center, Bangkok, Thailand

C. Margottini et al. (eds.), *Landslide Science and Practice*, Vol. 4,
DOI 10.1007/978-3-642-31337-0_30,

often triggered by meteo-climatic events that are in excess of some thresholds.

Except for few cases, almost all landslides in this region that have been investigated to date are known to be rain induced. Therefore, it is indeed necessary to investigate the possibility of interpreting landslide events in terms of the rainfall patterns immediately preceding the slide event. This can be further enhanced by taking the geological formation too in to account.

Rainfall threshold values vary from region to region due to differences in exiting soil characteristics and climatological patterns in different areas. Therefore, a complete study of the rainfall patterns in landslide prone areas and their records of landslides will help predict reasonable threshold values of rainfall and use them as a tool for landslide forecasting. With this, therefore, collection of critical rainfall values with sufficient geological data in the Asian region is of paramount importance for the benefit of the people who are vulnerable to landslides.

Regional Thresholds

Global Studies

Considerable efforts have been made to understand the triggers for landsliding in natural systems, with quite variable results. Rainfall, soil properties, and morphology are major factors controlling shallow landsliding. Crosta (1998) studied a series of meteorological events that triggered soil slips in northern Italy to define rainfall thresholds and to evaluate a possible regionalization. Soil properties, triggering rainfall, and local lithological and morphometrical settings of different sites had been used as input to an infiltration model. The approach allows the recognition of several triggering conditions in the Piedmont, Pre-Alpine and Alpine regions. This suggests the need for different rainfall thresholds with respect to those derived with other methods. Intensity versus rainfall duration relationships become particularly important when related to soil permeability and thickness, and demonstrate the role of antecedent precipitation.

Corominas and Moya (1999) found that the following thresholds (described below) exist for the upper basin of the Llobregat River, Eastern Pyrenees area in Spain. Without antecedent rainfall, high intensity and short duration rains triggered debris flows and shallow slides developed in colluvium and weathered rocks. A rainfall threshold of around 190 mm in 24 h initiated failures whereas more than 300 mm in 24–48 h were needed to cause widespread shallow landsliding. With antecedent rain, moderate intensity precipitation of at least 40 mm in 24 h reactivated mudslides and both rotational and translational slides affecting clayey and silty-clayey formations. In this case, several weeks and 200 mm of precipitation were needed to cause landslide reactivation. A similar approach is reported by Brand (1988) for Hong Kong, who found that if the 24 h antecedent rainfall exceeded 200 mm then the rainfall threshold for a large landslide event was 70 mm h^{-1}.

Caine (1980) established a worldwide threshold:

$$\mathbf{I} = 14.82\ \mathbf{D} - 0.39 \quad (1)$$

where: I is the rainfall intensity (mm h^{-1}), D is duration of rainfall (h)

This threshold applies over time periods of 10 min to 10 days. It is possible to modify the formula to take into consideration areas with high mean annual precipitations by considering the proportion of mean annual precipitation represented by any individual event.

Sri Lankan Thresholds

Bandara (2008) discussed the thresholds prepared after studying number of landslides in Sri Lanka with the correlation of the landslide occurrence and the daily rainfall of the incidence day or day before. According to the studies following generalized thresholds had been decided for the whole landslide prone areas of Sri Lanka.

Type one – Alert Warning – Rainfall exceed 75 mm within 24 h and continuing

Type two – Warning – Rainfall exceed 100 mm within 24 h and continuing

Type three – Evacuation warning – Rainfall exceed 150 mm within 24 h or 75 mm within an hour period and continuing

Those above three types of threshold limits are generally used all over Sri Lanka at present.

Indian Thresholds

Kuthari (2007) proposed a methodology in establishing precipitation thresholds for landslide initiation along with slope characterization using GIS-based modeling. The study had been carried out in the Alaknanda river catchment I Garhwal Himalayas, India. The catchment receives heavy precipitation between July and September. Thresholds were proposed based on 72-h precipitation and 15 days prior antecedent precipitation, if the daily rainfall is above a specified limit.

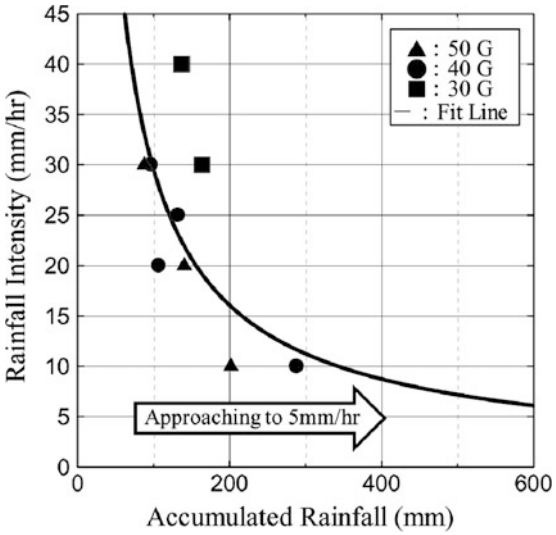

Fig. 1 Relationship between the intensity and the accumulated rainfall

Model Study in Japan

Although a number of rainfall threshold studies for landslide occuerences have been carried out in Japan, Kaneko et al. (2010) conducted centrifuge model tests to predict slope failures in sandy grounds and the Fig. 1 shows a variation between cumulative rainfall and rainfall intensity.

Studies Done in China

Tang et al. (2008) analyzed the mechanism of different rainfall infiltration at the loess plateau in the northeast of Shanxi province. The rainfall-triggered landslides had been summarized into the slow infiltration triggering mode, retarded infiltration mode and the fluent infiltration mode. The geohazards with accurate recording date and the corresponding rainfall data from 1960 to 2008 constitute the 298 cases which was filtered and grouped according to their application. For the first group, a regression model about relationship between the daily rainfall and landslide frequency in the previous 3 days was set up, a function of calculating the landslide frequency was obtained in the slow infiltration triggering mode. For the second group, the data of the accumulated rainfall from the day landslide happened to the previous 15 days was grouped every 10.0 mm. The rainfall threshold was obtained when the accumulated times of landslide reaches 25 % in the retarded infiltration mode; For the third group, the minimum and the maximum threshold were obtained after the analysis of the statistical data. Finally, the different rainfall thresholds were established at different rainfall triggering modes at loess plateau in the northeast of the Shanxi province. A plot between the times of the landslide occurrence and the times of the rainfall at different classes is shown in Fig. 2.

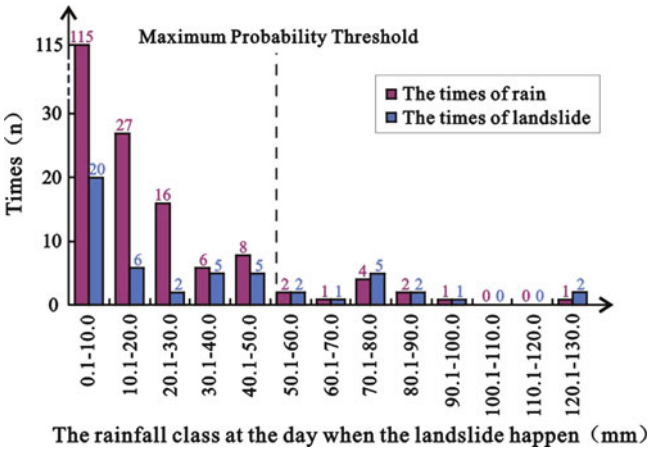

Fig. 2 The landslide times in each class

Methodology

A detailed tabular form was circulated to collect data among the partner countries of the Asian Program for Regional Capacity Enhancement for Landslide Impact Mitigation (RECLAIM). India, Bangladesh, Nepal, Thailand ,China, Bhutan and Sri Lanka contributed their data for the analysis. In addition to the data collection on landslides, the information including type and source, location and elevation, average rainfall, date of the event, effects, rock type, formation structure, soil type, thickness, slope angle, and length of slide were too collected as much as possible. However, it was found that the common availability of lithological information in the region is the simple classification of overburden as residual or colluvium.

Analysis

Results from Sri Lanka

Figure 3 shows the cumulative rainfall of those selected locations mentioned in Table 1. It clearly shows huge range of variation in the rainfall data. In this figure, seventh day corresponding to the day of disaster and the eighth day is the day after a particular disaster. To limit the variation from zero to unity Fig. 4 is prepared after normalizing the cumulative rainfall data by the the cumulative rainfall on the day of disaster.

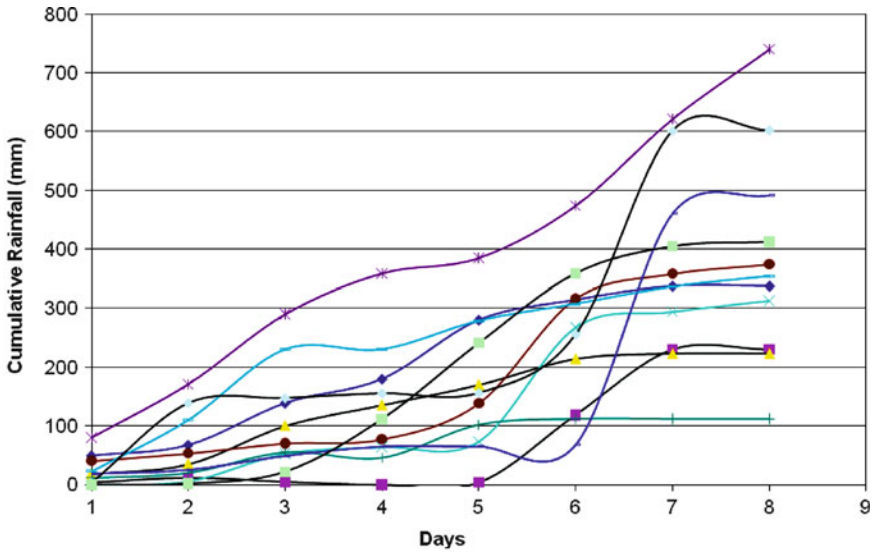

Fig. 3 Cumulative rainfall details of 12 landslide cases in Sri Lanka

Table 1 Daily rainfall records of 12 landslide cases in Sri Lanka NBRO (2010)

Location and date of the sediment disaster	6 days before	5 days before	4 days before	3 days before	2 days before	1 day before	The day of disaster	1 day after
Handurukanda, landslide 1982/12/20	50	18	71	41	100	34	22	–
Hetikande, 1989/5/30, earthslide	4	12	5	0	4	119	230	
Pattipola-Ohiya, landslide 1991/12/18	18.1	16.9	64.9	35.1	34.5	44.1	9.0	0.0
Watawala, earthslide 1992/6/3	0.0	5.6	47.1	11.3	9.4	194.2	26.4	18.9
Watawala, earthslide 1993/6/3	80.0	91.2	118.8	68.8	26.2	88.8	147.5	118.7
Helauda, debris flow 1993/10/8	40.8	12.8	17.0	7.0	61.2	177.6	41.6	16.1
Eheliyagoda, debris flow, 1994/5/28	11.4	20.3	55.2	46.0	102.0	112.0	87.0	
Navalapitiya, rockfall 1994/8/2	–	25.6	25.6	4.0	28.0	52.5	139.5	9.0
Holipitiya, landslide 1996/6/8	18.8	6.5	23.9	15.8	0.0	3.1	392.5	31.5
Neketiya, landslide 1997/11/19	22.9	87.4	120.0	0.0	48.5	28.6	28.6	17.7
Helauda, Palawela, earthslide etc. 2003/5/17	2.8	135.8	8.6	8.0	0.9	99.6	345.2	0.8
Walapane, earthslide 2007/1/12	0.0	1.4	20.3	89.7	129.6	117.9	45.9	7.3

The trendline shown in the Fig. 4 expresses the relationship between the normalized rainfall and the days till the disaster happened. The following procedure can be adopted to predict a possible landslide with the available rainfall data.

$$\mathbf{Y} = 0.\mathbf{1496X} - 0.16221 \quad (2)$$

To develop this equation, rainfall data from 6 days proir to the disaster has been considered. For an example, if the cumulative rainfall 4 days prior to the disaster, then it means, no. of days could be taken as 3.

E.g. Watawala earthslide on 3rd June 1993

(a) Cumulative rainfall 4 days prior to the disaster = 290
No. of days = 3
Predicted cumulative rainfall on the day of disaster = 943
Actual cumulative rainfall on the day of disaster from the available records = 621
Due to this gap between the actual and prediction, now, this can be further tested with more data.

(b) Cumulative rainfall 3 days prior to the disaster = 358.8
No. of days = 4
Predicted cumulative rainfall on the day of disaster = 780
Actual cumulative rainfall on the day of disaster = 621

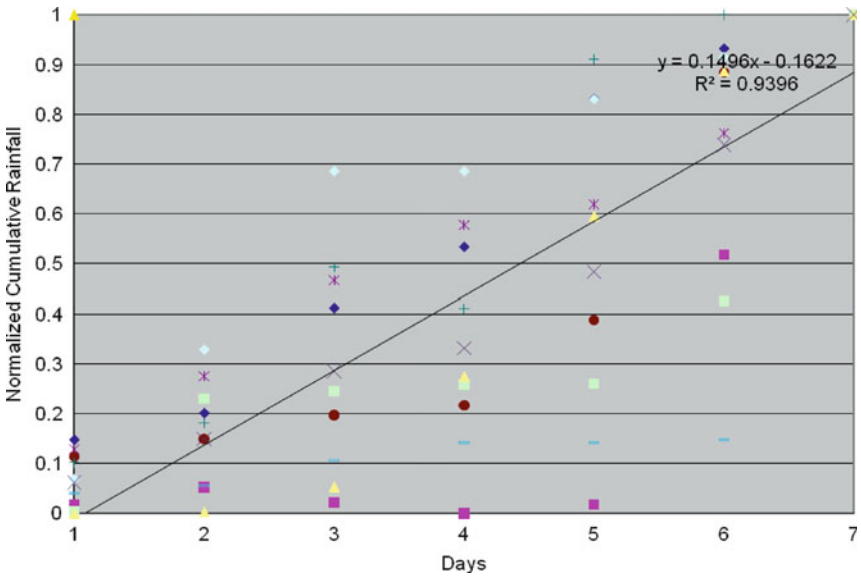

Fig. 4 Normalized cumulative rainfall details of 12 landslide cases in Sri Lanka

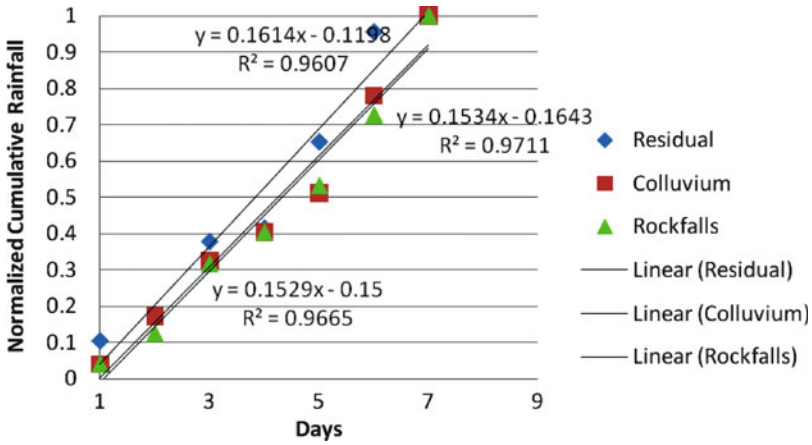

Fig. 5 Normalized cumulative rainfall details according to three different categories such as residual, colluvium and rockfalls

Answer is getting closer, however, it needs further improvements.

(c) Cumulative rainfall 2 days prior to the disaster = 385
No. of days = 5
Predicted cumulative rainfall on the day of disaster = 628
Actual cumulative rainfall on the day of disaster = 621
Answer is almost the same as the actual rainfall.
This means, 2 days prior to the disaster, threshold limit could be predicted with more accuracy indicating that the disaster can be predicted reasnbly well when it gets closer to the disastrous event.

These results can be further analyzed by grouping into three categories, such as residual, colluvium and rock falls. Figure 5 shows the differences among those three categories.

When Fig. 5 results are compared with Fig. 4, it can be found, once the overburden is grouped according to the formation, the better results could be obtained.

Data from Partner Countries

Figure 6 shows some regional rainfall data which were normalized by the cumulative rainfall on the day of landslide occurence. The trend in countries like Thailand, India and Sri Lanka shows the effect of longer duration rainfalls which caused the catastropies. However, countries like Bhutan, Bangladesh and Nepal show very different results as they had experienced extreme weather conditions such as heavy rainfalls within last 2–3 days prior to respective landslides.

This phenomenon can be studied when the last 3 days are considered for the analysis in such situations. Figure 7 shows their impact when only the last 3 days data are plotted similar to the previous plots. Table 2 gives the summary of R^2 (squared correlation between inputs and output – often called goodness of fit) values of 7 and 3 days situations for

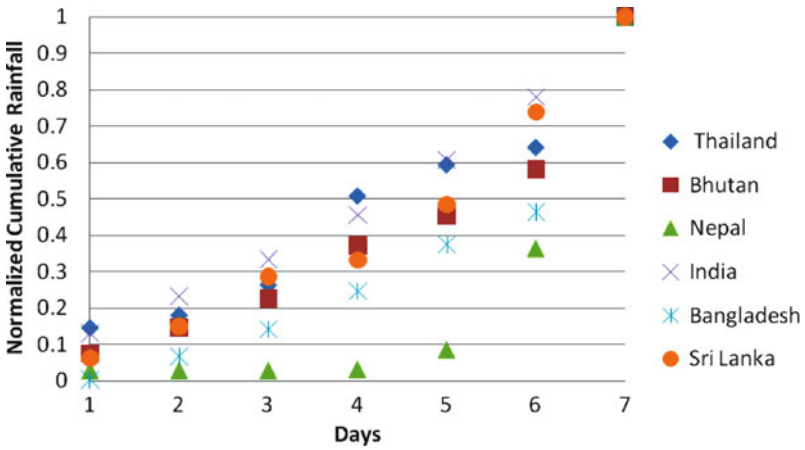

Fig. 6 Normalized cumulative rainfall details according to different countries

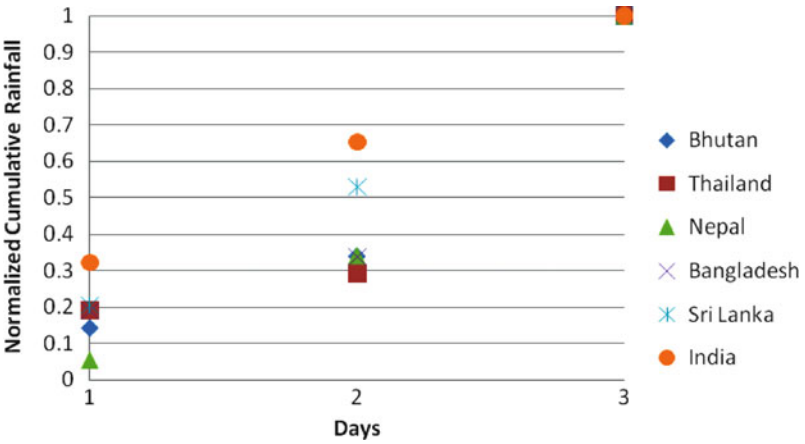

Fig. 7 Normalized cumulative rainfall details from partner countries considering the last 3 days data

Table 2 Goodness–of-fit for predicting landslides

	R^2 value	
Partner countries	7 days	3 days
Thailand	0.93	0.84
Bhutan	0.9	0.91
Nepal	0.6	0.95
India	0.98	1
Bangladesh	0.84	0.88
Sri Lanka	0.94	0.99

all the partner countries. All the countries show a very high goodness-of-fit confirming the last 3 days values a very important in predicting the landslides, though Thailand gives different results. This may be due to a prolonged rainfall having caused those landslides in Thailand. More important results are shown by Nepal; Nepal's goodness-of-fit has tremendously increased by considering the last 3 days results confirming those landslides should have been due to short-term high intense rainfalls. Table 3 can be referred to find the actual rainfall data in Nepal during 7 days prior to a particular landslide.

Concluding Remarks

Partner countries of the RECLAIM project contributed with data according to the format proposed in Table 1. However, due to non-availability of data in that pattern, the data received had to be analyzed with care. It also should be mentioned that finer conclusions could be made with more findings and data. Meanwhile, the results shown using Sri Lankan and Indian data are very promising for a better prediction of landslides using the proposed method. Developed countries use GIS-based predictions and still developing countries do not use the latest technology and those countries should be encouraged to apply such kind of new technique. Though this paper gives some concepts of early warning and threshold values, it should be emphasized that proper data collection is very vital in recommending such limits. Recent landslides due to short term high intense rainfalls in the region have caused devastated landslides. Therefore, hourly rainfall data related to landslides would be required and it can be recommended that more regional efforts must be made on this important subject.

Table 3 Seven days rainfall record for some landsldies in Nepal

Location	6 days before	5 days before	4 days before	3 days before	2 days before	1 day before	The day of disaster
1	7.8	0	0	0	5.2	49.1	135.5
2	0	0	0	5.2	49.1	135.5	179.4
3	7.8	0	0	0	5.2	49.1	135.5
4	7.8	0	0	0	5.2	49.1	135.5

Acknowledgments Asian Disaster Preparedness Center (ADPC) in collaboration with Norwegian Geo-technical Institute (NGI) has developed the Asian Program for Regional Capacity Enhancement for Landslide Impact Mitigation (RECLAIM) with the idea of promoting a dialogue between decision makers and professionals on the theoretical and practical aspects and issues related to landslide hazard mitigation. RECLAIM is being implemented with the funding support from Royal Norwegian Ministry of Foreign Affairs (MoFA) since 2004 with the aim to build national capacity on landslide disaster mitigation. Phase III of the project, which was started in autumn 2009, focuses on the use of early warning systems for landslide prone areas, which have advanced fairly rapidly over the last years. The project was implemented through gathering of data from existing approaches and through formation of joint working groups to identify critical factors for landslide initiation and to disseminate knowledge to participating countries. This paper is primarily prepared under this project for addressing the need of recommending threshold values for early warning for landslides in the region. All these agancies and partner countires are greatfully acknowledged for their efforts and MoFA for providing funds for successful completion of the mission.

References

Bandara RMS (2008) Landslide early warning in Sri Lanka, Regional seminar on experience of geotechnical investigations and mitigation for landslides, Bangkok, 13–14 Oct 2008

Brand EW (1988) Landslide risk assessment in Hong Kong. In: Proceedings of the 5th International Symposium on Landslides (Lausanne, Switzerland), vol 2, pp 1059–1074

Caine N (1980) The rainfall intensity-duration control of shallow landslides and debris flows. Geogr Ann 62A:23–27

Corominas J, Moya J (1999) Reconstructing recent landslide activity in relation to rainfall in the Llobregat River basin, Eastern Pyrenees, Spain. Geomorphology 30:79–93

Crosta G (1998) Regionalization of rainfall thresholds: an aid to landslide hazard evaluation. Environ Geol 35(2–3):131–145

Kaneko H, Tanaka H, Kudoh Y (2010) Prediction of slope failure of sand ground during rainfall by centrifuge model tests. In: 6ICEG, New Delhi, Nov 2010

Kuthari S (2007) Establishing precipitation thresholds for landslide initiation along with slope characterization using GIS-bases modeling. MSc thesis submitted to the International Institute for-Geo-information Science and Earth Observation, ITC, Netherlands

NBRO (2010) Rainfall in the Case of Some Major Landslides in Sri Lanka, a report prepared by NBRO. National Building Research Organization, Sri Lanka

Singh AK (2010) Landslide management: concept and philosophy. Disaster Prev Manage 19(1):119–134

Tang Ya-ming, Yin Yueping, Sun Ping-ping, Hu Wei, Xue Qiang (2008) Study of Loess Landslide Rainfall Triggering Model and thresholds, best practices and threshold values for landslide early warnings, Report prepared by Asian Disaster Preparedness Center (ADPC)

Flood and Slope Processes in the Scura Valley (Reatini Mts., Central Apennines, Italy). Meteo-climatic Analysis and Geomorphological Evolution

Paolo Maria Guarino, Riccardo Massimiliano Menotti, Guido Motteran, and Roberto Serafini

Abstract

The Scura Valley involves the eastern slope of the complex of the Reatini Mountains (Central Apennines, Italy); it is crossed in its entirety by the Scura Torrent, tributary of the Velino River.

Flood and gravitational phenomena in the Scura Valley occurred on December 1st and 2nd 2010, were attributable to extreme meteorological conditions. In the final days of November and in the early days of December 2010, abundant snowfalls occurred on the Reatini Mountains, accompanied by intense and prolonged rainfalls. Within a few days, the temperature plummeted to −1.5 °C and rapidly rose (Terminillo, Micigliano, Posta, Antrodoco and Leonessa meteorological stations).

The thermal rise favoured the melting of the snow that had accumulated in the higher parts of the valley, and the intense concomitant rainfalls determined the triggering of widespread debris flows.

Keywords

Debris flow • Snow melting • Rainfall • Scura Valley • Central Apennines • Italy

Introduction

The Scura Valley is a 16 km^2 square basin, that flows into the Velino River after having crossed the built-up area of Sigillo (Fig. 1), a hamlet near the town of Posta (Province of Rieti).

The articulated morphologic setting and the very high relief energy of the slopes cause frequent slope instabilities, mainly including rock falls from limestone cliffs and landslides in slope deposits (Amanti et al. 2009).

In the past, the Scura Valley was already involved in extreme alluvial phenomena. Particularly, in December 1999, an intense rainfall event triggered a very large landslide to the hydrographic right, and caused the destruction of the intake structure of the San Giuseppe spring.

On December 1st and 2nd 2010, a flood occurred that produced numerous and widespread erosion processes at the foot of both slopes, debris-flows and the moving of enormous quantities of debris. The watercourse deeply cut into the right slope of the valley, thus reactivating the landslide movement that had been triggered off in 1999. In the middle-low part, the bank erosion of the Scura Torrent carried away in large part the morphological terrace to the hydrographic left, destroying the route and temporarily isolating the locality of Le Casette.

In many places the torrent deviated its course, invading and destroying the route and the footpath that ascend from Sigillo towards the head of the Scura Valley.

The reinforced-concrete embankments, which had been built to safeguard Sigillo after the flood of 1999, intercepted and restrained the alluvial material, but were unable to prevent the water and fine sediments from invading the

P.M. Guarino (✉) • G. Motteran • R. Serafini
Soil Defence Department, ISPRA, 3 Curtatone street, Rome, Italy
e-mail: paolomaria.guarino@isprambiente.it

R.M. Menotti
Applied Physics, IFAC-CNR, Sesto Fiorentino, Florence, Italy

C. Margottini et al. (eds.), *Landslide Science and Practice*, Vol. 4,
DOI 10.1007/978-3-642-31337-0_31,

Fig. 1 Location of the study area

built-up area. Luckily, the realisation of the embankments in the inhabited stretch limited the damage to the houses.

Geological and Geomorphologic Setting

The catchment area of Scura torrent extends for around 16 km^2; the confluence with the Velino River to quota 621 m a.s.l. identifies the end section. The head of the Scura Valley is closed by mt. Porcini (1,982 m a.s.l.), mt. Iaccio Crudele (1,920 m), and mt. Elefante (2,015 m). From mt. Brecciaro (1,954 m) and mt. Ritornello (1,907 m) to the hydrographic right, and from mt. di Cambio (2,081 m) and Colle dei Tratturi (1,448 m) to the left, the valley slopes down towards the Velino River (Fig. 2).

The landscape is very uneven, sometimes steep and rugged. In the upper part of valley, the profile is characterised by morphological jumps attributable to the glacial erosion (Angelini et al. 2004), to Malopasso a fall with a jump of around 50 m sets the limit of probable maximum of the wurmian glacier; in the terminal line, the hydraulic works (embankments and weirs) have intercepted the alluvial material and formed sub-level areas.

The morphological setting above described is sharply conditioned by the tectonic structure, that is characterized by the Umbria-Sabina pelagic deposits tectonically overlap those of Gran Sasso-Cittareale Unit (Italian Geological Survey 1967; Bigi et al. 1992; Festa 2002 and references therein).

The calcareous and calcareous-dolomitic platform succession (so called "Massiccio") outcrops in the high and central parts of the Scura Valley, as does the Umbro-Sabine pelagic succession, which consists of limestone and marly limestone (Fig. 2). Moving valleyward to the Velino River, the marly-calcarenitic complex marks the passage between carbonatic and terrigenous sedimentation (Upper Eocene – Upper Miocene).

In the upper part of the valley, which is modelled by a group of glacial circles, the chaotic moraines deposits are formed by medium-fine elements which are slightly cemented and are characterised by the presence of very large blocks. In the middle and low parts, the slopes are covered with detritus and fans which consist of loose and extremely variable in size elements. The alluvial deposits present along the sides and on the valley bottom are represented by masses, more or less evolved pebbles, sands and silts.

The lithostratigraphic contacts and the geologic-structural order check the hydrogeological setting of the study area, that is part of the main pattern of the Reatini Mountains (Amanti et al. 2011): the meso-cenozoic calcareous-dolomitic unities and marly limestone unities (laziale-abruzzese shelf succession and umbro-sabina pelagic succession) are characterized by permeability from high to medium; the more marly and flyshoid unities (umbro-marchigiana succession) introduce permeability from low to nothing.

The contacts and the overlaps of these unities determine the drain toward the basic springs; generally, the groundwater flow is directed toward the Reatina plain, south of the study area.

In the Scura Valley, however, some minor springs related to the presence of a additional shallow aquifer are present, whose discharge values are reported in Table 1: Sorgente Porcini 1, Sorgente Porcini 2, Sorgente Cavalli, that supply the Rieti aqueduct and Sorgente S. Giuseppe, that supplies the Posta aqueduct.

The December 2010 Alluvial Event

The alluvial event of December 2010 has caused numerous instability phenomena in the median and lower sectors of the basin.

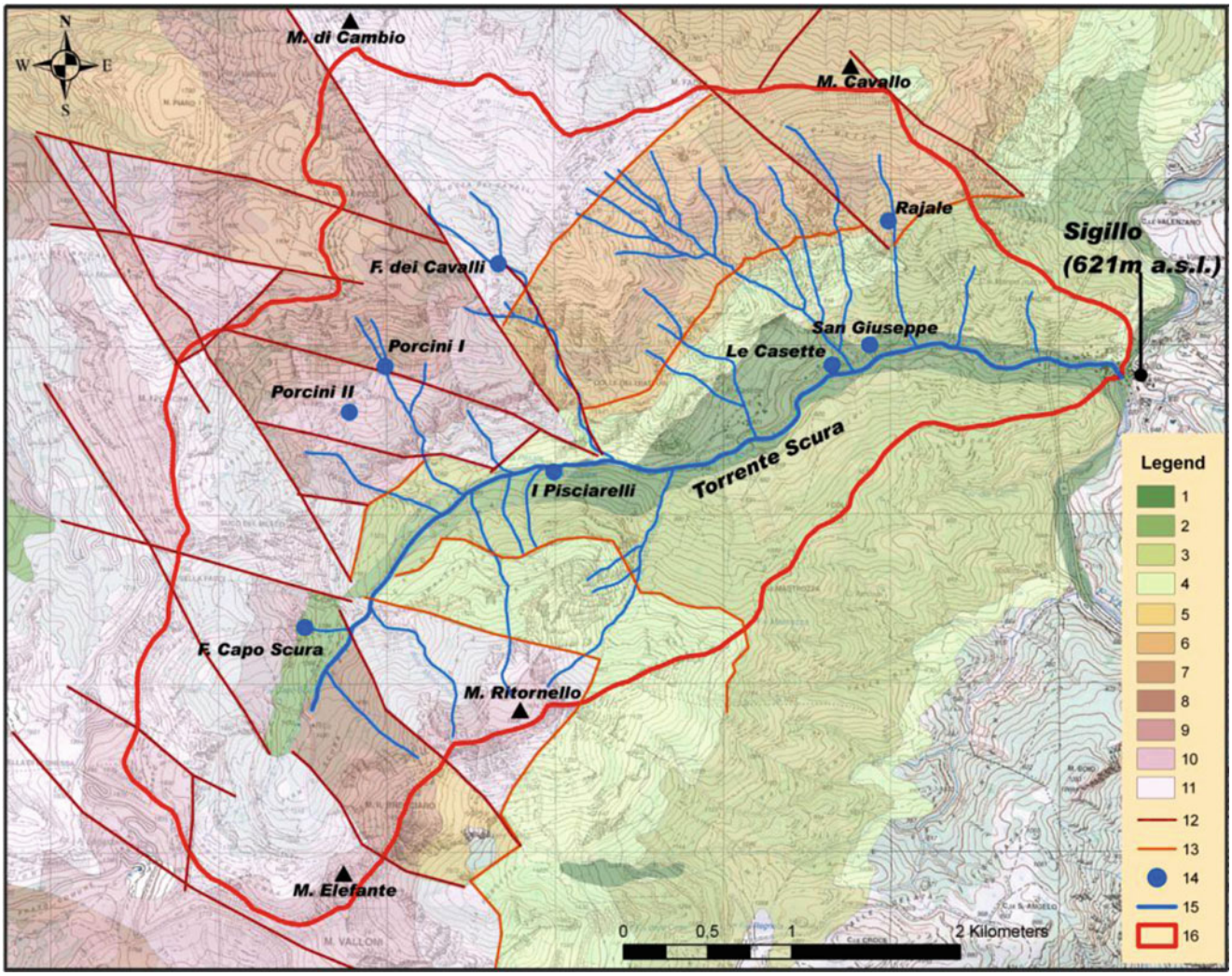

Fig. 2 Geological sketch map of the Scura Valley. Legend: *1* alluvial deposits (Holocene), *2* slope debris (Holocene), *3* marls of the Scaglia Cinerea formation (Miocene), *4* marly limestones of the Scaglia Rossa and Scaglia Variegata formations (Eocene-Cretaceous), *5* marls with Fucoidi (Lower Cretaceous), *6* limestones and marls of the Maiolica formation (Lower Cretaceous – Upper Jurassic), *7* limestones with chert of the Scisti ad Aptici formation (Upper Jurassic), *8* limestone (Jurassic), *9* limestones and marls of the Rosso Ammonitico formation (Lower Jurassic), *10* limestones with chert of Corniola formation (Lower Jurassic), *11* bioclatic calcarenites of the Massiccio formation (Lower Jurassic), *12* fault, *13*, thrust, *14* spring, *15* hydrographic net, *16* watershed (Adapted from Italian Geological Survey 1967)

Table 1 Springs and related discharge (From Amanti et al. 2011). The values marked with (*) are related to 1 only measure

Spring	Min (l/s)	Max (l/s)	Aver. (l/s)
S.Giuseppe	1.5	27	11.8
Le Casette	0.65	1.5	1.16
Capo Scura (*)	0.02	0.02	0.02
Porcini 1 (*)	6	6	6
Porcini 2 (*)	4	4	4
I Pisciarelli	5	36.8	15.8
F. dei Cavalli	–	–	–
Rajale	1	11	5.9

We have surveyed, particularly, phenomena of erosion of bank (Fig. 3), with erosion to the foot of the slopes, excavation and amplification of the riverbed (Fig. 4), overflow (with breakup of the road), flooding of the external areas

Fig. 3 Erosion of bank

Fig. 4 Excavation and amplification of the riverbed

Fig. 5 Flooding of the external areas of the riverbed

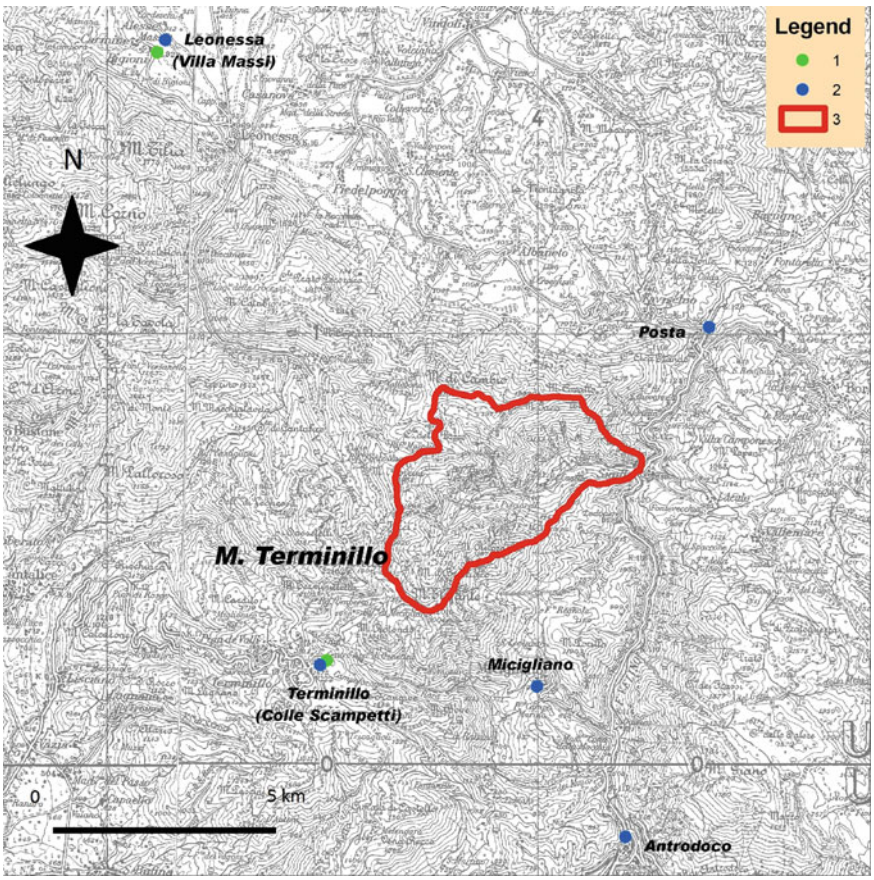

Fig. 6 Location of the meteorological stations. Legend: *1* Apenninic Centre "Carlo Iucci", *2* Hydrographical Agency of Latium Region, *3* Scura Valley basin

(Fig. 5), with partial burial of the existing works and re-erosion of the deposited material. We have not recorded, besides, particular conditions of instability in the slope areas, where the landslides are primarily activated to the foot because of the current erosion.

The picked elements allow us to affirm that the flood of the Scura Torrent has not been a purely hydraulic event, as been characterized by an elevated solid transport, in turn tied up to the erosive phenomena and the instability phenomena that have involved the stream bed.

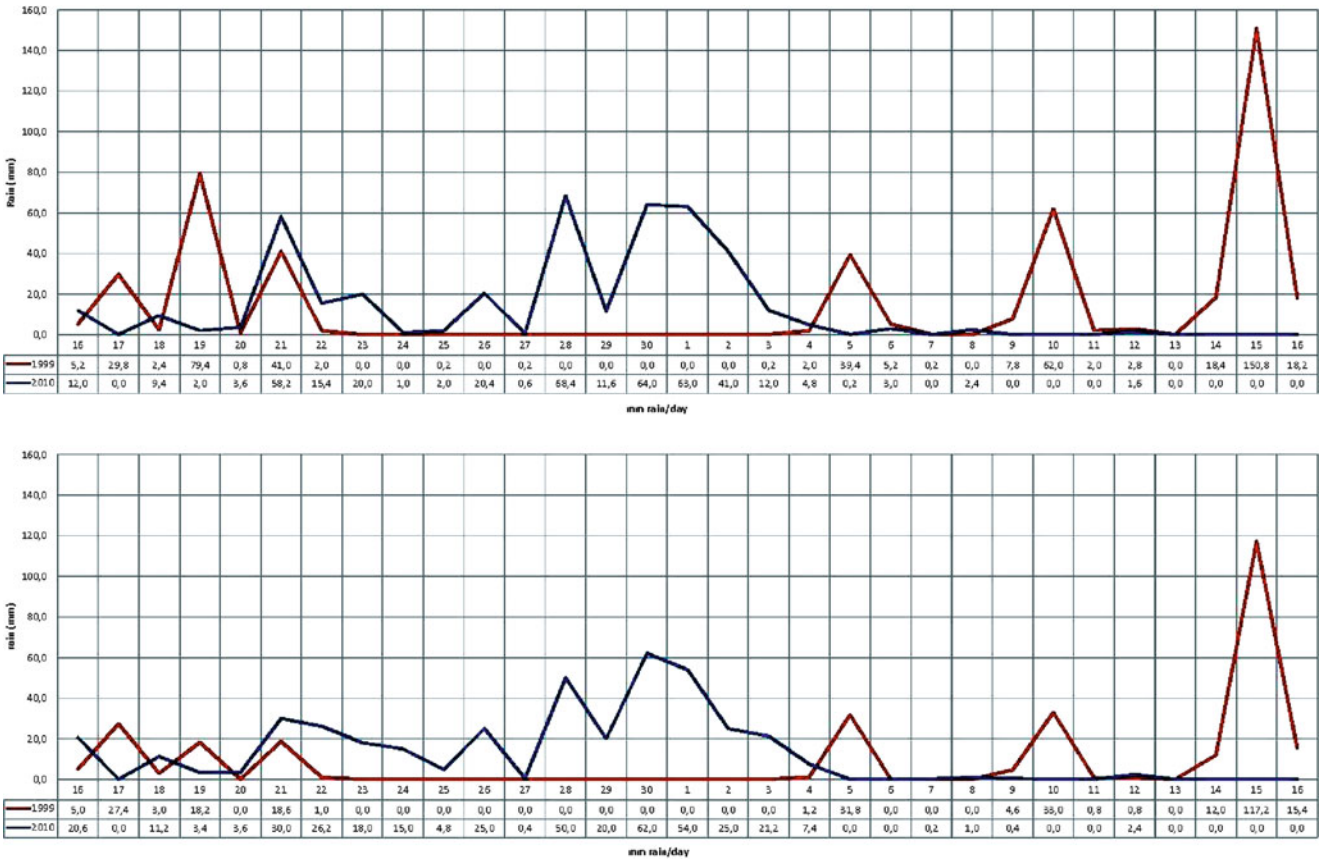

Fig. 7 Comparison of the daily rainfall for the months of November and December 1999 and 2010, referred to Leonessa Meteorological Station (*above*) and Terminillo Meteorological Station (*below*)

The erosion of bank has transported during flood great quantities of rocky material, and, additionally, large rocky blocks and trunks have caused the filling and the breakup of the wiers. The solid transport has probably determined the raising of the bed and has caused the deviation of the stream that subsequently has left the material in the lines to smaller inclination with overflooding phenomena.

Analysis of Rainfall Data

Analysis of meteorological data gathered from the agencies of Apenninic Centre "Carlo Iucci" (Università degli Studi di Perugia 2010) and from Tidal and Hydrografical Agency of Latium Region (http://www.idrografico.roma.it/) was carried out.

Particularly, data from the meteorological stations of Terminillo and Leonessa (Apenninic Centre "Carlo Iucci" of Terminillo) and of Posta, Antrodoco and Micigliano (Hydrografical Agency of Latium Region) were analyzed (Fig. 6).

The data collected show that, at the end of November 2010 there were 3 days of intense precipitations, with a mean of 120 mm of rain (Fig. 7). Likewise, during the first 3 days of December 2010, a mean of 110 mm of rain occurred, simultaneously with the melting snow.

Add to this that, in the month of November the snow cover that had been 25 cm thick (Terminillo Station, 1,700 m a.s.l.), dropped to only 3 cm as result of the temperature rising to a maximum of 6 °C.

The comparison with rainfall data for 1999 shows that in the latter case the rainfall event was shorter but more intense. In both cases, the amount of rain fell in the basin, which is characterized by a time of concentration very low (Tc = 1.3 h), has determined a flood wave much higher than what was calculated for a return period of 100 years (Municipality of Posta 1999, Technical Report).

Conclusions

The alluvial event of December 2010 in the Scura Valley was a consequence of 3 days of intense precipitations since the end of November, and the simultaneous melting snow due to a very rapid thermal rise.

This event shows many elements of similarity with what happened on November 1999.

Repeated flooding exposes the hamlet of Sigillo to a very high risk conditions; hence, a timely realization of risk mitigation works is required.

References

Amanti M, Chiessi V, Guarino PM, Serafini R (2009) Pericolosità per instabilità dei versanti del foglio 348 Antrodoco: distribuzione e tipologia dei fenomeni franosi. Rend Online Soc Geol It 6:7–8

Amanti M, Conte G, Marino M, Martarelli L, Monti GM, Motteran G, Perini P, Silvi A (2011) Hydrogeological features of high-altitude springs of the Monte di Cambio hydrostructure (Rieti, Lazio) and local meteo-climatic effects on their discharge processes. Italian J Eng Geol Environ 1:37–53

Angelini S, Farabollini P, Menotti RM, Millesimi F, Petitta M (2004) *Carta* geomorfologico-turistica di Monte Terminillo. Litografia Artistica Cartografica srl Firenze

Bigi S, Calamita F, Centamore E, Deiana G, Ridolfi M, Salvucci R (1992). Assetto strutturale e cronologia della deformazione della zona di incontro tra le aree umbro-marchigiana e laziale-abruzzese (Marche meridionali e Lazio-Abruzzo settentrionale). Studi Geol Camerti, vol. sp., 1991/2, CROP 11:21–26

Festa A (2002) Evoluzione strutturale del settore meridionale del sovrascorrimento dei monti Sibillini (Appennino Centrale). Mem Soc Geol It 57:369–377

Italian Geological Survey (1967). Geological map of Italy. Scale 1: 100,000. Sheet n. 139 "L'Aquila". Ist. Poligrafico e Zecca dello Stato, Rome

Municipality of Posta (RI) (1999) Technical Report: Studio Geomorfologico-idrologico dell'area di Vallescura-Sigillo per la realizzazione di interventi urgenti a seguito degli eventi alluvionali del dicembre 1999

Tidal and hydrographical agency of latium region (1999 and 2010) annals hydrologic. http://www.idrografico.roma.it/default.aspx. Accessed 21 May 2011

Università degli Studi di Perugia (2010) Centro Appenninico del Terminillo "Carlo Iucci". Dati meteorologici

Snowmelt Modelling for Improving the Forecasts of Rainfall Threshold-Based Landslide Triggering

Gianluca Martelloni, Samuele Segoni, Filippo Catani, and Riccardo Fanti

Abstract

In Central Italy a significant number of landslides occurrence have been triggered by rapid snow melt: recent seasonal events in the Northern Apennines, the study area, demonstrate that it is necessary to consider this phenomenon and to integrate snow precipitation within existing statistical models for landslide prediction. The proposed snow melt modeling (SMM) is divided in two modules depending on whether or not a threshold temperature is exceeded: the first one for the accumulation of solid rainfall in the snowpack and the latter for the snow melting. For the modeling identification we employ empirical data of depth of snow cover using an optimization algorithm to deduce the optimal values of the model parameters. This work is developed to increase the predictive capacity of the statistical models for landslide prediction based on rainfall thresholds. In the study area an improvement was achieved: several landslides, caused by snow melting, were correctly detected.

Keywords

Snow melting • Simplex • Optimization • Landslides • Threshold • Central Italy

Introduction

In mid-latitude areas landslides can be triggered by rainfall as well as snow melting: the modeling of the latter, which involves in particular shallow landslides, is the main topic of the present paper.

In literature, several snow accumulation and melting models are proposed. The nature and possible applications of snow melting models are varied and dependent on the purpose of use: for instance, in the hydrological modeling they are used for the analysis of runoff generated by the melting of the snowpack (Marks et al. 1999; Zanotti et al. 2004). In the prediction and study of avalanches some very sophisticated models are used which can provide a detailed representation of the internal structure of the snowpack (Brun et al. 1989). Essentially they are spatially distributed models based on equations of mass and energy balance. These models, based on digital elevation data (DEM) accounting for topography, generally require complex meteorological data: precipitation, air temperature, wind speed and direction, humidity, downwelling shortwave radiation, downwelling longwave radiation, cloud cover, surface pressure. Simplified approaches as degree-day or temperature-index models (Kustas et al. 1994; Hock 2003) show good results and it has been shown that "only little additional improvement in model performance is achieved when adopting an energy balance approach" (Hock 2003). The proposed model is built for the need of its integration with a statistical model for landslides prediction to take into account the correct computation of the rainfall and water

G. Martelloni (✉)
Earth Sciences Department, University of Florence, Via La Pira 4, Florence (IT), Italy

Department of Energy Engineering, University of Florence, Florence (IT), Italy
e-mail: gianluca.martelloni@unifi.it

S. Segoni • F. Catani • R. Fanti
Earth Sciences Department, University of Florence, Via La Pira 4, Florence (IT), Italy

C. Margottini et al. (eds.), *Landslide Science and Practice*, Vol. 4,
DOI 10.1007/978-3-642-31337-0_32,

resulting from snow melting. The statistical model for landslide forecasting, named SIGMA (Sistema Integrato Gestione Monitoraggio Allerta, that stands for "Integrated service for the managing and monitoring of the alert"), is based on a set of rainfall thresholds, whose overcoming defines different states of alert (Martelloni et al. submitted) and it is applied at regional scale in Emilia Romagna region (Italy). Moreover, the snow melt modeling is lumped for the integration with SIGMA, in which the study region is divided into 19 homogeneous areas, each one with a reference rain gauges. The adoption of a simple model for the snow melting is in our case necessary for the real time simulations in alert system of Civil Protection of Emilia-Romagna.

The proposed snow melt modeling is based on two equations: the conservation of mass (input–output balance) and an empirical equation for modeling the snow density variation. Also melting process is modeled with an empirical function based on chemical kinetics. From the conservation of mass, a differential equation of snow cover depth, depending on density and average temperature of the air, can be obtained. The second equation is an empirical function for the average density variation and depends on the snow cover depth (gravity effect) and the temperature of the air, which is variable in time. In the present form, this model depends on 13 empirical parameters, which are calibrated employing snow cover depth measures obtained through sensors located in the study area. Then we use an optimization algorithm (simplex flexible) to deduce the optimal values of the parameters. The latter include a threshold temperature switching precipitations between snowfall and rainfall. The meteorological data are gathered from the Emilia Romagna Regional network, which is composed by automated stations for the recording of rainfall, temperature and snow heights (all at hourly intervals).

Snow Melt Modelling (SMM)

Principal Model Equation

The model is based upon the balance of mass, so we can express the instantaneous change of mass contained in the snowpack m_s as the difference between the mass flow of input Q^{in} and output Q^{out}:

$$\frac{dm_s}{dt} = Q^{in} - Q^{out} \tag{1}$$

The terms of mass accumulated in the snowpack, in the input flow and in the output flow are given by the following equations:

$$\begin{cases} m_s &= \rho_s \cdot A \cdot H_s \\ m_s^{in} &= \rho_{so} \cdot A \cdot H^{in} \\ m_s^{out} &= \rho_s \cdot A \cdot H^{out} \end{cases} \tag{2}$$

where ρ_s, ρ_{so} are the densities of snowpack and of newly fallen snow, A is the generic section and H_s the depth of the snow layer.

As the experimental data of snowpack depth are available at hourly intervals, it is necessary to discretize the model. Using (1) and taking into account (2), we obtain:

$$\rho_s(t_1) \cdot H_s(t_1) - \rho_s(t) \cdot H_s(t) = \rho_{so} \cdot H^{in}(t) - \rho_s \cdot H^{out}(t) \tag{3}$$

where t is the discrete time variable and $t_1 = t + 1$.

Moreover, from the ratio between the density of water ρ_w and the density of newly fallen snow ρ_{s0} we obtain the equivalent height of snow H^{in} corresponding to a given amount of rain H_w:

$$\frac{\rho_w}{\rho_{so}} = \frac{\frac{m}{H_w \cdot A}}{\frac{m}{H^{in} \cdot A}} = \frac{H^{in}}{H_w} \Rightarrow H^{in} = \frac{\rho_w}{\rho_{so}} \cdot H_w \tag{4}$$

Finally, the height of the surface at time t + 1 is given by the following equation:

$$H_s(t_1) = \frac{\rho_s(t)}{\rho_s(t_1)} \cdot H_s(t) + \frac{\rho_w}{\rho_s(t_1)} \cdot H_w(t) - \frac{\rho_s(t)}{\rho_s(t_1)} \cdot H^{out}(t) \tag{5}$$

which expresses the total balance of mass. This single equation is not sufficient to completely characterize the model as in (5) some variables are still unknown, i.e. the average density of the snowpack and the term of output $H^{out}(t)$. So an empirical equation is introduced to take into account the variation in time of average snowpack density, as in other models (e.g. Kuchment and Gelfan 2001) and empirical function for melting. These functions are described in the next two paragraphs.

Accumulation Phase

When the temperature of the air T_a is under a threshold temperature T_0 the precipitation is considered solid and then the accumulation phase goes on. The new snow density depends on wind and T_a (Pahaut 1975) (Fig. 1), but as the available data is only temperature of the air

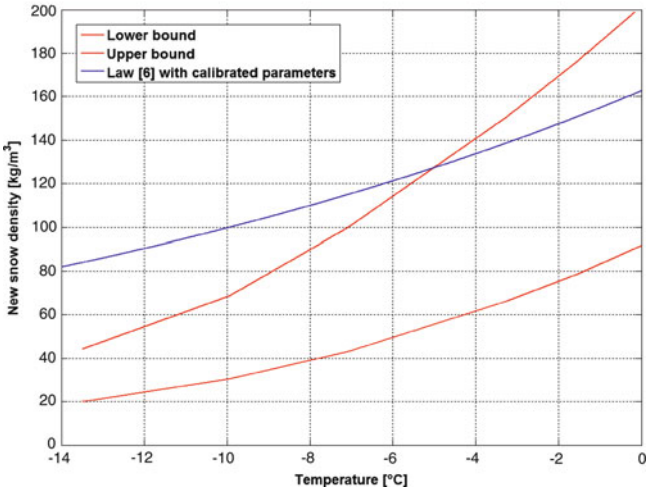

Fig. 1 Comparison between new snow density by parametric calibration of (6) and systematic measures by Pahaut (1975): the new snow density increases with temperature and wind.

and rainfall (in addition to snowpack depth), an approximation, expressed by an exponential equation depending on two empirical parameters ($k_{\rho 0}$ and k_{exp}), is adopted:

$$\rho_0(t_1) = k_{\rho 0} \cdot \exp\left(k_{\exp} \cdot (T_a(t_1) - T_0)\right) \tag{6}$$

where T_0 (thresholds temperature) and parameters $k_{\rho 0}$, k_{exp} are obtained by the model identification.

Note that (6) approximates sufficiently well for values of temperature superior to −5 °C, but this results is obviously due to temporal series of temperature used in calibration for model identification.

The average density of the snowpack ρ_s is updated at each time as a weighted average of the density in the time before and the density of new fallen snow:

$$\rho_s(t_1) = \frac{H_s(t)\left(\rho_s(t) + k_{\rho 1}\frac{H_s(t)}{k_{\rho 2}+H_s(t)}\frac{k_\rho}{k_\rho+\rho_s(t)}\right) + H_w(t_1)\rho_w}{H_s(t) + \frac{H_w(t_1)\rho_w}{\rho_0(t_1)}} \tag{7}$$

Where

$$k_{\rho 1}\frac{H_s(t)}{k_{\rho 2}+H_s(t)} \cdot \frac{k_\rho}{k_\rho+\rho_s(t)} \tag{8}$$

represented the term of compression in which the snowpack depth H is a limiter (terminology from chemical kinetics), i.e. large H implies more compression (due to a greater quantity of matter), while the density is an inhibitor of the compression process as a high density is opposed to the process of gravitational compression effect. In the function (8) $k_{\rho 1}$, $k_{\rho 2}$, k_ρ are empirical parameters.

Note, that by definition, a limiter X in a kinetics process is the ratio:

$$\frac{X}{k+X} \tag{9}$$

A third equation updates the height of the mantle based on the simple application of conservation of mass, obtained as the mass per unit area, which is the product between the density and the height of the snowpack:

$$H_s(t_1) = \frac{1}{\rho_s(t_1)}(H_s(t)\rho_s(t) + H_w(t_1) \cdot \rho_w) \tag{10}$$

Melting Phase

In the melting processes the equation of snowpack density is expressed like:

$$\rho_s(t_1) = \rho_s(t) + k_{\rho 1}\frac{H_s(t)}{k_{\rho 2}+H_s(t)}\frac{k_\rho}{k_\rho+\rho_s(t)}\frac{T_a(t_1)}{k_t+T_a(t_1)} \tag{11}$$

This equation is not a weighted average like the accumulation phase because the mass comes out of the system. Then the hypothesis, that the temperature influences the process as a limiting factor, is taken into account and it is expressed by:

$$\frac{T_a(t_1)}{k_t+T_a(t_1)} \tag{12}$$

this is a result of the melting process, or in other words the effect of water percolation in the snowpack causes an additional effect of compression and this process increases with temperature (k_t is an empirical parameter).

Then the equation of melting process is given by:

$$H_{ww}(t_1) = \left(k_2\Delta T^* + k_3\frac{H_w(t_1)}{k_w+H_w(t_1)}\right)\frac{k_{s1}}{k_{s1}+H_s(t)\rho_s(t)}$$
$$\Delta T^* = (T_a(t_1) - T_0)^{k1} \tag{13}$$

that expresses the amount of thawed mass per unit area and it is depended in this proposed model by a power term expressed by the difference between air temperature and the threshold T_0:

$$k_2 \cdot \Delta T^* \tag{14}$$

plus a term due to the influence of rain, if present, that contributes to the snow melting (this term is introduced as a limiter):

$$\frac{H_w(t_1)}{k_w + H_w(t_1)} \tag{15}$$

The melting process is also influenced by the amount of mass present and it can be assumed that the product high-density (ρ H) acts as an inhibitor of the dissolution process and can be expressed as the factor

$$\frac{k_{s1}}{k_{s1} + H_s(t)\rho_s(t)} \tag{16}$$

Which is contained in (13) to simulate the possible effects of refreezing that increases with the density and height of the mantle.

Then (17), which expresses the conservation of mass for the process, updates the height of the snow melting by subtracting the amount of water from melting (a term H_{ww}):

$$H_s(t_1) = \frac{1}{\rho_s(t_1)}\left(H_s(t)\rho_s(t) - H_{ww}(t_1)\right) \tag{17}$$

In (11) and (13) k_1, k_2, k_3, k_w, k_{s1} are empirical parameters.

The time step of SMM is hourly.

Methodology for Model Identification

Knowing the experimental depths of snowpack, obtained through sensors, we can calibrate the model with these data. The variable state H_s depends on the temporal series of temperature and rainfall, the variable state ρ_s, and the 13 constants of the model $P = p_1, p_2, \ldots, p_{13}$ $\Re^{13}$. The latter are the parameters of calibration. Indicating with x the independent variable of calibration we have the functional error E(P):

$$E(\mathrm{P}) = \frac{1}{N}\sum_{i=1}^{N} w_i \varepsilon_i^2 = \frac{1}{N}\sum_{i=1}^{N} w_i \left(H_i^{\exp} - H_i^{\mathrm{mod}}(\mathrm{x},\mathrm{P})\right)^2 \tag{18}$$

where apexes exp and mod indicate, respectively, the experimental data and the modeled heights; N represents the number of data; w_i are the weights of error ε_i: for example the experimental data can be weighted with derivate of variable state $H_s(t)$ or simply with the same $H_s(t)$. Ultimately, an appropriate optimization algorithm (Flexible Optimized Simplex) (Nelder and Mead 1965; Himmelblau 1972; Marsili-Libelli 1992) calculates the values of the parameters which minimize the difference between experimental data and output of the model like in (18) (Fig. 2).

The flexible simplex is an euristic search algorithm that implements a series of operations: in mathematics a simplex

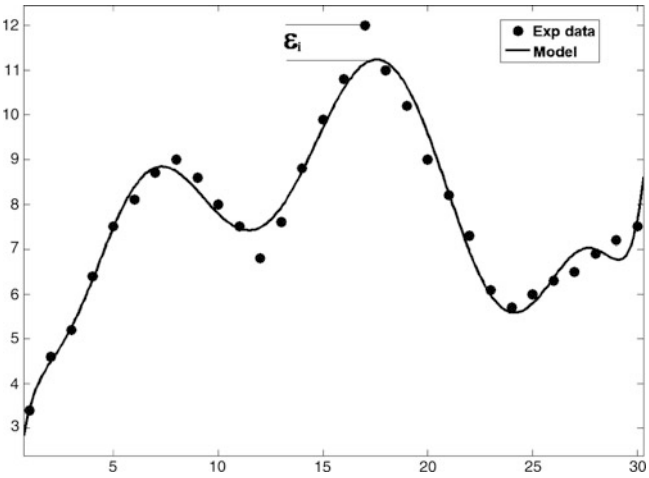

Fig. 2 The target of calibration is to minimize the sum of difference εi

is a n-dimensional polytope with the smallest number of vertices (n + 1), i.e. for example in 2 the simplex is a triangle. In our case the simplex is 13-dimensional (14 vertices), as the field (domain) of the functional error: once defined an initial simplex (by assigning an initial condition to each parameters), the algorithm updates the simplex step by step, replacing the worst point, i.e. the point with the higher functional error. This method brings several advantages:

- It does not fail in finding absolute minimum,
- It can handle problems with high "curvature" (different order of magnitude of parameters),
- Fewer functional assessments (in the case of dynamical systems each evaluation requires a simulation that can be computationally very demanding),
- Improved efficiency in the case of "narrow valleys" of the functional error, which are typical of dynamical systems,
- Better identification of the search direction at the bottom of the valleys.

The criterion for stopping the algorithm is based on a flatness test of simplex (all vertices of simplex must have the same functional error).

Results of Calibration and Validation of the SMM

The parametric identification of the model is obtained through validated data (2009) of Doccia di Fiumalbo rain gauge (1,371 m a.s.l.): this data are provided by ARPA ("Agenzia Regionale Prevenzione e Ambiente" – Regional Agency Prevention and Environment) Emilia Romagna region. In Table 1 the values of optimum parameters are shown, while in Fig. 3 the results of calibration with the errors are depicted.

Once the optimum parameters are found, we can validate the model, testing it with another data set: as the

Table 1 Optimum parameters of SMM obtained with parametric identification

Parameters	Optimum values
k_1	3.25031
k_2	0.000926091
k_3	15.8715
$k_{\rho 1}$	0.432043
$k_{\rho 2}$	1.40015
k_{ρ}	0.30003
k_t	0.110011
k_w	0.0400043
k_{s1}	200.02
$k_{\rho 0}$	165.016
k_{exp}	0.0490052
$k_{\rho m}$	94.011
T_0	0.300036

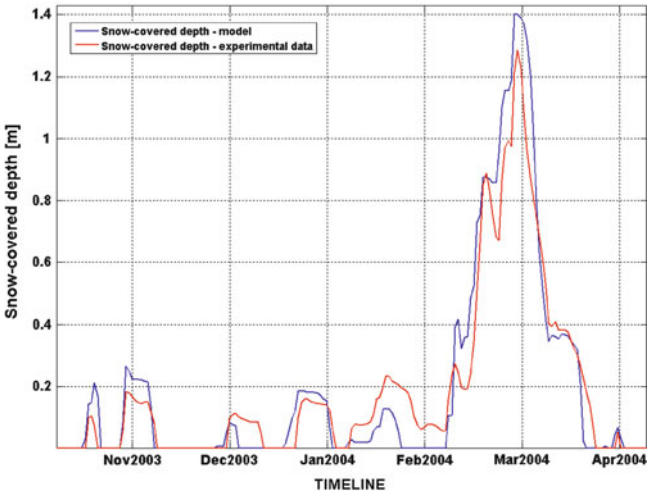

Fig. 4 Example of validation of the SMM with the event 12/2003-04/2004 registered with sensor of Febbio rain gauge (1,148 m a.s.l.)

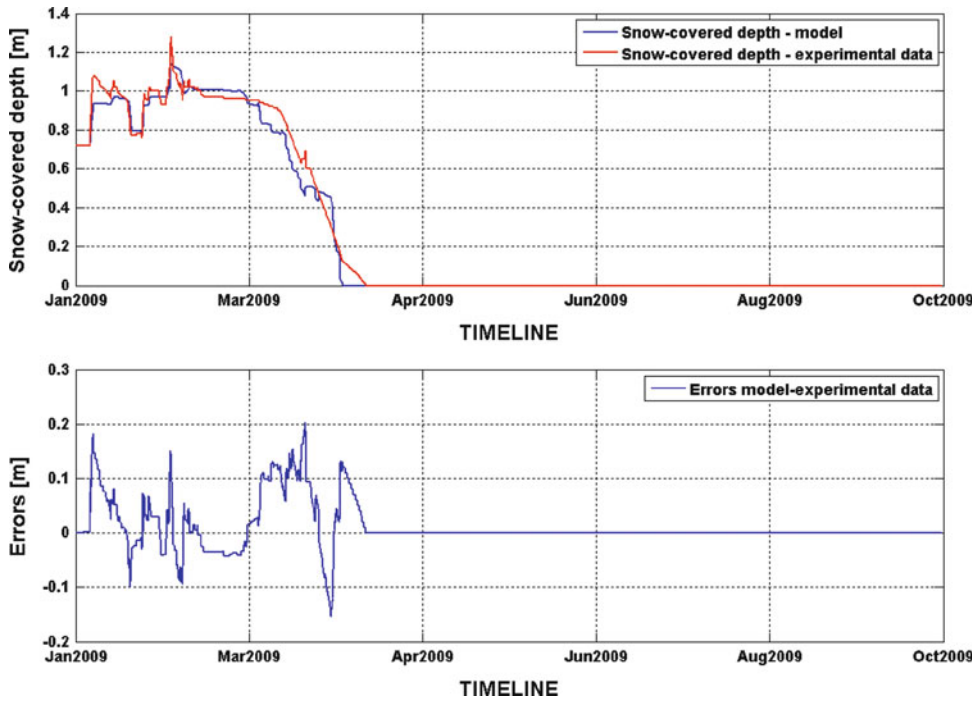

Fig. 3 Calibration of the model with the event 01/2009-03/2009 registered with sensor of Doccia di Fiumalbo rain gauge

experimental data of snowpack depths (hourly precision) are very noisy and we chose the best data and we used a 24-h mean and 10-day moving average with exponential weights to remove the noise from temporal series. The validation test proves that the snow model performance is quite satisfactory: Fig. 4 is an example of this validation.

The absolute mean error is 5.7 cm in calibration and 11.8 cm in all validation period; these results are below the measurement errors of the rain gauge sensors (Ryan et al. 2008).

Underestimation or overestimation of the height of the mantle is mainly due to the fact that some physical factors are not explicitly considered in the model: aspect, wind, cloud cover, etc.

Finally we test the resilience of the model with a sensitivity analysis (static and dynamic): in the studied range of values of parameters the errors are moderate, for example for values near the nominal value of k1 and for a large range of threshold temperatures the max errors is about 10 cm, which corresponds on average to 10 mm of equivalent

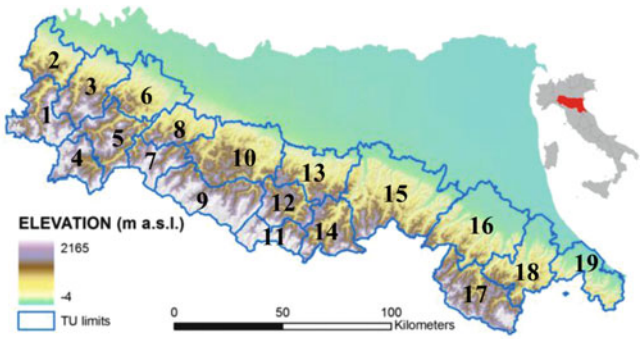

Fig. 5 The study area (Emilia Romagna region) with subdivision in TU (Territorial Unit)

rainfall. Then increasing the threshold temperature of 1°, a small error occurs in the melting phase and a negligible one occurs in the accumulation phase. Decreasing the temperature, the error becomes larger: this fact is confirmed by other models, where the threshold temperature varies in a range from −1 to +3 °C (U.S. Army Corps of Engineers 1956; Wigmosta et al. 1994).

Integration of the SMM with a Statistical Model for Landslides Prediction

The SIGMA Model

SIGMA (Sistema Integrato Gestione Monitoraggio Allerta, that stands for "Integrated service for the managing and monitoring of the alert") is a statistical model which is used in a landslide alert system by the Civil Protection of Emilia-Romagna region (Italy).

The region is partitioned into 19 Territorial Units (TU), each of them assembling areas with the same meteorological characteristics and the same prevailing lithology (Fig. 5).

Each TU has only one rain gauge reference whose temporal series of measurements was used to set site-specific rainfall thresholds. The latter are based on the amount of rain cumulated in the 3-days and a 60-days periods. The SIGMA model is based on a decision algorithm that, at daily steps, according to the rainfall forecasting and the measured antecedent rainfall, can provide four levels of increasing alert (Table 2). This statistical model is calibrated with the landslide events of period 2004–2007 and validated from the period 2008–2010. Further details on the SIGMA model are provided in Martelloni et al. (SIGMA WLF 2011) and Martelloni et al. (submitted to Landslides 2011).

Each level of criticality involves a specific operating procedure: since we should avoid as much as possible false alarms, the rainfall thresholds are properly calibrated on past rainfall events that resulted (or did not) in landslide triggering.

Table 2 SIGMA outputs and associated criticality of the Civil Protection System

SIGMA state	Criticality
0	Absent
1	Ordinary
2	Moderate
3	High

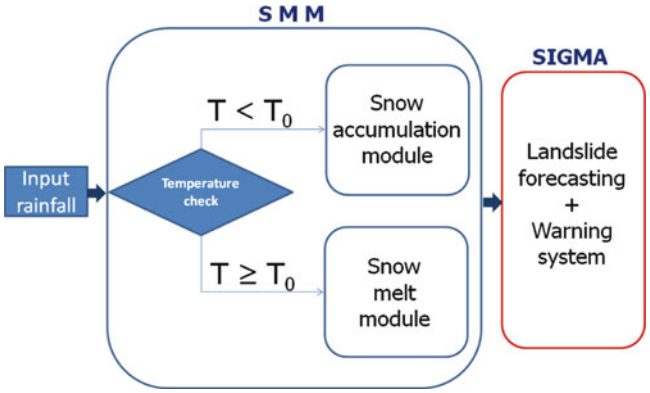

Fig. 6 Integrated system SMM–SIGMA for landslides forecasting

Table 3 The results of application of SMM to SIGMA model in all period 2004–2010 (calibration plus validation)

TU	Landslides identified without SMM	Landslides identified SMM + SIGMA	Difference
9	101	105	+4
12	84	112	+28
15	83	105	+22

Integration Between SMM and SIGMA (Results)

The integration between SMM and SIGMA is explained in Fig. 6, where the snow melt modelling acts like a filter depending on thresholds temperature T_0.

If $T \geq T_0$ the snow model returns to SIGMA the rainfall (if present) and the water equivalent of snow melting (if present) with a delay depending on the time that the temperature remains below the threshold (accumulation phase).

The SMM can be used only in those TU equipped with heated rain gauges (11 out of 19). With this application a marked improvement is obtained (see Table 3) in three TU, while in the remaining eight TU there are no substantial changes as snowfalls were not heavy at the altitude of these rain gauge.

Conclusion and Perspectives

The integration SIGMA – SMM allowed to detect 54 landslides in three TU due to snow melting in the period 2004–2010: these results was also verified by analysis of the landslide database in a GIS environment. In the remaining eight TU with heated rain gauge, as explained above, the snowfalls are low and some landslide triggering are due to combined effect rainfall – snowfall with the preponderance of the first one, while not many landslide triggering occurs in correspondence to not relevant snow melting for exceeding the thresholds.

Actually, the rainfall thresholds could be lowered in order to detect almost all landslides, but doing so would lead to a number of false alarms which is not tolerable in a civil protection alert system: the present configuration of the SIGMA – snow melt models represents an acceptable accommodation between correct predictions, false alarms and missed alarms.

The integrated module SIGMA-Snow melt model for landslides forecasting, however, has some weaknesses: first of all the use of one single rain gauge for each TU represents a coarse approximation as the environmental conditions of rain gauge (rain, temperature, ecc.) are considered valid for the whole TU. To get a more accurate modeling, a greater number of rain gauges should be used for each TU. Furthermore, the snow melting model would also gain in accuracy using a lumping scheme based on elevation as well. At present, the integrate module has some advantages: the extreme simplicity and rapidity of the forecast procedure; the limited number of input data that are derived from the values of precipitation and temperature, easily accessible in countries with sufficiently organised meteorological networks; the states of the model (0,1,2,3) can be placed in direct correspondence with the levels of criticality of the Civil Protection System to give a quick indication of the level of alert.

References

Brun E, Martin E, Simon V, Gendre C, Coleou C (1989) An energy and mass model of snow cover suitable for operational avalanche forecasting. J Glaciol 35(121):333–342

Himmelblau D (1972) Applied nonlinear programming. McGraw-Hill, New York

Hock R (2003) Temperature index melt modelling in mountain areas. J Hidrol 282:104–115

Kuchment LS, Gelfan AN (2001) Dynamic-stochastic model of snowmelt runoff generation and its application for estimating extreme floods. In: Proceedings of the 58th Eastern snow conference, Ottawa

Kustas WP, Rango A, Uijlenhoet R (1994) A simple energy budget algorithm for the snowmelt runoff model. Water Resour Res 30(5):1515–1527

Marks D, Domingo J, Susong D, Link T, Garen D (1999) A spazially distributed energy balance snowmelt model for application in mountain basins. Hydrol Process 13(12–13):1935–1959

Marsili-Libelli S (1992) Parameter estimation of ecological models. Ecol Model 62:233–258

Martelloni G, Segoni S, Fanti R, Catani F (2011) Rainfall thresholds for the forecasting of landslide occurrence at regional scale. Landslides, online first, doi:10.1007/s10346-011-0308-2

Nelder AJ, Mead R (1965) A simplex method for function minimization. Comput J 7:308–313

Pahaut E (1975) Les cristaux de neige et leur métamorphose. Météorologie nationale, Monographie n° 96, Paris, 58 p

Ryan WA, Doesken NJ, Fassnacht SR (2008) Preliminary results of ultrasonic snow depth sensor testing for National Weather Service (NWS) snow measurements in the US. Hydrol Process 22: 2748–2757

Segoni S, Martelloni G, Lagomarsino D, Fanti R, Catani F (2011) An operational warning system for the forecasting of landslide occurrence at regional scale. WLF2–2011–0385

U.S. Army Corps of Engineers (1956) Snow hydrology, summary report of the snow investigations. Technical report, U.S. Army Corps of Engineers, North Pacific Division, Portland

Wigmosta MS, Vail LV, Lettenmaier DP (1994) A distributed hydrology-vegetation model for complex terrain. Water Resour Res 30(6):1665–1679

Zanotti F, Endrizzi S, Bertoldi G, Rigon R (2004) The GEOTOP snow module. Hydrol Process 18(18):3667–3679

Defining Rainfall Thresholds for Early Warning of Rainfall-Triggered Landslides: The Case of North-East Sicily

David Johnny Peres and Antonino Cancelliere

Abstract

Extreme rainfall is the main cause of landslides and, depending on the magnitude of the rainfall event and the geomorphological characteristics of the landslide-prone area, its occurrence can lead to debris-flows, causing higher damage than floods. Empirical rainfall thresholds of landslide triggering have been proposed by researchers and used as a basis of early warning systems activated throughout the world. The present paper shows the results of an analysis aimed to formulate, in an empirical fashion, the landslide triggering conditions for the north-eastern region of Sicily, in which a catastrophic debris-flow has caused 37 deaths, on October 1, 2009. More specifically, we have investigated the possibility to exploit annual maxima of rainfall for fixed durations, available in the annual reports of the Water Observatory of the Department of Water and Waste of Sicily Region. Calibration of rainfall thresholds has been carried out using the National Research Council's AVI database of historical information on landslides developed by Guzzetti et al. (Environ Manage 18(4):623–633, 1994). Also the FLaIR model (Forecasting of Landslides Induced by Rainfall), proposed by Sirangelo and Versace (Atti del XXIII Convegno di Idraulica e Costruzioni Idrauliche, Firenze, pp D361–D373, 1992), and used as a basis in the realization of several early warning systems in Italy, has been implemented and tested on the case-study area. The results of the work can find application in view of the development of a landslide early warning system in the area.

Keywords

Early warning system • Debris-flow • Rainfall • FLaIR • Sicily

Introduction

Rainfall-triggered landslides are extreme events that can cause extended damage, especially when, depending on the magnitude of the rainfall event and the geomorphological characteristics of the landslide-prone area, they occur in the form of debris-flows. Rainfall thresholds of landslide triggering have been proposed by researchers and used as a basis of early warning systems activated throughout the world (Keefer et al. 1987; Baum et al. 2005).

Early warning of rainfall-triggered landslides has found widespread interest in literature (see e.g. reference list by De Vita and Reichenbach (1998)). Despite the theoretical advantage and high generalization capabilities of physically based approaches, yet their applicability is limited to individual slopes. Indeed, when the interest lies on local or regional scales, practical difficulties generally arise due to the lack of estimates of spatially distributed hydraulic and mechanical parameters, and to complexities of ground

D.J. Peres (✉) • A. Cancelliere
Department of Civil and Environmental Engineering, University of Catania, Viale A. Doria 6, Catania, Italy
e-mail: djperes@dica.unict.it; acance@dica.unict.it

C. Margottini et al. (eds.), *Landslide Science and Practice*, Vol. 4,
DOI 10.1007/978-3-642-31337-0_33,

conditions on susceptible slopes (Cepeda et al. 2011). Thus, empirical rainfall thresholds of landslide triggering have been developed. Since Caine (1980) proposed a rainfall intensity-duration (ID) empirical model, determining a relationship based on data collected worldwide, several site-specific ID models have been proposed, as well as refinements to better take into account antecedent soil moisture conditions via antecedent rainfall (Baum and Godt 2010), that seem to affect at significant degree soil slides rather than debris flows (Cepeda et al. 2011). An investigation by Guzzetti et al. (2007) showed that more than 125 site-specific empirical relationships have been formulated throughout the world (see http://rainfallthresholds.irpi.cnr.it/). Among these 54 are related to Italy.

A common finding of all studies is the conclusion that determination of landslide-triggering rainfall thresholds is strongly dependent on a sound database of observed landslides, which ultimately controls the reliability of calculated thresholds (Glade et al. 2000).

An attempt to generalize empirical models has been made by Sirangelo and Versace (1992), that have proposed the FLaIR model, which has found several applications in Italy, in particular to the Calabria region (Sirangelo et al. 1996; Sirangelo and Versace 1996; Iiritano et al. 1998), to Sarno in the Campania region (Sirangelo and Braca 2004) and to the Lanzo area in Piedmont, where an early warning system based on FLaIR is active (Capparelli et al. 2004).

In FLaIR model the definition of the warning threshold is based on the computation of a mobility function, that is the convolution between a rainfall time series at a representative location and a impulse response distribution, which characterizes the area with respect to its behaviour to landslides. Calibration of the model is done through the use of historical rainfall series and landslide events.

In the paper, preliminary results related to the determination of empirical rainfall thresholds for landslide triggering conditions in the Peloritan mountains, Sicily, are presented. First, empirical rainfall thresholds are derived making use of the FLaIR model. Then, a separate methodology based on maximum annual intensity rainfall data is outlined and applied. Such an approach attempts to better exploit rainfall data systematically collected for Italy, and to combine them with the landslide information of the AVI inventory (Guzzetti et al. 1994), the most complete archive of landslide events occurred in Italy. This landslide data is available through the SICI information system (Guzzetti and Tonelli 2004; http://sici.irpi.cnr.it/). The data of annual maximum intensity rainfall for sub-daily durations, available on the Hydrological Annual Reports of the Water Observatory of Sicily (formerly Hydrographic Service), are used to excerpt rainfall events in terms of total rainfall.

Methods

FLaIR Model

FLaIR model is based on the computation of a function Y of time t, denoted as *mobility function*, given by the convolution integral between rainfall intensity $p(t)$ at a representative location and an impulse response function $\psi(t)$:

$$Y(t) = \int_0^t p(\tau)\psi(t-\tau)d\tau \tag{1}$$

The role of the impulse response function should be to characterize the link between rainfall patterns and landslide occurrence in the given area.

In order to compute the mobility function starting from a rainfall time series at a Δt time scale, a discrete form of (1) (cfr. Sirangelo and Versace 1996)

$$Y_i = \sum_{j=1}^{i} h_j \psi[(i-j+0.5)\Delta t] \tag{2}$$

can be used, being h_j the total rainfall over time interval $[(j-1)\Delta t, j\Delta t]$ and Y_i the value of the mobility function at the current instant $i\Delta t$.

Regarding the impulse response function, Sirangelo and Versace (1992) suggest various parametric forms, among which there are the exponential (one parameter), the gamma (two parameters) and the beta (four parameters) distribution.

In particular, in the application carried out within this paper, the gamma distribution has been selected as impulse response function, hence:

$$\psi(t;a,b) = \frac{1}{b^a\Gamma(a)} t^{a-1} e^{-\frac{t}{b}} \tag{3}$$

Then calibration of the FLaIR model requires the identification of the two parameters a and b in (3).

After the form of the impulse response function is chosen, the calibration of its parameters can be carried out on the basis of a rainfall time series and the knowledge of landslide initiation instants within a past period, as explained in the following.

According to the *ranking criterion* (Sirangelo et al. 1996), a given set of parameters is admissible (i.e. the model is consistent with historical data evidence), if and only if the greatest K values, $Y_1 > \ldots > Y_k > \ldots > Y_K$ of the mobility function occur when landslides were observed. Due to

uncertainty in the knowledge of the instant of initiation of the slope movement and to the fact that in diffused landslides the various movements occur generally at different time instants, those K values must fall within time intervals δ_k that include the most representative instant of landslide initiation.

Since generally more than one parameter set is consistent with the above-described ranking criterion, a region of valid parameters results, called also admissibility field Ω (Sirangelo et al. 1996).

If θ^* is a valid parameter set, $F_U(\theta^*) = Y_K$ is the lowest value of the mobility function for which a landslide is triggered. Also the maximum value $F_L(\theta^*)$ outside the time intervals δ_k is important, since it indicates the maximum value of the mobility function for which no landslide was triggered.

Hence, the upper $F_U(\theta)$ and lower limit $F_L(\theta)$ functions result, being θ in the admissibility field Ω.

Due to the non univocal identification of the parameters of the model, a probabilistic approach has been proposed to identity the rainfall landslide-triggering thresholds and the conditions to issue the warnings (Sirangelo and Versace 1996; Sirangelo et al. 1996; Iiritano et al. 1998). Here a simpler approach is applied, based on the maximization of the difference between the upper limit and the lower limit function. In fact, assuming as best model criterion the capability to distinguish between critical (landslide triggering) and non critical (no landslide triggering) situations, the best value of the parameter may be the one that maximizes the difference $F_U - F_L$.

Once the model is calibrated, a critical value Y_{cr} of the mobility function is identified, as its lowest value for which a landslide was triggered. Y_{cr} is then equal to the value of the lower limit function for the best set of parameters. It could be assumed that the triggering condition for landslides is given by $Y = Y_{cr}$; however, as every historical sample does not contain all the possible patterns of rainfall that can trigger landslides, Sirangelo and Versace (1992) suggest to reduce the value of Y_{cr} multiplying it by a factor $s < 1$. Hence, alarms are to be issued when $Y = sY_{cr}$. Furthermore, as it is expected that the value of Y_{cr} will be reached gradually, the civil protection levels of advice and watch can be identified as fractions $s_{adv} < s_{wat} < s$, of Y_{cr}. For instance, in Versace and Capparelli (2008) it is suggested to assume: $s_{adv} = 0.40$, $s_{wat} = 0.60$ and $s = 0.80$, on the basis of the application of the model to several case studies.

Approach Based on High Intensity Rainfall Data

Derivation of reliable empirical rainfall-thresholds can be hindered by the lack of suitable precipitation data. For instance in Sicily, although long daily precipitation records are available starting from the early 1920s, yet no consistent datasets of sub-daily precipitation data are available. On the other hand, relatively long series of maximum annual rainfall of fixed durations (from 1 to 24 h) have been collected by the Water Observatory in several stations in Sicily. Therefore, an approach that capitalizes on such data is proposed here, with the objective of deriving cumulative rainfall thresholds for landslide triggering.

Table 1 Possible outcomes of an early warning system based on the comparison of total rainfall with total rainfall warning curves

	Landslide occurrence	
Comparison outcome	Landslide	No landslide
Warning $R(t) > R_w(t)$	True positive (TP)	False positive (FP)
No warning $R(t) < R_w(t)$	False negative (FN)	True negative (TN)

The approach is based on cross matching the high rainfall intensity events in the Water Observatory database with the landslide events that occurred during the years covered by available data in the area. In particular the objective is to define total rainfall warning curves $R_w(t)$ of the maximum total precipitation as a function of the duration t. Such critical curves can be selected based on the four possible outcomes of an early warning system scheme for which a prevention action is taken as the current total rainfall $R(t)$ exceeds the landslide warning curve $R_w(t)$. In Table 1 the possible outcomes of such warning system are outlined, in terms of correct / non correct warning. In principle, the best warning curve $R_w(t)$ is the one that maximizes the number of True Positive and True Negative occurrences, while minimizing the number of False Positive and False Negative occurrences.

Then, the best warning curve may be the one that maximizes the following function:

$$F = N_{TP} - N_{FN} + N_{TN} - N_{FP}, \tag{4}$$

being N_{XX} the number of the outcomes of the generic condition XX according to Table 1. A refinement of (4) can be obtained by observing that one may prefer to give different weights to the different outcomes, thus:

$$F = w_L(N_{TP} - N_{FN}) + w_N(N_{TN} - N_{FP}) \tag{5}$$

The above weights w_L and w_N simply take into account the fact that, for instance, one may give more importance to minimizing the number of False Negatives, rather than False Positives, since the costs related to a False Negative generally exceeds those of a False Positive.

Maximization of (5) depends on the ratio $w = w_L/w_N \leq 1$, so (5) can be expressed as a function of one parameter w only as:

Fig. 1 Location of the Fiumedinisi rain gauge managed by SIAS (Servizio Informativo Agrometeorologico Siciliano), used for FLaIR implementation

$$F = (N_{TP} - N_{FN}) + w(N_{TN} - N_{FP}). \quad (6)$$

Investigated Area and Data

The above described methodologies have been applied with reference to the Peloritan mountains located in the North-Eastern corner of Sicily island in Italy. The Peloritan mountains are amongst the areas of Italy with highest landslide risk, due to the high slopes, frequency of intense rainstorms and urbanization. Because of their geomorphology, characterized by small catchments and an high-density hydrographic network, landslides occur often in the form of debris-flows, with devastating effects. The most recent landslide event, occurred on 1st October 2009, caused 37 fatalities and huge economic losses.

For the implementation of the FLaIR model, the hourly data of rain gauge of Fiumedinisi (440 m a.s.l.) managed by SIAS (Servizio Informativo Agrometeorologico Siciliano, http://www.sias.regione.sicilia.it/) have been used (Fig. 1).

Within the period covered by such series (21st February 2002–9th February 2011), three sets of landslide events occurred in several locations in the investigated area: (1) 15th September 2006 (11:00), (2) 25th October 2007 (14:00), (3) 1st October 2009 (19:00). Among the three events, the most damaging has been the already mentioned event of October 2009. The time of occurrence in brackets has been determined analysing various documents available. The uncertainty of this time occurrence has lead to the choice of intervals δ_k equal to 7 h, i.e. 3 h after + 3 h before + the hour indicated above.

In order to apply the second methodology, based on warning curves derived from high intensity rainfall data, annual maxima of total rainfall for durations of 1, 3, 6, 12 and 24 h from 12 rain gauges in the area have been used (Fig. 2).

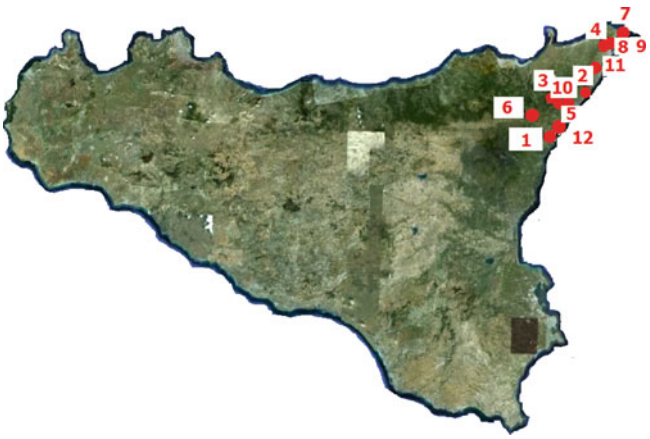

Fig. 2 Location of the precipitation stations of the Sicilian Observatory of Water used for collecting the high intensity rainfall data: *1* Alcantara, *2* Alì Terme, *3* Antillo, *4* Casalvecchio Siculo, *5* Camaro, *6* Francavilla di Sicilia, *7* Ganzirri, *8* Messina (Ist. Geofisico), *9* Messina (Osservatorio), *10* Ranciara, *11* S. Stefano di Briga, *12* Taormina

The data, available from 1924 to 2006, have been excerpted from the Hydrological Annual Reports of the Water Observatory of Sicily (formerly Hydrographic Service). Table 2 summarizes the main features of the selected data.

Information on landslides has been selected from the AVI inventory (Guzzetti et al. 1994), through the SICI information system (Guzzetti and Tonelli 2004). These data are available from 1990 to 2001.

Results

FLaIR Model

In Fig. 3 the admissible region for the parameters of the gamma impulse response function is shown, together with the values of the difference $F_L - F_U$ in a colorscale. The best pair of parameters is $a = 17.615$ and $b = B = 0.115$, as those values correspond to the maximum difference $F_L - F_U$.

The critical value of the mobility function, i.e. the lowest value for which a landslide was triggered, resulted:

$$Y_{cr} = 46.93.$$

Monitoring and eventually forecasting of rainfall and thus of the mobility function for the calibrated parameters, and comparison of this function with its critical value Y_{cr} can be the basis of the implementation of an early warning system in the case-study area.

Table 2 Summary of the high intensity rainfall dataset used for the development of landslide warning curves (z is the rain gauge altitude, N_d the sample size), and historical minima and maxima of rainfall (mm) for the various durations t

	Rain gauge	z		$t = 1$ h		$t = 3$ h		$t = 6$ h		$t = 12$ h		$t = 24$ h	
ID	Name	(m asl)	N_d	Min	Max	Min	Max	Min	Max	Min	Max	Min	Max
1	Alcantara	30	54	16.0	63.6	25.4	82.0	26.0	94.2	29.4	116.8	34.2	154.4
2	Ali Terme	7	60	14.8	64.6	19.0	154.2	22.0	165.2	27.6	166.4	34.8	199.6
3	Antillo	480	11	23.4	**112.8**	24.2	**207.2**	40.0	**240.2**	57.8	266.4	76.6	311.4
4	Camaro	568	100	16.0	100.0	18.4	189.0	31.4	196.0	39.0	208.0	47.4	245.2
5	Casalvecchio Siculo	500	21	13.8	75.8	14.0	118.2	19.0	121.4	28.4	141.6	36.4	158.0
6	Francavilla di Sicilia	463	40	14.0	84.4	20.0	120.0	36.4	232.0	47.8	**309.6**	48.0	**391.6**
7	Ganzirri	3	83	14.0	78.2	18.8	99.0	24.0	103.2	28.0	125.0	28.0	196.8
8	Messina (g)	50	79	11.0	81.4	14.2	108.0	16.8	108.6	26.6	108.6	29.0	195.8
9	Messina (o)	54	45	11.8	89.6	15.4	180.0	19.4	187.8	30.2	215.2	30.2	216.8
10	Ranciara	285	13	23.6	62.8	36.2	114.2	40.2	146.8	65.6	180.0	65.8	197.4
11	S. Stefano di Briga	139	5	19.0	53.5	32.6	123.1	37.2	211.5	47.4	226.4	58.8	226.4
12	Taormina	248	82	16.6	84.4	24.6	98.4	25.4	145.0	27.0	220.0	31.6	316.0
All			*593*	*11.0*	*112.8*	*14.0*	*207.2*	*16.8*	*240.2*	*26.6*	*309.6*	*28.0*	*391.6*

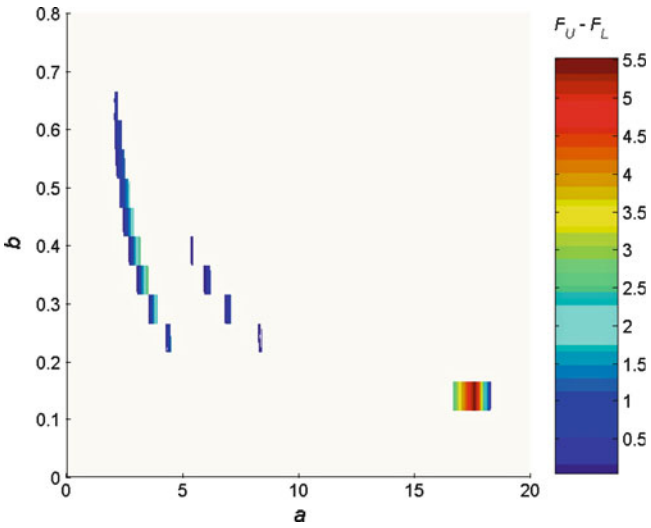

Fig. 3 Admissibility region for the parameters of the gamma impulse response function and difference between upper limit and lower limit functions. Best pair of parameters is $a = 17.615$, $b = 0.115$

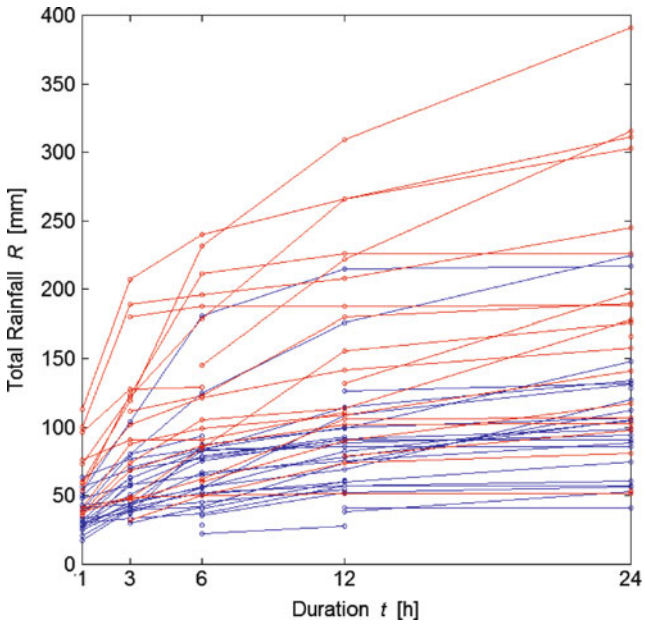

Fig. 4 Data of rainfall events measured by rain gauges 1–12 in dates of landslides. *Red curves* are relative to the rain gauge that measured the highest magnitude event ($R(t = 24\text{ h})$), while the *blue ones* are relative to the other available rain gauges

Warning Curves Based on High Intensity Rainfall Data

In Fig. 4, the total rainfall data of annual maxima per given durations observed in the same date of a landslide are shown. Total rainfall data measured at the same location and date are connected through a line, in order to show the events' pattern of total rainfall as a function of duration.

Since the same rainfall event (i.e. the event with maximum intensities at different durations in a given year) is often observed at several rain gauges, with different values due its spatial variability, more than one rain gauge may had measured an high intensity rainfall event whose date matches the one of the same landslide. In this case the most intense event has been isolated from the other ones by using the criteria that the most intense rainfall is the one with the highest value of total rainfall per duration of 24 h. The red curves in Fig. 4 represent such most intense event, while the blue ones the observations among the other available rain gauges. Hence Fig. 4 shows also the fact that bad located rain gauges can lead to an excessively high underestimate of the landslide-triggering rainfall value. Also the opposite could be true, as the triggering can occur for rainfall events of less magnitude observed at the maximum-rainfall-magnitude rain gauge.

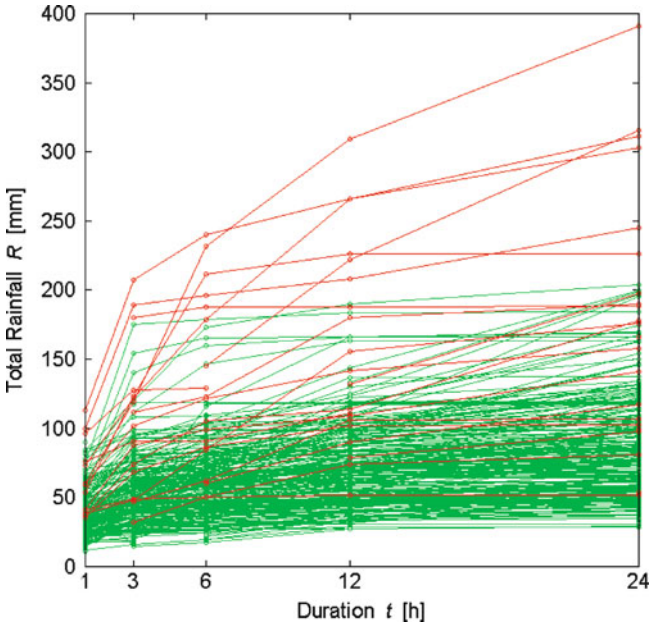

Fig. 5 Data of rainfall events measured by rain gauges 1–12 in dates for which no landslide occurred. Also the *red curves* of the previous figure are shown for comparison

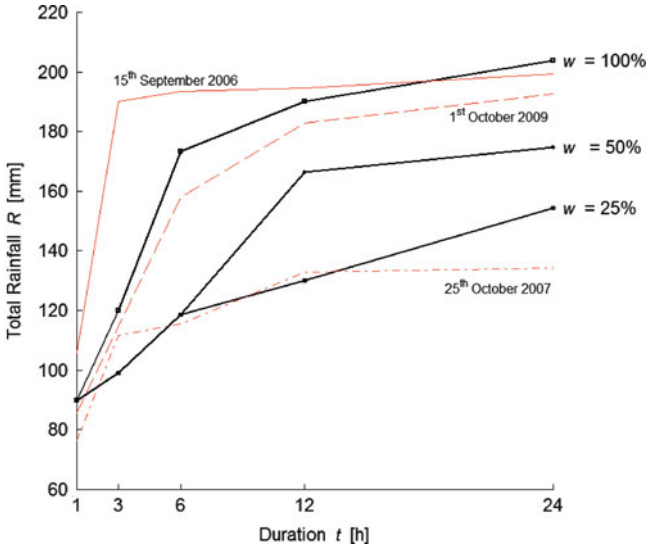

Fig. 6 Warning curves for $w = 0.25$, 0.50 and 1. The rainfall curves relative to the events of 15th September 2006, 25th October 2007 (14:00) and 1st October 2009 (19:00), observed at the Fiumedinisi rain gauge are also shown

Indeed, the combined use of landslide triggering and non-triggering rainfall data, could help to a more reliable assessment of the rainfall landslide-triggering values.

Rainfall events whose dates do not match with landslide dates are shown in Fig. 5 by green lines. The presence of green curves with relatively high precipitation to which correspond no landslides occurrence may be due to several causes, among which possible incompleteness of the AVI inventory cannot be excluded. Further research will also help in establishing whether or not that is the case.

Based on the red and green curves the maximization of the function in (6) has been carried out for different values of the weight w.

In Fig. 6 the best warning curves for the values of $w = 0.25$, 0.5 and 1 are shown. In the figure, the corresponding precipitation totals observed during the landslide events at Fiumedinisi raingauge (data used in FLaIR model implementation) are also shown. From the figure it can be inferred how the derived curves would have positively indicated the event of 15th September 2006 and of 1st October 2009 (for $w = 0.50$), while the event of 25th October 2007 would have been foreseen only in the case of a low value of the ratio w.

It may be worthwhile to note that the above results cannot be considered conclusive about the validity of the proposed approach since a proper validation, making use of extended precipitation data should be carried out. Such validation is the subject of ongoing research.

Conclusions

Efficient early warning of landslide occurrence represents one of the key issues in order to mitigate the most devastating effects of the phenomenon. In the case of rainfall triggered landslides, such early warning can be carried out by means of empirical precipitation thresholds, linking past landslides occurrences with the characteristics of the corresponding precipitation events.

In the paper, results related to the application of two approaches for early warning of rainfall triggered landslides have been illustrated, with reference to the case-study area of Peloritan Mountains, a particularly high landslide prone area in Sicily.

In particular the FLaIR model (Sirangelo and Versace 1992) has been applied with reference to three recent events that occurred in 2006, 2007 and 2009 in the area. One of the advantages of this methodology is that it is in principle applicable to every type of landslides, as it uses a whole measured rainfall time series.

Furthermore, a second approach, that derives rainfall threshold curves by combining annual maximum precipitation for fixed duration data with landslide occurrences observed in the past has been proposed and applied. The main advantage of this approach is the use of a large dataset of rainfall data (about 80 years long) available for all Italian territory, also in order to better exploit the AVI collection of landslide events (Guzzetti et al. 1994), that covers all the past century. Such an approach also

represents a preliminary attempt to take into account information related to both landslide occurrence and non occurrence, by considering the possible outcomes of a warning system in terms of correctly / not correctly warning for landslides. As this method is based on the analysis of subdaily data, it is reliable for shallow landslides, for which low influence of antecedent precipitation on landslide triggering can be supposed.

The results presented in the paper must be considered preliminary. Ongoing research is oriented to improve the high-intensity-rainfall-data-based methodology, as well as to carry out a thorough validation, also by comparing it with other methodologies (including FLaIR model).

References

Baum RL, Godt JW (2010) Early warning of rainfall-induced shallow landslides and debris flows in the USA. Landslides 7:259–272. doi:10.1007/s10346-009-0177-0

Baum RL, Godt JW, Harp EL, McKenna JW, McMullen SR (2005) Early warning of landslides for rail traffic between Seattle and Everett, Washington, USA. In: Hungr O, Fell R, Couture R, Eberhardt E (eds) Landslide risk management. In: Proceedings of the international conference on landslide risk management, Vancouver, Canada, 30 May–3 June 2005. Balkema, New York, pp 731–740

Caine N (1980) The rainfall intensity-duration control of shallow landslides and debris flows. Geogr Ann 62(1–2):23–27

Capparelli G, Sirangelo B, Versace P (2004) Realizzazione di un sistema di preannuncio delle frane innescate da pioggia. In: Atti del I Workshop MODECI – Modelli matematici per la simulazione dele catastrofi idrogeologiche, Arcavacata di Rende (Italy), pp 315–327

Cepeda JM, Malet JP, Remaître A (2011) Empirical estimates of precipitation conditions for landslide triggering in France and Norway. Geophysical Research Abstracts, vol 13, EGU2011-10550, EGU General Assembly 2011

De Vita P, Reichenbach P with contributions by Bathurst JC, Borga M, Crosta G, Crozier M, Glade T, Guzzetti F, Hansen A, Wasowski J (1998) Rainfall-triggered landslides: a reference list. Environ Geol 35(2–3):219–233

Glade T, Crozier M, Smith P (2000) Applying probability determination to refine landslide-triggering rainfall thresholds using an empirical "antecedent daily rainfall model". Pure Appl Geophys 157:1059–1079

Guzzetti F, Tonelli G (2004) Information system on hydrological and geomorphological catastrophes in Italy (SICI): a tool for managing landslide and flood hazards. Nat Hazards Earth Sys Sci 4 (2):213–232

Guzzetti F, Peruccacci S, Rossi M, Stark CP (2007) Rainfall thresholds for the initiation of landslides in central and southern Europe. Meteorol Atmos Phys 98:239–267

Guzzetti G, Cardinali M, Reichenbach P (1994) The AVI project: a bibliographical and archive inventory of landslides and floods in Italy. Environ Manage 18(4):623–633

Iiritano G, Versace P, Sirangelo B (1998) Real time estimation of hazard for landslides triggered by rainfall. Environ Geol 31(2–3):275–283

Keefer DK, Wilson RC, Mark RK, Brabb EE, Brown WM, Ellen SD, Harp EL, Wieczorek GF, Alger CS, Zatkin RS (1987) Real-time landslide warning during heavy rainfall. Science 238:921–925

Sirangelo B, Braca G (2004) Identification of hazard conditions for mudflow occurrence by hydrological model: application of FLaIR model to Sarno warning system. Eng Geol 73:267–276

Sirangelo B, Versace P (1992) Modelli stocastici di precipitazione e soglie pluviometriche di innesco dei movimenti franosi. In: Atti del XXIII Convegno di Idraulica e Costruzioni Idrauliche, Firenze, 1992, pp D361–D373

Sirangelo B, Versace P (1996) A real time forecasting model for landslides triggered by rainfall. Meccanica 31:73–85

Sirangelo B, Iiritano G, Versace P (1996) Il preannuncio dei movimenti franosi innescati dalle piogge. Valutazione della probabilità di mobilizzazione in presenza di indeterminatezza nell'identificazione dei parametri del modello FLaIR. In: Atti del XXV Convegno Nazionale di Idraulica e Costruzioni Idrauliche, Potenza, 3, pp 378–391

Versace P, Capparelli G (2008) Empirical hydrological models for early warning of landslides induced by rainfall. In: Proceedings of the first world landslide forum, Tokyo, 18–21 Nov 2008, pp 627–630

Mechanisms of the Recent Catastrophic Landslides in the Mountainous Range of Rio de Janeiro, Brazil

André S. Avelar, Ana L. Coelho Netto, Willy A. Lacerda, Leonardo B. Becker, and Marcos B. Mendonça

Abstract

Catastrophic mass movements occurred in January 2011 in a mountainous area of Rio de Janeiro leaving more than 1,500 dead people and large destruction. Heavy thunderstorms occurred on January 11th (~100 mm/day) and 12th (~150 mm/day) and triggered thousands landslides on steep slopes with trees and block rich debris materials converged into the river channels, hence avalanches down valley. Through fieldwork, mainly translational slides and debris flow types were observed, as well as some rotational slides and rock fall. Initial studies show that translational slides occurred in saprolite soil with 1–3 m depth and on more than 30° slopes. Debris flows initiated in small catchments with very steep slopes and run out along the valley bottom where colluvial soils are present. This study focuses geological analysis and correlation between soil properties and geotechnical behavior in order to explain this catastrophic slope movement mechanisms and processes.

Keywords

Shallow landslides • Intensive rainfall • Direct shear test • Rio de Janeiro

Introduction

On January 11th and 12th, 2011, 3,562 landslides occurred in the mountainous region of Rio de Janeiro State (RJ). These caused more than 1,500 deaths and severe damage to the urban and rural infrastructure of the municipalities of Nova Friburgo, Teresópolis, Petrópolis, Sumidouro and Bom Jardim. These landslides were observed in a regional band of around 20 × 80 km, where intense rainfall reached 325 mm within 48 h (Fazenda Mendes Station\CPRM). Precipitations over 24 h at various stations within the area with most destruction showed values of 200 mm over 24 h (more details on this can be found in Coelho Netto et al. 2011).

Although considered the most destructive landslides ever registered in Brazil, similar characteristic events already occurred in RJ in 1966, 1967, 1988, 1996 and 2010 (Meis and Silva 1968; Barata 1969; Jones 1973; Lacerda 1997, 2007; Coelho Netto et al. 2007, 2009). In this 2011 event, the majority of landslides were of shallow translational type with many occurrences of debris flows and few rotational

A.S. Avelar (✉)
Geoscience Institute, INCT-Reageo, Federal University of Rio de Janeiro, Av. Athos Ramos, 274, sala H1-015, CEP 21.941-916 Ilha do Fundão (RJ), Brazil
e-mail: andreavelar@acd.ufrj.br

A.L.C. Netto
Geoscience Institute, INCT-Reageo, Federal University of Rio de Janeiro, Av. Athos Ramos, 274, sala H1-015, CEP 21.941-916 Ilha do Fundão (RJ), Brazil

Civil Engineering Program\COPPE, INCT-Reageo, Federal University of Rio de Janeiro, Caixa Postal 68506, CEP 21945-970 Ilha do Fundão (RJ), Brazil

W.A. Lacerda
Civil Engineering Program\COPPE, INCT-Reageo, Federal University of Rio de Janeiro, Caixa Postal 68506, CEP 21945-970 Ilha do Fundão (RJ), Brazil

L.B. Becker • M.B. Mendonça
Civil Engineering, Politechnical School, INCT-Reageo, Federal University of Rio de Janeiro, Av. Athos Ramos, 149, CEP 21941-909 Ilha do Fundão (RJ), Brazil

C. Margottini et al. (eds.), *Landslide Science and Practice*, Vol. 4,
DOI 10.1007/978-3-642-31337-0_34,

Fig. 1 Aerial view of some landslides which occurred on January 12th, 2011 in the mountainous region of Rio de Janeiro State where shallow translational landslides were dominant

slides or rock falls. The most extensive debris flows moved along the most significant valley bottoms of the region and produced a trail of destruction of houses, farms, factories, roadways, bridges, drinking water networks, electricity and telecommunications. They were formed by the junction of diverse shallow translational slides occurring on slopes adjacent to rivers and originating from hollows in mountainous zones.

The geology of the State of Rio de Janeiro is associated with an ample fold belt from the Proterozoic Era, mainly composed of rocks with high metamorphic grades (gneisses) with well defined foliation in the SW-NE direction and fractures in diverse directions. Sin-tectonic igneous (granitoid) rocks, generated by anatexis also occur and are oriented in the same way as metamorphic rocks. The geomorphology of the State presents a predominance of hills and coastal plains with isolated rocky massifs, however the mountainous region of Rio de Janeiro contrasts sharply with this group (Fig. 1).

In the mountainous region, granites (post and tardi-tectonic), migmatites and gneisses with little foliation compose a province of highly weathering-resistant rocks which regionally produce a mountainous geomorphology called the Serra dos Orgãos. In this mountainous region of Rio de Janeiro, the valley bottoms are narrow and develop along persistent tectonic fractures in which only the larger-sized rivers are able to generate even fluvial deposits where the majority of the population is located. Adjacent to these valleys, escarpments with rocky outcroppings and steep slopes (more than 35°) are common; these can present deposits of talus or colluvium rich in rock blocks at the base. On the other hand, in the Serra dos Orgãos landscape, there are also many areas where intramontane hills grade to slopes of slighter declivity (between 15° and 35°). In these areas the regolith are composed by thick saprolitic and colluvial deposits that together can reach until 10 m in depth. Oly in few areas at Serra dos Orgãos range occur deep weathering profiles (saprolites) up to 50 m in thickness.

Colluvial soils in southeast Brazil have characteristic geotechnical features with high void ratio between 1.2 and 2.2, and frequently show a friction angle between 28° and 32° with a cohesion intercept of 2–10 kPa (Silveira 1993; Avelar 1996; Lacerda 2004). Saprolitic soils have variable geotechnical parameters according to the parent rock and the degree of weathering; however ,for saprolites originating from Rio de Janeiro granites described in the literature, a void ratio varying from 0.6 to 1.1, with a friction angle between 30° and 37° and cohesion intercept between 6 and 30 kPa are mentioned (Fonseca et al. 2004; Lacerda 2004). These soils also generally show highly saturated hydraulic conductivity with values between 10^{-2} and 10^{-4} cms^{-1} (Avelar and Coelho Netto 1992).

The region was originally covered continuously by the Atlantic rainforest, which was significantly removed and resulted in the vegetable plantings, grasses (pastures) and urban centers due to human occupation. Some parts with the original forest remain and, in various locations re-colonization by secondary forests occurred due to the impracticability of agricultural activity. These regenerated forests permit the entry of water into the soil, however they do not present deep root anchoring to increase soil resistance on the slopes. During the enlargement of urban and rural activity, cuts into the slopes were made to implant roadways and residences. Such factors increased vulnerability to landslides, as observed in various situations of this type.

The goal of the present work is to understand the geological, geomorphological and geotechnical mechanisms and processes related to the landslides located in the municipality of Nova Friburgo. In Teresópolis and Sumidouro the study focused the images interpretation.

Methods

Mapping the landslides in large portions of Nova Friburgo, Teresópolis and Sumidouro was undertaken by interpreting colored satellite images with a spatial resolution of 0.5 m, in a rectangle of 27.0 × 15.5 km (421 km^2). The landslide contours extracted from these images were entered into a topographic base of 1:50,000-scale over which a DEM was elaborated with a 20 × 20 m grid for later morphometric analyses using GIS. Using this map, fieldwork was undertaken to register the types of landslides which occurred according to the Varnes (1978) classification, and the characteristics of forms, especially length, width and depth of ruptured surfaces. Also the materials involved were observed.

Table 1 Statistical distribution of the slopes angles (degrees) obtained from DEM associated with landscape and landslides

Spatial element	Total	Q1 0–25 %	Q2 25–50 %	Q3 50–75 %	Q4 75–100 %	Mean	St. dv
Slopes on the landscape		0–9.5	9.6–17.3	17.4–24.5	24.5–71.1	17.2	9.8
Slopes with landslides	3,562	0–11.6	11.7–19.8	19.9–29.7	29.8–65.5	18.9	10.9
Landslides 20,000–100,000 m^2	140 (3.9 %)	0–12.9	13.0–21.0	21.1–27.7	27.8–58.4	20.0	11.1
Landslides 5,000–20.000 m^2	606 (17.0 %)	0–12.1	12.2–19.8	19.9–26.7	26.8–65.5	19.2	10.8
Landslides 32–5,000 m^2	2,816 (79.1 %)	0–9.5	9.6–17.6	17.7–24.8	24.9–54.9	17.1	10.6

After noting that there were materials which predominated in the landslides, four types of soil were selected for geotechnical characterization and realization of direct shear tests: grey saprolite, pink saprolite, slope colluvium and valley bottom colluvium.

The direct shear tests were performed on circular samples of 63.5 mm in diameter and 25.8 mm in height, submerged in water for around 20 h and placed in a ShearTracII Geocomp apparatus with a horizontal displacement rate of 0.05 mm. min^{-1}. Since the rupture surfaces of the majority of the landslides observed reached up to 2 m in depth, the values adopted for the initial normal vertical stress in the tests were 25, 50 and 100 kPa. At the end of the tests, the samples reached 12 mm of horizontal displacement representing an almost 18 % deformation. This deformation is enough to cause a rupture in the samples since the slope soils in southeast Brazil tend to reach failure near to 3 % deformation (Silveira 1993; Avelar 1996; Fonseca et al. 2004). In diagram σ (kPa) versus τ (kPa), the linear interpolation defined the equation of the failure envelope for each studied soil.

Results

The interpretation of the satellite images permitted observing the 3,562 landslides, in the rectangular area of 421 km^2, yielding an average density of 8.46/km^2. The GIS analyses enabled establishing landslide size classes (Table 1) grouped into large (from 20,000 to 100,000 m^2); medium (from 5,000 to 20,000 m^2) and small (from 32 to 5,000 m^2), for respective frequencies of 3.9 %, 17.0 % and 79.1 %.

Slopes and Landslides Morphology

Analyzing the DEM with GIS, it was also possible to extract the slope declivities both in the landscape and where landslides occurred (more details are in Coelho Netto et al. 2011). In the landscape, it was noted that there is a normal distribution of slope declivity classes with an average of 17.2° and a standard deviation of 9.8 (Table 1). In the same way, for the slopes with landslides an average declivity of 18.9° and a standard deviation of 10.9 were observed.

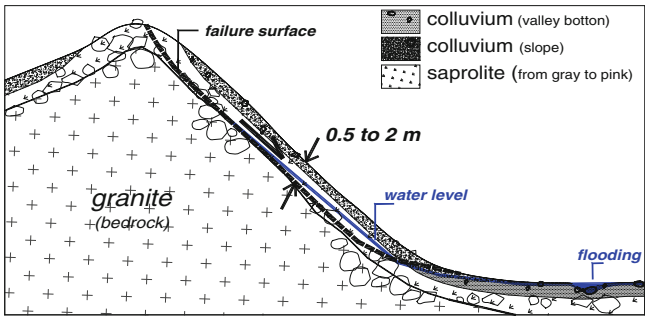

Fig. 2 Typical geological profile associated to the shallow translational slides

Moreover, the mode of slope declivities in the landscape was verified to be 17.3° (Table 1) with a relatively narrow declivity range as indicated by the second quartile (Q2) and third quartile (Q3) with angles between 9.6° and 24.5°. In the same way, the values for slopes with landslides were seen to be close, with a mode of 19.8° and an interval of Q2 and Q3 between 11.7° and 29.7°. This analysis treats landslides in general; however three size classes were considered and it was noted that large landslides show a mode (21.0°) slightly larger than medium (19.8) and small (17.6). This indicates that for a landslide to produce a larger area (or volume), it needs to be on a steeper declivity on the slope. However, in addition to the declivity, its association with slope materials is important.

Geology and Landslides Types

The survey of types of slope movements show that for the majority of shallow translational slides, debris flows also occur (mainly at the bottoms of large valleys) with few rotational slides and rock falls. In this way, it was possible to trace a typical geological profile for the predominant type (Fig. 2). The fieldwork indicated that the predominant rock in the region is an equigranular granite with grain between 3 and 5 mm, basically composed with quartz, k-feldspar and biotite. This rock is of Proterozoic Age and it is inserted in the regional geological maps as the Serra dos Orgãos Batolite and Nova Friburgo Granite units (DRM-RJ 1982).

Fig. 3 Shallow translational slide with failure surface on saprolite derived from granite

Geotechnical Behavior of Materials

The four soil types found in the landslides represent differentiated geotechnical characteristics and behaviors (Table 2 and Fig. 5), there are only similarities in the specific gravity of the grains. The void ratios clearly differentiates the saprolites from the colluvial. The saprolites present similar void indexes, varying between 0.77 and 1.03, which contrast significantly with the colluvium where the variation ranges from 0.97 to 1.61.

The grey-colored saprolite has elevated presence of biotite which indicates that is a slightly weathered soil and, hence, close to the unweathered rock limit (granite). Among the soils studied, it compared as being very sandy (69 %) and more resistant to shear stress, behaving as a granular material with a friction angle of 36.7° and a cohesion of 25 kPa. The pink-colored saprolite was similar to grey saprolite, especially in so far as the friction angle of 38.6°. This behavior pointed that pink saprolite is a material which suffered more chemical weathering, denoted by the transformation of biotites for the generation of clay minerals and iron oxides/hydroxides which influence its coloration and also reduce the sand content to 46 % and increase the clay fraction by 16 %. This chemical weathering action also reduces the cohesion intercept to 25 kPa.

The red colored colluvium presents less sand percentage than the other soils, with only 25 %, moreover, it does not present an increase in the clay content, which only reaches 17 %. These characteristics significantly affect the shear strength behavior of this soil which, despite presenting a friction angle of 38.3°, near to the saprolite values, shows zero cohesion intercept.

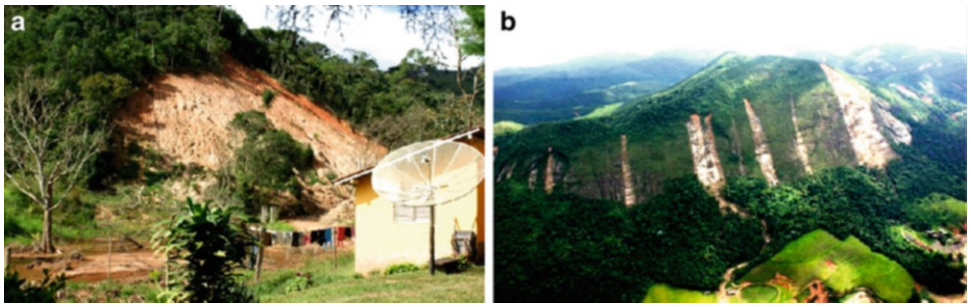

Fig. 4 Landslides with failure surface in colluvium (**a**) and along soil-rock boundary (**b**)

Table 2 Soil types and properties

Soil type	Gravel (%)	Sand (%)	Silt (%)	Clay (%)	Specific gravity	Void ratio
Valley botton colluvium	2	52	19	27	2.693	0.97–1.21
Slope colluvium	0	25	58	17	2.664	1.16–1.61
Pink saprolite	3	46	35	16	2.858	0.77–0.80
Gray saprolite	2	69	25	4	2.650	0.95–1.03

Observations on the materials involved in the shallow translational slides showed four types of different soils: (1) saprolites with grey coloring, representing the initial stage of granite weathering; (2) saprolites with pink coloring, which are in the most advanced stage of weathering; (3) colluvium of red coloring and intense laterization which cover the slope and (4) chestnut-colored colluvium with blocks of rounded rock filling the valley bottoms, generally in the hollows.

These predominant landslides present a rupture surface with a depth between 0.5 and 2.0 m, generally located within the saprolites (Fig. 3). In other cases, rupture surfaces were observed within the slope colluvium, with a depth of up to 1.0 m (Fig. 4). Also, they were observed ruptures along the soil-rock contact (Fig. 4b), with a small quantity mass of soil mobilized due to the thinness of this layer.

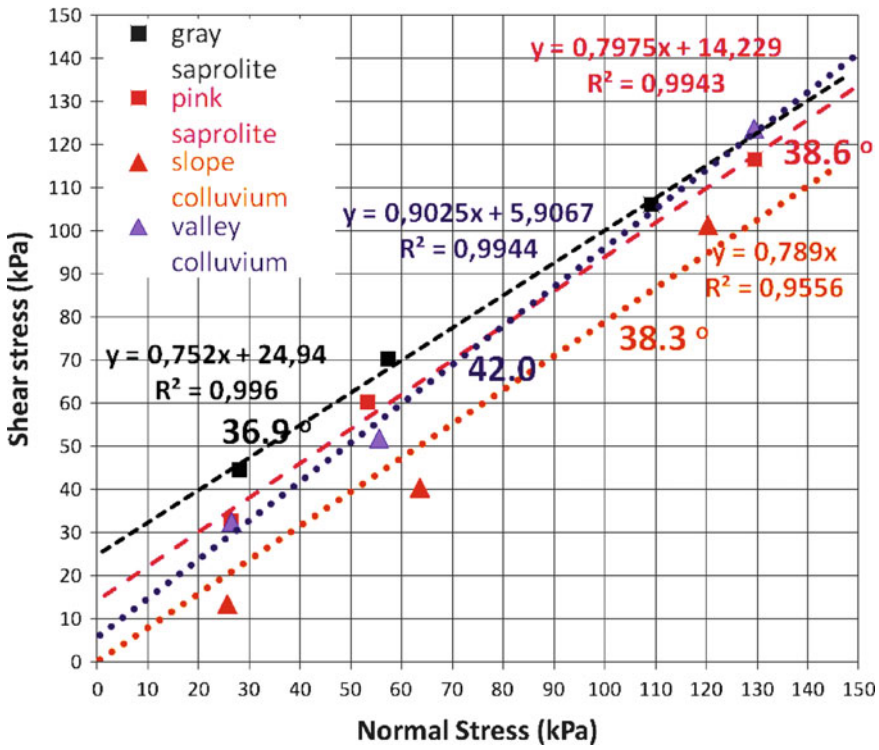

Fig. 5 Shear strength envelope for the four soils studied

The valley bottom colluvium shows a clear difference in relation to the previous soils, especially due to its grain size characteristics and resistance to shearing. It is a soil with high content of sand (52 %) and clay (27 %) which give it a larger friction angle than the others, with 42.0° and a small value for the cohesion intercept with only 6 kPa.

Conclusions

The occurrence of granite in the mountainous region of Rio de Janeiro makes the action of weathering processes difficult and permits the stability of steep slopes, which oftentimes present outcroppings of large-sized rocks. This situation was revealed in the statistical data on slope declivity with an average value of 18.9° and standard deviation of 10.9. On the other hand, with the geological time action and progressive increase of chemical weathering, in general more accentuated with granite fractures, the parent rock mass gives way to saprolitic soils with a gradation of weathering effect which will reduce the real cohesion (cementation) and generate rupture during prolonged rainfall events or during intense rainfall. In all, rock is not always completely weathered, as the occurrence of 'in situ' rounded rock blocks produced by spheroid exfoliation is common in the region.

In the recent landslides, as the saprolite soils present higher actual cohesion, in order for them to rupture in these soils it is probable that an initial saturated zone was formed during the rainy season after December, 2010. The infiltration gradually promoted expansion in the saturation zones into these soils with slowly increase of pore-pressure on the regolith-rock boundary. At the same time there was a moisture increase in the upper part of these soils (unsatured zones) and the suction was gently reduced. On January 11th and 12th, with the advent of intense rainfall, a sudden elevation of the phreatic level should have occurred and there was an rapid increase of pore-pressure with consequent significant reduction in effective stresses. This produced the failure conditions in the saprolites. Figure 2 represents a synthesis of this dominant slope failure mechanism.

The shallowest ruptures occurring in the colluvial soils could have been different. Due to the lack of true cohesion in the colluvium located on the region's slopes, it is probable that during the intense rainfall of January 11th and 12th 2011, there was sufficient infiltration to increase soil moisture, hence without creating a saturated zone. This increase in soil moisture could have caused significant reduction in suction and consequent soil rupture process.

Once the valley bottom colluvium was shown to be more resistant to shear stress than that located on the slopes, the conditions for its rupture also should have been different. The destruction at the valley bottoms in the area analyzed appears very similar to debris flows, however, due to the mechanical shear strength behavior of this soil, it seems that the destruction of these valley bottom soils relate to erosive effects produced by the passage of flows with high concentration of suspended solids. These concentrated flows would come from the superficial outflow generated by intense rainfall, added to the sediment available by shallow translational landslides, originating from the slopes of hollows and

steep slopes adjacent to the channels. Few cases in the studied region are debris flows originating in the slope areas or in the bottoms of steep valleys, that is, in these soils phenomena related to the sudden pore-pressure increase induced by sub-surface water flows were not common. It is possible that this erosive effect with debris flow appearance is more connected to phenomena of flood waves in the valley bottoms, due to outflow produced from rocky slopes located in the hollows.

Acknowledgments We would like to thank the Brazilian Research Council (CNPq), Rio de Janeiro Research Foundation (FAPERJ), Posgradute Program Foundation (COPPETEC), Hydrological Fund (CT-Hidro), Agriculture Fund (CT-Agro), and Brazilliam Science and Technology Institute for Geo-Rehabilitation (INCT-Reageo CNPq-FAPERJ) for their financial support and study grants. The authors would like to thank the students who participated in the different stages in the field and in the laboratory: Anderson Sato, Gabriela Vianna, Ingrid Araujo, Vitor Costa, Natália Lacerda, Ana Carolina, Pedro Lima, David LaCroix, George Teles, André Bastos and Matheus Leal. We would also like to thank engineer Sérgio Iorio and technician Luis Carlos Oliveira.

References

Avelar AS (1996) History and geotechnical investigation of the soberbo mass movement (RJ), (in portug.). M.Sc. dissertation, COPPE/UFRJ, 22 p

Avelar AS, Coelho Netto AL (1992) Subsuface water flow associated to hollows, (in portug.). In: Proceedings of the 1st Brazillian conference on slope stability, Rio de Janeiro, vol 2, pp 709–720

Barata FE (1969) Landslides in the tropical region of Rio de Janeiro. In: Proceedings of the 7th ICSMFE, Mexico, vol 2, pp 507–516

Coelho Netto AL, Avelar AS, Fernandes MC, Lacerda WA (2007) Landslide susceptibility in a montainous geoecosystem, Tijuca Massif, Rio de Janeiro: the role of morphometric subdivision of the terrain. Geomorphology 87(3):120–131

Coelho Netto AL, Avelar AS, Lacerda WA (2009) Landslides and disasters in Southeastern and Southern Brazil, cap 12, pp 223–243. In: Latrubesse E (ed) Natural hazards and human-exacerbated disasters in Latin America. Elsevier, Amsterdam, 550 p, ISBN 9780444531179

Coelho Netto AL, Sato AM, Avelar AS, Vianna LGG, Araujo IS, Croix D, Lima P, Silva AP, Pereira R (2011) January 2011: the extreme landslide disaster in Brazil. In: Proceedings 2nd world landslides Forum, Rome

DRM-RJ (1982) Geological map of nova friburgo. Dept Recursos Minerais, 1:50.000; Niterói (RJ)

Fonseca AP, Lacerda WA, Futai MM (2004) Thoths on residual strength of lateritic soils. In: Proceedings of the 9th international symposium on landslides, Rio de Janeiro, vol 1, pp 669–673

Jones FO (1973) Landslides of Rio de Janeiro and the Serra das Araras escarpment, Brazil, USGS. Prof. Paper 697, 42 p

Lacerda W A (1997) Stability of natural slopes along the tropical coast of Brazil. In: Proceedings of the internatinal symposium on recent developments in soil and pavement mechanics, Almeida, M.M.S (org), Brookfield, Rio de Janeiro, pp 17–39

Lacerda WA (2004) The behavior of colluvial slopes in a tropical environment. In: Proceedings of the 9th international symposium on landslides, Rio de Janeiro, vol 2, pp 1315–1342

Lacerda WA (2007) Landslide initiation in saprolite and colluvium in southern Brazil: field and laboratory observations. Geomorphology 87(3):104–119

Meis MRM, Silva JX (1968) Mouvements de masse r´ecents ‘a Rio de Janeiro: Une etude de geomorphologie dynamique. Revue de Geomorphologie Dynamique 18:145–152

Silveira GC (1993) Geomechanic characteristics of the residual and colluvial soils in the Soberbo road landslide, Rio de Janeiro, (in portug.). M.Sc. dissertation, COPPE/UFRJ, 295 p

Varnes DJ (1978) Slope movement types and processes. In: Schuster RL, Krizek RJ (eds) Landslides—analysis and control, Transport Research Board, Special Report (176). National Research Council, Washington, pp 11–33

A Regional Real Time Landslide Warning System Based on Spatially Variable Rainfall Thresholds

Samuele Segoni, Ascanio Rosi, Alessandro Battistini, Guglielmo Rossi, and Filippo Catani

Abstract

In the Tuscany region (23,000 km^2, Central Italy) landslides triggered by rainfall are a recurring phenomenon. We set up a regional warning system for the prediction and monitoring of the occurrence of landslides, which is based on statistical intensity–duration rainfall thresholds. Since a single regional threshold would be affected by a too large uncertainty, the region was partitioned into 25 alert zones and for each of them an independent set of thresholds was defined analyzing with an automated and objective procedure the rainfall measurements connected to the triggering of 2,132 past landslides.

Keywords

Landslide • Threshold • Rainfall • Warning system • WebGIS • Tuscany

Introduction

Rainfall induced landslides are a recurrent phenomenon that causes damages and casualties, therefore great efforts are being made to set up early warning systems able to forecast their occurrence. Regional warning system for the forecasting of landslide occurrence are often based on intensity–duration (I-D) rainfall thresholds (Caine 1980; Wieczorek and Glade 2005; Guzzetti et al. 2008, and references therein).

Although widely used, this approach is currently affected by a high degree of subjectivity in the procedures used to obtain the I-D relationship (Guzzetti et al. 2008; Segoni et al. in preparation).

Concerning Tuscany region (Central Italy), previous works assessed the possibility of defining a warning system based on rainfall thresholds (Rosi et al. 2010) and highlighted that a single threshold would be affected by large uncertainties, due to large variability of geological, morphological and meteorological factors (Segoni et al. 2010; Rosi et al. submitted). For example, the thresholds defined by Giannecchini (2005) for the Northwestern part of Tuscany resulted in a marked underestimation of hazard if used in other areas of the region (Rosi et al. submitted).

In the present work, to overcome these limitations, the following innovations were introduced:

- The whole territory was partitioned into 25 alert zones (AZ) on the basis of their climatic and geographical settings and for each AZ an independent set of I-D thresholds was defined;
- A newly developed automated procedure (Segoni et al. submitted) was applied to define statistical thresholds with the lowest possible degree of subjectivity.

The set of thresholds was then implemented in a WebGIS system with an intuitive graphical interface which provides a useful tool to help decision makers in assessing the warning level over the whole Tuscany region and at specific locations.

Material and Methods

Test Site

Tuscany is a 23,000 km^2 wide region located in Central Italy, characterized by a mainly hilly and mountainous territory (Fig. 1).

S. Segoni (✉) • A. Rosi • A. Battistini • G. Rossi • F. Catani
Department of Earth Sciences, University of Firenze,
Via G. La Pira 4, Florence, Italy
e-mail: samuele.segoni@unifi.it

C. Margottini et al. (eds.), *Landslide Science and Practice*, Vol. 4,
DOI 10.1007/978-3-642-31337-0_35,

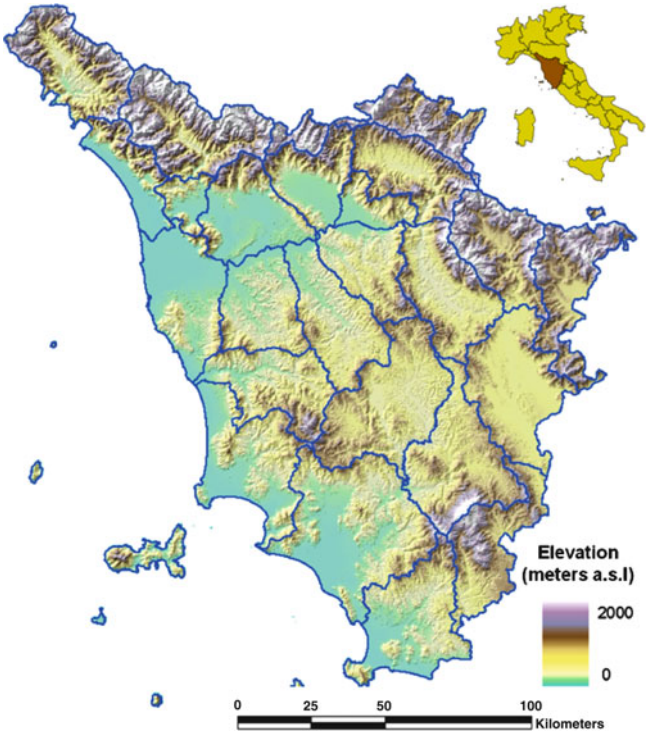

Fig. 1 Tuscany Region and boundaries of the 25 alert zones (in *blue*)

Tuscany has a typical Mediterranean rainfall regime with mild and moist winters, hot and dry summers and two peaks of precipitation (the main one in autumn and the secondary one in spring or winter), while summer is always the driest period of the year. Areal distribution of rainfalls is markedly influenced by the relief: in the North-western part of the region, in particular, mean annual precipitations (MAP) are above 2,000 mm/year (with peaks of 3,000 mm/year), while southern Tuscany is characterized by very lower rainfall amounts (MAP lower than 600 mm/year).

To account for this high variability and to get more accurate rainfall thresholds, the test site was partitioned into 25 Alert Zones (Fig. 1), which were independently analyzed.

Input Data

To define the rainfall thresholds, over 4,200 rainfall paths leading to the initiation of 2,132 dated and georecorded landslides were analyzed. Rainfall paths were obtained combining the hourly rainfall recordings from a regional network of about 360 rain gauges with a geodatabase containing 2,132 dated and georecorded landslides (Fig. 2).

Automated Analysis for Zonal Statistical Thresholds

The large amount of collected data has been analyzed using a newly developed procedure (Segoni et al. in preparation) which is largely automated and which allows the definition of intensity-duration rainfall thresholds with the lowest possible degree of subjectivity. The procedure is largely carried out with the software MaCumBA (Massive Cumulate Brisk Analyzer) (Segoni et al. in preparation), developed with the aim of processing in a short time large amounts of data to obtain statistical I-D warning thresholds.

For each landslide, MaCumBA analyzes the recordings of each rain gauge located in the same AZ. The software automatically carried out the following tasks, otherwise traditionally performed manually and in a subjective way over a limited number of rainfall paths:

- Identification, in the rainfall data, of the beginning of the antecedent rain.
- Definition of the critical parameters used to describe the rainfall event (in the present study: critical intensity I and critical duration D).
- *A posteriori* selection of the most appropriate rain gauge for the characterization of each landslide event.
- The selected ID values are plotted in a graph, where each point represents the rainfall conditions that in the past resulted in the triggering of a landslide.
- Two thresholds are automatically defined making use, in the frequentist statistics approach, of two distinct statistical intervals: the confidence interval and the prediction interval.

The thresholds are defined considering a power law function in the form (Caine 1980)

$$I = a\, D^{-b}$$

where I is intensity, D is duration and a and b are empirical parameters.

An advantage of the proposed methodology is that the complete automation of the procedure allows to iteratively perform several runs of the model using different parameters. The latter influence e.g. the definition of the critical rainfall (and thus the resulting I and D values), the choice of the proper rain gauge or the methodology to draw the threshold.

The optimal setting configuration is chosen with an objective procedure: an extension of the program is used to perform a back-analysis over historical rainfall data, in order to identify the threshold that minimizes both false positive errors (false alarms) and false negative errors (missed alarms).

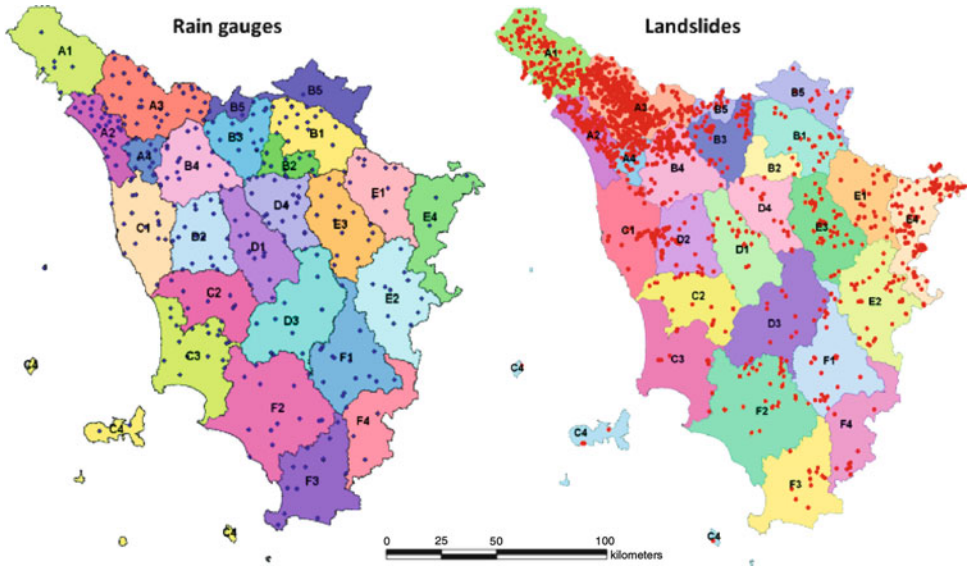

Fig. 2 Location of rain gauges and landslides within the study area. The partition into 25 alert zones is also displayed

The whole procedure (MaCumBA analysis and back-analysis) was applied separately for every alert zone: the final result is a dataset in which each AZ is characterized by:
- Its local I-D threshold (defined by the local values of *a* and *b* parameters of eq. 1)
- Its *no rain gap*, defined as the amount of time without precipitation required to consider a rainfall event as separated from the previous (and subsequent) one.

Those fundamental parameters were used for the definition of the WebGIS warning system.

WebGIS Warning System

In order to achieve an effective monitoring system, we set up a connection to real-time rainfall data collected by the regional network of 360 rain gauges. Rain gauge network data are distributed using a Comma Separated Value (CSV) file stored on a secure FTP site. The file contains rainfall intensity measured in mm/h for each rain gauge. The file contains the last 60 min rainfall recordings and it is updated with the same time rate.

Information about each rain gauge are collected from another CSV file (stored in the same FTP site) containing data about name, geographical coordinates and elevation of rain gauges.

To implement a real-time warning system a proper procedure was developed using PHP scripting (http://www.php.net/). A script takes care of downloading data from the FTP site. In agreement with Shannon's theorem (Shannon 1948, 1949; Jerri 1977), the connection frequency must be at least double than the update rate of rain gauges, so the script is set to check every 30 min the time of creation of the CSV file. If the file is newer than the local one, the file is downloaded an its data are transferred to a local DBMS (Data Base Management System). A MySQL Database (http://www.mysql.com) replicates the information of the CSV file, ensuring the continuity among rain gauge data. The same database stores also information about the Alert Zone each rain gauge belongs to and the local threshold parameters (as explained in the previous section).

On every update, the cumulative rainfall is calculated and compared with the thresholds of the area where the sensor is located. Depending on the value of cumulative rainfall, each rain gauge is labelled with one of the following states:
- Inactive: rain gauge does not provide any data (it is malfunctioning or temporarily dismissed)
- No rain: no rain was recorded during at least the last X hours, where X represents the *no rain gap* of the AZ
- Normal: cumulative rainfall is below the thresholds
- Alert: cumulative rainfall is above alert threshold (if present)
- Danger: cumulative rainfall is above danger threshold.

If an amount of hours equal to the *no rain gap* is passed without recording any rainfall, the event is considered concluded and the cumulative path is reset to zero. The data in the database are deleted so as to reduce the amount of used resources.

A WebGIS was developed to monitor the temporal evolution of the rain gauges. The WebGIS is continuously connected to the database, showing the rain gauge status, marked by different colours (Fig. 3).

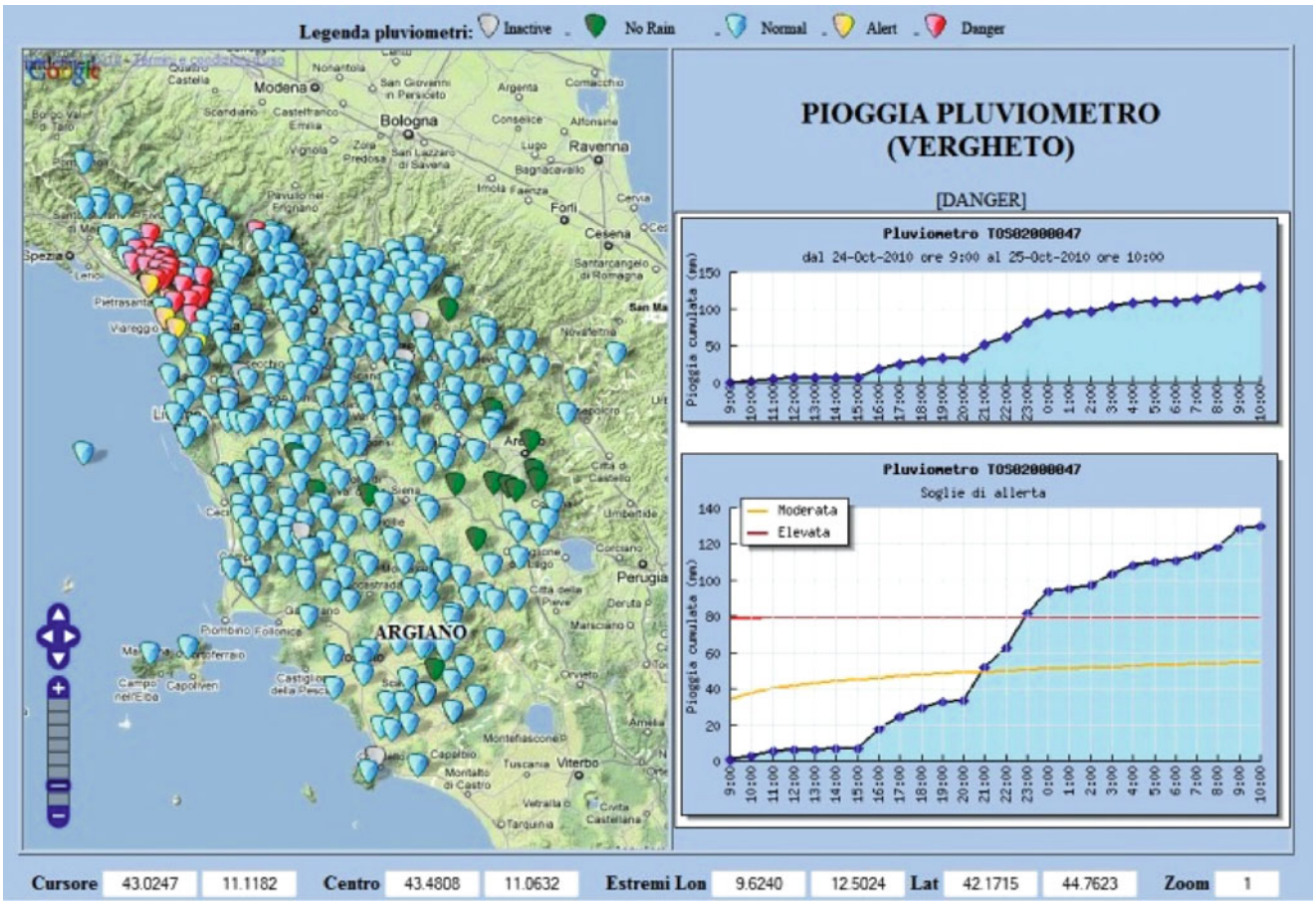

Fig. 3 WebGIS interface showing a rain gauge exceeding the danger threshold

The scripts embedded in the WebGIS store a steady stream of rain information on DB and CSV files. Noteworthy rain events (rainfalls with cumulative value greater than 20 mm) are stored as well for future reference.

For each rain event the scripts store a range of fundamental information, which can be used to recreate the event in future analyses (Fig. 4). Stored parameters are:

- IDStazione: unique ID of the rain gauge station (used as link to other data)
- t_start: time when the rainfall event starts
- t_end: time when the rainfall event starts
- status: severity of alarm (none, alert, danger)
- cumulRain: final value of cumulative rainfall, in mm
- maxSovrCum: maximum value exceeding the danger threshold (or minimum distance from it if the threshold was not exceeded)
- t_maxSovrCum: time of occurrence of the maximum value exceeding the danger threshold (or minimum distance from it if the threshold was not exceeded)
- t_over_thres: eventual time when the threshold was first exceeded
- rainMax: maximum rainfall intensity, measured in mm/h
- t_rainMax: time when the maximum hourly rainfall intensity occurred.

It is possible that the whole event "t_start–t_end" is not the most dangerous one: a shorter sub-event could be characterized by a more intense rainfall which could be related to a higher degree of hazard. To take this possibility into account, a script calculates the cumulative rainfall starting the event at each time-step between t_start (first rain) and t_end (current time), and compares it with the corresponding thresholds. The combination that exceeds the threshold by the largest amount (or that is below it by the shortest distance) is considered the worst scenario: it is selected and shown in the graphics.

Current developments of the systems include the connection of the WebGis with the LAMI Meteorological Model (Cacciamani et al. 2002), which provides 72 h rainfall forecasts. The future configuration will combine the possibility of using the WebGIS as a real-time monitoring system with the possibility of using it as a complete forecasting warning system.

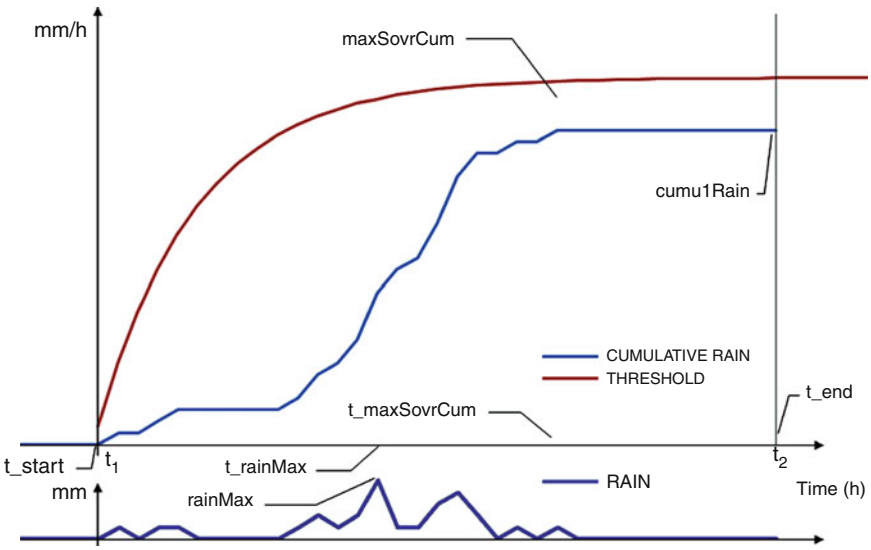

Fig. 4 Parameters used to characterize rain events

Discussion and Conclusion

We set up a warning and monitoring system for rainfall induced landslides in the Tuscany region. Rather than a single regional rainfall threshold, we used a combination of local intensity–duration thresholds. The latter were defined using a highly automated statistical procedure which minimizes subjectivity and reduces the occurrence of false alarms (Segoni et al. submitted).

The system was implemented in a WebGIS for operational use in civil protection procedures. It is easy and intuitive to consult and it provides different outputs, related to different observation scales: it can be used to quickly have an overview of the general situation of the whole Tuscany region or it can be used to monitor the situation at specific locations observing the rain-path recorded by each rain gauge and constantly comparing it with the local threshold.

The system is still on a test phase and further refinements (such as the combined use of nearly real-time recorded rainfall data and weather forecasts) will be soon undertaken.

References

Cacciamani EP, Ferri M, Minguzzi E (2002) High resolution verification of hydrostatic and non-hydorstatic LAM precipitation forecasts in Italy. In: Doms G, Shatter U (eds) COSMO newsletter, vol II. Offenbach, Germany, pp 176–186

Caine N (1980) The rainfall intensity-duration control of shallow landslides and debris flows. Geogr Ann A 62:23–27, 362

Giannecchini R (2005) Rainfall triggering soil slips in the southern Apuan Alps (Tuscany, Italy). Adv Geosci 2:21–24

Guzzetti F, Peruccacci S, Rossi M, Stark CP (2008) The rainfall intensity-duration control of shallow landslides and debris flows: an update. Landslides 5:3–17

Jerri AJ (1977) The shannon sampling theorem—Its various extensions and applications: a tutorial review. Proc of the IEEE 65(11): 1565–1596

Rosi A, Segoni S, Catani F, Casagli N (submitted) Statistical and environmental analyses for the definition of a regional rainfall thresholds system for landslide triggering in Tuscany (Italy). J Geogr Sci

Rosi A, Segoni S, Casagli N, Catani F (2010) Definition of a regional rainfall threshold for landslide triggering in Tuscany. In: Malet JP, Glade T, Casagli N (eds) Mountain risks: bringing science to society, proceedings of the 'mountain Risks' international conference, Firenze 24–26 Nov 2010, CERG, Strasbourg, pp 135–139

Segoni S, Rossi G, Rosi A, Catani F (2010) A regional landslide warning system based on spatially variable rainfall thresholds. Geophysical research Abstracts, EGU General Assembly 2010, vol 12, EGU2010-13767

Segoni S, Rossi G, Catani F (in preparation) Landslides triggered by rainfall: avoiding subjectivity and reducing uncertainty using an automated procedure to define intensity-duration thresholds. To be submitted to environmental modeling and software

Shannon CE (1948) A mathematical theory of communication. Bell System Tech J 27:379–423

Shannon CE (1949) Communication in the presence of noise. Proc IRE 37:10–21

Wieczorek GF, Glade T (2005) Climatic factors influencing occurrence of debris flows. In: Jakob M, Hungr O (eds) Debris flow hazards and related phenomena. Springer, Berlin/Heidelberg, pp 325–362

GIS Analysis of Debris Volume Mobilized by Heavy Rainstorm in North-Eastern Sicily

Nathalie Morey, Giuseppe Tito Aronica, Gabriele Leone, and Claudio Puglisi

Abstract

On October 1st 2009, after a very rainy season, a violent rainstorm poured down Giampilieri, in North-Eastern Sicily with damages to property, buildings, roads, bridges and moreover, loss of human lives. The main focus of this work concerns the analysis of debris volume that has been carried out during this event through the definition of methodologies and determination of techniques that can be applied to evaluate assessment, define crisis scenarios and predict situations of possible debris-mud flows. Here, a series of open-source GIS-based algorithms using spatial analysis has been used in order to perform the calculation of debris-mud flows volume moved during rainstorm. By comparing the volume and run out of past events Rickenmann(Nat Hazards 19(1):47–77, 1999), it is possible to identify empirical site-specific formulas to estimate run out distance of potential events. The analysis issue helps in assessing risk for establishing policies of land planning and civil protection activities.

Keywords

Debris-mud flows • LiDAR • Open-source GIS • Volume evaluation • North-Eastern Sicily

Case Study

Introduction

In the past few decades, the North-Eastern part of Sicily (Italy) has been severely struck by rainfalls inducing devastating debris-mud flows. The night between the 1st and the 2nd of October 2009, a vicious rainstorm accompanied by strong winds and lightning lashed Giampilieri, 10 km southward the city of Messina causing severe debris-mud flows in many villages around, such as Giampilieri Superiore, Briga Superiore, Scaletta Zanclea, Altolia and Molino. The debris-mud flows flooded most roads, ground floors and basements of buildings, underpasses and tunnels of the areas involved, blocking traffic for many hours. The assessed number of victims caused by disaster amounts to 38, with more than an hundred injured people and the evacuation of 2,000 people. The damages to property, buildings, roads and bridges were estimated close to 550 millions Euro.

The whole Giampilieri catchment was affected by a number of debris-mud flows that hit the population and caused the collapse of building dragging all kinds of debris downhill. In the adjacent catchments, only localized landslides occurred.

Earlier, in 2007, a similar event occurred in this area causing only physical damages and no casualties. In this region, most of catchments are small, with a steep slope, and characterized by short concentration times. Moreover,

N. Morey (✉)
Department of Physics, University of Messina, Messina, Italy
e-mail: nathalie@informatica.unime.it

G.T. Aronica
Department of Civil Engineering, University of Messina, Messina, Italy

G. Leone
University of Roma 3, Rome, Italy

C. Puglisi
ENEA, Rome, Italy

C. Margottini et al. (eds.), *Landslide Science and Practice*, Vol. 4,
DOI 10.1007/978-3-642-31337-0_36,

most of the slopes are poorly vegetated and, consequently, rainfall that is normally absorbed by vegetation can run off almost instantaneously.

The 2009 rainfall had a duration of about seven hours; the Sicilian Agro-meteorological Informative Service estimated that the rainstorm dumped more than 200 mm of rain in this time interval. The recorded damages and casualties occurred in the first three hours of rainfall with a registered peak of over 120 mm/h in 10 min.

The lithological, morphological and hydrological conditions has meant that, triggered by the heavy rainfall, more than 1,000 of debris-mud flows reached the valley bottoms and polygenic fans (fluvial and gravitational), in few minutes and with a high energy.

Geological, Morphological and Hydrographical Characteristics of the Basin

The studied region is located inside the Peloratani Mountains, a ridge along the Ionian coast, characterized by narrow and steep catchments of small size (5–10 km^2) with a high relief energy (up to 1,000 m drop in about 5 km) and a short concentration time (few minutes). The morphology of the Peloritani was mainly influenced by metamorphic lithology, complex geo-structural conditions related to the orogenic tectonics and the recent uplift, active in the area since the late Miocene. All the steep slopes are covered by debris and colluvium with a soil layer thickness of few decimetres. According to recent tectonico-stratigraphic outlines and geological-petrologic reviews proposed in recent scientific publications the Peloritani chain is composed of seven overlapped stratigraphic-structural units with an "anti-formal stack" type of geometry. It consists of a reversed metamorphic sequence, where the crystalline units with the highest metamorphic degree are in the higher geometric position (Vignaroli et al. 2008). The outcrop formations in the Peloritanian sector are primarily composed of schistose-crystalline rocks of different metamorphic grades (phyllite, schist, marble, gneiss) widely covered by detritus; some cover sedimentary deposits are also present.

The catchment area of interest is approximately 10 km^2, rising to around 1,021 m above sea level, and the main branch of the river is some 8.5 km long. The basin is predominantly rural with woods and sparse shrubs in the upper mountainous part, while the areas next to the outlet are highly urbanised. The topography is very rugged and the slope is steep, like that of a number of its tributaries, some of which are incised into narrow pathways as they approach the main channel. As a consequence, short concentration times are to be expected with fast hydrological response. The river network of the catchment is quite divided, especially in the mountainous area where a number of secondary river branches are present. These follow a short, twisted and quite steep main course that flows straight into the valley where the urbanisation affected not only the floodplain but also the riverbed itself, posing a serious risk to the village of Giampilieri Marina whose main roads were previously part of the torrent.

The territory conditions show a poorly developed geomorphologic state that generated a considerably strong erosion activity, particularly intense during significant and long lasting hydrometric events.

The climate of the area is typically Mediterranean, with heavy rainfalls during the winter period, and almost no precipitation during spring and summer. Moreover, the substantial load of solid material that these rivers carry following heavy rainfall poses a serious problem particularly when overflow occurs in the most densely populated areas.

Technology Used

For volume calculation, open-source GIS solutions have been chosen like *QuantumGIS* for map representation, *GRASS* for spatial operations and analysis on raster and vectors. Free cartographic libraries, as *Gdal*, helped in raster data transformation and merging. The *Traspunto* software developed by the Ministry of Environment in Italy has been successfully used for the vector coordinate transformation.

Volume Computation Process

The volume of moved material has been estimated by comparing data collected before and after the event (Fig. 1). Pre-event data was provided by existing 3D contour maps issued of an aero-photogrammetric flight performed in 2002. The data had the following characteristics: a resolution of 2 m in urban areas and 5 m in other areas. In some cases, a resolution of 1 m has been reached in situation where both resolutions were available. A laser flight performed a few days after the event produced the post-event data. The LiDAR technology used generated a 1 m resolution digital elevation model (DEM) and orthophotos with a 15 cm pixel. The LiDAR data was structured into a total of 11 sheets covering all the Giampilieri catchment. For the volume computation, a DEM was elaborated from the contour lines data and interpolated into a 1 m resolution map to perform comparison with the post-event one.

The calculation process (Fig. 2) faced coordinate transformation and elevation problems between data using different projection systems and moreover datum types. In this specific study, the LIDAR data used global datum WGS84

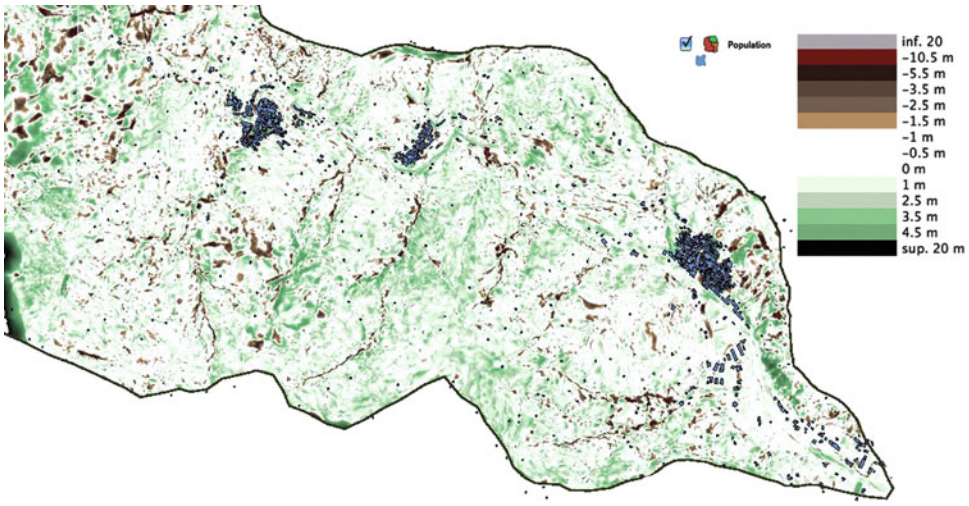

Fig. 1 Debris volume maps of the Giampilieri catchment

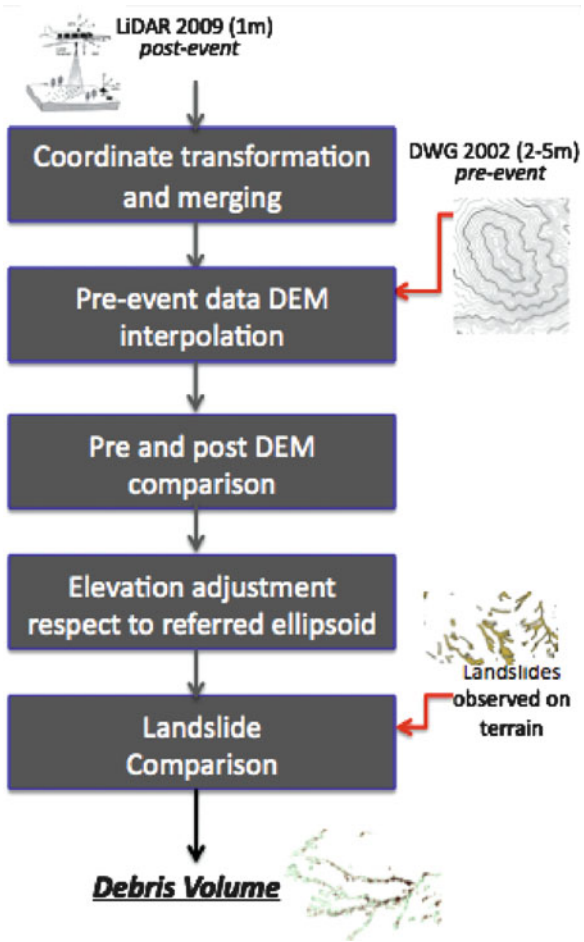

Fig. 2 Volume calculus process

while existing geo-data information, which is the case of most national geo-information, used a local one. Most of the data in Italy, and especially in Sicily are expressed in the *Gauss-Boaga* system reference, as the existing contour lines available for comparison. For this particular study, the volume of debris was determined using the difference between the land elevation before and after the event. The main troubles were that the elevation was referred to as ellipsoid in the global datum system while as geoid for the local one.

In the area of study, no data reference was available for the altitude conversion. Also, no formula has been found regarding the relationship between sheet maps and coordinates. However it was observed in main cases, inside the catchment, that the elevation was estimated around 40.3 m higher in *WGS84*. The resulting map also evidenced differences in zones of major/minor elevation (Fig. 3). These zones were digitalized. The calculation has been successively readjusted with respect to the catchment mean elevation of 40.3 m and zones of differences were then generated.

At the same time of the volume computation, ENEA produced the maps of source areas indicating zones of debris-mud flows inside the basin. Data were produced from a terrain analysis survey performed a few days after the disaster and, in situation of inaccessible places, through the analysis of the orthophotos that were generated by the LiDAR flight.

Debris flow volume results were matched with these source area maps (Fig. 4). Only the areas inside a buffer of 10 m around these observed debris-mud flows zones have been considered in the calculation (Fig. 5). In rare cases, some contour lines were missing in populated areas like Giampilieri Superiore. However, this lack of information was not concerned by the buffer vectors taken into account since referred locations were not involved by material mobilized.

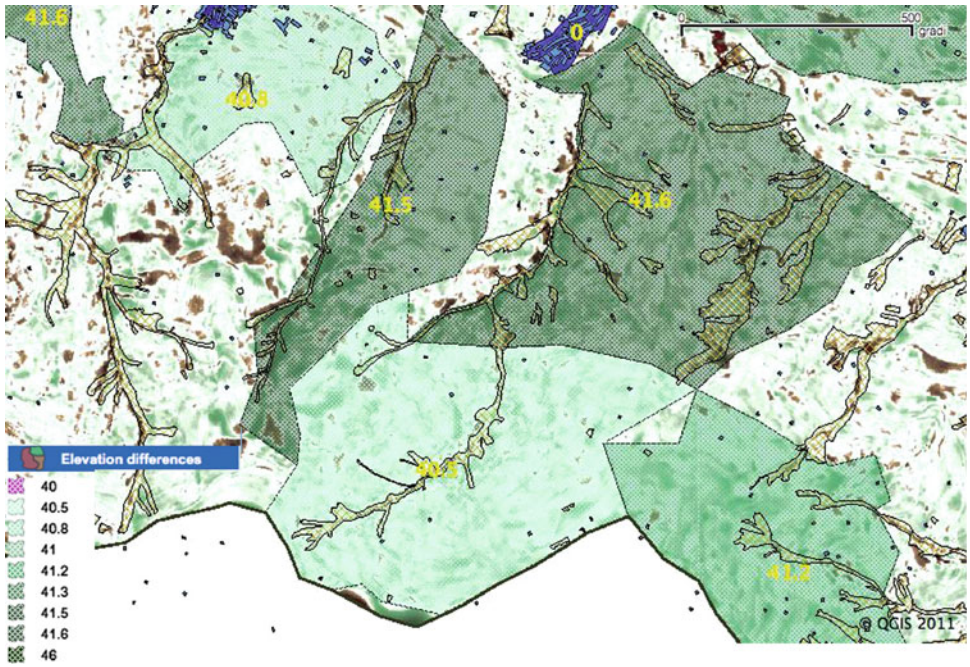

Fig. 3 Identification of major/minor elevation zones

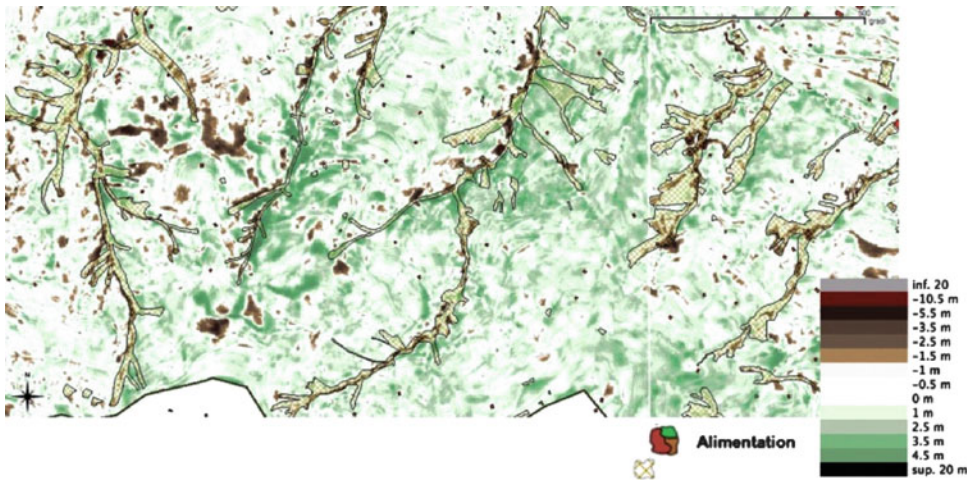

Fig. 4 Comparison between resulting volume and alimentation areas

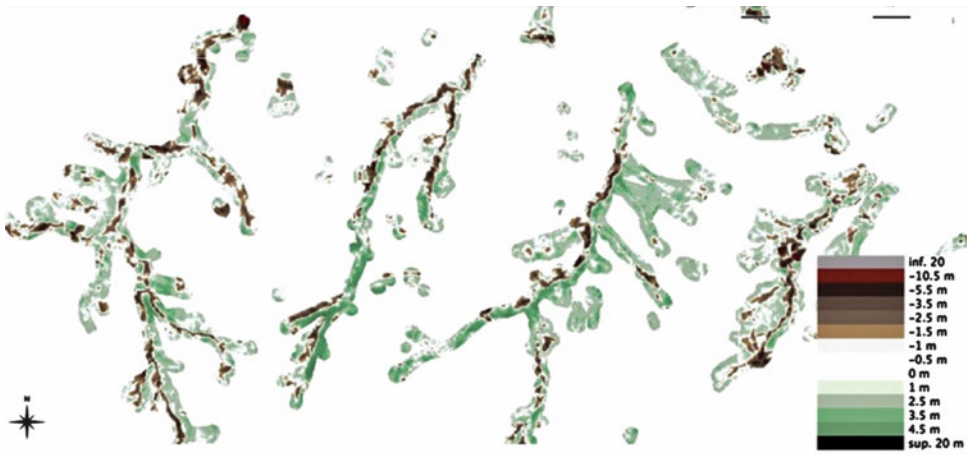

Fig. 5 Details on clipped volume

The calculated debris volume has been estimated about 780,000 m^3 for an area of 600,000 m^2.

Limits of Volume Calculation and Available Data

The requested volume was calculated using multitemporal DEMs. A first debris volume was estimated by comparing the post-event LiDAR data with maps provided by a digital flight performed and acquired by the regional department of environment in Sicily in 2007. The produced ortophotos and DEM had a resolution of respectively 25 cm and 2 m in horizontal. Unfortunately, although the maps were more current to debris-mud flows event, the calculation produced unreliable data. Some debris materials were indicated in zones where no landslides occurred, especially in the northwest of the basin in the upper mountainous part. Similar observations were recorded in shadow-facing slope with a deep calculus sometimes 5 m over the real one. Only the orthophotos were available in the analysis. The contour lines maps from 2002, although dated and with a lower resolution, seem to better fit reality.

The study points out the importance of working with validated and accurate data. The INSPIRE (Infrastructure for Spatial InfoRmation in Europe) directive which establishes spatial data infrastructure recommends the application of the ISO standard 19115:2003 on geographic information metadata. This standard concerns the knowledge of information resources and their description in a metadata catalogue based on an international standard. The ISO assures the quality of geographic data information.

Also, use of a standard format of data as well as common coordinate system reference is necessary for data integration. That is the case of the elevation considered in different system of datum as illustrated in our application. The problem is resolved in GPS application where *WGS84* has become the standard coordinate system reference. Moreover, standard data avoids loss of time and error generation in raster map coordinate transformations.

The volume calculation does not take into account the event occurred in 2007, when few debris-mud flows occurred in the studied basin, in particular in Giampilieri Superiore, Altolia and Molino.

Conclusion

The study points out the importance of establishing a standard of data and coordinate reference in the specific case of the debris-mud flows risk analysis field.

Determining mobilized material volume during remote events is fundamental to forecast future potential phenomena. In fact, plotting the results of debris volume multiplied by the height differences between trigger areas and the start of the material accumulation fans *vs* their flow, helps in improving empirical formulas (Rickenmann 1999; García-Ruiz et al. 2002) from which potential run out could be predicted.

Considering the large number numbers of debris-mud flows and the precision obtained through the described method to estimate the debris volume, the formulas that can be deduced for the Ionic Peloritani Mounts result to be statistically significant. The flow estimation of a potential future phenomenon is even more important in the estimation of the intensity, the hazard and the risk the area is exposed to.

As a last analysis, the information related to the volume estimation provides a framework of the degree of landslide hazard and represents a necessary basis for subsequent phases of vulnerability assessment of exposed elements and, ultimately, for the definition of risk scenarios aimed at risk mitigation. The morphology of Messina territory, the development of town and villages up to creek outlet, the transformation of riverbeds in streets and the abandonment of terracing, altogether contributed to increase geomorphological risk of urban areas. Knowledge of actual landslides impact may promote sustainable planning of risk mitigation for mountain source and transit areas as well as for urban areas prone to landslide invasion.

To mitigate the risk it has been considered important to schedule public events to disseminate to technicians and to population about the hazard level of municipal territory and the mitigation measures that can be implemented for the protection of the territory.

References

Baiocchi V, Bortolotti C, Crespi M, Del Moro MA (2004) Accuratezza delle trasformazioni tra Datum e Sistemi Cartografici Nazionali implementate nei software di maggiore utilizzo nelle applicazioni GIS. In: Atti 8° Conferenza Nazionale ASITA, Roma 2004, vol I, pp 195–200, ISBN 88- 900943-6-2

Aronica GT, Brigandì G (2010), Analisi idrologica ed idraulica degli eventi del 1 ottobre 2009 nel messinese: il caso del torrente Giampilieri. In: Atti del XXXII Convegno di Idraulica e Costruzioni Idrauliche, Palermo, 14–17 settembre 2010

García-Ruiz JM, Beguería S, Lorente A, Martí C (2002) Comparing debris flow relationships in the Alps and in the Pyrenees. Instituto Pirenaico de Ecología, Zaragoza, Spain

INSPIRE Data Policy & Legal Issues DPLI Working Group (2002) INSPIRE data policy & legal issues working group position paper. Environment agency for England and Wales

INSPIRE project. URL:http://Inspire.ec.europa.eu/

Rickenmann D (1999) Emprical relationships for debris flows. Nat Hazards 19(1):47–77, Kluwer Academic Publishers

Vignaroli G, Faccenna C, Jolivet L, Piromallo C, Rossetti F (2008) Subduction polarity reversal at the junction between the Western Alps and the Northern Apennines. Italy Tectonophysics 450:34–50

Space-Time Hazard Assessment of Rainfall-Induced Shallow Landslides

Lorella Montrasio, Roberto Valentino, Gian Luca Losi, Angela Corina, Lauro Rossi, and Roberto Rudari

Abstract

The paper deals with the application of a physically-based stability model that has been adopted by the Department of National Civil Protection as a prototype early warning system for rainfall-induced landslides in Italy, using rainfall data and geospatial datasets. The main features of the model are briefly recalled and particular attention is devoted to the discussion of the input data. The slope-stability analysis has been carried out on national scale, concerning some case-histories occurred between October 2009 and March 2011, on the basis of observed rainfalls. The comparison between observed landslide localizations and model back analysed results is finally presented.

Keywords

Soil slip • Case history • GIS platform • Shallow landslides • Warning system • Stability analysis

Introduction

Rainfall-induced shallow landslides, which can be triggered either by short intense or prolonged light rainfalls, have been widely described by many authors, referring to widespread phenomena occurred both in temperate and tropical regions. This kind of landslide generally involves small portions of shallow soils and is characterized by a high density of spatial distribution, thus causing damages to structures and infrastructures and, sometimes, human losses (Fig. 1). In the framework of risk management on regional scale, shallow landslide hazard maps are frequently used. Many authors have applied statistical correlations, which are based on the knowledge of previous events and take into account, beside rainfalls, other important variables, such as geology, geometry, groundwater, and geotechnical characteristics of the soil (Carrara et al. 1991; Bai et al. 2009; Cervi et al. 2010). As stated by Terlien (1998), such maps usually indicate the possible location of the landslides and not the triggering conditions. Therefore, it is not possible to use them to make decisions, such as evacuations or road closures. For this reason, the use of real-time early warning systems for shallow rainfall-induced landslides is attracting the attention of the scientific community, even if effective landslide warnings are far from reality in most landslide-prone areas. Some of these systems, allow a "dynamic" (time varying) monitoring on regional scale. It is clear that these innovative systems require coupling between rainfall amounts, hydrological models, and slope-stability analyses.

Most of the early warning systems, which are used, for the time being, as prototypes, are based on statistical rainfall-triggering thresholds by considering the main hydrological aspects of the problem (Crosta 1998; Borga et al. 2002; Aleotti 2004; Guzzetti et al. 2007, 2008; Tiranti and

L. Montrasio (✉) • R. Valentino • G.L. Losi
Department of Civil, Environmental, Territory Engineering and Architecture, University of Parma, Viale G.P. Usberti 181/A, Parma, Italy
e-mail: lorella.montrasio@unipr.it

A. Corina
Department of National Civil Protection, Via Vitorchiano 2, Rome, Italy

L. Rossi • R. Rudari
CIMA Research Foundation – International Centre on Environmental Monitoring, Via A. Magliotto 2, Savona, Italy

C. Margottini et al. (eds.), *Landslide Science and Practice*, Vol. 4,
DOI 10.1007/978-3-642-31337-0_37,

Fig. 1 Example of shallow landslide occurred at Casamicciola Terme (Ischia Island – Naples) on November 10th 2009 (From Prof. F. Ortolani, www.climatemonitor.it)

Rabuffetti 2010; Capparelli and Tiranti 2010; Capparelli and Versace 2011).

Since shallow landslides always occur as a result of rainfall infiltration, for many authors it is reasonable to evaluate this type of slope instability using physically based models of hillslope hydrology to simulate the processes involved (Montgomery and Dietrich 1994; Wu and Sidle 1995; Iverson 2000; Qiu et al. 2007; Baum et al. 2008; Lu and Godt 2008; Baum and Godt 2010). The formulation of such models, together with the wide availability of GIS, has led to the development of methods that appear suitable to determine both the time and the localization of soil slips, in response to rainfall, on a regional scale (Borga et al. 1998; Burton and Bathurst 1998; Iiritano et al. 1998; Aleotti 2004; Salciarini et al. 2006, 2008; Godt et al. 2008a, b; Schmidt et al. 2008; Simoni et al. 2008; Apip et al. 2010; Liao et al. 2010; Vieira et al. 2010). These methods are characterized by different levels of complexity and their results are strictly correlated with the quality of input data.

The model named SLIP (Shallow Landslides Instability Prediction) (Montrasio 2000; Montrasio and Valentino 2007, 2008), falls within this context: it will be briefly described in the next section. This model allows taking into account dynamically the connection between the stability condition of a slope, the characteristics of the soil and the rainfall amounts, also including previous rainfalls. The model was designed so that it can be easily implemented in a territorial monitoring system, which aims to provide warning messages to the population (Montrasio et al. 2009).

Case Histories

Very frequent disasters occurred in Italy in the last decades have sensitized the public and the emergency management agencies, such as the National Civil Protection Department (DPC), to the vulnerability of populations living in hazardous areas and to the need for more effective warnings and emergency preparedness. More recently, the SLIP model has been adopted by DPC as a prototype early warning system for rainfall-induced landslides in Italy, using rainfall data and geospatial datasets, as part of the monitoring system called DEWETRA. In order to carry out a validation process, the most important soil slips occurred in Italy between October 2009 and March 2011 have been considered. Among other events, 17 case histories have been chosen for the analysis.

The analysed events, which are summarized in Table 1, have been selected on the basis of the possibility to determine the exact date of each landslide occurrence. The localization of different sites is scattered on the entire Italian territory (Fig. 2) and the occurrence time generally corresponds with very intense rainfalls. In the following, for the sake of conciseness, only results corresponding to four of the 17 analyzed events are presented (Figs. 4, 5, 6, 7 and 8).

All the analysed shallow landslides occurred on hilly areas and, in most cases, the soils involved were represented by the colluvial deposits, derived by the weathering of the bedrock. Most of the slides had a thickness between 0.5 and 2 m, with the failure surface located along the contact between the colluvial cover and the weathered bedrock.

The geotechnical properties of the shallow soils can be considered as mean values of those characteristic of sandy-silt or clayey-silt. Very often in the northern Apennine, at the interface between the shallow soil cover and the bedrock, there is a thin layer of silty clay derived from the direct weathering of the bedrock. In a large number of cases, this thin layer represents the sliding surface of the landslide. Extensive perched water table development is common on these colluvial soil slopes, especially during the rainy season.

Slope angle seems to be a crucial factor for slope stability, even if the available Digital Terrain Model (DTM) with a resolution of 20 m doesn't allow to consider specific topographic conditions. Parameter values for the model are summarized in Table 2. Since soil values are the most difficult parameters to assess, we both used the soil information from literature and sparse, locally measured data generalized to a large area. Furthermore, we assume a nil value both for the root cohesion and the effective cohesion of the soil. Due to the large geographic area considered as well as the limited high resolution datasets for the entire Italian territory, we make several assumptions: (1) detailed geological information was not included in this model due to the limitations of the simplified physical model and lack of homogeneous information at realistic spatial resolution over the large study area. However, this information may be incorporated into the model when data become available; (2) the soil layer subject to sliding is generally characterized

Table 1 Main case histories from October 2009 and March 2011

Site	Province	Date	Major effects
1) Giampilieri	Messina	01/10/2009	37 victims
2) Casamicciola Terme-Ischia	Napoli	10/11/2009	1 victim
3) Tarcento	Udine	24/12/2009	Blocked roads
4) San Fratello	Messina	14/02/2010	Blocked roads
5) Maierato	Vibo Valentia	15/02/2010	Blocked roads
6) Germignaga	Varese	04/04/2010	Blocked roads
7) Monzuno	Bologna	15/05/2010	Damaged house
8) Uscio	Genova	08/09/2010	Blocked roads
9) Atrani	Salerno	09/09/2010	1 victim
10) Genova	Genova	04/10/2010	Blocked motorway
11) Pordenone	Pordenone	05/10/2010	Blocked roads
12) Villasimius	Cagliari	10/10/2010	Blocked roads
13) Scilla	Reggio Calabria	13/10/2010	Blocked motorway
14) Northern Italy	Massa Carrara	31/10/2010	3 victims
	Pordenone		
15) Avezzano	L'Aquila	01/12/2010	Blocked railway
16) Tellaro	La Spezia	23/12/2010	Isolated city
17) Marche Calabria	Ascoli Piceno Reggio Calabria	01/03/2011	Blocked roads

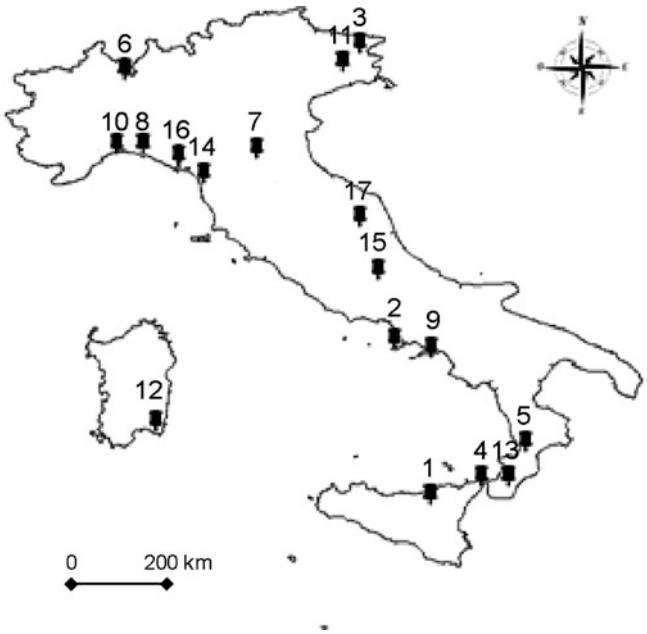

Fig. 2 Localization of the events analysed in the present work

by a certain degree of heterogeneity, but in this study it is considered homogeneous; (3) run-off and evapo-transpiration were globally considered in the water balance in 30 % of total rainfall. Therefore, we assume that 70 % of rainfall infiltrates into the soil. All above assumptions were useful to make the model easily applicable over large areas and able to employ various available datasets.

The SLIP Model

To determine the stability condition for shallow landslides, with a maximum depth of approximately 1.5÷2 m, the infinite slope model can be reasonably applied. Moreover, field information from the sites under study revealed that the shallow unstable layer thickness was rather thin with respect to the superficial extent of the scars. The model used to describe the triggering mechanism assumes that the potential failure surface is located, with respect to the ground level, at depth H, i.e. where the base layer is less permeable than the upper one (Fig. 3).

The model assumes that the main hydro-geotechnical process that leads to failure is the saturation of parts of the soil, which can be either immediately above the assumed failure surface or even in an upper position.

The slope is initially stable, due to the partial saturation of the soil, which contributes to its shear strength. The rain water can flow very easily through the macro-pores and reach the deeper parts of the many natural micro-channels. The hypothesis is that the water starts to flow in different directions through the micro-pores of the soil matrix, in the zones surrounding the macro-pores. The process continues until the rainfall persists, and larger and larger portions of soil become saturated. The sliding process starts when a relatively wide continuous stratum of saturated soil (mH) has formed.

The stability of a slope is evaluated through the definition of the safety factor (F_s), calculated using the limit equilibrium method, as the ratio between stabilizing and

Table 2 Input parameters for the SLIP model

β (°)	H [m]	ϕ′ (°)	c′ [kPa]	n (−)	G_s (−)	A (−)	λ (−)	α (−)	K_T [d^{-1}]
DTM	1.2	30–45	0	0.48	2.7	80	0.4	3.4	0.086

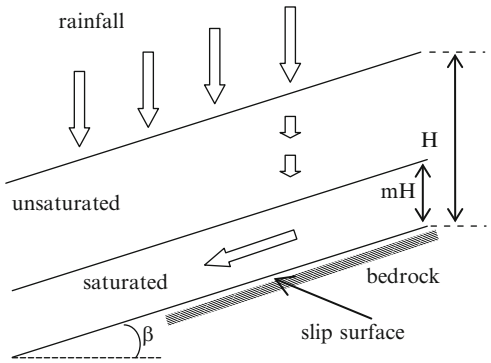

Fig. 3 Sketch of the infinite slope

destabilizing forces. Stabilizing forces are evaluated on the basis of the Mohr-Coulomb strength criterion. The contribution, to the soil shear strength, given by the partial saturation, in terms of apparent cohesion of the soil, is also included. This fact allows to consider stable, in unsaturated conditions, even those slopes characterized by non-cohesive soils, but with a slope angle steeper than the friction angle. The safety factor can be defined as follows:

$$F_s = \frac{\cot\beta \cdot \tan\phi' \cdot [\Gamma + m \cdot (n_w - 1)] + C' \cdot \Omega}{\Gamma + m \cdot n_w} \quad (1)$$

where

$$\Gamma = G_s \cdot (1 - n) + n \cdot S_r \quad (2)$$

$$n_w = n \cdot (1 - S_r) \quad (3)$$

$$\Omega = \frac{2}{\sin 2\beta \cdot H \cdot \gamma_w} \quad (4)$$

$$C' = \left[c' + c_\psi\right] \cdot \Delta s = \left[c' + A \cdot S_r \cdot (1 - S_r)^\lambda \cdot (1 - m)^\alpha\right] \cdot \Delta s \quad (5)$$

$$m = \frac{\xi}{nH(1 - S_r)} \cdot \sum_{i=1}^{\omega} h_i \cdot \exp[-K_T(t - t_i)] \quad (6)$$

where β is the inclination of the slope, ϕ' is the shear strength angle of the soil, γ_w is the water weight per unit volume, H is the thickness of the potentially unstable layer, Δs is the length of the soil slice, m represents the saturated fraction of the soil layer with respect to its thickness H, n is the porosity of the soil, G_s is the specific weight of the soil, S_r is the degree of saturation of the soil, c' is the effective cohesion of the soil, c_ψ is the apparent cohesion given by the partial saturation of the soil, A, λ and α are numerical calibration parameters, ξ is a runoff coefficient, K_T is the discharge capacity of the soil slice, t is the instant of time being considered, t_i is the time instant (day) to which the rainfall depth h_i corresponds. The direct correlation between the safety factor F_s and the rainfall depth is achieved by considering the factor m as a function, at each time step, of previous rainfalls and of parameter K_T, which represents the hydraulic discharge capacity of the slope and is linked to the drainage capability coefficient of the soil (6). A detailed description of the model is contained in Montrasio and Valentino (2008) and Montrasio et al. (2011).

Available Data and Application of the Model

The SLIP model has been implemented in a GIS platform, named DEWETRA, which is the system aimed to prevent, detect and mitigate potential weather related risks. The system is operatively used by the Italian Civil Protection Centers and has been tested on the entire Italian territory. The territory is divided into a 20 × 20 m grid, where each cell is independently modeled considering its own soil features. In this research, data sets information such as elevation, soil, land use, and precipitation were derived from the maximum available detail on national scale.

Elevation and Soil Parameters

The slope angle is derived from a DTM having a resolution of 20 m, whereas geotechnical data are elaborated starting from the geological map (scale 1:500,000).

In particular, for the geotechnical characteristics of shallow soils, due to the lack of information about soil covers, a unique set of mean parameters has been assumed. The geotechnical average parameters of the potentially unstable shallow layers have been estimated and assigned as functions of the soil type, on the basis of both laboratory tests (where available) and literature data. The soil input parameters assigned to the shallow soils over the entire area are shown in Table 2. The degree of saturation (S_r) is influenced by climatic conditions and seasonal weather. Experimental measurements show that in the study areas, for the soil at concerned depths, S_r generally ranges from a minimum of 0.6 in summer and a maximum of 0.9 in winter

Table 3 Input values for the degree of saturation (S_r)

Season	Period	S_r
Summer	July-August	0.60
Autumn	Sept-Oct-Nov	0.75
Winter-Early Spring	Dec-Jan-Feb-Mar-Apr	0.90
Late Spring	May-June	0.75

(Meisina and Scarabelli 2007; Montrasio et al. 2010; Valentino et al. 2011). For this reason, the value of S_r has been considered constant during each season and uniform on the entire analyzed area. Table 3 summarizes the values of S_r, which have been assumed in the model for each season, in relation with the weather conditions. All input data are acquired, by the system, from a GIS data-base. For each parameter used in the model, a map is generated at the same spatial resolution (20 × 20 m).

The input data are inserted into a "raster" form and refer to both soil characteristics (ϕ', c', α, λ, A, k_T, G_s, n) and slope geometry (β, H). In particular, for this application, H has been considered equal to 1.2 m everywhere, and the geotechnical parameters of the potentially unstable soil covers have been assigned according to the values shown in Table 2.

Land Use

By considering a map reporting the use of different areas (CORINE MAP – Scale 1:100,000), the following areas have been disregarded for the slope-stability analysis: unbroken urban areas, industrial and commercial areas, urban gardens and parks, rice-fields, coppices, conifer woods, beaches, rock outcrops, and bodies of water. In particular, conifer woods and unbroken urban areas have been disregarded because field surveys on actual landslides revealed that soil slips did not occur on these kind of areas. Moreover, conifer woods give a great resistance contribution to the shear strength of shallow soils thanks to their roots, while unbroken urban areas can be considered rather impervious to rainfall water.

Precipitation

The model is forced by precipitation maps, obtained from real-time rain gauges data. A rainfall input datum, in terms of rainfall depth, is associated with each cell. The interpolation method used for the definition of the rainfall pattern is based on the inverse-square distance weighting method, applied to each point with respect to the position of the rain gauges, disregarding the altitude.

Output

As of today, the model runs operatively twice a day, producing a detailed safety factor map on the basis of rainfall conditions of the last 30 days. The accumulation time step, currently set to 12 h, can be modified and reduced, in case of warning situations, to increase the refresh rate. In the following figures, for the sake of conciseness, only the results of daily runs are presented (Figs. 4, 5, 6, 7 and 8).

The output of the model can be represented both in terms of safety factor maps, which give the safety factor for each elementary cell 20 × 20 m at a certain time (non-aggregated results) like in Fig. 4b, and instability index maps (aggregated results), like in Fig. 4c. The latter, have been formed in order to obtain an index for soil slip occurrence on a wide area: the results obtained on elementary cells have been aggregated considering reference areas having width within one hundredth of degree of latitude and longitude (reference area of about 1 km^2). The instability index has been defined as the ratio between the number of elementary cells where $F_s \leq 1$ (instability condition) and the total number of cells where F_s is calculated in each reference area. Different classes of instability index have been defined and to each class a different color has been assigned (an example is Fig. 4c). In these maps, the results of the model are condensed and presented in a time-varying GIS environment through appropriated color maps corresponding to different levels of critical conditions.

Back Analysis for Some Case Histories

Figure 4 shows the result given by the DEWETRA system in correspondence of the 10th of November 2009, when a shallow landslide occurred on the Isle of Ischia, causing a human loss. In particular, Figure 4a shows the rainfall map on the entire Italian territory. Figure 4b shows the hotspot of F_s map corresponding to the Isle of Ischia: red areas, referring to elementary cells 20 × 20 m, correspond to unstable conditions. Figure 4c shows the SLIP results in the Isle of Ischia, on the same date, in terms of instability index, i.e. referring to elementary cells of about 1 km^2 each.

Figure 5 shows the result given by the DEWETRA system in correspondence of the 9th of September 2010, when the town of Atrani was flooded by a great mass of slush, in consequence of a sudden soil slip, occurred on the mountain behind the build-up area. In particular, Figure 5a represents the rainfall map of the Italian territory: it is evident how a particularly intense rainfall is over the area of interest.

Figure 5b shows the hotspot of the F_s map corresponding to the municipal territory of Atrani: red areas on the hill tops correspond to unstable conditions.

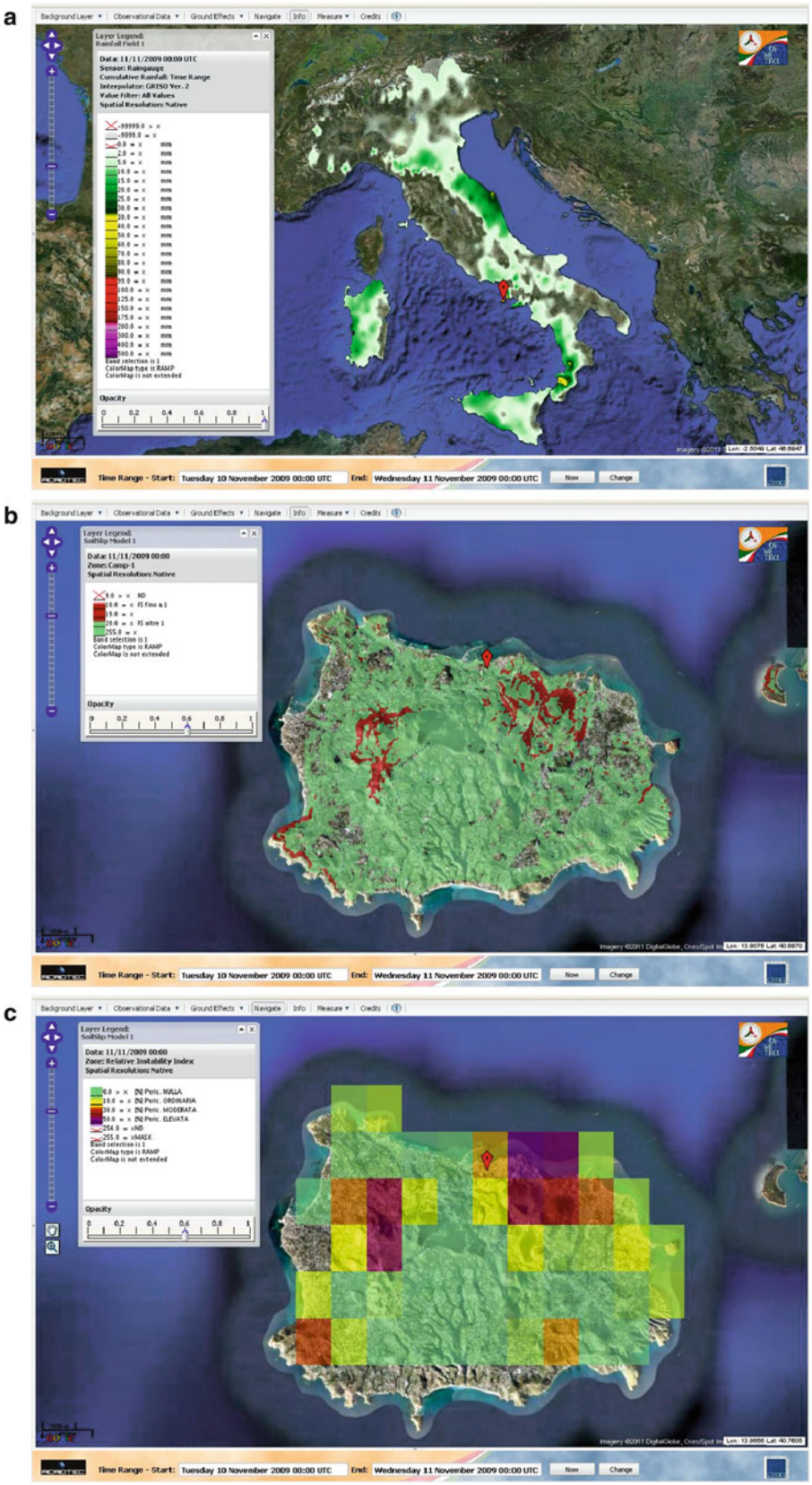

Fig. 4 Event occurred at Casamicciola Terme (Isle of Ischia) on the 10th of November 2009: (**a**) rainfall map; (**b**) F_s map (*red areas* correspond to unstable condition); (**c**) map of instability index

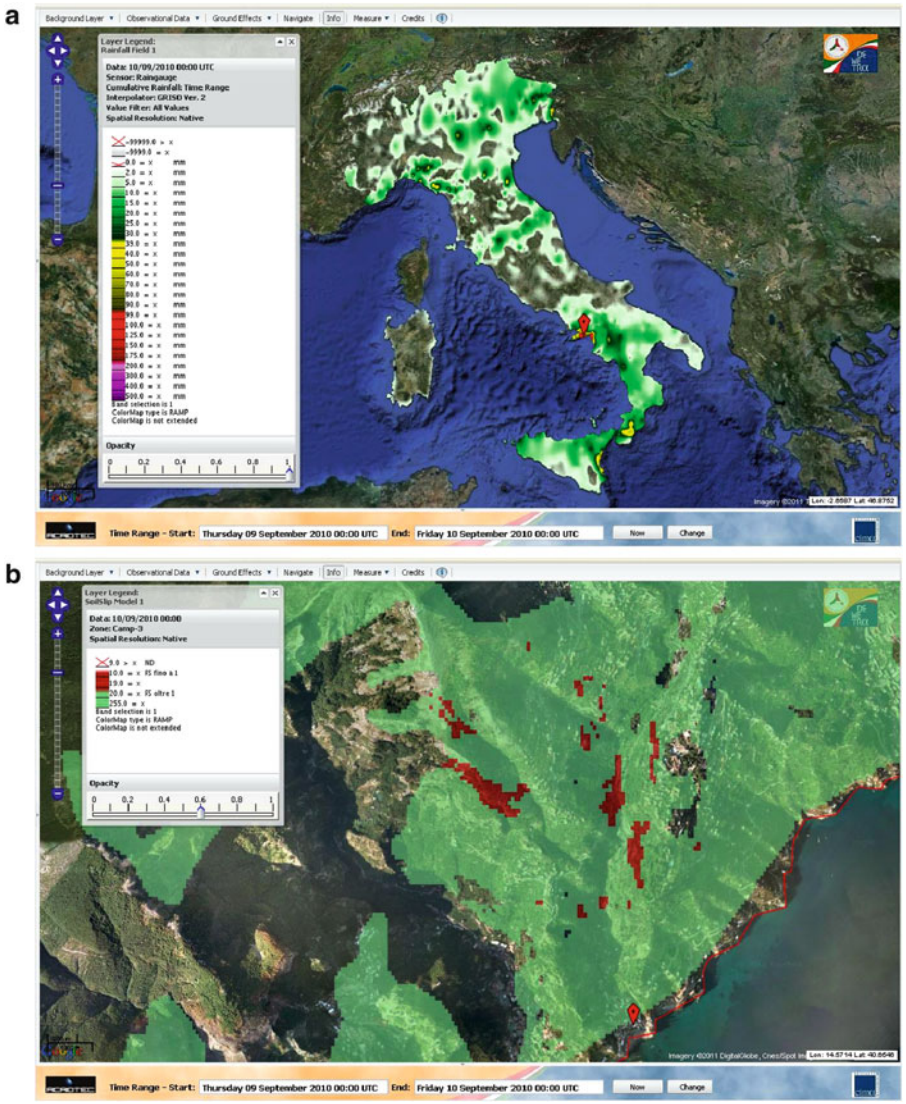

Fig. 5 Event occurred at Atrani on 9th of September 2010: (**a**) rainfall map; (**b**) F_s map (*red areas* correspond to unstable condition)

Figure 6 shows the result given by the DEWETRA system in correspondence of the 13th of October 2010, when in the area of Reggio Calabria, a motorway was blocked by a great mass of shallow soil, slipped down from the steep sides of the road. In particular, Figure 6a shows the rainfall map on the entire Italian territory, and Fig. 6b shows the hotspot of the F_s map corresponding to the area of interest: red areas represent unstable conditions. Figure 6c shows the results of the model in the area of Reggio Calabria, on the same date, in terms of instability index.

Another analyzed event is that corresponding to widespread soil slips triggered by heavy rainfalls, occurred in Northern Italy on the 31st of October 2010, which provoked three victims. Figure 7 shows the result given by the DEWETRA system in correspondence of that date. In particular, Fig. 7a shows the rainfall map, evidencing how particularly intense were the rainfalls over the area of interest. Figure 7b shows the hotspot of the instability index map and it is clear the good correspondence between landslide localization and model results.

Figure 8 shows the result given by the DEWETRA system in correspondence of the 1st of March 2011, when in two Italian regions, namely Marche and Calabria, many widespread soil slips occurred, blocking a great number of important roads. In particular, Fig. 8a shows the rainfall map on the national territory, evidencing heavy rainfalls even in correspondence of other wide areas in the southern part of Italy, where no soil slip occurred and where the model correctly does not reveal instability conditions. Figure 8b shows the instability index map of the entire Italian territory and, even in this case, the correspondence between landslide localization and model results is quite good.

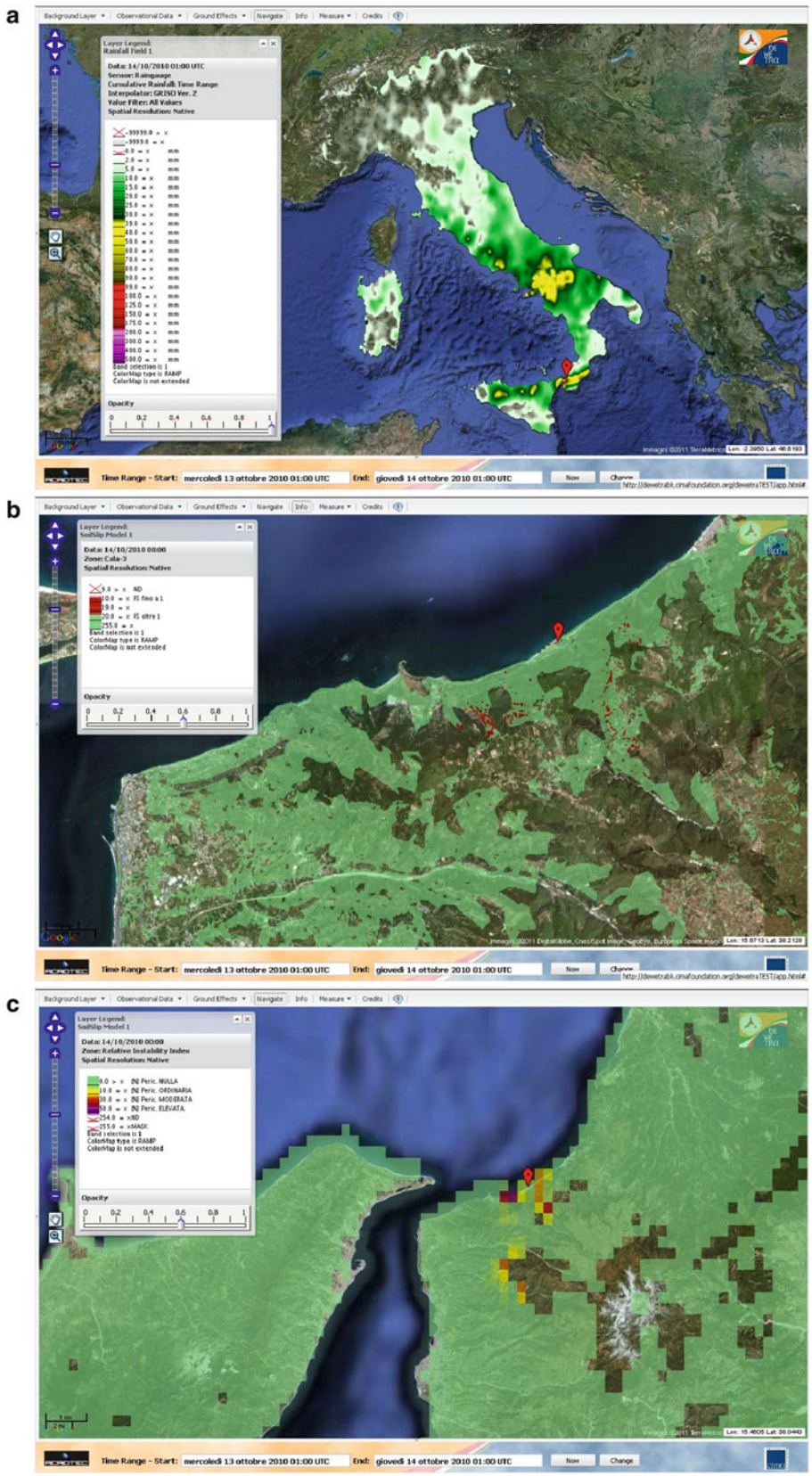

Fig. 6 Event occurred at Reggio Calabria on the 13th of October 2010: (**a**) rainfall map; (**b**) hotspot of F_s map (*red areas* correspond to unstable condition); (**c**) hotspot of the map of instability index

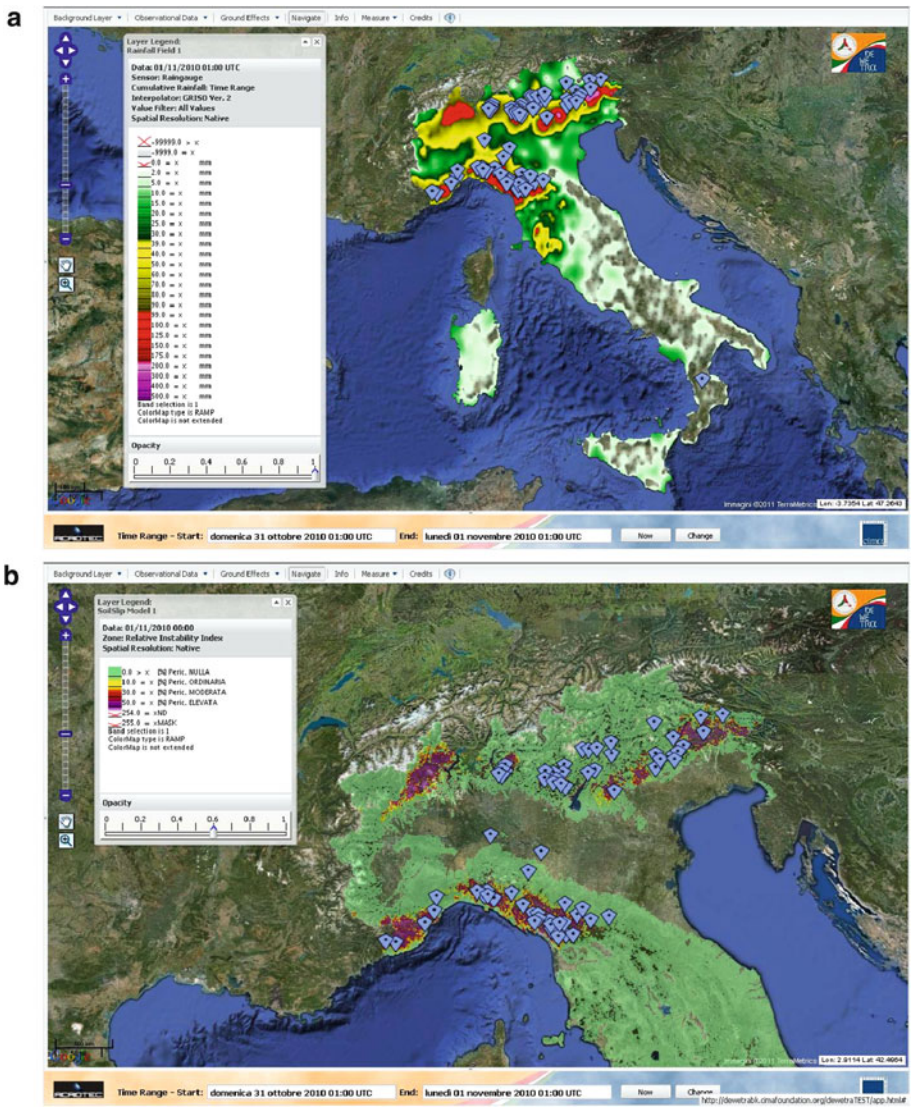

Fig. 7 Event occurred in Northern Italy on the 31st of October 2010: (**a**) rainfall map; (**b**) hotspot of the map of instability index

Concluding Remarks

This study tests the SLIP model performance, implemented in the DEWETRA system, for a gamut of specific real events, in order to evaluate, through a hind cast study, the capabilities of the system applied at national scale. Notwithstanding the lack of a quantitative evaluation of model results, the analysed case studies indicate that the model demonstrates good predictive skill when compared to the landslide inventory over the study area.

The input data used in the SLIP model represent the most important factors influencing the slope movement, and serve to simplify the model calculations and decrease the computational load. However, over-prediction is rather evident, though it is possibly due to a number of model assumptions and the limitation of physical models. It must be considered, in fact, that there are several limitations of simplifying the physically based relationships and employing input data at a such wide scale. These shortcomings can limit model accuracy and should be improved for future applications. For example, scarcely detailed geological information of slopes are assumed as initial conditions, which could lead to potential errors of model results. Neglecting various geological features within the model calculations greatly limits the forecast ability of the physical models. In the future application, more detailed information of geological structures from high risk prone areas could better enhance the hazard assessments.

Furthermore, the negative effects that decrease the accuracy of model results by applying the same soil values to the regional scale cannot be neglected. A same type of soil from different places reveals various physical and mechanical properties in a certain range, regardless of the vegetation roots and the rainfall infiltration. In this study, the soil was considered homogeneous and the same set of input data of

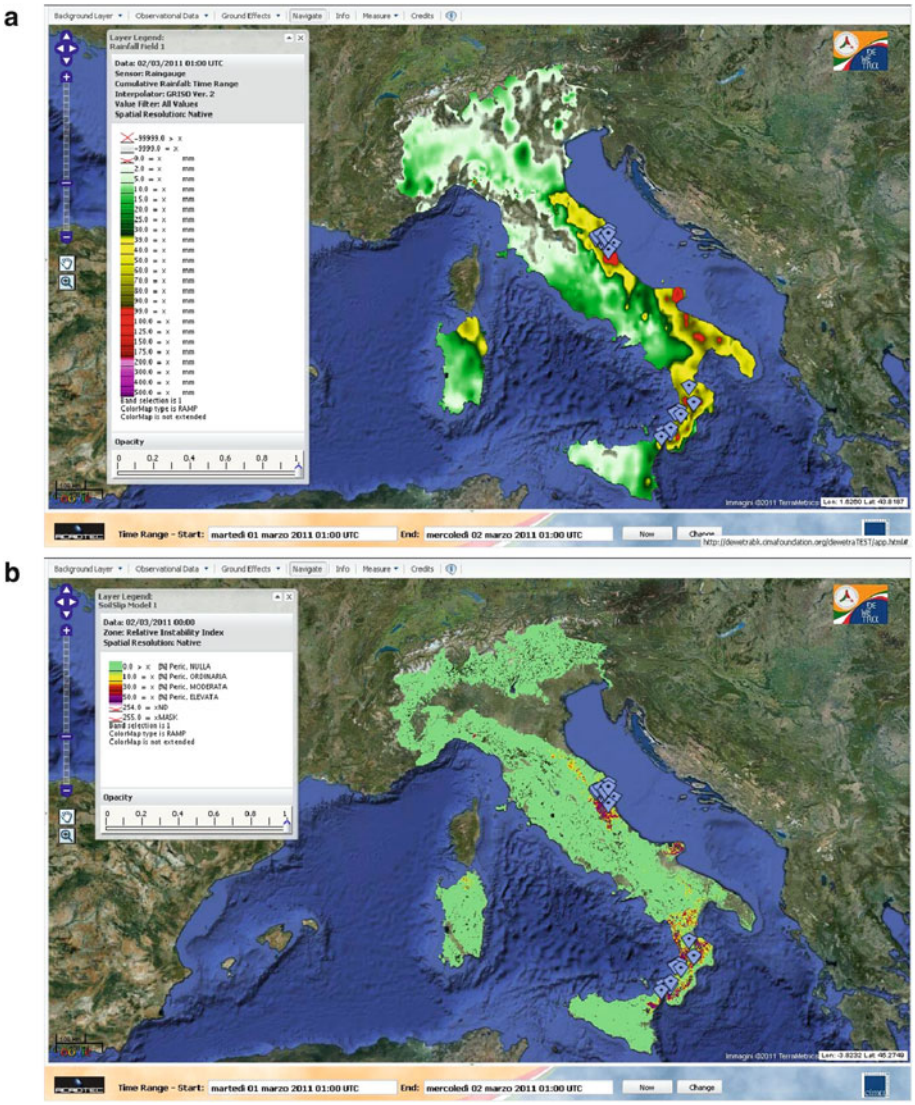

Fig. 8 Events occurred on the 1st of March 2011 in Marche and Calabria regions: (**a**) rainfall map; (**b**) map of instability index

physical and mechanical values have been assumed everywhere. This procedure obviously does not take into account the spatial variances. A study of the real distribution of soil properties would overcome this problem.

Higher spatiotemporal resolution of rainfall, DTMs, and accurately validated soil information are expected to better account for landslide-prone regions. On the other hand, over-prediction of landslides are difficult to reduce due to different triggering mechanisms, unpredictable mass volume of sliding and specific geomorphologic variations. Furthermore, landslide-prone areas can also largely be affected by other human activities such as improper building and roads, which have not been incorporated within the physically based model approach.

The model's overestimation and the lack of spatial accuracy suggest to consider the results predicted by the SLIP model "acceptable" not in an "absolute" sense, but only with respect to time-varying results and, especially in its use as a predictive tool, with respect to the low spatial resolution of forecast rainfall information. The presented model can be considered generally useful for preliminary assessments of slope stability over large areas, but it cannot provide assessments of stability for specific sites, with the exception of its application at a local scale, on the basis of more detailed data.

While there are several limiting factors affecting the accuracy of model forecasting, these results suggest that the output of the SLIP model and the DEWETRA system could be used to define different levels of "dynamic" susceptibility. In fact, thanks to its simplified formulation, the SLIP model allows a time-varying stability analysis on large scale with a very fast computation. This fundamental feature allows to consider the SLIP model as a potential real-time tool for territory management. Moreover, if coupled with a

model of forecast rainfall, SLIP could be the basis for the development of an early-warning alert system against soil slip phenomena.

Acknowledgments The financial support to the present study by CIMA Foundation (Savona – Italy) and by the Department of National Civil Protection is gratefully acknowledged.

References

Aleotti P (2004) A warning system for rainfall-induced shallow failures. Eng Geol 73:247–265

Apip TK, Yamashiki Y, Sassa K, Ibrahim AB, Fukuoka H (2010) A distributed hydrological-geotechnical model using satellite-derived rainfall estimates for shallow landslide prediction system at a catchment scale. Landslides 7(3):237–258

Bai SB, Wang J, Lü GN, Zhou PG, Hou SS, Xu SN (2009) GIS-based and data-driven bivariate landslide-susceptibility mapping in the three gorges area. Pedosphere 19(1):14–20

Baum RL, Godt JE (2010) Early warning of rainfall-induced shallow landslides and debris flows in the USA. Landslides 7(3):259–272

Baum RL, Savage WZ, Godt JW (2008) TRIGRS – A FORTRAN program for transient rainfall infiltration and grid-based regional slope stability analysis, version 2.0. US Geological Survey Open-File Report 2008–1159. 75 p

Borga M, Dalla Fontana G, Da Ros D, Marchi L (1998) Shallow landslides hazard assessment using a physically based model and digital elevation data. Environ Geol 35(2–3):81–88

Borga M, Dalla Fontana G, Cazorzi F (2002) Analysis of topographic and climatic control on rainfall-triggered shallow landsliding using a quasi-dynamic wetness index. J Hydrol 268:56–71

Burton A, Bathurst JC (1998) Physically based modeling of shallow landslide sediment yield at a catchment scale. Environ Geol 35 (2–3):89–99

Capparelli G, Tiranti D (2010) Application of the MoniFLaIR early warning system for rainfall-induced landslides in Piedmont region (Italy). Landslides 7(4):401–410

Capparelli G, Versace P (2011) FLaIR and SUSHI: two mathematical models for early warning of landslides induced by rainfall. Landslides 8(1):67–79

Carrara A, Cardinali M, Detti R, Guzzetti F, Pasqui V, Reichenbach P (1991) GIS techniques and statistical models in evaluating landslide hazard. Earth Surf Proc Land 16(5):427–445

Cervi F, Berti M, Borgatti L, Ronchetti F, Manenti F, Corsini A (2010) Comparing predictive capability of statistical and deterministic methods for landslides susceptibility mapping: a case study in the northern Apennines (Reggio Emilia Province, Italy). Landslides 7 (4):433–444

Crosta G (1998) Regionalization of rainfall thresholds: an aid to landslide hazard evaluation. Environ Geol 35(2–3):131–145

Godt JW, Baum RL, Savage WZ, Salciarini D, Schulz WH, Harp EL (2008a) Transient deterministic shallow landslide modeling: requirements for susceptibility and hazard assessments in a GIS framework. Eng Geol 102:214–226

Godt JW, Schulz WH, Baum RL, Savage WZ (2008b) Modeling rainfall conditions for shallow landsliding in Seattle, Washington. Rev Eng Geol 20:137–152

Guzzetti F, Peruccacci S, Rossi M, Stark CP (2007) Rainfall thresholds for the initiation of landslides in central and southern Europe. Meteorol Atmos Phys 98:239–267

Guzzetti F, Peruccacci S, Rossi M, Stark CP (2008) The rainfall intensity-duration control of shallow landslides and debris flows: an update. Landslides 5(1):3–17

Iiritano G, Versace P, Sirangelo B (1998) Real-time estimation of hazard for landslides triggered by rainfall. Environ Geol 35 (2–3):175–183

Iverson RM (2000) Landslide triggering by rain infiltration. Water Resour Res 36(7):1897–1910

Liao Z, Hong Y, Wang J, Fukuoka H, Sassa K, Karnawati D, Fathani F (2010) Prototyping an experimental early warning system for rainfall-induced landslides in Indonesia using satellite remote sensing and geospatial datasets. Landslides 7(3):317–324

Lu N, Godt JW (2008) Infinite-slope stability under steady unsaturated seepage conditions. Water Resour Res 44:W11404

Meisina C, Scarabelli S (2007) A comparative analysis of terrain stability models for predicting shallow landslides in colluvial soils. Geomorphology 87:207–223

Montgomery DR, Dietrich WE (1994) A physically based model for the topographic control of shallow landsliding. Water Resour Res 30:1153–1171

Montrasio L (2000) Stability analysis of soil slip. In: Brebbia CA (ed) Proceedings of international conference "Risk 2000", Wit Press, Southampton, pp 357–366

Montrasio L, Valentino R (2007) Experimental analysis and modelling of shallow landslides. Landslides 4:291–296

Montrasio L, Valentino R (2008) A model for triggering mechanisms of shallow landslides. Nat Hazards Ear Syst Sci 8:1149–1159

Montrasio L, Valentino R, Losi GL (2009) Rainfall-induced shallow landslides: a model for the triggering mechanism of some case studies in Northern Italy. Landslides 6:241–251

Montrasio L, Valentino R, Quintavalla C (2010) Estimation of the degree of saturation of shallow soils from satellite observations to model soil slips occurred in Emilia Romagna Region of Northern Italy. Int J Geosci 1:58–65

Montrasio L, Valentino R, Losi GL (2011) Towards a real-time susceptibility assessment of rainfall-induced shallow landslides on a regional scale. Nat Hazards Ear Syst Sci 11:1927–1947

Qiu C, Esaki T, Xie M, Mitani Y, Wang C (2007) Spatio-temporal estimation of shallow landslide hazard triggered by rainfall using a three-dimensional model. Environ Geol 52:1569–1579

Salciarini D, Godt JW, Savage WZ, Conversini P, Baum RL, Michael JA (2006) Modeling regional initiation of rainfall-induced shallow landslides in the eastern Umbria Region of central Italy. Landslides 3:181–194

Salciarini D, Godt JW, Savage WZ, Baum RL, Conversini P (2008) Modeling landslide recurrence in Seattle, Washington. USA Eng Geol 102:227–237

Schmidt J, Turek G, Clark MP, Uddstrom M, Dymond JR (2008) Probabilistic forecasting of shallow, rainfall-triggered landslides using real-time numerical weather predictions. Nat Hazards Ear Syst Sci 8:349–357

Simoni S, Zanotti F, Bertoldi G, Rigon R (2008) Modelling the probability of occurrence of shallow landslides and channelized debris flows using GEOtop-FS. Hydrol Process 22(4)

Terlien MTJ (1998) The determination of statistical and deterministic hydrological landslide-triggering thresholds. Environ Geol 35 (2–3):124–130

Tiranti D, Rabuffetti D (2010) Estimation of rainfall thresholds triggering shallow landslides for an operational warning system implementation. Landslides 7(4):471–481

Valentino R, Montrasio L, Losi GL, Bittelli M (2011) An empirical model for the evaluation of the degree of saturation of shallow soils in relation to rainfalls. Can Geotech J 48:795–809

Vieira BC, Fernandes NF, Filho OA (2010) Shallow landslide prediction in the Serra do Mar, Sao Paulo, Brasil. Nat Hazards Ear Syst Sci 10:1829–1837

Wu W, Sidle RC (1995) A distributed slope stability model for steep forested hillslopes. Water Resour Res 31(8):2097–2110

Tertiary Creep Reproduction by Back-Pressure-Controlled Test in DPRI-7

Atitkagna Dok and Hiroshi Fukuoka

Abstract

Fukuzono (Proceedings of 4th international conference and field workshop on landslides, Japan, pp 145–150, 1985) developed a method for predicting final failure time of a slope based on the findings derived from large scale flume test series that log of acceleration is proportional to log of velocity of surface displacement suddenly before failure. He proposed a simple method for predicting the failure time by plotting the inverse velocity of surface displacement ($1/v$). Yet, its mechanism is still unknown. To investigate the tertiary creep mechanism in soils, a series of back-pressure-controlled test on saturated sands were undertaken in ring shear apparatus. The tests were conducted under particular normal stress and shear stress with pore-water pressure changes to simulate the potential sliding surface condition in heavy rainfall. Sand and its mixture with clay material were used for specimen. Consequently, these tests could reproduce tertiary creep to failure, in which similar log v-log a relationship and α value range was found. While, linear relationship of α and A values was found.

Keywords

Tertiary creep • Ring shear apparatus • Back-pressure-controlled test • Rainfall–induced landslides

Introduction

Landslides are complex geo-disasters frequently triggered by earthquake and/or intense heavy rainfall or other related natural/anthropogenic impacts. Such catastrophic disasters have not only claimed residents' lives, but also resulted in property damages and other socio-economic consequences, which significantly interrupts the development of the communities and nations. Since the social resources for preventing those threatening potential landslides is limited in every country, the best solution recently met is safe evacuation immediately before the final catastrophic failure of the landslide. To realize an effective evacuation, reliable prediction methodology must be established.

Accordingly, in landslide fields, failure-time prediction methods of landslide have been widely developed by many researchers including Saito and Uezawa (1961) as an initiation, Saito (1965), Fukuzono (1985), Voight (1988, 1989), Azimi et al. (1988), Hayashi et al. (1988). However, only two methods developed by Saito and Uezawa (1961) and Fukuzono (1985) were accepted world-wide. Based on tertiary creep deformation theory through the findings getting from large scale flume tests for landslide studies, Fukuzono (1985) found logarithm of acceleration is proportional to the logarithm of velocity of surface displacement immediately before the failure, expressed as $d^2x/dt^2 = A(dx/dt)^{\alpha}$, where x is surface displacement, t is time, and A and α are constant. Besides, he proposed a simple method for predicting the time of failure by the inverse velocity ($1/v$) mean. The

A. Dok (✉)
Department of Technology and Ecology, Kyoto University, Yoshida-hommachi, Sakyo-ku, Kyoto 606-8501, Japan

Research Centre on Landslides, Kyoto University, Uji, Japan
e-mail: dok@landslide.dpri.kyoto-u.ac.jp

H. Fukuoka
Research Centre on Landslides, Kyoto University, Uji, Japan

C. Margottini et al. (eds.), *Landslide Science and Practice*, Vol. 4,
DOI 10.1007/978-3-642-31337-0_38,

curve of inverse velocity is concave at $1 < \alpha < 2$, linear at $\alpha = 2$, and convex at $\alpha > 2$. In spite of such exceptional achievements as well as great ability in estimating the failure time of a slope, these methods still need to be improved for higher accuracy, and the mechanism of creep deformation is not yet well-understood.

Lately, to understand the story behind the empirical relationship discovered by Fukozono, Minamitani (2007) has accomplished further research on tertiary creep deformation by increasing shear-stress development in ring shear apparatus. He got consistent α value distribution (1.95–2.46) as declared by Fukuzono and a strong relationship between A and α values, $\alpha = 0.1781A + 1.814$. He concluded that α value is not always constant throughout a test with proof of quite different variation trends of α value of dry and saturated samples in normal stress and Bentonite content test series, and even in OCR test series. Based on his research findings on tertiary creep corresponding to the period of forming a sliding surface, Minamitani named α progressive acceleration parameter which alters depending on type of material and its condition in the initial and final stages of tertiary creep.

Objective of Study

This study aims at figuring out the mechanism of landslides in tropical soils with respect to tertiary creep deformation theory by stress-controlled ring shear apparatus through back-pressure-controlled test series in help issue warning of rainfall–induced landslides in Southeast Asia countries.

Creep in Soils

In most landslide cases, failures are preceded by accelerated trend of displacement, which is associated with crack growth, soil particles rearrangement and shear surface evolution, namely progressive failure. Creep rupture theory was derived from material science, termed a time-dependent deformation.

Soils also result in a series of creep deformation: primary, secondary, and tertiary (Saito and Uezawa 1961), as demonstrated in Fig. 1. Primary creep is the initial stage of deformation when the strain rate is relatively high with minimum displacement. The strain rate eventually reaches a minimum and becomes nearly constant in secondary creep, meaning that the mass is continuously deforming at constant volume, normal effective stress and velocity. Tertiary creep is when strain rate exponentially increases through time shortly before final failure. In some cases of deep seated and lunar landslides, harmful failure does not proceed after a few maters of displacement, reaching tertiary creep.

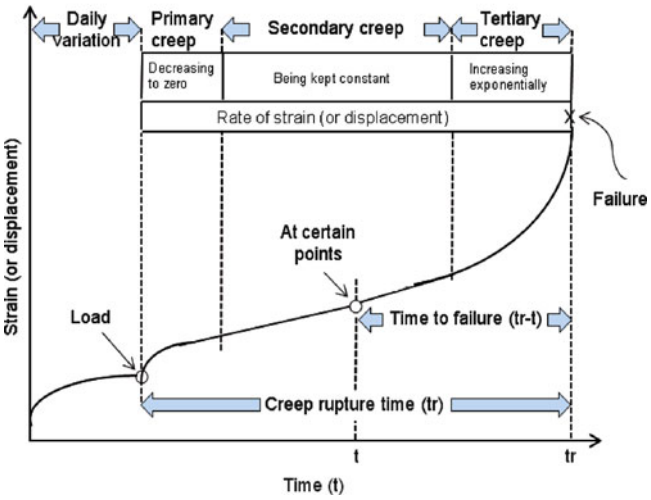

Fig. 1 General relationship of strain and time of a series of creep deformation (Saito and Uezawa 1960)

Ring Shear Apparatus

The un-drained and monotonic stress-controlled ring shear apparatuses are unique and most advanced geotechnical simulation apparatus invented by Sassa, Fukuoka and their colleagues at the Disaster Prevention Research Institute (DPRI), Kyoto University. The latest device in the DPRI ring shear series, DPRI-7, is employed to reproduce tertiary creep deformation in this study. It was designed with special ability to simulate quantitatively the entire process of failure of a soil sample from initial static or dynamic loading through shear failure, pore pressure changes and possible liquefaction to large displacement, steady-state shear movement. The DPRI-7 were developed to simulate the formation of the shear zone and the post failure mobility of high speed landslides and to observe the consequence of mobilized shear resistance, as well as the post failure shear displacement and generated pore-water pressure (Sassa et al. 2004) as simplified in Fig. 2.

Typical designed features of the DPRI-7 are obviously described as following:

- Shear box: inner and outer diameters: 27 and 35 cm.
- Unlimited shearing
- Un-drained testing under rapid shearing and pore pressure monitoring.
- Shear speed: 33–300 cm/s.
- Rapid loading and high-speed data acquisition 12–1,000 readings/s.
- Transparent shear box made of acrylic basin enables observation of shear zone during the initiation and post-failure motions of landslide.

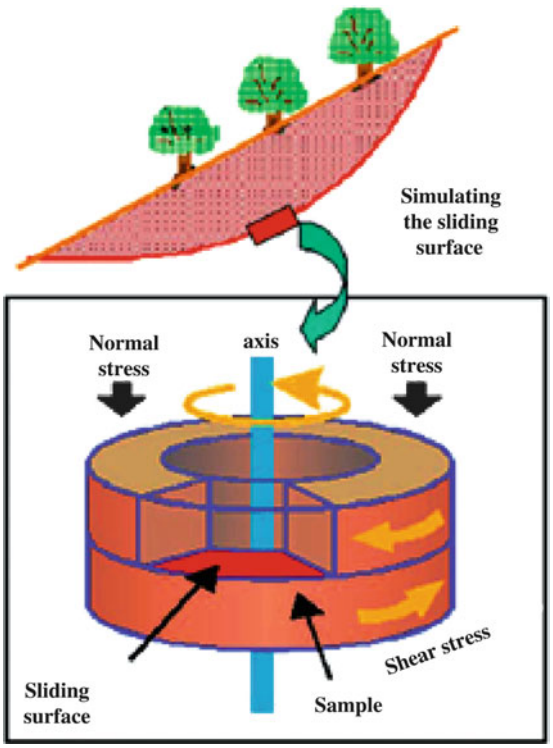

Fig. 2 Design concept of the ring shear apparatus (Sassa et al. 2004)

– Cyclic shear-displacement control, torque control, and shear speed control tests are possible.

Back-Pressure-Controlled Test

Sample Characteristics

Commercial fine grained silica sand No.8 (SS8), Bentonite and natural soil samples taken from sliding surfaces of actual landslide sites were utilized in back-pressure controlled test series of this study. There are four types of specimen: (I) SS8, (II) SS8 with 10 % Bentonite, (III) SS8 with 20 % Bentonite, and (IV) volcanic and silty soils taking from El Salvador, Shobara and Tandikat cities.

Test Conditions

25 back-pressure-controlled tests were undertaken in this study under combined conditions of particular normal stress and shear stress with pore-water pressure changes to simulate the potential sliding surface condition in heavy rainfall. The tests were performed with different over consolidation ratios (OCR = 1, 2, 4, and 5) and pore-water pressure increase rate (100 and 150 kPa) in drained condition that the sample can change its volume, with slope inclination $\theta = 30°$. Table 1 outlines initial conditions of each test depending on sample types. In addition, 1–14 time shear test were repeatedly implemented for a specimen to produce reactivated motion landslide.

Test Procedures

There five steps to be followed in back-pressure-controlled test as briefly described below and illustrated in Fig. 3. For the repeated test for a specimen, consolidation has to be restarted after failure occurrence, as well as shear stress and pore water pressure reductions.

Sample Setting

The ready-mixed dry sample was freely placed into the shear box layer by layer with the insertion of filter papers on the top and bottom of the sample.

Sample Saturation

The sample was saturated with help of carbon dioxide (CO_2) and de-aired water. After the sample was completely packed, the CO_2 gas was gradually percolated through the sample to expel the air in the sample pores for about 30 min until all air was replaced by CO_2. De-aired water was then infiltrated from the lower part of sample box and kept circulating into the sample to drive out the CO_2 from the sample pores. This injection process has to be at a very low rate, which takes at least one overnight to finish. Small amount of the remaining gas will be easily dissolved when normal stress is applied.

Checking Degree of Saturation

Saturation degree was checked by B_D value. As proposed by Sassa (1988), B_D is a pore pressure parameter which is related to the degree of saturation in the direct-shear state, formulated as $B_D = \Delta u/\Delta\sigma$, where Δu and $\Delta\sigma$ are increments of pore pressure and normal stress respectively in un-drained condition. While checking, the sample was initially consolidated under normal stress of 50 kPa in drained condition. Next, the normal stress increment of $\Delta\sigma = 50$ kPa was successively applied under un-drained condition, and the resultant increment of excess pore pressure was accordingly measured. Hence, the saturation degree was determined indirectly by the ratio of excess pore pressure and normal stress increments ($\Delta u/\Delta\sigma$), which is preferably to be $\geq$0.95 due to necessity in acquiring correct monitoring data. The B_D value acquired in this test series varies from 0.95 to 0.99.

Sample Consolidation

In this test series, all the samples were consolidated with respect to the targeted value of OCR as denoted in Table 1. After checking the B_D value, the normal stress was decreased to a value where the excess pore pressure is

Table 1 Back-pressure-controlled test conditions and results

Test no.	Samples	OCR	Pore pressure increase rate (du/dt, kPa/h)	Initial shear displacement (cm)	A value	A value
1	SS8	1.0	100	717	2.00	189.10
2	SS8	1.0	100	967	2.02	1,310.34
3	SS8	1.0	150	1	2.11	146.87
4	SS8	1.0	150	239	2.12	245.00
5	SS8	1.0	150	473	2.00	183.33
6	SS8	2.0	100	1,028	1.98	140.00
7	SS8	2.0	100	1,285	1.98	172.73
8	SS8	2.0	100	0	2.16	200.00
9	SS8	2.0	150	255	2.08	220.83
10	SS8	2.0	150	510	2.01	166.67
11	SS8	2.0	150	767	2.00	164.29
12	SS8	4.0	150	513	2.06	253.33
13	SS8	4.0	150	0	2.02	80.00
14	SS8	4.0	150	258	1.99	143.64
15	SS8 + Ben10 %	1.0	150	0	2.59	600.00
16	SS8 + Ben10 %	1.0	150	135	1.77	8.33
17	SS8 + Ben10 %	1.0	150	250	1.63	1.00
18	SS8 + Ben10 %	5.0	150	668	2.32	540.00
19	SS8 + Ben20 %	1.0	75	146	2.52	1,000.00
20	El Salvador	1.0	25	23	2.38	289.29
21	Shobara	1.0	150	0	2.32	400.00
22	Tandikat 1	1.0	100	256	2.09	200.00
23	Tandikat 1	1.0	150	0	2.41	462.50
24	Tandikat 2	1.0	100	260	1.96	100.00
25	Tandikat 2	1.0	150	0	2.46	600.00

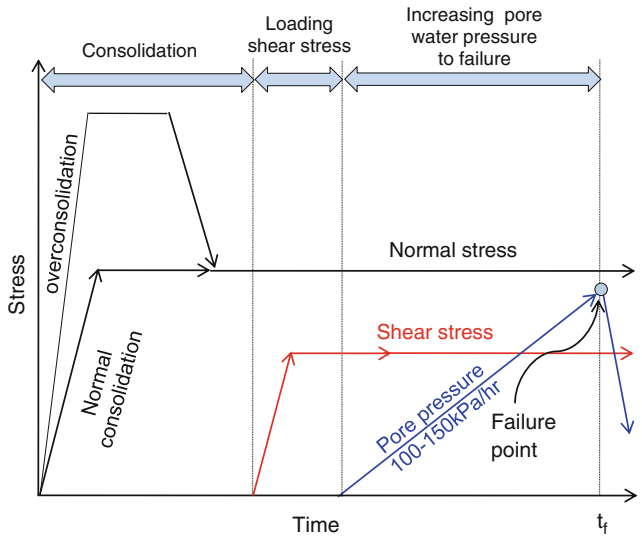

Fig. 3 Schematic illustration of back-pressure-controlled test procedure

reaching zero, then switch on the upper drainage valve. Afterward, slowly load the normal stress to a decided value, and then subsequently reduced applied normal stress to the predefined normal stress ($\sigma = 100$ kPa) in case the OCR > 1.0. A particular shear stress $\tau = 50$ kPa was applied soon after some time of consolidation process. It takes longer time for sticky material while consolidating.

Pore-Water-Pressure Increase to Failure

Pore water pressure inside the shear box was progressively increased up to 95 kPa with various increase rates united with constant normal stress and shear stress as written in Table 1. It is to form the potential sliding surface condition corresponding to rain storms in naturally drained condition. The pore pressure is monitored from the controlled computer to water tank connected to the nearby air tank with a servo-controlled air regulator (Fig. 4). The water pressure was provided through the soil sample via the tube linked between the water tank and the sample box of the ring shear apparatus. Failure may occur at any time while stress condition is attaining the failure criteria. Maximum shear displacement was limited to 200 cm to stop shearing automatically after failure.

Test Results and Discussions

Ring Shear Test Results

In each test, the investigation is principally focused on the curve of inverse velocity and shear displacement in several seconds immediately before failure, and the increment of

Fig. 4 Frontal view of the employed ring shear apparatus DPRI-7

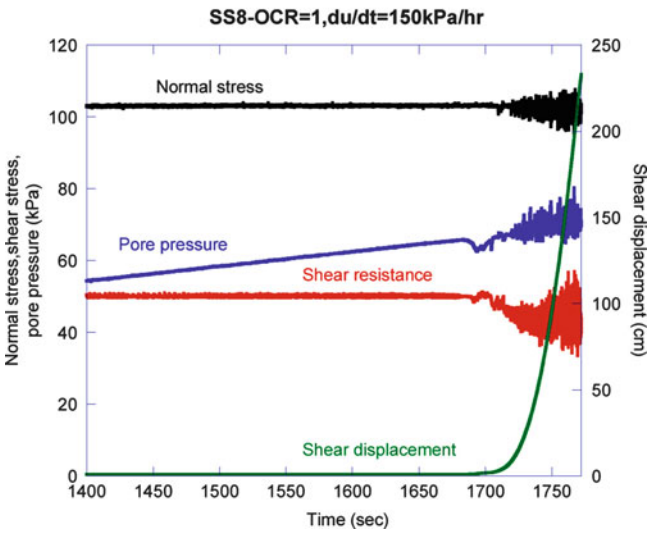

Fig. 5 Temporal change of shear displacement

acceleration and velocity observed in a few thousand seconds before failure to quantify Tertiary creep deformation analysis. Failure point is the point at which shear resistance is reaching its peak and after which shear displacement

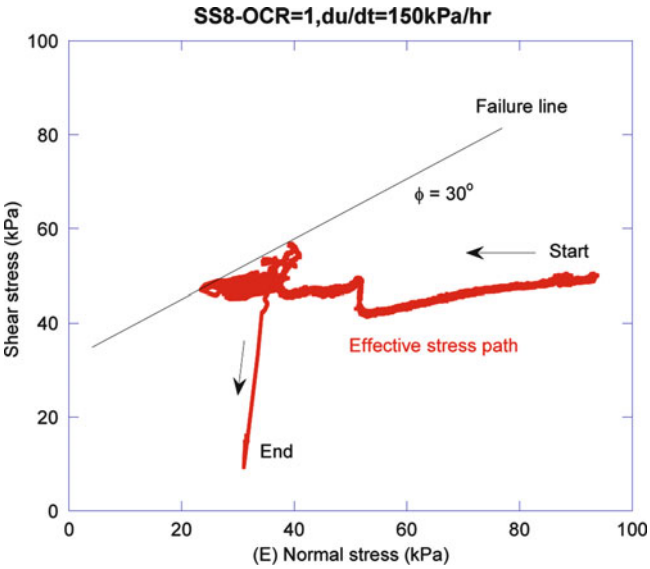

Fig. 6 Stress path propagation

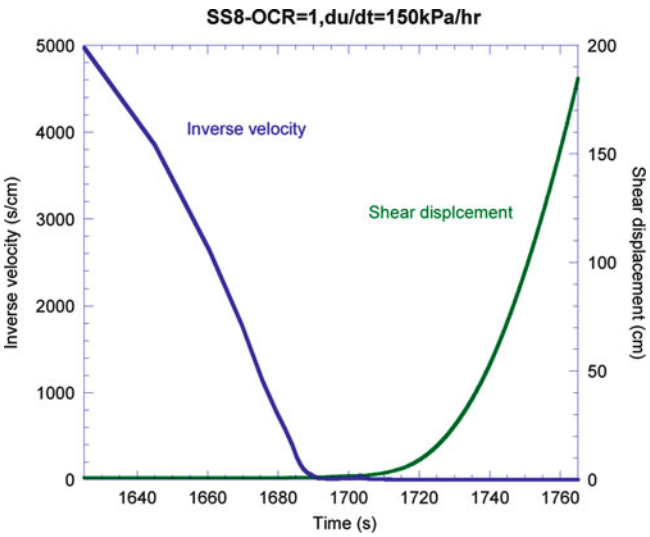

Fig. 7 Inverse velocity and shear displacement at final stage of tertiary creep

starts to increase cumulatively through constant time interval.

The examined outputs of this test series are initial shear displacement, A and α values getting before failure of every test as summarized in Table 1. Figures 5, 6, 7 and 8 show a selected test results–test No.3. Figure 5 views the overall test record that appears the accelerating displacement curve of typical Tertiary creep, while Fig. 6 indicates relationship between shear stress and effective normal stress before and after reaching failure line. Figure 7 exaggerates inverse velocity and shear displacement at the final stage of Tertiary creep from 1,625 to 1,765 s. The inverse velocity displays almost linear decreasing trend, which is also observed in

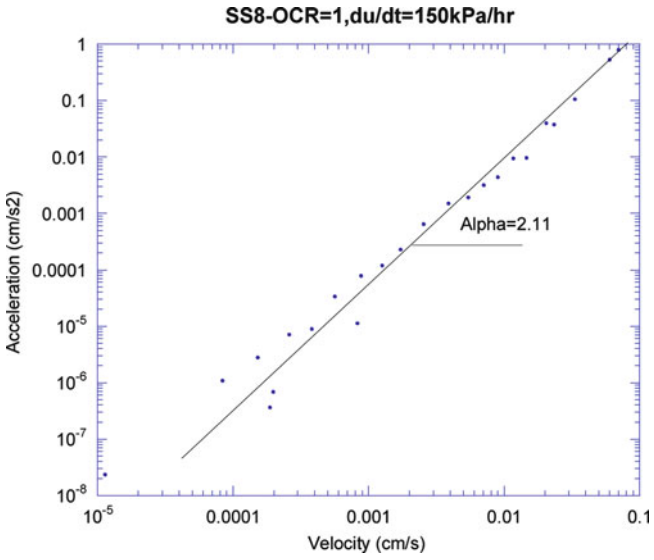

Fig. 8 Acceleration and velocity relationship in log scale

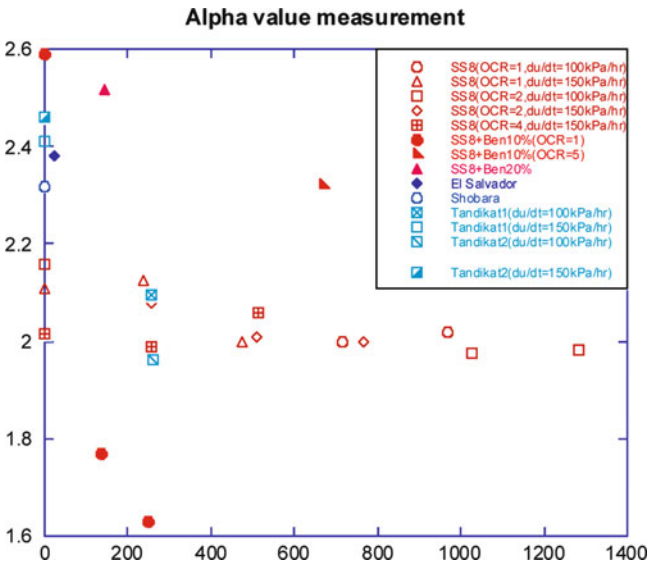

Fig. 9 Summary of α value measurement

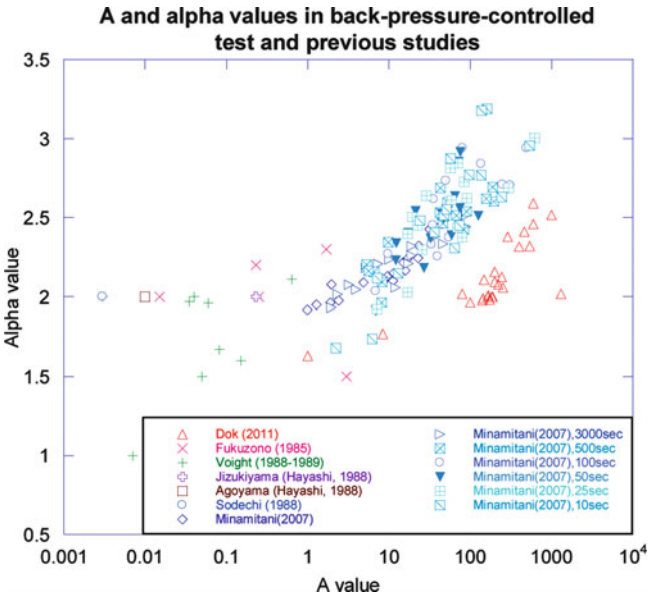

Fig. 10 *A* and α value relationship of this test series and previous studies

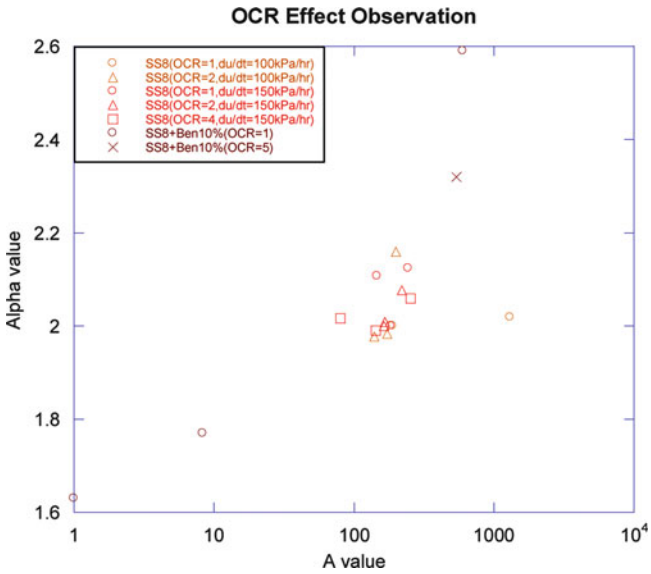

Fig. 11 Examination of OCR effect on α value

Fukuzono's flume tests. Figure 8 illustrates the logarithm of acceleration and velocity. Linear relationship appeared 0.00008–0.07 cm/s and the α value was calculated to be 2.107 in this range.

Velocity-Acceleration Analysis

The values of *A* and α produced in this study are in range of 1–1310.345 and 1.63–2.59, chronologically. The inverse velocity curve and the relationship between velocity and acceleration in doubled-log scale are almost linear in all tests. Variation of α value vs. initial shear displacement showed a big scatter (Fig. 9), including repeated creep tests of same specimens. When longer shear displacement, less variation was observed. *A* and α values obtained in this test series showed obvious relationship, and they are no longer independent. Their values follow nearly identical trend with that revealed in the shear-stress development test by Minamitani and with those found by previous researchers despite variation of *A* value (Fig. 10). Figure 11 interprets the OCR effect on α value that greater OCR results in smaller α value. However, the variations of α value

corresponding to OCR effect inspected in various sample types draw very wide range, which is commonly correlated with soil sample density.

Conclusions

The primary attempt in reproducing the tertiary creep behaviour of sands similar to previous flume tests with artificial rainfall and previous progressive failure tests under shear stress development conditions was succeeded by raising back pressure in ring shear apparatus. The power-law relationship of velocity and acceleration was found to be similar to Fukuzono's law in spite of certain variation of A value. The reason of A value variation could be attributed by: (1) finer grain portion, (2) slightly higher rubber edge friction of the shear box compared to previous ring shear tests, (3) increase rate of pore water generation due to time. In addition, the repeated test revealed that A and α values are not much dependent to displacement after large shear displacement. More, obvious relationship of A and α values point out that they are no longer constant and independent. Alpha value does parallel alter depending on OCR as confirmed in Minamitani's shear stress development test.

References

Azimi C, Biarez J, Desvarreux P, Keime F (1988) Forecasting time of failure for a rockslide in gypsum. In: Proceedings of the 5th international symposium on landslides, Lausanne, pp 531–536

Fukuzono T (1985) A new method for predicting the failure time of a slope. In: Proceedings of 4th international conference and field workshop on landslides, Japan, pp 145–150

Hayashi S, Park B, Komamura F, Yamamori T (1988) On the forecast of time to failure of slope (II)-approximate forecast in the early period of the Tertiary creep. J Landslide Soc 23(3):11–16

Minamitani T (2007) An experimental study on the parameter affecting tertiary creep deformation of soils. Master thesis, DPRI, Japan

Saito M (1965) Forecasting the time of occurrence of a slope failure. In: Proceedings of 6th international conference on soil mechanics foundation engineering, Montreal, Canada, vol 2, pp 537–541

Saito M, Uezawa H (1961) Failure of soil due to creep. In: Proceedings of the 5th international conference on soil mechanism and foundation engineering, vol 1, pp 315–318

Sassa K, Fukuoka H, Wang G, Ishikawa N (2004) Undrained dynamic-loading ring-shear apparatus and its application to landslide dynamics. Landslide J Springer-Verlag, No.1. pp 7–19

Sassa K (1988) Geotechnical model for the motion of landslides. In: Proceedings of the 5th internationl symposium on landslides, vol 1, Lausanne, pp 37–55

Voight B (1988) A method for prediction of volcanic eruptions. Nature 332:243–273

Voight B (1989) A method for describe rate-dependent material failure. Science 243:200–203

Part V

Landslides as Sediment Sources

Introduction by Giovanni Crosta[1], Matjaž Mikoš[2], and Zieaoddin Shoaei[3]

1) Dipartimento di Scienze Geologiche e Geotechnologie, Università degli Studi di Milano-Bicocca, Milan, Italy
2) Faculty of Civil and Geodetic Engineering, University of Ljubljana, Ljubljana, Slovenia
3) Department of International Scientific and Research Affairs, Agricultural Research, Education and Extension Organization, Teheran, Iran

Introduction

This session was proposed as a new session to the WLF2, and was accepted to be held within the general theme *Impact of landslides* together with three other sessions. Especially the thematic session *Landslides and reservoirs* with many more contributions was a strong competitor when discussing impacts of landslides. Nevertheless, the conveners of the proposed session are convinced that a wider view of landslide impacts (Mikos et al. 2006) should be discussed at the forum, not just the classical one with regard to problems of silting of reservoirs (Batuca and Jordaan 2000) but to see landslides as sediment sources (Korup et al. 2004). Their impacts on river regime and river morphodynamics are to be included into integrated river basin management. This integrated approach was in Europe introduced by the Water Framework Directive (WFD 2000).

Sediments also gained special recognition through the International Sediment Initiative (ISI; www.irtces.org/isi/) that has been launched by UNESCO as a major activitiy of the International Hydrological Programme (IHP) and that foster international cooperation in the field of erosion and sediment management, as well as in sediment-related research and education.

SedNet is a European network aimed at incorporating sediment issues and knowledge into European strategies to support the achievement of a good environmental status and to develop new tools for sediment management (www.sednet.org). They focus on all sediment quality and quantity issues on a river basin scale, ranging from freshwater to estuarine and marine sediments. For sediment management issues at river basin scale see Owens (2008).

Following these international developments, the text in the following paragraph was announced in the first forum circular and researcher, engineers, administrative officers, and practitioners were invited to submit a paper to this session:

> There is much variability of sediment yield in mountain river systems because it is influenced by both periodic and episodic events (snowmelt, high-intensity rainstorms, earthquakes . . .). Landslides (rock falls, slumps, deep-seated slides, debris flows . . .) are the most effective event that conveys large amounts of debris to the river channels through their frequent activities. Therefore, they should be treated within the framework of the integrated water management in catchments. After strong earthquakes or during typhoons and flash floods, many landslides occur and

contribute large amounts of fresh sediments to the river network and influence river morphology and unbalance sediment budget. Contributions, such as:

- Landslide case studies and analyses of corresponding erosion rates as well as estimations of sediment supply rates to watercourses from headwaters and slopes;
- Natural landslide dam outbursts and their impact on river morphology and sediment transport;
- Assessment of landslides' contribution to overall erosion rate of landscape compared to other erosion agents and
- Well described countermeasures undertaken in torrents and rivers after increased sediment supply from landslides.

Session Highlights

In the following section, the main conclusions drawn from the papers submitted to this session are presented.

Erdogan et al. (2012) stressed the importance of landslides as erosion agents within the context of the EU Soil Thematic Strategy and the related proposal for a Soil Framework Directive. Using the Tessina Landslide in Italy as a case study, the impacts of this landslide on on-site erosion and sediment delivery to the fluvial network was assessed using the RUSLE and stressing the importance of vegetation recovery in the landslide area on soil erosion.

Brambilla et al. (2012) aimed at showing how to evaluate debris volume that, in a certain time, reaches watercourses due to erosion, presence of geological weak zones and shallow landslides. Rather than choosing from either an empirical-statistical or a physically based model, they developed a hybrid distributed model to forecast sediment yields in river basins. They tested the model in the Val Rossiga basin in Northern Italy.

Brardinoni et al. (2012) stressed the fact that historical landslide inventories are critical for quantifying landslide sediment dynamics through time and for assessment of relevant contributions to regional sediment budgets. They mapped deep-seated gravitational slope deformations (DSGSD) and shallow landslides in Val di Sole in eastern Central Alps, Italy. They used historical sequence of aerial photographs and LiDAR derived hill shade rasters, together with field measured landslide depths, to obtain a volumetric transformation factor for remotely-sensed landslide areas. By integrating the two methods, a historical inventory of DSGSD and shallow landslides can be successfully developed and used to analyze landslide sediment dynamics through time.

Simoni et al. (2012) performed a catchment-scale assessment of sediment budget in the Reno River catchment in Italy over historical (Holocene) and post-glacial times. They combined available geological data with data on recent landslides (main relief-shaping agent) and on measured sediment rates. They estimated the present-day sediment delivery rates to the channel network by combining historical landslide frequency and landslide velocities and geometries measured by means of monitoring networks and inclinometers. The case study confirmed that the connectivity between hillslopes and fluvial network is well developed.

Shugar et al. (2012) studied sedimentology and geomorphology of rock avalanches and tried to link debris sheet sedimentology to observed large-scale flow features. Their idea was that to understand flow mechanics of large landslides a thorough characterization of rock avalanche debris is a necessary step. They used digital photo-sieving to describe the debris of three landslides on Black Rapids Glacier, Alaska, and the Frank Slide in Alberta, Canada. This interesting contribution was a bit out of the scope of the session.

Cepeda et al. (2012) discussed a conceptual framework for sediment-supply dependent rainfall thresholds used for early warning systems for rainfall-induced landslides. As a case study to test this concept, the Mt. Soufriere Hills volcano and its volcanic ash eruptions were used to show that variable rainfall thresholds should be used to avoid false early warning alarms. The topic of this contribution was a bit out of the scope of the session.

Conclusions

The session was one of the smallest sessions during the WLF2. One reason may well be that this session was new and was not part of the programme during the WLF1 in Tokyo in 2008. Another reason may be that this topic was at least partially covered by many papers that were due to their main focus submitted to other sessions of the WLF2. We, conveners of this special session on landslides as sediment sources firmly believe that this session will gain higher attention during the next WLF3 that will be held in Beijing in China in 2014. We heartily invite all researchers, practitioners, and administrative officers to join this highly interesting session in Beijing and in doing so stress the importance of landslides for river (and sediment) management of river basins worldwide.

Acknowledgments

The session conveners would like to thank all authors for their contributions to this session in all forms; especially for presentations and discussions during the parallel session.

References

Batuca DG, Jordaan JM (2000) Silting and desilting of reservoirs. Balkema, Rotterdam, 353 p. ISBN 90-5410-477-5

Brambilla D, Longoni L, Mazza F, Papini M (2012) An automated distributed method for solid transport evaluation in mountain basins. The Second Landslide Forum Abstracts, Rome, 3–9 Oct 2011, pp 417

Brardinoni F, Crosta G, Lamonaca S, Peretti L, Elli D, Valbuzzi E (2012) Landslide sediment transfer in Val di Sole, eastern Central Alps. In: Proceedings of the Second Landslide Forum, Rome, (this volume), 3–9 Oct 2011

Cepeda J, Barclay J, Devoli G (2012) A conceptual framework for sediment-supply dependent rainfall thresholds. In: Proceedings of the Second Landslide Forum, Rome, (this volume), 3–9 Oct 2011

Erdogan EH, Hervás J, Van Den Eeckhaut M, Pasuto A, Marcato G (2012) Assessment of soil erosion in areas affected by landslides. In: Proceedings of the Second Landslide Forum, Rome, (this volume), 3–9 Oct 2011

Mikos M, Fazarinc R, Ribicic M (2006) Sediment production and delivery from recent large landslides and earthquake-induced rock falls in the Upper Soca River Valley, Slovenia. Eng Geol 86(2–3):198–210

Korup O, McSaveney MJ, Davies TRH (2004) Sediment generation and delivery from large historic landslides in the Southern Alps, New Zealand. Geomorphology 61(1–2):189–207

Owens PN (ed) (2008) Sustainable management of sediment resources: sediment management at the river basin scale, vol 4. Elsevier, Amsterdam, (ISBN 978-0-444-51961-0) 280 p

Shugar D, Clague J, Giardino M (2012) A quantitative assessment of the sedimentology and geomorphology of rock avalanches. In: Proceedings of the Second Landslide Forum, Rome, (this volume), 3–9 Oct 2011

Simoni A, Picotti V, Ponza A, Berti M (2012) Landslide-related sediment yield rate in a large apenninic catchment. In: Proceedings of the Second Landslide Forum, Rome, (this volume), 3–9 Oct 2011

WFD (2000) Directive 2000/60/EC of the European Parliament and of the Council establishing a framework for the Community action in the field of water policy. Official J. L 327 (22.12.2000):1–73

Landslide-Related Sediment Yield Rate in a Large Apenninic Catchment

Alessandro Simoni, Alessio Ponza, Vincenzo Picotti, and Matteo Berti

Abstract

Diverse sources of information, which describes landslide movement, hillslope-channel connectivity and sedimentation rates, are analyzed to detect trends that took place during the last 12,000 years. We estimate the landslide-related sediment production rates by combining measured landslide velocities and geometries and historical landslide frequency. Coarse sediment deposition rates are measured throughout the Holocene by means of dating and stratigraphy of the alluvial fan and terraced deposits. The comparison between present-day hillslope sediment production and Holocene averaged sediment deposition rates confirms that landsliding is the main agent conveying sediments to higher order trunk streams. The connectivity between hillslopes and the stream network is well developed and no significant sediment sinks influence the sediment transport process. However fluctuations of sediment delivery rates at the outlet of the catchment took place during Holocene and are likely associated to periods of increased hillslope sediment production and channel discharge caused by climatic forcing.

Keywords

Earthflow • Sediment flux • Holocene record

Introduction

The sediment budget of large mountainous catchments is the result of the interaction of many different processes acting along the channels and over the hillslopes and interacting between themselves. The quantification of the contribution of each process to the sediment budget is, indeed, very complicated and involves the measurement or estimate of several variables.

The importance of landsliding as relief-shaping agent has long been recognized (Korup et al. 2010). The amount of total sediment produced by landslides within a given catchment is a function of their magnitude and frequency (Reid and Page 2002). Inventories of landslides show that the frequency of landslide is a function of landslide magnitude both in space and time (Brardinoni and Church 2002; Guzzetti et al. 2002). Such properties can be used to extrapolate predictions, though substantial uncertainty is still not resolved for extreme ends. In general, it can be said that the rate of sediment production from landslides vary greatly depending on the observation period and impact of extreme events (Korup et al. 2010).

Slow-moving, periodic landslides like earthflows (Hungr et al. 2001) have been seldom treated as source of sediment to regional sediment budget. Only very recently, Mackey and Roering (2011) made an effort to quantify earthflow movement over significant spatial and temporal scales. By taking a 60 years observation period, they measured earthflow movements exceeding 5 m (> 80 mm/year) and estimated the sediment production from earthflows in a weak-rock basin. Results demonstrate that earthflows are capable to generate a sediment yield that is more than half the estimated total sediment yield.

A. Simoni (✉) • A. Ponza • V. Picotti • M. Berti
Dip.to di Scienze della Terra e Geologico-Ambientali, Università di Bologna, Via Zamboni 67, Bologna, Italy
e-mail: alessandro.simoni@unibo.it

C. Margottini et al. (eds.), *Landslide Science and Practice*, Vol. 4,
DOI 10.1007/978-3-642-31337-0_39,

In this work, we analyse earthflow activity over a large portion of the Reno river catchment, where clay shales outcrop. The estimate of hillslope sediment delivery rate to the channel network is based on mapped connectivity, mean earthflow velocity (inclinometer readings), and geometric similarities describing the depth of sliding. We take advantage of peculiar lithological characteristics of the rocks involved in earthflow, to isolate the volumetric fraction of the Holocene deposits (fan and terraces) that can be ascribed to the Ligurian units. We then compare present day hillslope sediment yield rates and Holocene deposits to assess the contribution of earthflow movement to regional erosion rates and their control of landscape evolution.

Regional Study Area: Reno River

The Reno river catchment is located in the Northern Apennines of Italy (Fig. 1). Its mountainous portion extends over an area of 668 km^2, rising from an elevation of 56 m to the highest point at 1,922 m. A large alluvial fan dominated by gravel deposits is present at the basin outlet.

About 42 % of the catchment is made of geological units pertaining to the Ligurian domain. In the remaining portion, the bedrock mainly consists of stratified sedimentary rocks, dominated by arenaceous flysch.

Ligurian units consist mainly of chaotic clay shales and include limestone clasts (gravel to boulder size) embedded into the clayey matrix as a reminiscence of original calcareous beds (Pini 1999). The clay-shale bedrock shows a structure made of small iso-oriented particle aggregates (scales) with dimension ranging from millimeters to centimeters. Getting close to the surface, the clay-shale is subject to stress relief, swelling and weathering which progressively cancel the scaly structure and induce a color change from dark grey to brown.

The style of landsliding, on Ligurian Units, is dominated by complex earth slides-earthflows (Cruden and Varnes 1996). Hereafter, we use the term earthflow (Hungr et al. 2001) to describe slow-moving landslides with flow-like morphology. Earthflows typically have a bowl-shaped source area, an elongate transport zone and a lobate toe that reaches the trunk stream at the bottom of the slope or, alternatively, merges to other earthflows generating coalescent multiple phenomena.

Earthflow bodies slowly move downslope. The movement generally exhibits a seasonal pattern and mostly develops along discrete sliding surfaces with internal deformation of the sliding mass. Most often, failures are observed in the source area where they determine the progressive retrogression of the main headscarp and feed the earthflow body. Paroxistic reactivations of the whole deposit are much less frequent and probably related to the downslope transfer of undrained loading (van Asch 2005).

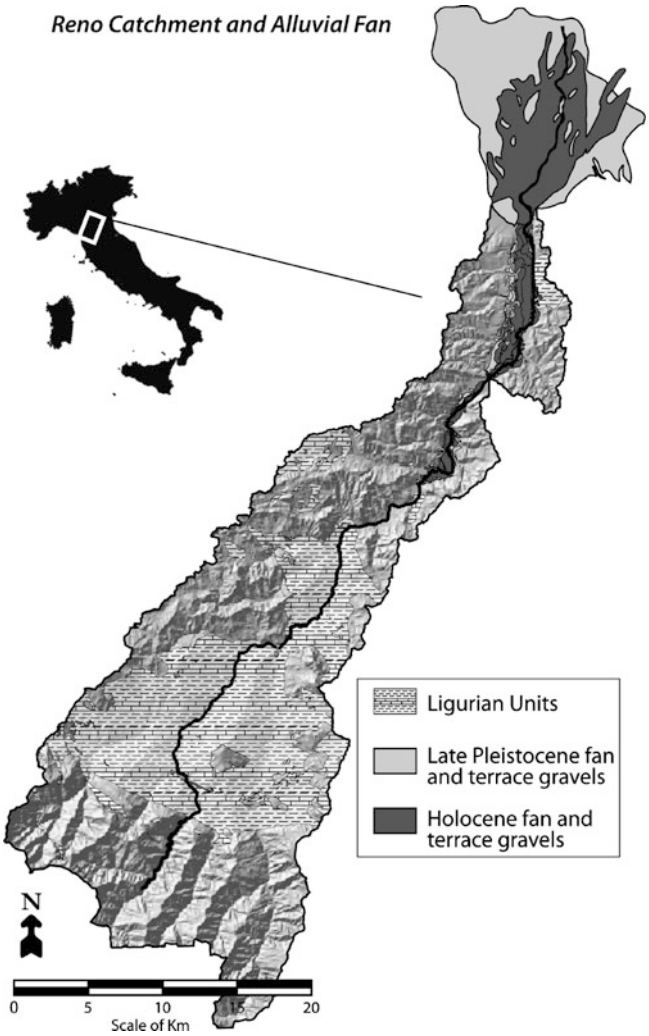

Fig. 1 Sketch map of the Reno river intramontane catchment and alluvial fan

The regional landslide inventory (Regione Emilia-Romagna 2011) reports 2,454 earthflows that cover 40 % of the Ligurian units areal extent. The mean area is 45,414 m^2 and the largest earthflow is 1.8 km^2. The analysis of the non-cumulative frequency area distribution of earthflows (log bin size = 1/16) shows that higher frequencies are associated to areas of about 20,000 m^2 (Fig. 2). The frequency of landslides of a particular size often follows a power-law relationship and the area below which the data set deviates or breaks in scaling between landslide area and frequency is called the roll-over (Guzzetti et al. 2002). In our case, the onset of the power-law dependence is located at 40,000 m^2 (R^2 value of 0.97) and the power law exponent is -1.16. Compared to other literature data (Goswami et al. 2011; Guzzetti et al. 2002, 2009), our data set is described by a large roll-over and a small exponent that we attribute to the peculiar features of earthflows. In fact, small size (100–10,000 m^2) phenomena

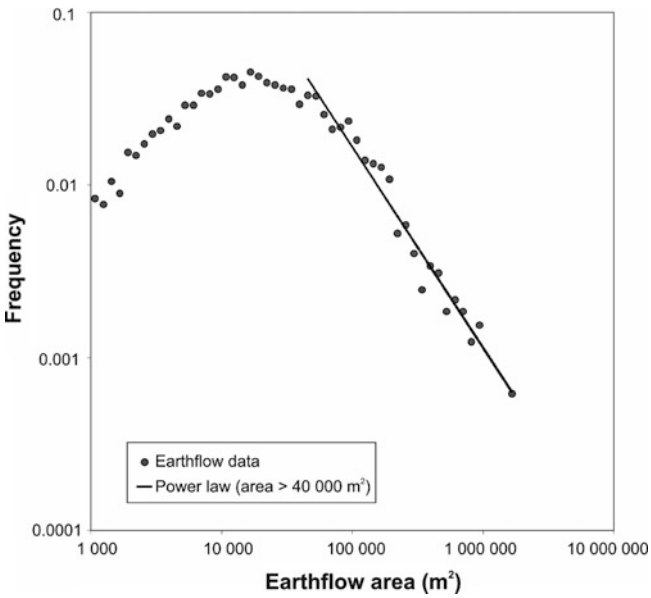

Fig. 2 Area-frequency statistics of earthflows

typically occur in the source area of larger phenomena or coalesce to generate a larger earthflow. Similar results were found by Mackey and Roering (2011) on a smaller data set of earthflows mapped over a time frame of 60 years.

Motivation

As outlined above, landsliding is the main agent shaping the landscape in the Reno catchment. A striking feature is that nearly all hillslopes in the Ligurian units appear to have been affected by mass movement. The drainage network is dense but poorly developed. Beside the main river and few tributaries, ephemeral gullies develop over extensive low-gradient slopes (10–15°) where erosion is dominated by earthflows.

Several approaches have been used to constrain background levels of rock uplift and erosion in Northern Apennines. Thermochronometric data (Zattin et al. 2002) show rapid exhumation (1.2 ± 0.24 mm/year) over the past 5 My which contrast with lower uplift rates (1 ± 0.2 mm/year) measured by geodetic methods (D'Anastasio et al. 2006), and erosion rates of 0.12–0.53 mm/year derived from basin sedimentation data (de Vente et al. 2006). Cyr and Granger (2008), based on cosmogenic nuclide, constrained the recent erosion rate between 0.28 and 0.58 mm/year. They suggested that dynamic equilibrium between uplift rates and both the hillslope and fluvial systems was achieved within a few million years from emergence of the Apennines and still persists today. The morphological features of the Reno catchment also strongly support the hypothesis of steady state landscape evolution. The widespread landslide activity demonstrates that hillslope are close to their limiting angle. The main trunk streams are bedrock-incised with exceptions mainly located in the lowest portion of the catchment. We therefore assume that landscape evolution proceeds with substantial equilibrium between local uplift, mean erosion and river incision rates. Such condition implies that relief doesn't change and that hillslope processes largely outpace channelized bedrock erosion in terms of contribution to the overall sediment yield.

The reconstruction of the sediment budget at catchment scale is far beyond the scope of this paper. We focus on landslide-dominated hillslope sediment fluxes and compare them to the alluvial sediment record. The comparison is possible because (1) Ligurian units contain the only calcareous rocks of the catchment; (2) the geometry of coarse Holocene deposits can be reconstructed; and (3) the relative abundance of limestone clasts measured.

The original calcareous beds of the Ligurian units were disrupted by tectonic deformation and can now be found as large angular fragments embedded into the clay shale matrix. Earthflows transport limestone clasts to the stream network where they are efficiently evacuated by fluvial processes. Sparse gravel deposits are present only in the lower part of the intramontane basin (Picotti and Pazzaglia 2008) while the vast majority of coarse deposition takes place on the fan.

Data

We use the extensive archive of information collected by the relevant territorial authority (Regione Emilia-Romagna). In order to characterize earthflow activity, we used the following: (1) 1:10,000 landslide inventory map; (2) historical landslide archive (Rossi et al. 2010); (3) inclinometer readings (collection of data and analysis performed by the authors). The Holocene fan geometry was reconstructed based on the data set of borehole logs (inclusive of ^{14}C datings) made available from Regione Emilia-Romagna. Terraced deposit mapping from Picotti and Pazzaglia (2008).

Methods and Results

Contribution of Earthflows to Regional Sediment Flux

We aim to quantify the transfer of sediment from slope failures to active channels. As previously stated, we focus on Ligurian units where earthflows largely dominate hillslope evolution.

Individual earthflows continue moving and actively supplying sediment to a channel for thousands of years (Bertolini et al. 2005). Paroxistic reactivations can periodically interrupt the persistent seasonal background movement (Iverson and Major 1987). The distinction between active and dormant

phenomena (Cruden and Varnes 1996) only supplies qualitative information about the distance in time from the last reactivation and is not related to the present deformation rates nor to the possibility of future reactivation.

The measurements of earthflow displacement (72 inclinometers) confirm that deformation takes place preferentially along discrete sliding surfaces (76 % of data). Mean velocities range widely, from virtually zero to tens of mm per month. Based on velocity, there is no statistically significant difference between earthflows mapped as active or dormant. Therefore, we do not adopt any distinction based on the state of activity and jointly analyze the data to characterize the landslide velocity and its variability. The frequency distribution (Fig. 3) can be approximated by a lognormal peaking at 1.68 mm/month and associated to significant variability. We found no relationship whatsoever between velocity and geometry of phenomena (i.e., area, width, depth) and therefore assume the mean velocity (V_{av}) as representative of the displacement taking place in earthflows.

Inclinometer data supply precious information also about the geometry of gravitational movements. They confirm the existence of geometric similarities between earthflows of different sizes. Scaling relationships were observed in different contexts and generally described by area-volume power-law equations (Guzzetti et al. 2009; Larsen et al. 2010; Parker et al. 2011). Figure 4 reports a selection of our data, regarding the median-lower part of earthflow deposits, where we observe a relationship ($R^2 = 0.63$) linking the depth of sliding surface (D) and planar area (A), across 2.5 orders of magnitude:

$$D = 0.07 \cdot A^{0.44} \tag{1}$$

The relationship is in general agreement with similar relationships in the literature. Some of them have been reported in Fig. 4 by simply equating the depth of sliding surface to the average landslide depth (Volume/Area).

In calculating sediment production from earthflows, we distinguished earthflows that discharge sediment directly into a channel or major gully from flows that are disconnected from the channel network and do not represent active sediment sources. In other terms, we map the earthflow-river connectivity based on their relative position. Figure 5 reports a schematic example that illustrates how the regional landslide inventory map is used to measure the width of each connected earthflow (W). A total of 1,314 earthflow-river connectivity segments were mapped and measured, and associated to the planar area of the corresponding earthflow.

The average annual sediment flux from earthflows of the Ligurian units (Q_{EF}) was simply estimated using the following:

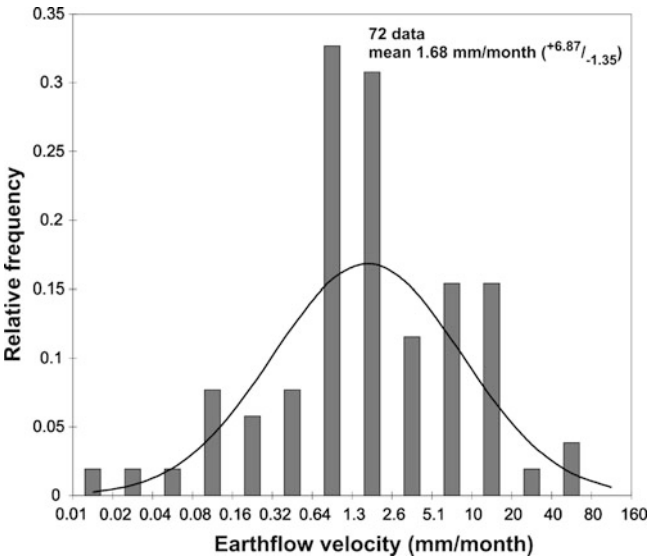

Fig. 3 Frequency distribution of earthflow velocities measured through inclinometers. A lognormal distribution described by mean and st.dev of the data is over imposed

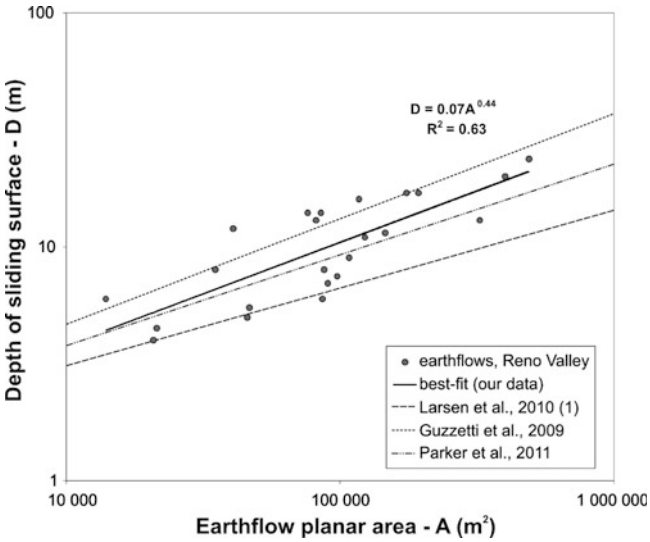

Fig. 4 Earthflow depth versus planar area. Data are from inclinometers positioned in the medium-lower part of the earthflow. When multiple inclinometers are available, the average value of depth is reported. Our data are compared to similar relationships reported in the literature

$$Q_{EF} = \sum_{i=1}^{i=n} (W \cdot D(A)) \cdot V_{av} \tag{2}$$

where n is the number of earthflows and D is estimated for each earthflow based on (1).

We estimated an average sediment flux of 61,124 m^3/year for 1,314 earthflows that can be considered tightly connected to the fluvial system.

As previously stated, we do not distinguish dormant and active earthflows. We believe that a discrete boundary

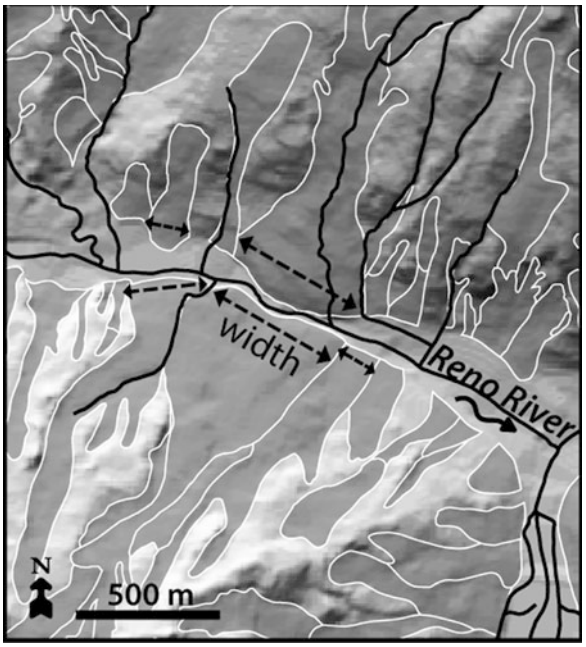

Fig. 5 DEM-derived hillshade map and landslide inventory illustrating the measurement of earthflow width

between the two does not exist and available data (Fig. 3) tend to confirm such view. Nevertheless, we know that earthflows periodically experience paroxistic reactivations causing the sudden increase of velocities up to tens of centimeters to meters per day. In such cases, displacements may reach values of tens of meters. Available historical information was used to make a tentative assessment of the frequency of paroxistic earthflow reactivations. Despite inherent uncertainties associated to the historical descriptions, we identified 111 events occurred between 1900 and today (1 event/year). We used such frequency together with the mean values of our earthflow population (W, D), and 20 m of total displacement to estimate a sediment flux of ~38,000 m^3/year due to the contribution of paroxistic reactivations.

The total sediment flux sum up to ~ 100,000 m^3/year and includes weathered clay-rich regolith, clay shales, and limestone clasts whose relative abundance was measured (24 % averaged over four sites) to quantify the specific contribution to the channel network. The simple procedure gives an estimated 24,000 m^3/year of limestone sediment flux.

Holocene Fan and Terraced Deposits

The Reno River deposited a large alluvial fan at the outlet of the intramontane valley. The fan deposits are mostly composed of gravels with subordinate sand and silt. Thanks to the availability of a large number of borehole logs (Fig. 6), including scattered ^{14}C datings, we could define the areal extent of Holocene coarse deposits together with the associated thicknesses. Here, we refer to Holocene deposits intending those younger than 12ky. Point-wise data describing the base and top where interpolated and subtracted to estimate the total volume of coarse sediments deposited through Holocene (Table 1). Terraced deposits of the same age (Picotti and Pazzaglia 2008) were also considered based on their extent and field-estimated thickness. As expected, the vast majority of coarse deposit is stored in the fan, and intramontane deposits account for less than 4 %.

In order to compare data with earthflow sediment flux, we converted the total volume of sediments into corresponding volume of limestone clasts. Experimental measurements of porosity, grain-size and limestone abundance (Table 1) were used. Overall, the results lead to an estimate of 170,000,000 m^3 of limestone gravel sediments deposited through Holocene by the Reno River.

Discussion and Conclusion

Our results show that earthflows are the primary erosion process in weak rock lithologies dominated by clay shales. Slow-moving gravitational movements contribute to deliver sediments to the channel network at a rate of ~100,000 m^3/year. Coarse calcareous fragments floating in the clay shales make up 24 % of such flux (~24,000 m^3/year) and can be tracked down to the end of the intramontane valley where terraces and alluvial fan store the coarse deposits. Their volume is used to calculate the Holocene-averaged deposition rate (~14,000 m^3/year) that reveals that hillslope sediment production and river deposition are similar to one another to within a factor of two. Considering that some fraction of limestone fragments are dissolved along the course of the river (ongoing assessment), we can state that a substantial equilibrium exists.

The sediment yield from the 278 km^2 of earthflow-prone Ligurian units (350 m^3/km^2/year) corresponds to an averaged erosion rate of 0.36 mm/year that is very similar to millennial-scale cosmogenic nuclide data (0.28÷0.58 mm/year) of nearby Apennine valleys (Cyr and Granger 2008). Our results are much likely under-estimated because they do not include hillslope erosion and creeping of stable slopes. Anyhow, they indicate that that present-day erosion proceeds at a pace similar to that recorded by sedimentation in post-glacial times. This argument suggests that the landscape evolution of the Reno catchment is a state of dynamic equilibrium.

Steady-state conditions were punctuated, through Holocene, by episodes of higher sedimentation that are recorded in the terraced deposits of the lower intramontane valley (Picotti and Pazzaglia 2008). Such pulses may be related to climate-driven variations of hillslope and channel sediment yield that rapidly propagated downslope to the fan.

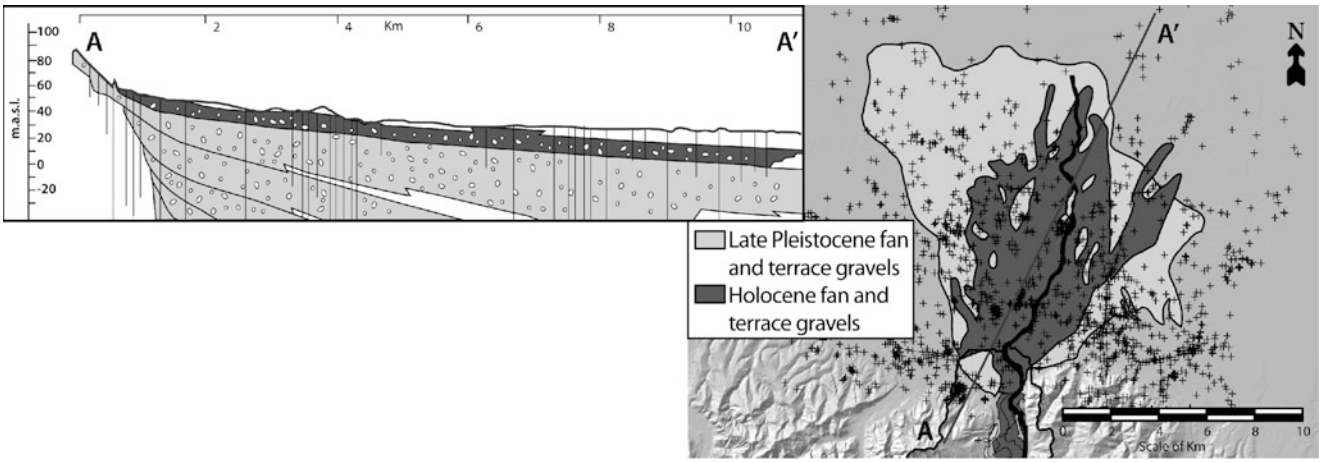

Fig. 6 Map and longitudinal section of Reno alluvial fan. *Cross-symbols* indicate the location of available borehole logs and cone-penetration tests

Table 1 Summary of data regarding Holocene coarse deposits of the Reno river

Variable	Mean value	St. dev.	Samples/ measurements	Methods
Volume of Holocene coarse deposits in the fan (m^3)	670,908,670	–	–	Areal extent and thickness based on borehole logs and ^{14}C datings
Volume of Holocene terraces (m^3)	26,204,080	–	–	Mapping + field estimated thickness
Soil porosity	0.24	0.02	3	In-situ volume measurements
Gravel fraction (% by volume)	83.88	1.86	6	Grain-size analysis (in situ measurements + lab sieving)
Limestone fraction (% by volume)	55.83	3.13	6	Qualitative clasts-counting

Among future developments, we intend to refine temporal correlations within the fan deposits to obtain intra-Holocene sedimentation rates that can be compared to studies of past climate scenarios.

Acknowledgments This work has been done in the framework of the Sedymont Project (TOPO-EUROPE) and we would like to thank all the participants who shared our opinion and promoted fruitful discussions.

We would like to thank Emilia-Romagna Region for kindly supplying the following data: landslide inventory map and historical archive, inclinometer readings, borehole logs and dating results on the alluvial fan.

References

Brardinoni F, Church M (2004) Representing the landslide magnitude-frequency relation: Capilano River basin, British Columbia. Earth Surf Process Land 29:115–124

Bertolini G, Guida M, Pizziolo M (2005) Landslides in Emilia-Romagna region (Italy): strategies for hazard assessment and risk management. Landslides 2:302–312

Cruden DM, Varnes DJ (1996) Landslide types and processes. In: Turner AK, Schuster RL (eds) Landslides: investigation and mitigation. National Academy Press, Washington, DC, pp 36–71

Cyr AJ, Granger DE (2008) Dynamic equilibrium among erosion, river incision, and coastal uplift in the northern and central Apennines, Italy. Geology 36(2):103–106. doi:10.1130/G24003A.1

D'Anastasio E, De Martini PM, Selvaggi G, Pantosti D, Marchioni A, Maseroli R (2006) Short-term vertical velocity field in the Apennines (Italy) revealed by geodetic levelling data. Tectonophysics 418:219–234. doi:10.1016/j.tecto.2006.02.008

de Vente J, Poesen J, Bazzoffi P, van Rompaey A, Verstraeten G (2006) Predicting catchment sediment yield in Mediterranean sediment sources and basins. Earth Surf Process Land 31:1017–1034

Goswami R, Mitchell NC, Brocklehurst SH (2011) Distribution and causes of landslides in the eastern Peloritani of NE Sicily and western Aspromonte of SW Calabria, Italy. Geomorphology 132(3–4):111–122. doi:10.1016/j.geomorph.2011.04.036

Guzzetti F, Malamud BD, Turcotte DL, Reichenbach P (2002) Power-law correlations of landslide areas in central Italy. Earth Planet Sci Lett 195:169–183

Guzzetti F, Ardizzone F, Cardinali M, Rossi M, Valigi D (2009) Landslide volumes and landslide mobilization rates in Umbria, central Italy. Earth Planet Sci Lett 279:222–229

Hungr O, Evans SG, Bovis MJ, Hutchinson JN (2001) A review of the classification of landslides of the flow type. Environ Eng Geosci 7(3):221–238

Iverson RM, Major JJ (1987) Rainfall, groundwater flow, and seasonal movement at Minor Creek landslide, northwestern California: physical interpretation of empirical relations. Geol Soc Am Bull 99:579–594

Korup O, Densmore AL, Schlunegger F (2010) The role of landslides in mountain range evolution. Geomorphology 120:77–90

Larsen IJ, Montgomery DR, Korup O (2010) Landslide erosion controlled by hillslope material. Nat Geosci 3:247–251. doi:10.1038/NGEO776

Mackey BH, Roering JJ (2011) Sediment yield, spatial characteristics, and the long-term evolution of active earthflows determined

from airborne LiDAR and historical aerial photographs, Eel River, California. GSA Bulletin 123(7/8):1560–1576. doi:10.1130/B30306.1

Parker RN, Densmore AL, Rosser NJ, de Michele M, Li Y, Huang R, Whadcoat S, Petley DN (2011) Mass wasting triggered by the 2008 Wenchuan earthquake is greater than orogenic growth. Nat Geosci, advance online publication, 4 pages, doi:10.1038/NGEO1154

Picotti V, Pazzaglia FJ (2008) A new active tectonic model for the construction of the Northern Apennines mountain front near Bologna (Italy). J Geophys Res 113, B08412, 24 pages, doi:10.1029/2007JB005307

Pini GA (1999) Tectonosomes and olistostromes in the Argille Scagliose of Northern Apennines, Italy. Geological Society of America Special Paper 335, 70 p

Regione Emilia-Romagna (2011) Inventario del dissesto. URL: http://www.regione.emilia-romagna.it/wcm/geologia/canali/cartografia/sito_cartografia/web_gis_dissesto.htm. Last accessed 17 June 2011

Reid LM, Page MJ (2002) Magnitude and frequency of landsliding in a large New Zealand catchment. Geomorphology 49:71–88

Rossi M, Witt A, Guzzetti G, Malamud BD, Peruccacci S (2010) Analysis of historical landslide time series in the Emilia-Romagna region, northern Italy. Earth Surf Process Land 35:1123–1137. doi:10.1002/esp. 1858

Van Asch TWJ (2005) Modelling the hysteresis in the velocity pattern of slow-moving earth flows: the role of excess pore pressure. Earth Surf Process Land 30:403–411

Zattin M, Picotti V, Zuffa GG (2002) Fission-track reconstruction of the front of the northern Apennine thrust wedge and overlying Ligurian Unit. Am J Sci 302:346–379. doi:10.2475/ ajs.302.4.346

Landslide Mobility and Landslide Sediment Transfer in Val di Sole, Eastern Central Alps

Francesco Brardinoni, Giovanni B. Crosta, Samuel Cucchiaro, Elena Valbuzzi, and Paolo Frattini

Abstract

We examine preliminary data from a landslide inventory that combines the mapping of landslides and deep-seated gravitational slope deformations (DSGSDs) in Val di Sole, eastern Central Alps, Italy. Landslide identification and classification was conducted via interpretation of sequential airphotos (API), LiDAR shaded-relief rasters. Landslide geometries were measured in the field for a sample of events. Seeking to evaluate landslide-driven sediment flux, we consider landslides as sediment sources and we classify them into rapid, full-mobility failures and slow, partial-mobility ones. The corresponding sediment flux, solely associated with rapid failures, exhibits clear lithologic controls, with metamorphic rocks displaying markedly higher landslide activity. DSGSDs occur exclusively in metamorphic terrain and landslides tend to cluster around them. Accordingly, these large-scale slope deformations could play a prominent role in modulating the contemporary landslide sediment flux. In the compilation of the inventory, the use of LiDAR and airphotos did not prove to be mutually exclusive. We recommend the two methodologies be employed in an integrated framework.

Keywords

Landslides • Deep-seated slope deformations • LiDAR • Aerial photography • Lithology

Introduction

Landslides exert prominent controls on the morphology of mountain drainage basins and drive the overall sediment flux across mountain environments. In this context, landslide inventories represent a critical base for quantifying landslide sediment dynamics and assessing relevant contributions to regional sediment budgets (e.g., Brardinoni et al. 2009).

Airphoto interpretation (API) is a convenient and efficient way to compile regional landslide inventories (e.g., Reid and Dunne 1996; Hovius et al. 1997; Martin et al. 2002), especially in steep terrain with difficult access. However, in densely forested regions identification and measurement of slope failures by remote sensing is hampered by the forest canopy so that a population of events cannot be detected (Brardinoni et al. 2003; Turner et al. 2010). Today LiDAR (Light Detection and Ranging) technology gives us the opportunity to detail in rugged, vegetated terrain critical process-geomorphology features like landslide scars, channel heads, and first-order streams (e.g., Ardizzone et al. 2007; Passalacqua et al. 2010), as well as delineate structural controls and deep-seated gravitational deformations (e.g., Jarman et al. 2011) over large landscape areas.

In this contribution, we present new data from a landslide inventory that combines the mapping of landslides and deep-seated gravitational slope deformations (DSGSD) in Val di Sole, eastern Central Alps, Italy. The inventory, compiled by means of API, 2 m-gridded LiDAR DEMs (acquired in 2006 by the Autonomous Province of Trento), and fieldwork,

F. Brardinoni (✉) • G.B. Crosta • E. Valbuzzi • P. Frattini
Department of Geological Sciences and Geotechnologies, University of Milano-Bicocca, Piazza della Scienza 4, Milan, Italy
e-mail: francesco.brardinoni@unimib.it

S. Cucchiaro
Monza, via della Taccona 42/B, Milan, Italy

C. Margottini et al. (eds.), *Landslide Science and Practice*, Vol. 4,
DOI 10.1007/978-3-642-31337-0_40,

represents an opportunity to critically evaluate advantages, limitations, and research needs that have arisen during this mapping exercise in relation to the identification of sediment sources and the estimation of landslide sediment flux.

Study Area and Data Collection

Val di Sole (708 km^2), located in the north-western corner of the Trentino Province, coincides with the upper half of the Noce River basin. The area is characterized by high relative relief, with elevations ranging from 553 m a.s.l. at the study basin outlet (Santa Giustina Lake), to 3,769 m (Cevedale Mountain), and 3,558 m (Presanella Mountain) of the main mountain tops. Bedrock geology includes metamorphic rocks of the Australpine Basement unit (mainly pre-Permian paragneiss and minor orthogneiss between the Tonale and Pejo lines, micaschists north of the Pejo line), Tertiary tonalites of the Adamello Batholith, and Triassic sedimentary rocks (mainly limestones and dolostones) in the Southern Alps unit (Fig. 1a). The whole Noce River basin was overridden by the Pleistocene Alpine ice cap, and as such typically presents oversteepened valley walls, cirques, hanging valleys, and well developed troughs. In places, thick glacial and glacio-fluvial deposits blanket the lower-to-mid portions of the slopes.

The altitudinal distribution of vegetation is characteristic of the Central Alps (Landolt 1992; Sartori et al. 2005) and includes deciduous forests below 1,000 m a.s.l., and conifer forests between 1,000 and 2,200 m. The latter, in turn, can be subdivided into: (1) a Montane belt (1,000–1,600 m) dominated by European silver fir with spruce fir; (2) a Subalpine belt (1,600–1,900 m), in which spruce fir and scots pine prevail; and (3) a Suprasubalpine belt (1,900–2,200 m), with Swiss stone pine, larch, and shrubs setting the timberline.

Selection of the study area was guided by: (1) the composite geological setting, which provides the opportunity to evaluate lithological effects on landslide activity and visibility; (2) the large extension of forested terrain, which allows to track landslide occurrence in relation to vegetation patterns of regrowth and to test the benefits of LiDAR technology; and (3) the limited portion of landscape occupied by rock walls and sedimentary linkages (e.g., active talus slopes and cones). On such landforms, typically characterized by a chronic flux of sediment with little potential for vegetation development, the identification of fresh landslide scars in sequential photosets is difficult and unreliable, because of the subtle contrast between the substrate and freshly eroded debris. In such conditions, an evaluation of the visibility time window for clusters of landslides on the hillslopes and debris flows along the channels would become virtually impossible.

During the compilation of the inventory landslides were classified according to Cruden and Varnes (1996) in relation to the velocity of the failure type and the mobility of the displaced material. In addition, seeking to evaluate landslide-driven sediment flux, we further simplified our landslide classification into: (1) rapid, full-mobility failures (e.g., rock avalanches, debris slides, and debris flows); and (2) slow, partial-mobility ones (e.g., deep-seated rotational and translational movements). For the former typology, one can generally estimate the depth of the mobilized material, and distinguish an initiation, transportation, and deposition zone. For slow, partial-mobility landslides, which typically present a well-defined headscarp, but an unclear/poorly developed runout zone, the relevant failures depths cannot be measured in the field unambiguously, the timing of movement initiation is uncertain (e.g., induced by deglaciation, or seismically related), estimating discrete travel distances is problematic, and to evaluate contemporary rates of movement would require detailed monitoring (e.g., Colesanti and Wasowski 2006). Therefore, although both full- and partial-mobility failures are sediment sources, because of the foregoing limitations, we restrict volume estimation of mobilized material to rapid, full-mobility events only.

Stereoscopic inspection of sequential airphoto sets (1959, 1969, 1973, 1983, 1996, 2000, and 2006, with nominal scale ranging from 1:15,000 to 1:27,000) formed the basis for compiling the multi-temporal landslide inventory for rapid full-mobility failures. During API, inspection of LiDAR topography was critical for delineating the complex morphologies created by DSGSDs, and for refining the API-derived inventory, especially in forested terrain. In this context, LiDAR resolution allowed resolving uncertainties in terms of landslide connectivity to the drainage network, and the partitioning of full-mobility failure tracks into initiation, transportation, and deposition zones. In particular, inspection of LiDAR shaded-relief rasters formed the basis for compiling the inventory of slow, partial-mobility failures and deep-seated gravitational slope deformations (Fig. 1). During this procedure, API was used as a subordinate source of information, mainly aiming at double-checking the landslides identified and classified during inspection of LiDAR shaded-relief maps.

Finally, during fieldwork we measured depth (d_L) of 173 full-mobility failures, which yielded the following volume-area relation:

$$V_L = 3A_L^{0.69} \quad (1)$$

Notwithstanding the high scatter in the relation ($R^2 = 0.51$), we applied (1), transformed landslide areas (A_L) into relevant volumes (V_L), hence could estimate rates of sediment transfer. The trend describes a peculiar

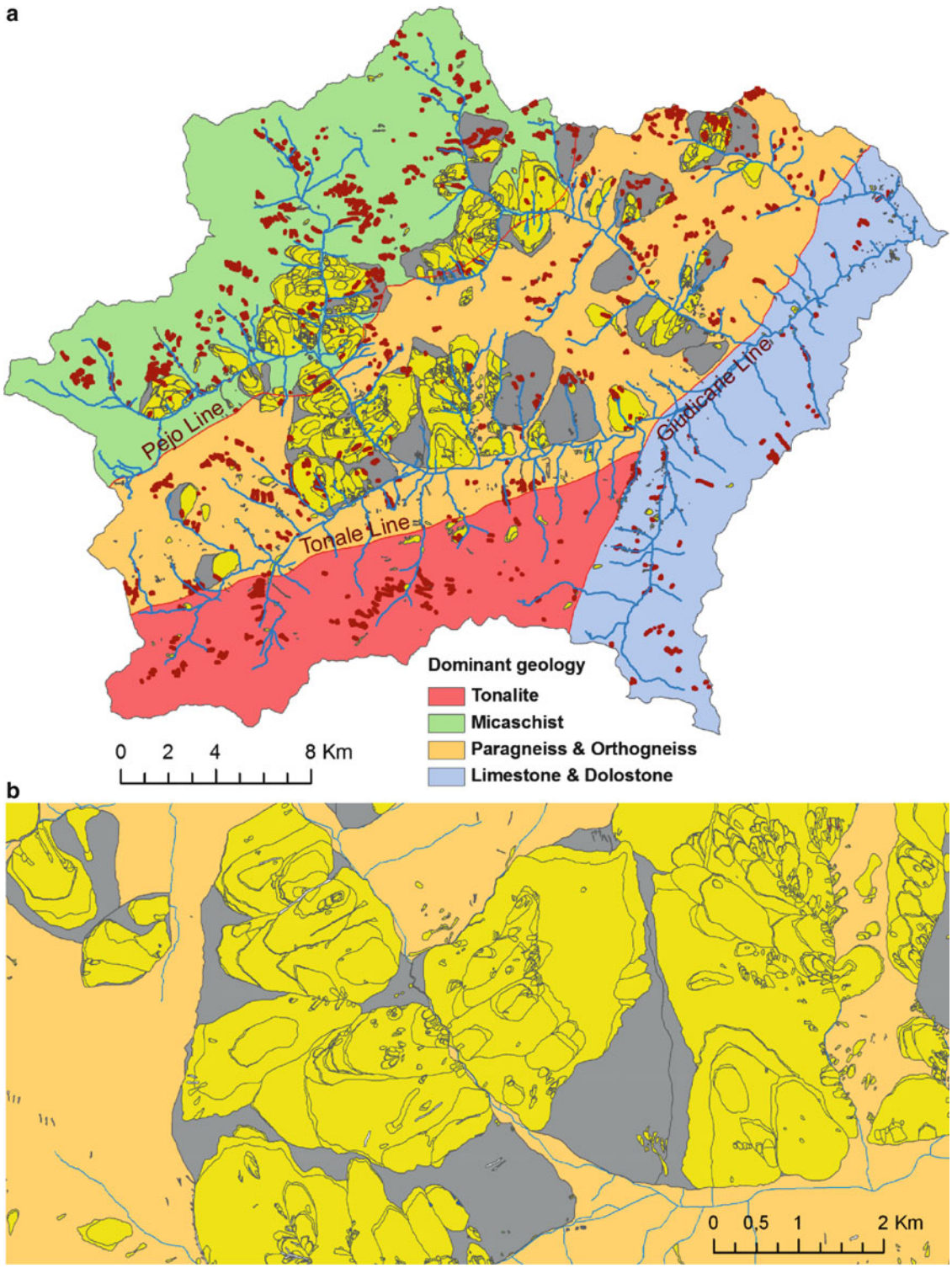

Fig. 1 (**a**) Dominant bedrock geology and main tectonic lines in Val di Sole. *Dark brown polygons* indicate rapid failures identified by multi-temporal API. Deep-seated gravitational slope deformations (*grey polygons*) and landslides (*yellow polygons*) were mapped primarily via interpretation of LiDAR shaded relief. (**b**) Close-up view of the LiDAR-based landslide mapping

allometric behavior, that is, for progressively larger events, landslide volume increases at slower pace than area. Interestingly, this relation contrasts with recent compilations of landslide geometry (e.g., Guzzetti et al. 2009; Larsen et al. 2010) that reports a scaling exponent between landslide area and volume ranging between 1.33 and 1.45.

Landslide activity is examined in terms of the following variates: landslide count (#LS), landslide density (#LS per km^2), total landslide area (km^2), specific landslide area (total landslide area in m^2 divided by terrain area in km^2), and landslide volumetric specific yield (m^3/km^2/year).

Results

In the presentation of the results, we first illustrate the crude numbers of the inventory, differentiating between events identified by API and the supplementary set mapped through observation of LiDAR-derived rasters (Table 1). We then consider how landslide types (i.e., full- and partial-mobility ones) are distributed across the four main lithological categories that underlie Val di Sole (Tables 2 and 3), estimating sediment fluxes for rapid, full-mobility failures only. Finally, we examine topological correlations between DSGSDs and landslide types (Table 4).

The multi-temporal API-based landslide inventory includes 1786 rapid, full mobility events. To this figure, inspection of LiDAR-derived shaded-relief rasters allowed identifying a large number of supplementary sediment sources: 2,514 full- and 404 partial-mobility failures (Table 1). However, because we have no time constraint on the occurrence of the "LiDAR landslides", these events cannot be included in the evaluation of landslide-derived sediment yield for the 1959–2006 period (Table 3).

Lithologic Controls and Landslide Typology

Lithologic controls on landsliding are apparent and metamorphic lithologies are associated to higher mass wasting activity. Analysis of API-based rapid failures documents that in the 1959–2006 period landslide density and specific landslide area are highest in terrain underlain by micaschist and paragneiss/orthogneiss, about two to five times those recorded in intrusive and sedimentary areas. In volumetric terms, full-mobility failures mobilize about twice as much material in terrain underlain by micaschist (10.76 m^3/km^2/year) than in intrusive (4.64 m^3/km^2/year) and sedimentary lithologies (3.79 m^3/km^2/year), with paragneiss/orthogneiss rocks showing intermediate denudation rates (7.04 m^3/km^2/year). Values in the intrusive terrain of Val di Sole are respectively one and two order of magnitude smaller than in similar lithologies of coastal (Brardinoni et al. 2003) and insular British Columbia (Brardinoni et al. 2009).

When LiDAR-derived sediment sources are added, full-mobility statistics increase across lithologies between two and four times in terms of simple landslide counts and between four and eight times in terms of total landslide area (Tables 2 and 3). For slow, deep-seated, partial-mobility failures the lithologic control is even more pronounced, in that they are an order of magnitude more frequent in metamorphic rocks than in intrusive and sedimentary ones. If on one hand this failure typology is marginal in terms of landslide numbers (Table 2), it clearly affects large parts of metamorphic terrain, and can make up from 22 % (tonalite) to 89 % (paragneiss) of the total area covered by landslides (Table 3).

Table 1 Number of landslides inventoried by multi-temporal API and inspection of a LiDAR-derived shaded-relief rasters

Survey type	Full mobility	Partial mobility	Combined
Multi-temporal API	1,786	n.a.	1,786
LiDAR	2,514	404	2,918
Total	4,300	404	4,704

The Geomorphic Significance of DSGSDs

In the study area DSGSDs occur exclusively in metamorphic rocks (Fig. 1). To explore potential causal linkages between DSGSDs and landslide occurrence we compare landslide counts of events that are topologically related and unrelated to DSGSD polygons (Table 4). It turns out that landslide densities of events that intersect or are completely within DSGSDs are higher than those recorded for topologically unrelated events.

This effect, which is particularly apparent for slow, partial-mobility failures – landslide density increases about 16 times within DSGSD areas – provides a reasonable explanation for the lithologic correlations, presented in Table 3. In Val di Sole, the presence of DSGSD structures seems to destabilize unchannelled topography and to a lesser extent those mountain streams setting part of a DSGSD perimeter. In this context, unchannelled topography is characterized by complex clusters of slow, partial mobility failures (Fig. 1b). Steep mountain streams appear to experience long series of shallow, rapid, full-mobility failures that deliver material directly to the channels.

Discussion and Conclusions

The present work seeks to critically evaluate how LiDAR technology can improve the reliability of airphoto-based landslide inventories, and should not be regarded as an attempt to replicate and contrast inventories using different remote sensing techniques. API and LiDAR technology share advantages and disadvantages. If on one hand, the use of LiDAR shaded-relief rasters reduces uncertainty in the identification and delineation of DSGSD and landslide features, on the other, it is too expensive to be replicated

Table 2 Number of landslides and landslide densities (#LS/km^2) as identified from API and LiDAR-based survey, by dominant geology types and landslide mobility

Dominant geology		Full mobility (API)		Full mobility (API + LiDAR)		Partial mobility (LiDAR)		Total	
(Number of events)	Terrain area (Km^2)	# LS	LS density	# LS	LS density	#LS	LS density	#LS	LS density
Tonalite	103	147	1.43	264	2.57	7	0.07	271	2.64
Micaschist	202	777	3.85	1,272	6.30	167	0.83	1,439	7.12
Paragneiss and Orthogneiss	290	742	2.56	2,282	7.87	218	0.75	2,500	8.62
Limestone and Dolostone	113	120	1.06	482	4.27	12	0.11	494	4.37

Table 3 Total landslide area (km^2), specific landslide area (m^2/km^2, values in brackets) and volumetric specific yield (m^3/km^2/year) as estimated from API and LiDAR-based survey, by dominant geology types and landslide mobility

Dominant geology	Full mobility (API)	Full mobility (API + LiDAR)	Partial mobility (LiDAR)	Total	Specific yield (Full mobility, API)
Tonalite	0.17 (1,687)	0.97 (9,417)	0.98 (9,514)	1.95	4.64
	8.7 %	49.7 %	50.3 %		
Micaschist	0.75 (3,710)	3.37 (16,683)	27.85 (137,871)	31.22	10.76
	2.4 %	10.8 %	89.2 %		
Paragneiss and Orthogneiss	0.71 (2,441)	5.71 (19,690)	44.18 (152,345)	49.89	7.04
	1.4 %	11.4 %	88.6 %		
Limestone and Dolostone	0.16 (794)	1.05 (9,292)	0.29 (2,566)	1.34	3.79
	11.9 %	78.3 %	21.6 %		

Table 4 Number of landslides in metamorphic terrain that are topologically related and unrelated to DSGSDs

	#DSGSD-related			#DSGSD-unrelated		
	Full mobility			Full mobility		
Dominant geology	(API)	(LiDAR)	Partial mobility (LiDAR)	(API)	(LiDAR)	Partial mobility (LiDAR)
# LS	388	1,146	327	557	889	58
LS densities (# LS/km^2)	3.12	9.24	2.64	1.51	2.41	0.16
DSGSD acceleration factor	× 2	× 4	× 16	1	1	1

over time and obtain multi-temporal datasets across large study areas. By contrast, airphotos have limitations in terms of landslide identification (e.g., Brardinoni et al. 2003; Turner et al. 2010), but they are relatively affordable, they are available for a number of regions from 1950s onward, and allow to analyse landslide sediment dynamics through time (e.g., Brardinoni et al. 2002; Imaizumi and Sidle 2007; Galli et al. 2008).

Overall, the Val di Sole inventory shows how the two techniques can be integrated in a convenient and efficient way. For example, they can be employed to (1) evaluate long-term (e.g., postglacial) versus contemporary landslide activities; and (2) establish landslide visibility thresholds for aerial photo detection using landslide scars delineated on LiDAR hillshades as true reference.

The classification of landslides into full- and partial-mobility types, even though simplistic, highlights the importance of stratifying inventories according to sedimentary dynamics; and identifies knowledge gaps that currently prevent us from making quantitative statements about colluvial sediment flux in mountain environments.

Lithologic correlations with landslide occurrence display high variability in relation to landslide type. The generalized increase of landslide activity in metamorphic terrain shows acceleration factors ranging between two and three times for full-mobility failures, and between 7 and 14 times for partial-mobility ones. The former typology exhibits a distinctively higher degree of connectivity to the drainage network.

High landslide activity in metamorphic terrain appears, at least in part, to be explained by the spatial distribution of DSGSDs. These large-scale deformations, which occur on metamorphic rocks only, are associated with higher numbers of slow, partial-mobility landslides (16-fold increase). Following this logic, DSGSDs, by weakening the structure of entire valley sides, would trigger further destabilization of the hillslopes, which then tend to fail into smaller portions (via slow, partial-mobility landslides) especially at convex-like topographic locations.

In order to improve our understanding of the factors controlling landslide activity and sediment transfer in Val di Sole, future work will integrate the spatial distribution of

lithology, with that of surficial materials (e.g., till, bedrock, colluvium, and lacustrine), land use/cover, and landslide connectivity to stream channels.

Acknowledgments This work was funded through EU-FP7 Marie Curie Actions IEF (project 221051 – Slidelaws). Paolo Campedel of the Geological Survey of Trento provided critical comments on landslide data and made available to us LiDAR data and the airphoto sets (1973, 1983, 1996, and 2000). Giuseppina Zambotti provided useful logistical information.

References

Ardizzone F, Cardinali M, Galli M, Guzzetti F, Reichenbach P (2007) Identification and mapping of recent rainfall-induced landslides using elevation data collected airborne Lidar. Nat Hazards Ear Syst Sci 7:637–650

Brardinoni F, Hassan MA, Slaymaker O (2002) Complex mass wasting response of drainage basins to forest management in coastal British Columbia. Geomorphology 49:109–124

Brardinoni F, Slaymaker O, Hassan MA (2003) Landslide inventory in a rugged forested watershed: a comparison between remotely sensed and field survey data. Geomorphology 54:179–196

Brardinoni F, Hassan MA, Rollerson T, Maynard D (2009) Colluvial sediment dynamics in mountain drainage basins. Earth Planet Sci Lett 284:310–319

Colesanti C, Wasowski J (2006) Investigating landslides with space-borne Synthetic Aperture Radar (SAR) interferometry. Eng Geol 88:173–199

Cruden DM, Varnes DJ (1996) Landslide types and processes. In: Turner AK, Schuster RL (eds) Landslides, investigation and mitigation, Transportation Research Board Special Report 247. Washington, DC, pp 36–75

Galli M, Ardizzone F, Cardinali M, Guzzetti F, Reichenbach P (2008) Comparison of landslide inventory maps. Geomorphology 94:268–289

Guzzetti F, Ardizzone F, Cardinali M, Rossi M, Valigi D (2009) Landslide volumes and landslide mobilization rates in Umbria, central Italy. Earth Planet Sci Lett 279:222–229

Hovius N, Stark CP, Allen PA (1997) Sediment flux from a mountain belt derived by landslide mapping. Geology 25:231–234

Imaizumi F, Sidle RC (2007) Linkage of sediment supply and transport processes in Miyagawa Dam catchment, Japan. J Geophys Res 112: F03012. doi:10.1029/2006 JF000495

Jarman D, Agliardi F, Crosta GB (2011) Megafans and outsize fans from catastrophic slope failures in Alpine glacial troughs: the Malser Haide and the Val Venosta cluster, Italy. Geol Soc Lond Spec Public 351:253–277

Landolt E (1992) Unsere Alpenflora. Gustav Fischer Verlag, Stuttgart/Jena, 320p

Larsen IJ, Montgomery DR, Korup O (2010) Landslide erosion controlled by hillslope material. Nat Geosci 3:247–251

Martin Y, Rood K, Schwab JW, Church M (2002) Sediment transfer by shallow landsliding in the Queen Charlotte Islands, British Columbia. Can J Ear Sci 39(2):189–205

Passalacqua P, Tarolli P, Foufoula-Georgiou E (2010) Testing space-scale methodologies for automatic geomorphic feature extraction from lidar in a complex mountainous landscape. Water Resour Res 46:W11535. doi:10.1029/2009WR 008812

Reid LM, Dunne T (1996) Rapid evaluation of sediment budgets. GeoEcology Paperback. Catena Verlag, Reiskirchen/Germany, 164p

Sartori G, Mancabelli A, Wolf U, Corradini F (2005) Atlante dei suoli del Parco Naturale Adamello-Brenta. Suoli e Paesaggi. Museo tridentino di Scienze Naturali, Trento, 350 p

Turner TR, Duke SD, Fransen BR, Reiter ML, Kroll AJ, Ward JW, Bach JL, Justice TE, Bilby RE (2010) Landslide densities associated with rainfall, stand age, and topography on forested landscapes, southwestern Washington, USA. For Ecol Manage 259:2233–2247

A Quantitative Assessment of the Sedimentology and Geomorphology of Rock Avalanche Deposits

Dan H. Shugar, John J. Clague, and Marco Giardino

Abstract

We use digital photo-sieving and spatial statistics to quantify the debris of three landslides on Black Rapids Glacier, Alaska, and the non-glacial Frank Slide, Alberta. The debris sheets on Black Rapids Glacier have clusters of large blocks in parts of their distal rims; small clusters of large blocks also occur elsewhere, including the proximal side of a high medial moraine. Longitudinal flowbands formed by shearing within the debris and marked by different block sizes characterize all three Black Rapids debris sheets. In contrast, no flowbands are evident on the Frank Slide debris sheet. Especially large blocks form a conspicuous cluster in the middle of the Frank Slide debris sheet. The distal edge is composed of small blocks. The presence of many of the largest blocks at the peripheries of the three Black Rapids Glacier debris sheets indicates that the landslides spread without confinement. The lack of a coarse distal rim at Frank may indicate that the irregular topography over which the debris traveled influenced the distribution of the largest blocks. Patches of different types of carbonate rock within the Frank Slide debris sheet indicate that source-zone stratigraphy is preserved within the debris sheet. Differences among the studied debris sheets reflect different paths and substrates over which the landslides traveled: unconfined spreading and continuous, progressive thinning of debris traversing a relatively flat surface of snow and ice at Black Rapids Glacier; and topography-controlled spreading over an irregular rising and vegetated surface at Frank.

Keywords

Rock avalanche • Glacier • Sedimentology • Geomatics • Frank Slide • Black Rapids Glacier

Introduction

Many researchers have qualitatively described geomorphic features of rock avalanche deposits, including raised rims, flowbands, and lithologic zonation. Little quantitative work, however, has been done to link debris sheet sedimentology to observed large-scale geormorphic features. A thorough characterization of rock avalanche debris is a necessary step in understanding the flow mechanisms of large landslides. Rock avalanche sedimentology is also important because diamictons, previously thought to be glacial in origin, have been reinterpreted as landslide debris with little or no climatic significance (Porter and Orombelli 1980; Hewitt 1999; Larsen et al. 2005; Shulmeister et al. 2009).

In this paper we describe the sedimentology of four rock avalanche debris sheets and evaluate whether runout over glacier ice affects their characteristics. We studied deposits of three rock avalanches on Black Rapids Glacier, Alaska, and the deposit of the non-glacial Frank Slide, Alberta.

D.H. Shugar (✉) • J.J. Clague
Department of Earth Sciences, Centre for Natural Hazard Research, Simon Fraser University, Burnaby, BC, Canada
e-mail: dshugar@uvic.ca

M. Giardino
Department of Earth Sciences, University of Torino, Torino, Italy

C. Margottini et al. (eds.), *Landslide Science and Practice*, Vol. 4,
DOI 10.1007/978-3-642-31337-0_41,

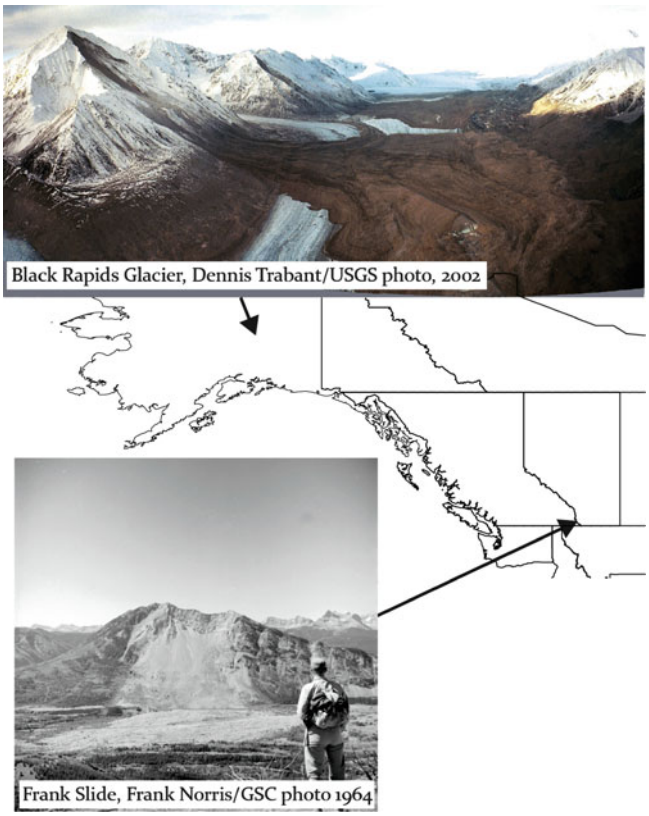

Fig. 1 Locations of Black Rapids Glacier, AK, and Frank Slide, AB, and photographs of the landslide debris sheets

Study Areas

Black Rapids Glacier is a 40-km-long, surge-type glacier in the central Alaska Range of interior Alaska (Fig. 1). It has a mean slope of 2° and an average width of 2.3 km. The 3 November 2002 Denali earthquake (M 7.9) triggered three large rock avalanches that deposited ~25 × 10^6 m^3 of granitic debris over 11 km^2 of the glacier's ablation zone to an average depth of 2–3 m (Shugar and Clague in press). Slabs of rock 30–50 m thick broke along orthogonal joints and rapidly fragmented as they moved down the 35–38° slopes and onto Black Rapids Glacier (Jibson et al. 2004). We refer to the deposits of the three landslides as BRG-west, BRG-middle, and BRG-east.

The Frank Slide is located on the east slope of Turtle Mountain in the Crowsnest Pass region of southwest Alberta (Cruden and Hungr 1986). The landslide occurred on the morning of 29 April 1903 and destroyed part of the mining town of Frank, killing about 70 people; it was Canada's worst landslide disaster. The debris sheet has a volume of ~37 × 10^6 m^3 (Nicoletti and Sorriso-Valvo 1991), an area of ~2.7 km^2 (McConnell and Brock 1904), and an average thickness of 14 m (Cruden and Hungr 1986). It consists mainly of limestone of Paleozoic age (Langenberg et al. 2007).

Methods

We digitally photo-sieved blocks at the surface of the debris sheets on orthorectified aerial photographs. Photo-sieving is a method of grain-size analysis of coarse sediment, in which the outline of each clast is manually traced on photographs (Ibbeken and Schleyer 1986). Shugar and Clague (in press) adapted the method for use with digital images in a GIS. Field surveys were conducted (at Black Rapids Glacier in 2007; at Frank Slide in 2010) to verify the quantitative photogrammetric assessments and to support sedimentological and geomorphological interpretations.

Vertical aerial photographs of the Black Rapids Glacier landslides were flown on 7 September 2004. We produced a 10-m DEM and a 0.25-m orthophoto mosaic from the photographs. For Frank Slide, we used a 0.25-m orthophoto flown in 2002 and provided by the Geological Survey of Canada.

Individual blocks ≥1 m^2 were manually digitized in ArcGIS. More than 194,000 blocks were digitized at Black Rapids Glacier, and more than 69,000 blocks were digitized at Frank Slide. Block lengths (a-axis) and widths (b-axis) were determined using the Bounding Containers ArcGIS toolbox (Patterson 2008). We analysed results using neighborhood analysis, which allows calculation of an output value for each non-overlapping neighborhood. Median (D_{50}) and maximum (a-axis) block sizes and a-axis standard deviation were calculated for 25 × 25 m neighborhoods.

Results

Deposit Geometry and Physical Characteristics

The three Black Rapids Glacier landslides originated on steep, north-facing rock slopes on the south side of the valley occupied by the glacier. The landslides flowed across the glacier, overtopping a medial moraine up to ~25 m high (Table 1). Conspicuous longitudinal stripes, or flowbands (sensu Dufresne and Davies 2009), reveal the flow direction of the landslides (Fig. 2).

BRG-west had the simplest deposit geometry – the debris traveled directly across the glacier and came to rest at its northern margin, 3.4 km from the source. BRG-middle initially traveled directly across the glacier, but on reaching the distal side, changed course and traveled downglacier to the east. The total runout distance is 5.6 km. Flowbands at BRG-east indicate that some of the debris traveled directly across the glacier and then, as at BRG-middle, turned to the east. Much of the debris however, took a more direct route, traveling directly 4.1 km to the northeast.

Table 1 Characteristics of the four rock avalanches

Name	Height (km)	Distance (km)[a]	Length (km)[b]	Width (km)[c]	Deposit thickness (m)	Area (km^2)	H/L	Fahr. (°)	L_e (km)[d]	Dimensionless spreading[e]	Volume (m^3)[f]
BRG-west	0.73	3.4	3.4	1.0	2–3	2.5	0.21	12.1	2.3	1,430/ 300 = 4.8	4.9–7.4
BRG-middle	0.80	3.0	5.6	1.5	2–3	3.9	0.14	8.1	4.4	3,050/ 400 = 7.6	7.7–11.6
BRG-east	0.98	3.6	4.1	1.4	2–3	4.7	0.24	13.4	2.6	3,420/ 400 = 8.6	9.3–14.0
Frank Slide	0.80	3.3	3.3	1.3	14	2.7	0.24	13.6	2.1	2,150/ 700 = 3.1	36.5

[a]Distance measured from the highest point of the head scarp to the highest point of the deposit at the distal edge of the landslide
[b]Total travel distance measured along the centreline of the rock avalanche
[c]Width measured on orthophotos at half the runout distance
[d]Excess travel distance, $L_e = L - H/\tan(32°)$
[e]The quotient of maximum deposit width and initial width. Initial (scar) width measured on Google Earth
[f]Volumetric calculations differ widely between studies. Volume is here calculated as the product of deposit area and average thickness

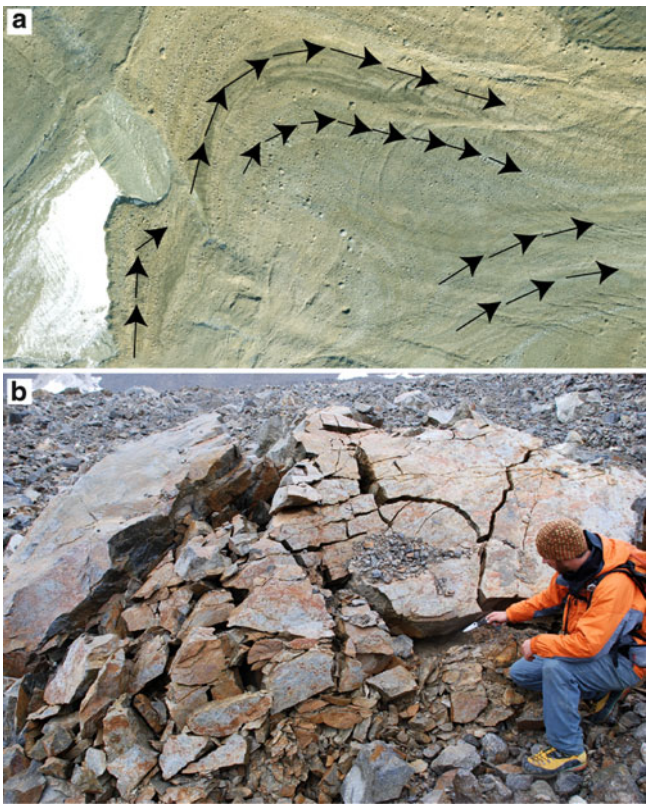

Fig. 2 Photographs of rock avalanche debris on Black Rapids Glacier. (**a**) Aerial photograph of the northwest corner of BRG-middle, showing longitudinal flowbands (*arrows*) turning to the east near the glacier margin. (**b**) Large jigsaw brecciated block on BRG-west. (Modified from Shugar and Clague in press)

The surface debris of the Black Rapids Glacier landslides is composed of coarse angular blocks. So-called "jigsaw" blocks of brecciated, but otherwise intact bedrock are common within the middle of the debris sheets. The coarse carapace of the debris sheet overlies a massive deposit of finer, matrix-supported muddy sandy blocky debris.

The Frank Slide, which became airborne as it crossed the Old Man River, flowed 3.3 km across the floor of the valley, spreading laterally to a maximum width of 2.1 km on a rising topographic slope. The debris sheet covers 2.7 km^2 and has an average thickness of 14 m. Exposures along the railway right-of-way were studied by Cruden and Hungr (1986). The debris sheet lacks the longitudinal stripes that are common at Black Rapids Glacier; instead it has an irregular hummocky surface. The distal part of the debris sheet, termed the "splash zone" by McConnell and Brock (1904), consists mainly of mud and sand with scattered blocks (Cruden and Hungr 1986).

Excess travel distance, defined by Hsü (1975) as the horizontal projection of the travel distance beyond what one expects of a rigid mass sliding down an inclined plane with a normal coefficient of friction ($L_e = L - H/\tan(32°)$), ranges from 2.3 to 4.4 km for the Black Rapids Glacier landslides, and 2.1 km for Frank Slide. The three glacier landslides have fahrböschungs ranging from 8.1° to 13.4°, whereas the Frank Slide fahrböschung is 13.6°. Dimensionless spreading indices (maximum slide width divided by initial width) for the Black Rapids Glacier landslides range from 4.8 to 8.6; the index for Frank Slide is only 2.1 (Table 1).

Block Patterns

Block-size patterns of the four landslide debris sheets, although not identical, have some similarities (Figs. 3, 4, and 5). All three Black Rapids debris sheets have clusters of large blocks in their distal rims, although clusters of large blocks also exist elsewhere. Many 25 × 25 m neighborhoods in the distal rim of BRG-west have blocks ranging from 7 to 16 m in length (Fig. 3b). However, the largest block on BRG-west, which is 26 m long, is located near the middle of the debris sheet. And most of the >20 m-long blocks are found near the middle of BRG-middle.

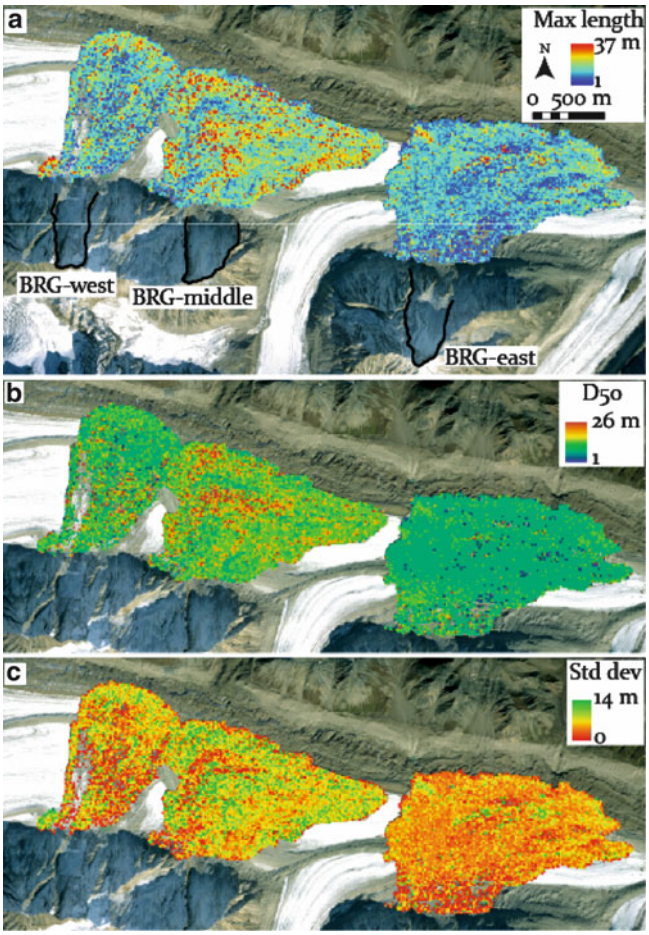

Fig. 3 Maps of (**a**) maximum block size, (**b**) median block size, and (**c**) standard deviation of block length per 25 × 25 m neighbourhood for the Black Rapids landslides

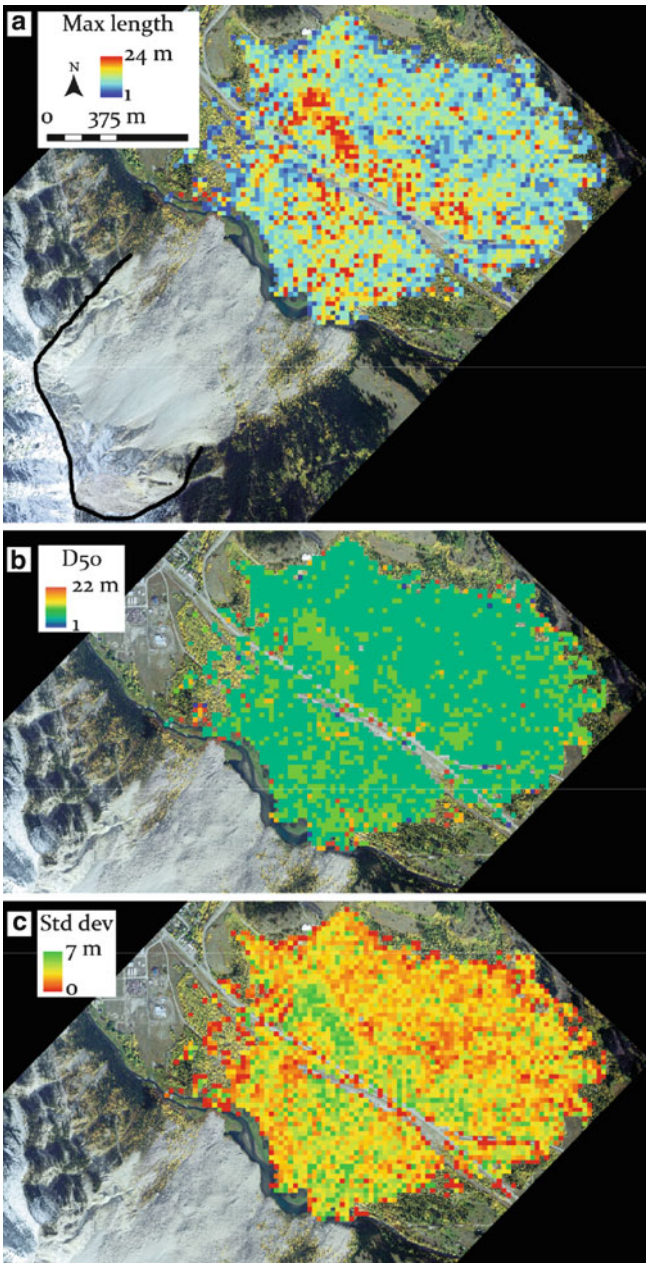

Fig. 4 Maps of (**a**) maximum block size, (**b**) median block size, and (**c**) standard deviation of block length per 25 × 25 m neighbourhood for the Frank Slide

Most neighborhoods on BRG-west have maximum block sizes <5 m long. The neighborhood median block size ranges from 2 to about 9 m. The area of relatively high D50 in the proximal, southeast corner of the debris sheet has relatively low block density compared with other areas. Thus, the high median values here should be viewed with caution.

Large blocks similarly characterize the distal parts of the BRG-east debris sheet, although most are smaller than at BRG-west – mainly 4–6 m long, with some up to 10 m in length. The largest block at BRG-east is 23 m long and is located within a train of very large blocks (>12 m) in the distal half of the debris sheet. Elsewhere, maximum neighborhood block length is typically ~4 m. Median block size on BRG-east is consistent across the debris sheet; most neighborhoods have a D50 of ~2 m.

The typical maximum neighborhood block size on BRG-middle is larger than at either BRG-west or BRG-east (e.g. Fig. 5). Blocks 6–10 m in length cover much of the debris sheet. Narrow flowbands of finer debris separate areas of large blocks, and longitudinal stripes of very large blocks (>10 m) exist locally. The largest block (37 m) is located in the distal, northwest corner where much debris stalled as the landslide decelerated and changed direction.

Maps of neighborhood median and maximum block length at Frank Slide are shown in Fig. 4. The proximal region of the debris sheet, south of Highway 3, is characterized by neighborhood maximum block sizes ranging from 4 to 10 m, with isolated larger blocks. A large cluster of very large blocks, >10 m in length, occurs in the

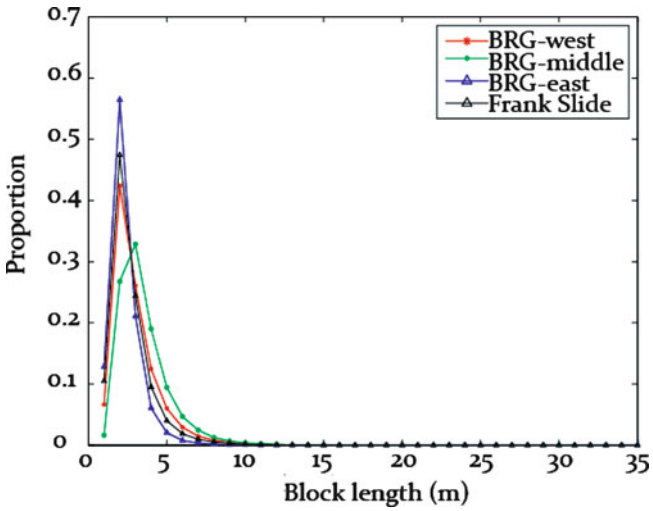

Fig. 5 Block size distribution for the four debris sheets

middle of the debris sheet and is bisected by Highway 3 and the railway; the largest block (24 m long) is located here. The distal parts of the debris sheet are composed almost entirely of smaller blocks, generally <5 m. The map of 25 × 25 m neighborhood median size (Fig. 4b) shows little difference in d50 values over much of the debris sheet; the typical value is ~2 m.

The Frank Slide debris sheet is also characterized by lithological differences. South of the highway, most surface blocks are massive to fractured fine- to coarse-grained limestone ranging from grey to black in color. Dissolution features along fractures on these blocks are especially common on smaller blocks located in topographic lows. Within the cluster of large blocks along the highway, blocks are mainly massive, light-gray crystalline limestone, with distinctive striped faces. Coarse-grained fossiliferous limestone blocks are also common. Decreasing block size and darker limestones characterize a transition zone towards the distal parts of the debris sheet. Elongated patches of chert-banded limestone blocks are present along the western edge of the debris sheet.

Discussion

The Frank Slide and BRG-west debris sheets are similar in morphology, although Frank Slide debris sheet is much thicker than the BRG debris (ca. 14 vs. 2 m). The Frank Slide debris sheet also has a smaller spreading index (Table 1), which suggests lower mobility.

The surfaces of the landslide debris sheets on Black Rapids Glacier are characterized by conspicuous flowbands, which Dufresne and Davies (2009) argue are fundamental characteristics of granular flows on glaciers. Similar features on other glaciers separate bands of different lithologies (e.g. Shreve 1968). At Black Rapids Glacier, the flowbands record differences in grain size rather than lithology. The flowbands on BRG-middle and BRG-east match differences in block size (e.g. compare Figs. 2a and 3a).

No flowbands are evident at Frank Slide, and there is not a distal rim of large blocks, as at Black Rapids. McConnell and Brock (1904) reported a prominent distal rim, 2–9 m high at Frank Slide, but Cruden and Hungr (1986) found only three sites where large blocks are exposed at the perimeter. More commonly, they observed a digitate scarp, bordered by a 100-m-wide hummocky deposit of fine sediments and scattered blocks ("splash" area of McConnell and Brock 1904). Similarly, our analysis does not reveal a cluster of particularly large blocks at the periphery of the Frank Slide. The rim described by McConnell and Brock (1904) is composed, not of unusually large blocks, but of a large number of average- or even smaller-than-average blocks bulldozed into tall piles by the advancing rock avalanche.

The cluster of large blocks near the centre of the Frank Slide debris sheet is puzzling in the context of many other rock avalanches that have concentrations of large blocks near their margins (e.g. Locat et al. 2006; Hewitt 1999; Porter and Orombelli 1980). One possible explanation is that debris at the front of a rock avalanche flowing over glacier ice fragments more slowly than debris traveling over vegetated terrain, such as at Frank. It is also possible that the irregular topography over which the Frank Slide traveled influenced the distribution of the larger blocks. The debris at Frank climbed 100 m over a distance of 1.5 km east of Oldman River; in contrast the Black Rapids Glacier landslides traveled over nearly flat surfaces. Interestingly, at both Black Rapids Glacier and Frank, areas of especially large blocks are also characterized by large standard deviations (Figs. 3c and 4c), implying that large blocks are mixed with much smaller blocks.

Conclusions

We use digital photo-sieving to quantify the block size distribution and map large-scale geomorphic features in the debris sheets of four historic rock avalanches. Clusters of large blocks occur within all four debris sheets, although those at Black Rapids Glacier are most common in rims near the margins of the debris. Longitudinal flowbands in the Black Rapids Glacier debris sheets mark differences in block size and are the result of differential shear with the streaming debris. In contrast, the largest blocks in the Frank Slide debris occur in a cluster in the middle of the debris sheet; no distal rim or flowbands are present. Differences in block-size patterns among the four debris sheets are likely due to differences in the surfaces over which the rock avalanches traveled. The lack of a coarse distal rim at Frank may indicate that

the irregular topography over which the debris traveled influenced the distribution of the largest blocks. Patches of different types of carbonate rock within the Frank Slide debris sheet suggest that source-zone stratigraphy is preserved within the debris sheet.

Acknowledgments This work was funded through an NSERC Discovery Grant to Clague and an NSERC-PGS doctoral scholarship, a GSA Bruce 'Biff' Reed research grant, Northern Scientific Training Program grants and an Arctic Institute of North America Grant-in-Aid to Shugar. Giardino was supported by ICCS-FEP 2009. EACEA and HRSDC provided funds through the EU-Canada cooperation project "geoNatHaz", whose participants are acknowledged for assistance in the field in 2010. We thank Steve Sparks (Aero-Metric, Fairbanks, Alaska) for providing aerial photographs of Black Rapids Glacier, and the Geological Survey of Canada for providing the orthophotograph of Frank Slide. Mark Hird-Rutter helped in producing the digital elevation model of Black Rapids Glacier. Jon Pasher (Environment Canada, Ottawa, Canada) and Dan Patterson (Carleton University, Ottawa, Canada) provided assistance with digital photo-sieving.

References

Cruden DM, Hungr O (1986) The debris of the Frank Slide and theories of rockslide-avalanche mobility. Can J Earth Sci 23(3):425–432

Dufresne A, Davies TR (2009) Longitudinal ridges in mass movement deposits. Geomorphology 105(3–4):171–181

Hewitt K (1999) Quaternary moraines vs catastrophic rock avalanches in the Karakoram Himalaya, Northern Pakistan. Quaternary Res 51(3):220–237

Hsü KJ (1975) Catastrophic debris streams (sturzstroms) generated by rockfalls. Geol Soc of Am Bull 86(1):129–140

Ibbeken H, Schleyer R (1986) Photo-sieving – a method for grain-size analysis of coarse-grained, unconsolidated bedding surfaces. Earth Surf Proc Land 11(1):59–77

Jibson RW, Harp EL, Schulz W, Keefer DK (2004) Landslides triggered by the 2002 Denali fault, Alaska, earthquake and the inferred nature of the strong shaking. Earthquake Spectra 20(3):669–691

Langenberg CW, Pana D, Richards BC, Spratt DA, Lamb MA (2007) Structural geology of the Turtle mountain area near Frank, Alberta. Alberta Energy Resources Conservation Board/Alberta Geological Survey, Earth Sciences Report 2007–03. Edmonton

Larsen SH, Davies TRH, McSaveney MJ (2005) A possible coseismic landslide origin of late Holocene moraines of the Southern Alps, New Zealand. New Zeal J Geol Geophys 48(2):311–314

Locat P, Couture R, Leroueil S, Locat J, Jaboyedoff M (2006) Fragmentation energy in rock avalanches. Can Geotech J 43(8):830–851

McConnell RG, Brock RW (1904) Report on the great landslide at Frank, Alta. 1903. Annual report. Part VIII. Department of the Interior Dominion of Canada, Ottawa

Nicoletti PG, Sorriso-Valvo M (1991) Geomorphic controls of the shape and mobility of rock avalanches. Geol Soc Am Bull 103 (10):1365–1373

Patterson DE (2008) Bounding containers ArcGIS toolbox. http://resources.arcgis.com/gallery/file/geoprocessing/details?entryID=3D230972-1422-2418-34A5-2F3FFF97C238. Accessed 1 Oct 2008

Porter SC, Orombelli G (1980) Catastrophic rockfall of September 12, 1717 on the Italian flank of the Mont Blanc massif. Z Geomorphol 24:200–218

Shreve RL (1968) Sherman landslide. In: The great Alaska earthquake of 1964 – hydrology, Pt. A. National Academy of Sciences, Washington, DC, pp 395–401

Shugar DH, Clague JJ (in press) The sedimentology and geomorphology of rock avalanche deposits on glaciers. Sedimentology. doi:10.1111/j.1365-3091.2011.01238.x

Shulmeister J, Davies TR, Evans DJA, Hyatt OM, Tovar DS (2009) Catastrophic landslides, glacier behaviour and moraine formation – a view from an active plate margin. Quaternary Sci Rev 28(11–12):1085–1096

Part VI

Advances in the Understanding of Cold Region Landslides

Introduction by Marten Geertsema[1], Marta Chiarle[2,3], and Wei Shan[4]

1) Ministry of Forests, Lands, and Natural Resource Operations, Prince George, Canada
2) University of Northern British Columbia, Prince George, Canada
3) CNR-IRPI Italian National Council of Research, Institute for Research for Hydrogeological Protection, Torino, Italy
4) Northeast Forestry University, Harbin, China

Introduction

Session 26, on landslides in cold regions, brought together scientists from around the world with representatives from Canada, China, France, Italy, New Zealand, Pakistan, Switzerland, and Russia. Presentations could be grouped into broad categories. The overarching keynote address by Stephan Gruber (Zurich) stressed the importance of understanding permafrost dynamics in the context of a changing climate as a key to landslide hazard assessments in cold regions. Stephan stressed concepts such as heterogeneity, non-linear trajectories of change, and unexpected results with respect to mountain permafrost, and that these conspire to make hazard analysis difficult.

Chinese, Swiss Italian and Russian papers discussed aspects of landslides in cold **soil**, whereas the remaining papers discussed aspects cryospheric landslides (mainly) in **rock**. A subset of these last papers dealt with rock instabilities on the Mont Blanc massif.

Landslides in Cold Soils

Five papers discussed landslides in cold soils.

Two papers from northeastern China, presented by Wei Shan and Ying Guo highlighted the role of seasonal movements of wet thawed soil at the upper boundary of frozen ice rich layers.

Oxana Masyagina (Russia) described Siberian thaw flows from an ecosystem recovery perspective. She concluded that full ecosystem recovery (soil respiration) takes decades in Siberian forests in the permafrost zone.

Vanessa Wirz (Switzerland) presented a paper on a methodology for measuring (and preliminary results) high elevation debris movements in the Swiss Alps. Using GPS devices, she and colleagues measured daily movements of rock glaciers and other undifferentiated debris deposits in the permafrost zone. The daily readings, combined with temperature, snow cover and precipitation data, help tease out what drives the movement of these deposits.

Maria Christina Rulli (Milano) presented a snowmelt landslide initiation model which she and colleagues applied to the mountainous Basilicata region of Italy. The model incorporates snowmelt, precipitation and soil water fluxes with stability equations. The model, GALLIUS, shows promise in its predictive capabilities.

Cryospheric Landslides in Rock

A number of presenters discussed high elevation rock slope failures. Philip Deline (France) presented on the December 2008Crammont rock avalanche in the Mont Blanc Massif (Italy). He and colleagues suggested that seepage water in the detachment zone, modelled warm permafrost, and the fact that no other Holocene rock avalanche had occurred, pointed to a permafrost degradation trigger. Ludovic Ravanel and Philip Deline presented additional Mont Blanc rock slide data pointing to permafrost degradation. While they acknowledged that glacial conditioning, such as debuttressing plays a role in rockwall instability, the presence of massive ice, modelled permafrost, and 98 % of rock fall during the warmest periods, points strongly to a permafrost degradation driver.

In separate studies, Marco Giardino (Italy) and Michèle Curtaz (Italy) used integrative approaches to assess rock instability. Marco and colleagues used structural geological and geomorphological map data, with a LiDAR DEM, orthophotos, a mobile GPS unit and Coltop3D software to characterize slopes in the Mont Blanc massif. Curtaz and colleagues combined photogrammetric surveys and geostructural surveys to investigate strength properties due to permafrost changes. Both studies linked rock instability to permafrost degradation.

Christian Huggel (Switzerland) presented a conceptual model for five different approaches to detect climate change derived rock instability, cautioning that detection of changes is fraught with difficulties. These included (1) event inventories, (2) damage and loss data, (3) case studies, (4) causative and trigger factors, and (5) process models.

While most landslides in cold regions can be linked glacial conditioning, not all can be linked to permafrost degradation. In the case of Ken Hewitt's (Canada) studies of massive rock slides in the Karakoram, Pakistan, the antiquity of the landslides renders causation elusive. Mauri McSaveney's and Chris Massey's (New Zealand) account of New Zealand's 2007 Young River rock slide rules out a permafrost trigger. Rather they suggest that a strong diurnal temperature variation, allowing melting and freezing of the rock face, played a strong role. Trapped water and elevated pore pressures combined with a progressive weakening rock mass led to failure.

Landsides in Cold Regions: Making a Science that can be put into Practice

Stephan Gruber

Abstract

The assessment of landslide hazard in cold regions (i.e. influenced by snow, glaciers, permafrost) is faced with a twofold challenge: The magnitude of climate change is expected to be greater here that in many other regions, enabling strong shifts in e.g., the probabilities of triggering events such as intense precipitation or snow melt. Additionally, rapid changes such as permafrost degradation, warming firn areas or vanishing glaciers can fundamentally alter system behaviour and thus strongly change its response to a given forcing. As a consequence, the known difficulties of understanding low-frequency high-magnitude events such as landslides are intensified by continued and nonlinear change. Using concrete example from permafrost research, I will discuss general strategies to nevertheless arrive at conclusions that may be of practical relevance. This presentation, of course, heavily draws from the work of collaborators.

Keywords

Landslide • Permafrost • Glacier • Climate

Introduction

What is special about cold regions landslides? An answer can be nicely structured by following the review of Varnes (1984), who summarized knowledge and common practice in a pre-climate-change setting. Based on the time scale of their changes, he distinguished two groups of causative conditions and processes: "Inherent or basic conditions" and "Factors producing unfavourable changes in conditions". The latter can be used to structure cryosphere-moderated climate impacts into its two categories. Changes to the stress conditions prominently include the de-buttressing by glacier melt. Changes in the strength of materials include the effect that the warming and thaw of permafrost can have on material properties and the effect of diminishing glacier cover and ground ice on recharge and routing of sub-surface water. While glacial de-buttressing is comparably straightforward to observe and understand, the effects of changes to sub-surface ice and water movement are extremely difficult to detect or quantify. This is because they occur at depth and because of the highly nonlinear nature of the involved phase-change processes. At the same time, their effect can be large enough to locally become a dominating control of stability. In dealing with landslides in cold regions under sustained climate change, we are thus faced with a system that is extended by one important and, unfortunately, very dynamic unknown.

To reduce human or economic losses, it is important to investigate this new unknown in order to better constrain the location and timing of future landslides and to provide means to put this into practice. While differing definitions could be conceived, for this contribution I define research as "put into practice" if it has transformed the way in which people deal with, or understand and perceive natural hazards. In this context, it is rather obvious that there is a need to improve our understanding of (a) the mechanisms that link climate and slope stability via cryosphere systems;

S. Gruber (✉)
Department of Geography, University of Zurich, Winterthurerstrasse 190, Zurich 8057, Switzerland
e-mail: stephan.gruber@geo.uzh.ch

C. Margottini et al. (eds.), *Landslide Science and Practice*, Vol. 4,
DOI 10.1007/978-3-642-31337-0_42,

(b) the current spatial patterns of relevant cryosphere phenomena; and (c) the changes that those phenomena undergo. What is less obvious, and certainly debatable, is where we can have the greatest practical impact with the research we perform. With this paper I aim to contribute to this debate using examples from my own research that is largely concerned with mountain permafrost.

Heterogeneity and Trajectories of Change

Permafrost is a good example showing how heterogeneity in both space and temporal behaviour conspire to fundamentally challenge our ability to estimate future environmental states.

The current conditions and spatial patterns of permafrost systems are strongly governed by heterogeneity. Sub-surface properties however, are not easily observable and in combination, this drastically limits our ability to characterize relevant present properties of landscapes. These unknown properties include temperature and ice content of the sub-surface as well as other material characteristics. Because they span diverse scales (e.g., small ice-filled clefts or topography-induced shading of slopes) some of those properties can be described well with current data and methods while others likely will remain elusive.

Due to the nonlinear nature of cryosphere phenomena, (even small) differences in conditions and properties can cause drastic differences in the response trajectories (i.e. the temporal changes of response variables, Fig. 1). Differing ice content, for example, can subdue the temperature change experienced by one slope for extended periods but increase its change in mechanical strength. Differing surface characteristics may render one slope more sensitive to changes in winter temperatures and the other more to summer temperatures.

The determination of present permafrost conditions is thus subject to large uncertainty, and for the estimation of future conditions (of permafrost or related slope stability) unknown material characteristics further amplify this effect by non-uniform change.

Hazard Zonation

Varnes (1984) names three principles of landslide hazard zonation, all of which are challenged in permafrost environments: (1) "The past and present are keys to the future." This common paradigm of geologic sciences is complicated by the object of interest being a transient and nonlinear system that is likely to soon evolve beyond historic and Holocene precedence. Furthermore, the remoteness of most cold regions limits observations and the clandestine and heterogeneous nature of permafrost systems always

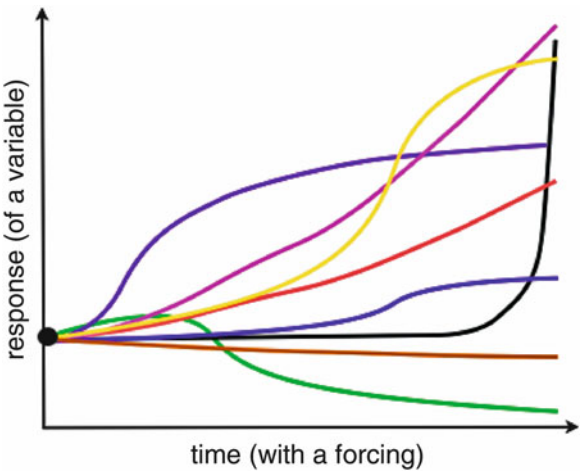

Fig. 1 Schematic of differing trajectories of change: depending on initial conditions as well as near- and sub-surface properties, the responses of neighbouring slopes to the same climate forcing may differ strongly

complicates their analysis. In many instances, we thus hardly have that key to the future. (2) "The main conditions that cause landsliding can be identified." In contrast to the general statements made, the basic causes of slope instability related to climate-change effects on permafrost are largely unknown and case-studies of specific failures are rare and limited not the least by the uncertainty of determining their permafrost conditions. As a consequence of the poor knowledge of causes and the uncertainty in characterising spatial patterns and conditions of permafrost, in a given area it is difficult to recognize relevant conditions or to rate or weigh their effects. (3) "Degree of hazard can be estimated." This is based on the concept that if conditions and processes that promote instability can be identified, it is often possible to derive a summary of the degree of potential hazard in an area. While I have argued above that precisely this is very difficult, there is nevertheless a promising avenue to make a contribution, here.

A number of studies (e.g., Harris et al. 2009; Gruber and Haeberli 2007; Geertsema et al. 2006) point to the possible role of permafrost and its degradation in the conditioning or release of landslides. While studies to understand the location, timing and possible processes of landslides from permafrost exist, for the reasons outlined in the previous section, this is in many regions or circumstances not at a level that can be translated into hazard zonation practice. For most practitioners, current knowledge can simply be summarized as "areas that are subject to permafrost conditions have an elevated potential for surprise and require (continued) extra attention in hazard assessment". Surprise here may refer to landslides originating from unexpected locations, during unexpected times, or having mechanisms that are surprising. Because permafrost is usually invisible at the land surface and in many places heterogeneous, the provision of permafrost maps is the basic step in extending

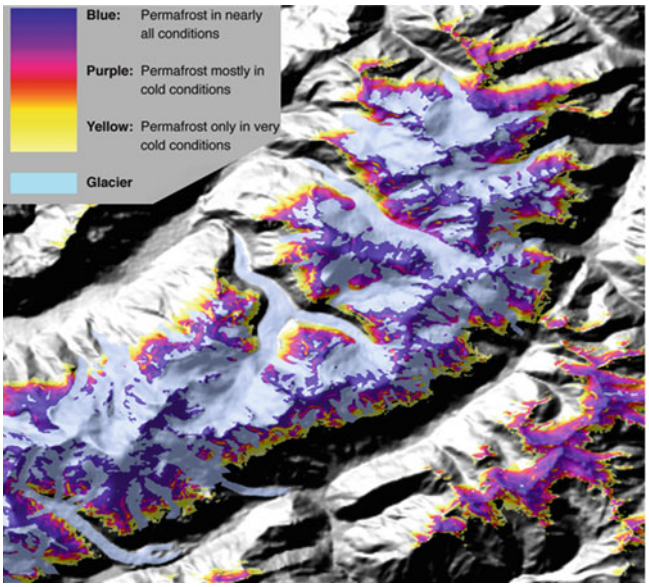

Fig. 2 Sample of the Alpine Permafrost Map in the Mont-Blanc massif near Chamonix, France. The map shown is 25 km wide

hazard zonation with a permafrost-related element. It allows the zonation into areas that likely do and that likely do not require special attention. This also is a simple message that can be communicated alongside the dissemination of maps.

A high-resolution example is the recent pan-Alpine permafrost map of which a sample is shown in Fig. 2. Based on a homogenized inventory of permafrost evidence (Cremonese et al. 2011), a statistical model (Boeckli et al. 2012) and a set of assumptions that is currently being published, a consistent map of about 30 m resolution has been derived. This map that has been developed in collaboration with public authorities from several Alpine countries is accompanied by a legend and interpretation guide. At a coarser scale and with a grid-resolution of about 1 km (Fig. 3), a global model and map of permafrost zonation (Gruber 2012) now provides the level of detail necessary for investigating permafrost in remote mountain regions. Both maps are available as overlays for Google Earth: http://www.geo.uzh.ch/microsite/cryodata/.

While these maps are not a zonation with respect to permafrost-related hazard (but often misinterpreted in this way), they do provide important information for practitioners dealing with climate change effects: A division of the land surface according to the potential for permafrost-related phenomena and corresponding potential for surprise. And, they are an intuitive tool to communicate, to the public as well as to relevant authorities, the importance and approximate spatial pattern of a phenomenon that usually is invisible.

For several other phenomena, a similar mapping of conditions that are prone to change or of the changes themselves, but without actual hazard mapping may be a promising step into practice. Examples include glacier inventories (Paul et al. 2007), elevation change of glaciers (Paul and Haeberli 2008) that qualitatively relates to de-buttressing, and the estimation of newly-forming lakes (Frey et al. 2010).

The value of a spatial model or a map is greatest in the areas with least prior information, whereas for scientists, it is attractive to model in areas where ample data exists. For marginalized populations in remote regions, this is further aggravated by the fact that a large proportion of measurements, research and publications only exist because of their connection to economic development of limited spatial scope. Given the ever-increasing amount of (freely available) spatial data, I am convinced that by extending and applying knowledge to remote regions, we can put some of our science into practice very effectively, even if it is at a low level of detail and coarse scale.

Unexpected Phenomena

Examples of exceptional phenomena of movement are diverse and include accelerating rock glaciers (e.g., Roer et al. 2008), the detachment of rock fall from ice-filled clefts (e.g., Ravanel et al. 2010), rock/ice avalanches from cold conditions or extremely large and far-reaching events (e.g., Haeberli et al. 2004). Although the event dimensions are modest, Fig. 4 illustrates well the concept of unexpected events. It is the recognition of these as potential new kinds of events that is important.

While some of the effects caused by transient cryosphere systems will conform to previous knowledge and expectations, we also have to expect types of events and landslides that have not or only rarely been observed and described before. Because these may well gain practical relevance in the future, their fast recognition and scientific scrutiny is important. This can best be achieved if traditional landslide experts and cryosphere researchers work together. While in the majority of corresponding landslide case-studies, the precise role of permafrost and other cryosphere phenomena cannot be determined with certainty, one can hardly afford to wait for this certainty if we aim at putting into practice the insight we gain. The stage of investigating possible mechanisms of observed unusual events is already a great step forward because it helps to reflect our current understanding. It would be naïve to assume that what we characterize as a complex and non-linear system that is about to leave the ranges of documented boundary would behave as we predict.

New Technology in Research and Practice

Preferred and accepted methods for investigating individual landslides, for hazard zonation or warning have been established over decades, but sometimes, these may not be ideal in cold regions.

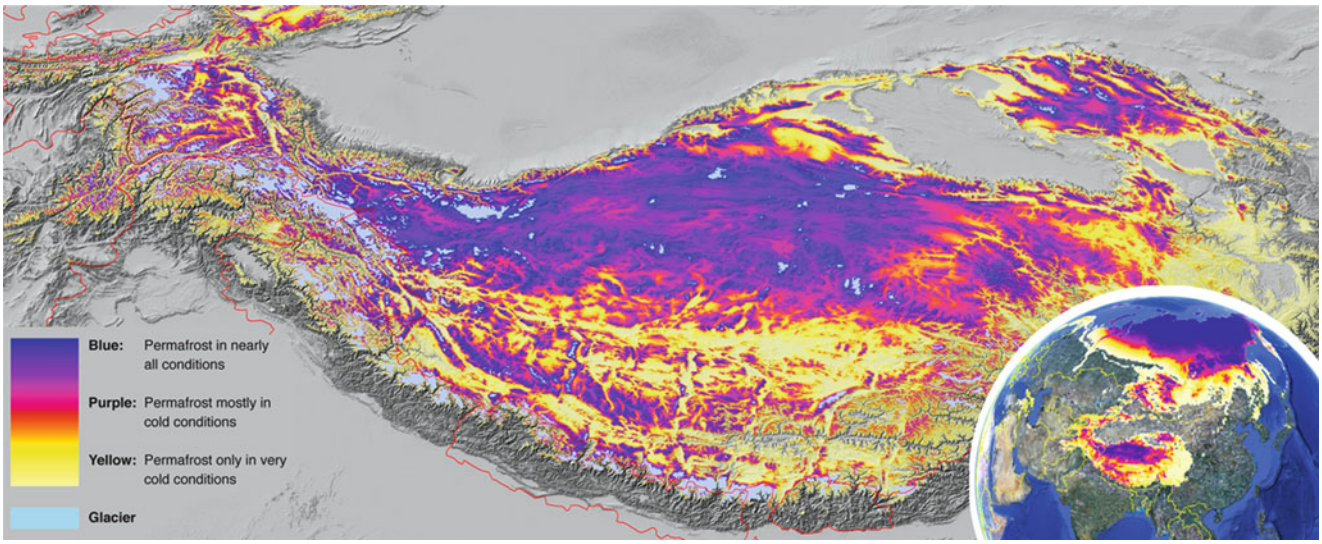

Fig. 3 Sample of the 30 arc-second (~1 km) global permafrost zonation map. It is obvious that large populations in Asian mountain ranges live in proximity to or in permafrost areas

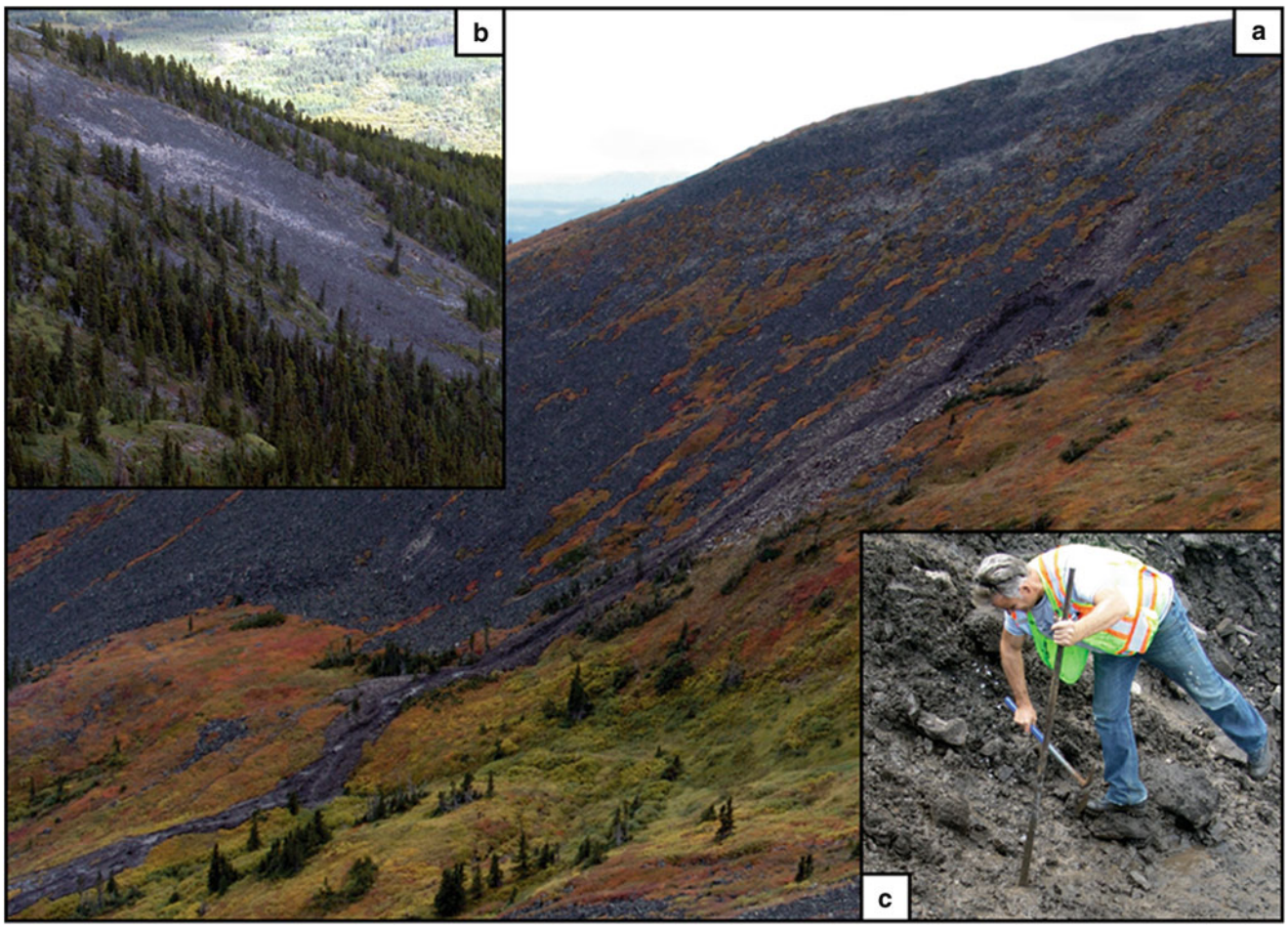

Fig. 4 The possibility for new and unexpected phenomena is illustrated well by this landslide from a block slope on Pink Mountain (122.86°W/57.05°N), British Columbia, Canada, that happened shortly before 4 September 2008. The overview (**a**) shows a slope with a coarse block surface. Dark lichen cover and spreading vegetation indicate a long period of stability. Following heavy rainfall a landslide detached on a planar surface that upon inspection (**c**) revealed high content of ice and fine material. A second surprising phenomenon, the recent development

This may be because environmental conditions are more severe or because unusual phenomena call for alterations of established protocol and equipment as well as for investigations with a strongly explorative character.

Here, the collaboration with various engineering and geosciences disciplines can constitute a key advantage for research projects through individual customization of measurement systems and, more importantly, by making available and developing technology that would otherwise not, or not yet, be accessible commercially. Besides benefits for research projects or enabling more relevant insight into natural processes, this type of collaboration may help to put into practice also technology more effectively and to develop surveillance and warning systems that incorporate recent technology.

Two examples from the PermaSense consortium of projects (www.permasense.ch) illustrate this: For steep bedrock permafrost, the work of Hasler (2011) demonstrates the potential of spatially-distributed measurements of both cleft dilatation and rock/cleft temperature to better understand modes of rock movement and their environmental controls. For debris slopes, Wirz et al. (2011) aim to better understand cryosphere control on slope movement based on spatially-distributed continuous GPS measurement.

Concluding Remarks

With this contribution I hope to provide food for thought in the debate whether or not landslides in cold regions are special and how we can best put our research into practice. The arguments and examples presented strongly reflect my own background – I am a cryosphere researcher, not a landslide specialist – and projects. I would certainly be happy if this helped to spark increased debate and contact between the many differing scientific communities involved in landslide and cryosphere research.

Acknowledgments The work presented in this keynote draws heavily on the work of colleagues and collaborators. It has been decisively supported by the SNF NCCR-MICS project PERMASENSE, the nanotera.ch supported project X-SENSE, the SNF project CRYOSUB, the EU-Alpine-Space project PERMANET, the Swiss Federal Office for the Environment as well as the International Foundation High Altitude Research Stations Jungfraujoch and Gornergrat. Marten Geertsema has enabled and led the field campaign on which the Pink Mountain slide was documented.

References

Boeckli L, Brenning A, Gruber S, Noetzli J (2012) Permafrost distribution in the European Alps: calculation and evaluation of an index map and summary statistics. The Cryosphere 6:807–820

Cremonese E, Gruber S, Phillips M, Pogliotti P, Boeckli L, Noetzli J, Suter C, Bodin X, Crepaz A, Kellerer-Pirklbauer A, Lang K, Letey S, Mair V, Morra di Cella U, Ravanel L, Scapozza C, Seppi R, Zischg A (2011) Brief communication: an inventory of permafrost evidence for the European Alps. The Cryosphere 5:651–657

Frey H, Haeberli W, Linsbauer A, Huggel C, Paul F (2010) A multi-level strategy for anticipating future glacier lake formation and associated hazard potentials. Nat Hazards Earth Syst Sci 10:339–352

Geertsema M, Clague JJ, Schwab JB, Evans SG (2006) An overview of recent large catastrophic landslides in northern British Columbia, Canada. Eng Geol 83:120–143

Gruber S (2012) Derivation and analysis of a high-resolution estimate of global permafrost zonation. The Cryosphere 6:221–233

Gruber S, Haeberli W (2007) Permafrost in steep bedrock slopes and its temperature-related destabilization following climate change. J Geophys Res 112:F02S18

Haeberli W, Huggel C, Kääb A, Zgraggen-Oswald S, Polkvoj A, Galushkin I, Zotikov I, Osokin N (2004) The Kolka-Karmadon rock/ice slide of 20 September 2002: an extraordinary event of historical dimensions in North Ossetia, Russian Caucasus. J Glaciol 50:533–546

Harris C, Arenson LU, Christiansen HH, Etzelmüller B, Frauenfelder R, Gruber S, Haeberli W, Hauck C, Hölzle M, Humlum O et al (2009) Permafrost and climate in Europe: monitoring and modelling thermal, geomorphological and geotechnical responses. Earth Sci Rev 92:117–171

Hasler A (2011) Thermal conditions and kinematics of steep bedrock permafrost. Ph.D. thesis, University of Zurich, Switzerland

Paul F, Haeberli W (2008) Spatial variability of glacier elevation changes in the Swiss Alps obtained from two digital elevation models. Geophys Res Lett 35:10–1029

Paul F, Kaab A, Haeberli W (2007) Recent glacier changes in the Alps observed by satellite: consequences for future monitoring strategies. Glob Planet Change 56:111–122

Ravanel L, Allignol F, Deline P, Gruber S, Ravello M (2010) Rock falls in the Mont Blanc Massif in 2007 and 2008. Landslides 7(4): 493–501

Roer I, Haeberli W, Avian M, Kaufmann V, Delaloye R, Lambiel C, Kääb A (2008) Observations and considerations on destabilizing active rock glaciers in the European Alps. In: Ninth international conference on permafrost, Fairbanks, Alaska, pp 1505–1510

Varnes DJ (1984) Landslide hazard zonation: a review of principles and practice. UNESCO, Paris

Wirz V, Limpach P, Buchli B, Beutel J, Gruber S (2011) Temporal characteristics of different cryosphere-related slope movements in high mountains. In: Proceedings of the second world landslide forum, Rome

Fig. 4 (Continued) of slow movement can be inferred. Near the top of slope in (**a**), bright across-slope stripes as well as small, double-ridge-like features are visible and here interpreted as signs of down-slope extension. The bright stripes made up of blocks overturned to their lichen-free and un-weathered side are interpreted as a sign of recent onset of the responsible movement after a long and stable period. The bulge at the foot of slope below inset (**b**) provides additional evidence for movement. Similar bright stripes have also been visible on a neighbouring slope (**b**) and have been reported and investigated elsewhere (M Geertsema, personal communication of 23 February 2009)

Large, Topography-Constrained Rockslide Complexes in the Karakoram Himalaya, Northern Pakistan

Kenneth Hewitt

Abstract

The paper looks at six catastrophic rockslides in the upper Indus Basin with original volumes between 5 and 45 km^3. They have distinctive morphologies and composition related to run out constrained and blocked by rugged terrain. All include long run-out debris lobes, but most of their mass remained as deep-seated, rotational or compound movements with relatively limited and stalled run-out. Their mobility as measured by 'equivalent angles of friction' lies well below that typical for their volumes; essentially an effect of topographic blocking. Even so, the landslide material consists almost entirely of highly fragmented and comminuted bedrock. Stratigraphic relations of the original bedrock are preserved, however. Such intense crushing and pulverizing in minutes or less, of intact bedrock hundreds of meters thick is pertinent to debates of the mechanisms of rock fragmentation. These are landslide 'complexes' in having two or more interrelated units and events at each site, and two or more types of mass movement. The deep-seated nature of failure in the main events suggest earthquake triggering, possibly rare, Himalayan mega-quakes. All sites were deeply undercut during major Pleistocene glaciation(s) and/or by stream incision, suggesting a paraglacial connection. Post-glacial climate change may have affected pre-conditions for failure. These are also topography-changing events. Detachment zones show significant reductions and displacements of interfluves. In run out zones, landslide deposits caused extended valley floor and valley-junction disturbances, stream realignment and drainage fragmentation.

Keywords

Mega landslide • Karakoram Himalaya • Topographical-constrained rockslide • Runout

Introduction

Some 380 massive rock slope failures (MRSF) with long run out of debris, have been identified in the trans-Himalayan upper Indus Basin (Hewitt 2006, 2009a). They belong to a landslide type sometimes called *rockslide-rock avalanches* implying two main phases of movement; an initial sliding or collapse of the failed mass from the detachment zone, changing to flow-like movement of crushed and pulverized rock; a *rock avalanche* or *sturzstrom* (Hewitt 2002).

This paper looks at a small sub-set having original volumes over 1 km^3 called *megaslides*: in fact, six of between 5 and 50 km^3 and some of the largest yet found in the upper Indus Basin (Fig. 1.). The discussion highlights their distinctive composition, morphologies, and post-emplacement histories. Four of the events occurred in diverse rocks of the Kohistan-Ladakh Batholith (Searle 1991), and two in the Karakoram Metamorphic Complex. The combination of large size, massive crushing and compacting forces and sudden, valley-blocking

K. Hewitt (✉)
Department of Geography and Environmental Studies, Cold Regions Research Centre, Wilfrid Laurier University, Waterloo, ON N2L 3Z9, Canada
e-mail: khewitt@wlu.ca

C. Margottini et al. (eds.), *Landslide Science and Practice*, Vol. 4,
DOI 10.1007/978-3-642-31337-0_43,

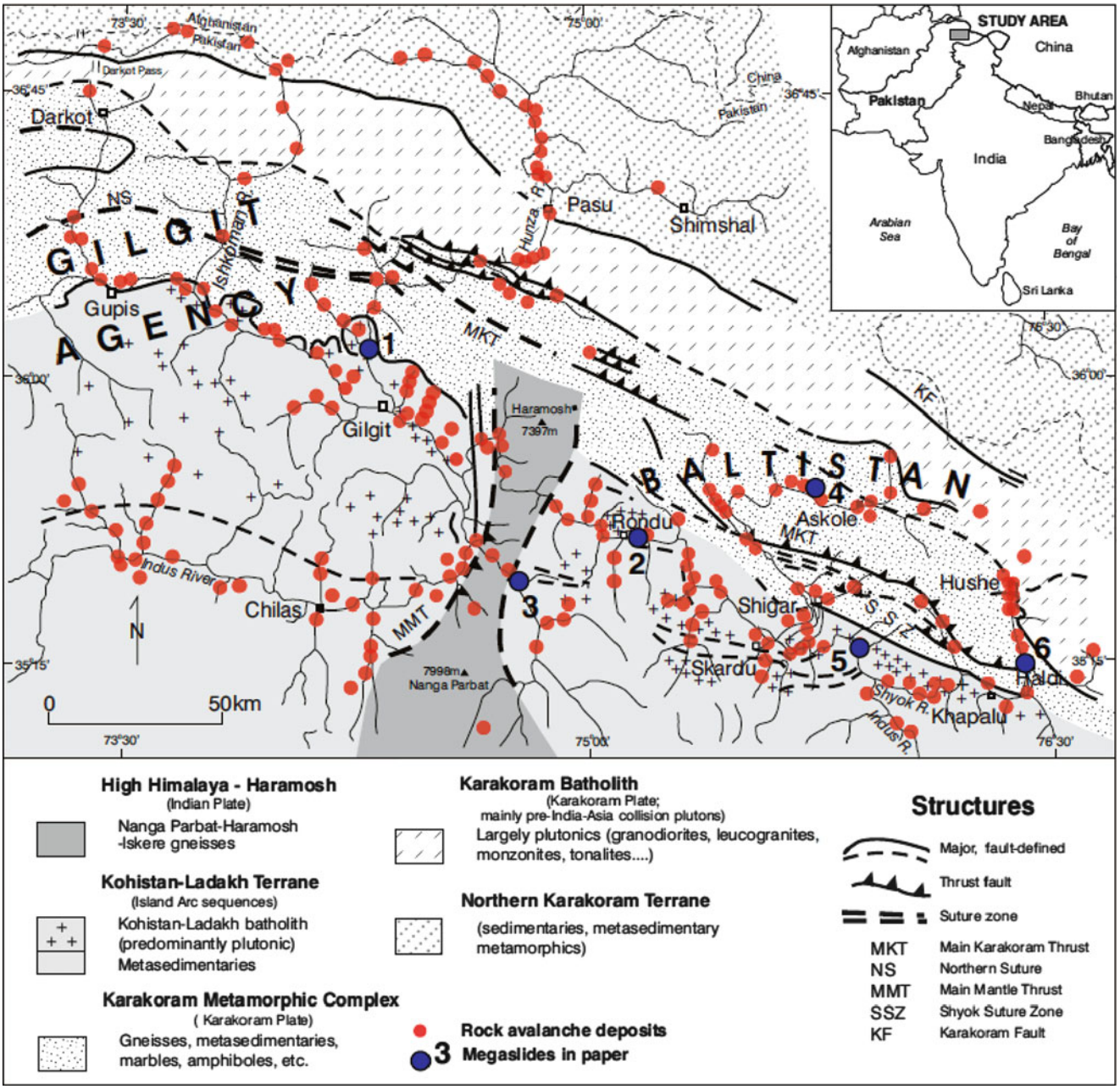

Fig. 1 Geological base map of the Central Karakoram and Nanga Parbat Haramosh massif (after Searle 1991), with rock avalanches identified to date, and locations of the six megaslide complexes discussed in the text.: *1* Nomal (Hunza), *2* Rondu-Mendi (Haramosh), *3* Pharashing (Astor), *4* Ghomboro (Braldu), *5* Gol-Ghone "N" and "S" (Indus), and Haldi (Saltoro)

emplacement has led to extended disturbance in landform developments. All gave rise to large lakes that persisted for centuries, at least, and major episodes of intermontane sedimentation. A sense of related landform developments is essential to recognizing and interpreting the landslides. For the last 150 years the landslide complexes, or those parts not mapped as *in situ* bedrock, were considered to be moraines. They, and related landform developments had been attributed to major climate change, glaciation and/or tectonic disturbances. Here, they are shown to be post-, or inter-glacial megaslides whose distinctive morphologies and composition are partly due to exceptional size, mainly to constraints and blocking of run out by topography.

The Events

In addition to being megaslides, certain common features of the landslides suggest a distinct sub-set of massive rock slope failures (Table 1). The main landslide masses involved deep-seated rotation or sagging in bedrock and sudden, catastrophic collapses. They are landslide *complexes* in two

Table 1 Dimensions of six megaslide events estimated from ground observations and satellite imagery and, where available, detailed contour maps (Fig. 1)[a]

#	VALLEY landslide	Volume (km^3) Original (remains)	Area (km^2) Total (deposit)	Fall (km)	Runout (km)	Highest (masl)
1	HUNZA	45.0	76.0	2.4	11.0+	3 450
	Nomal	(35.0)	(65.0)			
2	INDUS	24.0	56.0	2.3	10.0	3 870
	Rondu A	(15.0)	(49.0)			
3	ASTOR	6.0	15.0	2.2	8.5	4 420
	Pharishang	(4.5)	(10.5)			
4	BRALDU	5.5	41.0	3.0	7.0	5 640[b]
	Ghomboro	(3.0)	(24.0)			
5	INDUS	5.0	25	2.0	8.5	4 120
	Gol-Ghone 'N' and 'S'	(3.5)	(18)			
6	SALTORO	2.2	27	2.2	7.0	4 200
	Haldi	(1.0)	(23)			

[a]These figures are substantially larger than some early estimates (Hewitt 1998, 2002), thanks to further ground surveys, improved satellite coverage, and a better sense of the whole events
[b]The only megaslide to originate higher than Ghomboro is the Iskere-Sassi event

senses. Within a common slope failure 'system', the main masses show evidence of two or more distinct events or phases of movement, and areas or units that move(d) along differing trajectories, or that separated from each other during run out. Secondly, each 'system' involves two or more distinct types of mass movement that include translational slide blocks, rotational slump, rockfall, rock avalanche, debris avalanche, and debris flow.

However, three other characteristics of the landslide masses are a focus of interest here; their geometries of emplacement, deposit composition and relations to landform developments. In each case the main body remained hundreds of meters thick (Fig. 2a, b). Although all parts must have traveled at high speeds for a time, and over some kilometers, only small fractions spread into the more typical, relatively thin, long run out debris sheets.

With respect to composition, the main body in each case consists of thoroughly crushed and fragmented materials hundreds of meters thick and many square kilometers in area. Indications are that the bedrock was largely intact and not significantly weathered before failure occurred. In the landslide it then became completely shattered and crushed, creating a brecciated, or cataclastic-like facies. There are large boulders on the surface, but most of the landslide mass was reduced to granule-, sand-, and silt-grades; although entirely of local bedrock. There is internal faulting, over-thrusting, and splitting into distinct units or lobes, but stratigraphic relations of the original bedrock are preserved. Lithologies within the main body have not mixed.

Thirdly, the landslides brought major modifications to local terrain and topography, and even basin-wide developments. They have reorganized interfluve geometries and must contribute to significant shifts in crest-line, mountain and drainage basin morphology. The run out, valley blocking and relative resistance of the landslide materials to erosion, have massively disturbed valley evolution along the Indus streams, as described at length elsewhere (Hewitt 1998). All six megaslides dammed large lakes for some centuries at least, leading to large scale intermontane sedimentation. While subsequently breached and trenched they remain incompletely cut through and continue to act as local base level controls for much of the upper Indus basin (Hewitt et al. 2011). These particular features will be discussed after introducing each event.

Nomal Complex

This comprises the largest landslide system yet identified in the region, involving a collapse of the west flank of the Hunza valley at and below the junction with Naltar valley (Hewitt 2001) (Fig. 3). The entire area involved likely exceeded 75 km^2, the landslide debris covering some 65 km^2, and with a volume of around 45 km^3. More than one-third of the original mass has been removed or buried.

The bedrock comprises volcanics and plutonics of the Kohistan Batholith (Petterson et al. 1990). Parts of the headwall and some rotational blocks below it, are from their "late undeformed" Shirot pluton; the main mass from his "early deformed plutonics" of the Nomal-Matum Das pluton. Petterson (personal communication) also attributes the distinctive range of yellow, orange and pink bands to original geochemical alteration. However, the landslide mass was mapped as *in situ* bedrock.

The landslide is an interconnected series of rock slumps beneath an 8 km semi-circle of irregular cliffs, 300–1,000 m high from which it slid down to form a wide plateau. Parts of this landslide surface are eroded by streams and it ends in a cliff some 6 km long and 1,000–1,400 m high, overlooking the Nomal villages and the Hunza River. The landslide

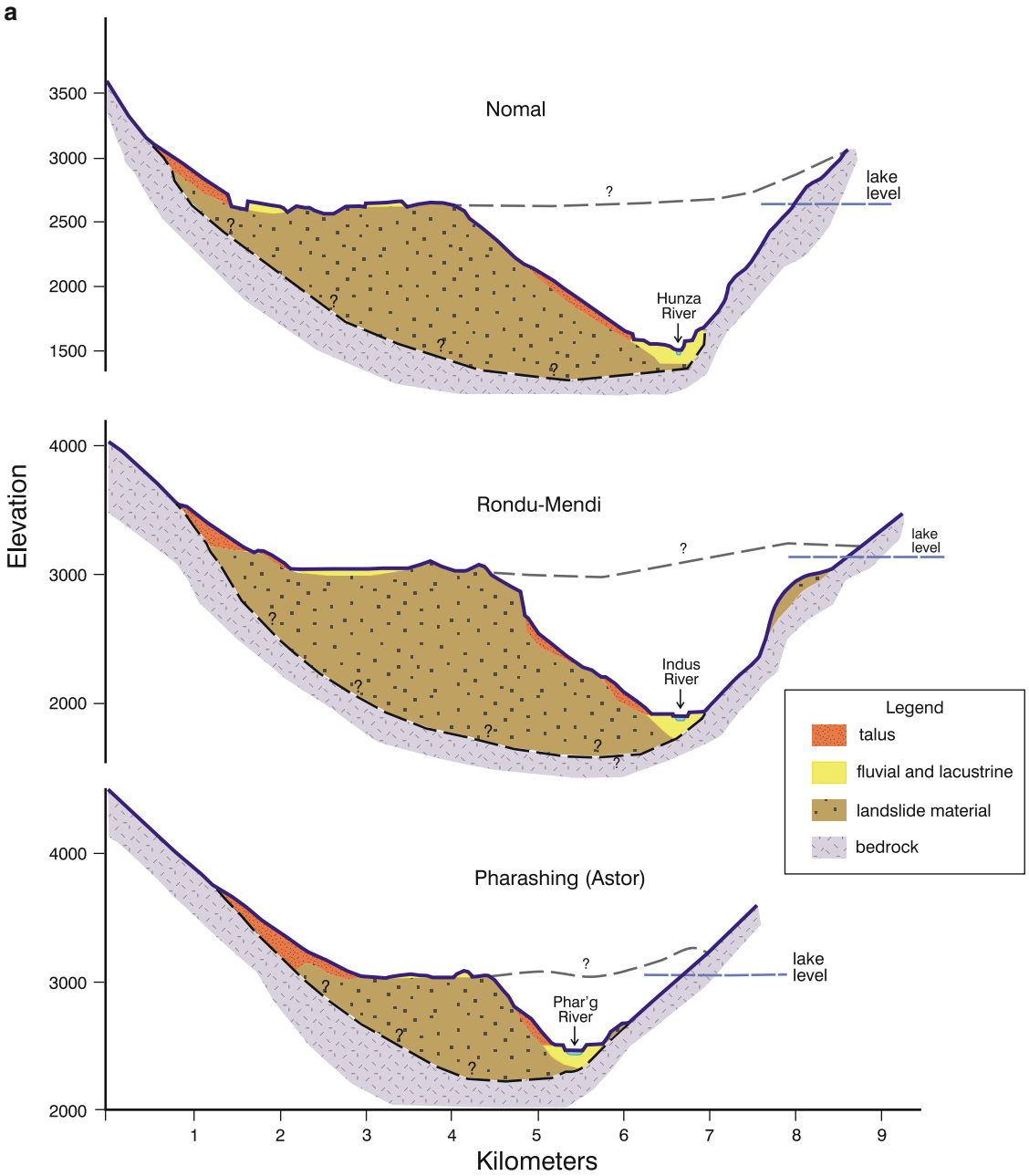

Fig. 2 (continued)

originally sealed the mouth of the Naltar and dammed the Hunza to a depth of about 1,000 m (Hewitt 2009b, 244). The focus here is on the main mass that stalled against the opposing slope, but there were fast-moving lobes that split off and travelled far up and down the Hunza valley.

Rondu

This resembles Nomal in many respects, but is about two-thirds its size. The landslide again comprises a huge slump block that fills most of the Indus valley around Rondu, which it blocked (Fig. 4). It also left a broad plateau-like surface in front of the village of Lustung, 1,100 m above the Indus River which has eroded a huge cliff in the landslide debris but not yet cut down to the pre-landslide river channel. The landslide material consists of Ladakh batholithic rocks, originally continuous with the Kohistan batholith, but cut by the Nanga Parbat Haramosh Massif (Searle 1991). The only detailed geological investigation was by Zanettin (1964, his Fig. 2). However, much of what he maps as bedrock is landslide material, including most of his "Twar basic mass, diorites, norites, gabbros, granodiorites and amphibolites". He did not identify the landslide, but shows about 10 km^2 of the 'plain'

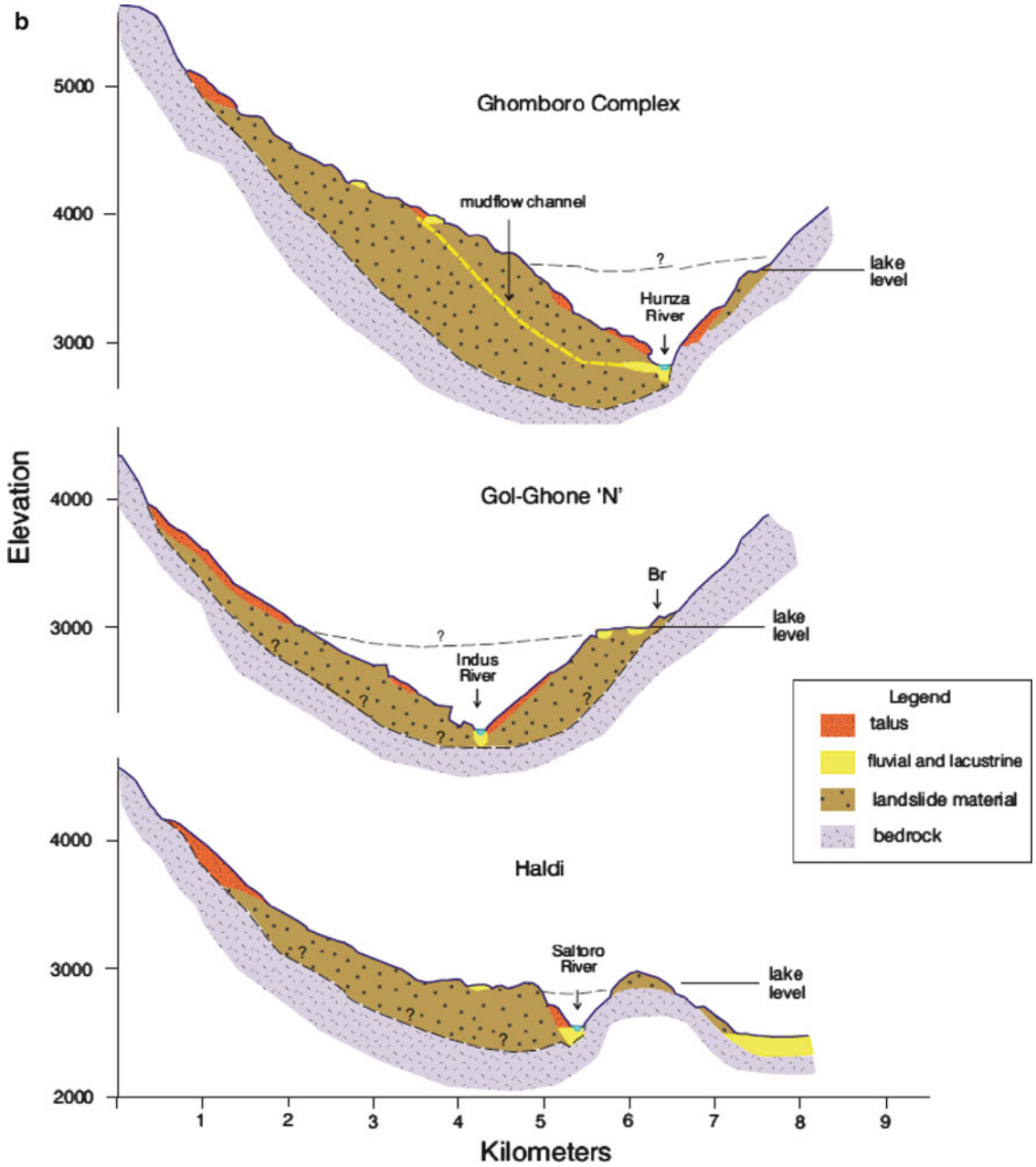

Fig. 2 (**a**) and (**b**). Cross-valley long profiles of the six events arranged in order of magnitude (cf Table 1). The profiles are from where the landslides descended directly from mid-points along the detachment zones and at right angles to valley they belong to and blocked. They do not represent the highest source nor lowest run out elevations, but roughly bisect the landslides at their greatest mass and, probably, thickness. The actual basal failure surfaces, pre-landslide valley profiles and outer surface profiles of the deposits are not known and shown schematically

around Lustung and the Twar valley as "moraine, alluvium and debris. . .[and] thick moraine" (ibid, 34–35).

Pharishang Gah

This complex is an order of magnitude smaller than Nomal and Rondu, but of similar geometry. It represents a collapse of the south wall of the Pharashing at and just above the junction with the Astor River which a lobe of the landslide also blocked. Again the deep seated collapse has left an extensive 'plateau' below the source slope, its outer part cut by a 500 m cliff where the river cuts through (Fig. 5). The source and most of the run out area are placed in the Ladakh batholith, immediately east of the north trending fault boundary of the NPHM gneisses. Earthquakes and movements along this fault may have triggered the landslide from slopes destabilized by the retreat of Deosai and Nanga Parbat glaciers which filled the valleys in the last major glaciation. It also provides a striking example of Strom and Pernik's (2005) "secondary

Fig. 3 View of Nomal Complex from the opposite flank of Hunza valley, showing the cliff cut by the river in brightly coloured landslide materials, and line of cliffs comprising the visible detachment zone in the far distance. Horizontal span shown is about 6 km and, vertical from the river to head of detachment zone about 2,000 m

Fig. 4 Rondu Complex from plateau-like surface looking down the cliffs in thoroughly crushed rock cut in the landslide by the Indus. The opposite slope has many remnants of the landslide scattered over it and evidence of the river's breaching of the high dam it once formed

Fig. 5 View along the north side of the Pharishang Gah main landslide surface towards the headwall. The coarse landslide material is buried in finer wind-blown dust, and fluvial and lacustrine deposits when the river overflow channels and landslide-dammed lakes covered parts of the surface

rock avalanche". A large section of the original mass of the main cross-valley lobe has collapsed and moved away at right angles from the west, downstream flank. It too created a small 'plateau', the remnant about 1 km^2 in area below a bowl-shaped cliff in landslide material about 300 m high (Fig. 6). Most of this secondary mass entered and blocked the Astor valley covering what is now the site of Astor town, and blocking the outlet valley of Sachen Glacier.

Ghomboro

This is the highest, steepest and most unstable of the landslide complexes; and largest of at least seven megaslide complexes that descend into the Braldu River gorge between Surongo and Dassu (Hewitt 1998) (Fig. 7). The bedrock which failed is part of the Ganschen Unit of the Karakoram Metamorphic Complex consisting mainly of metasedimentaries but with abundant intrusives and quartz veins (Searle 1991). It occurs along a very narrow deep section of the Braldu, once filled by ice over 1,500 m thick, from what remains today the highest, most heavily glacierized part of the Karakoram. The entire ridge crest above has collapsed, and the Complex appears as a shovel-shaped amphitheatre of rock walls with steep landslide materials burying the lower two-thirds. The main body of rock slope failure materials is mostly buried by later rockfall, debris flow, avalanche and wind-blown material. Perennial debris flow channels enter the Braldu from the surface of the landslide and large debris flows frequently block the river. Four separate rock avalanche lobes can be detected that climbed the left/south/opposing slope. It cannot be said with certainty whether they occurred at different times and as distinct events, or were part of a single, major collapse.

Gol-Ghone Complex

This complex consists of two massive rock slope failures from a common source on the left/west flank of the Indus,

Fig. 6 View westwards from the upper surface of Pharishang Gah landslide across the secondary lobe that travelled across the Astor River, in the middle ground, which it dammed. The landslide also plugged the entrance of the valley opposite, where the town of Astor lies, blocking the exit of the Sachen Glacier in the upper right corner

20 km upstream of Skardu, and between the villages of Gol and Ghone (Hewitt 2002, 363–365). The bedrock is again in the Ladakh Batholith, mainly granodiorites, whose light colored rock is seamed with darker and paler intrusions, and many quartz veins. The main mass is stalled against the opposing, east wall of the Indus gorge, forming a hummocky upper surface 0.5–1.0 km wide, 400–600 m above the river, and continuing for 4.5 km (Fig. 8). Cliffs in the landslide debris and talus cones derived from it fall to the river's edge. At the northern and southern limits, separate lobes shot off along the valley floor for some 5 km or more up and down the Indus leaving deposits more typical of sheets of rock avalanche debris, 3–10 m thick.

Haldi

The rock slope failure forming the Haldi Complex was on the right/north wall of the Saltoro valley, just before its junction with the Hushe (Hewitt 2002). The visible parts of the detachment zone are on the southern flank of the Kande plutonic unit, but lower outer parts of the landslide include masses of Hushe Gneiss rocks (Searle 1991). The section shown in Fig. 2 is where the debris was stalled against the opposing valley slope, creating a morphology similar to the other examples, but it comprises a relatively smaller part of the whole landslide complex (Fig. 9). The spur between the Saltoro and Shyok valleys is fairly low here and part of the landslide climbed as much as 500 m to cross the opposing interfluve and deposit debris on it. In this regard the Haldi megaslide is closest of the six events to the Koefels landslide, in the Oezthal of Austria, and their volumes were similar (Erismann and Abele 2002, 36). However, right and left of the cross-valley mass major lobes diverged westwards across the Hushe, and eastwards up the Saltoro to create an even more complex morphology.

Fig. 7 View into the embayment of the Ghomboro Complex showing the snow-covered detachment zone in the upper distance, debris flow channels that originate in the mid-regions of the landslide mass (see Fig. 2), and the Braldu River cutting through. The terraces record impoundment episodes by later or secondary landslides suggesting the river breached the main Ghomboro mass and was again dammed on several occasions

None of these landslides had been recognized as such in 150 years of scientific investigations and apart from Nomal, evidently regarded as a bedrock feature, they were previously classified as glacial deposits (Hewitt 1999). Since the detachment zones occur at or near the upper limits of ice in the last major glaciation, it seems likely glacial oversteepening and debutrressing may be a factor in their location and instabilities (Hewitt 2009b). Most are located at or near valley junctions and ice movement in preceding glaciation may have been critical for the scale and geometries of instability. However, all are post-glacial, possibly interglacial in the case of Rondu, and descended over ice-free valley floors.

Topographical Constraints

The landslide masses are so large and planes of failure reach such depths, that in some respects they resemble tectonic more than subaerial processes. Nevertheless, the geometry and settings leave no doubt they are mass movements. Failure was mainly or wholly rotational or slope-parallel, reflecting stress concentration, rather than collapse along pre-existing lines-of-weakness in the bedrock. Only Pharishang is near a known active fault.

On the one hand, the heights of fall ('H') are greater than most examples elsewhere; for instance, considerably more than Saidmarreh, Flims and Mayanmurca (Table 2). On the other hand, they seem small given the available relief and steepness of surrounding terrain. Vertical spans of 4,000–6,000 m occur within 20 km or less of the megaslides. Peaks between 6,500 and 8,000 m are nearby. While rockslide-rock avalanches have been identified with start zones above 7,000 m elevation (Hewitt 2002), the six

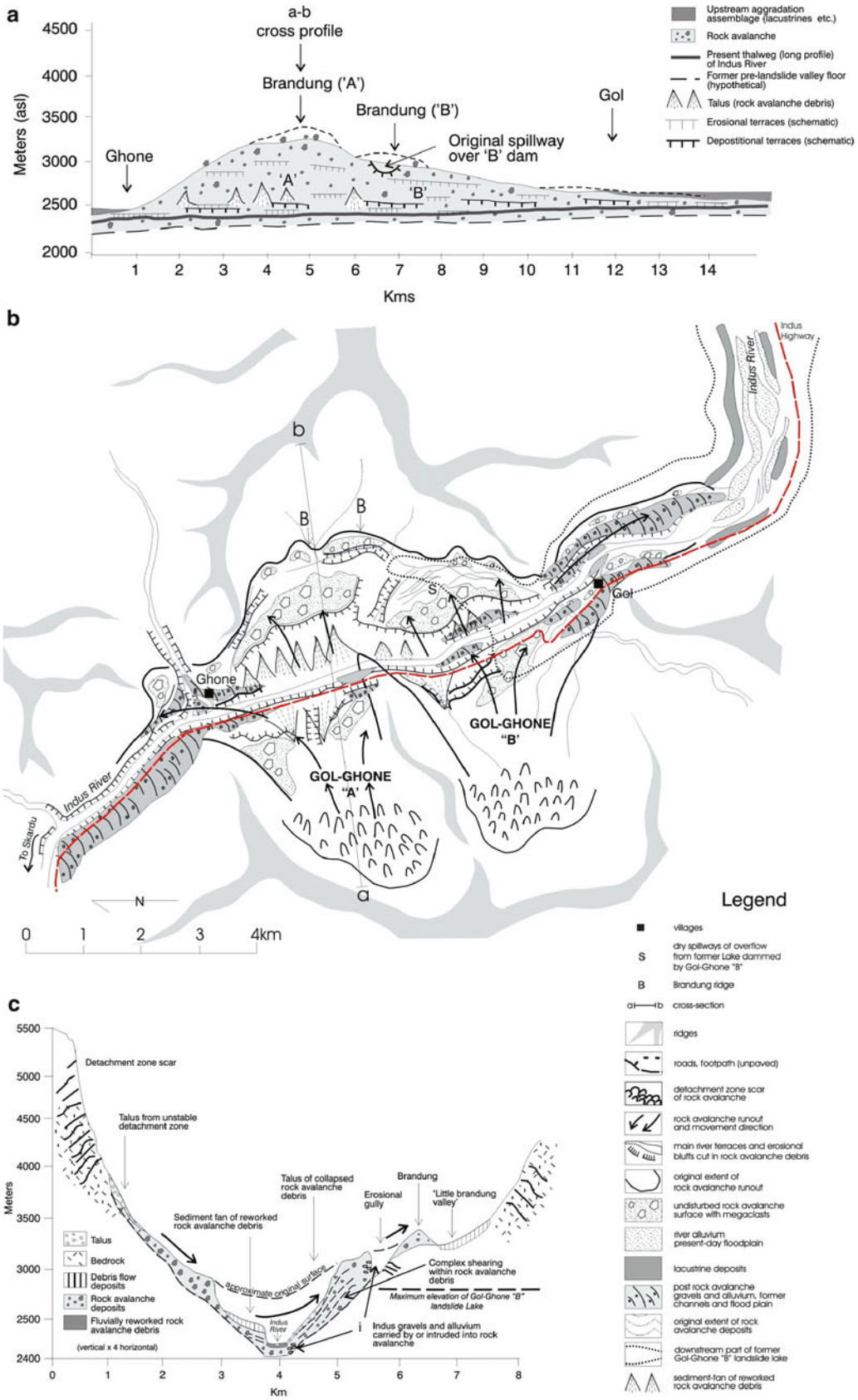

Fig. 8 The Gol-Ghone Complex showing: (**a**) the long profile along the Indus and main mass that stalled against the opposing slope and subsequent terracing as the river gradually incised the landslide barrier, (**b**) a plan view of the two parts of the landslide and relations to the Indus River, (**c**) a schematic transverse profile

Fig. 9 The Haldi Complex, which forms most of the middle ground in this view looking east from the Hushe valley, up the Saltoro valley. The profile in Fig. 2b is from left to right of the photograph in the middle distance where the landslide encountered and climbed over the interfluve south of the Saltoro. Remnants of the lobe that separated and traveled westward across the Hushe is in the foreground

megaslides are largely confined to the lowest one-third of the elevation range of the mountains.[1] In the six megaslides, size and the geometries of failure and movement in relation to valley topography, seem critical. Detachment zones are on the flank of deeply excavated valleys, and initial landslide movement was transverse to the valley such that the bulk of the deposits were emplaced in front of the detachment zone and against the opposing valley slope.

Rugged terrain influences and complicates debris emplacement in most rock avalanches in the region. Topographic irregularities in the path concentrate, disperse, or split the debris streams (Hewitt 2002, 2006). In the present cases, however, the main landslide mass is stalled rather than being dispersed as mobile debris lobes. Descriptively, there is an unusual relation to Heim's (1932) proposal that all landslides involve three elements, in today's language:

1. *Detachment zone* or source where failure occurs;
2. *Transport zone/travel path/slope* ". . .through which the rock mass passes on the way down. . ." and,
3. *Deposit area,* ". . .where the rubble comes to a halt".

These three zones are not spatially distinct or functionally separate in the six megaslides. The main depositional mass is not fully separated from the detachment zone and there is little or no visible 'transport slope'. The main mass remains of relatively uniform thickness across the valley floors with, in some cases, thickening against, or climbing of, the opposing wall.

Analytically, the third of Heim's proposed controls over rock avalanche movement assumes singular importance; ". . . the [ir]regularity of the path [and] obstructions. . ." (Heim 1932, 100). The other two are size of the mass in movement (V), and height of fall (H). He found, as a general rule, the larger the mass the further the rock avalanche will travel, and the lower the angle between the head of the detachment zone and furthest deposit rim. His *'fahrboschung'* or 'path angle', H/L has been treated as the "equivalent angle of friction" (Hsü 1978, 79). Scheidegger (1973) applied this concept to a world-wide set of catastrophic landslides of more than 0.75×10^6 m^{-3}. He showed a log-normal relation between H/L and landslide volume. However, the six megaslides, although relatively mobile long-run events, have 'equivalent angles of friction' more than one standard deviation, outside Scheidegger's relation, and more than two standard deviations in some (Fig. 10). Evidently, this is not simply a matter of size. Saidmarreh (#4) in the Zagros Mountains of Iran, for example, is less than half Nomal's size, while Flims (#5), on the upper Rhine is half Rondu's. However, they plot around one standard deviation *below* Scheidegger's correlation, and their depositional bodies are more typical of rock avalanches.

The apparent reduced mobility of the six examples is essentially an effect of topographic blocking. The direction of run out and conditions in the run out zone are more significant that size. The graph also shows that they are more extreme cases, not completely separate from other upper Indus catastrophic rockslides. Most rock avalanche deposits in the region exhibit styles of emplacement constrained by topography (Hewitt 2002).

'Sedimentary' Properties and Bedrock Fragmentation

Lithology is a key to recognizing and analyzing rockslide-rock avalanches. The characteristic materials in their deposits come from a local bedrock source and, if the source involves two or more rock types, they do not mix and retain their relative positions: the "remnant stratigraphy" of Heim (1932).

Near the surface of the megaslides is a carapace of broken rock and clast supported finer materials, familiar in the relatively thin, run out lobes of typical rock avalanches (Fig. 11). However, below about 25 m depth, and up to 1,000 m at Nomal and Rondu, the material has more the appearance of deformed and faulted bedrock – for which it has been mistaken. Close inspection reveals that it is really intensely crushed, shattered and comminuted. There may be folding in the direction of movement giving a macroscopic appearance of ductile responses, but microscopically the material turns out to be thoroughly fragmented by brittle breakage (Fig. 12). Stratigraphic relations of the original bedrock are preserved, however so that it closely resembles intensely brecciated or cataclastic facies. These developments occurred within the landslides mass, so that landslide activity is responsible for the highly fragmented and comminuted bedrock. Intact

[1] The only megaslide to originate higher than Ghomboro is the Iskere-Sassi event (H = 5,850+; L = 25 km; H/L 0.23) from the walls of Haramosh (7,409 m). It is not included here because it first descended over glaciers for about 10 km and became a debris avalanche, which helps to explain the exceptional mobility.

Table 2 Dimensions of known upper Indus megaslides in order of volume estimates. The six discussed in the text are in bold. Several examples from other regions are included in italics (Rouse 1984, 500). Note that the values are for the whole landslide, not the cross-valley sections for main masses shown in Fig. 2

#	BASIN landslide	Volume (original) Original (km^3)	Fall (km)	Runout (km)	H/L	Comment
1	**HUNZA Nomal**	**45**	**2.4**	**11.0**	**0.22**	
2	**INDUS Rondu**	**24**	**2.3**	**10.0**	**0.23**	
3	INDUS Gor-Th.	24	3.1	15.5	0.2	
4	*SAIDMARREH*	*20*	*0.9*	*14.5*	*0.1*	*Iran*
5	*FLIMS*	*12*	*1.22*	*16.5*	*0.14*	*Swiss*
6	**ASTOR Pharashing**	**6.0**	**2.2**	**8.5**	**0.26**	
7	**BRALDU Ghomboro**	**5.5**	**3.0**	**7.0**	**0.43**	
8	INDUS Basho I	5.4	2.3			
9	**INDUS Gol-Ghone**	**5.0**	**2.0**	**8.5**	**0.24**	
10	INDUS Harban	4.5	1.9	8.9	0.21	
11	TANGIR Sheko	3.7	2.6	10.3	0.25	
12	INDUS Bachahaloi	3.5	2.4	7.0	0.34	
13	INDUS Shatial	2.6	2.2	8.5	0.26	
14	GILGIT Batkor	2.5	1.8	9.5	0.19	
15	**SALTORO Haldi**	**2.2**	**2.2**	**7.0**	**0.31**	
16	INDUS Katzarah	2.1	2.7	10.8	0.25	
17	*MAYUNMURCA*	*1.6*	*1.9*	*8.2*	*0.23*	*Peru*
18	INDUS Jalipur	1.5	1.5	6.9	0.22	
19	INDUS Doian	1.5	1.5	5.8	0.26	
20	INDUS Satpara-Sk.	1.4	1.9	9.0	0.21	
21	GILGIT Dhak Chauki	1.1	2.1	6.5	0.32	
22	STAK Stak III	1.1	1.9	5.7	0.33	
23	INDUS Lichar 1	1.1	2.1	4.5	0.47	
24	HUNZA Baltit-Sum.	1.0	3.1	9.5	0.33	
25	INDUS Gine	0.9	2.3	9.2	0.25	
26	HUNZA Jaglot	0.9	2.4	6.3	0.38	
27	BUNAR Bunar	0.8	2.2	5.6	0.39	
28	STAK Stak II	0.8	1.9	5.7	0.33	

(*continued*)

Table 2 (continued)

#	BASIN landslide	Volume (original) Original (km^3)	Fall (km)	Runout (km)	H/L	Comment
29	GILGIT U. Henzul	0.8	1.4	5.0	0.28	
30	KARGAH Kargah I	0.8	2.3	4.5	0.5	
31	BALAS Balas I	0.5	1.5	6.0	0.25	

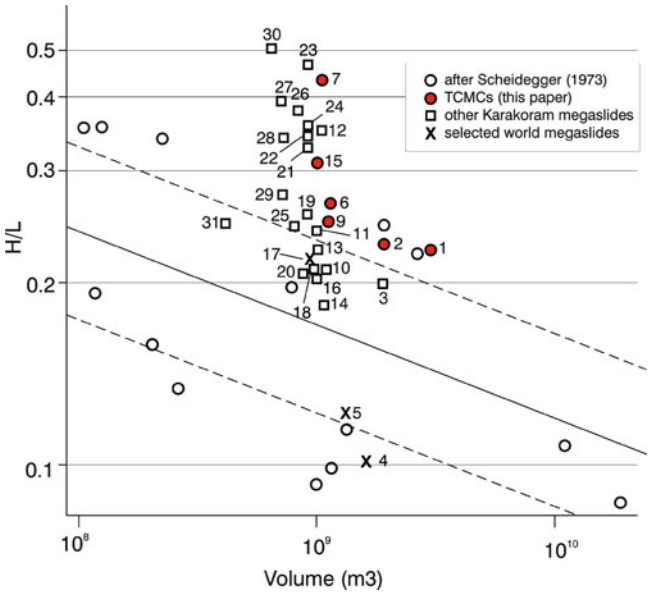

Fig. 10 The graph plots landslide volumes (arithmetic scale) against the ratio of descent to furthest run out distance (H/L) on a logarithmic scale. The *diagonal line* is the average relationship determined for a set of world-wide landslides by Scheidegger (1973). The *broken diagonal lines* represent an upper and lower standard deviation. Clearly, all six upper Indus megaslides lie well outside this and on the side of apparent greater frictional resistance and reduced mobility. Moreover, the set of all upper Indus megaslides and a small number that are almost as large, suggests the six chosen are not particularly eccentric there. I suggest this is a consequence of topographical constraints rather than any other factor

bedrock hundreds of meters thick was reduced to fragments in minutes or less. To reduce it so quickly to fragments predominantly smaller than cobble-size and with between one- and two-thirds sand-grades or less, the crushing forces applied must exploit the micro-level flaws as well as major discontinuities, and lines of weakness. Given that run-out is highly constrained and the mass remains so thick, the problem is pertinent to debates of the mechanisms of rock fragmentation (McSaveney and Davies 2006).

Several phenomena seem to reinforce or be at odds with what specialists in landslide mechanics and modeling have proposed. In this case fragmentation must result from one, or a combination of;

1. The initial collapse and descent,
2. The (limited but) high speed run-out,
3. The sudden shocks of blocking and stalling against the opposing wall.

There are problems with proposals and models that either seek explanation in presumed, friction-reducing conditions at the base of the landslide or within the rubble. The material in the megaslides involves fragmentation happening tens to hundreds of meters above and below the base and upper surfaces where neither frictional sliding of one over the other, nor rolling of clasts are possible. The crushing and pulverizing takes place within the rock mass through internal forces and/or inter-grain impacts. While this would mean some dilation even under the huge static loads at such depths of rock, nothing prevents intense compaction or over-consolidation at the moment when movement stopped by 'frictional freezing'. The main body of the landslide materials is much more compacted and has fewer voids or cavities than most bedrock outcrops. If there had been basal, friction-reducing layers of moisture, vapour or other gases, these would counteract rather than explain the forces needed for the comminution or granulization that occurs in the body of these landslides.

Topography-Changing Events

The megasides also strongly modify terrain and topography. There is displacement of interfluves in the detachment zones where headwalls 'daylight' beyond the former watershed or ridge-crest. This slope migration, 'eating into' the adjacent drainage basin, is especially large at Ghomboro Complex and Gol-Ghone, but applies to some extent in all cases. It contrasts with an impression in many landslide diagrams where falls, slides, slumps and flows are shown to originate on and below pre-existing slopes or scarps (Selby 1993). In addition, it is likely that the maximum height of headwall evident in the terrain now, is lower than the height-of-land before the collapse. This applies to ridge collapses as at Ghomboro, but even more where a pre-existing peak or salient collapsed. At Nomal, Rondu-Mendi and Pharashing, there is a distinct sense of 'missing mass' to drive these enormous displacements had they descended only from existing headwalls.

In each case, the relatively thick cross-valley barriers created large dams of densely packed material resistant to erosion and failure (Costa and Schuster 1988, 10; Korup et al. 2010). These have disturbed and modified valley evolution along the Indus streams, as described at length elsewhere (Hewitt 1998; Hewitt et al. 2008). The large

Fig. 11 The *right side* of the photo shows a section eroded in the upper 20 m or so of the Gol-Ghone 'S' rock avalanche with typical boulder-supported fabric of a rock avalanche 'carapace'. (cf Fig. 12)

Fig. 12 A section about 50 m across, eroded through the Gol-Ghone landslide some 450–500 m below the surface as shown in Fig. 11. Here the material resembles the bedrock from which it is derived, is strongly compacted and able to stand in near-vertical cliffs. However, on close inspection it turns out to be crushed to cobble-, and smaller grades, mainly sand and dust sizes. The strung-out quartz veins are original but distorted, crushed to powder and sheared in places. Several seeming 'faults' run through the mass, notably the one from *lower left* to *upper right* marked by a conspicuous band of fine-milled 'goudge'. These are landslide-generated separations and lines of shear

lakes lasted for some centuries, generating intermontane sedimentation on a large scale, followed by breaching and trenching for many millennia, and still incomplete. They continue to act as local base level controls for much of the upper Indus basin (Hewitt et al. 2011).

References

Costa JE, Schuster RL (1988) The formation and failure of natural dams. Geol Soc Am Bull 100:1054–1068

Erismann TH, Abele G (2002) Dynamics of rockslides and rockfalls. Springer, Berlin, 684pp

Heim A (1932) Bergsturz und Menschenleben. Fretz and Wasmuth, Zurich

Hewitt K (1998) Catastrophic landslides and their effects on the Upper Indus streams, Karakoram Himalaya, Northern Pakistan. Geomorphology 26:47–80

Hewitt K (1999) Quaternary moraines vs. catastrophic rock avalanches in the Karakoram Himalaya, Northern Pakistan. Quaternary Res 51:220–237

Hewitt K (2001) Catastrophic rockslides and the geomorphology of the Hunza and Gilgit basins, Karakoram Himalaya. Erdkunde 55:72–94

Hewitt K (2002) Styles of rock avalanche depositional complex in very rugged terrain, Karakoram Himalaya, Pakistan. In: Evans SG, DeGraff JV (eds) Catastrophic landslides: effects, occurrence, and mechanisms, Reviews in engineering geology. Geological Society of America, Boulder, CO, pp 345–378

Hewitt K (2006) Rock avalanches with complex run out and emplacement, Karakoram Himalaya, Inner Asia. In: Evans SG et al (eds) Landslides from massive rock slope failure, NATO science series. Springer, Dordrecht, pp 521–550

Hewitt K (2009a) Catastrophic rock slope failures and late quaternary developments in the Nanga Parbat-Haramosh Massif, Upper Indus basin, Northern Pakistan. Quaternary Sci Rev. doi:10.1016/j.quascirev.2008.12.019

Hewitt K (2009b) Paraglacial rock slope failures, disturbance regimes and transitional landscapes, Upper Indus Basin, northern Pakistan. In: Knight J, Harrison S (eds) Periglacial and paraglacial processes and environments, vol 320, Geological society special publication. Geological Society, London, pp 235–255

Hewitt K, Clague J, Orwin J (2008) Legacies of catastrophic rock slope failures in mountain landscapes. Earth Sci Rev 87:1–38

Hewitt K, Gosse J, Clague J (2011) Rock avalanches and the pace of late quaternary development of river valleys in the Karakoram Himalaya. Geol Soc Am Bull. doi:10.1130/B30341.1. Published online on 14 June 2011, p 16

Hsü KJ (1978) Albert Heim: observations of landslides and relevance to modern interpretations. In: Voight B (ed) Rockslides and avalanches; 1, natural phenomena. Elsevier, Amsterdam, pp 70–93

Korup, O, Hewitt, K, Montgomery, DR (2010) Glacier and landslide feedbacks to topographic relief in the Himalayan syntaxes, Proceedings of the National Academy of Sciences (USA) www.pnas.org/cgi/doi/10.1073/ pnas.0907531107 plus supporting information online at www.pnas.org/cgi/content/full/0907531107/DCSupplemental

McSaveney MJ, Davies TRH (2006) Rapid rock mass flow with dynamic fragmentation: inferences from the morphology and interna;l structure of rocksldies and rock avalanches. In: Evans SG, Scarascia-Mugnozza G, Strom AL, Hermanns RL (eds) Landslides from massive rock slope failure, (proceedings, NATO advanced workshop, Celano, Italy, June 2002). Springer, Dordrecht, pp 285–303

Petterson MG, Windley BF, Sullivan M (1990) A petrological, chronological, structural and geochemical review of Kohistan Batholith and its relationship to regional tectonics. Phys Chem Earth 17:47–70

Rouse WC (1984) Flowslides. In: Brunsden D, Prior DB (eds) Slope Instability. Wiley, New York, pp 491–522

Scheidegger AE (1973) On the prediction of reach and velocity of catastrophic landslides. Rock Mech 5:231–236

Searle MP (1991) Geology and tectonics of the Karakoram mountains. Wiley, New York

Selby MJ (1993) Hillslope materials and processes, 2nd edn. Oxford University Press, Oxford, p 466

Strom AL, Pernik LM (2005) Utilisation of the data on rockslide dams formation and structure for blast-filled dams design. ItalJ Eng Geol Environ, Special issue I, Rome, "Security of natural and artificial rockslide dams: NATO advanced research workshop, Bishkek, Kyrgyzstan, June 8–13, NATO-OTAN, 2004", pp 133–137

Zanettin B (1964) Geology and petrology of Haramosh-Mango Gusor area, Scientific reports of Italian expeditions to the Karakorum (K2) and Hindu Kush, III/I. E.J. Brill, Leiden

Did Radiative Cooling Trigger New Zealand's 2007 Young River Landslide?

Mauri McSaveney and Chris Massey

Abstract

The 11 million m^3 Young River landslide (44° 08′ 44.6 ″S, 169° 06′ 46.0″ E) fell at 4:40 h on 29 August 2007 in New Zealand's Mt Aspiring National Park. It fell from an extensive mass of dilated closely jointed schist with pre-existing evidence of rock-mass creep and prior rockfalls. The remaining slope has only marginal stability, as had the prior slope for a long time. It required very little change to trigger rapid failure. The fall left a seismic record indicating a lack of an earthquake trigger. The landslide fell in winter, and the deposit shows evidence of much groundwater in the source, hence we dismiss a permafrost-thaw trigger. The failure occurred just before the usual coldest time of night. Rainfall and daily maximum and minimum temperatures at climate stations in the region suggest that the landslide fell on a night with extreme radiative cooling to a dry, clear, night sky (the largest diurnal temperature drop that winter), after several weeks of clear, cold nights. We suggest that the immediate trigger was an abnormal rise in groundwater pressure when springs froze on the face of the landslide source area. Since freezing of springs is likely to be frequent in winter, we suggest that the rise in pore pressure on the night of 28–29 August 2007 affected a progressively lowering threshold of rock-mass strength from mass creep. Hence failure was inevitable, and the particular trigger was irrelevant.

Keywords

Landslide • Alpine • Nocturnal radiation cooling • Freezing • Pore-water pressure • New Zealand

Introduction

A large new landslide (Fig. 1) was sighted in the headwaters of Lake Wanaka on 26 September, 2007 by a helicopter pilot, Mr Harvey Hutton. The landslide had dammed the north branch of Young River in southern South Island, New Zealand (Fig. 2). At the time of first sighting, the landslide had already impounded a 2-km long lake which was within a week of overflowing. The middle reaches of the north branch of Young River were an untracked, little visited area of Mt Aspiring National Park prior to the landslide.

A search of seismic records from southern New Zealand, revealed the distinctive signature of a rapid fall of a large rock avalanche in the Young River catchment at 4:40 h, 29 August, 2007 (NZST)(UT + 12 h). This time of fall was consistent with realistic water inflows to fill the lake in a month.

The Young River landslide is one of many large landslides which have fallen in the Southern Alps of New Zealand in recent decades (McSaveney 2002; Hancox et al. 2005; Cox and Allen 2009). Attempts to link an increase in alpine landslide frequency to recent climatic warming (Allen et al. 2011) are thwarted by a very incomplete observational record prior to the 1990s and knowledge that truly random

M. McSaveney (✉) • C. Massey
GNS Science, Lower Hutt, New Zealand
e-mail: m.mcsaveney@gns.cri.nz

C. Margottini et al. (eds.), *Landslide Science and Practice*, Vol. 4,
DOI 10.1007/978-3-642-31337-0_44,

Fig. 1 Winter (August 2008) aerial view of the August 2007 Young River landslide. The summit of Haunted Spur above the landslide headscarp is at 1,680 m and the valley floor below the landslide is at 480 m (above mean sea level datum). Note the presence of many steep, rocky bluffs on the side of the valley (*north facing*) from which the landslide fell (Photo: MJ McSaveney)

events must occur in clusters. More time is required to tell if we are not experiencing a random cluster.

The present study arises because although warming may be invoked for a number of alpine rockfalls in the warm summer of 2008 (Cox and Allen 2009), it was one mechanism that could be eliminated as a possible trigger for the Young River landslide which fell in late winter on a clear cold night. Herein, we discuss how we can eliminate several typical landslide trigger mechanisms, and speculate on how a clear cold night might have triggered the Young River landslide. Of course, the landslide itself destroyed all on-site physical evidence of a trigger. Our speculation is based entirely on inference.

Physical and Climatic Setting

The alpine Young River valley is cut in Haast Schist, which extends throughout the Lake Wanaka headwaters. Several strands of the Siberia fault (White 2002), a part of the north-east south-west trending Moonlight fault zone pass to either side of the landslide source juxtaposing garnet and biotite schist. White (2002) maps a pseudotachylyte outcrop in the north branch of Young River. Fragments of pseudotachylyte occur in the landslide deposit. Foliation on Haunted Spur in the vicinity of the landslide dips at about 52° NNE-NE, but does not feature as a major defect in relation to slope stability.

Some rock-mass defects in the landslide source area are aligned to the trend of the Siberia fault, but the highly fractured nature of the source area does not appear to be

Fig. 2 Location of the Young River landslide near the Main Divide of the Southern Alps in southern South Island, New Zealand, at 44° 08′ 44.6″ S, 169° 06′ 46.0″ E

because of the fault which probably is inactive. Instead, the very dilated, very closely jointed rock mass appears to be part of a large-scale Sackung feature now exposed in section in the source area, and extending both up slope and along valley. Extensive Sackungen are widespread along mountain ridges in the region (Fig. 3).

The Young River valleys formerly were glaciated, and all retain major glacial imprints of glacially steepened valley walls despite many post-glacial rockfalls. The deglaciation history is largely unknown, but the last cirque glacier probably melted from the Young River scene in the late nineteenth century. Very little snow persists from year to year around catchment summits (Fig. 4).

The true right (NNE-facing) valley wall of the north branch of Young River in the vicinity of the landslide has many steep rocky bluffs (Fig. 1). The history of previous slope instability in the area is largely unknown. The forested valley floor and river channel are littered with many large rockfall boulders. The site of the present Young River landslide deposit is known to have been a rockfall talus prior to 2007 (Fig. 3), and the now-lake floor was formerly a wide alluvial flat of gravel deposited upstream of the rockfall talus.

The volume of the new lake (~ 20.6 million m^3) was determined from pre- and post-landslide digital terrain models, and the surveyed lake level at low flow (579.7 m).

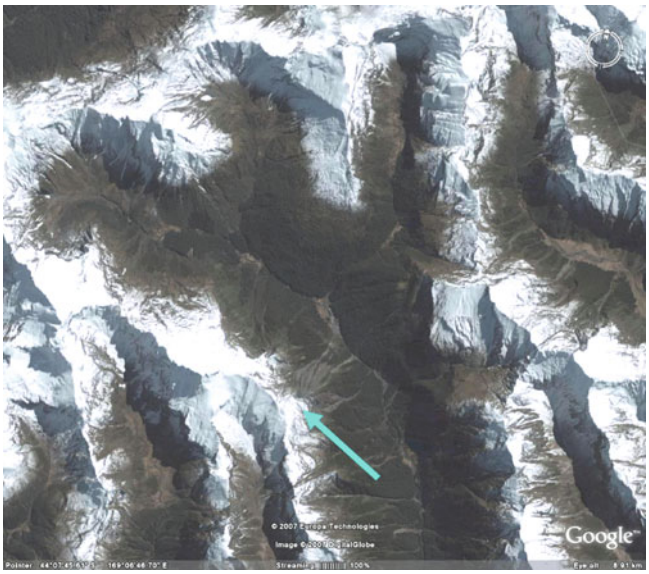

Fig. 3 Rectified satellite image of the North branch of Young River prior to the 2007 landslide (22 September 2005). *Arrow* points to the now-missing rock mass. Note the presence of rockfall talus from past instability of the slope. Note also extensive Sackung slopes in the *upper right quadrant* of the image. A similarly disrupted slope was present at the *arrow head*

Fig. 4 Aerial view of Young River landslide. Note highly fractured rock mass at the apex of source area and fine textured talus apron which overlaps onto coarse debris at toe adjacent to lake. Lobes in fine textured debris suggested that the debris was saturated when it fell on 29 August 2007. Note also minimal snow persisting in catchment headwaters in late summer (Photo: GT Hancox)

The catchment drainage area above the dam is ~ 33.9 km^2, and the lake overflowed at about 18:00 on 5 October 2007. Hence the lake took 37.6 days to fill at an average inflow of 7.1 m^3/s; this is a catchment mean runoff of 678 mm (about 18 mm/day) which is not an unusual winter runoff in this area.

The Southern Alps experience a mid-latitude, super-humid, maritime climate; precipitation is not seasonal. The headwaters of Young River can experience heavy rain or snow at any time of year. The coldest time of year is June to August. Persistent blocking anticyclones with clear skies, little wind, and severe nocturnal frosts are a common occurrence in August.

Predisposing Instability Factors

Topography and Prior History of Slope Instability

Most of the Young River drainage basin retains a strong imprint of past glacial erosion, with minimal post-glacial erosional modification. High, steep rocky bluffs abound on the north-facing side of the north branch of Young River. The Young River landslide fell from a steep slope on Haunted Spur (informal local name). The apex of the landslide headscarp is at about 1,600 m and the toe of the source area daylighted at the base of a steep bluff at about 850 m (Figs. 5 and 6). Most of the rock mass that fell appears on pre-landslide historical images (22 Sept., 2005) on Google Earth® as a highly fractured and dilated rock mass. A largely vegetated rockfall talus at the toe of the slope on the valley floor (Fig. 3) attests to prehistorical and historical slope instability on the site.

The opposing (south-facing) valley wall is demonstrably less stable than the north-facing one, but the style of landsliding there is very different. The gentler slopes on this side are formed by deep-seated rock mass creep which reaches to the valley floor.

Eliminated Triggers

Earthquake

Young River lies within a region of New Zealand with very high seismic hazard. It is frequently shaken by earthquakes associated with the nearby Puysegur subduction zone and the off-shore extension of the New Zealand Alpine fault (Reyners et al. 2003). Seismic records from around 28 to 29 August, however, are clear and unambiguous; the only significant seismic event in the region was the event (#2786576) recorded at 4:40 h on 29th August (NZST)(M_L 2.9), which is unambiguously a surface seismic event in the Young River area with the distinctive emergent spindle shape of a large avalanche (rock) (Fig. 7).

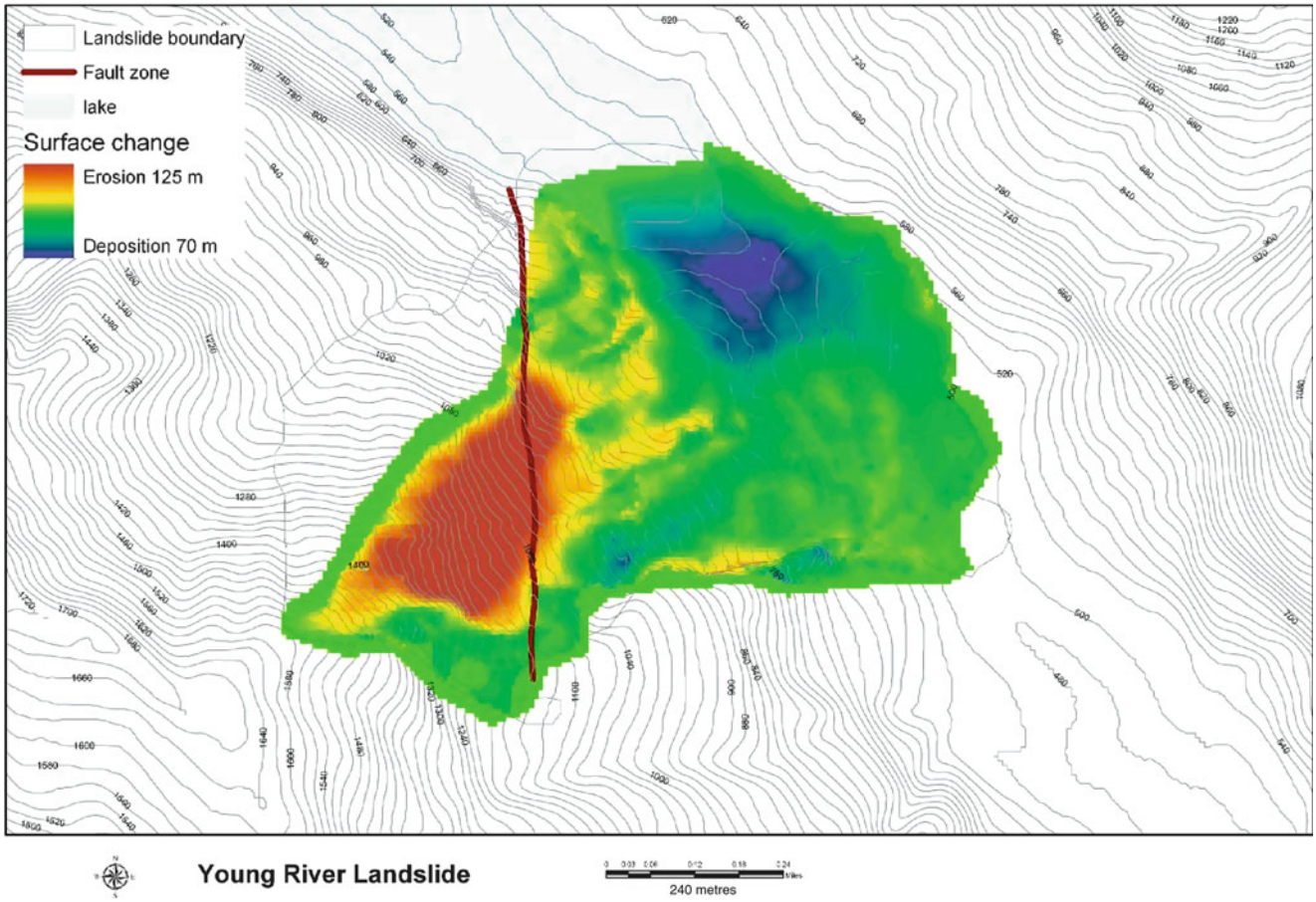

Fig. 5 Difference map of the Young River Landslide indicating a deposit volume of 11 million m^3. Pre-failure topography is from 1:50,000 Topographic Map 260-F38 (Wilken); post-failure topography is from Terrestrial laser scan surveys (Image prepared by Sam McColl). Note that the "Fault zone" is a 100-m wide zone of schist-derived cataclasite

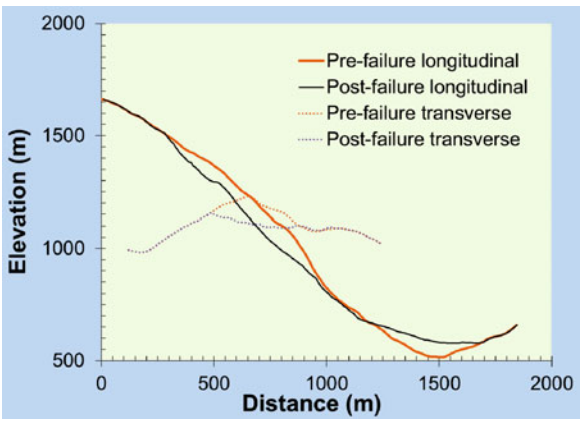

Fig. 6 Pre- and post-failure longitudinal and transverse topographic profiles of the Young River landslide. Orientation of transverse profile is NW (*left*) SE (*right*) approximately through the the section of greatest loss of mass. Note that failure took away a spur and rocky bluff, with failure daylighting at the base of the bluff

Although the source scar continued to spall minor rockfalls for months after the initial failure, the shallow (20 km) Mw 6.7 George Sound Earthquake of 15 October 2007, at a distance of about 145 km, did not trigger further significant rockfalls at Young River. The landslide source is known to have experienced moderate ground shaking in the Mw 7.2 Fiordland earthquake of 21 August 2003 when a strong-motion seismometer at Makarora (13.5 km ESE of the landslide) recorded peak ground accelerations above 0.35 m/s^2 190 km from the epicentre (Reyners et al. 2003) without initiating major rockfall from the rock buttress that failed in 2007. The upper section of the slope has always been a rockfall source and still sheds minor rockfalls into the new lake. We cannot establish that rockfalls fell from here in the earthquake of 2003, but that is a reasonable surmise. The space image of 22 Sept. 2005 establishes that nothing major fell from the site in 2003.

An earthquake did not trigger the failure in August 2007, but earthquakes (brittle tectonic deformation) certainly were involved in preparing the scene for it.

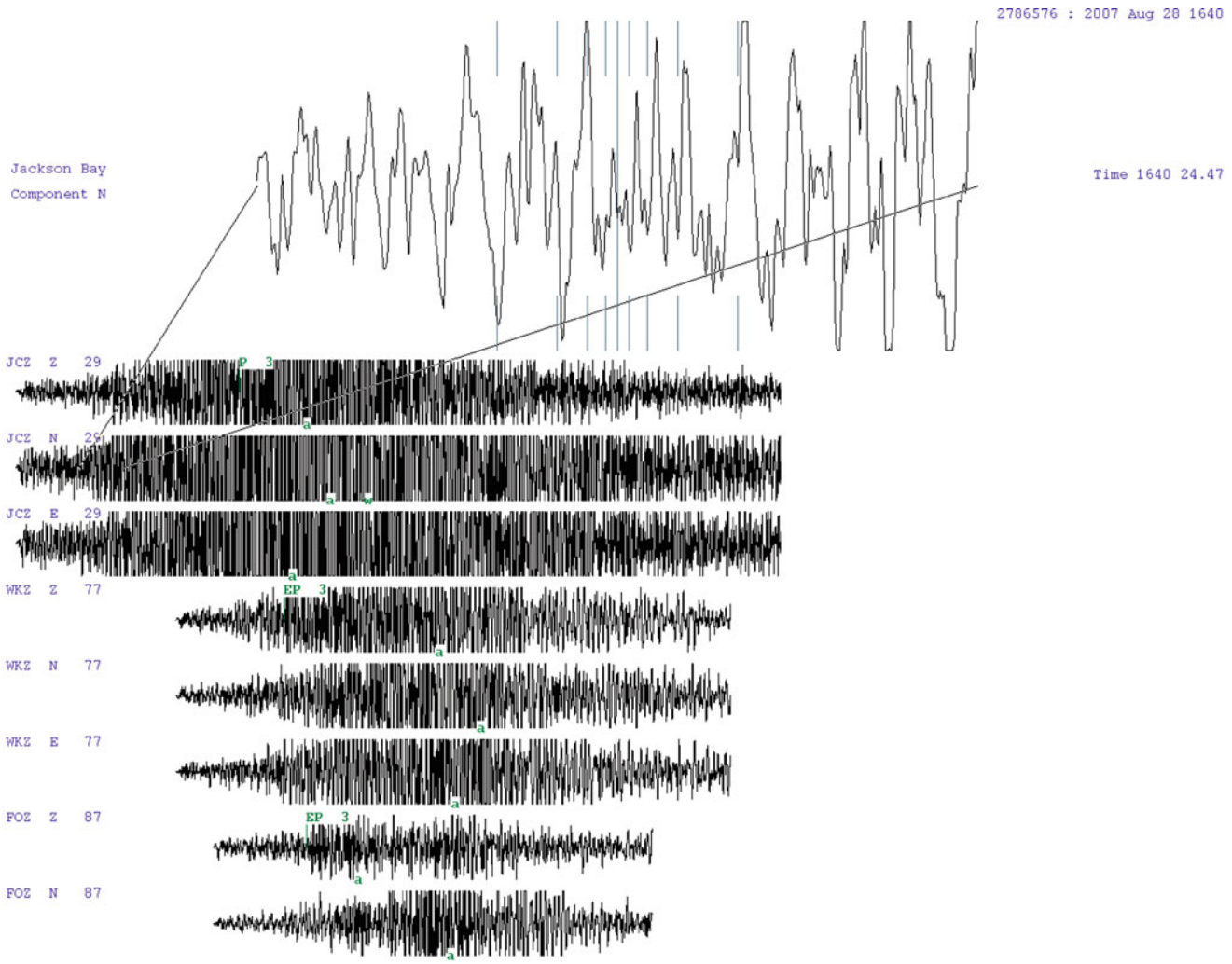

Fig. 7 Coda from selected three-component broad-band monitoring sites (JCZ = Jackson Bay, WKZ = Wanaka, and FOZ = Fox Glacier) in the New Zealand Seismological network recording the fall of the Young River landslide (Event # 2786576). Date and time are Universal Time (UT); NZST is UT + 12 h. Note: Coda are truncated at larger amplitudes for display (Data from the GeoNet Project)

Rainfall

There were no rain gauges in the Young River catchment prior to the landslide, but two automatic recording gauges nearby are in the same climatic regime; Makarora (13.5 km ESE) and Dragonfly Flat (23.5 km S) are operated by the Otago Regional Council as part of routine hydrological monitoring.

Since August 2008, a rain gauge on the Young River landslide has routinely caught about twice the rainfall recorded at Makarora, as it is closer to the Tasman Sea, source of most of the precipitation that falls on the region. There are very steep precipitation gradients across the Otago region, rising from less than 500 mm per year in Central Otago, to over 5,000 mm around the Main Divide of the Southern Alps (to over 10,000 mm per year in the Western Southern Alps).

The nearly 187 mm of rain in 70 h at Dragonfly Flat on 9th–11th August (Fig. 8) is unexceptional for the area. As much, or more precipitation would have fallen on the landslide source area, mostly as "warm" rain on a melting winter snowpack, although the storm must have ended with snow at Young River, followed by clear cold weather (Fig. 9).

No significant precipitation fell in the region in the 18 days prior to the landslide (Fig. 8), due to a very stable "blocking" anticyclone over South Island. We infer that the Young River landslide was not triggered by heavy rain or snowfall.

Inferred Trigger

Pore-Pressure Change

Although rainfall can be eliminated as a possible trigger of the Young River landslide, the rainfall records provided us with the first suggestion of another weather-related process

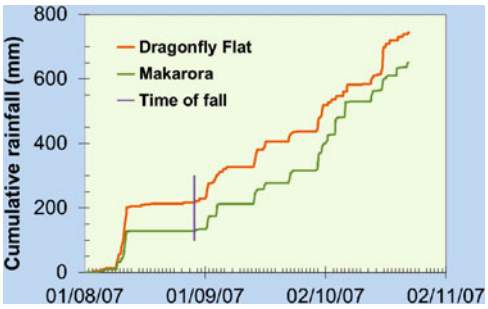

Fig. 8 Cumulative hourly rainfall at the two closest recording rain gauges (Dragonfly Flat and Makarora). Minor August "rainfall" at Dragonfly Flat occurs at similar times (9:00–11:00) on a number of August mornings and likely represents thawing of hoar when direct sunlight reaches the automatic rain gauge. This interpretation is consistent with our interpretation that the night of 28–29 August was clear and very cold in the vicinity of springs fed by groundwater draining from within the rock mass of the landslide source area at Young River

capable of changing pore-water pressure within the source rock mass of the landslide. The evidence is the lack of significant recorded precipitation. Few areas of New Zealand are so cold that they do not experience winter rain, and so 18 days with no measured precipitation was seen as an indicator of a stable anticyclone over southern New Zealand, which was confirmed from other weather records.

Daily temperatures at the closest full climatological station to the landslide (Wanaka Airport, 345 m asl, 65 km S) show a large diurnal range with ground frost on most nights (Fig. 9). The night of 28th–29th August had the largest diurnal temperature range for the winter of 2007 at Wanaka Airport. It is not realistic to extrapolate temperatures from Wanaka Airport to Haunted Spur in the Young River catchment because the airport region is affected by a very strong temperature inversion on still winter nights, and the steep slopes of Haunted Spur are not. Nevertheless, it is reasonable to infer that the area was at about 5 °C colder, and that the heat flux from the bare rock on the mountain slope that night was abnormally negative, radiating through clear dry air to deep space. With radiation cooling, minimum temperatures are commonly experienced an hour or so before dawn, before sunlight begins to warm the outer atmosphere above the site.

We do not invoke significant freezing of groundwater to affect pore-water pressure within the granular materials of the landslide source, because the thermal conductivity of the rock materials is too low for the low temperature of the night to have penetrated to any significant soil depth. Instead, we suggest that freezing of water at springs on the rocky bluff was gradually blocking outflow. Since any spring outflow would have been advecting heat from the interior of the spur, we reason that on the night of the failure, the recession curve from the 9th–11th August rainfall had reduced the advective heat flux from the interior to lower than the radiative heat flux to free space,

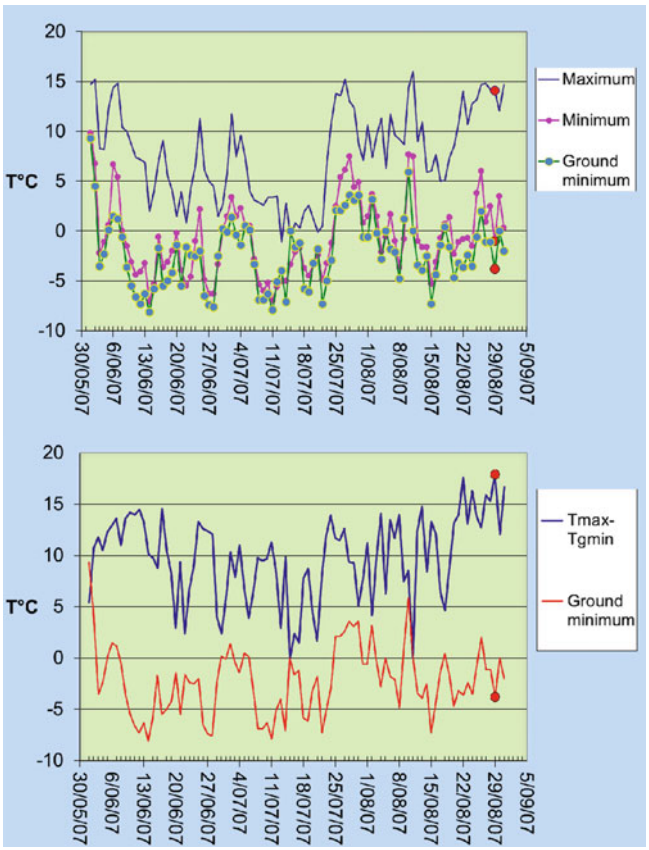

Fig. 9 Maximum, minimum, and ground-surface temperatures at Wanaka Airport (345 m asl). Red dots mark values recorded at 9:00 am, 29th August 2007. Note the large diurnal temperature range of 17.9 °C (T_{max}-T_{gmin}) indicating high radiation losses during the night. Note also the maximum temperature spike for 10th August supporting rain at Young River. Plunging temperature on 11th August indicate that the event ended in snow followed by clear cold weather

allowing the spring outflow to reduce significantly as the spring became increasingly sealed by ice formation. The scenario then is that continuing groundwater flow raises the water table in the rock mass behind the rocky bluff. The rising water table then encounters sub-freezing rock and is unable to find an exit. As the phreatic surface behind the frozen spring flattens, the pore-water pressure in the most stressed and least stable portion of the potential landslide mass rises, until slope failure is induced (Fig. 10).

We infer that the failure of the Young River landslide released a substantial groundwater reservoir because the fine-textured landslide deposit (rockfall talus) that reaches the lake in Fig. 4 appears to have been cohesive when it fell, flowing as a series of wet lobes to overlap coarser debris. It should be noted, however, that the landslide was not discovered until more than 3 weeks after it fell, and substantial rain had fallen on it by then.

The above freezing scenario can reasonably be expected to have repeated often on this slope, possibly several times

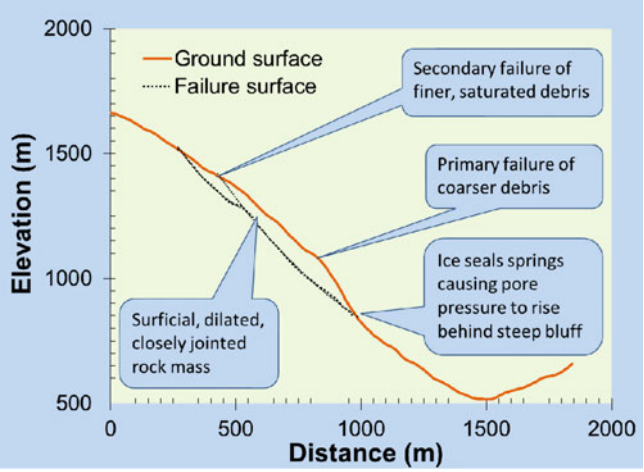

Fig. 10 Our interpretation is that on the clear cold night of 28–29 August springs at the base of the mid-slope bluff froze, causing pore-water pressure to rise in the rock mass at the base of the bluff where a reduction in frictional resistance in the rock mass could have maximum effect in destabilising the slope

each winter, but previously without causing failure. Three varying factors have to coincide to cause failure. The advective heat flux from the interior has to reduce to be less than the radiative heat flux to free space, and the factor of safety of the slope has to have diminished over time (through any cause including static fatigue) to a value that allowed a relatively small rise in pore-water pressure to trigger failure.

We can only speculate that such a scenario could have triggered the landslide, because any direct evidence was destroyed in the landslide. Given that the stability of the slope must have been marginal for some time before 29th August 2007, and that static-fatigue cracking accelerates as the moment of failure approaches, we infer that the probability of the above scenario, or of any other scenario triggering the Young River landslide was increasing relatively rapidly, and that static fatigue alone could have triggered failure if no other trigger had intervened. Indeed, we cannot eliminate static fatigue as the true trigger. Perhaps the weather at the time of fall was pure coincidence.

Conclusions

The Young River landslide fell at 4:40 h on a clear cold night in late winter after several weeks without precipitation. The only recorded seismic disturbance was that of the failing rock mass. The landslide could not have been triggered by an earthquake, by precipitation or by thawing permafrost. We speculate that the trigger was rising pore-water pressure behind frozen springs. The evidence for this is entirely circumstantial, as all physical evidence was destroyed in the failure, and the landslide was not discovered until 3 weeks after it fell.

Acknowledgments This research was supported by the New Zealand Public Good Science Fund. We acknowledge the New Zealand GeoNet project and its sponsors EQC, GNS Science and LINZ, for providing the seismic data used in this study. Hydrological data was provided by the Otago Regional Council. Temperature data were from the National Water and Atmospheric Research Institute (NIWA).

References

Allen SK, Cox SC, Owens IF (2011) Rock avalanches and other landslides in the central Southern Alps of New Zealand: a regional study considering possible climate change impacts. Landslides 8:33–48

Cox SC, Allen SK (2009) Vampire rock avalanches of January 2008 and 2003, Southern Alps, New Zealand. Landslides 6:161–166

Hancox GT, McSaveney MJ, Manville VR, Davies TR (2005) The October 1999 Mt Adams rock avalanche and subsequent landslide dam-break flood and effects in Poerua River, Westland, New Zealand. NZ J Geol Geophys 48:683–705

McSaveney MJ (2002) Recent rock falls and rock avalanches in Mount Cook National Park, New Zealand. Geol Soc Am Rev Eng Geol XV:35–70

Reyners M, McGinty P, Cox S, Turnbull I, O'Neill T, Gledhill K, Hancox G, Beavan J, Matheson D, McVerry G, Cousins J, Zhao J, Cowan H, Caldwell G, Bennie S, the GeoNet team (2003) The MW 7.2 Fiordland earthquake of August 21, 2003: background and preliminary results. Bull NZ Nat Soc Earthq Eng 36:233–248

White SR (2002) The Siberia Fault Zone, northwest Otago, and kinematics of mid-Cenozoic plate boundary deformation in southern New Zealand. NZ J Geol Geophys 45:271–287

Soil Sliding in Continuous Permafrost Terrain of Siberia: The Case Study of Soil Respiration and Soil Microbial Activity Dynamics During Ecosystem Re-establishment

Oxana Masyagina, Svetlana Evgrafova, Stanislav Prokushkin, and Anatolii Prokushkin

Abstract

In forested ecosystems developed on permafrost, solifluction processes are widespread, occur in years of above average summer-autumn precipitation and can cover up to 20 % of total area of slopes adjacent to rivers. This process is the most destructive natural disturbance event resulting in complete disappearance of initial ecosystems (vegetation cover and soil). To analyze postsliding ecosystem succession, sites of two ages (5 and 35 years old) after solifluction were chosen along with Nizhnyaya (Lower) Tunguska River valley. Results show that regeneration of soil respiration and eco-physiological status of microbial communities in soil during postsolifluction succession starts with vegetation re-establishment. As long as ecosystems regenerate, accumulated litter contains the main pool of microorganisms, though microbial biomass of 35-year-old solifluction area does not reach the value of microbial biomass in control plots. Therefore, forested ecosystems in permafrost zone after landsliding requires decades for final successful restoration of soil respiration and the microbial community.

Keywords

Landslide • Permafrost • Soil respiration • Microbial respiration • Boreal ecosystems • Siberia

Introduction

Solifluction or landsliding is one of the main destabilizing factors in boreal forest ecosystems. Its dramatic effect on the forest vegetation of the Siberian permafrost region can be considered on a similar level with forest fires and cuttings. However, solifluction processes, in contrast to forest fires and harvesting, result in the full destruction of initial ecosystems. During solifluction, sliding of an active layer of soil (together with vegetation) occurs on a rupture surface of permafrost under the soil. Thus, ecosystem development starts on parent material. New ecological conditions at postsolifluction areas lead to changes in species composition as well as soil respiration fluctuations and soil microbial associations. The most widespread landslide type in the Siberian permafrost region near Yenisei River is differential solifluction (at slopes with middle steepness of 8–15° and more), characterized by slow, fast and sometimes catastrophic land sliding events with groove formation (Gigarev 1967). Soil sliding events usually occur on the slopes with the thickest active layers (e.g., south and west slopes). Forest fires, overwetting of seasonally thawed layers, excessive precipitation in summer, or intensive nival thawing can be the main causess of solifluction events. In river valleys, landsliding is an important landscape forming factor (Abaimov 1997; Katina 1965; Pozdnyakov 1986). At present, the development and consequences of solifluction processes and soil-vegetation regeneration patterns attracts little scientific attention.

Various heterogeneous conditions (microclimatic and edaphic) are at play on a landslide, especially on permafrost

O. Masyagina (✉) • S. Evgrafova • S. Prokushkin • A. Prokushkin
Siberian Branch, V.N. Sukachev Institute of Forest, Russian Academy of Sciences, Akademgorodok 50/28, Krasnoyarsk, Russia
e-mail: oxanamas@ksc.krasn.ru

C. Margottini et al. (eds.), *Landslide Science and Practice*, Vol. 4,
DOI 10.1007/978-3-642-31337-0_45,

Fig. 1 Cross section profile of 2001-solifluction site (S2001) in the middle part of slope: *we* and *ee* – western edge and eastern edge, *m* – alluvial bare ground, *s* – temporal stream bed

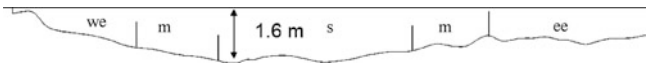

Fig. 2 Cross section profile of 1972-solifluction site (S1972) in the middle part of slope: *we* and *ee* – western edge and eastern edge, *m* – alluvial bare ground, *s* – temporal stream bed

soils; pH, biogenic elements (N, P, K, Ca) and carbon contents decrease, sharp changes of C:N occur especially on alluvial bare ground. All these factors initialize the first phase of regenerative succession for newly forming biogeocenosis. Therefore soil microbial activity, vegetation regeneration and soil respiration are highly variable at different microsites (e.g. depending on microrelief).

In this research, we attempt to assess how ecological conditions formed after solifluction influence soil respiration and microbial activity.

Objects and Methods

We have selected two solifluction sites of different age on south-east-facing slopes in a valley of Nizhnyaya (Lower) Tunguska River (64° N, 100° E) as described in Bugaenko et al. (2005). One site was destroyed by landsliding in 2001 (S2001, Fig. 1), another in 1972 (S1972, Fig. 2). The total areas affected (zone of depletion and accumulation) is about 11,200 m^2 for S2001 and 5,700 m^2 for S1972 (Table 1). Our surveys have been conducted in the mid slope position on the postsolifluction landslides. The chosen zones are characterized by different forest types, amount of mineral and organic matter and ecological conditions and described elsewhere (Prokushkin et al. 2010). Both sites are characterized by successful regeneration by Gmelin larch (*Larix gmelinii* (Rupr.) Rupr.) (Fig. 3).

In the middle part of slope, western and eastern edges, representing soil-vegetation complexes between the edge of solifluction site and undamaged forest, and central part (bare ground) have been selected along with the direction of solifluction progressive movement. Under solifluction impact, edges and central zones have been drastically changed by concentration of nutrients and ecological conditions (Prokushkin et al. 2010). Undamaged forests neighbouring solifluction sites of 2001 and 1972 were used as a control sites to estimate the effect of soil sliding on ecosystem processes.

Table 1 Site characteristic

Parameter	S2001	S1972
Date of solifluction event	2001	1972
Prescription of disturbance on the moment of 2007, years	6	35
Slope, °	19–27	11–20
Slope length, m	390	290
Maximal width of a site, m	33	37
Minimal width of a site, m	12	7
Site area, m^2	11,200	5,700
Withdrawal soil volume, m^3	5,365	3,725

Fig. 3 2001- (S2001) and 1972-solifluction site (S1972) in 2007 (Photo by Masyagina O.V.)

In the middle part of the slope both in solifluction and control sites, soil temperature at 5 cm depth was measured in the afternoon every 3–5 days in July of 2005–2007. Water content was measured at 10 cm depth in July of 2006–2007.

To assess how soil sliding affects ecosystem re-establishment, CO_2 emission from soil surface, soil heterotrophic respiration (basal respiration, BR) and soil microbial biomass in the mineral soil layer (0–10 cm) have been

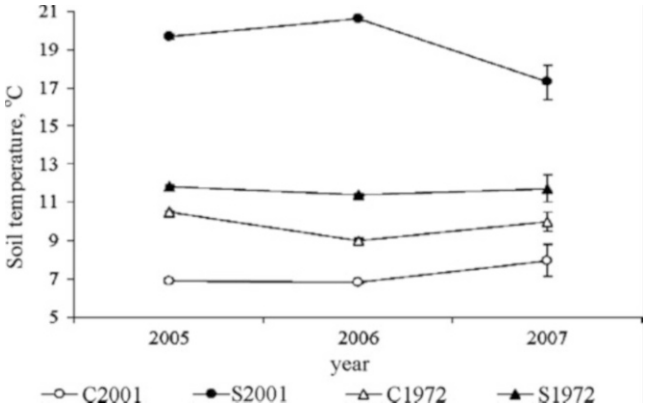

Fig. 4 July average soil temperature at 5 cm depth at 2001-solifluction, 1972-solifluction and control sites

Table 2 Soil temperature at 5 cm depth (°C) at microsites in July 2007

Microsite type	2001-solifluction site	1972-solifluction site
Bare ground	19.5	12.1
Eastern edge	16.2	12.9
Western edge	16.1	10.0
Control site	8.0	10.0

measured. Soil respiration rates were measured at subplots on the base of 3–5 replications with Li-Cor 6200 (LI-COR, USA) at solifluction and control sites. In parallel, soil temperature and water content were measured at 5 cm depth, and height of vegetation cover and litter was determined.

Soil heterotrophic microbial biomass (Cmic, mg C g soil^{-1}) was assessed with kinetic method implying soil microbiota substrate-induced respiration (SIR, mg CO2-C g soil^{-1} h^{-1}) determination with subsequent recalculation on carbon of microbial biomass basis, C-CO_2 according to (1) (Sparling 1995).

$$C_{mic} = 50.4 \times SIR \quad (1)$$

At the same time, basal respiration (BR) of soil microorganisms as a CO2 emission rate in 24 h of soil incubation at 22 °C and 60 % of soil water capacity has been studied. Coefficient of microbial activity qCO2 was calculated with the (2) (μgCO2-C mg−1Cmic h−1).

$$\frac{BR}{C_{mic}} = qCO_2 \quad (2)$$

Results and Discussion

Three-year research of temperature regime (at 5 cm depth) revealed increased soil temperature at solifluction sites comparing to control sites (Fig. 4). Moreover, at 2001-solifluction site of initial successional stage soil temperature two to three times higher than that of control site. Such a big difference, first of all, results from the lack of tree cover. Soil temperature differences between the 1972-solifluction site and respective control site were much less – about 1–2°°C, which points possibly to the final successional stage.

Soil temperature at microsites (bare ground, western and eastern edges) has been registered in July 2007 (Table 2). According to data, at 2001-solifluction site maximal soil temperature was at bare ground, whereas at 1972-

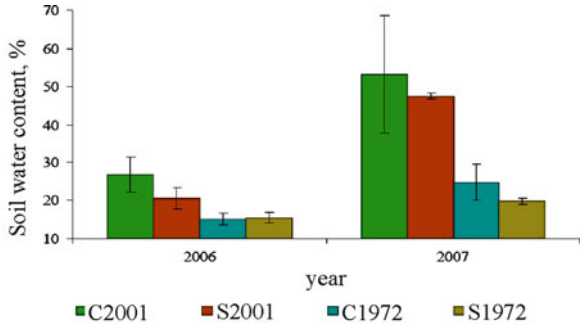

Fig. 5 Soil water content at 5 cm depth at 2001-solifluction, 1972-solifuction and control sites in July

Table 3 Plant association characteristics at initial state and its dynamics during succession in July 2006 (Bugaenko et al. 2005)

Site	Number of species	Vegetation type		
		Vascular plants	Mosses	Lichens
Control site of 2001-solifluction site	26	18	6	2
2001-solifluction site	30	27	3	0
Control site of 1972-solifluction site	26	11	9	6
1972-solifluction site	26	16	6	4

Table 4 Soil respiration and height of vegetation cover and litter at solifluction and control sites

Site	Respiration rate, μmol CO_2 m^{-2} s^{-1}	Height of vegetation cover and litter, cm
Control site of 2001-solifluction site	6.3 ± 0.2	8.5 ± 1.3
2001-solifluction site	5.8 ± 1.4	1.1 ± 0.6
Control site of 1972-solifluction site	11.8 ± 0.2	5.3 ± 1.4
1972-solifluction site	13.8 ± 0.9	5.7 ± 0.9

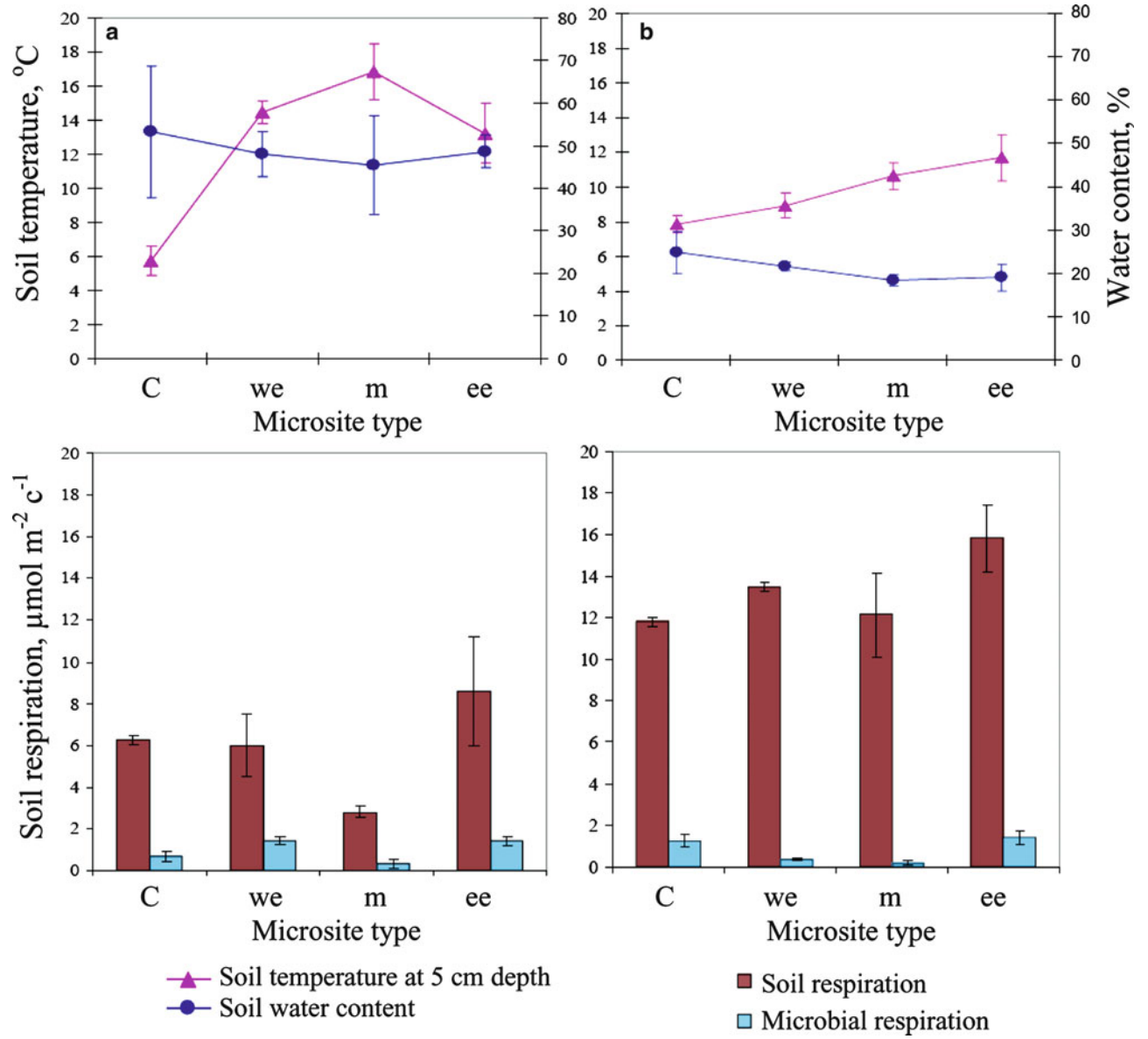

Fig. 6 Hydrothermal conditions, soil and microbial respiration at 2001-solifluction (**a**) and 1972-solifuction (**b**) sites. *C* – control site, *ee* – eastern edge, *m* – bare ground, *we* – western edge

Table 5 Microbial respiration contribution (%) in total carbon dioxide emission from soil surface

Microrelief type	2001-solifluction	1972-solifluction
Control site	11	11
Western edge	24	2
Bare ground	12	1
Eastern edge	17	9

solifluction site soil temperature did not differ among solifluction microsites and control site.

Soil water content is one of the most important ecological factors influencing regeneration of disturbed ecosystem. Our research revealed lower values of water content at solifluction sites comparing to control sites (Fig. 5). Though the differences were insignificant, as Fig. 5 shows, water content at control site was 1.1–1.3 times higher then that of 2001-solifluction site. Between older solifluction site (of 1972) and control site, the differences in water content were minimal.

Thus, ecological conditions of solifluction sites were sharply different among types of microsites as well as control sites and were dependent on prescription of land sliding disturbance. Ecological conditions formed at solifluction microsites affected regeneration processes of newly establishing forest in different ways: on the one hand, wood species (larch and *Dushekia*) regeneration occurred during

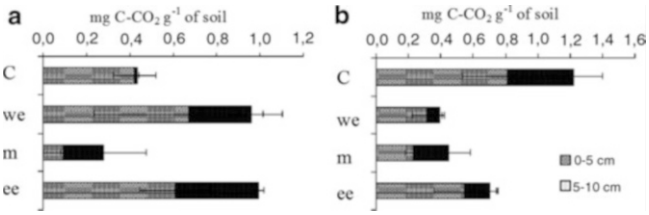

Fig. 7 Microbial biomass in mineral soil at 2001-solifluction (**a**) and 1972-solifuction (**b**) sites. *C* – control site, *ee* – eastern edge, *m* – bare ground, *we* – western edge

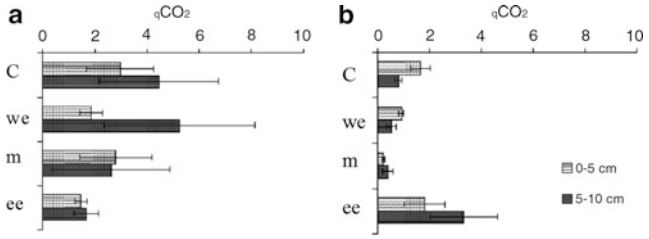

Fig. 8 Coefficients of microbiological activity (qCO_2) in mineral soil at 2001-solifluction (**a**) and 1972-solifuction (**b**) sites. *C* – control site, *ee* – eastern edge, *m* – bare ground, *we* – western edge

postsolifluction period, on the other hand, unrepresentative live vegetation cover for native larch stands have formed.

There were also important differences in vegetation cover. The control larch stand was characterized by an understory of *Ledum*-crowberry-green mosses larch stand with undergrowth *Duschekia fruticosa* (Rupr.) Pouzar. was dominated (Table 3). Four vegetation cover association types were found after 3 years of successional regeneration at 2001-solifluction site (Bugaenko et al. 2005). Vegetation biodiversity at 2001-solifluction site was higher than that of control site: at solifluction site, there were found 27 species of vascular plant, whereas at control – only 18. Concerning moss species there was reverse situation: at solifluction site there were three moss species and at control site – 8. Similar tendencies on species biodiversity were found at the 1972-solifluction site, but differences between solifluction and control were not so pronounced especially regarding to species composition of mosses and lichens. Thus, 16 species of vascular plants were found at 1972-solifluction and this value is 1.5 times higher then that of control. Number of species of mosses and lichens at 1972-solifluction site was 1.5 times lower then that of control (Table 3).

Counting of regrowth amount and seedlings of *Larix gmelinii* (Rupr.) Rupr. and other wood species showed that at 2001-solifluction their amount is 3.5 times higher (2,744 stems per ha) than that of 1972-solifluction site (626 stems per ha) (Bugaenko et al. 2005).

Soil respiration measurements showed that its value was significantly higher at 1972-solifluction site than that of 2001-solifluction site as well as control sites (Table 4). Thus, soil respiration at "old" solifluction and its control site was about 11.8–13.8 μmol CO2 m^{-2} S^{-1}, whereas in "young" solifluction and its control site was much lower (5.8–6.3 CO2 m^{-2} S^{-1}). Concerning changes of height of vegetation cover and litter (Table 4) after landsliding event, its values at 1972-solifluction and control sites are comparable, whereas in 2001-solifluction and its control there is an eight times difference between values, that indicates the disturbance of ecosystem. Respiration rate at 2001-solifluction site was lower then that of control site due to vegetation cover disturbance or its disappearance at some places.

Microrelief is a factor that intensifies variation of the studied parameters, especially soil temperature and water content. Soil temperature and water content at 2001-solifluction varied depending on microrelief type (Fig. 6) which is in contrast with 1972-solifluction pattern of these factors. Moreover, at 1972-solifluction site values of soil respiration between microrelief types did not differ and were very close to control site (Fig. 6). Whereas at young solifluction site (of 2001) there was high variation of CO2 emission between microrelief types: maximal soil respiration was at eastern edge (8.6 CO2 M^{-2} c^{-1}) and minimal – at bare ground (2.8 μmol CO2 M^{-2} c^{-1}).

At control sites of solifluction of different age, contribution of microbial respiration in total soil CO_2 emission occurred to be the same – about 11 % (Table 5). At younger solifluction site (of 2001), this value is higher then that at control site, especially at edges (about two times higher). At the older solifluction site, on the contrary, microbial respiration contribution was lower than that of control site. Low contributions of microbial respiration at the older site was due to low soil microbial biomass; possibly, the main contribution to soil CO2 emission was due to physical diffusion of CO2 from the soil at this site.

Microbial biomass (MB) measurements in mineral soil layers of different age solifluction and control sites revealed that microbial biomass at control site of 2001-solifluction is located mainly (up to 80 %) in 0–5 cm layer. Whereas at 2001-solifluction its value at 0–5 cm layer was much lower (about 30–60 %) and widely varied depending on disturbance degree: maximum at edges and minimum at bare ground (Fig. 7a). Total microbial biomass at 2001-solifluction is higher, than that of control due to changed ecological conditions and enhanced substrate availability after event. At 1972-solifluction total microbial biomass is lower than that of control. Moreover, its value at bare ground at 1972-solifluction site was comparable to values at edges, which indicates gradual regeneration of microbiota in mineral soil.

One of the main parameter of eco-physiological status of microbial population is coefficient of microbiological activity qCO2 that is varying in the range of 1.0 at normal conditions. Therefore, its deviation from 1.0 points to disturbance of normal functioning of soil microbiota. Analysis of coefficient of microbiological activity values revealed intensive disturbance of microflora functioning at western edge

and bare ground at 2001-solifluction site (Fig. 8a), and at eastern edge and bare ground of 1972-solifluction site (Fig. 8b). The degree of disturbance of soil microbiota is much lower at the 1972-solifluction site than that of the 2001-solifluction site. So, the restoration of eco-physiological status of microflora at solifluction sites is very slow.

Conclusion

Microecological conditions developed at the initial phase of postsolifluction succession are far different from those in undisturbed stands. Spatially they are also very heterogeneous at landsliding sites. The extreme conditions for vegetation regeneration are formed on bare ground. High variation of hydrothermal conditions at the younger solifluction site resulted in increasing of soil respiration variation. Also at the initial phase of postsolifluction succession there was bigger microbial biomass as well as microbial respiration contribution compare to control or the older solifluction site (of 1972).

At the 35-year old solifluction site, hydrothermal conditions were very close to control conditions. Soil respiration and microbial respiration contribution here are comparable to control site, however microbial biomass is higher at 1972-solifluction site than that of control. The coefficient of microbiological activity qCO2 points on stabilization of microbial association at the 1972-solifluction site and approaches control site conditions, except for eastern edge plots.

Results showed that in permafrost conditions of Central Evenkia it is necessary to at least 35 years for larch stands to regenerate to control state after solifluction events.

Acknowledgments Research was supported by Russian Foundation for Basic Research (RFBR) (grants 11-04-01884-, 11-05-00374-, 10-04-01003).

References

Abaimov AP (1997) Larch forests and open woodlands of Siberian North (Diversity, ecological and forest development traits). DB thesis, Central Siberian Botanical Garden of the Siberian Branch of the Russian, Novosibirsk

Bugaenko TN, Oreshenko DA, Shkikunov VG (2005) Regeneration of forest vegetation after solifluction events in permafrost region. In: Proceedings of young scientists conference on studies on components of Siberia forest ecosystems, Krasnoyarsk, 21–22 March 2005, pp 12–14

Gigarev LA (1967) Reasons and mechanisms of solifluction development. Nauka, Moscow

Katina TN (1965) Cryogenic slope processis. Nauka, Moscow, p 296

Pozdnyakov LK (1986) Permafrost forest science. Nauka, Novosibirsk, p 191

Prokushkin SG, Bugaenko TN, Prokushkin AS, Shkikunov VG (2010) Succession-driven transformation of plant and soil cover on solifluction sites in the permafrost zone of Central Evenkia. Biol Bull 1:80–88

Sparling GT (1995) The substrate-induced respiration method. In: Alef K, Nannipieri P (eds). Methods in applied soil microbiology and biochemistry Academic Press, London, pp 397–404

Detecting Potential Climate Signals in Large Slope Failures in Cold Mountain Regions

Christian Huggel, Simon Allen, John J. Clague, Luzia Fischer, Oliver Korup, and Demian Schneider

Abstract

Concern and interest are rising that climate change may have an adverse impact on slope stability in mountain regions. Rock slopes in high mountain areas with glaciers and permafrost are particularly sensitive to atmospheric warming. In fact, several large rock slope failures have been observed in high mountain areas around the world in recent years. However, the detection of changes in the frequency or magnitude of such slope failures is fraught with a number of difficulties and has only recently been addressed. Here we outline several approaches that could be used to detect a change in high mountain slope failure activity. Rather than present research results, we provide a conceptual design of how research in this field could be strengthened.

Keywords

Slope failure • Climate change • Detection and attribution

Introduction

Rock slope failures span a wide range of sizes from tens of cubic meters to many cubic kilometers. Depending on magnitude, location, fall or flow dynamics and runout, rock slope failures may pose significant hazards in mountain regions. Small- to medium-size slope failures (<100,000 m^3) commonly have small areas of impact but still can be destructive, for example where ski or other tourism infrastructure is affected. Large rock slope failures (up to tens of millions m^3) may evolve into rock avalanches with long runout distances (Legros 2002), and, consequently, more damage potential. In populated mountain valleys, towns may be impacted or even completely destroyed. Furthermore, process cascades can considerably increase the reach of damage, for example when a landslide enters high mountain lakes, triggering far-reaching lake outburst floods (Clague and Evans 2000).

Small rock slope failures have been regularly observed over historic time and are well known landslide processes to local residents and authorities. Large slope failures, however, are rare and generally are a poorly appreciated hazard. Due to their relatively low probability and large size, and related uncertainties over causes and triggers, large landslides pose challenges to researchers and to public authorities charged with managing associated hazards and risks.

In this context a fundamental problem that has arisen in recent years are potential changes in hazards due to (anthropogenic) climate change or other transient drivers. From a risk management perspective there are two aspects of concern: (1) robust detection of changes in mountain slope

C. Huggel (✉) • D. Schneider
Department of Geography, University of Zurich, Winterthurerstr. 190, Zurich CH-8057, Switzerland
e-mail: christian.hugggel@geo.uzh.ch

S. Allen
Climate and Environmental Physics, University of Bern, Bern, Switzerland

J.J. Clague
Department of Earth Sciences, Simon Fraser University, Vancouver, BC, Canada

L. Fischer
Geological Survey of Norway (NGU), Trondheim, Norway

O. Korup
Earth and Environmental Sciences, Potsdam University, Potsdam, Germany

C. Margottini et al. (eds.), *Landslide Science and Practice*, Vol. 4,
DOI 10.1007/978-3-642-31337-0_46,

stability, both in the past and in the future, and (2) development of risk management strategies that adequately consider changes in hazards.

In climate sciences, as defined in the IPCC Assessment Reports, 'detection' is the process of demonstrating that climate has changed in some defined statistical sense, without providing a reason for that change, whereas 'attribution' establishes the most likely causes for the detected change with some defined level of confidence (Hegerl et al. 2007). Research on detection and attribution is rooted in the field of physical climate sciences, but is now becoming increasingly important in impact studies as well (Rosenzweig et al. 2008). A recent IPCC report distinguishes different methods of attribution to climate change, including single-step and multi-step attribution that explicitly model the response of a system or variable to an external forcing and drivers, such as increased greenhouse gas emissions and related temperature increase (IPCC 2010). Single- and multi-step attribution studies of climate change impact are difficult to achieve due to incomplete understanding of how systems respond to climate change and the many confounding factors that complicate the response. Nevertheless, Pall et al. (2011) have recently successfully applied a multi-step approach for flood risks in the UK. More common in the field of climate change impacts is an associative pattern approach, where spatial patterns of observed impacts are compared with observed climate trends using statistics on large numbers of data series (Rosenzweig et al. 2008).

In the case of landslide research, detection and attribution to climate change is in its infancy. Reasons include a traditionally strong focus on geologic and geomorphologic aspects of landslides, lag effects with respect to contemporary climate change, and the general difficulty of detecting changes in landslide occurrence and its relation to climate change. Nevertheless, the response of alpine rock slopes to glacier downwasting has a longer history of scientific interest. It has been found that rock slope failure may result from slope steepening by glacial erosion and unloading or debuttressing due to glacier retreat (O'Connor and Costa 1993; Augustinus 1995). Ballantyne (2002) suggests that a rock slope may respond to glacier downwasting by failing in (1) large rock avalanches, (2) large-scale, progressive, yet slow rock mass deformation, and (3) frequent rock fall. Furthermore, it has been recognized that warming and thawing of permafrost can have an effect on the stability of steep rock slopes. Reduction of shear strength in ice-filled clefts due to thawing permafrost (Davies et al. 2001), water infiltration and advective heat transport processes in cleft systems (Gruber and Haeberli 2007), or thickening of the active layer (Gruber et al. 2004) are among the identified slope destabilization processes associated with climate change and permafrost. At shorter time scales, it has recently been demonstrated that particularly warm periods days and weeks prior to large slope failures likely affect slope stability (Huggel et al. 2010).

Here we present a conceptual model for five different approaches that can be used to rigorously detect changes in high-mountain rock slope failures in relation to climate change: (1) event inventories, (2) damage and loss data, (3) case studies, (4) causative and trigger factors, and (5) process models simulating climate change impact chains. The model provides a possible avenue for attribution studies. Each approach is briefly described, and existing studies reviewed to the degree they exist. Unfortunately, in many instances relevant studies applicable to high mountain slope failures do not exist. However, analogues from related research fields can be useful in providing guidance for future studies in high mountain environments.

Detection and Attribution Approaches

Slope Failure Inventories

Inventories of rock slope failures and other landslides provide data that are required to document change in the frequency or magnitude of events. Several difficulties have to be overcome, however, to detect any significant change over time. The source of documented events differs over long periods of time. Evidence of Holocene landslides generally derives from deposits identified in the field, whereas recent landslides, decades to centuries before present, can be documented from historic sources, media and scientific reports. The level of documentation has typically not been the same over the historic period; documentation becomes increasingly complete with time, which must be considered to avoid deriving erroneous trends. Small- and medium-size rock slope failures show a strong increasing trend of documentation for about the past two decades (Fischer et al. subm.).

A reasonable approach to avoid this documentation bias is to focus on large (>100,000 m^3) slope failures that can be assumed to be documented with higher consistency over the past 100 years in populated mountain regions such as the Alps in Europe. Alternatively, in remote mountain regions, archived aerial and satellite imagery can be used to retrospectively observe and map larger slope failure deposits (e.g., Allen et al. 2011). Geertsema et al. (2006) for instance analyzed 38 large landslides in rock and soil and found an increase from 1.3 to 2.3 landslides per year over 30 years, although the relation to potential effects of climate change over that period has not yet been clarified. There has also been a strong increase in the number of rock slope failures from glacial and periglacial areas in the Swiss Alps and

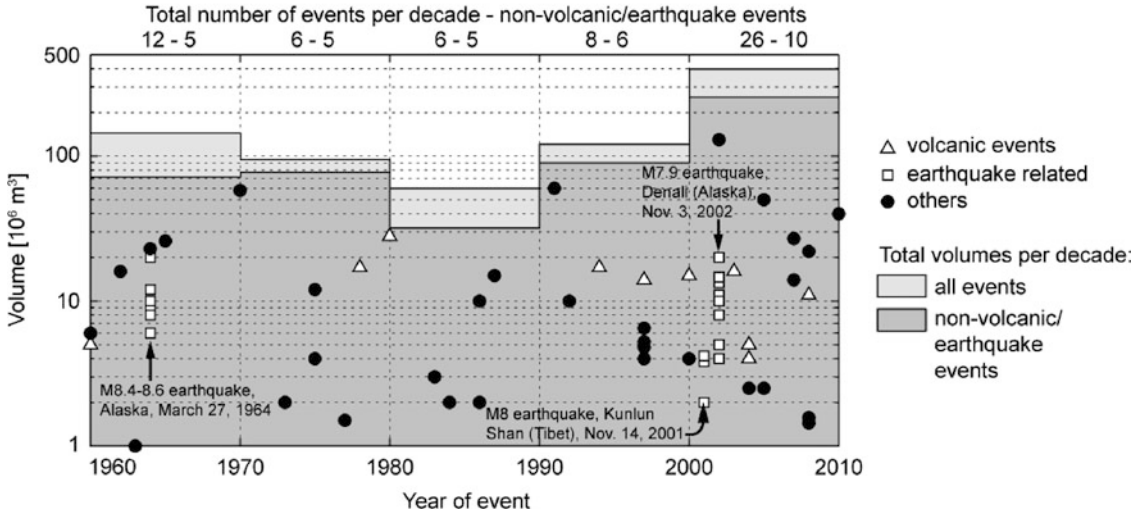

Fig. 1 Temporal distribution of worldwide large ($> 1 \times 10^6$ m^3) rapid mass movements in glacial environments. Events on volcanoes and related to seismic activity are marked. Note that the data can be biased due to non-uniform documentation throughout the past decades on a global scale

adjacent areas over the past two to three decades as compared to the rest of the twentieth century (Fischer et al. subm.). The trend hold true when only large events are considered although the sample then is reduced to about 20 events only. Interestingly, there is a second peak of increased rock slope failures around the 1940s that coincides with a warm period in the Alps.

Such regional-scale inventories include slope failures with a variety of different geology, topography, local climate and other factors that are known to influence slope instability. Local-scale studies are therefore important since to isolate the effects of these factors. Ravanel and Deline (2011) analyzed rock slope failures over the past ~150 years on high-mountain walls in the Mont Blanc area and found trends that are consistent with regional-scale studies: a large increase in slope failure activity during the past two to three decades and a second minor peak around the 1940s. The increase in event frequency during the past two decades as compared to the past 150 years is evident over the full range of magnitude (Ravanel and Deline 2011).

Figure 1 shows a global-scale inventory of 59 large ($>$ 1 million m^3) rapid mass movements in glacial environments between 1960 and 2010 based on Schneider et al. (2011). Both, number of events and volume, are significantly higher between 2000 and 2010 than in previous decades which would be consistent with the aforementioned findings at the regional- and local-scale (Fischer et al. subm., and Ravanel and Deline 2011, respectively). However, even though only large events are included here, it is not clear whether at the global scale any documentation bias can be excluded over the past 50 years. Furthermore, slope failures triggered by earthquakes and in volcanic environments have to be distinguished. In principle, climate change effects could lower the strength of rock slopes and thus make them prone to failure to lower-magnitude earthquakes, thus increasing the event frequency. However, we have no data that could provide corresponding evidence. Yet, it is interesting to note that even when subtracting seismically and volcanically related events, the increase in total failure volume over the past three decades holds true (Fig. 1). Overall, this analysis underlines that care is required when trying to extract potential climate signals based on slope failure inventories.

Inventories of high-mountain rock slope failures generally contain a limited number of events, typically $<$100 over the past ~100 years. Rigorous statistical analysis is therefore limited. Larger inventories of several hundred landslides (e.g. Korup et al. 2007; Guzzetti et al. 2009) offer opportunities for more sophisticated analysis. To test whether changes in boundary conditions such as climate change are detectable in landslide frequency-magnitude relationships, Huggel et al. (2013) created 100 random inventories, each containing 10,000 landslide events. They concluded that frequency-magnitude distributions are likely not adequate to detect potential changes in triggering conditions due to climate. For example, frequency-magnitude scaling statistics may render even a twofold increase of slope failure volume due to enhanced landsliding undetectable.

Damage and Loss Data

Data on damage and loss from natural hazards is systematically collected on national, regional/continental and global scales by a number of international, governmental and

private companies, in particular the insurance sector (e.g. MunichRe 2008). Durham University maintains a global catalogue of fatal landslides (Durham Fatal Landslide Database; Petley et al. 2005). A number of landslide catalogues that provide information on damage and loss also exist at the national level, for instance in Italy (Guzzetti 2000). Based on the Durham landslide database, Petley (2010) documented an increase in landslide casualties or losses in south, east and south-east Asia between 2003 and 2009. Landslides in these regions are predominantly triggered by monsoon and tropical cyclone activity, but Petley (2010) attributed the increasing trend to changes in exposure, i.e. population growth, and not to climate change.

Over the past years several researchers have examined potential trends in disaster loss data. They have documented a strong increase in disaster losses over the past several decades, ascribed largely to ime-variant socio-economic factors (Pielke et al. 2005). An adjustment procedure must be applied to detect any significant signal of change in disaster loss series. This implies an inflation correction as well as a normalization of disaster losses for changes in population and wealth. Indicators used for changes in wealth include Gross Domestic Product (GDP) per capita, property values and size of property market (Barredo 2010; Changnon 2011).

A recent assessment of disaster loss trend studies concluded, that although economic losses from weather-related disasters have increased worldwide over the past several decades, most studies have not found any trend in normalized losses that could be attributed to anthropogenic climate change (Bouwer 2011). Important uncertainties, howver, remain with respect to changes in exposure and vulnerability. Similarly, factors offsetting disaster losses, such as improved building codes, early warning systems, defense measures, disaster preparedness and response, and land-use planning, are still poorly quantified (Neumayer and Barthel 2011).

No systematic study on damage and loss exists for high-mountain slope failures, but both global and national event catalogues include some pertinent data. For instance, the Working Group on Glacier and Permafrost Hazards in Mountains (GAPHAZ) of the International Association of Cryospheric Sciences (IACS) and the International Permafrost Association (IPA) maintains a global catalogue of glacier hazards that includes, but is not limited to, high-mountain slope failures. The Swiss Permafrost Monitoring Network (PERMOS) has an inventory of rock slope failures in permafrost areas that includes damage information, although not systematically.

In conclusion, it is unlikely that any sound trend analysis can be performed with existing damage and loss data, largely due to the relatively rare occurrence of damaging high-mountain slope failures.

Case Studies

Although inventories and loss data may reveal changes in frequency or magnitude of events, they tell us nothing about the causes of the changes. Analysis of case studies, on the other hand, should provide insights into the driving processes at specific locations. Although there have been several media reports in recent years of mountaineers commenting on changes in rock fall activity along high-mountain climbing routes, little scientific evidence on such changes has yet been gathered.

In the Alps the record-breaking heat wave in the summer of 2003 coincided with strongly enhanced rock fall activity from permafrost areas, probably in relation with rapid thawing processes (Gruber et al. 2004). At Monte Rosa at the Swiss-Italian border, the frequency and magnitude of slope failures from bedrock and steep glaciers on the 2,500 m high east face significantly increased in the 1990s (Fischer et al. 2006). This change in mass movement activity was interpreted as a response to mass changes in relation with atmospheric warming in the 1980s and 1990s. Fischer et al. (2011) showed that the mass failures in rock and ice were coupled processes. Massive ice loss from steep glaciers mechanically and possibly thermally destabilized major rock slopes that had low rock strength or unstable geologic structures, and subsequently failed (Fischer et al. 2011).

Interesting evidence of a systematic change of rock slope failures from permafrost areas comes from the central Swiss Alps. Frequent rock falls started to occur in 2009 from the northeast face of Ritzlihorn (3,263 m asl) in the Grimsel area. Running water in bedrock couloirs together with numerous small-scale slope failures from the summit area during warm summer days (D. Tobler, personal communication, 2011) are likely evidence for the influence of thawing permafrost. Rock fall debris accumulates on less steep parts of the northeast face and on the apex of the large Holocene debris fan on which the community of Guttannen is located. At the time of the beginning of rock fall activity, repeated and large debris flows initiated at the fan apex. Antecedent soil saturation due to long-lasting snow is probably an important factor in triggering the debris flows. The largest debris flows, in July and August 2010, had volumes of ~100,000 m^3 and a peak discharge of ~500 m^3/s (Hählen 2010). A highway and a transnational gas pipeline were damaged by the debris flows and mitigation measures costing tens of millions Euros were initiated.

It is noteworthy that there were no historic damaging debris flows on the debris fan at Guttannen prior to 2009. This case study thus signals a dramatic change in a coupled high-mountain geomorphic system, with a possible attribution to impacts of climate change, although the attribution is difficult to quantify. Similarly, as at Monte Rosa, the

Table 1 Selected major rock slope failures and avalanches of the past two decades around the world. Events related to earthquakes are excluded. Existence of permafrost at the failure area is indicated, as well as occurrence of warm periods with temperatures close to or above freezing days and weeks before failure

Location	Date of occurrence	Approx. Volume (10^6 m^3)	Max. failure elevation (m asl)	Permafrost occurrence at failure	Warm period days-weeks before failure
Mt. Cook, New Zealand	14 Dec 1991	60	3,755	Yes	Yes
Brenva, Italy	18 Jan 1997	6.5	3,725	Yes	No
Kolka, Russia	22 Sept 2002	130	4,300	Yes	No data
Thurwieser, Italy	18 Sept 2004	2.5	3,570	Yes	No data
Mt. Steller, Alaska	14 Sept 2005	50	3,100	Yes	Yes
Tinguiririca	~Jan 2007	14	3,900	–	Yes
Mt. Rosa, Italy	21 April 2007	0.3	4,000	Yes	Yes
Mt. Steele, Canada	24 Jul 2007	27–80	4,640	Yes	Yes
Mt. Miller, Alaska	6 Aug 2008	22	2,200	Yes	Yes
Mt. Dampier, New Zealand	First week April 2010	0.5	3,400	Yes	Yes
Mt. Meager, Canada	6 Aug 2010	45	2,400	Likely	Yes

Ritzlihorn case study also indicates that an initial stimulus of climate change may be sufficient to alter a system in such a way that it can subsequently evolve independently of further climate impacts.

Causative and Trigger Factors

Another approach to detect changes in slope failures is to analyze potential changes in landslide predisposition and triggering factors and processes. For shallow landslides, intense and prolonged rainfall events with rapid infiltration into the soil, saturating it and generating high transient pore pressures are a main trigger (Iverson 2000). Important triggering parameters are total rainfall, rainfall intensity, rainfall duration, and antecedent rainfall (Wieczorek and Glade 2005; Sidle and Ochiai 2006). An important body of research exists on empirical rainfall landslide triggering (e.g. Guzzetti et al. 2007).

Rainfall is also recognized as a trigger of rock slope failures through mechanisms such as water infiltration and pressure variations in cleft systems (Wieczorek and Jäger 1996; Chau et al. 2003). Precipitation has been considered to be a likely trigger of high-mountain slope failures through water infiltration and possibly lock-off effects after refreezing (Fischer et al. 2010).

Temperature can have an important indirect effect on triggering or predisposing slopes to failure in high- mountain glacial and periglacial environments, where surface and subsurface ice is sensitive to short and longer term changes in temperature.

Related to longer term processes, inventory-based studies in the New Zealand and European Alps (Allen et al. 2011; Fischer et al. subm.,), have identified a prevalence of recent slope failure occuring from zones of warm, thawing permafrost (ca. >-1.5 °C) and/or from bedrock slopes influenced by recent glacial recession. Such studies have therefore provided an indirect, partly qualitative demonstration that predispositional processes related to climate warming have altered the distribution although not necessarily the frequency of recent high-mountain failures.

Concerning shorter time scales, recent studies of several large rock slope failures in Alaska, New Zealand and the Alps have shown that virtually all of the events were preceded by very warm temperatures, clearly above the freezing point, i.e. generating melt conditions (Huggel et al. 2010). Because these events are rare, it is difficult to detect a change in their frequency, and therefore attribute any direct influence of extreme temperature or precipitation as trigger mechanisms. However, very high temperatures, commonly expressed as the 90th or 95th percentile of the long-term record, have increased over the past 50–100 years over most land regions worldwide (Trenberth et al. 2007). In Europe, for instance, the frequency of hot days almost tripled between 1880 and 2005 (Della-Marta et al. 2007). Precipitation extremes have also increased in many parts of the world over the past several decades, but the changes vary more with season, and between regions (Trenberth et al. 2007). There is currently a lack of studies that specifically look at changes of extreme temperature and precipitation events in high mountain regions, partly due to limited long-term observation data (Table 1).

Climate Impact and Process Models

Detection and attribution of changes in landslides could, in principle, also be addressed through climate impact and

process models along the lines of single-step or multiple-step attribution studies (IPCC 2010). For shallow landslides, where the link between slope failure and climate variable (rainfall intensity or duration) is reasonably clear, such an approach may be successful. In the case of past landslide events triggered by intense precipitation, one must demonstrate an attribution of high-intensity rainfall events to effects of anthropogenic greenhouse gas emissions, such as done by Zhang et al. (2007) for mean precipitation trends. The second step is to examine the attribution of landsliding to greenhouse-gas-induced heavy precipitation. This step would probably be done using multiple realizations, resulting in a probability-based assessment of attribution (Pall et al. 2011).

The attribution of high-mountain rock slope failures to anthropogenic warming is much more complicated and probably not feasible because the link between the climate variable (temperature or precipitation) and slope failure is not yet sufficiently understood or modeled. Models of permafrost distribution at the surface and depth have been used in combination with regional climate models, and past and future three-dimensional permafrost distribution could be modeled (Salzmann et al. 2007). Limited applications of mechanical slope stability models exist for rock slope failures in permafrost areas (Fischer et al. 2010), but explicit modeling of different effects of permafrost on rock slope stability has not yet been achieved. Thus, although the human influence on increasing temperatures is detectable in different regions around the world (Hegerl et al. 2007), any anthropogenic effect on high-mountain slope failures cannot yet been quantified.

Conclusions

The primary objective of this paper was to outline a number of approaches that potentially can be used to detect a change in landslide activity, more specifically, landslide activity in high mountains. Although recent studies have found changes in the occurrence of alpine rock slope failures over the past several decades, the research is in its infancy. A limited number of studies, have examined possible changes in frequency or magnitude of shallow landslides or debris flows. The methodological approaches described here have not been rigorously tested in high-mountain environments. However, several of the presented approaches, including the analysis of slope failure inventories, case histories and trigger factors, are promising avenues for detection studies. The last methods presented here, which refer to attribution of observed changes to anthropogenic climate change, might currently hardly be applicable for complex high mountain slope stability problems. They could be used, however, if our under standing of processes improves.

Acknowledgments Some of the data presented here has been generated in projects funded by the Swiss National Science Foundation (SNF).

References

Allen SK, Cox SC, Owens IF (2011) Rock avalanches and other landslides in the central Southern Alps of New Zealand: a regional study considering possible climate change impacts. Landsldies 8:33–48

Augustinus PC (1995) Glacial valley cross-profile development: the influence of in situ rock stress and rock mass strength, with examples from the Southern Alps, New Zealand. Geomorphology 14:87–97

Ballantyne CK (2002) Paraglacial geomorphology. Quater Sci Rev 21:1935–2017

Barredo JI (2010) No upward trend in normalised windstorm losses in Europe: 1970–2008. Nat Hazards Ear Syst Sci 10:97–104

Bouwer LM (2011) Have disaster losses increased due to anthropogenic climate change? Bull Am Meteorol Soc 92:39–46

Changnon SA (2011) Temporal distribution of weather catastrophes in the USA. Climatic Change 106:129–140

Chau KT, Wong RHC, Liu J, Lee CF (2003) Rockfall hazard analysis for Hong Kong based on rockfall inventory. Rock Mech Rock Eng 36:383–408

Clague JJ, Evans SG (2000) A review of catastrophic drainage of moraine-dammed lakes in British Columbia. Quatern Sci Rev 19:1763–1783

Davies MCR, Hamza O, Harris C (2001) The effect of rise in mean annual temperature on the stability of rock slopes containing ice-filled discontinuities. Permafrost Periglac Process 12:137–144

Della-Marta PM, Haylock MR, Luterbacher J, Wanner H (2007) Doubled length of Western European summer heat waves since 1880. J Geophys Res-Atmos 112(D15103)

Fischer L, Amann F, Moore JR, Huggel C (2010) Assessment of periglacial slope stability for the 1988 Tschierva rock avalanche (Piz Morteratsch, Switzerland). Eng Geol 116:32–43

Fischer L, Eisenbeiss H, Kääb A, Huggel C, Haeberli W (2011) Monitoring topographic changes in steep high-mountain flanks using combined repeat airborne LiDAR and aerial optical imagery – a case study on climate-induced hazards at Monte Rosa east face, Italian Alps. Permafrost Periglac Process 22:140–152

Fischer L, Kääb A, Huggel C, Noetzli J (2006) Geology, glacier retreat and permafrost degradation as controlling factors of slope instabilities in a high-mountain rock wall: the Monte Rosa east face. Nat Hazards Ear Syst Sci 6:761–772

Fischer L, Purves RS, Huggel C, Noetzli J, Haeberli W (subm.) On the influence of geological, topographic and glaciological factors on slope instabilities: analyses of recent Alpine rock avalanches. Nat Hazards Ear Syst Sci 12:241–254

Geertsema M, Clague JJ, Schwab JW, Evans SG (2006) An overview of recent large catastrophic landslides in northern British Columbia, Canada. Eng Geol 83:120–143

Gruber S, Haeberli W (2007) Permafrost in steep bedrock slopes and its temperature-related destabilization following climate change. J Geophys Res 112:F02S18

Gruber S, Hoelzle M, Haeberli W (2004) Permafrost thaw and destabilization of Alpine rock walls in the hot summer of 2003. Geophys Res Lett 31:L13504

Guzzetti F (2000) Landslide fatalities and the evaluation of landslide risk in Italy. Eng Geol 58:89–107

Guzzetti F, Ardizzone F, Cardinali M, Rossi M, Valigi D (2009) Landslide volumes and landslide mobilization rates in Umbria, central Italy. Earth Planet Sci Lett 279:222–229

Guzzetti F, Peruccacci S, Rossi M, Stark CP (2007) Rainfall thresholds for the initiation of landslides in central and southern Europe. Meteorol Atmos Phys 98:239–267

Hählen N (2010) Murgänge Spreitgraben Guttannen. FAN Herbstkurs 2010: Objektschutz p 11. FAN

Hegerl GC, Zwiers FW, Braconnot P, Gillett NP, Luo Y, Marengo Orsini JA, Nicholls N, Penner JE, Stott PA (2007) Understanding and attributing climate change. Climate change 2007: the physical science basis. In: Solomon S, Qin D, Manning M, Chen Z, Marquis M, Averyt KB, Tignor M, Miller HL (eds) Contribution of working group I to the fourth assessment report of the intergovernmental panel on climate change, Cambridge University Press, Cambridge, United Kingdom/New York, pp 663–745

Huggel C, Korup O, Gruber S (2013) Landslide hazards and climate change in high mountains. In: James AC, Harden, Clague JJ (eds). Treatise on geomorphology: hazards, applied, anthropogenic and cultural geomorphology. Academic Press, San Diego

Huggel C, Salzmann N, Allen SK, Caplan-Auerbach J, Fischer L, Haeberli W, Larsen C, Schneider D, Wessels R (2010) Recent and future warm extreme events and high-mountain slope stability. Philos Trans Roy Soc A 368:2435–2459

IPCC (2010) Meeting report of the intergovernmental panel on climate change expert meeting on detection and attribution related to anthropogenic climate change. In: Stocker TF, Field CB, Qin D, Barros V, Plattner G-K, Tignor M, Midgley PM, Ebi KL (eds) IPCC Working Group I Technical Support Unit, University of Bern, Bern

Iverson RM (2000) Landslide triggering by rain infiltration. Water Resour Res 36:1897–1910

Korup O, Clague JJ, Hermanns RL, Hewitt K, Strom AL, Weidinger JT (2007) Giant landslides, topography, and erosion. Earth Planet Sci Lett 261:578–589

Legros F (2002) The mobility of long-runout landslides. Eng Geol 63:301–331

MunichRe (2008) Topics Geo, natural catastrophes 2007: analyses, assessments, positions. Munich Reinsurance Company, Munich

Neumayer E, Barthel F (2011) Normalizing economic loss from natural disasters: a global analysis. Global Environ Change 21:13–24

O'Connor JE, Costa JE (1993) Geologic and hydrologic hazards in glacierized basins in North America resulting from 19th and 20th century global warming. Nat Hazards 8(2):121–140

Pall P, Aina T, Stone DA, Stott PA, Nozawa T, Hilberts AGJ, Lohmann D, Allen MR (2011) Anthropogenic greenhouse gas contribution to flood risk in England and Wales in autumn 2000. Nature 470:382–385

Petley DN (2010) On the impact of climate change and population growth on the occurrence of fatal landslides in South, East and SE Asia. Quart J Eng Geol Hydrogeol 43:487–496

Petley DN, Dunning SA, Rosser NJ (2005) The analysis of global landslide risk through the creation of a database of worldwide landslide fatalities. In: Hungr O, Fell R, Couture R, Eberhardt E (eds) Landslide risk management. A.A. Balkema, Rotterdam, pp 367–374

Pielke RA, Agrawala S, Bouwer LM, Burton I, Changnon S, Glantz MH, Hooke WH, Klein RJT, Kunkel K, Mileti D, Sarewitz D, Thompkins EL, Stehr N, von Storch H (2005) Clarifying the attribution of recent disaster losses: a response to Epstein and McCarthy. Bull Am Meteorol Soc 86:1481–1483

Ravanel L, Deline P (2011) Climate influence on rockfalls in high-Alpine steep rockwalls: the north side of the Aiguilles de Chamonix (Mont Blanc massif) since the end of the'Little Ice Age'. Holocene 21:357–365

Rosenzweig C, Karoly D, Vicarelli M, Neofotis P, Wu Q, Casassa G, Menzel A, Root TL, Estrella N, Seguin B, Tryjanowski P, Liu C, Rawlins S, Imeson A (2008) Attributing physical and biological impacts to anthropogenic climate change. Nature 453:353–357

Salzmann N, Nötzli J, Hauck C, Gruber S, Hoelzle M, Haeberli W (2007) Ground surface temperature scenarios in complex high-mountain topography based on regional climate model results. J Geophys Re 112: F02S12

Schneider D, Huggel C, Haeberli W, Kaitna R (2011) Unraveling driving factors for large rock-ice avalanche mobility. Earth Surf Process Land (in press)

Sidle RC, Ochiai H (2006) Landslides: processes, prediction, and land use. American Geophysical Union, Washington, DC

Trenberth KE, Jones PD, Ambenje P, Bojariu R, Easterling D, Klein Tank A, Parker D, Rahimzadeh F, Renwick JA, Rusticucci M, Soden B, Zhai P (2007) Observations: surface and atmospheric climate change. Climate change 2007: the physical science basis. In: Solomon S, Qin D, Manning M, Chen Z, Marquis M, Averyt KB, Tignor M, Miller HL (eds) Contribution of working group I to the fourth assessment report of the intergovernmental panel on climate change, Cambridge University Press, Cambridge, United Kingdom/New York, pp 235–336

Wieczorek GF, Glade T (2005) Climatic factors influencing occurrence of debris flows. In: Jakob M, Hungr O (eds) Debris-flow hazards and related phenomena. Springer, Berlin/Heidelberg, pp 325–362

Wieczorek GF, Jäger S (1996) Triggering mechanisms and depositional rates of postglacial slope-movement processes in the Yosemite Valley, California. Geomorphology 15:17–31

Zhang X, Zwiers FW, Hegerl GC, Lambert FH, Gillett NP, Solomon S, Stott PA, Nozawa T (2007) Detection of human influence on twentieth-century precipitation trends. Nature 448:461–465

Landslides Characteristic of Northwest Lesser Khingan Range China

Wei Shan, Hua Jiang, Ying Guo, Zhaoguang Hu, and Chunjiao Wang

Abstract

Since the late 1990s, with the construction of the highway in Heilongjiang province, the problems of ground deformation and subgrade stability caused by the permafrost have been seriously recognized. Currently, there was little research on Landslides caused by permafrost melting and human factors. We took K177 + 100 to K179 + 300 section of Bei'an to Heihe highway expansion project as the research object. Through site surveys, geological drilling, shallow ground water content and temperature monitoring, slope and subgrade deformation monitoring, laboratory test methods, the formation mechanism of classic landslides in the research area have been comprehensive studied. The results show that: the terrain, geological conditions and the change of moisture content in hillside slope were the main reasons to generate landslides. Atmospheric precipitation, seasonal freezing and thawing of shallow slope ground and the melting of island permafrost scattered in the mountain valley provided continuous landslides water. Artificial disturbance to slope soil in the road construction process accelerated the slope sliding. This research can provide reference for slope design and assessment of similar conditions in northeast China.

Keywords

Lesser Khingan Range • Frozen soil • Seepage • Landslides • Soil moisture changing

Introduction

In response to the global economic crisis, the Chinese government strengthens the focus on infrastructure construction to expand domestic demand since 2008. Heilongjiang Province decided to widen and expansion the highway from Bei'an to Heihe into expressway.

During the construction process of the Bei'an to Heihe highway from 1999 to 2002, there were some subgrade and slope landslides occurred from K159 + 000 to K184 + 000 when through the Lesser Khingan Range, the most serious section was from K176 + 500 to K178 + 300. After the subgrade construction was complete, the landslides caused whole subgrade instability and had to change the line to re-build (see Fig. 1). At present, there were some other highways in the similar situation in Heilongjiang province.

The field surveys and geological topographic mapping work of Bei'an to Heihe highway expansion project from K177 + 100 to K179 + 300 were carried out since June 2009, the survey and mapping results shown in Fig.2.

Previous Studies

Yang and Lin studied the characteristics of ground water's formation, burial conditions and distribution in permafrost regions (Yang and Lin 1986). Zhou reviewed the history of permafrost research, discussed the formation conditions, zoning principles and evolution of trends of frozen soil in "China's permafrost"(Zhou et al. 2000). Wu studied on the stability of the Qinghai-Tibet Highway induced by the

W. Shan (✉) • H. Jiang • Y. Guo • Z. Hu • C. Wang
Northeast Forestry University, Harbin 150040, China
e-mail: shanwei456@163.com

C. Margottini et al. (eds.), *Landslide Science and Practice*, Vol. 4,
DOI 10.1007/978-3-642-31337-0_47,

Fig. 1 The bird's eye view of Bei'an to Heihe highway expansion project from K176 + 500 to K179 + 300 sections

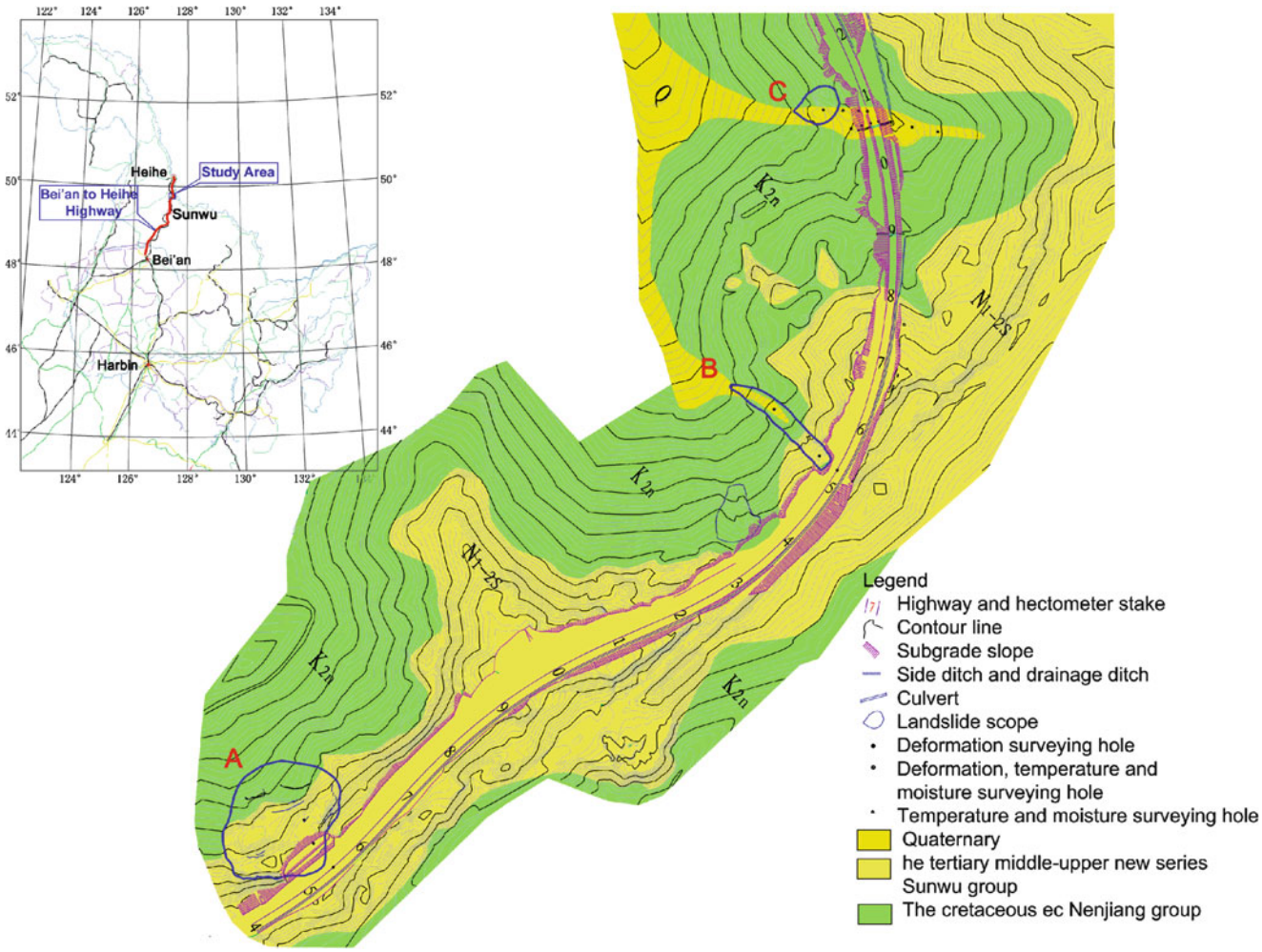

Fig. 2 The topographic and geologic map of Bei'an to Heihe highway expansion project from K177 + 100 to K179 + 300 sections

climate warming (Wu and Tong 1995). Zhang Jinzhao, Wu summed up the construction techniques in Qinghai-Tibet permafrost regions (Zhang et al. 1999). Yuan studied subgrade subsidence reasons in permafrost regions of northern Greater Higgnan Mountains (Yuan 1999). Sun taken the regions in Greater Higgnan Mountains China as an example, discussed symbiotic mechanism of swamps and permafrost (Sun 2000). Niu Fuchun etc. monitored slope failure induced

by permafrost thaw slumping in Qinghai-Tibet plateau (Niu et al. 2004). Jin Dewu etc. studied the formation mechanism of two kinds of low angle Landslides disaster in the Qinghai-Tibet Plateau (Jin et al. 2005).

At the initial construction of Bei'an to Heihe highway in 1999, cold region and arid region research institute of the Chinese academy of sciences and Heilongjiang provincial expressway construction bureau jointly carried out investigation on geological conditions and permafrost distribution in the region routes passing by. The preliminary studies were carried out on the poor geological conditions may affect the stability of the subgrade. Wang Biao, Meng Fansong, Zhang Yan etc. described the distribution of permafrost, degradation status and Subgrade defect state of Bei'an to Heihe highway, and provide the subgrade design principles(Wang et al. 2001; Meng et al. 2001; Zhang et al. 2001).

Site Conditions and Geologic Background in Research Area

Landslides areas of Bei'an to Heihe highway were located at the border of Anhui district Heihe City and Sun Wu County, at northwest of Lesser Khingan Range's. This area is hilly landscape, undulating terrain, the relative height difference is little, and some sections are steep slopes. The tectonics belongs to the Wuyun to Yaxin fault zone, the south of the Shu River uplift, and the north side of the rare atmosphere folding beams.

This area belongs to cold temperate continental monsoon climate, long and cold winter, windy spring, mild and rainy summer, cool autumn, and often with early frost damage. Average annual temperature is −0.6 °C. Annual average precipitation is 400–650 mm. More concentrated rainfall in the summer from July to September. Average annual sunshine time is 2551.5 h. Average annual period of snow is 215 days. It crosses the fourth, fifth and sixth accumulated temperature zone. Frost-free period is 90–120 days. The annual effective accumulative temperature between the 1571.1 °C and 2117.4 °C. Vegetation is divided into forest and meadow vegetation. There belongs to cold temperate coniferous forest zone. The forest coverage rate reached 45 %.

The exposed stratums of the study area by the old to the new formation are: the upper cretaceous nenjiang group, Tertiary group of Sun Wu in the Pliocene, Quaternary Holocene modern river alluvium. Layered Weakly cemented rock resist weathering ability is poor, it has larger weathering depth and basic fully weathered near surface.

The area is in uplift phase, valley cutting relatively strong. The upper part is high permeability tertiary pebbly sandstone, the lower part is whole weathering Cretaceous weakly cemented mudstone or silty mudstone both water and water-barrier. The ground slope generally between 10° and 25°,

Fig. 3 Carex tato distribution under forest

Fig. 4 Permafrost soil samples under carex tato

tertiary pebbly sandstone and mudstone of Cretaceous or weakly cemented silty mudstone contact surface with the tertiary pore water. Water often seeping along the contact surface, eroding the lower weak cementation Cretaceous mudstone or silty mudstone, especially in the July to August becomes more apparent.

Moisture Content Changes and Landslides Mechanism

In the study area through the coniferous forest zone, there are oak, birch, poplar, linden tree and the majority is birch tree. There are cracked turfs under trees. Carex tato, moss and other vegetation distributed in the valley. It has obvious vegetation distribution characteristics of permafrost region, and permafrost was found under Carex tato by drilling, as shown in Figs. 3, 4 and 5.

The permafrost under carex tato under trees and the collection of precipitation within the valley provide water source for the increase in water content of slope. The cracks in cracket turfs on slope provide the infiltration condition for the increase in water content of slope.

Slope soil moisture content change is a complicated process, including slope surface precipitation infiltration,

Fig. 5 Cracked turfs

Fig. 6 Interface of sandstone and mudstone at K177 + 500 section

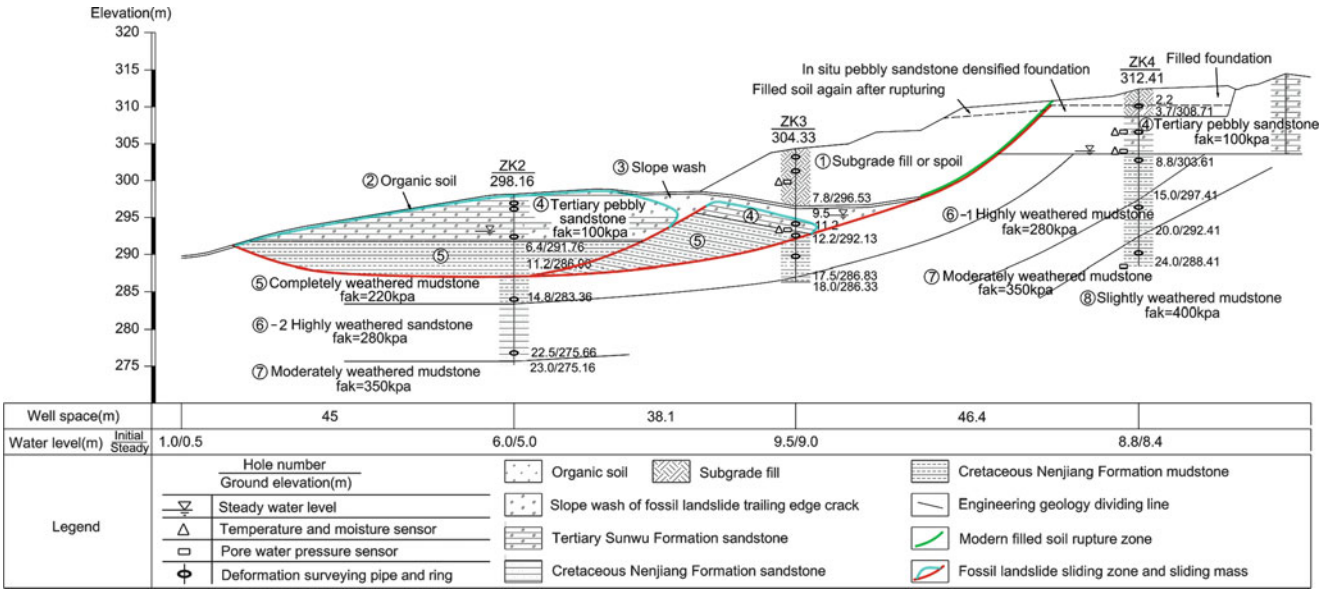

Fig. 7 The geological profile and monitoring equipment layout at K177 + 550 section

thawing permafrost supplies, fissure seepage, seepage in soil under gravity conditions and other forms. When the water infiltration intensity greater than the infiltration rate of slope soil, infiltration moisture make the shallow slope soil to reach saturation. It makes the dynamic water load and still water load increased, the soil shear strength reduced. So, the slope is instability, the slope slide produced.

The water content of slope soil increased can reduce the suction of soil particles, decrease cementation bate between grains and adsorption cohesion. Most slope soil in unsaturated condition, the seepage in unsaturated soil make matric suction decrease, soil generate transient saturated. It makes soil in plastic state, so, the shearing strength of soil decreased.

The groundwater seepage process can generate pressure on soil particles, and can make the soluble cementing things between particles run away, so, the cohesion and internal friction coefficient of soil reducing. When water infiltration process stagnant when water reach the surface of weathering bedrock or all sorts of impermeable clay layer, the underpart soil form weak sliding surface by soaking and softening, it can prompt and accelerate the upper soil move along the weak sliding surface. In addition, water table elevates due to water infiltration, the upward buoyancy reduce the normal pressure on the sliding surface induced by potential sliding body weight.

The interface of sandstone and mudstone at K177 + 500 section in retaining wall foundation construction process was described in Fig. 6, the geological profile and monitoring equipment layout at K177 + 550 section were described in Fig. 7, combined with soil parameters in Table 1, the surface soil is sandy clay, higher porosity, existence local fissures. Whose integrity is not strong, can provide good channel for water infiltration. The strong weathering mudstone soil below it has visible obvious fissure. The layered sandstone is below the strong weathering mudstone. By indoor test, the surface soil and strong weathering mudstone

Table 1 Soil composition and soil parameters at ZK2 point

Soil type	Distance to surface (m)	Water content (%)	Volume weight (kN/m)	Permeability coefficient (cm/s)	Cohesion (kPa)	Internal friction angle (°)
Sandyclay	2	29.39	16.7	2.74×10^{-4}	1.73	5.4
Mudstone	4	35.29	16.7	1.74×10^{-4}	19.23	20.4
Mudstone	8	25.57	17.5	4.55×10^{-5}	19.52	20.1
Sandstone	10	20.99	18.3	2.23×10^{-5}	6.38	14.47
Sandstone	12	23.12	18.9	1.90×10^{-5}	1.07	23.63
Sandstone	14	22.45	23.7	2.02×10^{-5}	0.77	26.7

Fig. 8 Surface crack development at section A. (**a**) Crack in the south of the section A. (**b**) Crack in the north of the section A. (**c**) Landslide frontier at section A

soil with fractures have bigger permeability coefficient than sandstone. The surface water through the crack down to the mudstone, the soil suction reduces and adsorption cohesion between soil particle decrease. The permeability coefficient of sandstone is less than mudstone's, mudstone layer moisture content increases gradually, so, the soil shear strength reduces.

In the process of soil deformation, the edge dropping firstly, then it moves forward gradually. When the slope fractures have not yet had time to fully develop, the entire slope slide, it showed Landslide feature. In addition, as a kind of soft rock, mudstone's strength in saturated condition is only 10% of the strength in dry state, with mud Characteristics. The disintegrating, softening and strength decreasing of Mudstone led to the collapse of slope and affect the stability of the subgrade.

Site Monitoring of Research Section

In the research sections, we choose the K177 + 550, K178 + 530, K179 + 060 as monitoring sections, shown in Fig.2a–c. Foundation and subgrade deformation monitoring devices, foundation soil temperature, moisture, pore water pressure sensors were laid since May 2009, and related data were monitored.

Take the K177 + 550 section as an example, Fig.2 presents the occurrence and development situation of the Landslide by the monitoring data changing. The geological survey and monitoring equipment lay out were completed in July 2010. Relevant monitoring data were collected since 22 July. A month later, the deformation monitoring tube of 10m (ZK3) and 40 m (ZK2) were broken at the location 10 m to

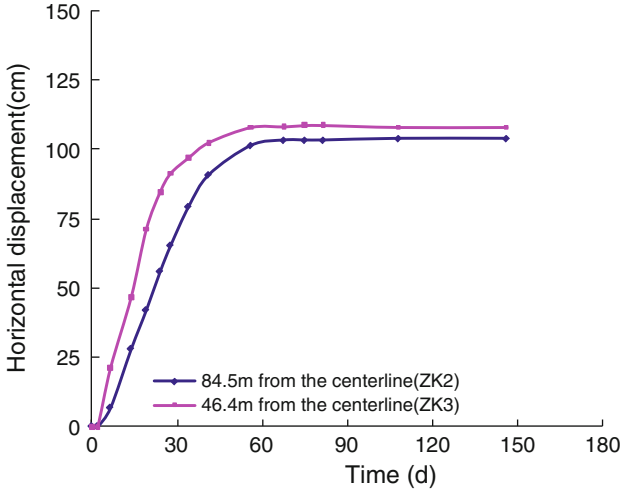

Fig. 9 Horizontal displacement at section A

surface, wires of temperature, moisture, and water pressure sensor were also cut off, and measuring device did not show monitoring data. According to the relevant phenomenon, we judged that the relevant soil layer disturbed. At the same time, mobile data of the nozzle monitored by GPS were started. Many cracks on the excavation and filling junction mountain surface in the monitoring section were found in late August 2010. The slope body was shear slid under the slope, as illustrated in Fig. 8. Its development is very fast. At the same time, we paid attention to collecting the relevant data of the monitoring point (ZK4) in the junction of old and new subgrade which did not damaged.

Monitoring Date Analysis

From Aug.22 to Nov.4, in 70 days, the Horizontal displacement of ZK2 and ZK3 is 100 cm or so respectively (see in Fig. 9). The move speed was fast when beginning then slows down. Without increasing external load conditions, Vertical deformation of ZK2 and ZK3 is 2cm and 20 cm respectively in 30 days (July 20 to August 22). Maximum fill thickness is not more than 2 m. When the total monitoring period to 100 days or so, cumulative vertical deformation reaches 30 and 80 cm respectively (see in Fig. 10). The surface cracks around the mountain were observed, and showed the development trend. At the same time, Attention was paid to the monitoring data of ZK4 which located at 50 m from ZK3. The vertical and horizontal displacements are very small. But the pore water pressure about 9 m from the surface increased and then decreased, and the peak values occurred at 22 August (see in Fig. 11). According to the above monitoring data,

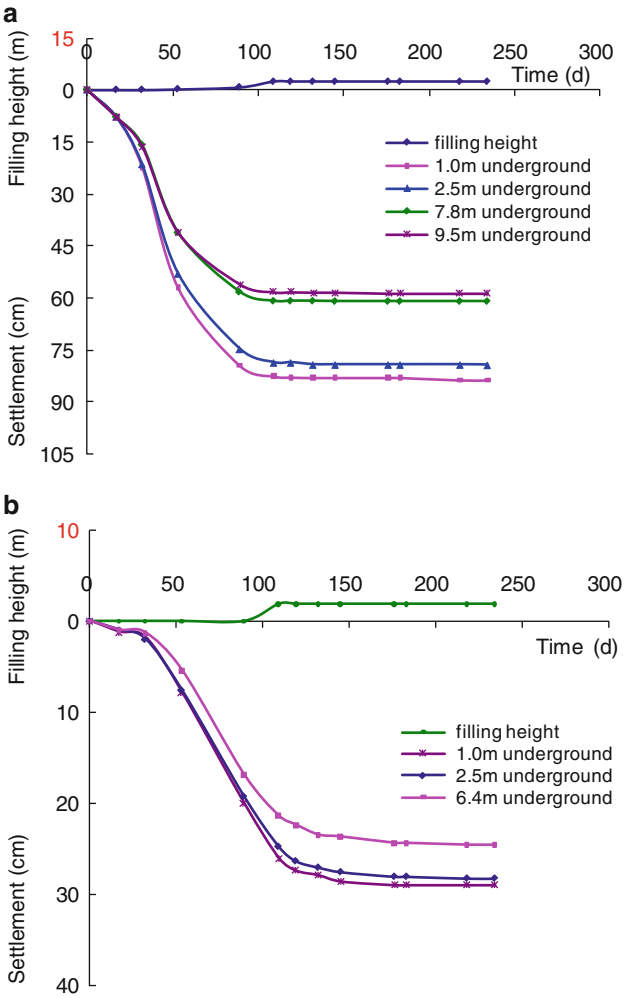

Fig. 10 Vertical displacement at section A (**a**) ZK2 (**b**) ZK3

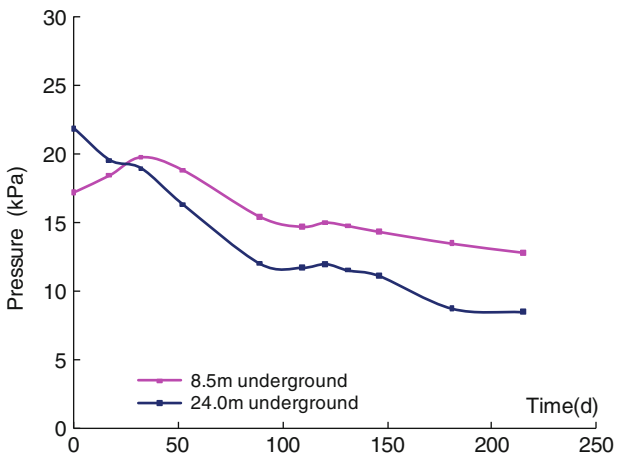

Fig. 11 Porewater pressure of central dividing strip at section A

combined with the surface crack that happen and the development situation, on August 20, shallow mountain slope happening squirming Landslide was concluded.

Conclusions

The project research is ongoing, according to the research work already undertaken and the results have been obtained, the following preliminary conclusions can be drawn:

1. Permafrost melting and the valley slopes of precipitation provide water supply conditions for slope deformation.
2. Slope surface temperature shrinkage cracks and the high permeability of shallow slope provide a channel for water infiltration and percolation.
3. The low permeability mudstone under loose slope cover and the top of frozen earth that don't melt in spring melting period, formed impermeable layer, infiltration water flow along it, which reduced the soil's shear strength of soil. The seepage layer within the slope formed slide zone.
4. The soil above the slide zone sliding along the slide zone under the action of gravity, Landslide was formed. Because of the discontinuity of permafrost distribution and differences in geological conditions, landslide in the region have the property of progressive, the end point, creeping slowly and so on.

Acknowledgments The authors would like to thank the financial supports provided by the project of Heilongjiang provincial transportation department and the subproject of Chinese western transportation technology research on "Research on roadbed stability technology of highway expansion and widening project at melting permafrost and landslide sections".

References

Jin D, Sun J, Fu S (2005) Discussion on landslides hazard mechanism of two kinds of low angle slope in permafrost regions ofQinghai2Tibet plateau. Rock Soil Mech 26(5):774–777

Meng F, Liu J, Liu Y (2001) Design principles and frost damage characteristics of frozen soil roadbed along the Heihe – Bei'an highway. J Glacol Geocryol 23(3):307–311

Niu F, Cheng G, Lai Y et al (2004) Instability study on thaw slumping in permafrost regions of Qinghai2Tibet plateau. Chin J Geotech Eng 16(3):403–406

Sun G (2000) Discussion on the symbiotic mechanisms of swamp withpermafrost–Taking Da-Xiao Xing'an mountains as examples. J Glaciol Geocryol 22(4):309–316

Wang B, Sheng Y, Liu J (2001) Distribution and degradation of permafrost in Xiao Xing'an Mountains along the Heihe-Dalian highway. J Glacol Geocryol 23(3):302–306

Wu Q, Tong C (1995) Permafrost change and stability of the Qinghai-Xizang plateau. J Glaciol Geocryol 17(4):350–355

Yang R, Lin F (1986) Permafrost hydrogeology and engineering geology. Northeast Forestry University Press, Harbin

Yuan X (1999) Study on thaw settlement of subgrade in permafrost regions in the northern part of Da Hinggan Mountains. J Glaciol Geocryol 21(2):155–158

Zhang J, Wu J, Li Z (1999) The study of highway construction techniques on plateau permafrost regions: review and prospect. J Glaciol Geocryol 21(2):187–191

Zhang Y, Wu Q, Liu J (2001) Distribution characteristics of the permafrost in the section from Heihe to Bei'an in the Xiao Xing'an Mountains. J Glaciol Geocryol 23(3):312–317

Zhou Y, Guo D, Qiu G et al (2000) Geocryology in China. Science Press, Beijing

Landslides and Moisture-Temperature for Cutting Slope Soil in Freeze-Thaw Cycles

Ying Guo, Wei Shan, Chengcheng Zhang, and Yuying Sun

Abstract

It is the main problem for highway in seasonal frozen regions that soil cutting slope instability causing by freeze-thaw, which affected traffic safety and the environment seriously. Relying on the silty clay slope, which is in the Tong-San highway expansion project from Jiamusi to Harbin, using triaxial shear tests, field monitoring, the mechanism of slope instability causing by freeze-thaw was studied. Triaxial test results show that: when the soil water content is less than the optimum water content, the soil cohesion is increased with the increase of moisture. The soil cohesion is decreased with the increase of moisture, when the soil water content is bigger than the optimum water content. The peak value of soil cohesion is near the optimum water content. The internal friction angle of soil is decreased with the increase of moisture. Soil cohesion is decreased with the increase of times of freeze-thaw cycles. Field monitoring results indicates that, during the process of soil freezing, moisture migrates to the freezing-front. In the melting period of spring, because of the accumulating water within the cracks of temperature shrinkage, and longer duration of zero temperature below the slope surface, the melting water was hampered, as well as the water frozen within the soil body melt rapidly when soil body temperature reaches 0.1 °C, all of these results in the water content in shallow slope is too high, and soil shear strength decreases, then occurs cutting slope landslides.

Keywords

Highway • Cutting slope • Silly clay • Freeze-thaw • Soil moisture • Soil temperature

Introduction

Soil cutting slope shallow landslides occurs frequently in seasonal frozen areas of Northeast China (Wu et al. 2006; Liu and Wang 2006). The main reason is the moisture tranfer to the freezing front during the freezing period, result in water content increasing in somewhere of shallow slope, then frost heaving occurs under subzero temperature. In the melting period of spring, the frozen layers in shallow slope thawed influenced by kinds of factors such as precipitation, increasing temperature and so on. The melting water was hampered by unfrozen layer under them during their infiltration downward, result in the water content in the layer between melt layer and frozen layer increasing rapidly, and reach saturation or over-saturated state, then the effective stress within the slope reduced, the partial or whole of the shallow slope slide down along the "water saturation layer" under gravity (Niu et al. 2004).

In August 2009 survey, Tong-San highway expansion project from Jiamusi to Harbin, was found seven landslides on the left cutting slope, landslide locations was shown in Fig. 1. The study area is from K560 + 090 to K565 + 690. The terrain graph fluctuation of study area is bigger, the soil

Y. Guo (✉) • W. Shan • C. Zhang
Northeast Forestry University, Harbin 150040, China
e-mail: samesongs@163.com

Y. Sun
Heilongjiang Institue of Technogly, Harbin 150090, China

C. Margottini et al. (eds.), *Landslide Science and Practice*, Vol. 4,
DOI 10.1007/978-3-642-31337-0_48,

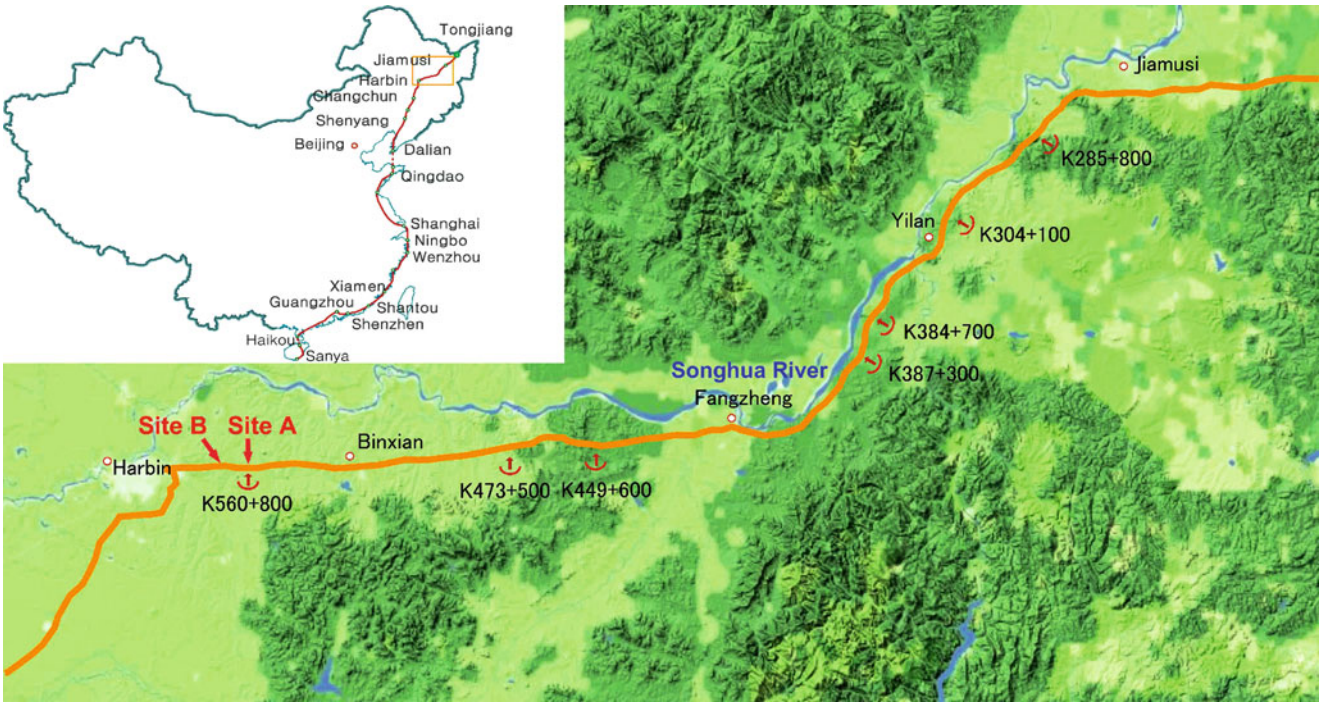

Fig. 1 Site map and the distribution of the shallow slope failure along the Ha-jia highway

of it is sandy clay, whose natural density is 1.8–2.1 g/cm^3, the average height of the cutting slope is 5–15 m, and the average ratio of the slope is 1.5–1.75.

The study of the stability of permafrost slopes appeared earlier (Tarr 1897; McRoberts and Morgenstern 1974; Clark 1988; Zhou and Guo 1982), but mainly is in the permafrost plateau (Zhu et al. 1996; Wang and French 1995; Niu et al. 2002; Li and Zhao 2002). There is different between instability in seasonal frozen region and instability in permafrost, mainly is larger changes in temperature and repeated freezing-thawing cycles, which has obvious seasonal characteristics.

Through on-site investigation, monitoring water content and ground temperature in shallow slope, and laboratory of soil physical and mechanical, the physical and mechanical nature of the soil varied with water content and freeze-thaw cycle was studied, the relationship between soil moisture and soil temperature during the freeze-thaw cycles was studied, and landslides mechanism of shallow slope was also studied.

Effect of Freeze-Thaw Cycles on Soil Shear Strength

In order to study the effect of freeze-thaw cycles and moisture and compaction of the soil on the shear strength of slope body, the basic physical parameters of the soil in the slope were measured and shown in Table 1. With the same 85 % compaction degree, the soil samples with different water content and different freeze-thaw cycles were conducted indoor triaxial test, the results are shown in Fig. 2.

Table 1 Basic physical properties indicators of silty clay

Liquid Limit (%)	Plastic limit (%)	Plasticity index	Maximum dry density (g/cm^3)	Optimum water content (%)
32.5	18.7	13.8	1.90	13.3

For silty clay with 85 % compaction degree, Fig. 2a shows the relationship curve (M-C curve) between soil moisture and soil cohesion under different freeze-thaw cycles. It can be seen that when soil moisture is close to the optimum moisture, soil cohesion reach the peak value. Soil cohesion decreases gradually with the increase of freeze-thaw cycles, especially when soil compaction degree is bigger. Under the optimum moisture, after 1, 5 freeze-thaw cycles, the soil cohesion decreases by 45.91 % and 54.08 % separately.

For silty clay with 85 % compaction degree, Fig. 2b shows the relationship curve (M-IFA curve) between soil moisture and soil internal friction angle under different freeze-thaw cycles. It can be seen that soil internal friction angle decreases with the increase of soil moisture. When soil moisture increased from 9 % to 22 %, after 1, 5 freeze-thaw cycles, the reduction value of soil internal friction angle is 26.63 %, 17.46 %, 21.51 %, separately.

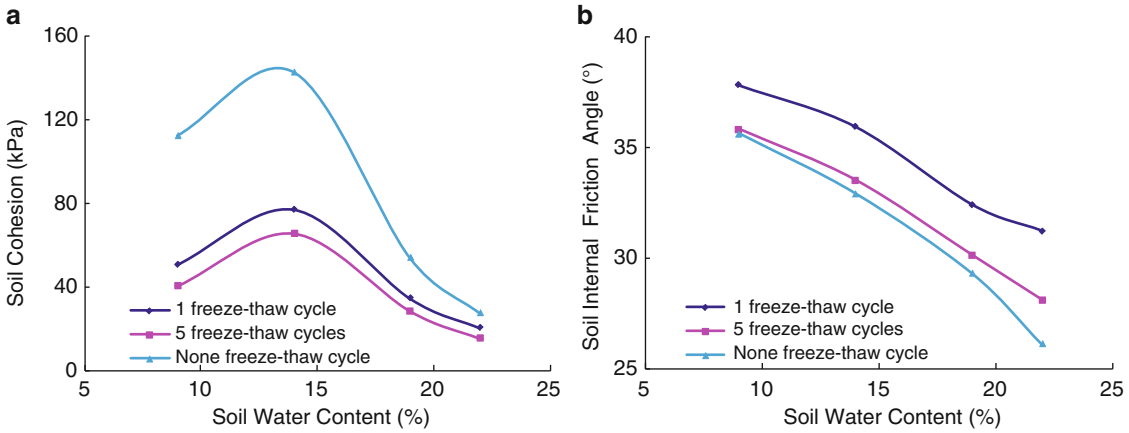

Fig. 2 Soil shear strength curves before and after frozen-thaw with 85 % soil compaction (**a**) M-C curves (**b**) M-IFA curves

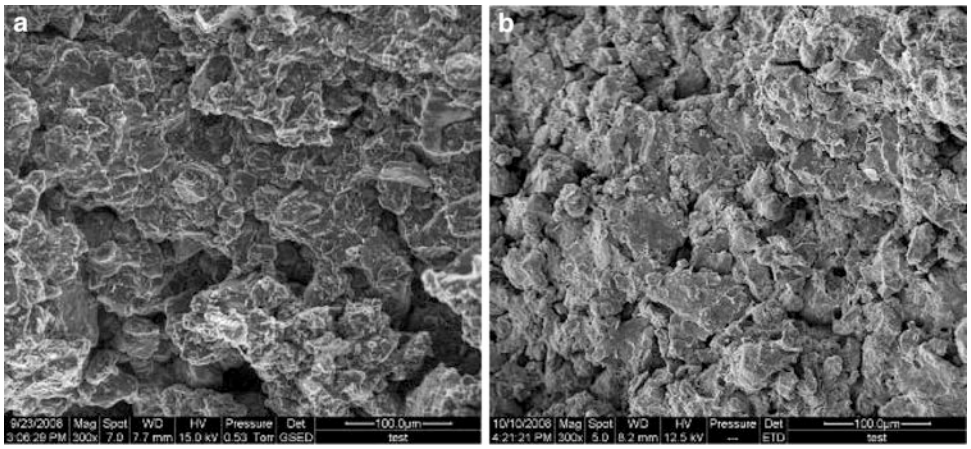

Fig. 3 Three hundred times magnification electron micrograph for silty clay sample with 90 % soil compaction. (**a**) Befor freeze (**b**) After first freeze-thaw cycle

Soil cohesion decreases with the increase of freeze-thaw cycles. Soil internal friction increases after the first freeze-thaw cycle, and then decreases gradually in later freeze-thaw cycles. The reason is, the association and arrangement among soil particles was changed by frost heaving, and then the mechanical properties of the soil changed also(Shan et al. 2009). During the first freezing period,there will appear the cracks caused by temperature shrinkage, and the soil was divided into units by the cracks(see Fig. 3),the original soil cohesion between soil particles is destroyed. With the times of freeze-thaw cycles increasing, soil units continue to be divided by new cracks, soil cohesion continue to reduce, but declines slowly. On the other hand, after first freeze-thaw cycle,the interlocking function between soil particles has been strengthened because new soil unites appearance, then soil friction angle increased. the later freeze-thaw cycles, the soil unites was devided by new cracks and became smaller, soil friction angle decrease gradually.

Monitoring of Ground Temperature and Soil Moisture on the Slope

According to meteorological data in Heilongjiang Province, for the ground within 20 cm below the surface, subzero temperature begins to appear in early November every year, and above zero temperature appears in end of March of next year. The maximum freezing depth is about 1.9 m. According to field investigation, the sliding surface of the cutting slope is about 1–1.5 m deep from the slope surface, and the thickness of slip zone is 10–25 cm.

In order to study the effect of weather temperature and plant on the ground temperature and soil moisture on the slope, two study sites were selected(Fig. 1.), one is in K560 + 700 (site A) which planted grass, anther is in K563 + 870 (site B) which planted Lespedeza. On both sites, temperature sensors and moisture sensors were buried in the depth of 0.6, 1.4, 2.2 m separately. The sensors in

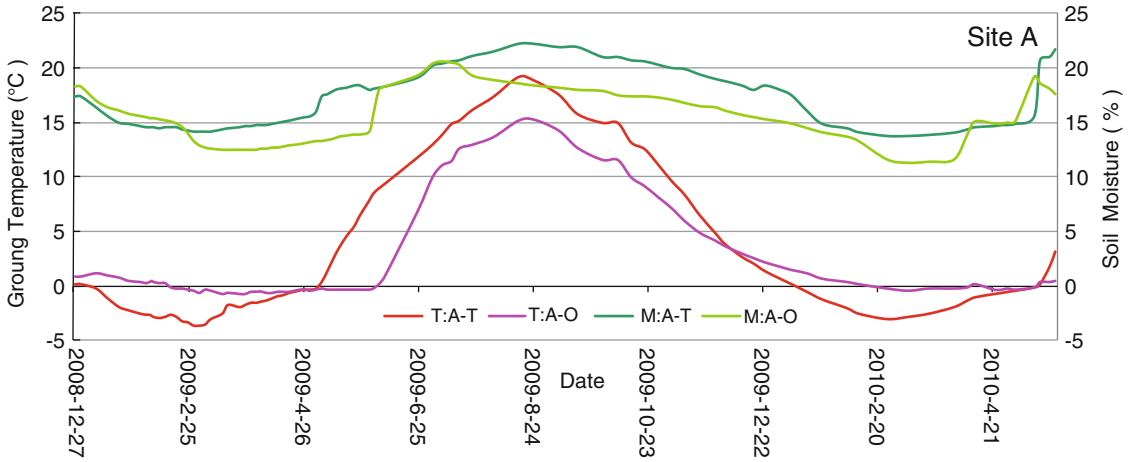

Fig. 4 The curve of ground temperature and soil moisture of site A in 1.4 m depth

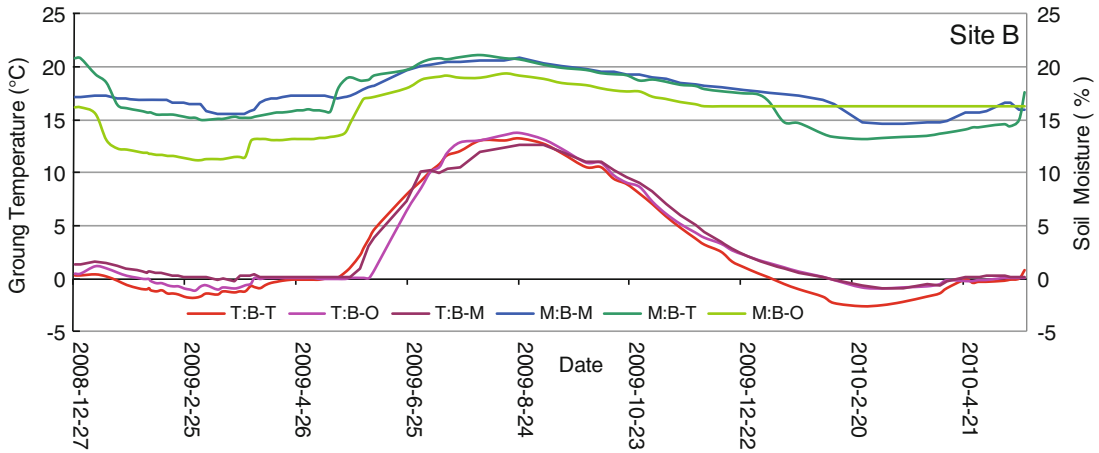

Fig. 5 The curve of ground temperature and soil moisture of site B in 1.4 m depth

different depth are all in the same drilling hole, site B has three drilling holes which located on top(B-T), in middle (B-M) and on foot(B-O)of the slope separately. Site A has only two holes(A-T, A-O) and hasn't the hole in middle of the slope. From January 2009 to June 2010, the monitoring of ground temperature and soil moisture of five drilling holes was conducted. Among them, the value of the 1.4 m depth has the most representative, because it is above the maximum freezing depth, as well as near the sliding surface which was known from the field investigation above. The next analysis is about the value of 1.4 m depth, and the curves can be seen in Figs. 4 and 5.

Variation of Ground Temperature of the Slope

In spring of 2009 and 2010, it can be seen from Figs. 4 and 5 that, in site A, the lowest ground temperature of two springs was −3.7 °C, −3.1 °C, which is found in A-T, and happened on March 1st, 2009 and February 25th 2010. The lowest ground temperature of A-O was −0.6 °C and −0.3 °C, which happened on March 2nd, 2009 and April 23rd 2010. In site B, the lowest ground temperature of two springs was −1.8 °C, −2.6 °C, this is found in B-T, and happened on the same date with A-T. The lowest ground temperature of A-M was −1.1 °C, −0.9 °C which happened on March 2nd, 2009 and March 8nd 2010. The lowest ground temperature of A-O was −0.9 °C, −1.6 °C which happened on March 1st, 2009 and March 3rd 2010. Since after these dates, the ground temperature of the measuring point begins to go up slowly, and goes into the stage of above zero temperature one by one. The order of appearing above zero temperature for five drilling holes is A-T,B-T,B-M,A-O,B-O, and corresponding appearing time is May 5th,, May 11th, May 25th, June 4th, June 7th in 2009. Since after these dates, the ground temperature of five drilling holes begins to rise significantly. It's worth noting that, firstly, from top to toe of the slope, the time interval of appearing above zero temperature is about 30 days, secondly, there is a longer duration of zero temperature.

In summer of 2009, It can be seen from the Figure, in site A, the highest ground temperature was 19.1 °C, 15.3 °C, which happened on August 16th and August 24th. In site B, the highest ground temperature was 13.2 °C, 12.6 °C and 13.8 °C, which all happened on August 24th. It's worth noting here, the difference of the highest ground temperature between site A (with turf) and site B (with Lespedeza) is 6.5 °C.

As the weather turns to autumn, the order of appearing subzero temperature for five drilling holes in is A-T,B-T, B-M,B-O,A-O, and corresponding appearing time is January 8th, January 10th, February 7th, February 7th, February 17th in 2010. Since after these dates, the ground temperature of the measuring point begin to go down continuously.

It can be seen from the above analysis that, for the ground temperature in 1.4 m depth, the top of the slope is affected by the weather temperature mostly, then is in middle of and on toe of the slope. Secondly, the type and density of the plant on the slope also affect the ground temperature in 1.4 m depth. Thirdly, it is in spring that there is a longer duration of zero temperature in 1.4 m depth of the slope, but in autumn there hasn't.

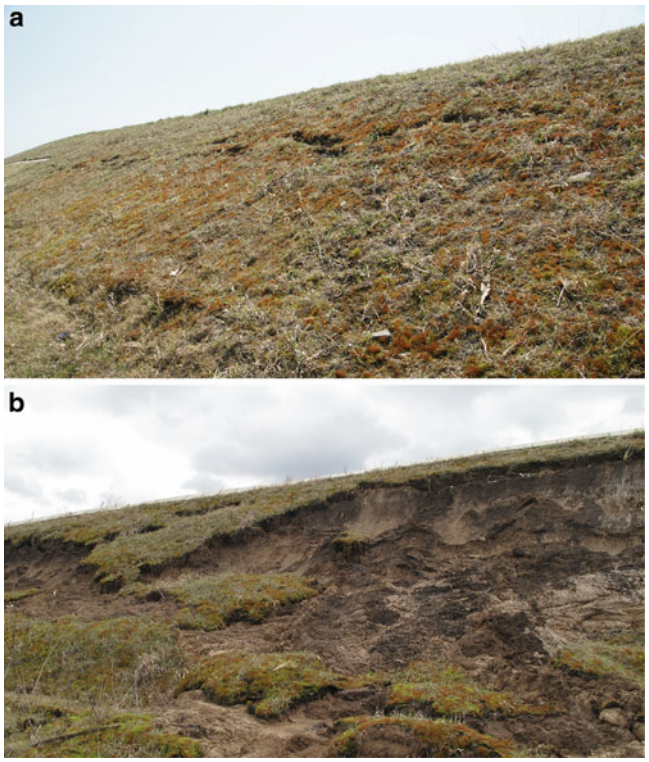

Fig. 6 The slope with turf (Site A). (**a**) The cracks on the slope before landslide. (**b**) The landslide causing by freeze-thaw

Variation of Soil Moisture of the Slope

It can been seen from Figs. 4 and 5 that, during the freezing period, the soil moisture curve has a sharp declining when ground temperature is about 0 °C. After that, the ground temperature declines gently until reaching a minimum value, then the curve rise again slowly, as soon as ground temperature is over the zero temperature, the curve goes up rapidly.

For site A, in 2009 spring, the soil moisture of A-T goes up from 16 % (May 2nd) to 17.4 % (May 5th), at same time, corresponding ground temperature goes up from −0.3 °C to 0.3 °C. The soil moisture of A-O goes up from 13.9 % (May 30th) to 18 % (June 4th), the corresponding ground temperature goes up from −0.2 °C to 0.2 °C. After that, the curve of soil moisture goes up slowly until close or over the value of plastic limit of the soil. The scene situation is, after 2009 spring, there appears cracks near site A (K560 + 420–K560 + 550), as shown in Fig. 6a, then there occur landslide on 7th May 2010, as shown in Fig. 6b.

For site B, in 2009 spring, the moisture curve of B-T has one uplift process, which like site A, but the moisture curve of B-M and B-O have two uplift processes, details are as follows, The soil moisture of B-T go up from 15.8 % (May 14th) to 19 % (May 25th), then the rise turn to gentle, at same time, corresponding ground temperature goes up from 0 °C to 0.1 °C, and keep straight up till to late July. The soil moisture of B-M first goes up from 15.6 % (March 29th) to 16.9 % (April 9th), corresponding ground temperature go up from −0.2 °C to 0.1 °C, next follows a smooth uplift process, then goes up again from 17.3 % (May 25th) to 19.6 % (June 24th), corresponding ground temperature go up from −0.1 °C to 1 °C. The soil moisture of B-O go up from 11.5 % (March 29th) to 13.2 % (April 3th), corresponding ground temperature go up from −0.9 °C to 0.1 °C, next also follows a smooth uplift process, then goes up again from 13.8 % (May 22nd) to 17.2 % (May 30th), corresponding ground temperature goes up from 0.1 °C to 6.4 °C.

It can be seen from above analysis that, soil moisture rises up quickly when ground temperature is above 0.1 °C. The moisture of B-T and A-T begin to rise as soon as ground temperature is larger than zero, and turns to gentle in 3–10 days. The moisture of B-M and B-O increased 1.3 % and 1.7 % when ground temperature rises up to 0.1 °C, but the difference is that the ground temperature here continued to maintain near 0.1 °C for 19 days and 65 days separately, then rise up again, during this period, the moisture of B-M and B-O rise up again for 2.3 % and 3.4 % separately.

The cause of above phenomenon is, during the freezing period, as freezing-front extends to deep slope, there will appear the cracks caused by temperature shrinkage. The new freezing-front in the soil along the cracks was formed, and then the moisture in soil body migrated to the cold freezing-front (Fig. 7), so the curve of moisture here is decline. In spring, the ground temperature rises up, when it reaches

Fig. 7 The migration of moisture in soil body

about 0 °C, the moisture near the freezing-front began to migrate again under the function of gravity and surface tension, and then there is the first uplift process of the moisture curve. When ground temperature was over 0.1 °C, the melting water from snow and infiltrating water make the moisture curve to have the second uplift process.

Conclusion

1. Laboratory test results showed that: For the silty clay slope, the soil cohesion increases with the increase of soil moisture. When soil water content is bigger than the optimum water content, soil cohesion decreases with the increase of moisture. The internal friction angle of soil decreases with the increase of moisture. Freeze-thaw had a significant effect on soil cohesion and internal friction angle. Soil cohesion decreases gradually with the increase of freeze-thaw cycles, soil internal friction increases after the first freeze-thaw cycle, then decreases gradually in later freeze-thaw cycles.
2. Field monitoring results show that, for the ground temperature in 1.4 m depth, whose on the top of the slope is affected by the weather temperature mostly. The kind and density of the plant on the slope also affect the ground temperature in 1.4 m depth.

   During the freezing period, as freezing-front extends to deep slope, there will appear the cracks caused by temperature shrinkage. The new freezing-front in the soil along the cracks is formed, and then the moisture in soil body migrates to the cold freezing-front, so the curve of moisture here is decline. In spring, there is a longer duration of zero temperature in the seasonal active layer of the soil, the moisture near the freezing-front begins to migrate again under the function of gravity and surface tension, and then there is the first uplift process of the moisture curve. When ground temperature is over 0.1 °C, the melting water from snow and infiltrating water near the freezing-front make the moisture curve have the second uplift process.

   In melting period, accumulated water in the temperature shrinkage cracks, as well as long time of zero ground temperature, make water infiltration not be in time, resulting in high moisture in shallow slope, and shear strength of the soil decreasing. The soil body begins to slide along the slip zone under gravity function.

Acknowledgments The authors would like to thank the financial supports provided by the research project of Heilongjiang provincial Science and Technology Department (GZ07 C401), and the Key project of Heilongjiang provincial Transportation Department "Highway Slope Stability and Greening by Vegetation in Cold Regions".

References

Clark MJ (1988) Advance in periglacial geomorphology. Wiley, New York, pp 325–359

Li Y, Zhao K (2002) The analysis of landslide in k2023 of QING-Zang highway. J Geol Hazards Environ Preserv 13(4):33–35

Liu H, Wang P (2006) Stability analysis of instability caused by freeze-thaw for highway earthen side slopes. J Harbin Inst Technol 38 (5):764–766

McRoberts EC, Morgenstern NR (1974) The stability of thawing slopes. Can Geotech J 11:447–469

Niu FJ, Cheng GD, Xie Q (2002) Study on instability of slopes in permafrost regions of Qinghai-Tibet High plateau. In: Yakutsk C (ed) Proceedings of the 5th international symposium on permafrost engineering, Permafrost Institute/SB RAS Press, pp 192–197

Niu F, Cheng G, Lai Y et al (2004) Instability study on thaw slumping in permafrost regions of Qinghai-Tibet plateau. Chin J Geotech Eng 26(3):402–406

Shan W, Guo Y, Liu H (2009) Effect of freeze-thaw on strength and microstructure of silty clay. J Harbin Inst Technol 16(Sup. 1):207–211

Tarr RS (1897) Rapidity of weathering and stream erosion in the arctilatitudes. American Geologist 19:131–136

Wang B, French HM (1995) In situ creep of frozen soil. Tibet pleateau. China Can Geotech J 32:545–552

Wu H, Gao W, Wang G et al (2006) Cause and control of soil-cutting's sliding collapse in frigid zone. J Nat Disasters 15(3):66–70

Zhou Y, Guo D (1982) Principal characteristics of permafrost in China. J Glaciol Geocryol 4:1–19

Zhu C, ZhangJ X, Cheng P (1996) Rock glaciers in the central Tianshan Mountain, China. Permafrost Periglac Process 7:69–78

Temporal Characteristics of Different Cryosphere-Related Slope Movements in High Mountains

Vanessa Wirz, Jan Beutel, Bernhard Buchli, Stephan Gruber, and Philippe Limpach

Abstract

Knowledge of processes and factors affecting slope instability is essential for detecting and monitoring potentially hazardous slopes. The overall aim of this study is to detect and characterize different slope movements in alpine periglacial environments, with the ultimate goal to understand the broad range of phenomena and processes encountered. In this article, our measurement-setup and our strategy for analyzing the spatio-temporal (seasonal and intra-annual) velocity fluctuations of various slope movements is explained and initial results are presented.

GPS (Global Positioning System) devices have been developed and deployed to continuously measure the velocity of slope movements within an Alpine study site. The measurement devices have the potential to operate for several years. Since December 2010, first devices are successfully measuring. Based on these measurements, high-accuracy daily differential GPS-positions and the corresponding velocities are calculated. A steep rock-glacier tongue showed a steady decrease in velocity in winter and a strong acceleration in May during the snowmelt period. These first results demonstrate the importance of continuous (here daily) measurements over longer periods and their potential to enable the inference of factors and processes controlling slope movement.

Keywords

Mass movements • Cryosphere • Differential GPS

Introduction

Permafrost slopes are sensitive to climate change and permafrost degradation can develop or accelerate slope instabilities. With predicted global climate change, it must be anticipated that instabilities of rock slopes and movement of ice-rich debris will increase (Haeberli and Burn 2002).

V. Wirz (✉) • S. Gruber
Glaciology, Geomorphodynamics and Geochronology, Department of Geography, University of Zurich, Zurich, Switzerland
e-mail: vanessa.wirz@geo.uzh.ch

J. Beutel • B. Buchli
Computer Engineering and Networks Laboratory, ETH, Zurich, Switzerland

P. Limpach
Institute of Geodesy and Photogrammetry, ETH, Zurich, Switzerland

In the last decades an increasing number of slopes in periglacial environments developed into fast mass movements (e.g. Lewkowicz and Harris 2005). Further, for many rock glaciers, acceleration could be observed (e.g. Roer et al. 2008; Delaloye et al. 2008), probably due to increasing air-temperatures (e.g. Roer 2006). Additionally, it seems that the number of large rock falls (e.g. Ravanel and Deline 2010) and debris flows (e.g. Jomelli et al. 2004) starting in permafrost areas has increased. While some factors controlling slope stability, such as topography or lithology, remain rather constant over time, others undergo rapid changes in response to climate forcing and may cause unexpected types of lope movements (Gruber 2011). Examples of these are ground temperature, precipitation or melting of surface and subsurface ice.

Hazard assessment and early warning can be improved when it is understood where and when slopes can develop

C. Margottini et al. (eds.), *Landslide Science and Practice*, Vol. 4,
DOI 10.1007/978-3-642-31337-0_49,

into destructive mass movements. So far, most scientific studies concentrate on one specific type of mass movement (e.g. rock glaciers, solifluction, debris flows or fast landslides). In contrast, the overall aim of this study is to analyze slope movements in alpine environment within a broader range of phenomena and processes.

Newly developed methods of terrestrial and aerial surveying increase the ability to observe slope movements in alpine regions (e.g. Kääb et al. 2005; Strozzi et al. 2010). GPS devices allow to continuously measuring the displacement of single boulders (Limpach and Grimm 2009) and, therefore, to analyze the temporal variability of slope movements. This study is part of *X-Sense*, a joint research project between different research groups (geodesy, computer engineering, remote sensing and geography). Within *X-Sense*, new low-cost GPS devices suitable for high mountain environments have been developed (Beutel et al. 2011). The measurement-setup (described in a later section) allows continuously measuring highly accurate positions and tilt-angles of moving boulders with high temporal resolution and coverage (several years). Based on these measurements at least one highly accurate position fix per day can be achieved.

To increase process-understanding of slope movements, the high temporal resolution and coverage are of great value. Mainly because short-term velocity fluctuations of permafrost creep are still poorly understood (Haeberli et al. 2006), although it has been recently discovered that they can be higher than inter-annual variations (Perruchoud and Delaloye 2007). Moreover it has been investigated that seasonal variations can even occur when no inter-annual variability can be observed (Matsuoka 2003; Delaloye et al. 2008). Thus the high temporal resolution allows detecting velocity-variations within short time-period, e.g. seasonal or even sub-seasonal variations. Detecting the timing of acceleration and deceleration of various measurements points allows building and testing hypotheses concerning influencing factors, such as melt water infiltration.

In the following, we explain the research strategy to analyse the spatio-temporal variability of cryosphere-related slope movements, with the main focus on the seasonal and intra-annual velocity-fluctuations. Further, we give an overview of the study site and the setup of the GPS-stations. In addition, preliminary results are shown.

Research Strategy

Studied Phenomena

A range of different types of slope movements will be investigated. While some movements can be clearly related to a certain geomorphological feature, for others the underlying processes are unknown. The term ***c**ryosphere-related slope movements in high **m**ountains (CM-movements)* is therefore introduced to describe slope movements studied within this work. Slope movements in steep bedrock are excluded. Investigated CM-movements have the following common characteristics:

- Located in high mountains
- Cryosphere-related: i.e. strongly influenced by the occurrence of permafrost, glacier-debuttressing and/or snow
- At least partly debris-covered

Planed Methodology

A schematic overview of planned methods is given in Fig. 1. We will include various CM-movements in the analysis, and for each movement type several GPS-locations are chosen. To investigate if the velocities of one single GPS location are representative for the whole feature, the GPS solutions will be compared to other displacement-measurements (e.g. InSAR-derived velocities or mobile periodical GPS measurements of additional boulders). In comparison to previous studies (e.g. Delaloye et al. 2008; Delaloye 2010), the main advantages of our measurements are the high temporal resolution and temporal coverage. Our measurement-setup allows detecting the exact time of velocity-changes and learning about important common characteristics of various CM-movements. This helps to increase the understanding of controlling factors and processes. The setup of the GPS stations is described in a later section.

The GPS-data analysis will have two parts: In *Part A*, statistical methods will be used to describe the temporal characteristics. Mainly intra-annual and seasonal velocity-changes will be analyzed together with auxiliary data (e.g. measured subsurface temperature and data from weather-stations). We will on the one hand analyze the temporal characteristics of each movement type. On the other hand we will study the differences and common characteristics of various movement types in the test site (e.g. rock glacier vs. open fractures). In *Part B*, we will investigate the factors and processes causing CM-movements. This will partly be based on explorative data analysis, but mainly based on hypotheses-testing with statistical models, e.g. multivariate regression models. Hypotheses will be formulated based on first results (of Part A) and literature study. Auxiliary data for the analysis will include measured as well as modelled variables. The model GEOtop (Rigon et al. 2006; Dall' Amico et al. 2011), a physics-based distributed energy balance model, will be applied for this. Modelled auxiliary data include factors, which are rather difficult to measure in the field, but have an influence on movements, e.g. pore water pressure or ground temperature at various depths.

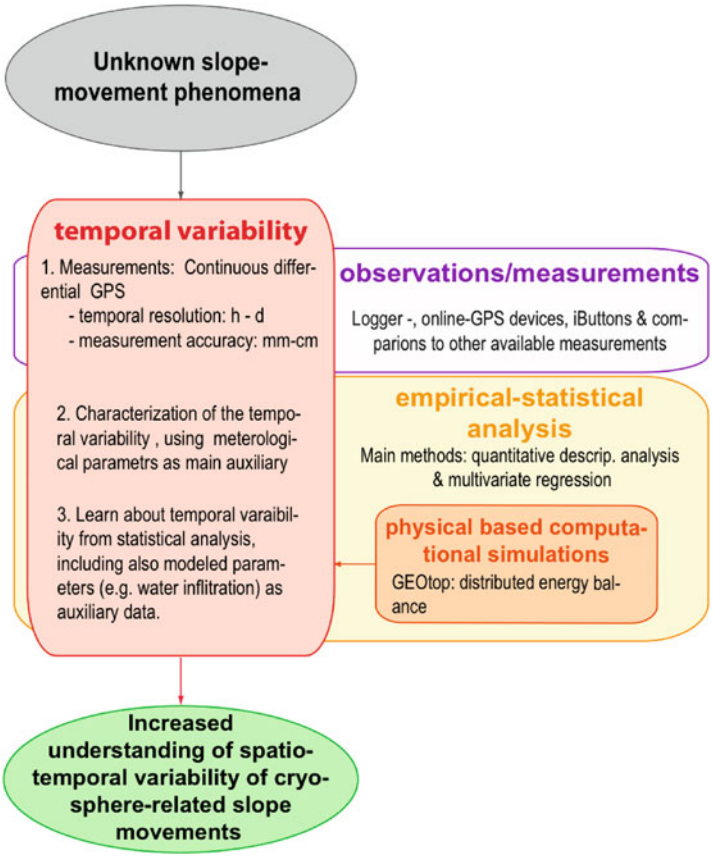

Fig. 1 Schematic overview of the methods, which are included in the study, and how we will combine them

Study Site and Field Instrumentation

The main study site is the *area of Dirruhorn,* located at the orographic right side of the Matter Valley, above Herbriggen/Randa, Switzerland (Fig. 2). The mainly westerly exposed slopes range from 2,600 to 3,200 m a.s.l.. Permafrost is abundant in this area (BAFU 2006; Böckli et al. 2011). The lithology is strongly weathered Gneiss and the main geological structure is oriented approximately parallel to the main slope. The field area includes various CM-movements: e.g. exceptionally fast and potentially dangerous rock glaciers moving up to 10 m/a (Delaloye 2010), and slopes where clear evidence for movement exists but the underlying mechanisms are unclear. Figure 3 shows the geomorphological map of the main study site.

Figure 2 gives an overview of installed GPS stations in the *area of Dirruhorn*. In December 2010, the first three GPS stations were installed (DI2, DI7 and Base). The station *Base* serves as GPS reference station. In March 2011 an additional GPS station was deployed at position DI5. Since May 2011, 11 more GPS stations, mounted on moving boulders continuously measure position and tilt-angle. Additional equipment, such as a base-station for data transmission purposes, a webcam and a weather station, were installed. Nearby each GPS station five iButtons (simple temperature data loggers) were distributed, following the procedure outlined by Gubler et al. (2011), to measure the near-surface ground temperature. The GPS stations are placed in the field such that various types of slope movements are covered. Within the area of one movement type the stations are positioned in such a way that the displacement is as representative as possible (e.g. in the middle of the rock glacier; not at the front). It is planned to expand the setup with further GPS stations and one to two high-resolution cameras. The cameras will deliver important information about actual surface characteristics, such as snow cover. Since 2007 Delaloye (2010) has made mobile GPS-measurements twice per summer in the *area of Dirruhorn*. In the following description of our GPS locations, all given velocities refer to the measurements of Delaloye (2010).

GPS stations DI2, DI5 and DI7 are located on the *Dirru* rock glacier (Fig. 2), which consists of different tongues (Fig. 3). DI5 and DI7 are located on the lower part of *Dirru*, with a slope angle between 30° and 40°. DI5 is located on an inactive tongue, as we assume based on the existing sparse vegetation and as can be seen from the GPS results in Delaloye et al. (2008). DI7 is located on an active steep tongue, which potentially became destabilized in the last years. In 2009 the mean velocity of locations close to

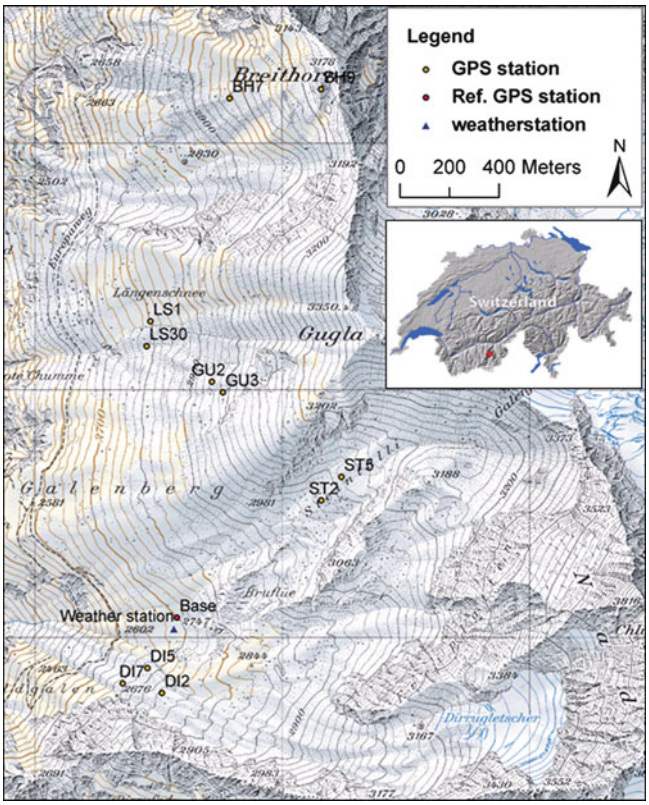

Fig. 2 Overview of the study site *area of Dirruhorn*. The study site is located in the Matter valley, Valais, Switzerland. Topographic map LK 1:25'ooo of Swisstopo

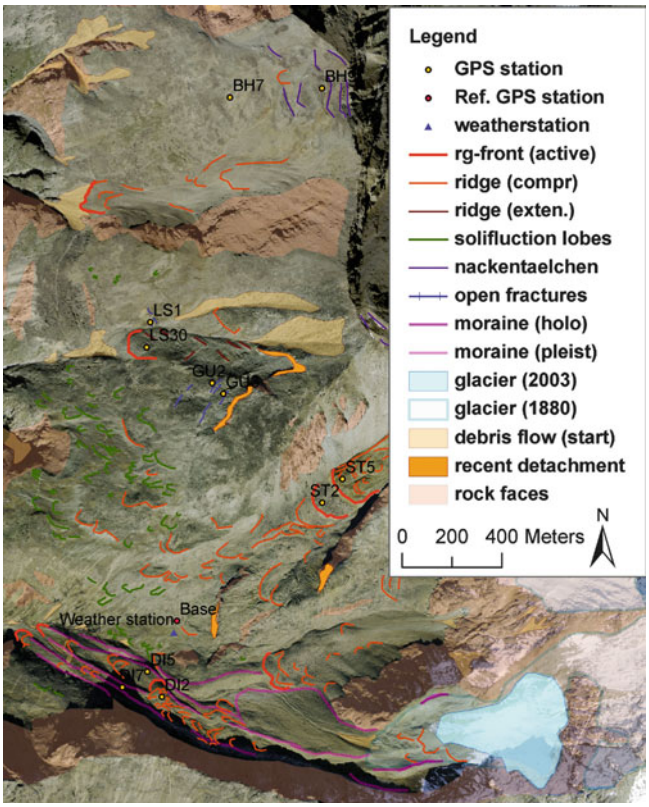

Fig. 3 Geomorphological map of the study site *area of Dirruhorn*. Orthophoto from the year 2005 of Swisstopo

DI7 was assessed to be more than 9 m/a. DI2 is located on the upper part of Dirru, with a gentle slope ($< 15°$) and mean velocity of approximately 3 m/a (measured in summer 2009). Since 2009 the velocities of *Dirru* rock glacier have been observed to be slightly decreasing at all measured locations.

GPS station LS30 is positioned on the *Gugla* rock glacier. This rock glacier has depressions, which indicate extensive flow (Figs. 2 and 3).

GPS stations ST5 and ST2 are mounted on two rock glaciers in the Steintälli (Figs. 2 and 3). The upper rock glacier (ST5) overrides the lower one (ST2). Both rock glaciers have typical ridges and furrows, indicating compressive flow.

GPS stations GU2 and GU3 are mounted upon "Nackentälchen", located below a recent slope failure zone, in the westerly exposed slope of *Gugla* (Figs. 2 and 3). The geomorphological feature "Nackentälchen" is similar to a double-ridge with a small valley in between, but is not located close to a mountain-ridge.

At *Breithorn* (BH9 and BH7) geomorphological features (e.g. Kellerer-Pirklbauer et al. 2010) indicate a deep-seated gravitational slope deformation. BH9 is positioned upon a double-ridge (Figs. 2 and 3), BH7 in the central part of the landslide. Velocities measured in 2008/2009 at Breithorn were between 0.05 and 0.3 m/a.

GPS Devices and Data-Processing

Measurement-Devices

The measurement system consists of distributed GPS loggers that autonomously collect and log GPS data, inclination of the antenna, and system status information over extended periods. At selected positions (DI5, DI7), powerful testbeds (Buchli et al. 2011) have been installed along with the loggers. These prototype sensors, equipped with wireless radios, permit design investigation of a planned online GPS system to provide real-time data for on-the-fly analysis.

The custom GPS logger electronics feature an off-the-shelf GPS receiver that can output data suitable for the differential post-processing algorithm employed within this study. GPS data is currently logged at a sampling interval of 30 s. All sensors are mounted elevated on a mast of 0.5–1.5 m to allow the reception of GPS signals also in deep snow cover. To disambiguate between lateral displacement and tilting of the mast, two inclinometers, for X- and Y-axis, are also logged periodically.

Fig. 4 GPS station at position DI7, on the destabilized tongue of the *Dirru* rock glacier. Station DI7 includes a logger, two inclinometers and a prototype online sensor, all mounted on the same mast. Energy supply is given by a photovoltaic energy harvesting system

The energy to operate the device is provided by a photovoltaic energy harvesting system, and backed by a battery (Fig. 4). The battery acts as buffer that permits running the system during times without solar input. To handle energy fluctuations, the devices have two operating modes. The high-power mode logs continuously to the SD card as long as the battery has an energy content above a given threshold (>11.8 V for 12 V AGM cells). Once the battery capacity drops below this threshold, the device enters an energy-saving mode. In this mode, the GPS receiver is powered only during a statically configured fraction of the measurement period, e.g. 2 h/day. With this setup, the lifetime of the logger is limited only by the SD card capacity.

GPS Data Processing

The GPS data processing is based on single-frequency differential carrier phase techniques. A local GPS reference station, placed within a stable area, is used for the differential computation of the coordinates of the moving GPS stations. Kinematic coordinates with sampling intervals down to 30 s (the sampling interval of the GPS devices) are computed, as well as daily station coordinates. The achieved positioning accuracies are at mm-level for the daily solutions and cm-level for the 30 s solutions (Limpach and Grimm 2009). Based on the GPS station displacements (Fig. 5), 3D-velocities (Fig. 6) are computed using *least-squares smoothing spline* parameterizations and their analytical derivatives.

Preliminary Results and Interpretation

Here we present first results of the GPS stations DI5, DI7 and the reference station *Base*. The data cover the time period from 19 December 2010 until 25 May 2011. The temporal resolution of the preliminary displacement solutions shown is 24 h (Fig. 5). For all GPS stations the standard deviation of the daily GPS solutions was 1 mm in the horizontal and 2 mm in the vertical. The inclinometer measurements were not yet included in the analysis.

The position of the reference station (629575/108081, 2,697 m a.s.l., Swiss coordinate system CH1903) was stable over the entire observation period.

The GPS station DI5, positioned on an inactive tongue of the *Dirru* rock glacier, did not move either and the position (629456/107877, 2,706 m a.s.l.) remained static. This observation is consistent with previous GPS results of Delaloye et al. (2008). The mm-level standard deviation of the daily solutions with respect to the static mean position over the entire period demonstrates the excellent repeatability of the GPS results.

In contrast, measurements of GPS station DI7 showed a total displacement (3D) of 1.43 m from 19 December 2010 to 25 May 2011 (Fig. 5). The total vertical displacement was 0.69 m. Until the middle of April the velocity was approximately linearly decreasing. The mean 3D-velocity (velocity along the main displacement) was ~1.0 cm/day in December and ~0.6 cm/day during the first half of April (Fig. 6). At the end of April the velocity started to increase. The 3D-velocity reached a value of 1.9 cm/day in the middle of May. The acceleration again decreased towards the end of May to a 3D-velocity of 1.5 cm/day.

Air temperatures were measured at the weather station (Fig. 2) since March 2011. Until the end of March, the daily mean air temperature in the area *Dirru* rock glacier was mainly below zero degrees, with the exception of a short period in March (Fig. 7). At the beginning of April, air temperatures increased and were mainly positive for 2 weeks, dropping again to below zero degree in the middle of April. During May air temperatures mostly remained above zero degrees. On webcam images of the *Dirru* rock

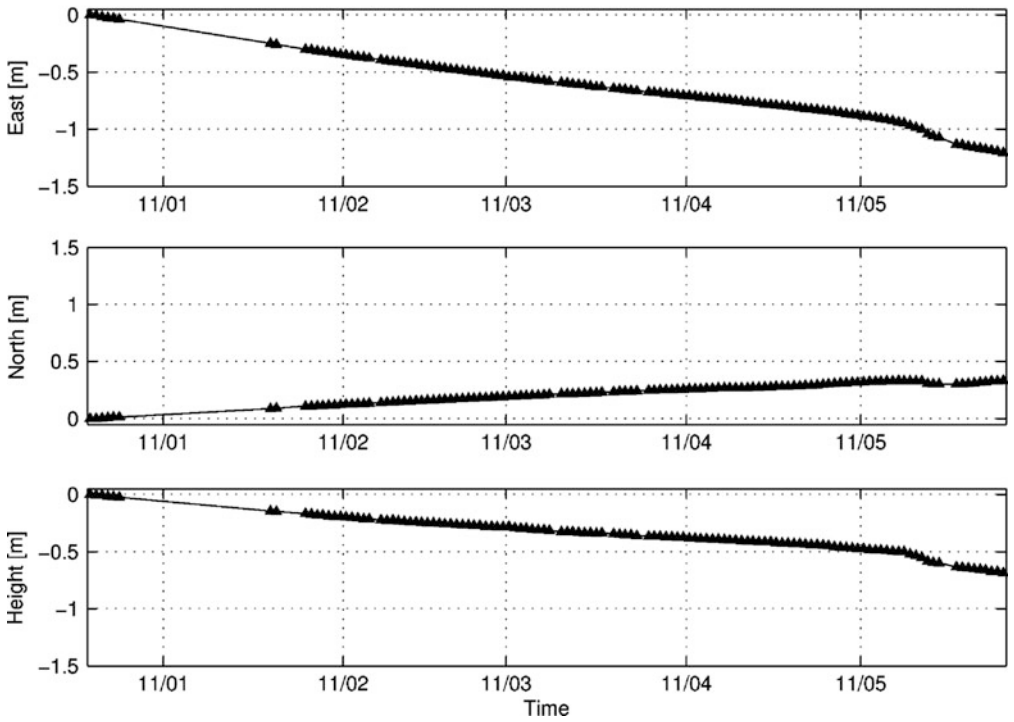

Fig. 5 Daily solutions of displacements of the GPS-device DI7, from differential GPS processing

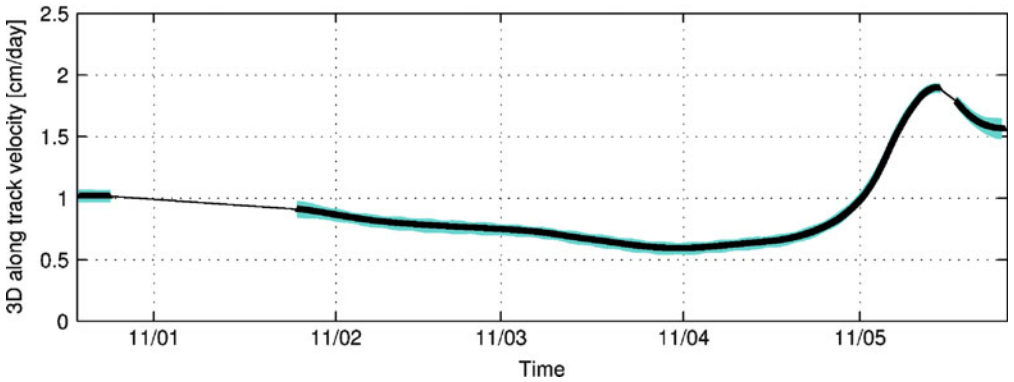

Fig. 6 3D-velocity along the main direction of displacement of GPS-device DI7. The blue error bar shows the uncertainty interval

glacier it is visible, that snow started to disappear in April. In the middle of May many parts of the rock glacier were already snow free.

Our results support previous findings (e.g. Delaloye et al. 2010) that the tongue of *Dirru* rock glacier, where the GPS-device DI5 is located, is inactive. Further, based on first observations we formulate the hypotheses, (a) that the acceleration at position DI7 at the end of April and middle of May was caused by the infiltration of snow meltwater. And (b) that in May due to the lack of meltwater from snow the velocity decreased. (c) The high acceleration in May most probably was accompanied by a tilt of the mast. This rotation of the boulder can explain the sudden change of displacement from north to south around May 20 (Fig. 5). We assume therefore that actual velocity was slightly smaller in the middle of May than shown here.

Conclusions

Within the *X-Sense* project new low-cost GPS devices including two inclinometers have been developed to continuously measure the position and tilt angle of moving boulders. The novelty of obtained data is that they have a high temporal resolution and can cover several years.

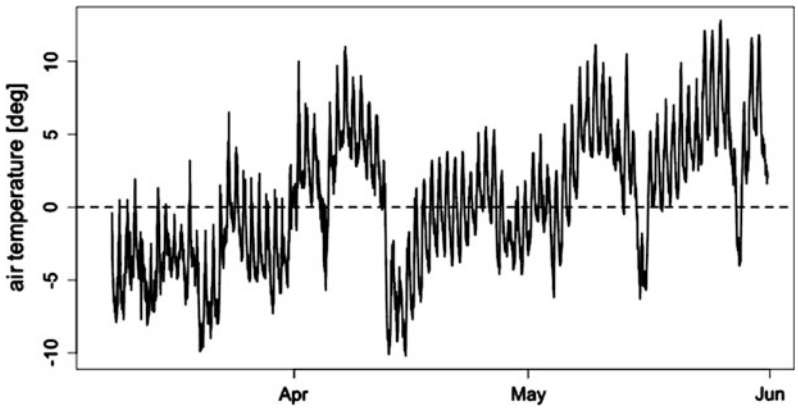

Fig. 7 Air temperatures measured at the weather station next to the *Dirru* rock glacier at 2,697 m a.s.l

This makes it possible to identify both velocity variations (a) within a short period (e.g. week or season) and (b) between different years. The exact timing of acceleration can help to detect influencing factors, such as snowmelt. The low costs per GPS-device allow measuring at many locations. The high number of measurement points, located upon various slope movement types, will help to find common characteristics of cryosphere-related slope movements in high mountains.

First results show high short-term velocity fluctuations in spring. The velocity of a potentially destabilized tongue was slightly linearly decreasing in winter. From the end of April, with increasing air-temperature and the disappearance of the snow cover, velocities increased up to nearly 2 cm/day in the middle of May, but again decreased to ~1.5 cm/day.

Outlook

So far we could only present data from two locations on two different tongues of Dirru rock glacier without inclination-measurements. Nevertheless, the acceleration of position DI7 in May confirms the importance of high temporal resolution and coverage to increase process understanding. The observation that the displacement at station DI7 was most probably accompanied by a rotation of the boulder depicts the importance of measuring the tilt-angle of the GPS-mast. The next analysis will include a more quantitative comparison of GPS data from the different locations and meteorological data, using descriptive statistical methods. To increase process understanding, we will apply statistical methods to combine measured data with physical modelling. Data will cover a longer time-span (from spring to summer).

Acknowledgments This study was funded by Nano-tera.ch. We acknowledge data provided by H. Raetzo from the Swiss Federal Office for the Environment (FOEN) and the unpublished report 2010 made available by R. Delaloye.

References

Beutel J, Buchli B, Ferrari F, Keller M, Thiele L, Zimmerling M (2011) X-Sense: sensing in extreme environments. In: Proceedings of design, automation and test in Europe, 2011

Buchli B, Yuecel M, Lim R, Gsell T, Beutel J (2011) Demo abstract: feature-rich experimentation for WSN design space exploration. In: Proceedings of the 10th international conference on information processing in sensor networks (IPSN 2011), ACM/IEEE, Chicago, April, 2011

Böckli L, Brenning A, Gruber S, Nötzli J (2011) Potential permafrost distribution in the European Alps. Cryosphere Discussion 5:1419–1459

Bundesamt für Umwelt BAFU (2006) Übersicht über die potenzielle Permafrostverbreitung in der Schweiz. www.bafu.admin.ch. Last accessed 21 June 2011

Dall'Amico M, Endrizzi S, Gruber S, Rigon R (2011) A robust and energy-conserving model of freezing variably-saturated soil. Cryosphere 5:469–484

Delaloye R, Strozzi T, Lambiel C, Perruchoud E, Raetzo H (2008) Landslide-like development of rockglaciers detected with ERS-1/2 SAR interferometry. In: Proceedings of the 8th international conference on permafrost, Zürich

Delaloye R (2010) GPS Messungen Mattertal 2010. Bericht. Department of Geosciences, University of Fribourg, Fribourg, Switzerland, unpublished report

Gubler S, Fiddes J, Keller M, Gruber S (2011) Scale-dependent measurement and analysis of ground surface temperature variability in alpine terrain. Cryosphere 5:431–443

Gruber S (2011) Landsides in cold regions: making a science that can be put into practice. In: Proceedings of the Second World Landslide Forum, Rome, 3–9 Oct 2011

Haeberli W, Burn C (2002) Natural hazards in forests: glacier and permafrost effects as related to climate change. In: Sidle R (ed) Environmental change and geomorphic hazards in forests. IUFRO Research Series, CABI Publishing, Wallingford/New York (2002), pp 167–202

Haeberli W, Hallet B, Arenson L, Elconin R, Humlum O, Kääb A, Kaufmann V, Ladanyi B, Matsuoka N, Springman S, Vonder Mühll D (2006) Permafrost creep and rock glacier dynamics. Permafrost Periglac Process 17(3):189–214

Jomelli V, Pech V, Chochillon C, Brunstein D (2004) Geomorphic variations of debris flows and recent climatic change in the French Alps. Climatic Change 64(1–2):77–102

Kääb A, Huggel C, Fischer L, Guex S, Paul F, Roer I, Salzmann N, Schäferli S, Schmutz K, Schneider D, Strozzi T, Weidmann Y (2005) Remote sensing of glacier and permafrost-related hazards

in high mountains: an overview. Nat Hazards Earth Sys Sci 5:527–554

Kellerer-Pirklbauer A, Proske H, Strasser V (2010) Paraglacial slope adjustment since the end of the Last Glacial Maximum and its long-lasting effects on secondary mass wasting processes: Hauser Kaibling, Austria. Geomorphology 120(1–2):65–76

Lewkowicz A, Harris C (2005) Frequency and magnitude of active-layer detachment failures in discontinuous and continuous permafrost, Northern Canada. Permafrost Periglac Process 16:115–130

Limpach P, Grimm D (2009) Rock glacier monitoring with low-cost GPS receivers. In: Abstract Volume 7th Swiss Geoscience Meeting, November 2009, Neuchatel

Matsuoka N, Ikeda A (2003) Contemporary periglacial processes in the Swiss Alps: seasonal, inter-annual and long-term variations, In: Proceedings of the 8th international conference on permafrost, Zürich, pp 735–740

Ravanel L, Deline P (2010) Climate influence on rockfalls in high-Alpine steep rockwalls: the north side of the Aiguilles de Chamonix (Mont Blanc massif) since the end of the 'Little Ice Age'. Holocene. doi:10.1177/0959683610374887

Perruchoud E, Delaloye R (2007) Short-term changes in surface velocities on the Becs-de-Bosson rock glacier (western Swiss Alps). Grazer Schriften der Geographie und Raumforschung 43:131–136

Rigon R, Bertoldi G, Over TM (2006) GEOtop: a distributed hydrological model with coupled water and energy budgets. J Hydrometeorol 7(3):371–388

Roer I (2006) Rockglacier speed-up throughout European Alps – possible controls and implications. Geophys Res Abstracts 8:06022

Roer I, Haeberli W, Avian M, Kaufmann V, Delaloye R, Lambiel C, Kääb A (2008) Observations and considerations on destabilizing active rock glaciers in the European Alps. In: Proceedings of the 9th international conference on permafrost, Fairbanks, 2, pp 1505–1510

Strozzi T, Delaloye R, Kääb A, Ambrosi C, Perruchoud E, Wegmüller U (2010) Combined observations of rock mass movements using satellite SAR interferometry, differential GPS, airborne digital photogrammetry, and airborne photography interpretation. J Geophys Res 115(F1):F01–014

Test of a Procedure to Assess the Stability of Permafrost Rock Walls: The Case of the Pellaud Basin, Rhêmes Valley (Aosta Valley, Italy)

M. Curtaz, A.M. Ferrero, G. Forlani, M. Migliazza, R. Roncella, and M. Vagliasindi

Abstract

The present paper illustrates a working methodology for the stability evaluation of slopes in permafrost conditions in order to draw up an hazard map. The method developed has been applied to a basin named Pellaud, located in the Rhêmes Valley (Aosta Valley Autonomous Region, Northwestern Italy), where several instability phenomena have been recorded in the past. The study is based on an aerial photogrammetric survey performed from helicopter, geo-structural and stability analysis executed using the Digital Surface Model derived from the survey, the regional DTM model and the geotechnical parameters obtained from laboratory tests. Results are shown in terms of thematic maps for an easier and more direct basin hazard visualization.

Keywords

Permafrost • Rock stability • Hazard

Introduction

During the last decades an increase in frequency and intensity of rockfalls and numerous debris flow events have been recorded throughout the Alps (Ravanel and Deline 2010; CENSI CRO 2009). These facts seem to be related to permafrost degradation due to climate change. The challenge is therefore to consider these impacts on natural risks evaluation and management in high mountains. Therefore, new methods need to be finalized and improved in order to bypass the difficulties due to environmental conditions of high mountain territories. Such a methodology has been elaborated and tested in the frame of the Alcotra 2007–2013 "RiskNat" project, in particular in the context of activities B1-C1 "Hazards deriving from high mountain environment evolution" on a little catchment basin in the Aosta Valley, affected by mass wasting processes (rockfalls and debris flows).

The studied area is the Pellaud basin in the Rhêmes Valley (Aosta Valley Autonomous Region, Northwestern Italy). This small basin (Fig. 1) is surrounded by rock cliffs which stand on steep slopes where the fallen rock material accumulate, until strong precipitations carry and transport it to the valley floor, causing debris flows and mass wasting events. In 2005, some rockfalls at the basin's head triggered some debris flows that hit the alluvial fan and left some unstable parts in the rock walls that needed barring interventions.

During helicopter surveys some ice was seen in the unstable rock mass; this fact led to consider that permafrost degradation and instability phenomena could be correlated. The study has been conducted in order to identify the potentially unstable zones, on the basis of the geostructural and morphological characteristics of the rock slopes, but also to evaluate the effects of a possible permafrost degradation on the stability of the cliff sectors. In this paper, the working methodology elaborated and tested on the Pellaud site is

M. Curtaz (✉) • M. Vagliasindi
Fondazione Montagna sicura, Cormayeur, Italy
e-mail: mcurtaz@fondms.org

A.M. Ferrero • G. Forlani • R. Roncella
Department of Civil Engineering, Environmental and Territory and Architecture, University of Parma, Parma, Italy

M. Migliazza
Earth Science Department, University of Milan, Milan, Italy

C. Margottini et al. (eds.), *Landslide Science and Practice*, Vol. 4,
DOI 10.1007/978-3-642-31337-0_50,

Fig. 1 Pellaud basin with 2005 detachment area in evidence

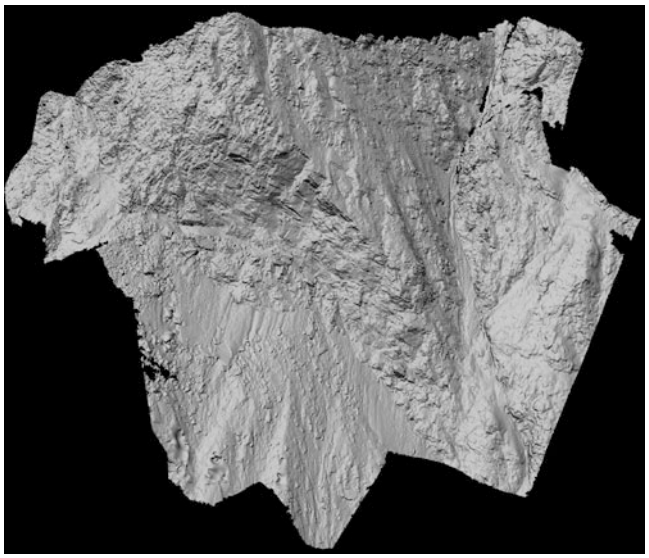

Fig. 2 DSM 3D representation of the slope

presented as an example of stability assessment at a basin scale.

Aim of the work is, in particular, to address the following issues:

1. The geostructural conditions of the slopes;
2. The slope stability conditions as a function of the variation of the strength properties of the discontinuities due to permafrost changes.

The importance of these two issues is particularly relevant in high mountain basins because:

- The existing discontinuities tend to be open and to be affected by thaw-freezing cycles, thus exposing potentially unstable blocks;
- The assessment of stability is linked not only to the orientation of the geo-structural planes and of the slope, but also to the hydraulic and mechanical properties of the rock mass;
- Thaw-freezing cycles induce changes in the strength of the planes and in hydraulic conditions;
- Permafrost degradation can lead to a deepening of the active layer and to an increase of the depth concerned by thaw-freezing cycles;
- The orientation of the planes of discontinuity is often very difficult and dangerous to assess because of environmental conditions;
- Dimensions of the rock walls to examine are often wide;
- The basin geometry is a fundamental basis for all zoning issues (stability, danger etc.).

Photogrammetric Survey

The photogrammetric survey was carried out from a helicopter using a Nikon D3× camera (format 36 × 24 mm, resolution 6,048 × 4032) with a 35 mm lens; two strips were collected with very high forward overlap (more than 80 %); the GSD (Ground Sampling Density) is about 7 cm. Block orientation has been performed by automatically finding tie points with a Structure from Motion algorithm implemented in EyeDea (Barazzetti et al. 2011); in each image, an average of about 500 tie points were measured; each point was imaged on average in eight photos: in such a way, the inner block structure is very strong and a fair amount of reliable seed points is provided for the DSM generation.

Block georeferencing was performed by measuring about 30 ground control points from two theodolite stations in the valley. The estimated average accuracy for the tie points is about 2 cm in North and Elevation and about 6 cm in East direction. A dense point cloud of about $2 \cdot 10^6$ points with an average spacing of 15 cm has been produced using Dense Matcher, a software using image correlation techniques developed at Department of Civil Engineer of University of Parma (DICATeA). In Fig. 2 the 3D representation of the slope is reported.

Geostructural Survey

In order to carry out a stability analysis, it was necessary to survey the number and respective orientations of the discontinuity families in the examined rock mass. For this purpose a geostructural survey of the discontinuities was conducted using the ROCKSCAN programme (Voyat et al. 2006; Ferrero et al. 2009), which allows to determine the orientation and position of conveniently chosen surface discontinuities automatically identified on the basis of the results of the photogrammetrical survey of the walls. The programme, through opportune geometrical segmentation

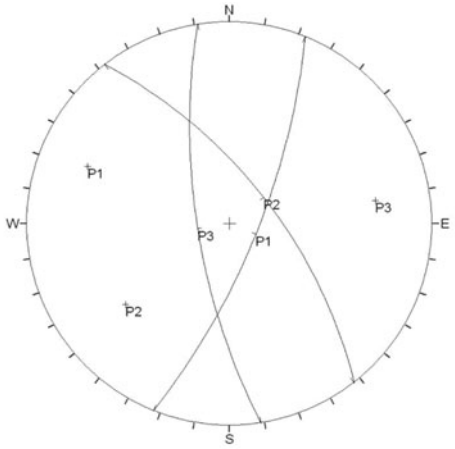

System Pi Intersection Rij	P1	P2	P3	R12	R13	R12
Dip [°]	74	66	72	66	42	32
Dip Dir [°]	112	052	261	060	186	339

Fig. 3 Stereographic projection and orientation angles of discontinuity systems

processes of the DSM, has made it possible to determine the equation of the plane that best approximates the geometry of the selected zone. The discontinuity planes were then identified on the photographs and, thanks to the coupling of these with the DSM of the examined wall, their position in space, and their immersion and dip values were defined.

Altogether 500 planes were identified, and the orientation (dip-dip direction), position and spacing were identified for each of these. The surveyed data were treated statistically using the DIPS 5.1 programme (DIPS 5.1, 2009) in order to identify the discontinuity systems, their mean orientation and the characteristic spacing values. Three main discontinuity systems were identified (Fig. 3). It was then possible to analyse their kinematics and verify their stability.

Stability Analysis and Thematic Maps

Kinematics analyses study the geometric possibility of a block to move, without taking into consideration the forces that determine the movement. Then, through a comparative analysis of the attitude of the discontinuity systems in the rock mass and the orientation of the slope, it is possible to identify the movements that could occur (possible kinematics) and to distinguish them from those that cannot occur (impossible kinematics). It is therefore possible, according to the geometric characteristics, to identify possible movements, such as: planar sliding, tri-dimensional sliding (or wedge sliding), overturning of blocks and flexural overturning. The kinematics analyses were conducted through the Markland test, which consists in using a stereographic grid on which the slope face, the discontinuity families and their relative poles are represented. Once the possible cases of kinematics have been identified for each plane, it is possible to analyze the stability conditions, considering the forces that could cause the block moving.

The stability verifications are then conducted by applying the limit equilibrium method (LEM) for each example of kinematics identified as being possible, considering the forces at play that tend to mobilize the block and the resistant ones that oppose such a mobilization. The result of these analyses is expressed through a safety factor that quantifies the propensity to mobilize of the possible cases of kinematics.

Analysis of Grid Effect

The stability analysis was carried out by dividing the basin into a regular square mesh grid and defining a mean local orientation value for each mesh (dip and dip direction). Initially meshes of 5, 4, 3, 2, 1 and 0.5 m were considered, and a parametric analysis was conducted in order to identify the representative dimensions (Fig. 4).

In order to perform this analysis, the Markland test was first carried out for each cell and then the presence of possible cases of kinematism was evaluated. The kinematisms were verified for all three discontinuity planes and for the corresponding intersection networks (in the case of wedge sliding), in other words: planar sliding along planes P1, P2 and P3; tri-dimensional sliding along the R12, R13 and R23 intersection networks; the block overturning with respects to the basic P1 planes (and intersection line R23), P2 (and intersection line R13) and P3 (and intersection line R12); flexural overturning with sliding along P1, P2 and P3. The safety factor for the cells in which a case of potential kinematics was identified was calculated by applying the limit equilibrium method. If the safety factor resulted to be lower than 1, the cell was considered unstable; instead, if it resulted to be higher than 1, the cell was considered stable. This process was repeated for all of the six cell dimensions.

In this first stage, the analyses were conducted without considering the hydraulic underpressure or the presence of rock bridges, but considering a friction angle of the discontinuities equal to 35°. Comparing the results of unstable areas obtained for different cell sizes, it emerged that the percentage variation of the area was minimum: the results of the analyses were therefore not affected to any significant extent by the scale effect. It was therefore decided to adopt the 5 m side cell as a representative dimension in order to limit the number of cells that would be necessary to work on.

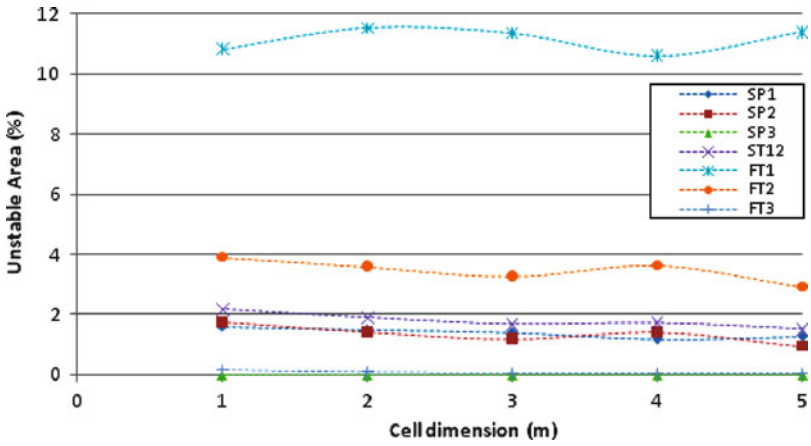

Fig. 4 Grid size effect on the unstable area

Parametric Analysis

The study was then continued using only the representative 5 m cell mesh and it consists in parametric analyses varying the strength characteristics of the discontinuities and the hydraulic underpressure conditions, in order to simulate the freeze-melting effect.

The first step was to repeat the Markland test considering friction angle values of the discontinuity of 30°, 35°, and 40°, respectively. As previously mentioned, the considered kinematisms were planar sliding, tri-dimensional sliding, flexural toppling and the toppling of blocks. It was therefore investigated whether there were conditions, in each of the cells, that could trigger one or more of these types of kinematism. A thematic map of the examined area (Fig. 5) was then drawn up to represent the results for each type of kinematism; the cells in which no cases of potential kinematism were observed were colored green, while the cells with potential cases of kinematism were colored red. The test pointed out that 39.2 % of the examined cells can be considered potentially unstable. This value includes cells in which at least one type of potential kinematism was identified. Some showed signs of the coexistence of different possible types of kinematism.

Once the results of the Markland test were known, it was then possible to conduct the parametric analyses for the cells where potential kinematism had been identified.

The first parametric analysis carried out consisted in evaluating the influence of the decrease in discontinuities friction angle value on the safety factor value. As already mentioned, the safety factors were calculated with formulas derived from the analysis of the limit equilibrium. From these analyses it emerges that the types of kinematism in the examined basin with the highest percentages of probability of occurrence are flexural toppling with sliding along P1, flexural toppling with sliding along P2 and tri-dimensional sliding along the R1–3 intersection line. Furthermore, the values of the safety factors decrease with the friction angle of the discontinuity, both in the case of planar sliding and tri-dimensional sliding. However, it is possible to note that the percentage of actually unstable cells does not vary with a variation of the friction angle of the discontinuity. This means that when the safety factor is below 1, it remains so, even with a variation of the friction angle of the discontinuity. On the other hand, where the safety factor is above 1, it remains so, although the value varies. This is not the case when flexural toppling is considered, as there are more noticeable variations in the safety factor, and therefore in the percentage of unstable area, for variations of the friction angle of the discontinuity.

Again in this case, thematic maps were drawn up in which the unstable cells (FS $<$ 1) were colored red, the stable ones, but which come close to the limit equilibrium condition (1 $>$ FS $>$ 1.5) were colored yellow, the stable cells (FS $>$ 1.5) were colored green and the cells in which no kinematism was previously pointed out were colored blue.

The second parametric analysis evaluated the influence of rock bridges (and therefore an apparent cohesion) on the safety factor values and therefore the influence of the discontinuity persistence.

Persistence represents the ratio between the discontinuous areas and the total reference area. Therefore, a persistence of 100 % corresponds to an infinitely extended discontinuity condition, while a persistence of 0 % corresponds to an intact rock condition. In order to conduct this analysis, it was necessary to know the cohesion value to be associated to the rock matrix and therefore the geology of the examined area. As this area is made up of minute gneiss and schists, it was decided to adopt a cohesion value of 39 MPa. This value was derived from laboratory analyses and it corresponds to an intact rock condition. However, if one wishes to increase the persistence of the discontinuity, it is necessary to refer to an apparent cohesion value that needs to be associated to this value. A precautionary estimation is usually carried out in stability analyses considering a persistence of 100 %. The persistence was then gradually

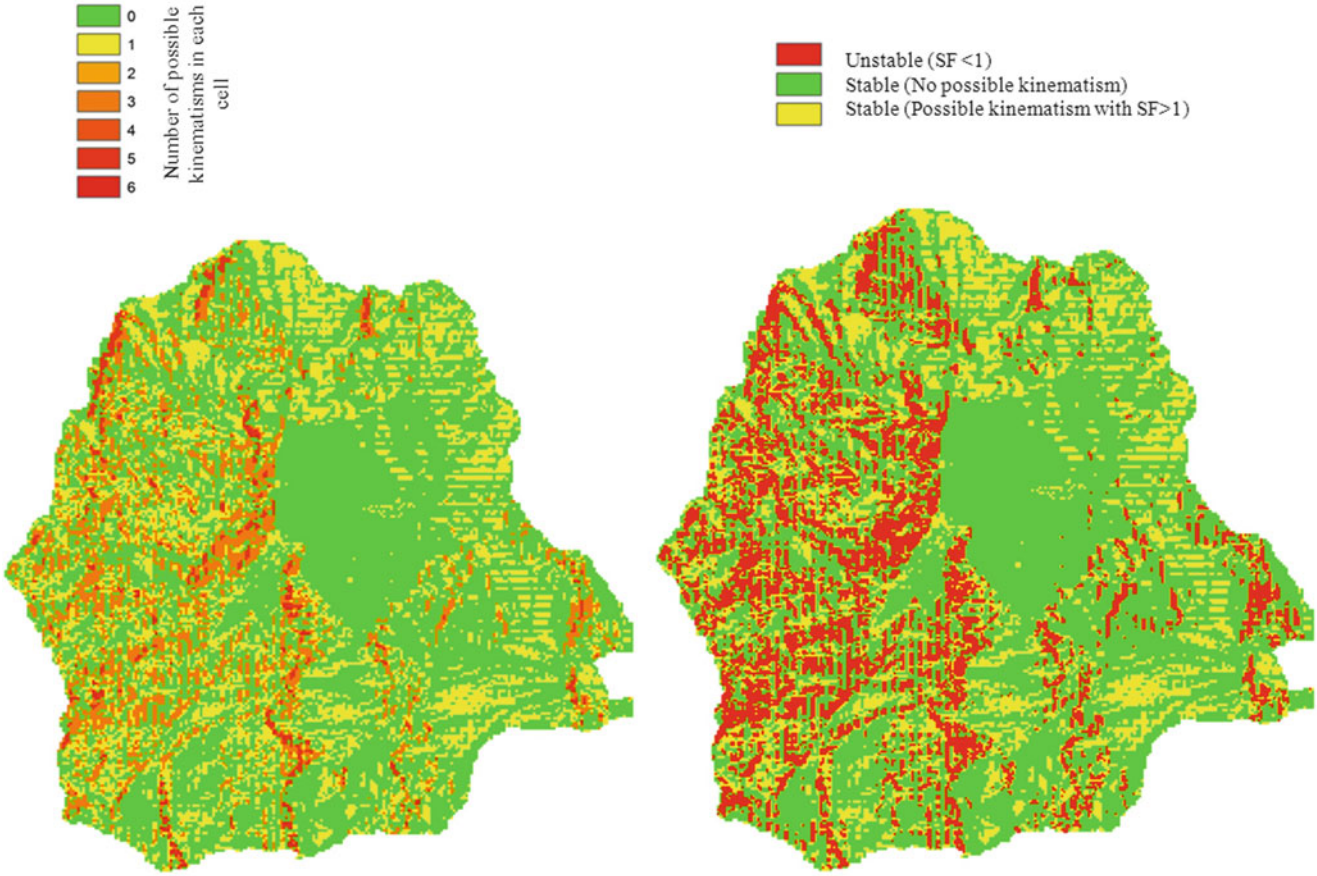

Fig. 5 Maps of kinematism and instability zones

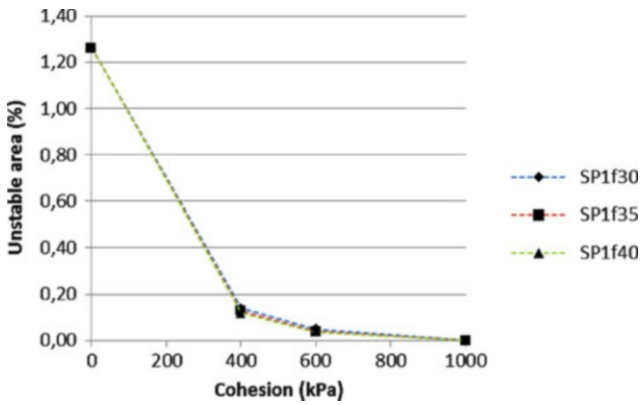

Fig. 6 Unstable area versus apparent cohesion obtained for sliding along plane P1 by varying the value of discontinuity friction angle

diminished in order to identify the value corresponding to the total stability. Apparent cohesion values of 0.40, 0.60, and 1.0 MPa, which represent persistence values of 98.9 %, 98.4 % and 97.4 %, respectively, were considered. The analysis was conducted with friction angle values of the discontinuity of 30°, 35° and 40°, but only for planar sliding phenomena. The results have clearly shown how the presence of even very small rock bridges can drastically reduce the percentage of the unstable area; for example, the unstable area of 1.26 % for planar sliding along plane P1 (Fig. 6) with a friction angle of the discontinuity of 35° in infinitely extended conditions, is reduced to 0.13 % (decrease of 89.05 % compared to the previous situation) for a persistence of 98.9 %. The same was verified for planar sliding along the P2 plane, with a friction angle of the discontinuity of 35°, as there is an unstable area percentage of 0.94 % in infinitely extended discontinuity conditions, while for a persistence of 98.9 %, the unstable area is reduced to 0.04 %, with a decrease of 95.74 %. For planar sliding along P3, instead, there are no cases of potential kinematics, therefore the unstable area results to be nil. The analysis has also pointed out that, with a persistence of 97.44 % (apparent cohesion of 1,000 kPa), total stability conditions are reached for all the considered cases of kinematism.

Finally, observing the results, it is also possible to note a slight variation in the percentage of stable area, in function of the friction angle of the discontinuity (Fig. 7), something which does not occur for planar sliding in the absence of cohesion. Again in this case, thematic maps were drawn up, with the same characteristics as the previous ones, to represent the results.

The third parametric analysis investigated the role of water presence, and therefore different hydraulic underpressure

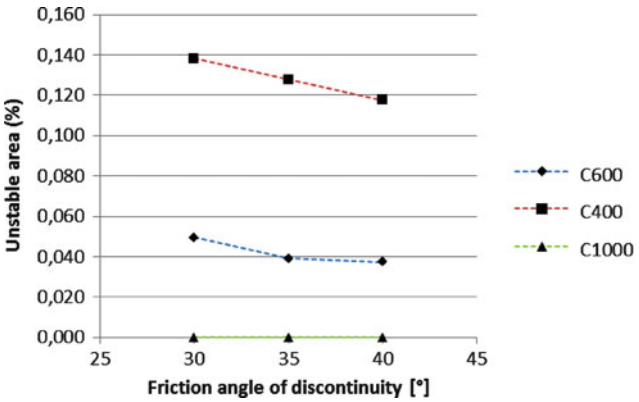

Fig. 7 Unstable area versus discontinuity friction angle obtained for sliding along plane P1 by varying the value of apparent cohesion

hypotheses. The following configurations were considered in particular:

- The presence of hydraulic underpressure along the sliding plane (U);
- The presence of hydraulic underpressure along the sliding plane + tension crack (U + V).

The analysis was only performed for planar sliding and the presence of rock bridges was not considered.

For each examined kinematism, the percentage of unstable area does not depend on the two hydraulic configurations or in consideration of the friction angle of the discontinuity. In fact, all the cells where a potential kinematism was identified, (both for planar sliding along plane P1 and for planar sliding along plane P2) resulted to be unstable, while no example of kinematism was found for planar sliding along plane P3. What does vary between the two configurations is obviously the safety factor value, FS, which, however, always remains below 1 and sometimes even takes on negative values. As in the other two cases, thematic maps were drawn up to represent the results.

Putting together the results of the different stability analyses, it results that 52.3 % of the cells in which potential kinematisms were identified, are unstable. Overall, the unstable area is equal to 20.5 % of the total area of the examined basin.

In conclusion, the substantial importance of cohesion on the discontinuities, from the mechanical point of view, has been pointed out. This cohesion is due to the strength of the rock bridges: in many cases, a very low percentage of rock bridges (less than 2 %) is sufficient to guarantee stability of the blocks. This result confirms the probable progressive mechanism of block detachment, due to the rupture of rock bridges, because of cyclic loading phenomena caused by alternations of freezing and melting of the water inside the fractures. The presence of hydraulic underpressure is in fact due to the possibility of a greater water circulation during the melting phases, and the variations in temperature influence the evolution of instability, at least in an indirect manner.

Conclusions

The methodology tested for the Pellaud basin, described in the present paper, can be applied to other basins in order to draw up a picture of the instability at a basin scale and to detect most unstable sectors of rock walls. This procedure answers to some critical points related to performing stability analysis in high mountain areas.

Using a photogrammetric survey from helicopter as basis for the geostructural analysis done by means of ROCKSCAN software allows to get detailed data, avoiding direct contact with the rock face, often instable.

The survey time is reduced and a wider area can be inspected. The availability of high resolution DTM model allows to extend the study to all the basin and to recognize which type of kinematisms can produce, where and which could be the influence of permafrost degradation inside the rock mass. The results show the major role of the presence of rock bridges on stability and the susceptibility of these to permafrost degradation due to freeze-melting cycles solicitation and water circulation and underpressure inside the fractures. Comparing the maps with the position of past events, like the rockfalls of 2005, an agreement is found: the sector of 2005 rockfall scar is still one of the unstable areas.

Acknowledgments This work has been realized and funded in the framework of the project RiskNat (2007–2013 Operational programme for cross-border cooperation Italy – France, Alps – ALCOTRA) in particular in activity B.1-C.1 “Hazards deriving from high mountain environment evolution” in collaboration with Fondazione Montagna sicura.

References

Barazzetti L, Forlani G, Remondino F, Roncella R, Scaioni M (2011) Experiences and achievements in automated image sequence orientation for close-range photogrammetric projects. Proc SPIE 8085:80850F. doi:10.1117/12.890116

CENSI CRO (2009) Censimento dei Crolli in Roccia in alta quota. Relazione tecnica finale Ing. Michèle Curtaz. Internal report

DIPS 5.1 (2009) Software M.S. Diederichs e E. Hoek – Rock Engineering Group Department of Civil. Owned and distributed by Rocscience

Ferrero AM, Forlani G, Roncella R, Voyat HI (2009) Advanced geo structural survey methods applied to rock mass characterization. In: Rock mechanics and rock engineering, Springer, Wien/New York. Available on line DOI 10.1007/s00603-008-0010-4

Ravanel L, Deline P (2010) Climate influence on rockfalls in high-Alpine steep rockwalls: the north side of the Aiguilles de Chamonix (Mont Blanc massif) since the end of the ‘Little Ice Age’. The Holocene Online First, published on 15 July 2010 as doi:10.1177/0959683610374887, pp 1–9

Voyat IH, Roncella R, Forlani G, Ferrero AM (2006) Advanced techniques for geo structural surveys in modelling fractured rock masses: application to two Alpine sites. In: GoldenRocks 2006: 41st U.S. Rock mechanics symposium, Golden

Permafrost Degradation and Destabilization of Alpine Rockwalls: A Very Close Link in the Mont Blanc Massif

Ludovic Ravanel and Philip Deline

Abstract

The number of rockfalls actually seems to rise in the Alps, while vulnerabilities are increasing in high altitude and in valleys. Due to a lack of systematic observations, frequency and magnitude of rockfalls, as well as their triggering factors remain poorly understood. We here analyse different inventories of rockfalls acquired in the whole Mont Blanc massif by three innovative methods in order to emphasize the role of permafrost. Permafrost degradation appears to be the most likely triggering factor. In particular, almost all of the recorded rockfalls occurred in a context of permafrost, a very good correlation exists between climate (temperatures) and rockfalls, the other temperature-dependent factors may only explain a little part of the rockfalls, and topographic factors are highlighting the importance of permafrost in rockfall trigger. Within the context of global warming scenarios for the twenty-first century, these results raise the question of risk assessment and management in high mountain regions.

Keywords

Rockfalls • High mountain • Permafrost • Global warming • Mont Blanc massif

Introduction

It is a well-known fact that climate and evolution of alpine glaciers are closely related. The relationship between climate and rockfalls in high mountain rockwalls is not so clearly understood, even though rockfalls may have strong impacts on people, infrastructures, and landscape (Haeberli et al. 1997). This misapprehension is partly explained by a lack of rockfall data, while back analysis of past events is fundamental to assess the role of rockwall permafrost degradation in triggering rockfalls in high mountains – whereas the geological structure makes the rock face more or less prone to rockfalls.

The term 'permafrost' refers to any subsurface material at 0 °C or less for at least 2 years. In rockwalls, ice can form or melt in clefts, while air temperature evolves (Harris et al. 2009). Because the strength of the ice lowers as its temperature rises, especially when approaching the fusion point (Davies et al. 2001), rock slope stability can decrease by three processes, which have different consequences in terms of frequency and magnitude of related slope failures: (1) formation of an active layer (i.e. superficial layer with positive temperatures during each summer season) by heat conduction; (2) deepening of the active layer during one season or several years, by heat conduction; (3) deep thawing in cleft matrix by heat advection (heat supply by percolating water) – that may be delayed by decades, centuries, or millennia (Gruber and Haeberli 2007).

Here, we analyse different inventories of rockfalls acquired in the whole Mont Blanc massif by three innovative

L. Ravanel (✉)
EDYTEM Lab, University of Savoie, CNRS, Le Bourget-du-Lac F-73376, France

Institute of Geography, University of Lausanne, Anthropole, Lausanne CH-1015, Switzerland
e-mail: Ludovic.Ravanel@univ-savoie.fr

P. Deline
EDYTEM Lab, University of Savoie, CNRS, Le Bourget-du-Lac F-73376, France

C. Margottini et al. (eds.), *Landslide Science and Practice*, Vol. 4,
DOI 10.1007/978-3-642-31337-0_51,

methods, in order to emphasize the role of permafrost degradation.

The analysis of all those events aims at verify the hypothesis that permafrost degradation is the most likely triggering factor of slope instability.

The Mont Blanc Massif

The Mont Blanc massif, oriented SW-NE, has an area of approximately 550 km^2 and its highest point is at 4,810 m a.s.l. Bordered by the deep valley of Chamonix on the NW, the Val Veny on the E, and the Val Ferret on the SE, it is characterized by an extraordinary combination of peaks and ridges, with glaciers covering about 40 % of its surface (Fig. 1). Many of its granitic, fractured faces and summits stand well above 3,000 m a.s.l.

The Mont Blanc is mainly a granitic batholith formed during the Hercynian orogeny by granite intrusion in the gneissic basement (micaschists and gneiss). The granite changes from an intrusive position in gneiss in the SW to a tectonic contact in the NE. Tilted towards the NW, the massif is cut in panels by large subvertical Variscan, recurrent faults (north–south), and alpine faults (N40–N60 °E) with mylonitized zones (shear zones). The Mont Blanc granite has a very coarse-grained texture, with facies varying from microgranite to porphyroidic granite. Multiple tectonic phases have broken up the rock with multiple direction planes that may overlap.

Finally, the combination of past and present glaciations, steep and fractured rock walls, and strong relative relief results in high magnitude morphodynamics.

Methods

We photo-interpreted a series of photographs of two areas of the Mont Blanc massif (the west face of the Drus and the north side of the Aiguilles de Chamonix), which have been choosen because of the wide existing documentation since the end of the LIA. The first step consisted in setting up a documentary corpus. For the west face of the Drus, the oldest document used is a daguerreotype of 1854 (Ravanel and Deline 2008). For the north side of the Aiguilles de Chamonix, the first shots were realized between 1858 and 1860 (Ravanel and Deline 2011). Nearly 400 photographs have been gathered but only a few dozen could finally be used, the others having a poor lighting, an improper angle, a low clarity, a cloud cover, or were damaged. In the two studied areas, the reconstructions were not conducted in the same way because of different rockwalls dimensions and dynamics but both methods consisted in comparing and interpreting photographs in order to delineate

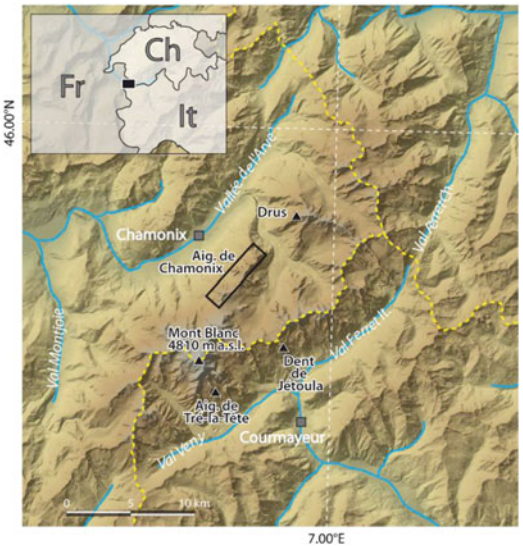

Fig. 1 The Mont Blanc massif

the rockfall scars, determine periods characterized by morphological and colour changes caused by rockfalls, and date the identified rockfalls. In both sectors, it was often necessary to diversify and cross-check information sources in order to precisely date collapses. Collapsed volumes were estimated by terrestrial laserscanning, laser surveying or indirect measurements (on maps or Digital Elevation Models).

Only a structured network of observation, coupled with fieldwork, can allow a nearly completecensus of current rockfalls. For this purpose, a network was set which consists in dozens of guides, hut keepers and mountaineers sensitized to rockfalls observation (Ravanel et al. 2010). The network is fully operational since 2007 and focused on the central part of the Mont Blanc massif (57 %) due to heavy workload in that area. The census is carried out with reporting forms, indicating the main features of the rockfalls and the conditions of the affected rockwalls. The network is reactivated every year. As such network guarantees a very good representation of data but can not ensure the completeness of the inventories, important fieldworks are also conducted every fall in order to check the reported observations and to complete them.

To compare the data obtained by the observation network with the exceptional morphodynamics related to the 2003 summer heatwave, the 2003 rockfalls were identified from their supra-glacial deposits through the analysis of the 051/257 SPOT-5 image taken at the end of the heatwave (Ravanel et al. 2011), which covers the entire massif.

The characteristics of each collapse (and deposit for 2003) were determined using several methods. The altitude of scars, slope/orientation of the affected rockwalls, and the surface of the deposits were calculated within a

Table 1 Main results of the three methods used in the Mont Blanc massif to document rockfalls

Site and period	Drus and Aiguilles de Chamonix End LIA – 2009	Whole massif 2003	Central part of the massif 2007–2009
Number of years	150	1	3
Rockwall area (m^2)	3.6×10^6	126×10^6	84×10^6
Number of rockfalls	50	182	139
Total volume ($\times 10^3$ m^3)	725 ± 120	355 ± 100	185 ± 45
Mean volume (m^3)	15.5	1.9	1.5
Mean altitude (m a.s.l.)	3,165	3,470	3,310
Max. altitude (m a.s.l.)	3,560	4,160	3,965

Geographical Information System. In case of lack of any direct measurement of the scars, the surface of the deposits was multiplied by the estimated thicknesses, in order to assess the collapsed volumes (Table 1). The possible or probable presence of permafrost was determined from the TEBAL model (Gruber et al. 2004) of Mean Annual Ground Surface Temperature distribution.

Results

Evolution of Rockfalls Since the End of the Little Ice Age

The Drus and the Aiguilles de Chamonix rockfalls are distributed with singularity over the last 150 years. Eight rockfalls have affected the Drus between 1905 and 2005, producing the retrogressive erosion of the Bonatti Pillar until its final collapse in June 2005 (265,000 m^3; Fig. 2). In the Aiguilles de Chamonix, 42 rockfalls were documented between 1947 and 2009, but most of them occurred recently.

From the end of the LIA until the mid-twentieth century, rockfalls were rare. In the Drus, the first post-LIA collapse involving a volume greater than 10,000 m^3 occurred in 1950. In the Aiguilles de Chamonix, the first rockfall occurred during the summer 1947. It is the most important rockfall of this area (65,000 m^3). In the late 1940s, two other collapses affected the Aiguilles de Chamonix. The mid-XXth century is thus a turning period marked by major collapses.

From the 1950s to the 1990s, the morphodynamic evolution of the Drus was low. In the Aiguilles de Chamonix, no rockfalls occurred between 1954 and the 1970s.

The 1990s and the 2000s differ from previous decades and are characterized by more and more frequent rockfalls, involving greater volumes. It is particularly true at the Drus where three major events occurred in September 1997 involving 27,000 m^3 of rocks, then 6,500 m^3 of rocks were mobilized during the 2003 heatwave, and finally the main collapse occurred in 2005 (Fig. 2). In the Aiguilles de Chamonix, the situation is more contrasted: if the 1990s were marked by large rockfalls, the 2000s experienced a high frequency of collapses of smaller dimensions. In 2003, a dozen of rockfalls affected the Aiguilles de Chamonix.

Fig. 2 Dust cloud related to the rockfall of June 2005 in the west face of the Drus (3,754 m a.s.l.)

Rockfalls from 2003 to 2009

In 2003, the 182 reported collapses were distributed fairly homogeneously throughout the massif, with a slightly lower density south of the Mont Blanc (Ravanel et al. 2011). The most affected sector was the central part of the massif. All but two of the rockfalls occurred in rockwalls where models suggest the presence of permafrost.

Forty-five rockfalls were reported in 2007. They occurred between January and late September. Only three events took place out of the modelled permafrost area, among which we find the most important identified event: the Dent de Jétoula rockfall (15,000 m^3).

Year 2008 was characterized by a lower rockfall frequency: only 22 events were reported, which occurred between June and September. The last one occurred at about 3,470 m a.s.l. at the Aiguille de Tré-la-Tête involving a volume of 33,000 m^3 of rocks. It was the largest event of the 2007–2009 period and probably the largest one since the 2005 little rock-avalanche of the Drus. Among the 22

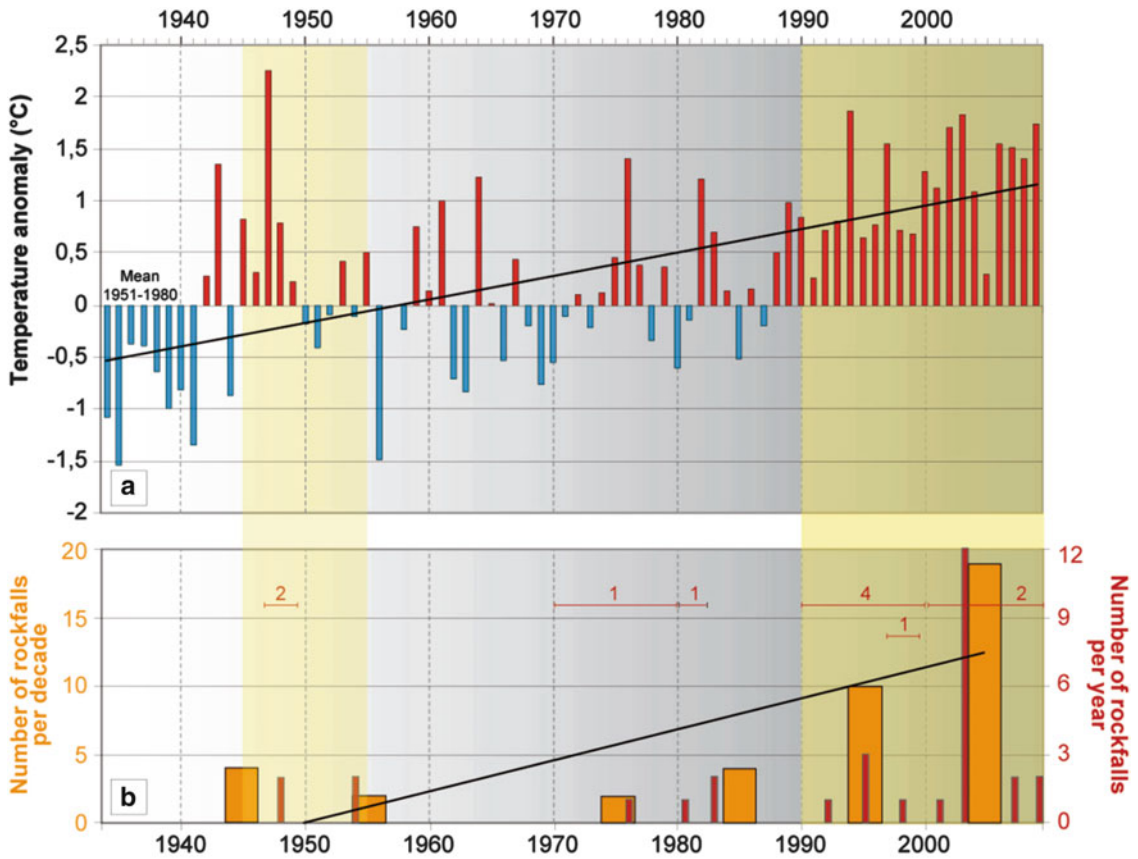

Fig. 3 Comparative evolution of climate in Chamonix (1,040 m a.s.l.) and rockfalls in the North side of the Aiguilles de Chamonix (Mont Blanc massif, France). (**a**): mean annual air temperature anomaly in relation to the 1951–1980 mean; (**b**) rockfalls number per decade and per year. *Black line*: trend; wide bars in (**b**) rockfalls not precisely dated (Meteorological dataset: Météo-France; Ravanel and Deline 2011 modified)

documented collapses, only one seems to have been triggered out of the permafrost area.

Year 2009 was marked by a high number of small size rockfalls (up to 7,000 m^3): 72 collapses were recorded between April and October, although morphodynamics really started in August. Only two rockfalls occurred out of the permafrost area.

To summarize, only 8 of the 321 documented events of 2003, 2007, 2008 and 2009 probably occurred out of the possible or probable permafrost area: ice was observed in more than 22 scars.

Discussion and Conclusions

Before discussing the link between rockfalls and permafrost, it is first necessary to verify the existing relationships between climate and rockfalls, in particular with periods of warming which are prone to degrade permafrost. To deal with the relationships between rockfalls and global warming, we first crossed the occurrences of the documented events of the Drus and the Aiguilles of Chamonix with

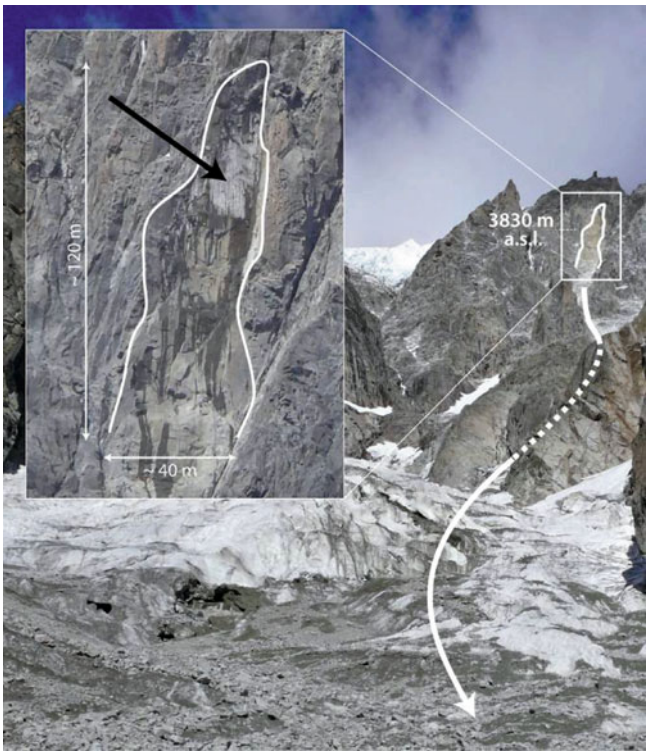

Fig. 4 The September 2007 rockfall of the Tour des Grandes Jorasses. The *black arrow* shows massive ice still present in the scar two weeks after the rockfall

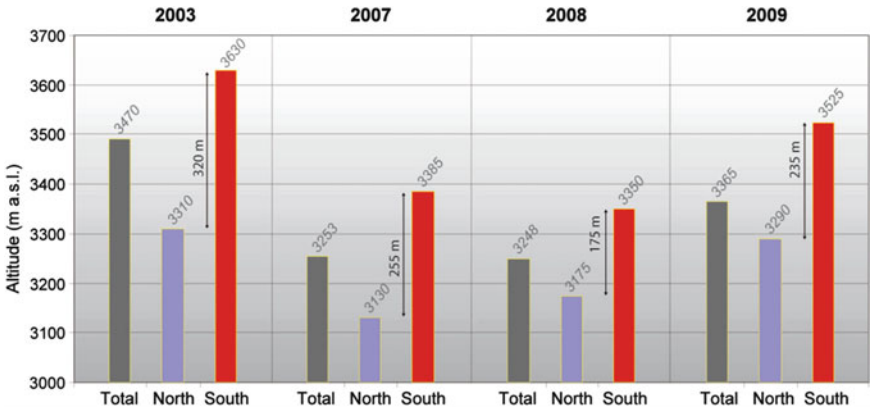

Fig. 5 Altitudinal asymmetry in the rockfalls trigger between the north faces and the south faces

climate data. The climatic factor – especially the thermal one – seems important in the triggering of rockfalls which occurred after the end of the LIA. The simultaneity of rockfall occurrences with the hottest periods has a good evidence (Fig. 3). 70 % of the documented events occurred during the past two decades, which were characterized by an acceleration of global warming. Heatwave periods are particularly prone to rockfalls: the largest number of rockfalls occurred during the summer 2003 heatwave. There are also concomitance between the 2003, 2007, 2008 and 2009 rockfalls and climatic conditions of those years – in particular with high temperatures.

Secondly, it has to be noted that also topographic factors are highlighting the importance of permafrost degradation in rockfall triggering. The average rockwalls elevation is around 3,000 m a.s.l., whereas the average elevation of rockfall scars is much higher (Table 1). Although rockwalls are very common below 3,000 m a.s.l., relatively very few collapses occur there. This observation indicates that the main triggering factor(s) is(are) not ubiquitous. The most affected altitudinal belt is 3,200–3,600 m a.s.l., which corresponds to areas of "warm" permafrost (undergoing fast degradation). Moreover, observations show that the hotter the summer, the higher the scar elevations, and that there is a sharp contrast in the scar elevations between north and south faces, which is consistent with permafrost distribution and evolution (Fig. 5). We also observed that rockfalls occur especially on topographies that are particularly affected by permafrost degradation, such as pillars, spurs and ridges (Ravanel et al. 2010).

Several other considerations lead to consider permafrost degradation as the most likely trigger of documented slope failures:

– The other cryospheric factors driving instability, which are glacial debuttressing and evolution of ice/snow rockwall covers, which are also temperature-dependent, may only explain a little part of the rockfalls;
– Almost all the recorded rockfalls (98 %) occurred in a context of possible/probable permafrost, according to the outputs of the TEBAL model;
– Rockfalls occur primarily during summer time, when permafrost degradation is enhanced;
– Among the 2007–2009 collapses, massive ice was observed in at least 22 scars (Fig. 4);
– Summer 2003 rockfalls were unusually numerous and could mainly be explained only by permafrost degradation (Ravanel et al. 2011).

Within the context of global warming scenarios for the twenty-first century, these results raise the question of risk assessment and management in high mountain regions.

Acknowledgments This paper is a contribution of the PermaNET project, that is part of the European Territorial Cooperation and co-funded by the ERDF in the scope of the Alpine Space Programme (www.alpine-space.eu).

References

Davies MCR, Hamza O, Harris C (2001) The effect of rise in mean annual temperature on the stability of rock slopes containing ice-filled discontinuities. Permafr Periglac Process 12(1):137–144

Gruber S, Haeberli W (2007) Permafrost in steep bedrock slopes and its temperature-related destabilization following climate change. J Geophys Res 112:F02S18

Gruber S, Hoelzle M, Haeberli W (2004) Rock-wall temperatures in the Alps: modeling their topographic distribution and regional differences. Permafr Periglac Process 15:299–307

Haeberli W, Wegmann M, Vonder Mühll D (1997) Slope stability problems related to glacier shrinkage and permafrost degradation in the Alps. Eclogae Geol Helv 90:407–414

Harris C and 21 co-authors (2009) Permafrost and climate in Europe: monitoring and modelling thermal, geomorphological and geotechnical responses. Earth-Sci Rev 92:117–171

Ravanel L, Deline P (2008) La face ouest des Drus (massif du Mont Blanc): évolution de l'instabilité d'une paroi rocheuse dans la haute montagne alpine depuis la fin du petit âge glaciaire. Géomorphologie 4:261–272

Ravanel L, Deline P (2011) Climate influence on rockfalls in high-Alpine steep rockwalls: the North side of the Aiguilles de Chamonix (Mont Blanc massif) since the end of the 'Little Ice Age'. Holocene 21:357–365

Ravanel L, Allignol F, Deline P, Gruber S, Ravello M (2010) Rock falls in the Mont Blanc Massif in 2007 and 2008. Landslides 7:493–501

Ravanel L, Allignol F, Deline P, Bruno G (2011) Les écroulements rocheux dans le massif du Mont-Blanc pendant l'été caniculaire de 2003. Géovisions 36:245–261

The December 2008 Crammont Rock Avalanche, Mont Blanc Massif Area, Italy

Philip Deline, Massimo Broccolato, Jeannette Noetzli, Ludovic Ravanel, and Andrea Tamburini

Abstract

Rock avalanching is a very hazardous process in high mountain area. Present climatically induced glacier shrinkage and permafrost degradation could increase its frequency and magnitude. A 0.5 M m^3 rock avalanche affected the 400-m-high North face of Mont Crammont (western Italian Alps) on 24/12/ 2008.

The main part of the rock mass settled at the rockwall foot, whereas a minor part travelled horizontal and vertical distances of 3,050 and 1,560 m, respectively. The mobility was enhanced by the channelization in two torrent gullies, and the incorporation of snow.

Three elements suggest that the rock avalanche could have been triggered by the current degradation of the rockwall permafrost: seepage water in the detachment zone; modelled 'warm' permafrost ($T > -2$ °C); no other Holocene rock avalanche deposit.

Collapsed volume was computed by comparison of pre- and post-event DTMs. Back analysis calculation of the rock avalanche runout suggests a two step event.

Keywords

Rock avalanche • Permafrost degradation • Climate change • Modelling • Crammont • Western Alps

Introduction

In inhabited mountain valleys, rock avalanching, i.e. the extremely rapid flow movement of fragmenting rock particles, represents a potential high risk for growing infrastructure and people living in in high mountain areas, as recently shown at Kolka-Karmadon, Caucasus (Huggel et al. 2005). This hazardous process is due to steep slopes, high relief, intensive rock fracturing, seismicity, paraglacial control, periglacial climatic conditions and the presence and interaction of snow, glaciers, and permafrost. Ice or/and snow on the surface enhances the mobility of rock avalanches because of a lower coefficient of friction and the incorporation of ice and snow into the moving rock mass (Evans and Clague 1988; Deline 2009). Present glacier shrinkage, and permafrost degradation in steep rockwalls (Gruber and Haeberli 2007) in the context of the current global climate change may increase the frequency and magnitude of rock falls and rock avalanches (Ravanel and Deline 2010).

Several rock avalanches recently occurred in the Mont Blanc massif (western European Alps; Deline 2009), as the small Drus rock avalanche in June 2005 (Ravanel and Deline 2008). The objective of this paper is to document the small rock avalanche that detached from Mont Crammont (2,749 m a.s.l.) in the Mont Blanc massif area in December

P. Deline (✉) • L. Ravanel
EDYTEM Lab, Université de Savoie, CNRS, Le Bourget-du-Lac 73376, France
e-mail: pdeli@univ-savoie.fr

M. Broccolato
Aosta Valley Geological Survey, Quart, Italy

J. Noetzli
Glaciology, Geomorphodynamics and Geochronology Group, University of Zürich, Zürich, Switzerland

A. Tamburini
Imageo S.r.l., Torino, Italy

C. Margottini et al. (eds.), *Landslide Science and Practice*, Vol. 4,
DOI 10.1007/978-3-642-31337-0_52,

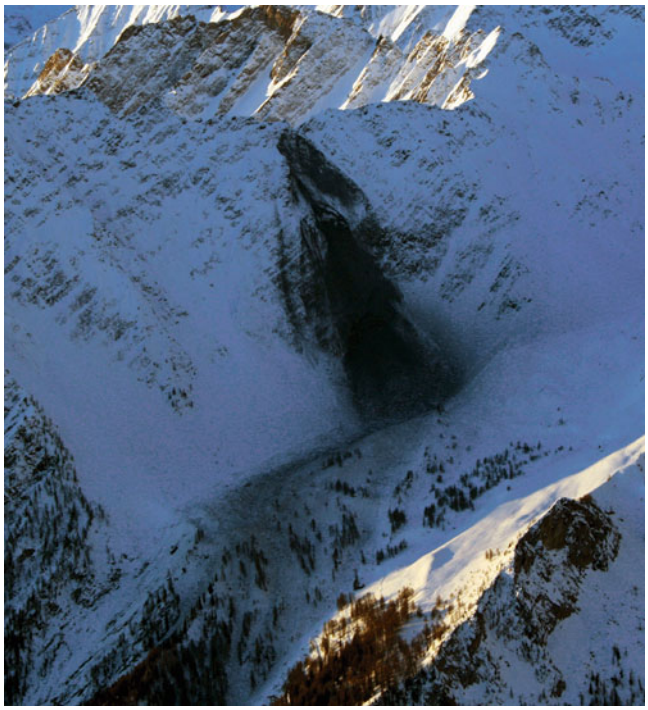

Fig. 1 North side of the Crammont 3 weeks after the rock avalanche (13/01/2009). Small rockfalls have affected continuously the scar, located in the upper half of the 400-m-high face; the rock debris accumulation on the plateau at the foot of the rockwall is snow-covered; the upper section of the two torrent gullies is visible in the lower left (Photo M. Broccolato)

2008 (Fig. 1), and to investigate and discuss its controlling factors.

Studied Area and Rock Avalanche Description

Geological Setting of Mount Crammont

Mont Crammont is towering 1,700 m above the Doire Baltée river (Fig. 2). Located 10 km south-east from the Mont Blanc summit, it is composed of the so-called 'Flysch de Tarentaise' Sequence, with massive beds of conglomerate without schistose interbedding, and alternate beds of limestones, black calcschists, and molassic sandstones.

The rock avalanche has affected the north face of the rock ridge that develops west of the Mont Crammont (2,749 m a.s.l.). This anaclinal north slope is a normal escarpment roughly perpendicular to the dip of the bedding plane, that culminates at 2,653 m a.s.l. in the detachment area, with a mean slope angle of 50°, and rises 400–550 m above a 100–150-m-high scree slope.

Characteristics of the Rock Avalanche

On 24 December 2008, preceded by several mixed rock-snow avalanches during the early afternoon, a small rock avalanche detached from the north face of the Crammont ridge (Fig. 2). It released a dense black aerosol cloud, which travelled across the Vallon d'Arp, divided into two arms because of the topography, and deposited the bulk of the collapsed rock mass mixed with snow on the snow-covered plateau located around 2,100 m a.s.l. A small part of this mass continued downstream, forming two branches channelled by the gullies of the Torrents de Planey and Arpettaz. The Arpettaz branch, containing a high proportion of snow, reached the Doire river at 1,090 m a.s.l., without damming it; rock debris material was more abundant in the Planey branch. Vertical and horizontal travel distances were 1,560 and 3,050 m.

After the melting of the larger part of the embedded snow in late Spring 2009, the deposit on the plateau was generally $>$ 0.60–1 m thick, reaching some meters in the largest boulder areas (Fig. 3); its non-uniform thickness is due to both pre-event topography and depressions resulting from snow melt. In the torrent gullies, the final rock deposit has a mean minimal thickness of c. 20 cm; unsorted large clasts are matrix-supported.

Methods

A geomorphological study of the area and the rock-avalanche deposit was carried during the first semester of 2009 (Fig. 3).

Collapsed volume was obtained by substracting in a 2.5D GIS a high resolution (20 cm) DEM of the Crammont area generated in June 2009 from helicopter-borne LiDAR from the 2 m resolution DEM of the Valley of Aosta Region generated from airborne LiDAR in 2007. The landslide volume was calculated both in the detachment and upper accumulation zones (Fig. 3). The ratio between the computed volumes in the detachment and accumulation areas is about 1.3 – a minimal ratio, as the deposit in the two gullies is not taken into account.

For the assessment of the permafrost conditions in the starting zone, a schematic temperature distribution of a N–S cross section through the summit ridge of the Crammont was modelled based on the approach by Noetzli (2008): the rock surface temperatures were estimated along the cross section based on the results from a distributed energy balance model (Noetzli and Gruber 2009) and respective elevation, aspect and slope, and for idealized conditions in steep rock that

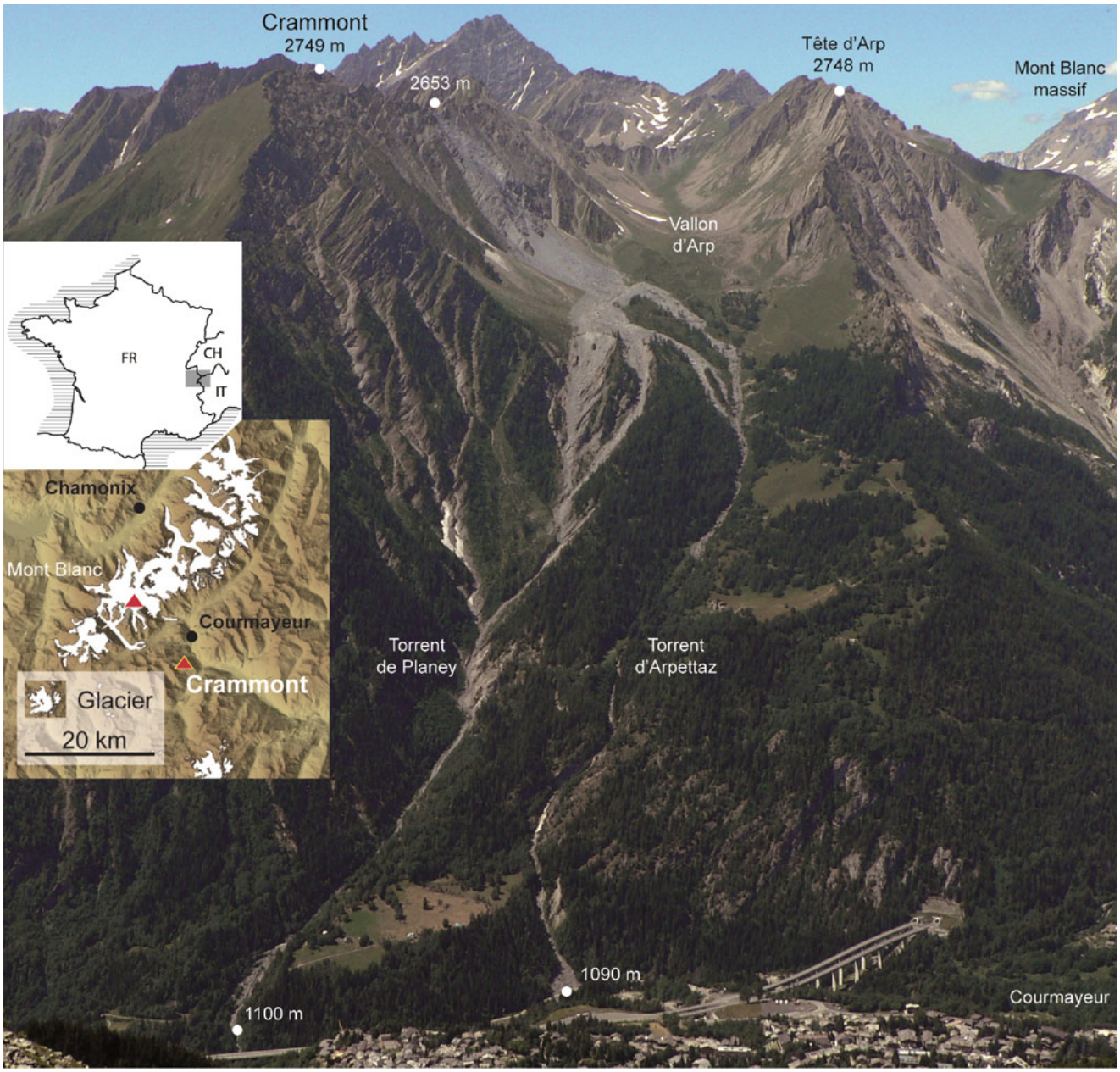

Fig. 2 General view of the rock avalanche from NE, and location maps. Source zone scar and main deposit (*light grey*) of the Crammont rock avalanche are in the top center; secondary deposit in the two narrow torrent streams down to the Doire River. Note highway and village at the foot of the opposite side of the Doire valley (From Deline et al. 2011)

does not retain a snow cover. The subsurface temperature field was then calculated based on heat transport by conduction using the modelling package COMSOL Multiphysics.

The runout of the Crammmont landslide was back-analyzed with DAN3D (McDougall and Hungr 2004), a relatively simple dynamic model which enables a simulation of the event in terms of flow distance, velocity and distribution of deposits. Two different rheologies were combined: a frictional model was used in the proximal path, and a Voellmy rheology in the distal path, in order to simulate the effect of the snow in increasing the landslide mobility. The transition between the frictional and Voellmy models was placed at the base of the scree slope. Taking into account the presence of snow, a bulk friction angle of 30° was adopted for the frictional model. The Voellmy resistance parameters were adjusted by trial and error to achieve the best fit with the observed extension of the rock-avalanche deposit.

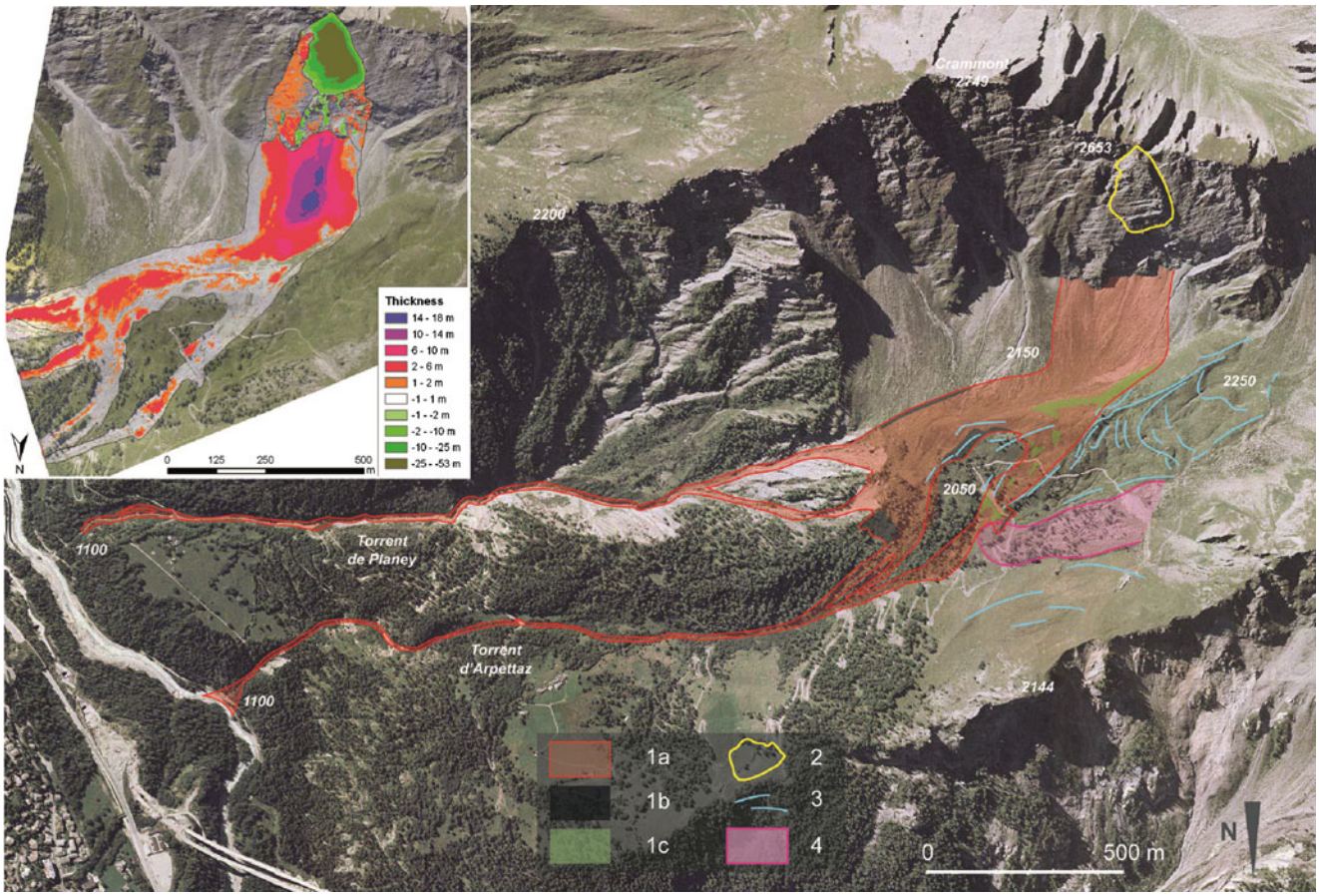

Fig. 3 Geomophological map of the Crammont area. *1*: 2008 rock-avalanche deposit (*1a rock deposit*, *1b splash area*, *1c scoured area*), *2* source zone, *3* Lateglacial moraines, *4* relict rock glacier. *White numbers*: elevation (m a.s.l.). Inserted map: thickness map of the detachment and upper accumulation zones (From Deline et al. 2011)

Results

Substraction of the scar DEMs gives a collapsed volume of 535,000 m^3. While this volume is half the volume defined by Hsü (1975) to consider a rock avalanche, the

Crammont apparent coefficient of internal friction (H/L) of 0.51, lower than the expected coefficient of 0.62 (Hsü 1975), highlights the high mobility of this rock avalanche.

The first runout simulation with DAN3D provided a good agreement in terms of flow distance but the results at the base of the scree slope were not consistent with the observed deposit thickness and distribution. A two-phase simulation was then carried out, with two separate sliding volumes of 370,000 and 200,000 m^3 respectively, released in sequence. Results show a better fit on the scree slope, with a deposit close to the observed one (Figs. 3 and 4). Thus, modelling and observations suggest a two-phase event: (1) the 24 December rock avalanche, that involved the bulk collapsed material and reached the Doire River; and (2) a continuous process of debris sliding and toppling from the scar during the following 7 months.

As suggested by modelling, permafrost may be present on the north slope of the Crammont ridge, with lowest temperatures mainly in the range above −2 °C (Fig. 5). The south side is estimated to be free of permafrost and the permafrost boundary is nearly vertical within the summit ridge of Crammont. The recent twentieth century warming has likely affected the uppermost ca. 50 m below the surface, as can be seen from the isotherms which are strongly bent towards the surface.

As shown by the shape of the Crammont side, rock slope failures due to glacial downwasting and consequent debuttressing have affected it after the Last Glacial Maximum. But no deposit of large Holocene rockfall prior to 2008 is observed in the Vallon de l'Arp – except the one from which formed a relict rock glacier –, where the Lateglacial morainic complex is fully preserved (Fig. 3). During the Holocene, the main active processes were frost-shattering and debris and boulder falls, as suggested by the large scree slope at the foot of the north side of the Crammont.

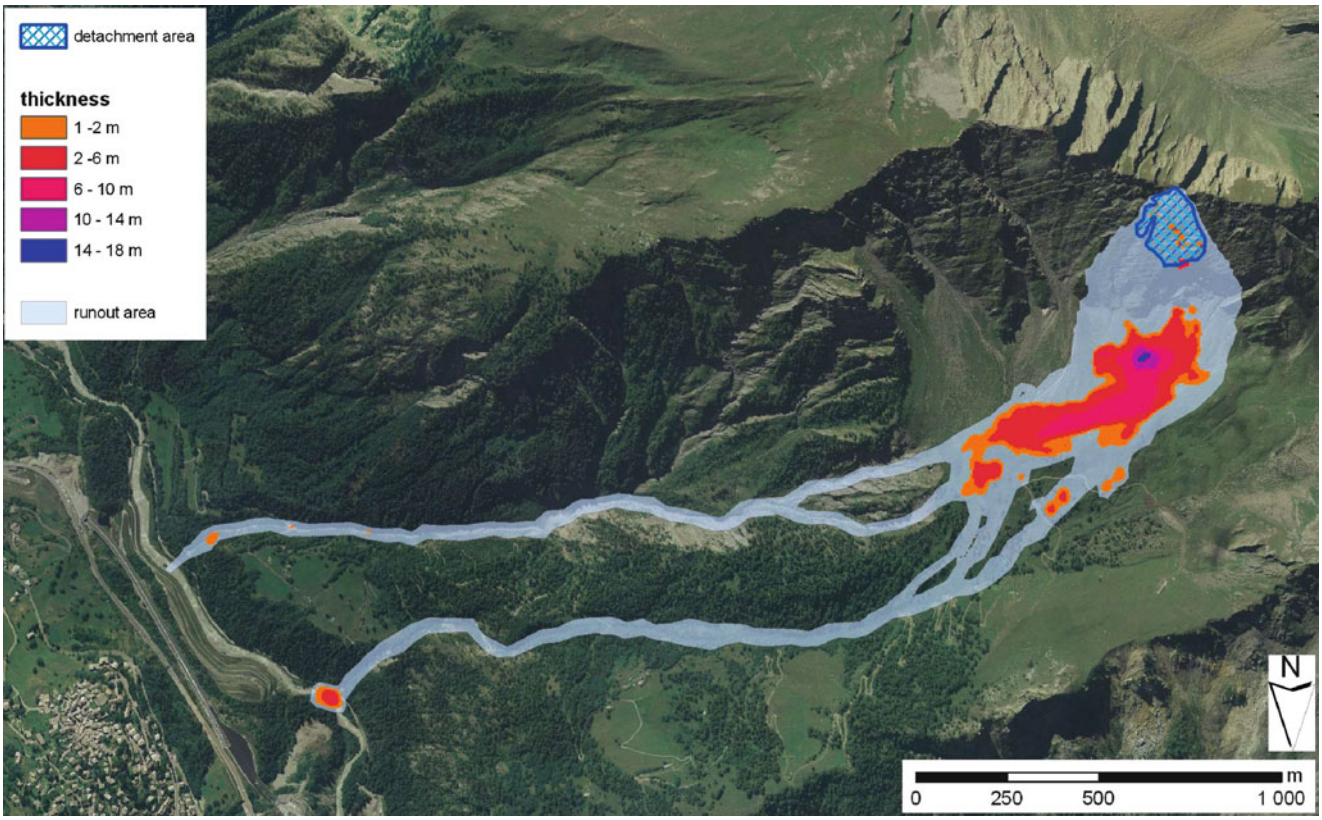

Fig. 4 Extension of the runout path and thicknesses of the accumulation computed by DAN3D considering a two-phase event. Compare with observed runout path on geomorphological map on Fig. 3 (Deline et al. 2011)

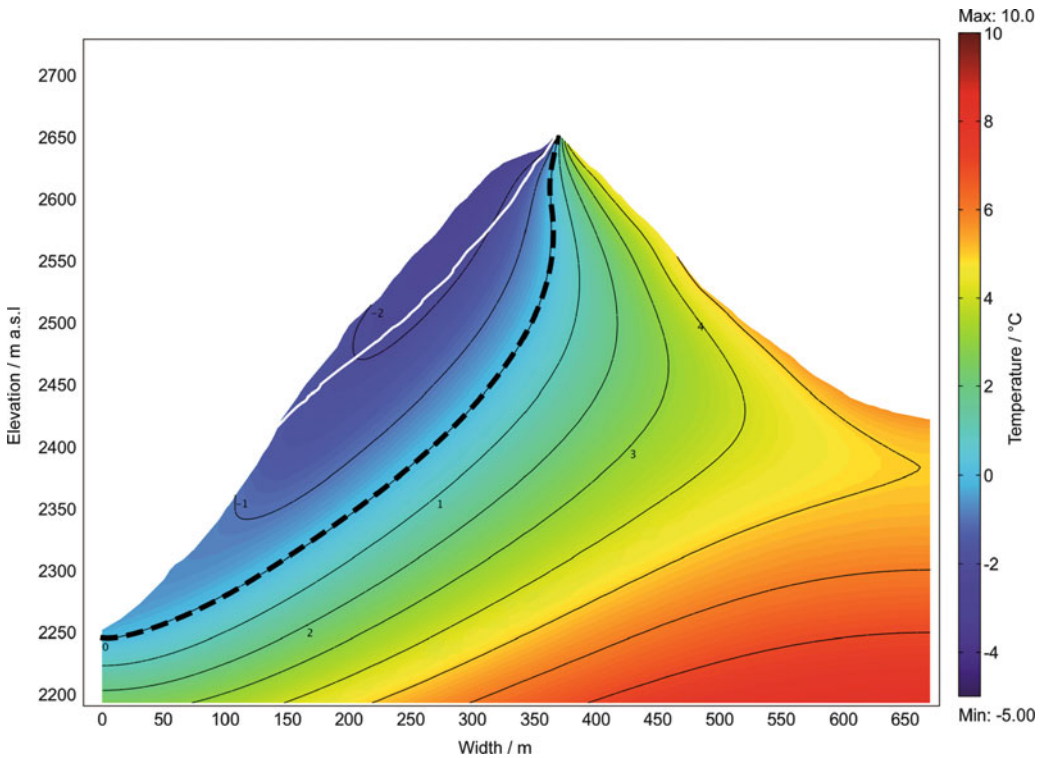

Fig. 5 Simulated subsurface temperature field in the Crammont rock ridge (N-S cross section; 2008 topography). *Black dashed line*: 0 °C isotherm, *white line*: bottom of the rock-avalanche scar (Deline et al. 2011)

Discussion and Conclusions

A small earthquake (11 November, ML: 2.7) with epicenter at Pré-Saint-Didier, ~ 8 km far from the Crammont, could have contributed to prepare the 24 December collapse, but no triggering seismic event was recorded during the failure itself.

While no rain was recorded in the previous week in the Crammont area, mean daily air temperature at the close Grand-Saint Bernard Pass (2,472 m a.s.l.) was negative during the period 25 November-24 December 2008 – yet regularly increasing from −13 °C to −1 °C.

Modelling of rock temperature distribution in the Crammont ridge indicates warm permafrost in the north face at the elevation range of the scar. Climate warming since the termination of the Little Ice Age likely degraded it, and heat advection by water circulation could have recently affected the rock mass at depth. As suggested by the geomorphology of the area, no other rock avalanche detached from Mont Crammont during the entire Holocene – in contrast to the close Mont Blanc massif where rock avalanches frequently occurred during the Holocene, probably in relation with the geological and topographical controls.

A small rock avalanche, the 2008 Crammont event is one of the major recent landslides in the Alps. Its low apparent coefficient of internal friction – especially by considering its relative small volume (0.5 M m^3) – results from its channelization, the incorporation of snow, and the snow-covered surface of its path. This should draw our attention to the importance of local conditions (e.g. snow cover, topography) in the consideration of this hazard in the context of risk management. Back-analysis of the motion of the rock avalanche confirms the important role of snow in increasing its mobility. Modelling is seen to contribute towards better understanding of the dynamics of this event, especially its two phases.

The Crammont rock avalanche highlights the importance of rock avalanches in shaping the alpine landscape. Occurring in a densely inhabited area of the Alps, close to one of the main international roads crossing the Alps, it emphasizes how this highly destructive process can place populations at risk. In the context of present global warming and further warming predicted for the twenty-first Century, permafrost degradation should accelerate. Therefore, more frequent rock avalanches could be triggered.

Acknowledgments The authors thank M. Ravello for information, W. Alberto, O. Hungr, and F. Villa for preparation and simulations with DAN3D. This paper is a contribution of the PermaNET project, that is part of the European Territorial Cooperation and co-funded by the European Regional Development Fund (ERDF) in the scope of the Alpine Space Programme (www.alpine-space.eu).

References

Deline P (2009) Interactions between rock avalanches and glaciers in the Mont Blanc massif during the late Holocene. Quat Sci Rev 28 (11–12):1070–1083

Deline P, Alberto W, Broccolato M, Hungr O, Noetzli J, Ravanel L, Tamburini A (2011) The December 2008 Crammont rock avalanche, Mont Blanc massif area, Italy. Nat Hazard Earth Syst Sci 11:3307–3318

Evans SG, Clague JJ (1988) Catastrophic rock avalanches in glacial environments. In: Proceedings of the 5th international symposium on landslides, Rotterdam, pp 1153–1158

Gruber S, Haeberli W (2007) Permafrost in steep bedrock slopes and its temperature-related destabilization following climate change. J Geophys Res 112:F02S18. doi:10.1029/2006JF000547

Hsü KJ (1975) Catastrophic debris streams (sturzstroms) generated by rockfalls. Geol Soc Am Bull 86:129–140

Huggel C, Zgraggen-Oswald S, Haeberli W, Kääb A, Polkvoj A, Galushkin I, Evans SG (2005) The 2002 rock/ice avalanche at Kolka/Karmadon, Russian Caucasus: assessment of extraordinary avalanche formation and mobility, and application of QuickBird satellite imagery. Nat Hazard Earth Syst Sci 5:173–187

McDougall S, Hungr O (2004) A model for the analysis of rapid landslide motion across three-dimensional terrain. Can Geotech J 41:1084–1097

Noetzli J (2008) Modeling transient three-dimensional temperature fields in mountain permafrost. Ph.D. thesis, Department of Geography, University of Zurich, Zurich

Noetzli J, Gruber S (2009) Transient thermal effects in Alpine permafrost. Cryosphere 3:85–99

Ravanel L, Deline P (2008) La face ouest des Drus (massif du Mont-Blanc): évolution de l'instabilité d'une paroi rocheuse dans la haute montagne alpine depuis la fin du petit âge glaciaire. Géomorphologie 4:261–272

Ravanel L, Deline P (2010) Climate influence on rockfalls in high-Alpine steep rockwalls: The North side of the Aiguilles de Chamonix (Mont Blanc massif) since the end of the 'Little Ice Age'. Holocene. doi:10.1177/0959683610374887

GALLIUS: GeomorphohydrologicAl Model for LandsLide Initiation Under Snowmelting

Maria Cristina Rulli, Federica Gobattoni, and Monia Santini

Abstract

Landsliding events are triggered not only by extreme rainfall, but often by rapid snowmelt, causing an increase in soil water pressure. It follows landslide risk spreading from regions dominated by liquid precipitation to sub-humid climate areas where the sudden raising of temperature, sometimes combined with rainfall events, melts the snowpack.

The snow melting influence on landslide initiation is here investigated via dynamic geomorfohydrological distributed modeling. The model, named GALLIUS (GeomorfohydrologicAl model for LandsLide Initiation Under Snowmelting conditions), evaluates the snowmelt by solving the energy and mass balance equations, accounts for soil water fluxes and their propagation and analyses slope stability. Model application for a case study in Italy highlights the role of snowmelt in increasing soil water pressure and in shallow landslides triggering

Keywords

Landslide • Snowmelting • Model

Introduction

Landslides are one of the most frequent and widespread natural hazards, representing high risk concern for ecosystem processes and for anthropogenic environment and activities. There is a threat in many watersheds around the world often associated to other natural hazards like earthquakes, floods or volcanic eruptions. Landslides are events consisting in more or less rapid descent of mud, debris or rocks in sloped terrains. From a geomorphologic point of view, landslides are a key-factor for hillslope evolution and sediment dynamics both at the hillslope and catchment scale. The soil detachment process can potentially turn into destructive mass flows that might be very dangerous for resources, properties and lives, given the absence of initial movement evidence and their high velocity (Montgomery and Dietrich 1994). As for other natural hazard, such hydrogeomorphic events are due to a combination of *predisposing* (e.g., geomorphologic settings), *quickening* (e.g., human activities) and t*riggering* (e.g., climatic forcing) factors (Santini et al. 2009).

A comprehensive evaluation of landslide risk requires a detailed historical reconstruction and a careful data collection regarding temporal incidence of landslides and their causes (precipitations, floods, earthquakes, volcanic eruptions and anthropogenic activities). Combining such information with ground-based landslide mapping allows to obtain landslide hazard mapping. This procedure having the advantage to make assumptions and supply predictions about which conditions can favour terrain instability phenomena. To this aim in the last decades empirical, probabilistic, statistical or deterministic approaches were developed. Empirical rainfall threshold methods (e.g., Caine 1980) were

M.C. Rulli (✉)
Politecnico di Milano, Piazza L. Da Vinci, 32, Milan, Italy
e-mail: cristina.rulli@polimi.it

F. Gobattoni
Università della Tuscia, DAFNE, Viterbo, Italy

M. Santini
Università della Tuscia, CMCC, Lecce, Viterbo, Italy

C. Margottini et al. (eds.), *Landslide Science and Practice*, Vol. 4,
DOI 10.1007/978-3-642-31337-0_53,

developed for landslide triggering analysis. These methods are able to account mainly for *predisposing* and *quickening* factors, whose temporal scale (medium and long term) allows assuming that derived statistical relationships represent well the environmental boundary conditions accompanying landslides. Anyway meteo-climatic forcings, playing essential role in slope instabilities triggering, are characterized by time and space high variability usually working at short-term scale. Such "event" nature of triggering factors limits the possibility to develop exhaustive and consistent statistical relationships linking the meteo-climatic event with the landslide hazard. This makes it difficult to reliably predict the effects of a specific meteorological event on landslide occurrence. Process based landslide models (Montgomery and Dietrich 1994; Wu and Sidle 1995; Borga et al. 1998; Rosso et al. 2006) are used for hazard forecast, prevention and mitigation. Such type of models allows reproducing those weather-soil combined processes that trigger landslides, in particular the increase of soil pore water pressure. This latter is usually considered due to liquid precipitation, albeit many authors (e.g. Naudet et al. 2008; Coe et al. 2003; Okamoto et al. 2004; Wang et al. 2005;) related landslides triggering to soil saturation produced by snowpack melting or by the combined effect of rain and snow melting (Eberhardt et al. 2005; Luino 2005). Snow melting induced landslides usually occur in sub-humid areas characterized by successive alternation of rapid temperature rise and snowfall events. The Italian territory is prone to landslide events due to its geologic, geomorphologic and climatic patterns (Caniani et al. 2008). In addition, mass movements are observed mainly in areas where vegetation cover was reduced by deforestation, fire, quarrying activities or land clearing (e.g., Glade 2003; Rosso and Rulli 2002; Rulli et al. 2006). Finally, extreme climatic events create a force disequilibrium that induces an increase in soil pore water pressure and reduces shear strength of loose, shallow sediments, leading to landslide triggering (Dehn et al. 2000) or landslide reactivation (Bertolini et al. 2005). The combination of the above factors produces in Italy a broad variety of instability phenomena in terms of typology, kinematic mechanism, evolution characteristics and dimensions (Caniani et al. 2008). Besides intense and/or prolonged rainfall, snow events followed by rapid increase of temperature causing snow melting episodes are common in Italy (Guzzetti et al. 2002; Luino 2005), as well as alternating periods of intense and continuous snowfall and high temperatures (Naudet et al. 2008). In particular Basilicata (Southern Italy) is one of the Mediterranean regions at highest landslide risk (Polemio and Sdao 1999). This region is well known as a landslide and intense erosion prone area because of its geology, relief, neo-tectonics, climate and vegetation (Valentini 1979). Indeed Basilicata exhibits an higher density of landslides than the rest of Italy (Guzzetti 2000), because of the combination of predisposing conditions such as fine and loose materials as well as sloping terrains, and due to particular conditions such as extreme precipitation events (Piccareta et al. 2004) or anthropogenic activity, such as cave excavation (Lazzari et al. 2006), deforestation (McNeill 2004) and deep urbanization and industrialization (Naudet et al. 2008). Moreover historical records show that the number of landslides has increased over recent centuries, this considered due to changes in land use and climate (Piccarreta et al. 2006).

In this paper the new model GALLIUS (GeomorphologicAl model for LandsLide Initiation Under Snowmelting conditions) is presented. It is a dynamic spatially distributed model aimed to analyse snowmelt induced landslides triggering. Gallius is built by adding to the hydrological spatially distributed model modular framework (Rulli and Rosso 2005; Rosso et al. 2007; Rulli 2010) two modules analysing snowmelting and landslide triggering.

The two new modules are described in detail and the Gallius model application to a case study is reported. The study area is located in Basilicata region, Italy, and belongs to the Tiera river basin, acknowledged as landslide-prone area and interested by landslide occurrence following the alternation of snowfall and temperature rise during the winter-spring 2005.

Materials and Methods

Study Area Description

The study site is located in the upper part of Tiera river basin (left hand tributary of Basento river), in the east side of the municipality area of Potenza (Basilicata region, Italy) (Fig. 1), covering an area of about 77 km^2. The study area is well representative of pedologic, geomorphologic and lithologic characteristics typical of Basilicata region. Basin elevations ranges from 643 to 1,214 m a.s.l., with an average slope of 16 %. It belongs to the southernmost part of Apennine Chain. Oligo-Miocenic formations are represented by clayey and marly scists, hosting thin layers of limestone and sandstone (Argille Varicolori formation). Such clays originated during the Miocene tectonic from the construction of the Apennine Chain (Caniani et al. 2008).

Over this formation they are present outcroppings of the well known Corleto-Perticara formation, again consisting in clayey and marly scists, but also comprising marly and calcareous-marly formations. Similar outcropping terrains comprise Miocenic limestone, clayey marly and sandstone formations, underlying molasses and flysch consisting in sandstone and conglomerates in alternation with limestone and marly. In some parts of the basin there are also stratified sandy sediments and arenaceous rocks with intercalation of clay, conglomerates and marly sediments (Pliocene). Along

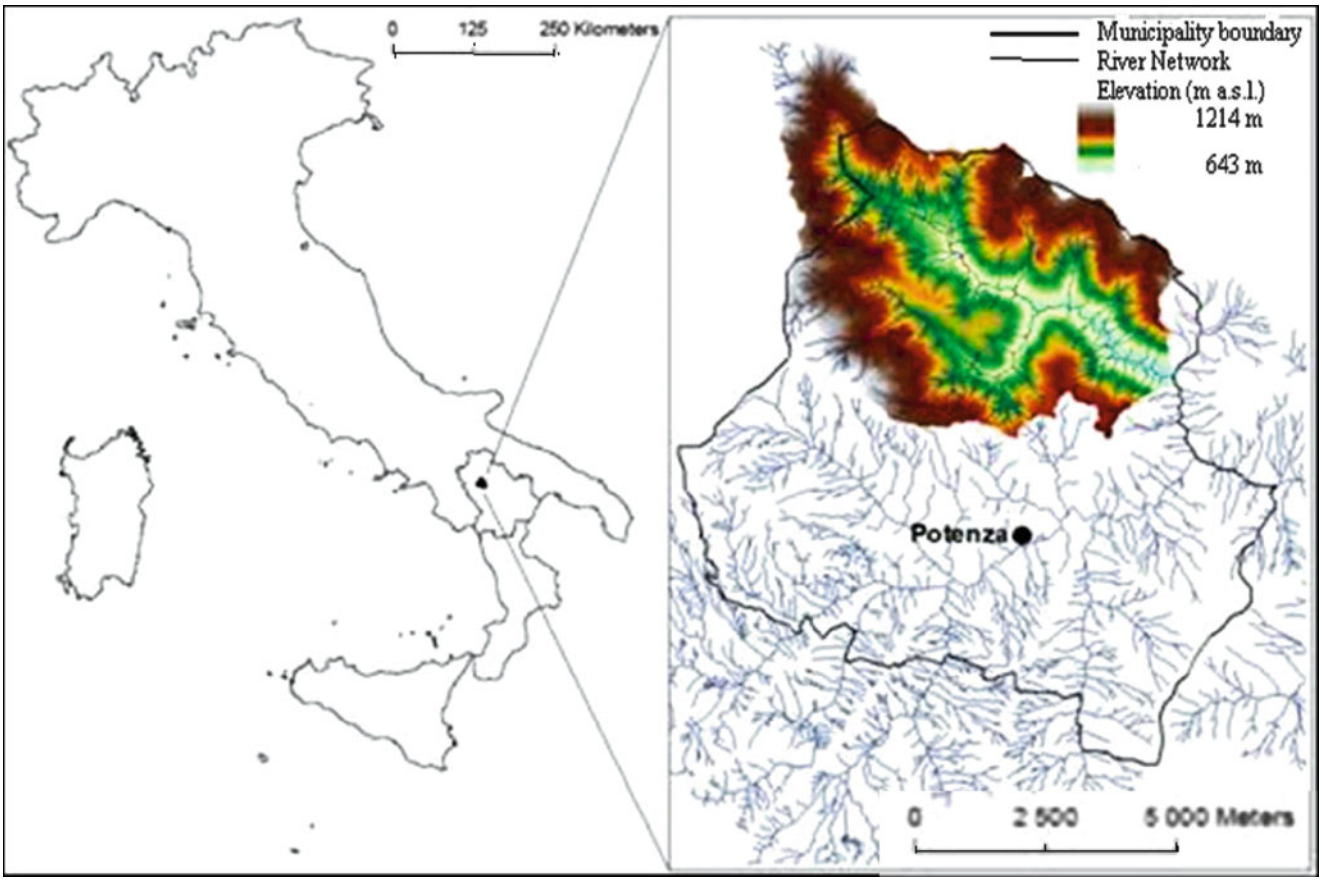

Fig. 1 Location of the basin under study and of surrounding hydrographic network

the river networks, Quaternary alluvial and debris flow deposits are present. Superficial loose soils derive from the weathering of above described formations and result in 11 % of the basin presenting a fine soil, while 74 % is fine-silty, 3 % is fine-loamy and 12 % is coarse-loamy. Concerning soil type, 12 % of the basin consists in mixed Cambisols-Leptosols while the remaining part presents Cambisols-Regosols, both with minor occurrence of Luvisols. Climate is typically Mediterranean, characterized by hot dry summers and mild wet winters. Yearly average rainfall is approximately 650 mm; yearly average temperature ranges from 16 to 17.5 ° C (Piccarreta et al. 2006). During the last decades, accordingly to the general trend due to climate changes, the weather conditions were characterized by an increase in frequency and intensity of rainfall and snowfall episodes, in alternation with higher temperature days. The basin is prone to slope instability phenomena, varying in types and dimensions, depending on its structural and lithologic characteristics. Landslide dataset, supplied by the Basilicata river agency allows to extrapolate information about the spatial distribution of landslide risk (Fig. 2b): 6 % of the basin area is at low landslide risk (R1), 3.1 % is at medium risk (R2), 7.1 % is at high risk (R3), while 2.7 % is a very high risk (R4); the risk being the results of combining terrain vulnerability due to the presence of properties and lives. In this context, the lithology of the substratum (clayey–marly–arenaceous) and the extreme meteorological events (snowfall) were recognized to be the two main factors causing landslides triggering on the hillslope of Bosco Piccolo village NW of Potenza at the end of February 2005 (Naudet et al. 2008).

In particular, from January to March 2005 snowfall events alternated to brief warmer periods have been recorded (Fig. 2a). At the end of February fast snowmelt occurred, increasing soil saturation and soil pore-water pressure,leading to hillslope failure. The observed landslide was complex (rotational and mudflow) landslide, followed by retrogressive evolution (Naudet et al. 2008).

Model Description

The combined action of water infiltrating from both rainfall and snow melting processes may activate slope failures by quickly saturating the soil and reducing its shear stress (Fredlund et al. 1978). GALLIUS (GeomorphologicAl model for LandsLide Initiation Under Snowmelting conditions) accounts for rainfall and snow cover thawing in

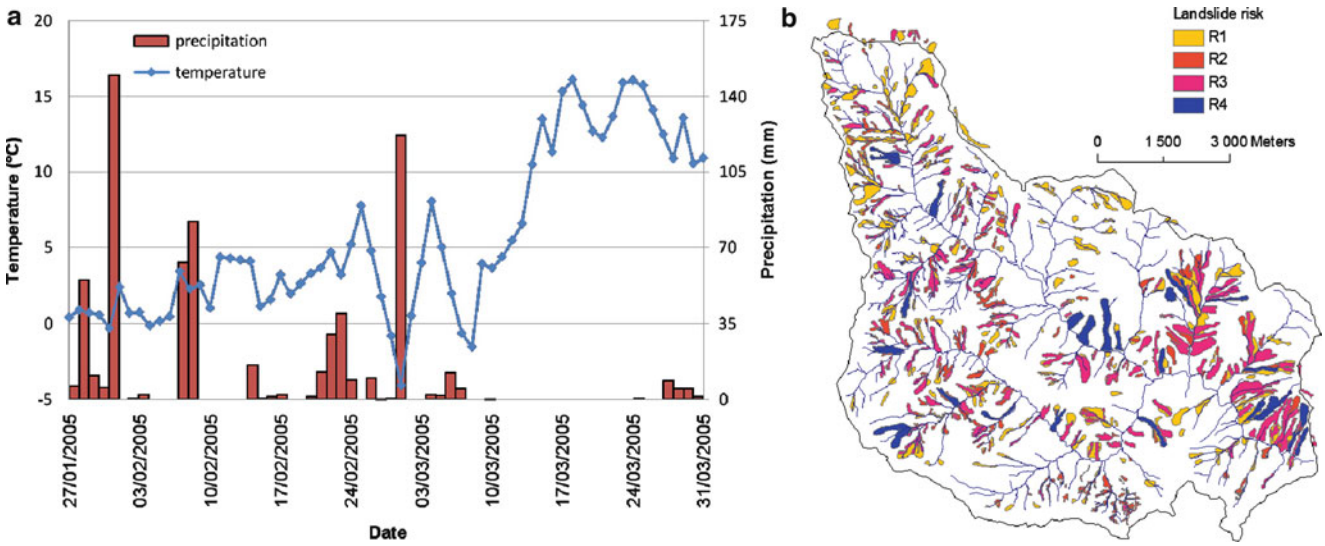

Fig. 2 (**a**) Precipitation and temperature versus time in the study time period. (**b**) Maps of (a) soil texture, (b) soil type and (c) landslide risk in the basin under study

landslide triggering. Such modelling approach is a dedicated version of the spatially distributed hydrologic model AUGUSTO (Rulli and Rosso 2007; Rosso et al. 2007) and it combines: (1) a catchment partitioning module, (2) soil water fluxes module, and (3) landslide triggering module.

The partitioning procedure here used (Rulli 2010) is an improvement of the method developed by Menduni et al. (2002). It consists on a preliminary identification of an Ideal Drainage Network (IDN) based on contour lines through a variable mesh size, and on a further extraction of the Actual Drainage Network (AND) from the IDN, using land morphology. In particular, the model first derives the steepest slope lines starting from the highest contour and then proceeds downslope. Further, the procedure defines polygons bounded by two subsequent contours and two adjacent steepest lines, orthogonal to the contour lines. Using this type of partition, the model defines the elements where the water flows into two classes: hillslope elements that are polygons, and channel elements, obtained by joining two or more stream tubes where surface runoff is channelized. The model can also automatically identify significant terrain characteristics (e.g. peaks and saddles) and account for their impact on streamflow. Watershed, subwatershed and draining area at any point can be automatically detected by using network elements interconnectivity, and also it is possible determine the Actual Drainage Network.

Overland flow is routed through stream tubes, formed by pairs of stream lines delineated normal to the contour lines (equipotential lines) of the watershed. This partitioning procedure allows to solve the equations describing the hydrological processes by a series of coupled one-dimensional equations. Soil water fluxes are considered due both to rainfall and snow melting and also to the joint action of the two processes. The snowmelt module (hereafter SM) provides the hydrological fluxes due to snowmelting. SM calculates snow melting by combining the energy balance and the mass balance (Wigmosta et al. (1994)). SM solves the energy balance incremental form Anderson (1968):

$$c_s W \frac{\Delta T_s}{\Delta t} = R_n + Q_s + Q_l + Q_p + Q_g + Q_m \qquad (1)$$

Where the left-hand term is the change in the snow pack cold content, being c_s the specific heat of ice (kJ kg^{-1} K^{-1}), W is the snow pack water equivalent accounted with proper measurement, ΔT_s the variation of snow temperature (°K), Δt the time step. On the right-hand side, R_n is the net solar radiation [kJ m^{-2}], Q_s is the sensible heat [kJ m^{-2}], Q_l is the energy loss by evaporation and sublimation processes or gained by condensation processes [kJ m^{-2}], Q_p is the heat advected by rainfall to snow cover [kJ m^{-2}], Q_g is the conduction heat from soil to snow cover [kJ m^{-2}], usually negligible, and Q_m is the latent internal heat lost during the snow melting or gained during liquid water refreezing [kJ m^{-2}]. See Wigmosta et al. (1994) for more details.

During snowmelting the pack is isothermal at 0 °C, Q_m can be calculated from (1) posing $T_s^{t+\Delta t} = 0$

The amount of snow melted is then evaluated through a mass balance equation considering water solid and liquid phases. The snowpack W is given by the volume of liquid water per unit area W_{liq} plus the ice phase water equivalent, W_{ice}.

$$W = W_{liq} + W_{ice} \qquad (2)$$

Where at each timestep Δt we have:

$$\Delta W_{liq} = \left[P_r + \frac{Q_l}{\rho_w \lambda_v} - \frac{Q_m}{\rho_w \lambda_v} \right] \quad (3)$$

$$\Delta W_{ice} = \left[P_s + \frac{Q_l}{\rho_w \lambda_f} + \frac{Q_m}{\rho_w \lambda_f} \right] \quad (4)$$

In (3) and (4), on the righ-hand side, the first terms represents the liquid and solid phase increments due to rain and snow precipitations, respectively; the second terms are the mass exchanges between air and snow, respectively, whereas the third terms represent the mass exchanges in melting and freezing processes. Water is removed from the snowpack when the liquid phase exceeds the snowpack water storage capacity (usually equal to 0.06 W), this condition is expressed as:

$$M_p = W_{liq} - 0,06W \text{ with } \mathrm{Mp} > 0 \quad (5)$$

Where M_p is the depth of the meltwater removed from the pack (m) per unit area. The SM module, integrated to the hydrologic flux module, provides the amount of water, due to snowmelting and/or rainfall, contributing to soil water content. Soil hydrological fluxes are modelled via Soil Bucket Model (SBM) (Vertessy and Elsenbeer 1999) where overland flow formation can be due to saturation excess or infiltration excess mechanism. Overland flow routing for each element is calculated by using the De Saint Venant equations with the kinematic wave approximation and Manning's resistance equation. Time and space variant soil water fluxes, that determine the depth of saturated soil, are input to the soil stability model module where soil stability is analysed in term of safety factor by using the Mohr-Coulomb criterion and the infinite slope stability theory.

Input Data

Study area topography was derived from the Digital Elevation Model (DEM) at 20 m of resolution (IGMI 2003). From the DEM 10 m contour lines were derived and then supplied as input to the catchment partitioning module. Daily climate inputs such as air temperature (°C), precipitation (mm), solar radiation (kJ/m^2) and wind speed (m/s), were derived from the local meteorological station (POTENZA, lat. 40.38, lon 15.48 and elevation 823 m a.s.l). Data gaps were filled by using data obtained from the NOAA database for a meteo station close to the previous (lat. 40.633, long. 15.8 and elevation 843 m). Information about effective eliophany was calculated by daylight duration, whereas the theoretical eliophany was computed from the effective one considering the latitude and the solar declination related to each day of the year. Vapor Pressure Deficit (VPD, kPa) was derived from the difference between the saturation vapor pressure (in kPa, calculated by air temperature and air relative humidity) and the actual vapor pressure (kPa). Initial snowpack thickness was derived from NOAA dataset and its temperature set to 0 °C as the air temperature in the starting day was 0.4 °C considering snow temperature slightly lower. LAI was obtained by using MODIS data. Gaps or low quality pixel for these images due to cloud cover or acquisition errors were corrected by considering relationships among LAI values and land cover type. Vegetation cover was derived from the Corine Land Cover dataset. Further soil parameters (e.g., depth, roughness, hydraulic conductivity etc.) were assessed by analyzing thematic maps (geologic, pedologic, etc.) and literature (Naudet et al. 2008).

Results and Discussion

In order to test GALLIUS in detecting snow melting induced landslides triggering, an event occurred during the winter-spring 2005 was considered. The period, lasting from the middle January and the end of March 2005, was interested by a series of snowfall events alternated with higher temperature days and rainfall episodes. In the north-eastern side of the Bosco Piccolo Village, mass movements occurred between February 25th, when a first detachment was observed, and March, 3rd, 2005 after a further snow fall and melting (Naudet et al. 2008). The chosen period for running GALLIUS ranged from January 27th to March 31st, 2005. The starting day was selected as the day with the highest snow thickness (about 40 cm) and the duration of period was selected to account for the complete snow melting.

Meteorological data analysis (Fig. 2a) show that at the beginning of the study period daily mean temperature was slightly above 0 °C and the falling precipitation was probably mixed between snow and rain, snowpack melted in these few days. After the day of the first detachment (February, 25th), temperature decreased within 3 days below or close to 0 °C, precipitations were solid with growing snowpack. On March 3rd, the temperature raised to 4 °C, an heavy rainfall event occurred, causing both the rapid snowpack melting and the second mass movement (Naudet et al. 2008). Although at the time of second detachment snowpack was more shallow (about 10 cm) than at the time of the first one, mass movement occurred due to the high soil water content already increased by the previous snow melting. In particular, starting from March 3rd soil water pore pressure strongly increased caused by snow melting, rainfall, runoff and subsurface flow, increasing soil stresses and leading to terrain displacement.

Model performances was checked by using both Bosco Piccolo event landslides map survey (Fig. 3b) and the landslide risk map (Fig. 2b). The last representing areas affected by landslide risk, and classifies such risk according to its general definition as the product of vulnerability, hazard and exposure

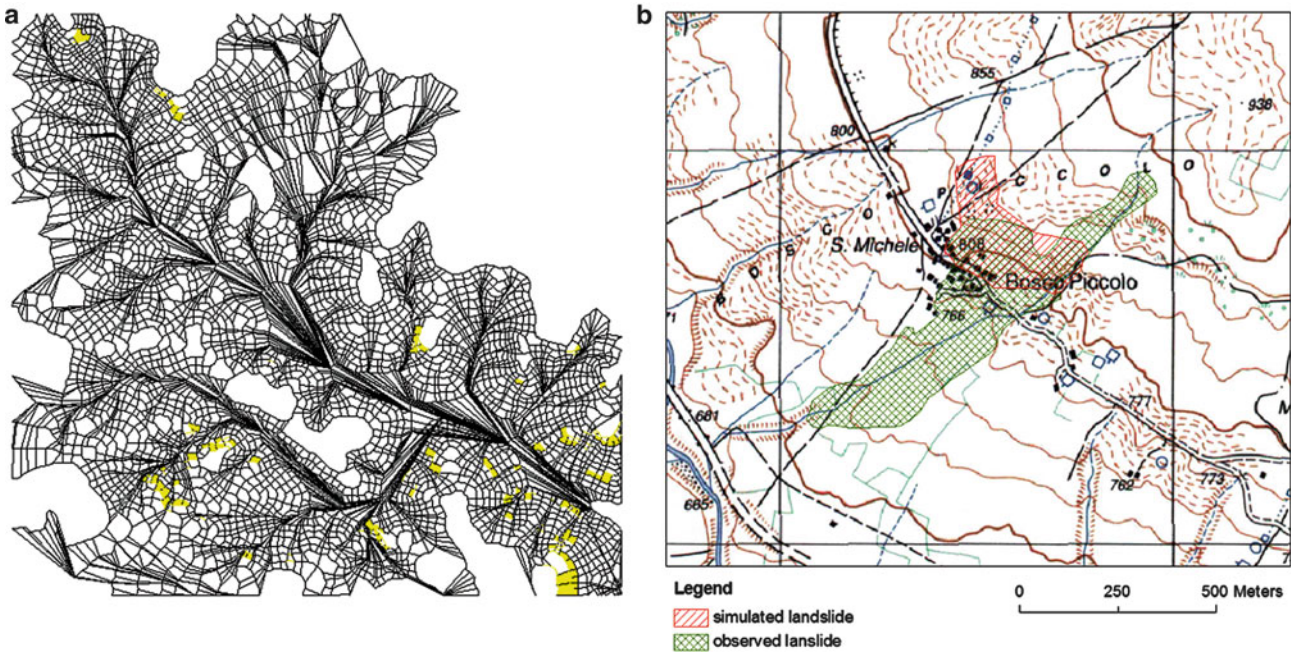

Fig. 3 (**a**) Modelling results showing shallow landslides triggered in the snowmelt study period. (**b**)Topographic map showing the survayed location of the landslide triggered during the period 25th February – March 3rd, 2005 (*green polygon*) and the one simulated by GALLIUS (*red polygon*)

(e.g. Varnes 1984). Some issues have to be considered when the landslide risk maps is used for landslide triggering model validation. First of all, the landslide triggering models simulation results are to be interpreted as instability initiation (landslide scar) whereas the landslide risk maps mainly delineate the whole landslide bodies moved and classifies them according to their activity degree and closeness to vulnerable elements. Then, several parts of landslide bodies, mainly the lowest ones, may be stabilized and in this case the model is not able to detect them as unstable areas (Santini et al. 2009).

Gallius model results (Fig. 3a) where overlaid with observed instabilities survey map (Fig. 3b). Focusing on the event of February-March 2005. the results show a substantial consistency with the observed data confirming that hydrogeomorphological distributed model like GALLIUS can reproduce landslide detachment area characterizing the complex precipitation event as the one happened in Bosco Piccolo Village on February-March 2005.

Conclusions

GALLIUS model, simulating snow melting processes and calculating soil hydrological fluxes due to liquid and solid precipitation, can represent, investigate and explain landslide triggering phenomena during snow cover and snow melting periods. Even though Gallius needs to be improved especially in his geomechanic component, the agreement between simulated and observed landslides, shows the quite good reliability of the presented model. It also point out the significance of coupling hydrological and landslide triggering modeling in prediction and assessment of meteorological forcing on landslides occurrence.

While several approaches are available for accounting for physical predisposing and quickening factors and they are reliably working at medium and long term scale, most of them can hardly consider and include meteo-climatic forcings variability at short-term scale. Spatially distributed hydrogeomorphological models, like GALLIUS, by accounting for every hydrological process affecting soil stability, can help to understand the role of snowmelt in landslide triggering and can be used for predicting landslides triggering

References

Anderson EA (1968) Development and testing of snowpack energy balance equations. Water Resour Res 4(1):19–37

Bertolini G, Guida M, Pizziolo M (2005) Landslides in Emilia-Romagna region (Italy): strategies for hazard assessment and risk management. Landslides 2:302–312

Borga M, Dalla Fontana G, Da Ros D, Marchi L (1998) Shallow landslide hazard assessment using a physically based model and digital elevation data. Environ Geol 35(2–3):81–88

Caine N (1980) The rainfall intensity-duration control of shallow landslides and debris flows. Geogr Ann Ser A 62A:23–27

Caniani D, Pascale S, Sdao F, Sole A (2008) Neural networks and landslide susceptibility: a case study of the urban area of Potenza. Nat Hazard 45:55–72. doi:10.1007/s11069-007-9169-3

Coe JA, Ellis WL, Godt JW, Savage WZ, Savage JE, Michael JA, Kibler JD, Powers PS, Lidke DJ, Debray S (2003) Seasonal movement of the Slumgullion landslide determined from Global

Positioning System surveys and field instrumentation, July 1998–March 2002. Eng Geol 68:67–101
Dehn M, Bürger G, Buma J, Gasparetto P (2000) Impact of climate change on slope stability using expanded downscaling. Eng Geol 55:193–204
Eberhardt E, Thuro K, Luginbuehl M (2005) Slope instability mechanisms in dipping interbedded conglomerates and weathered marls—the 1999 Rufi landslide, Switzerland. Eng Geol 77:35–56
Fredlund DG, Morgenstern NR, Widger RA (1978) The shear strength of unsurturated. Can Geotech J 15:313–321
Glade T (2003) Landslide occurrence as a response to land use change: a review of evidence from New Zealan. Catena 51(3–4):297–314
Guzzetti F (2000) Landslide fatalities and the evaluation of landslide risk in Italy. Eng Geol 58:89–107
Guzzetti F, Malamud BM, Turcotte DL, Reichenbach P (2002) Power-law correlations of landslide areas in central Italy. Earth Planet Sci Lett 195(3–4):169–183
Italian Military Geographical Institute (IGMI). www.www.igmi.org/download.php
Lazzari M, Geraldi E, Lapenna V, Loperte A (2006) Natural hazards vs. human impact: an integrated methodological approach in geomorphological risk assessing on Tursi historical site, southern Italy. Landslides 3(4):275–287
Luino F (2005) Sequence of instability processes triggered by heavy rainfall in the northern Italy. Geomorphology 66:13–39
McNeill JR (2003) Observations in the nature and culture of observational history. Hist Theory (Theme issue 42):5–43, Wesleyan University. ISSN 0018-2556
Menduni G, Pagani A, Rulli MC, Rosso R (2002) A non conventional watershed partitioning method for semidistributed hydrological modelling: the package Aladhyn. Hydrol Process 16:277–291
Montgomery DR, Dietrich WE (1994) A physically based model for the topographic control on shallow landsliding. Water Resour Res 30 (4):1153–1171
Naudet V, Lazzari M, Perrone A, Loperte A, Piscitelli S, Lapenna V (2008) Integrated geophysical and geomorphological approach to investigate the snowmelt-triggered landslide of Bosco Piccolo village (Basilicata, southern Italy). Eng Geol 98:156–167
Okamoto T, Larsen JO, Matsuura S, Asano S, Takeuchi Y, Grande L (2004) Displacement properties of landslide masses at the initiation of failure in quick clay deposits and the effects of meteorological and hydrological factors. Eng Geol 72:233–251
Piccareta M, Capolongo D, Boenzi F (2004) Trend analysis of precipitation and drought in Basilicata from 1923 to 2000 within a southern Italy context. Int J Climatol 24:907–922
Piccarreta M, Capolongo D, Boenzi F, Bentivenga M (2006) Implications of decadal changes in precipitation and land use policy to soil erosion in Basilicata, Italy. Catena 65:138–151
Polemio M, Sdao F (1999) The role of rainfall in the landslide hazard: the case of the Avigliano urban area (Southern Apennines, Italy). Eng Geol 56(3–4):297–309
Rosso R, Rulli MC (2002) An integrated simulation method for flash-flood risk assessment. 2. Effects of changes in land use under a historical perspective. Hydrol Earth Syst Sci 6 (2):285–294
Rosso R, Rulli MC, Vannucchi G (2006) A physically based model for the hydrologic control on shallow landsliding. Water Resour Res 42:W06410. doi:10.1029/2005WR004369
Rosso R, Rulli MC, Bocchiola D (2007) Transient catchment hydrology after wildfires in a Mediterranean basin: runoff, sediment and woody debris. Hydrol Earth syst Sci 11(1):125–140
Rulli MC (2010) A physically based watershed partitioning method. Adv Water Resour 33(10):1206–1215. doi:10.1016/j.advwatres.2010.06.011, 2010
Rulli MC, Rosso R (2005) Modeling catchment erosion after wildfires in the San Gabriel Mountains of Southern California. Geophys Res Lett 32:L19401. doi:10.1029/2005GL023635
Rulli MC, Rosso R (2007) Hydrologic response of upland catchments to wildfires. Adv Water Resour 30:2072–2086. doi:10.1016/j.advwatres.2006.10.012
Rulli MC, Spada M, Bozzi S, Bocchiola D, Rosso R (2006) Rainfall simulations on a fire disturbed Mediterranean area. J Hydrol 327 (3–4):323–338. doi:10.1016/j.jhydrol.2005.11.037
Santini M, Grimaldi S, Nardi F, Petroselli A, Rulli MC (2009) Pre-processing algorithms and landslide modelling on remotely sensed DEMs. Geomorphology 113(1–2):110–125
Valentini G (1979) I fenomeni di erosione e di frana nei depositi argillosi della fossa bradanica. Geol Appl e Idrogeol 14:126–141 (In Italian)
Varnes DJ (1984) Landslides hazard zonation: a review of principles and practice. Nat Hazard 3:63, UNESCO
Vertessy RA, Elsenbeer H (1999) Distributed modeling of storm generation in an Amazonian rain forest catchment: effects of model parameterization. Water Resour Res 35(7):2173–2187
Wang FW, Matsumoto T, Tanaka Y (2005) Two recent flowslides in Yamashina area, Kanazawa City, Japan. Landslides 2:229–234
Wigmosta M, Voil LW, Lettenmaier D (1994) A distributed hydrology-vegetation model for complex terrain. Water Resour Res 30 (6):1665–1679
Wu W, Siddle R (1995) A distributed slope stability model for steep forested basins. Water Resour Res 31(8):2097–2110

DSGSDs Induced by Post-Glacial Decompression in Central Apennine (Italy)

Domenico Aringoli, Bernardino Gentili, Marco Materazzi, Gilberto Pambianchi, and Nicola Sciarra

Abstract

During the last 30 years of studies in the field of mass movements located in the calcareous-marly and marly-sandy Apennines (Umbria-Marches and Latium-Abruzzi regions), over to a large number of landslides with different dimensions, even a lot of deep-seated gravitational slope deformations (DSGSDs) have been recognized and analysed. These phenomena are also located in that sector of central Italy affected by a cold climate during the past and actually temperate (central Apennine chain).

Keywords

DSGSD • Post-glacial decompression • Numerical modeling • Central Apennine

General Setting

The present note is addressed to the analysis of some deep-seated gravitational slope deformation (DSGSD) phenomena along the Umbria-Marches-Abruzzi slopes (Sibillini Mountains, Laga Mountains and Gran Sasso d'Italia) modeled by the late Pleistocene glacial morphogenesis and the post-glacial decompression effects. In particular, we recognized this kind of phenomena in the mounts located in Fig. 1 (Aringoli 1998; Aringoli et al. 1996; Dramis et al. 1988, 1995; Gentili et al. 1992).

The above phenomena are located in the calcareous-marly and marly-sandy Apennines (Umbria-Marches and Latium-Abruzzi regions) which main characteristics are shown in Fig. 2.

In this sector of central Italy, along the Gran Sasso d'Italia (the highest chain, reaching 2,912 m a.s.l.), the glacier of Calderone represents the only remaining trace of active glacial processes in the Apennine. In the past, however, glacial morphogenesis left numerous traces, modeling cirques and glacial valleys, also of great dimensions (Jaurand 1998). Although not comparables with the alpine ones, cirques characterized by "walls" of hundreds of meters and U-shaped valleys with difference in height from the top to the valley floor up to 600 m are visible.

Such geomorphological setting, together with the litho-structural one, favored the activation of large landslides and DSGSDs, in particular along the steepest slopes of the most elevated areas, at the valley heads, and in ancient cirques areas (Fig. 3).

State of the Art and Methodology

The fundamental genetic factors of the DSGSD phenomena have been identified in: (1) the specific geological setting (such as thrust fronts); (2) the high relief and the seismic activity (both related to the intense neo-tectonic uplift of central Italy). Evolutionary models have also been hypothesized: *lateral spreads* clearly prevail in the stony rocks intercalating or overlaying pelitic (or deeply tectonized or karstified) levels, sometimes driven by thrust planes, bedding or, more rarely, pre-depositional erosion surfaces (Aringoli 1998; Crescenti

D. Aringoli (✉) • M. Materazzi • G. Pambianchi
Scuola di Scienze Ambientali, Università di Camerino, Camerino, Italy
e-mail: domenico.aringoli@unicam.it

B. Gentili
Scuola di Architettura e Design, Università di Camerino, Camerino, Italy

N. Sciarra
Dipartimento di Geotecnologie per l'Ambiente ed il Territorio, Università di Chieti-Pescara, Chieti-Pescara, Italy

C. Margottini et al. (eds.), *Landslide Science and Practice*, Vol. 4,
DOI 10.1007/978-3-642-31337-0_54,

Fig. 1 Localization of DSGSD phenomena in central Apennine recognized by authors on valleys of glacial origin

et al. 2002; Cruden and Varnes 1996; Dramis 1984; Dramis and Sorriso-Valvo 1994; Hutchinson 1995; Pasuto and Soldati 1996; Savage and Varnes 1987; Ter-Stefanian 1977; Varnes 1978; Zischinsky 1969). Rare *sackungs* usually develop in the thick and fractured rock masses forming the slopes with the highest relief values (Fig. 4; Aringoli et al. 1996; Radbruch-Hall et al. 1976).

More in general along the glacial valleys, once the glacier died out or receded, DSGSDs occur where the glacier action has been more effective and has deeply modified the slope morphometry generating high relief valley sides (Agliardi et al. 2001; Crosta and Agliardi 2002). In these areas, after glacial retreat, high instability conditions occurred along the slopes, because of the absence of a lateral support; however, a fundamental role is also played by slope angle and local seismicity.

All the above conditions, together with the litho-structural setting of the slopes and the distribution/state of rock discontinuities (joints, karst features etc.) are, in general, factors predisposing to the activation of mass movements; in this case, rockfalls, slides (subordinately flows) and deep seated gravitational slope deformations (DSGSDs) occur along the slopes and on the area where glacier were present. The above phenomena may be present also as a combination.

Rockfalls, slides and flows are very rapid and sudden processes, while DSGSDs need a long period of preparation and show few superficial geomorphological evidences. If glacial retreat occurred recently, DSGSD activation may take place with minor and less evident superficial geomorphological evidences

In order to define the role played by deglaciation in the occurrence of mass movements and to characterize the dynamic evolution on significant sections of actual cases, in addition to the systematic and detailed geologic-geomorphologic surveys and to the processing of the relative models, in this study we used a complex numerical calculation methodology, already exploited in other studies (Crescenti et al. 2002).

The numerical code that has been used (FLAC_2D, 2000) is a finite differences bi-dimensional numerical analysis method. The examined slopes are discretized by tetrahedral elements, the physical-mechanical behaviour of every element has to answer to a pre-established rule of stress/deformation (linear or not-linear), in reply to the applied forces and/or to the contour conditions.

The numerical methods offers a lot of information on strain and stress conditions inside the system, optimizing the properties and the behaviours of the rock masses.

The study allows us to attribute to the decompression forces related to receding glacial tongues a predominant role in comparison with the other genetic factors; moreover, it aims to establish if these forces represent activation triggering or a predisposing factor (as pointed out for the Alps) of the above mentioned phenomena.

Study Cases

Different study cases have been analyzed. Some of them show very evident traces of glacial activity and slopes deformation caused by gravity, as a consequence of glacier retreat.

The case of Mount Bove (see Fig. 2 for location) is an excellent example (Fig. 5): the high relief and slope angle caused the occurrence of a DSGSD which involved the entire calcareous slope, with a shear zone which developed within a low-resistant marly bend. In this case, a fundamental role is played also by the structural setting of the slope, where the presence of significant discontinuities (a, and b in Fig. 5) partly bounded the phenomenon.

A numerical modeling has been attempted in other contexts. A beautiful example is the DSGSD of Campo Pericoli, near the Gran Sasso Massif (Figs. 6 and 7), where the last active glacier of central Apennine (Calderone Glacier) is present: this phenomenon will be briefly discussed in the present work.

From a lithologic point of view, the site is mainly characterized by calcareous formations, partly karstified, overlying marly levels with minor resistance characteristics (see Table 1).

The role of glacier dynamics in slope instability result from the combination of several processes: abundant circulation of groundwaters, deep karst, volumetric changes, forces of decompression; all these processes, connected to climate variations, must be considered as preparation factors.

The geotechnical parameters used for modeling are significant not so much for their absolute value as for the differences between the two categories.

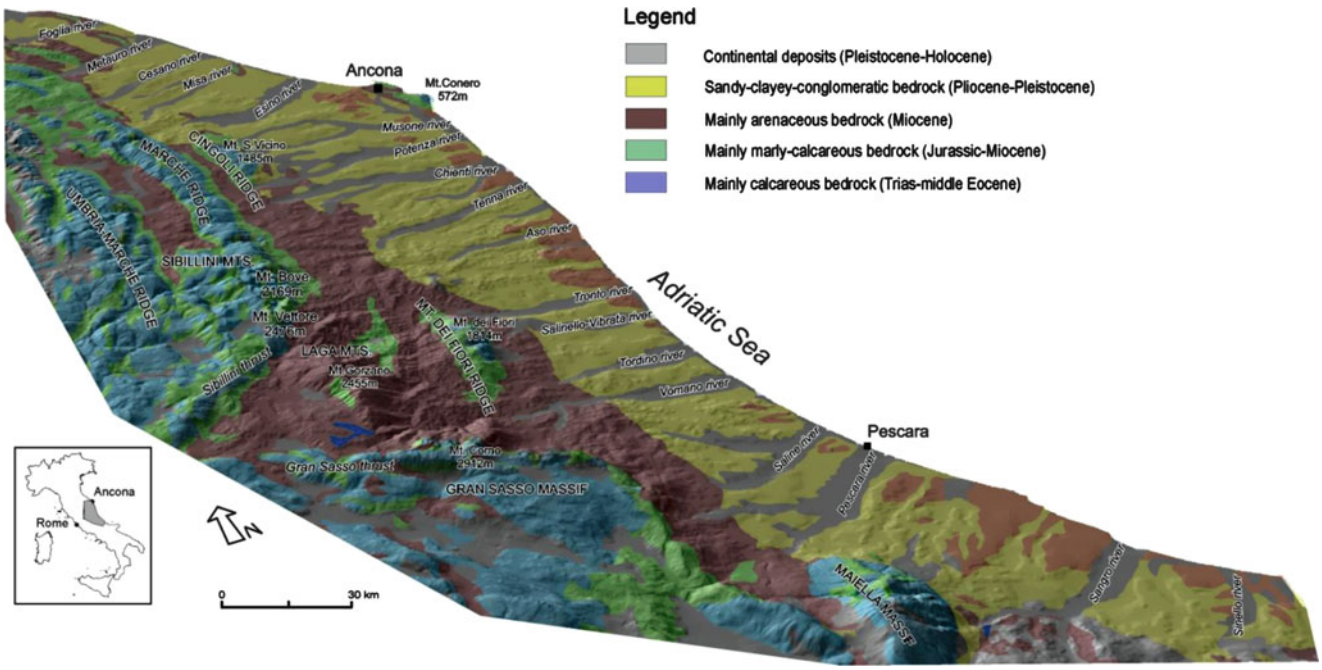

Fig. 2 The study sector of central Italy, with main geological formations (Modified from Dramis et al. 1995)

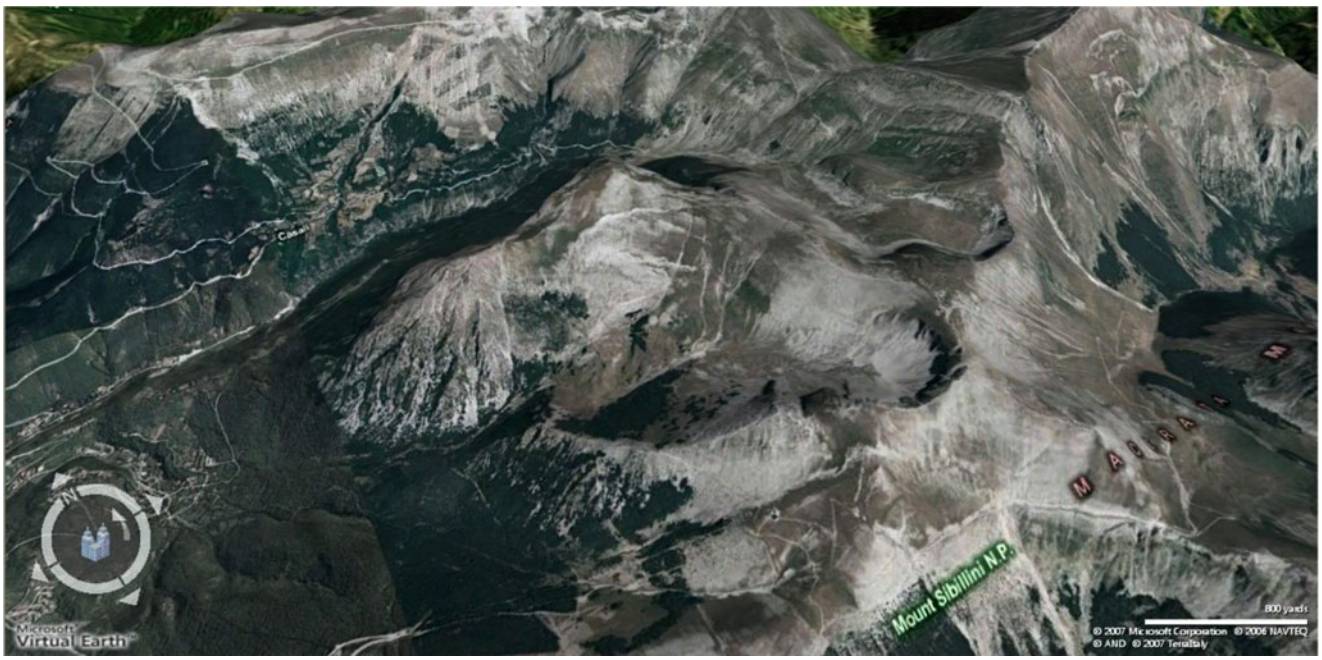

Fig. 3 Aerial 3D-view of the central sector of Sibillini Mountains with glacial macro-morphologies

The study of the deformation has been carried out by means of a 2D finite difference numerical modeling (FLAC_2D software distributed by Itasca) in order to determine the main elements which led to the present configuration. In the modeling, also the decompression connected to glacier retreat, supposed to change from 4.5 to 0.5 Mpa taking into account the maximum height reached by the glacier, has been simulated.

In the Figs. 8 and 9, some results obtained by the numerical simulation are shown; very interesting is the displacement observed along x and y, which is almost totally congruent with the morphologies observed in the field.

The study, which can be extend to analogous phenomena along the Apennine chain, allowed us to formulate a genetic-evolutive hypothesis (Fig. 10) where two different phases have been theorized: in the first one, occurred at the end of late

Fig. 4 Geomorphological evidences in the upper part of a DSGSD in central Apennine

Fig. 7 View from the North of the Campo Pericoli deformation and the Gran Sasso Massif

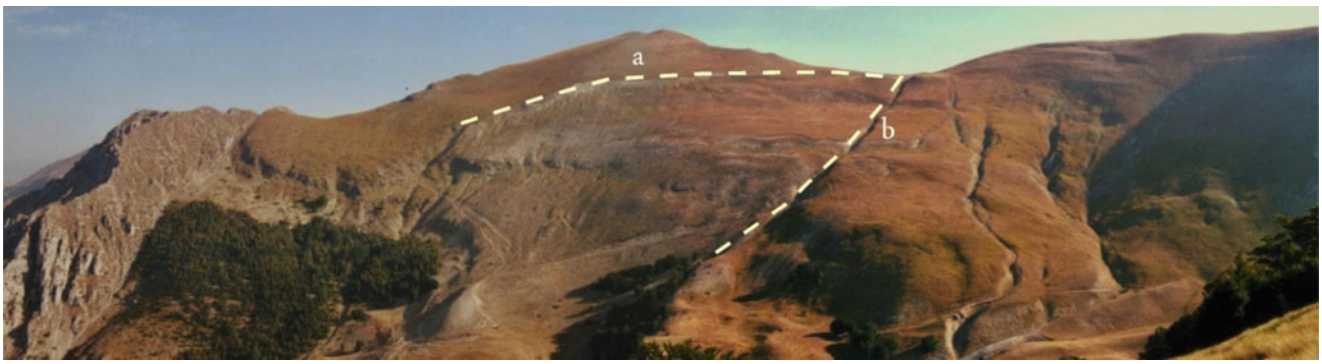

Fig. 5 The western slope of the Mount Bove shaped by geomorphological processes of different type, and the gravitational deformation in its central portion; *a* and *b* are the main discontinuities which bound the phenomenon

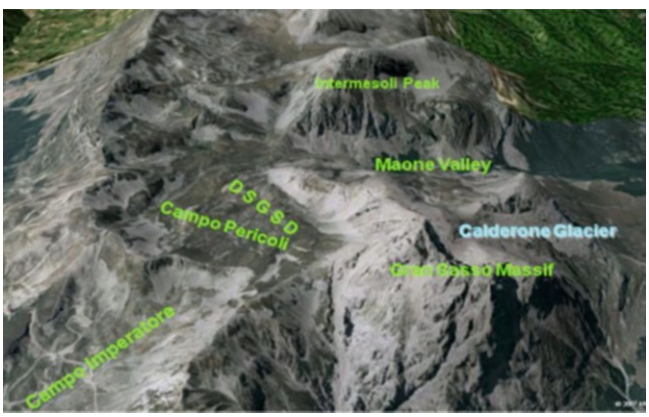

Fig. 6 The Gran Sasso Massif: main landforms and localities

Table 1 Main geotechnical parameters used in the numerical modeling (Limestones lithotypes correspond to the Maiolica and the Calcareniti a Entrochi formations; marly lithotypes are found in the Verde Ammonitico formation)

	γ unit weight KN/m^3	ϕ friction angle (°)	c cohesion MPa	E Young modulus GPa
Limestones	24	45	2.5	50
Marls	23	40	1.0	10

Pleistocene when the glacier was still present, the combined action of ice, sub-glacial waters and karst weathered and weakened the calcareous rocks; in a second phase, subsequent to glacial retreat, the lack of a lateral support and the high relief caused a strong decompression of the slopes and a slow deformation of the entire mass along the less resistant marly level and using the discontinuities previously reworked.

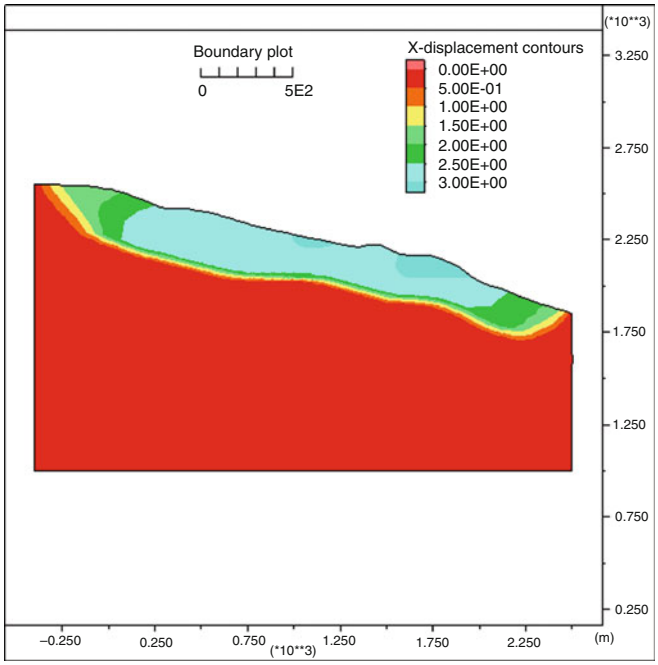

Fig. 8 X-displacement resulting from numerical modeling: the colors from red to cyan show an increasing horizontal displacement

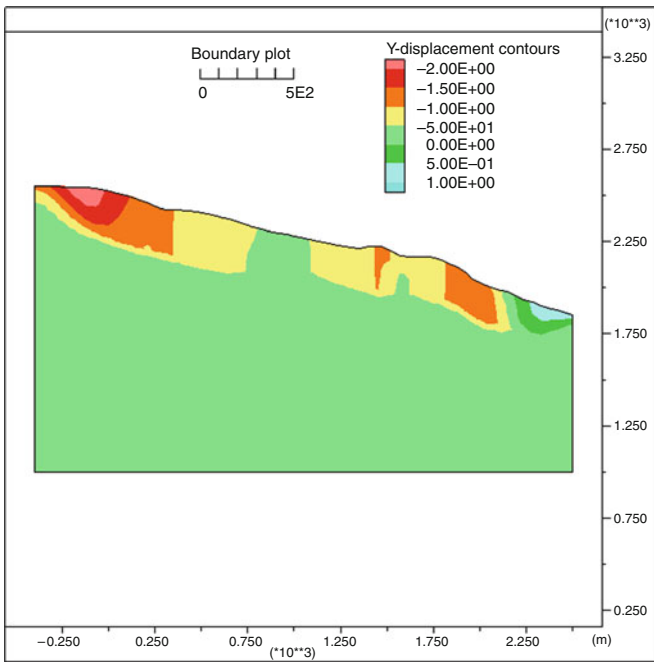

Fig. 9 Y-displacement resulting from numerical modeling: the colors from cyan to red show a progressive lowering (vertical displacement)

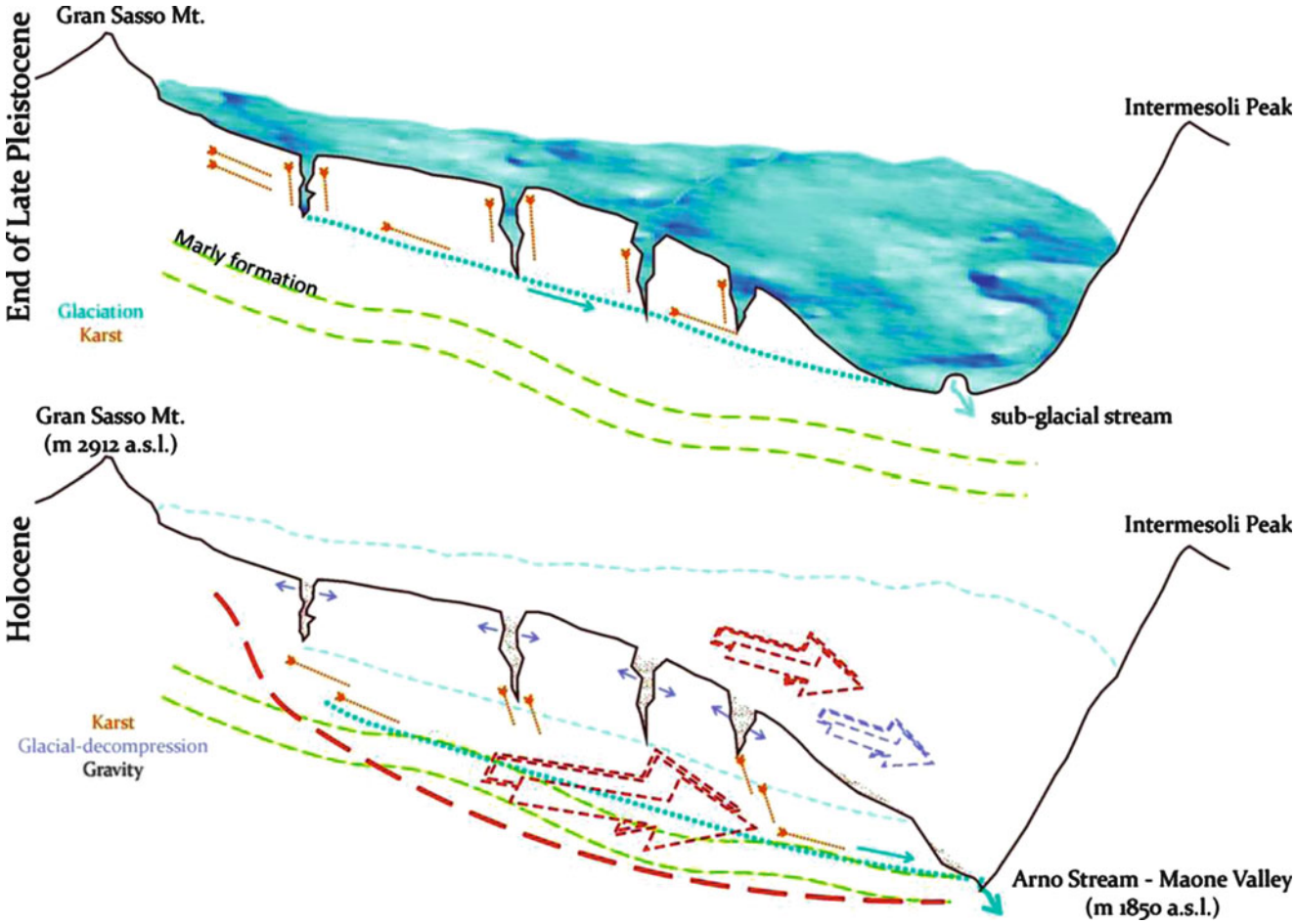

Fig. 10 Genetic-evolutionary hypothesis of the gravitational deformation in glacial valleys in central Apennine

Conclusions

The study, which used data coming from the DSGSD database built by the authors for central Apennine, allowed to recognize some cases (less than 10 % of the total DSGSD analyzed) in which glacial activity can be ascribed as a fundamental genetic factor.

A further intention was to establish if all the processes involved represent a predisposing or activation factors (as pointed out for the Alps). The present data, in agreement to other authors, let us to not attribute to the described factors a triggering role in the activation of the above mentioned phenomena.

References

Agliardi F, Crosta GB, Zanchi A (2001) Structural constraints on deep-seated slope deformation kinematics. Eng Geol 59(1–2):83–102

Aringoli D (1998) Studi morfotettonici e geomorfologico-applicativi: alcuni esempi nell'area umbro-marchigiana. Ph.D. thesis in applied geology, geomorphology and hydrogeology, X, University of Perugia, pp 220

Aringoli D, Gentili B, Pambianchi G (1996) The role of recent tectonics in controlling the deeep-seated gravitational deformation of Mount Frascare (central Apennines). Geogr Fis Dinam Quat 19:281–286

Crescenti U, Gentili B, Pambianchi G, Sciarra N (2002) Modeling of complex deep-seated mass movements in the central-southern Marches (Central Italy). In: Rybar J, Stemberk J, Wagner P (eds) Landslides. Swets & Zeitlinger, A.A. Balkema, Lisse, pp 149–155. ISBN 90 5809 393 X

Crosta GB, Agliardi F (2002) How to obtain alert velocity thres holds for large rockslides. Phys Chem Earth Parts A/B/C 27(36):1557–1565

Cruden DM, Varnes DJ (1996) Landslide types and processes. In: Turner AK, Schuster RL (eds) Landslide-investigation and mitigation, vol 247, National Academy of Sciences, Washington, DC, Trasportation Research Board Special Report, pp 36–75

Dramis F (1984) Aspetti geomorfologici e fattori genetici delle deformazioni gravitative profonde. Boll Soc Geol It 103:1–7

Dramis F, Sorriso-Valvo M (1994) Deep-seated gravitational slope deformations, related landslides, and tectonics. In: Oyagy N, Sorriso-Valvo M, Voight B (eds) Deep-seated landslides and large-scale rock avalanches. Eng Geol 38(3–4):231–243

Dramis F, Gentili B, Pambianchi G (1988) Deformazioni gravitative profonde e grandi frane in un tratto di valle trasversale

dell'Appennino marchigiano (F. Chienti). In: Atti Convegno: "I corsi d'acqua minori dell'Italia appenninica", Aulla, giugno 1987, Boll. Museo Storia Nat. Lunigiana, 6–7, pp 29–33

Dramis F, Farabollini P, Gentili B, Pambianchi G (1995) Neotectonics and large-scale gravitational phenomena in the Umbria-Marche Apennines, Italy. In: Slaymaker O (ed) Steepland geomorphology. Wiley, Chichester, pp 199–217

Gentili B, Pambianchi G, Aringoli D (1992) Rimodellamenti gravitativi del tratto di anticlinorio marchigiano compreso tra i fiumi Chienti e Fiastrone. Studi Geologici Camerti XII:105–115

Hutchinson JN (1995) Deep-seated mass movements on slopes. Mem Soc Geol It 50:147–164

Jaurand E (1998) Les glaciers disparus de l'Apennin. Publications de la Sorbonne. Geographie 10:382

Pasuto A, Soldati M (1996) Rock spreading. In: Dikau R, Brunsden D, Schrott L, Ibsen ML (eds) Landslide recognition. Wiley, Chichester, pp 122–136

Radbruch-Hall DH, Varnes DJ, Savage WZ (1976) Gravitational spreading of steep-sided ridge ("sackung") in Western United States. Bull Int Assoc Eng Geol 14:23–35

Savage WZ, Varnes DJ (1987) Mechanics of gravitational spreading of steep-sided ridges ("sackung"). Bull IAEG 35:31–36

Ter-Stefanian G (1977) Deep-reaching gravitational deformation of mountain slopes. Bull Int Assoc Eng Geol 16:87–94

Varnes DJ (1978) Slope movements type and processes. In: Schuster RL, Kriezek RJ (eds) Landslides – analysis and control. National Academy of Sciences, Washington, DC, Transportation Research Board

Zischinsky U (1969) Uber Sackungen. Rock Mech 1:30–52

Climatic and Structural Controls to Slope Instabilities in Val Veny (Italy)

Marco Giardino, Luigi Perotti, Marco Bacenetti, and Paolo Zamparutti

Abstract

Study of slope instabilities in high mountain regions is a challenge for scientists and professionals. A classic field-based geological/geomorphologic approach has been coupled with innovative geomatics techniques to collect data for slope instability factors characterisation in Val Veny (Mont Blanc, NW-Italy). Mobile-GIS application (SRG2) for geomorphologic mapping and LiDAR DEM plus Coltop 3D software for detailed structural analysis were used. A GIS system set up to store and manage field data and historical records for interpreting the "slope-system" behaviour, i.e. relationships between litho-structural constrain, meteo-climatic condition, glacier evolution and landslide activity. Landslides-prone sectors have been individualized in a morpho-tectonic map. Potential failure surfaces have been investigated with Markland kinematic test. GIS-integration of data allowed localizing preferred areas where local climate conditions, glacial dynamics, tectonic and geomorphologic settings strongly interact each other for producing movable materials and unstable slopes.

Keywords

Geomorphology • Geomatic • LiDAR • Coltop 3D • Slope instability

Introduction

Glacier retreat and permafrost degradation are extensively taking place during recent decades in the Western Alps, affecting geomorphologic processes and landforms on mountain slopes. In this context, the integration of classical field-based geological and geomorphologic approaches with innovative geomatics techniques may contribute significantly to a more detailed characterization of the controlling factors of slope instabilities. A better reconstruction of slope sensitivity under the forcing action of climatic fluctuations is possible too. This paper aims to a better comprehension of the "slope system" behaviour in the Veny Valley, where: (1) large amount of data is available for a high altitude environment and (2) a deeper knowledge on slope instabilities is needed for a territory of high natural and economic interests.

Lithological and Structural Setting

The study area is located in the Italian side of the Mont Blanc Massif (NW-Alps), close to the border of France and Suisse (Fig. 1). The massif has its highest elevation at 4,808 m.s.l., and many of its fractured granite faces, peaks and crests stand well above 3,000 m.

From the geological point of view the study area includes two main domains: Helvetic-Ultrahelvetic (Mont Blanc and cover units; mostly granites and clay-carbonatic schist) and Penninic Domain (Sion-Courmayeur Zone: quartzite, dolomite, limestone breccias and schist; Perello et al. 1999).

M. Giardino (✉) • L. Perotti
Earth Sciences Department, University of Torino, Torino, Italy

NatRisk Inter-department Centre, University of Torino, Torino, Italy
e-mail: marco.giardino@unito.it

M. Bacenetti • P. Zamparutti
Earth Sciences Department, University of Torino, Torino, Italy

C. Margottini et al. (eds.), *Landslide Science and Practice*, Vol. 4,
DOI 10.1007/978-3-642-31337-0_55,

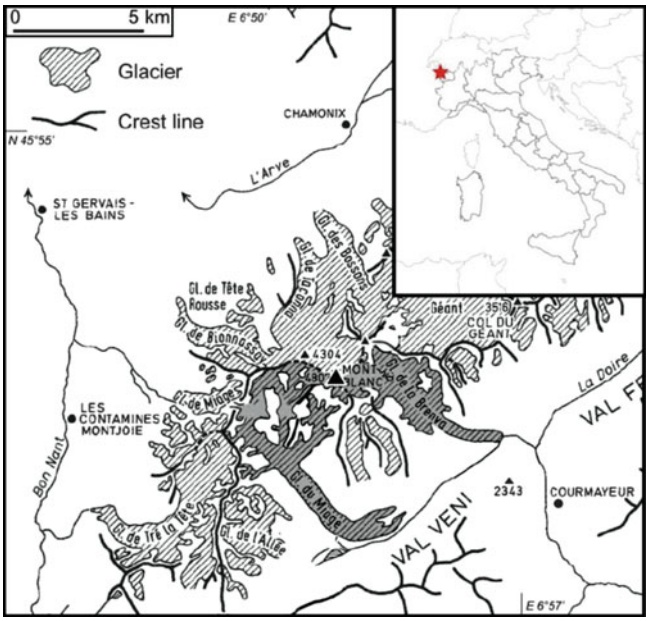

Fig. 1 Location of the Mont Blanc massif (After Deline 2009)

Structural setting is characterized by NW-dipping units separated by large subvertical Variscan N20°-striking faults, and Alpine N45°-striking faults with mylonitized zones. Due to the continuing collision of the Eurasian and African (Adriatic) tectonic plates, the massif is uplifting at few mm/a (Lemoine et al. 2000).

Geomorphologic and Climatic Conditions

From the geomorphologic point of view, the Mont Blanc massif shows a cross-range asymmetry. The Northwest side has relatively gentle slopes and the largest glaciers, fed by precipitation from the dominant westerly winds and protected by shaded North faces. The Southeast side is very steep, with smaller glaciers bounded by high, subvertical rock walls. In the Val Veny two main geomorphologic features dominate the landscape: debris-covered glaciers (Miage and Brenva) and steep rock slopes on the other side. The Miage Glacier is the third largest Italian glacier and the longest. It is fed by 4 tributary glaciers, flowing from the peak of Mont Blanc through a narrow valley surrounded by steep rock slopes. The glacial tongue of these glaciers built great moraines on the outlet of the valley. These landforms blocked the valley stream (Dora di Veny) and created two lakes, then filled by fluvio-glacial deposits, forming the Zerotta plain and the Combal plain.

Several stages of glacial advance and retreat are registered along Val Veny, most of the preserved landforms having been built after the LGM. Neogenic climate fluctuations strongly modify the geomorphology of the valley. Glacial variation during the Holocene interglacial is an important key for interpreting the palaeoclimatic conditions, although the transfer function between climate signals and glacier oscillations remains poorly understood (Orombelli and Deline 2002). Study of the sediments of moraines dammed lakes (i.e. Combal) suggests that the main moraines of the Miage and Brenva glacier have built since 5.0 kyr BP (Deline and Orombelli 2005)

Methods

Pocket PC and Mobile GIS

Simplicity, precision and rapidity of field survey techniques are some key-features of the pocket PC equipped whit dedicated GIS software. Mobile GIS is the combination of Geographic Information System (GIS) software, Global Positioning Systems (GPS), and mobile computing devices. Mobile GIS fundamentally changes the way information is collected, used in the field, and shared with the rest of an organization.

For faster and more suitable procedures of field mapping activities, we used the "SRG2" application: an ArcPad extension including a toolbar with several functions for a useful mapping and classification of geological and geomorphologic features.

LiDAR

Airborne LiDAR data provide new opportunities to overcome some of the problems associated with traditional, field-based, geomorphologic mapping, such as restrictions on access and constraints of time or cost. The combination of airborne LiDAR data and GIS technologies facilitates the rapid production of geomorphologic maps. Classification of LiDAR data according to elevation in a GIS enables the user to identify and to delineate geomorphologic features similarly to field mapping (Fig. 2); however it is necessary to use a range of classification intervals in order to map the various types of feature that occur within a single reach.

Digital Stereo and Ortophotos

Stereographic digital models were obtained from the scanned aerial photograms and then elaborated. Multitemporal stereo-models were useful to make considerations about the evolution of the area (Fig. 3). The use of photogrammetric software allowed faster management and updates of all the available data, if compared to traditional techniques. The stereo-pairs were exported from Leica Photogrammety Suite and imported

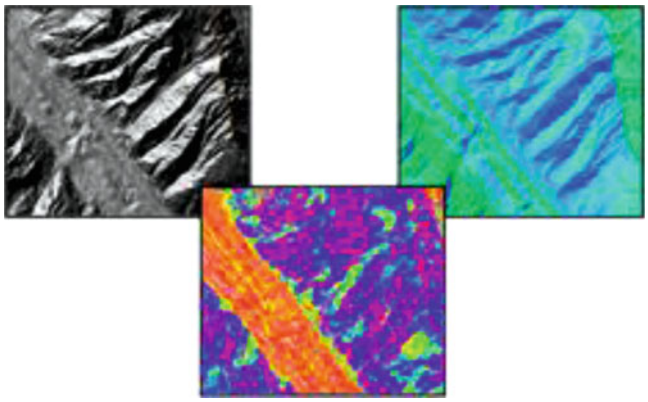

Fig. 2 Hillshade (*left*), Slope (*center*) and Aspect (*right*) maps of the central part of the Miage valley. Morphostructural (*tributary incisions*) and glacial (*debris cover*) features are enhanced

into ArcMap where it was possible to analyze the stereographic digital models through Stereo Analyst (GIS extension) and to visualize them by 2.5D ArcScene.

Coltop3D

Coltop3D is a software developed by Quanterra (University of Lausanne); the GeoSitLab (University of Torino) is part of the BetaTesters veryfying this software by data from field surveys. Coltop-3D computes the orientation of each cell of the DEM. The result is a coloured shaded relief map combining both terrain slope angle and slope aspect (direction of slope) in a unique representation. DEM LiDAR images were imported into Coltop 3D to analyse potential failure surfaces of the Mont Rouge de Peuterey (Fig. 4). The Coltop 3D data were then analysed for stability using the Markland test. Through back-analysis, the software allowed the determination of main areas of potential gravitational instabilities.

Results

"Around Site" Geomorphological Data

Three main glacial stages have been mapped along the Miage valley by means of trimlines (Fig. 5):

1. The highest in elevation could be referred to LGM: it is underlined by a slope change; bedrock above this trimline shows major effects of weathering processes (deepened incisions, open fractures, rock/mineral alteration, allowing decrease in geomechanical conditions);
2. The second trimline has been observed just a hundred meters above the present glacier surface: below the trimline, bedrock appears more smoothed than above and segmented only by structural discontinuities. Most of rock falls originate in the altitudinal belt between this and the highest trimline;
3. The last and lowest mapped trimline shows the evidence of recent glacial mass contraction.

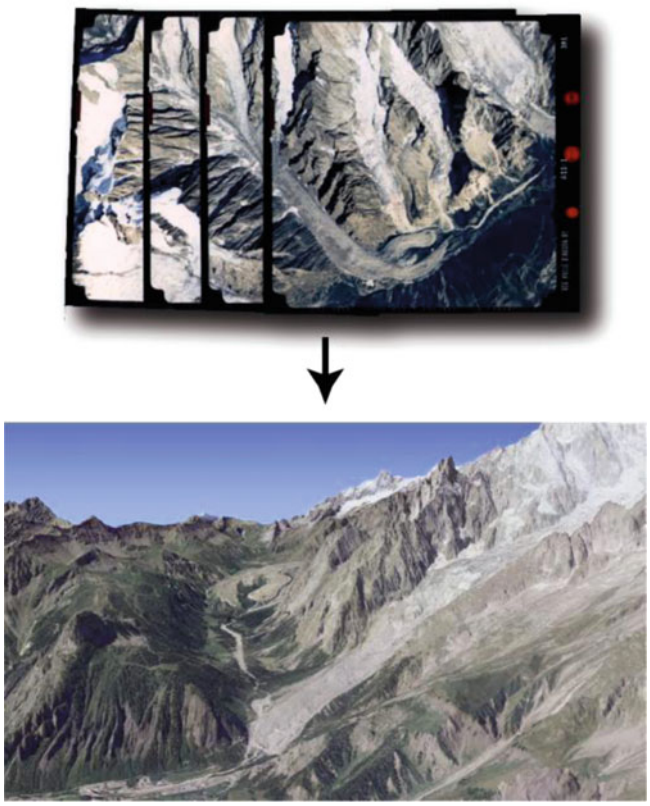

Fig. 3 Stereographic digital models of Val Veny

Other geomorphological features suggesting past glacial condition are: small glacial deposits and terraces on one side of the valley slopes. Morover two tributary suspended glacial valleys (actually free of ice), have been mapped at elevation of about 2650 m a.s.l..

From bibliographic data (De Saussures 1774; Baretti 1880) we know the surface of Miage glacier was free of debris until the end of XIX century. Now almost all the ablation tongue is covered by a layer of debris, from a few centimetres to around 2 m, originated mostly from rock falls (Deline 1998, 2002). Three main typologies of rock instability have been recognized by the author:

1. *ébulisation* (mainly small boulders $< 20 \div 30$ cm) located on recently deglaciated areas with gentle slopes (cirques);
2. *ébulment* (isolated blocks or > 100 m^3) located on recently deglacialized slopes and glacial ridges;
3. *écroulment* (<100 m^3) in high altitude areas on vertical faces.

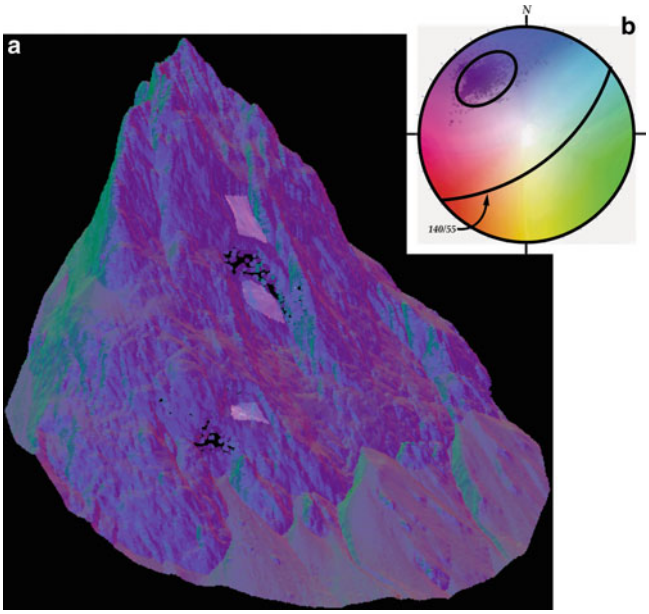

Fig. 4 Coltop 3D working envinronment **a**) polygon selection thru **b**) stereoplot Shmidt-Lambert - Joint set at 145/55

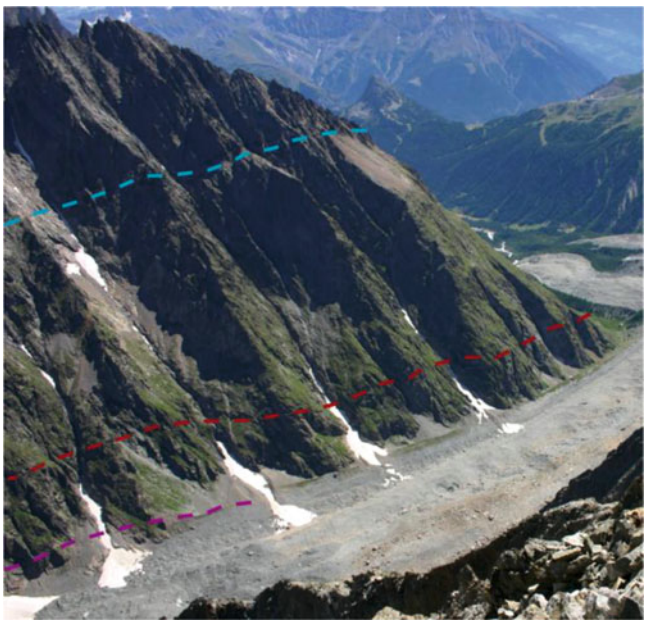

Fig. 5 Trimline on right slope of Miage valley

"Around Site" Structural Data

Previous geomechanical surveys (Chiarle 2000; Amerio 2004) individuated four main joint sets on the total Veny valley, in order of frequency:

1. E/NE-W/SW: parallel to the major tectonic lineaments;
2. N/NE-S/SW: high angle dip;
3. N/NW-S/SE: parallel to the Miage valley and to the reverse faults of the granitic units;
4. E-W: high angle dip.

The mesostructural data collected for the present paper update to five the joints systems on the on the Miage valley slopes, here indicated as Dip Direction/Dip, with the correspondent system of the Val Veny (Fig. 6):

1. (E/NE-W/SW): 173/57;
2. (N/NE-S/SW): 10/70;
3. (N/NW-S/SE): 293/67;
4. (E-W): 145/65;
5. 70/60

Discussion

Four sectors with different morpho-tecnonic behaviour have been recognized in Val Veny:

1. The *upper part of Val Veny* (Lex-Blanche valley), characterized by cryogenic processes and rock-glaciers, mainly affecting carbonate-type rocks;
2. The *middle-lower right side of Val Veny*, where: evaporitic rocks outcrops, slopes are affected by DSGSD and incisions show debris flow deposits;
3. The *lower left side of Val Veny* (Fig. 7): the granitic bedrock is affected by four major joint set; Markland tests on N70°/60° open fractures. underline the aptitude to toppling and wedge sliding; at the base of this sector, polygenic cones (Breuillat, Fréney, Combalet) are fed mainly by rock falls and avalanches.
4. The *Miage basin glacier*, the major tributary of Val Veny, crossing the Mont Blanc Massif for 7 km length, with a N/NW trend. Back analysis by Coltop 3D individuated unstable sectors on the left slope of Miage valley (Fig. 8); here all the joint sets interact and the Markland tests show the aptitude of wedge sliding.

This information has been summarized into a Morpho-Neo-Tectonic map of the dynamics of the area (1:15,000 in scale; Giardino et al. in press)

The field survey data for the Val Veny have been compared to the regional map showing possible occurrence of permafrost in the Aosta Valley coming from the PERMACLIM model (Guglielmin et al. 2003). This model calculates the mean soil annual surface temperature (MAGST) on the base of: historical climate series (TA), the snow high coverage (HS) from monitoring meteo stations and DTM parameters of aspect and slope.

Focusing on the Miage Glacier valley slopes, relationships between *écroulements* and permafrost distribution have been observed (Fig. 9). It appears clear that the degradation of sub surface-ice is one of the triggers of large rock fall events, while predisposing factors could be main

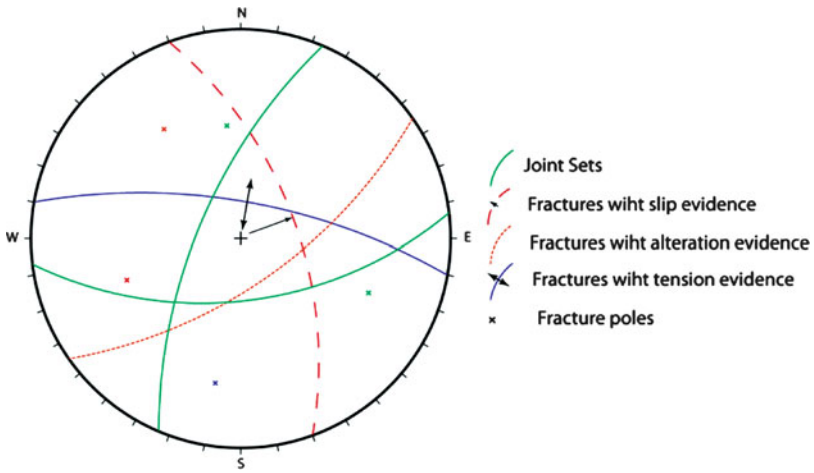

Fig. 6 Stereoplot of Miage valley joint sets (Shimidt net, lower hemisphere)

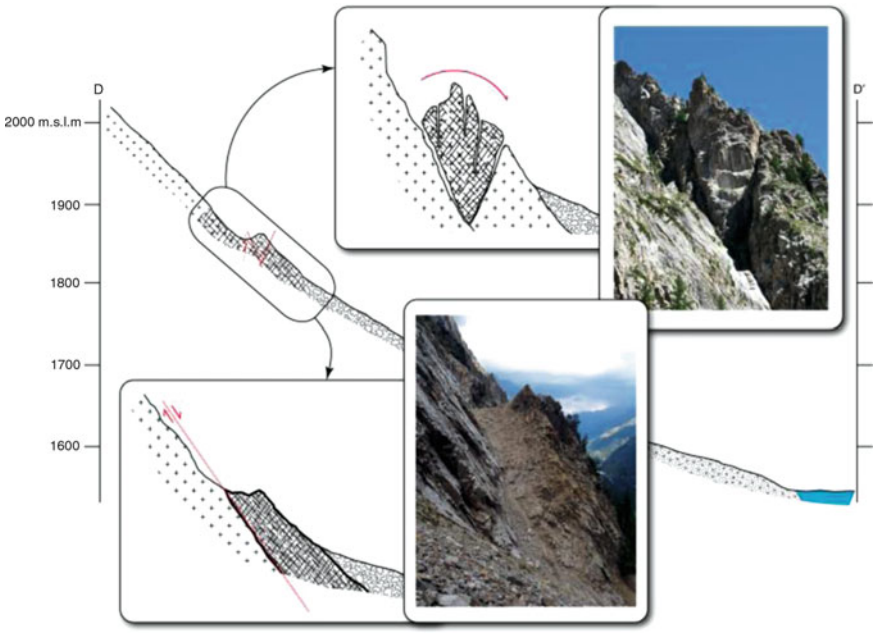

Fig. 7 Schematic morpho-tectonic setting and cross sections of the right side of the *lower left side of Val Veny*

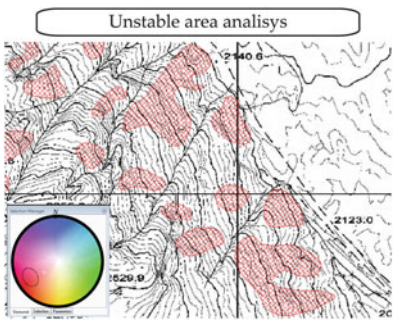

Fig. 8 Example of unstable areas detected by Coltop 3D analisys on the Miage Basin south slope. Dip and Dip direction limit in the stereo plot

structural discontinuities bounding the sectors. In effect the occurrence of these landslides should not be connected to annual temperature fluctuation, but to long-term climatic variations (i.e. Permafrost degradation).

Concerning *éboulement* and *éboulisation* phenomena, there is no clear relationships with PERMACLIM data, whose results in the Miage glacier Valley show "Permafrost possible" and, "Permafrost present" in both cases. On *éboulisation* sectors, the number of discontinuities and fractures is particulary high, while the gentle slope morphology is usually represented by recently deglaciated areas such as suspended glacial valleys or old glacial cirques. The compression and decompression actions exerted by the glacial masses and the water circulating through the discontinuities, favoured the fracturing of bedrock and the production of sparse debris feeding debris-avalanche cones.

Éboulement sectors are localized on steep slopes close to the tributary glacier outcomes on the main tongue. Annual fluctuation of the temperature and opening of pre-existing fractures produce unstable blocks and landslides that seasonally reach the glacier surface contributing to the debris coverage thickening.

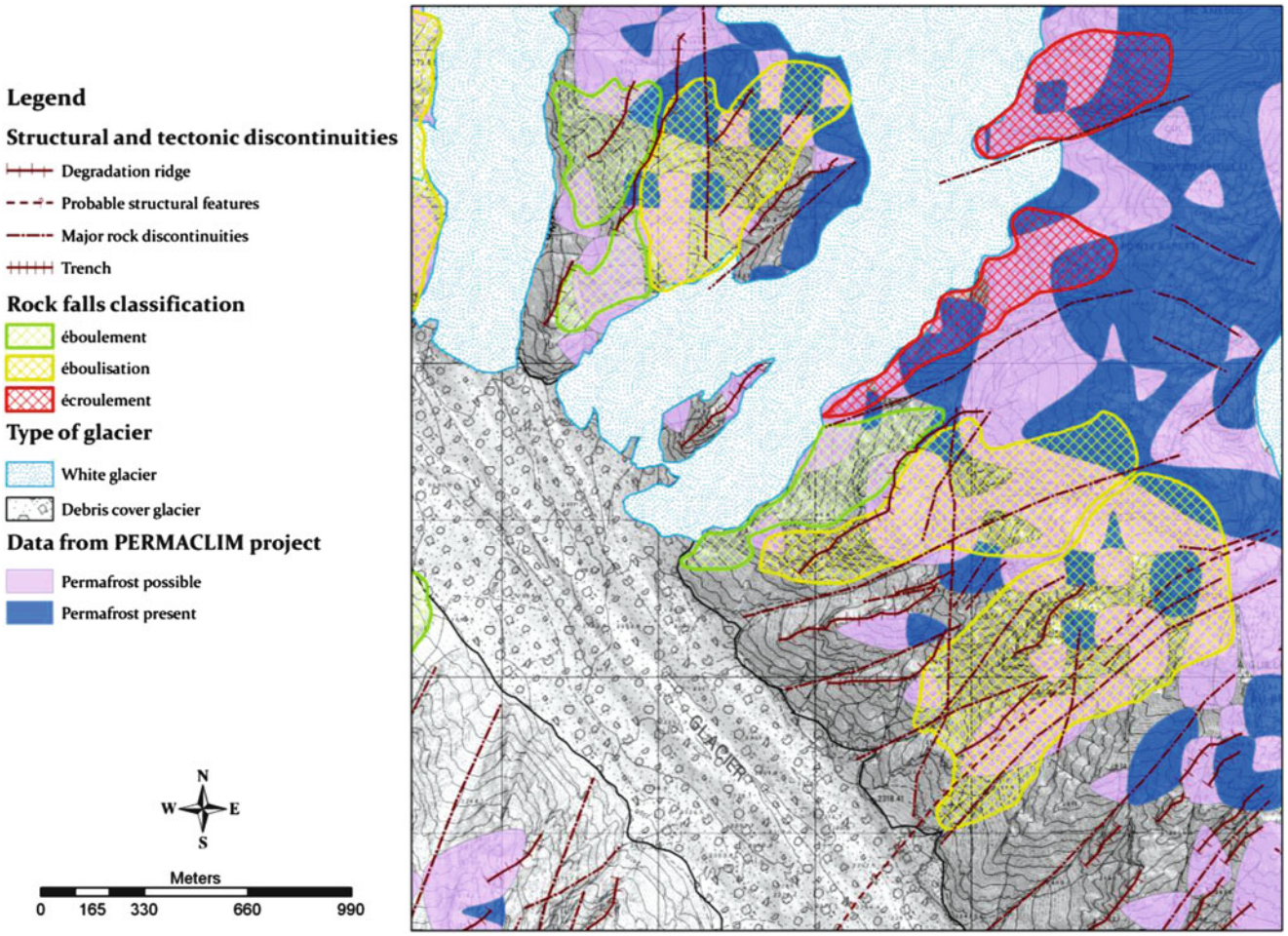

Fig. 9 Map of interaction whit structural setting, rock falls and permafrost

Conclusions

The application of these innovative methodologies has allowed the integration of the data and their geomorphologic interpretation. The remote sensing technologies applied in this work proved to be affordable for upgrading the usual field-based approach in the safe analysis of stability conditions in mountainous areas. A GIS system was set up to store and to manage data, each layer being used to interpret the landforms. The evolution of each sector of the Veny Valley was reconstructed by using the most important elements as keys for interpreting the relationships between landforms and bedrocks, glaciers evolution and landslides activity. Integration of all collected data inside the GIS allowed to understand the complete morpho-structural setting of the Val Veny area.

Interaction between climatic variation and geomorphologic processes is suggested by two lines of evidence:

1. Different sectors of the Val Veny show landforms with different evolutionary stages: evolution is more enhanced moving down stream;
2. Distribution of rock falls events is influenced by local geomorphology and permafrost degradation, as suggested by the data elaborated for the Miage valley.

Acknowledgments This work is part of the international research project "MIAGEO" ("Use of innovative topographical methods (Geomatics) for the study of morphodynamics of the Miage Glacier and Mont Blanc slopes") coordinated by Marco Giardino (GeoSITLab, University of Torino) and Philip Deline (Laboratoire EDYTEM, Université de Savoie). Funds were received by the Regione Autonoma Valle d'Aosta and the Earth Sciences Department (University of Torino). We thank Sara Ratto (Centro Funzionale Regionale, Regione Autonoma Valle d'Aosta), Andrea Tamburini (IMAGEO spin-off University of Torino) for providing tools and materials (aerial photographs, orthophotograph and LIDAR data) for the research. We thank Michael Jaboyedoff (IGAR, Université de Lausanne) for including geoSITLab within the BetaTesters verifying Coltop3d software.

References

Amerio M (2004) Pericolosità geomorfologica e interazioni con l'attività antropica in alta montagna: il caso del bacino glaciale del Miage e della bassa Val Veny (Monte Bianco). MS thesis, Università degli Studi di Torino, Torino

Baretti M (1880) Il ghiacciaio del miage, vol XXXII(II). Mem. R. Acc. Scienze Torino

Chiarle M (2000) Analisi dei pericoli naturali in ambiente glaciale. Ph. d. thesis, Politecnico di Torino, Torino

De Saussure H (1774) Voyages autour du Mont Blanc en 1774, 10 July. Brouillard en crayon. BPU Geneve. Manuscript, 46 + 33 p, Ms. Saussure, 14/1

Deline P (1998) L'étagement morphodynamique de la haute montagne alpine: l'exemple du valveny (vald'aoste, italie). Revue de Géographie Alpine 86(3):27–35

Deline P (2002) Etude géomorphologique des interactions entre écroulements rocheux et glaciers dans la haute montagne alpine: le versant sud-est du massif du Mont Blanc (Vallé d'Aoste, Italie). Ph.d. thesis, Université de Savoie, Chambery

Deline P (2009) Interactions between rock avalanches and glaciers in the montblanc massif during the late holocene. Quat Sci Rev 50:1070–1083

Deline P, Orombelli G (2005) Glacier fluctuations in the western Alps during the Neoglacial, as indicated by the Miage morainic amphitheatre (Mont Blanc massif, Italy). Boreas 34:456–467, Oslo. ISSN 0300-9483

Giardino M, Perotti L, Bacenetti M, Zamparutti P. Geomatic techniques contributing to understending geo-morpho-structural assessment of Veny valley (Courmayeur, Ao). In: Proceedings of 17th meeting of the association of European geological societies, geology in digital age, 14–16 Sep 2011, Belgrade (in press)

Guglielmin M, Aldighieri B, Testa B (2003) PERMACLIM: a model for the distribution of mountain permafrost, based on climatic observation. Geomorphology 51:245–257

Lemoine M, De Graciansky P, Tricart P (2000) De l'océan à la chaine de montagnes. Tectonique des plaques dans les Alpes. Gordon and Breach Science, Paris, p 208

Orombelli G, Deline P (2002) L'anfiteatro morenico del Miage (Courmayeur, Valle d'Aosta): nuovi dati sulla sua genesi. Istituto Lombardo (Rendiconti Scienze) B 134(2000):115–133

Perello P, Piana F, Martinotti G (1999) Neo-alpine structural features at the boundary between the penninic and helvetic domains (Pré S. Didiér – entrèves, Aosta valley, Italy). Eclo Geol Helv 92:347–359